STEREOSPECIFIC PHOTOCHEMICAL TRANSFORMATIONS INVOLVING AXIALLY CHIRAL ACRYLANILIDES AND α-OXOAMIDES

A Dissertation
Submitted to the Graduate Faculty
of the
North Dakota State University
of Agriculture and Applied Science

By

Anoklase Jean-Luc Ayitou

In Partial Fulfillment
for the Degree of
DOCTORATE OF PHILOSOPHY

Major Department:
Chemistry and Biochemistry

April 2013

Fargo, North Dakota

North Dakota State University
Graduate School

Title

STEREOSOECIFIC PHOTOCHEMICAL TRANSFORMATIONS INVOLVING AXIALLY CHIRAL ACRYLANILIDES AND α-OXOAMIDES

By

Anoklase Jean-Luc Ayitou

The Supervisory Committee certifies that this ***disquisition*** complies with North Dakota State University's regulations and meets the accepted standards for the degree of

DOCTOR OF PHILOSOPHY

SUPERVISORY COMMITTEE:

Prof. Sivaguru Jayaraman
Chair

Prof. Mukund Sibi

Prof. Pinjing Zhao

Prof. Kalpana Katti

Approved:

April 05, 2013 — Date

Prof. Gregory CookÍÍ — Department Chair

ABSTRACT

Asymmetric photochemical transformations have been under-explored due to the ineffectiveness of conventional methodologies/reagents/catalysts (point chiral auxiliaries and inductors) that were generally employed for thermal reactions. This limitation to use point chiral auxiliaries for asymmetric photochemistry is partly due to the asynchronous behavior of photo-excitation and chiral transfer/induction processes.

This dissertation describes a complementary approach to conventional methodologies involving light induced chirality transfer from atropisomeric *viz* axially chiral molecular reactants (acrylanilides and α-oxoamides) to enantiopure product(s) with point chirality. The study has revealed the importance of rotamers control in the ground state and how it can impact the stereospecificity during light induced excited state reactions leading to enantiopure product(s).

Con-rotatory 6π-photocyclization of axially chiral acrylanilides was explored under various reaction conditions. For example, α,β-unsaturated acrylanilides gave the expected 3,4-dihydroquinolin-2-one photoproduct(s) with enantiomeric excess (*ee*) values > 90% in both direct and triplet sensitized irradiations. On the other hand, the solution phase direct irradiations of α-substituted acrylanilides yielded racemic photoproduct(s) whereas the triplet sensitized reactions led to *ee* values > 90% in the expected photoproduct(s). By changing the reaction medium from isotropic media to solid state, α-substituted acrylanilides gave photoproducts with *ee* values as high as 70%.

In addition to the effect of the reaction medium and the reactive spin state on the enantioselectivity, preliminary evaluation of the role of Lewis acid(s) and heavy cations (Na^+, K^+ and Cs^+) were explored. The initial observations were quite promising with *ee* values up to 90% in the photoproducts upon direct irradiation in isotropic media.

The photochemical γ-hydrogen abstraction reaction involving axially chiral α-oxoamides leading to β-Lactam photoproducts was investigated. The enantiomeric ratio (*e.r.*) > 90:10 in the expected β-Lactam photoproducts was found to be dependent on the temperature under which the irradiation was performed. Furthermore, elevated pressure was employed to counter the effect of elevated temperature and slow the rotation around N-C(aryl) chiral axis leading enantioenriched β-Lactam photoproducts.

This dissertation details the overall mechanistic rationales and photophysical control studies during the photochemical transformations of atropisomeric acrylanilides and α-oxoamides leading to chirally enriched products.

ACKNOWLEDGMENTS

On one afternoon of fall 2006, I walked into the office of the Chair (Prof. John Hershberger) of the Department of Chemistry and Biochemistry at North Dakota State University (NDSU); I told him that I wanted to join a research group in order to have some research experience and laboratory skills. He directed me to a young faculty (Prof. J. Sivaguru), who had just joined the department…and mentioned to me that he may be looking for motivated undergraduate students. Here I am, from the first day I talked to Prof. Sivaguru about my ambitions on that day in his office. I sincerely and graciously wish to thank my advisor Prof. Sivaguru for his guidance and endless support for my research endeavors, to the preparation of this dissertation and for being a great mentor who knows his students' needs. I also want to thank him for having taught me integrity, perseverance and hard work in every aspect of research.

I would like to thank Prof. John Hershberger for having set me on the right path from the day I talked to him.

I would like to thank the committee members (Prof. Mukund Sibi, Prof. Kalpana Katti and Prof. Pinjing Zhao) who have supervised the research work described in this dissertation and for their useful advice that helped me overcome challenges in my projects.

I would like to thank the faculty in the Department of Chemistry and Biochemistry at NDSU for their support and advice that helped me achieve the best of myself.

For the past six years, I felt welcome and I enjoyed the collegial environment and camaraderie in the research lab of Prof. Sivaguru and in the entire Department of Chemistry at NDSU; I would like to thank my lab mates (Dr. Barry C. Pemberton, Elango Kumarasamy, Nandini Vallavoju, Ramya Raghunathan, Anthony Clay and Akila Iyer and past members of the group) and other graduate students whose path had crossed mine during this journey. I also thank other scholars and friends at NDSU who have made my journey a smooth one.

I would like to thank the staff scientists (Dr. Angel Ugrinov, Dr. John Bagu and Daniel Warner) and the clerical staff (Wendy Leach, Linda Stoetzer and David Tacke) in the department of Chemistry and Biochemistry for their support and help during this journey.

I would like to thank the following people who have been involved as collaborators in my research work:

- Prof. Nickolas Turro† and Dr. Steffen Jockuch at Columbia University, New York, NY for their collaborative work regarding photophysical aspects of this dissertation. A special thanks to this team of researchers who hosted me in their lab to complete key experiments that are part of this dissertation.
- Prof. Yoshihisa Inoue, Dr. Gaku Fukuhara and the staff in the Prof. Inoue's lab at Osaka University, Osaka, Japan for their collaborative work with photochemical transformation under elevated pressure. A special thanks to this team of researchers who hosted me in their lab to complete key experiments that are part of this dissertation.
- Prof. Anna Gudmundsdottir at University of Cincinnati, Cincinnati, OH and Prof. Svetlana Kilina at NDSU, Fargo, ND for their insights and help with the computational aspect of this dissertation.

I would like to thank the following agencies for providing me with the opportunity to perform my research at NDSU:

- The National Science Foundation (NSF) for a graduate fellowship and a research grant that was useful in successfully completing the topic related to this dissertation
- The National Science Foundation for the generous support of the research (CAREER CHE-0748525 and CHE-1213880).
- The National Science Foundation grant (NSF-CRIF) for purchase of XRD instrument (CHE-0946990).
- Merck and the United Negro College Fund (UNCF) for a financial support to the research described in this dissertation.
- GlaxoSmithKline and the National Organization for the Professional Advancement for Black Chemists and Chemical Engineers (NOBCChE) for a graduate research award to recognize my achievements.

- The Global Center Of Excellence (GCOE) for Eco-Chemistry and Environmentally Friendly Protocols at Osaka University, Japan for a student fellowship that helped me traveled to Japan for research work related to elevated pressure experiments described in this dissertation.

A smile and thanks, a kiss and a hug to my family:

My wife Adjo Delali Mlapa for her everyday love and patience

My son Warase Arsene-Kevin Ayitou for the joy he provided me during this journey. He is the leitmotiv and the driving force that encouraged me in this journey

My parents for their endless support during this journey

My family especially my wife and my son have been very understanding whenever I needed to stay late in the lab to collect data, which are presented in this dissertation.

TABLE OF CONTENTS

LIST OF TABLES

LIST OF FIGURES

LIST OF SCHEMES

LIST OF EQUATIONS

LIST OF CHARTS

ABBREVIATIONS

AcOH……..Acetic Acid

CD……...Circular Dichroism

Ch……..Cyclohexyl

$CHCl_3$/$CDCl_3$….....Chloroform/deuterated chloroform

Cp…….……Cyclopentyl

CPL……..Circularly Polarized Light

d.e..……..Diastereomeric Excess

DCM..……..……..Dichloromethane

DEPT……..……..Distortionless Enhancement by Polarization Transfer

DMSO……..Dimethylsulfoxide

ee/e.r……Enantiomeric Excess or Ratio

E_T..……Triplet Energy of an excited species

EtOAc...……..……Ethyl Acetate

EtOH……..……Ethanol

GC...……..……Gas Chromatography

HOMO…...……..….Highest Occupied Molecular Orbital

HPLC……....High Performance Liquid Chromatography

HRMS/HRMS-ESI……...High Resolution Mass Spectrometry (Electropray Ionization)

IPA……..Isopropyl Alcohol

ISC…..……..……..Intersystem Crossing

LUMO……Lowest Unoccupied Molecular Orbital

MBA……..…….. *S*-(-)-Methylbenzylamine

MCH……Methylcyclohexane

MeCN……..……...Acetonitrile

MeOH……..……...Methanol

NEER……..Non-Equilibrating Excited Rotamer *principle*

NMR……...Nuclear Magnetic Resonance *spectroscopy*

R*f*……..……Retention Factor

RT/r.t……..Room Temperature

S_1 or S_n……...……...First or n^{th} singlet excited state

SET……..……Single Electron Transfer

S_o……..……Ground state (singlet)

T_1 or T_n……First or n^{th} triplet excited state

TFE……..……...Trifluoroethanol

THF…….....Tetrahydrofuran

UV/VIS……....Ultra-Violet/Visible light

XRD……X-ray Diffraction

CHAPTER 1. INTRODUCTION TO PHOTOCHEMISTRY AND ADVANCES IN LIGHT INDUCED ASYMMETRIC SYNTHESIS

This chapter is divided into 3 parts to give an overview of the concepts/topics relevant to this dissertation.

Part 1

This section will first introduce the photosynthetic process and then make a connection to the field of photo-sciences. Photochemistry will be succinctly explained from the quantum theory point of view. This will then lead to the discussion on the interaction of light (as electromagnetic wave) and matter (in the form of electron *viz.* particle).

Part 2

The chronology of and strategies in asymmetric organic photochemical transformations will be detailed: starting from the use of circularly polarized light sources that have been employed to achieve asymmetric synthesis of some essential molecules to the recent advances in the preparation of chirally enriched molecules using non-polarized light sources. In this context, the need of chiral auxiliaries/inductors or/and chiral crystalline materials will also be discussed.

Part 3

This section will introduce non-biaryl atropisomeric substrates and their unique structural and stereodynamic features that are explored in thermochemical transformations. The discussion from this part of the dissertation will lead to the second chapter to demonstrate the effective chiral transfer using atropisomeric motifs during photochemical transformations in solution.

1.1. Introduction

Our ability to see many colors, shapes, and figures originates from the interaction of light with matter. This interaction of light with matter is the essence of life on earth with regard to species that use sunlight to "survive" commonly referred to as *phototrophs*. As a matter of fact, carbohydrates that are needed to sustain life are produced via the well-known process of *photosynthesis*, by which plants and other organisms convert sunlight into chemical energy. Under sunlight, chlorophylls from plants or other organisms for example are able to fix carbon dioxide to produce sugar molecules and oxygen as depicted in scheme 1.1.

$$6\,CO_2 + 6\,H_2O \xrightarrow{\text{Light}} C_6H_{12}O_6 + 6\,O_2$$

Scheme 1.1: Synthesis of glucose by photosynthetic process.

For million or even billion of years, nature has elegantly employed the photosynthetic process to sustain life on earth. To mimic nature and produce many other essential molecules, it is important to understand not only the composition of light, which is the most indispensable reagent in photochemical processes, but also its interaction with matter.

1.2. Photochemistry

During the early 20th century, groundbreaking advances led us to the understanding of "light" with both wavelike and particle-like properties. The wavelike theory suggests that light is a combination of electromagnetic (EM) waves from very low energy frequencies like radio waves, to radiations with very high-energy frequencies such as gamma rays (Figure 1.1). The visible region of light (400 – 700 nm) is what is available for humans' eyes to see colors, shapes and figures; while other species and organisms interact with the UV region of the light spectrum to function. This interaction is a consequence of the quantization of the energy of matter, which has a separation that is of the same order as the energy of visible or UV light.[1]

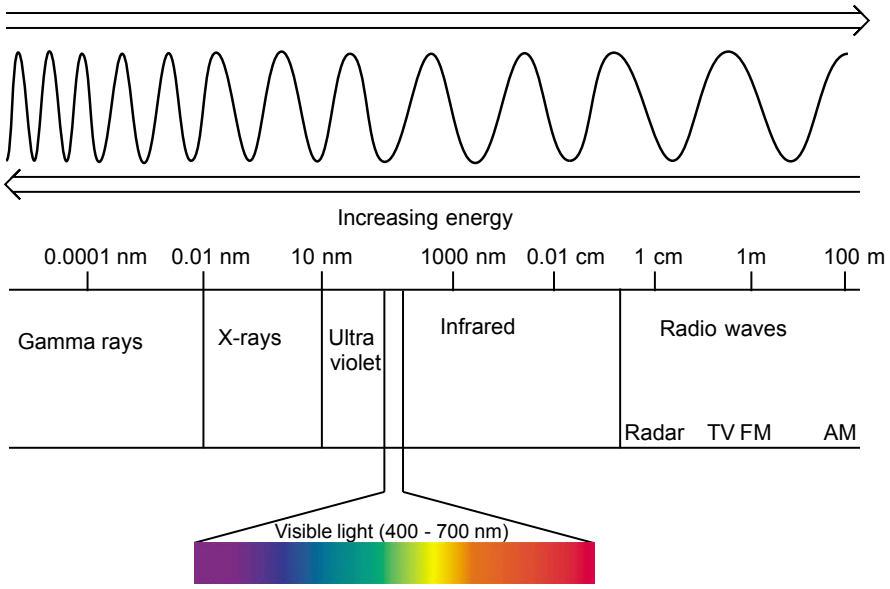

Figure 1.1: Electromagnetic wavelike representation of light.

It is a *universalis veritas* that matter at the sub-atomic level is constituted of electrons, which have both wavelike and particle-like properties. One of the processes by which matter would interact with light (or an energy level or a particular wavelength) is called absorption. Absorption of UV or visible light by matter can produce electronically-excited (or reactive) species, which is a consequence of electrons being excited to higher energy level as shown in figure 1.2.

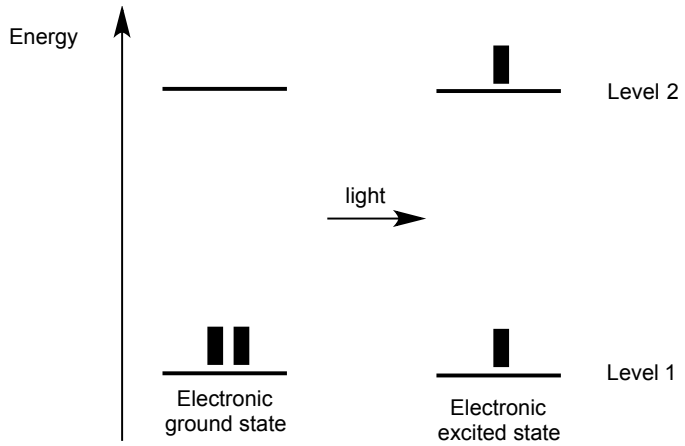

Figure 1.2: Energy levels of matter upon absorption of UV or visible light: Adapted from ref. 1.
(▮) Represents an electron.

The particle-like property of light suggests that light interacts with matter (e.g. chemical species) in the form of particles called *photons*, which have no rest mass and always travel at the speed $c \sim 3 \times 10^8$ m/s in vacua and whose probabilities of observation are predicted by the quantum theory.[2] The energy E of a photon necessary to cause the excitation of species to the upper level state(s) is defined by the Planck's law (Eq. 1.1):

$$E = h\upsilon$$

Equation 1.1: Planck's law defining the energy of a photon: h is the Planck's constant (6.63×10^{-34} Js) and υ is the frequency of the electromagnetic radiation in s^{-1}.

Chemical species that absorb light (a wavelength or set of wavelengths) are called chromophores. In a typical absorption process, quantization suggests that a photon having energy equal to the energy difference between two electronic states of a chemical species is absorbed. This process is followed by the production of electronically-excited chemical species, which could undergo a photochemical transformation according to the Grotthuss-Draper law (Principle of photochemical activation). Depending on the functional groups that are present in a given chromophore, the transition(s) from the ground state to the excited state(s), that is, the promotion of one electron from the *highest occupied molecular orbital* (HOMO) to the *lowest unoccupied molecular orbital* (LUMO) must follow certain rules with respect to electronic transitions. Depending on the chromophores in the molecule, one or more occupied and unoccupied orbital(s) may be present. Figure 1.3 shows plausible molecular orbitals encountered in organic photo-chromophores.

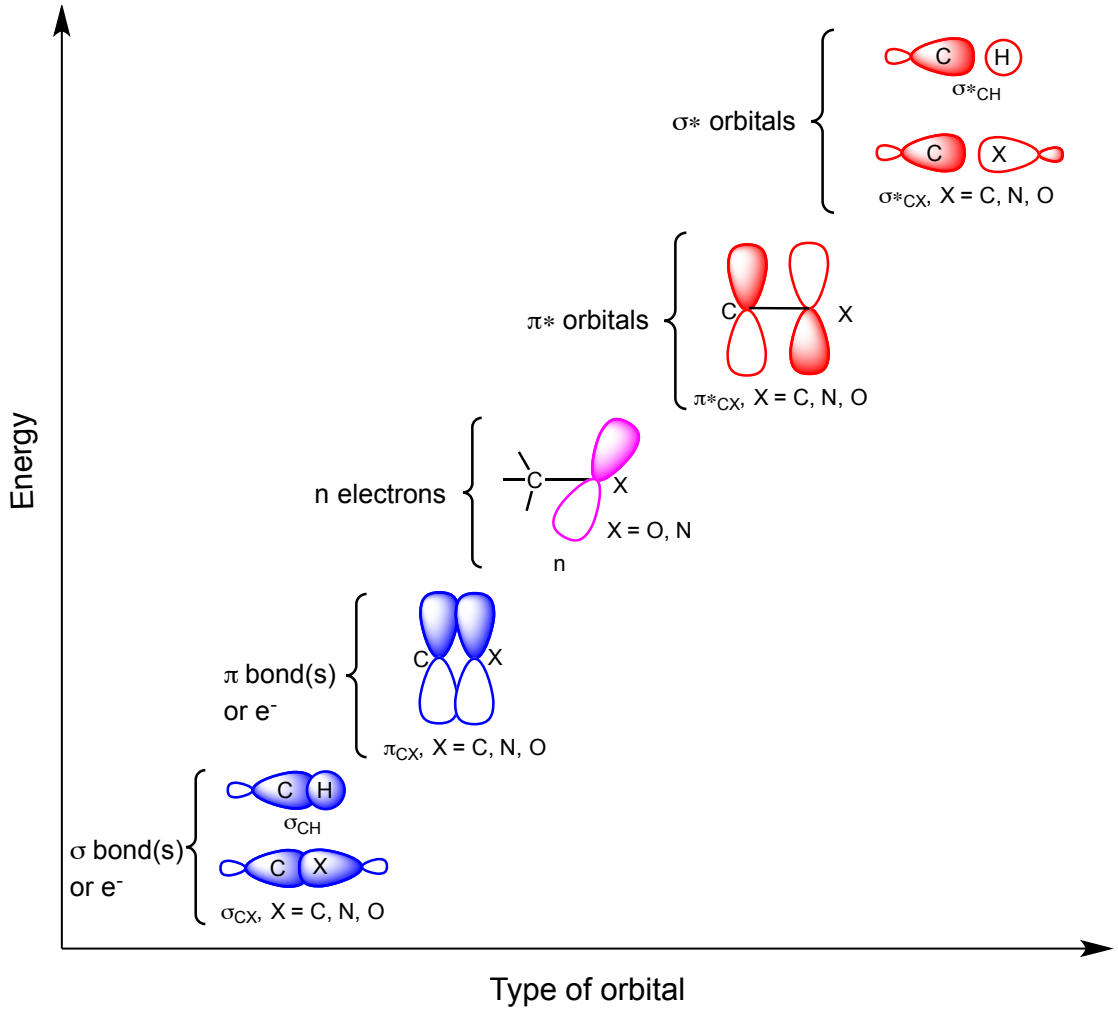

Figure 1.3: Molecular orbital for most occurring functional groups in organic chromophores.

In most chromophores, there are various electronic transitions with different energetics. For example, alcohols R – OH absorbing in the region 180 – 185 nm have n→σ* transition; isolated C=C alkenes having maximum absorption in the regions 170 – 178 and 185 – 205 nm are prone to undergo π→π* and π→σ* transitions and amide functional groups R–CO–NH_2 have exclusive absorption maximum at 175 nm with a n→π* and n→σ* transitions mainly localized on the amide carbonyl functionality.

A hypothetical molecule having combinations of chromophoric functional groups display characteristic absorption profile(s) with one or more transitions, which dictate the photophysical properties and allow exploring the photochemistry of the molecule of interest. The absorption of photons by the

hypothetical chromophore from the singlet ground state, S_0, with multiplicity $2q+1 = 1$ (where q being the total spin of e^-) to upper states (S_n or T_n, n = 1, 2, 3… for S_n, $q = 0$ and for T_n, $q = 1$) is termed as excitation. Depending on the type of functionality that is being excited, the transition from S_0 to S_n or T_n is accompanied by many processes summarized by the following diagram known as the Jablonsky's diagram (Fig. 1.4).

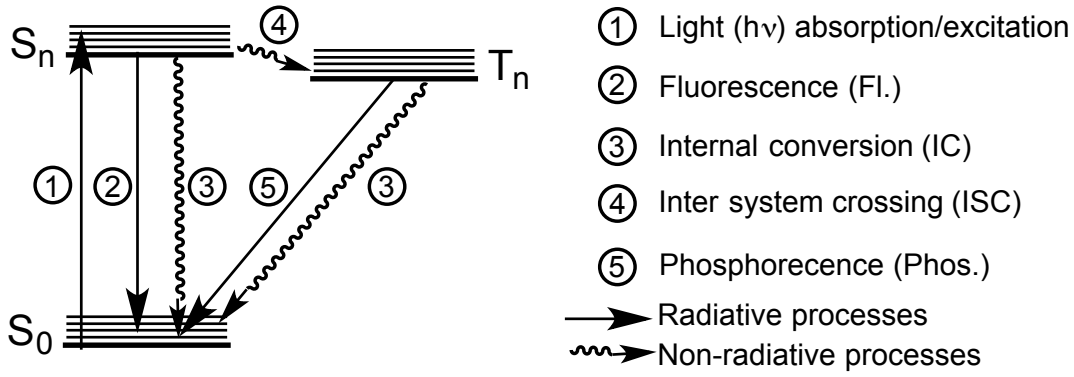

Figure 1.4: Simplified photophysical processes: Adapted from the Jablonsky's diagram ref. 3.

The events that follow can be generalized as a paradigm for the processes occurring upon interaction of a chemical species and photon(s) and illustrated in figure 1.5.

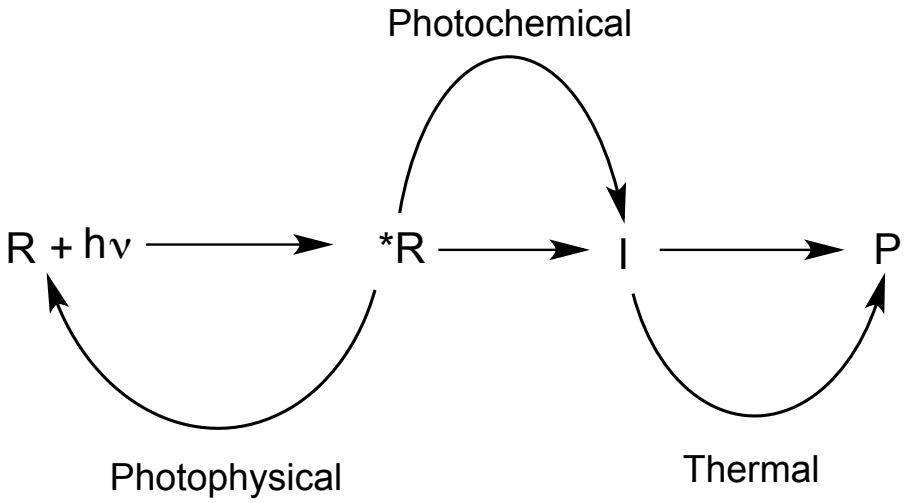

Figure 1.5: A global paradigm for photochemical pathways of *R to P and the overall photophysical pathways from *R to R:[3] Adapted from ref. 3.

According to the last two diagrams (Figure 1.4 and 1.5), photophysics would deal with radiative and non-radiative processes that occur upon absorption of a photon by chemical species “R” leading to the corresponding excited species “*R” and the physical phenomena that followed are decay(s) back to the ground state as illustrated by figure 1.5. From the excited state(s), species *R can also undergo other transformations *viz.* formation of new bonds and/or breaking of bonds or migration of group(s). Thus, photochemistry elucidates chemical transformations occurring from *R to P and studies the chemical reactions and physical changes that result from interactions between matter and light.

1.3. Asymmetric Reactions: Thermal vs. Photochemical Reactions

Over the years, many transformations of organic chromophoric molecules have been explored. The stereochemistry (spatial arrangement of atoms or groups of atoms that form the three dimensional features of molecules[4]) associated with these transformations depends not only on the substrate(s) but also on the type of transformation(s) as well. Most stereoselective or asymmetric transformations (thermal or photochemical) have hitherto required chiral auxiliaries or inductors. In thermally controlled reactions for example, a chiral auxiliary **X** is tethered to a reactant R in order to differentiate two transition state species with respect to a stereo-center. The asymmetry induced in the transition state favors one diastereomeric species over the other in terms of its activation energy. At 25 ^{o}C for example, a difference in activation energy of 2.81 kcal•mol^{-1} will lead to the formation of the expected product P with 99% of stereoselectivity as depicted in figure 1.6-A. Unlike thermally controlled reactions, the paradigm dictating photochemical transformations involves a reactant R that is promoted to the excited state upon absorption of a photon of light of appropriate wavelength/frequency; R, thus becomes *R, which has a short lifetime in the excited state to undergo a specific transformation. Even in the presence of a chiral handle, the reaction becomes a downhill barrier-less process, leading to poor stereoselectivity unless the reaction environment is pre-organized or preset to favor one stereoisomer as in organized environments/assemblies.

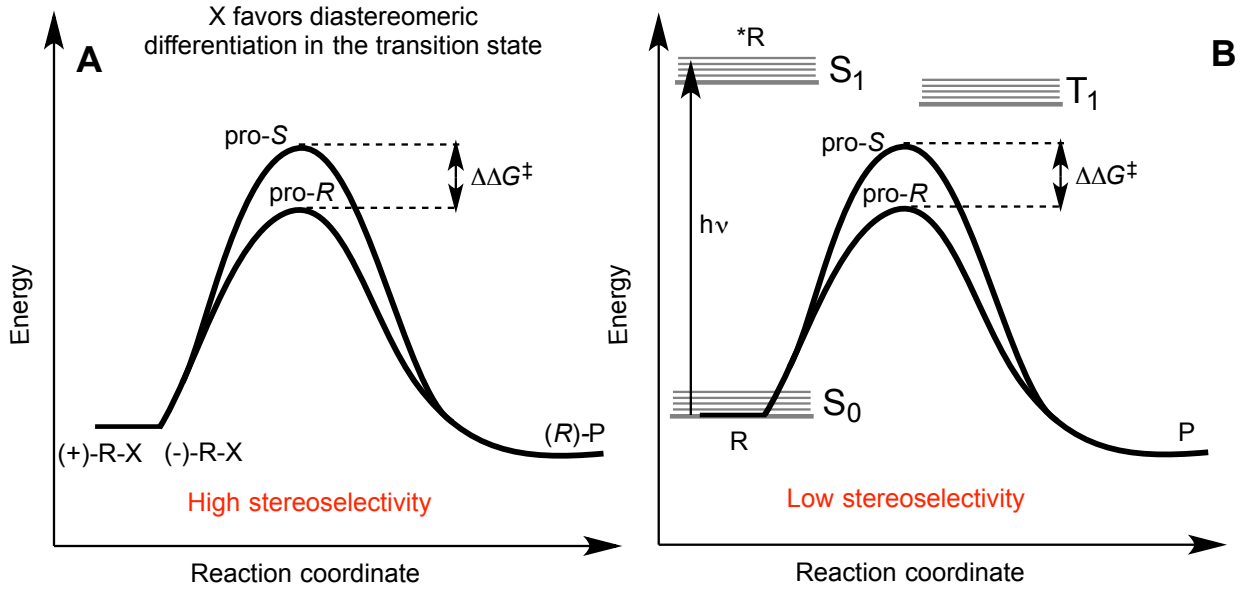

Figure 1.6: Schematic representation of diastereomeric differentiation in the transition state. **A**: thermal reaction, where the transition states energetics lead to asymmetric induction in the final product. **B**: photochemical transformation, where light excitation and chiral induction are asynchronous in terms of rates and energetics.

As illustrated in figure 1.6-B, the energetics in the excited state does not permit differentiation of pro-*R* and pro-*S* diastereomeric transition states. The short lifetime of the reactive species *R limits effective chiral transfer or induction during photochemical transformations. To achieve asymmetric during photochemical transformations, many elegant methodologies have been employed with varying degree of success. The next section details recent and useful advances in the field of asymmetric organic photochemical transformations.

1.4. Circularly Polarized Light or "Chiral Light"[5]

The EM nature of light has allowed scientists since 1860 to devise methodologies to polarize it. An unpolarized light is known to vibrate in all directions; nevertheless, we may simplify an unpolarized light with directed vertical and horizontal oscillations representing the electric and magnetic fields. When the electric field of an EM radiations passes through polarised media of different refracting indices (polarization by refraction) or when it is reflected off of two glass mirrors (polarization by reflection), it becomes polarized. A complementary approach is to use a polarizer such as the Nicol prism[6] to obtain

two directed (polarized) beams: one that is in the same plane as the incident beam and the other, which plane is perpendicular to the incident plane.

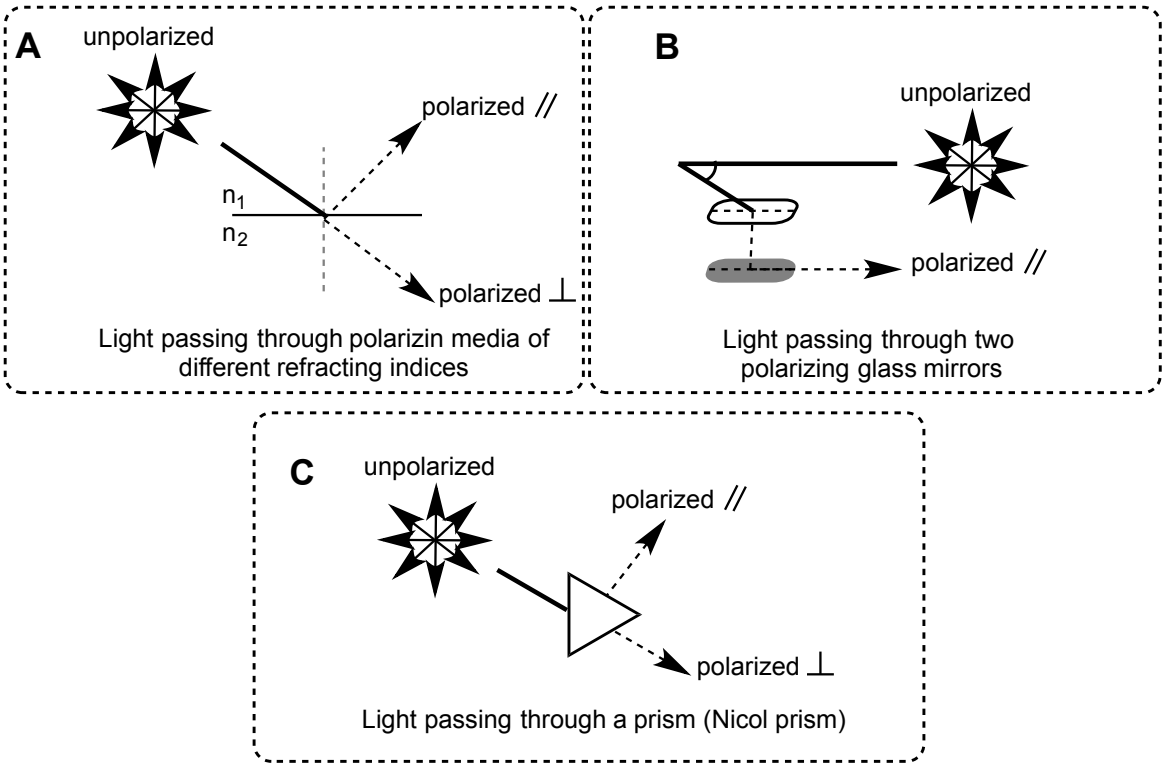

Figure 1.7: Techniques employed to generate polarized beams of light: Adapted from PPL and CD handout by Norma J. Greefield (September 09, 2004).

Circularly polarized light (left and right) is created superposition of plane polarized light with a dephased angle of 90^{o} between the two components (parallel and perpendicular). The original approach for creating circularly polarized light is to use a Fresnel rhomb.[7,8]

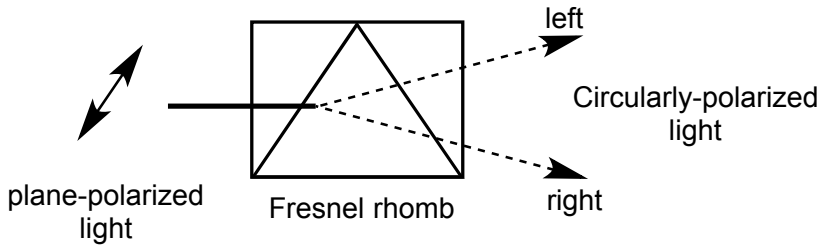

Figure 1.8: A Fresnel rhomb [7,8] is used to generate circularly polarized light (CPL): Adapted from PPL and CD handout by Norma J. Greefield (September 09, 2004).

The development of CPL has been of great importance in the early years, as it allowed chemists to transfer chiral information from the asymmetric field to racemic or pro-chiral organic molecules in order to obtain higher stereoselectivities during a transformation of interest.[5] Although a directed/polarized magnetic field could also be employed to achieve asymmetric photochemical transformations, we will concentrate on exploring how CPL has been employed to perform asymmetric photochemical transformations.

1.5. Strategies for Asymmetric Organic Photochemistry

1.5.1. Solution phase transformations using CPL

Chemical methods utilizing CPL are often called absolute asymmetric synthesis, as there is no net chirality in the molecular reactant.[5] Asymmetric photochemical transformations may also utilize pre-organized molecular reactants (crystalline or supramolecular assemblies) to obtain chirally enriched product(s) by using non-polarized light. Thus, by an absorption process, racemates or regioisomers of a given chromophoric substrate interact with R-CPL or L-CPL to end up with enantiomeric enrichment in the final photoproduct.

In 1897, Le Bel and Van't Hoff were the first to explain CPL (occurring in the universe) as a possible cause of the abundance of some forms of biomolecules: L-amino acids and D-sugars are tangible examples for this observation.[9-11] Many other theories have thereafter attempted to explain the homochirality of the universe until in 1929, Werner Kuhn, who has been working in the field of asymmetric photolysis, demonstrated the first enantioselective photolysis of racemates of ethyl-α-bromopropionate (**1**)[12] and *N,N*-dimethyl-α-azidopropionamide (**3**).[13] The transformation was presumed to go through homolytic cleavage of α-C–Br(N_3) bond followed by stereoselective recombination promoted by the asymmetric field of the light source. It was also mentioned that the anisotropy factor (g) of the molecular reactant played a crucial role in the enantioenrichment of the final product.

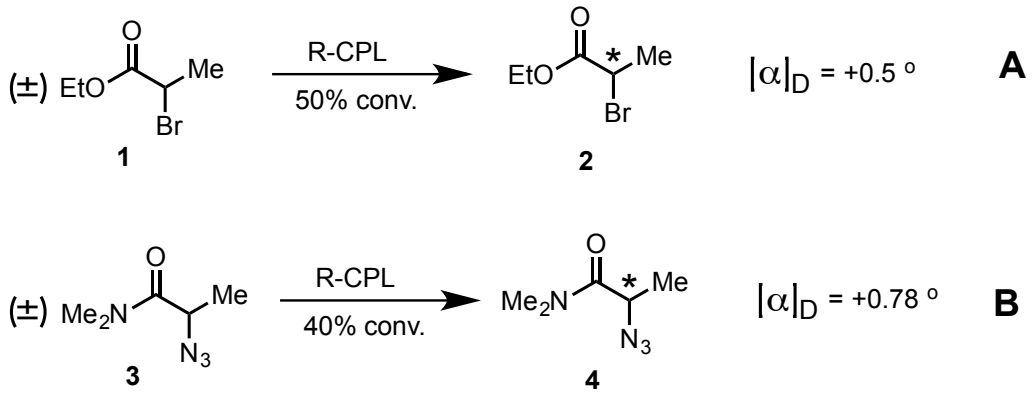

Scheme 1.2: CPL promoted enantioenrichment of ethyl-α-bromopropionate **1** and *N,N*-dimethyl-α-azidopropionamide **3**: Adapted ref. 13 and 14 and from a handout by Tehshik Yoon, Princeton University.

The discovery of CPL to be used in fundamental research prompted Henri Kagan and co-workers in 1971 at the University of Paris-Orsay to achieve the first asymmetric synthesis of optically active hexahelicene (having planar chirality) using R-and L-CPL. 1-(β-naphthyl)-2-(3-phenanthryl)ethylene (**6**) or 1-(2-benzo[c]phenanthryl)-2-phenylethylene (**7**) were photo-oxidized in the presence of iodine for 10 and 6 h respectively to afford optically active hexahelicene (scheme 1.3-A).[14] In 1974, the same research team reported the highest photochemically induced enantiomeric excess ever reported during that time frame. Racemates of camphor (**8**) were irradiated with CPL to 99% completion with up to 20% *ee.* (Scheme 1.3-B)[15]

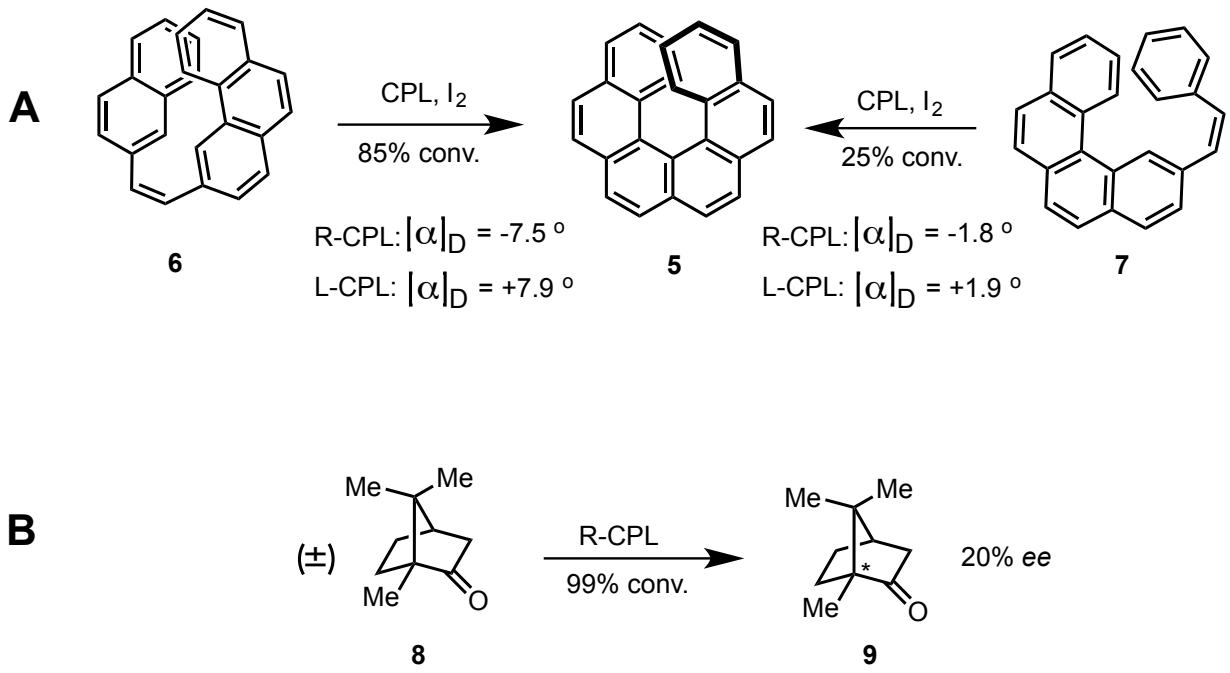

Scheme 1.3: CPL promoted synthesis of chiral hexahelicene (A) and camphor (B): Adapted from ref. 15 and 16.

In 1977, another distinguished investigation of asymmetric photolysis using CPL was achieved by Flores and co-workers.[16] Racemic samples of leucine (**10**) were photolyzed using a 218 nm R- or L-CPL to afford chirally enriched leucine (**11**) samples with 2.5% *ee* at a maximum conversion of 75%. The findings from this investigation support the role and contribution of asymmetric photochemistry in explaining the origin of optical activity and (homo)chirality in majority of biomolecules.

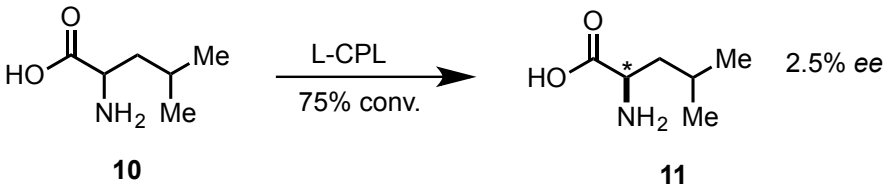

Scheme 1.4: Enantioenrichment of leucine (**10**) promoted by CPL: Adapted from ref. 17.

Indeed, the development of CPL impacted the field of asymmetric photochemistry and allowed chemists to utilize photochemistry as a complimentary tool for organic synthesis. In order to be useful and to serve as a mimic to nature (synthesizing optically pure molecules), asymmetric organic photochemistry has to comply with cost effective and environmentally benign reaction conditions. Thus, to make use of

broadband light sources and scale up photochemical processes, chemists have relied on the very simple idea of “chiral environments” instead of “chiral light” to achieve absolute asymmetric synthesis. In this picture, one may use chiral auxiliaries or inductors to create solution phase “chiral pockets” for the molecular reactant, although we have already provided ample evidence from literature that this methodology may not be successful/efficient (refer to section 1.2 Fig. 1.6). Starting from the pioneering works of Schmidt and co-workers (crystalline environments were shown to be effective in controlling photo-transformations) a chiral crystalline environment would allow transferring the chiral information from one pocket to the other even if the chromophoric unit is achiral. The next section will discuss solution phase asymmetric transformations followed by a comparison to their solvent free counterparts.

1.5.2. Asymmetric photochemical transformations in solution (unimolecular)

Asymmetric photochemical transformations using broadband light sources instead of CPL was achieved as early as 1965 by Hammond co-workers where *meso*-*cis*-1,2-diphenylcyclopropane (**12**) underwent stereochemical isomerization to the corresponding *trans*-isomer.[17] In the presence of optically active sensitizer naphthyl acetamide derivative (**14**), the *cis-to-trans* photoisomerization led to *ee* value of 6.7% compared to the direct irradiation (Scheme 1.5).[18] This elegant work became the bedrock for light induced asymmetric photochemistry. Since this report, various research groups have employed other sensitizers (chiral singlet, triplet and electron transfer) to ameliorate the *ee* value in the photoproduct during the *cis-trans* photoisomerization of the system under study. In the subsequent studies, sensitized *cis-trans* photoisomerization in the presence of chiral aromatic ketones (triplet) such as indenone and dihydronaphthalenone derivatives[19,20] and chiral *R*-menthylnaphtoate (singlet) afforded poor *ee* (1 – 3%).[21] The highest *ee* value (up to 10%) was achieved with chiral (poly)alkyl benzene(poly)carboxylates.[22,23]

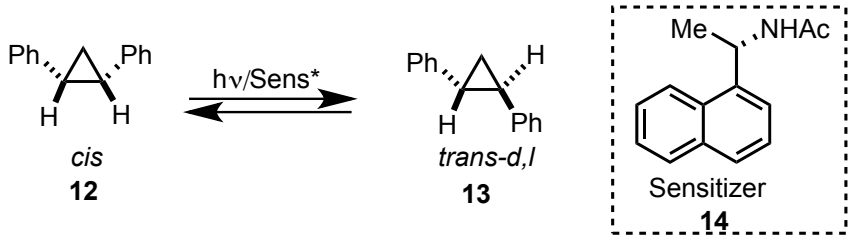

Scheme 1.5: Stereoselective photoisomerization of 1,2-diphenylcyclopropane: Adapted from ref. 22.

Since the pioneering work by Hammond and co-workers in 1965 with regard to the use of chiral sensitizers for asymmetric photochemical transformations, various elegant stereochemical photoreactions have been studied in solution at ambient conditions. Photoinduced lactonization of 5-methyl-1-hexenoic acid (**15**) for example was one of the most useful transformations, where cyanoaromatics sensitizers such as 1-cyanonaphthalene have been employed in a single electron transfer (SET) process to afford photocyclized product lactone derivatives.[24,25] The stereochemistry of the cyclization have been separately studied by García and co-workers who found that optically active 2,4,6-triphenylpyridinium tetrafluoroborates (**18**) could be used as electron-accepting triplet sensitizer to afford optically active isopropyl hydrofuranone (**16**) in 3 – 7% *ee* (Scheme 1.6).[26] The presumed mechanism of the transformation involved triplet energy transfer to reactive species of 5-methyl-1-hexenoic acid (**15**) that likely quench the triplet excited state of the pyridinium moiety (having a 1,4-cyclohexadiene character).

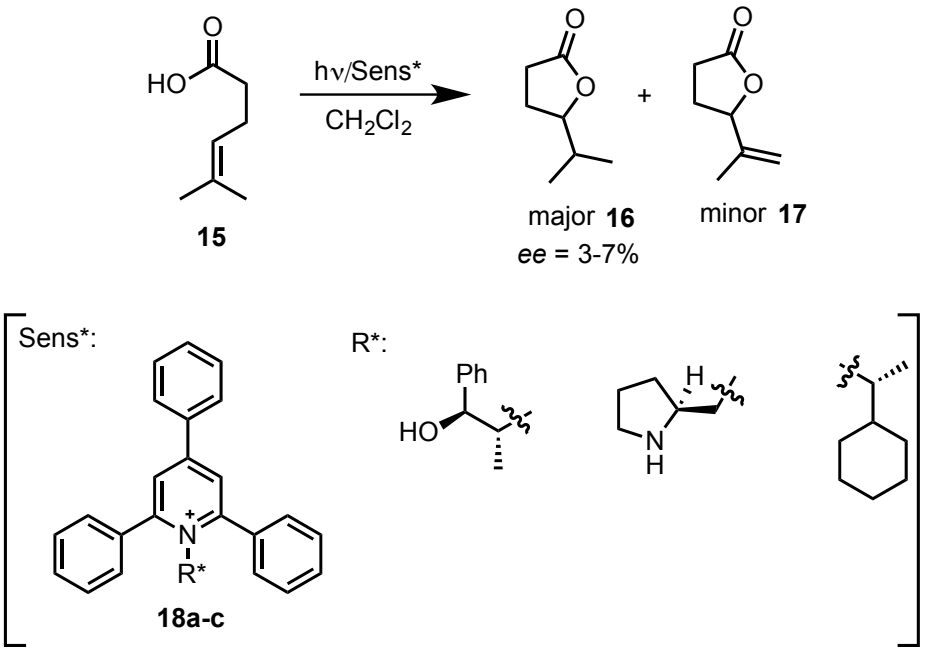

Scheme 1.6: Light induced lactonization of 5-methyl-1-hexenoic acid *via* SET: Adapted from ref. 27 and from Chiral Photochemistry book (127 – 177) edited by Yoshihisa Inoue and V. Ramamurthy.

1.5.3. Asymmetric transformations in confined media – transformations with supramolecular assemblies

Supramolecular scaffolds have been widely employed in thermally controlled asymmetric reactions. Similarly, various research groups have successfully employed supramolecular assemblies to perform asymmetric photochemical transformations with various degree of success. Recent advances in asymmetric supramolecular photochemistry involve the use of cyclodextrins, zeolites, octa-acid capsules and bidentate catalysts derived from Kemp triacid. For example, Bach and co-workers have demonstrated that amide catalysts prepared from readily available Kemp triacid could be used for supramolecular template with the ability to H-bonding for asymmetric photochemical transformations. Similar to the strategies with cyclodextrins and zeolites, the methodology employed by Bach and co-workers allows the host appended with a sensitizer (xanthone appended to Kemp triacid) to be excited by the light source followed by triplet energy transfer to the guest molecule.

As depicted in scheme 1.7, the guest molecule quinolone **19** undergoes an intramolecular [2+2] photocycloaddition to afford fused tetracyclic photoproducts **20** and **21** (two sets of enantiomers). In the presence of 5 mol% of the xanthone appended template, the transformation (at -25 ^{o}C and 1h irradiation

time) led to enantioenriched photoproducts (two regioisomers 79:21 ratio) in 94% *ee* and at 73% conversion.[27]

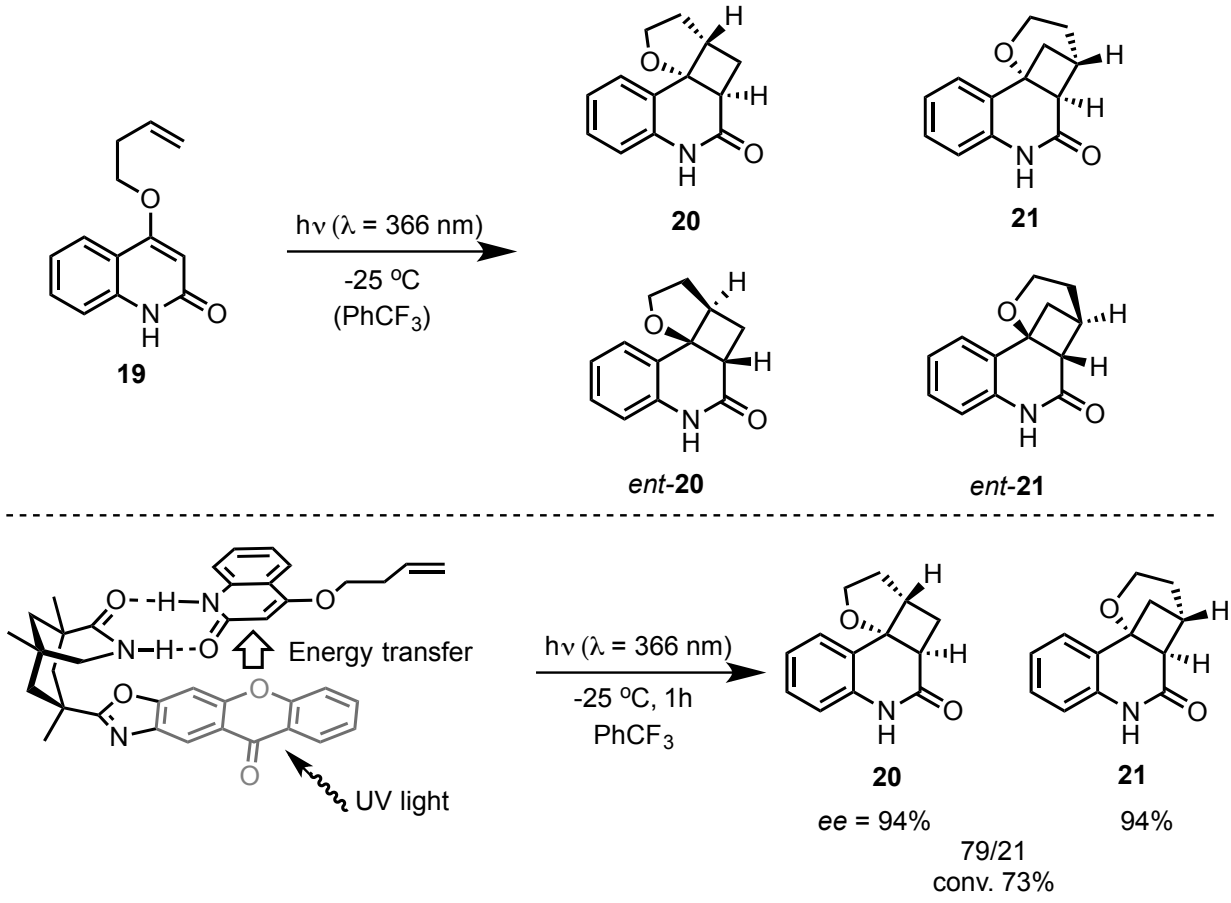

Scheme 1.7: Template mediated enantioselective [2+2] photocycloaddition: Adapted from ref. 28.

1.5.4. Solid state transformations

To achieve absolute asymmetric transformations without the help of CPL, chromophoric substrates may be recrystallized in chiral space groups; consequently, photochemical transformations in chiral crystals would lead to enantiomeric enhancement in the expected product(s). The idea of performing asymmetric photochemistry in crystalline state consists of spontaneous formation of chiral crystalline materials from achiral substrates. Once obtained, the chiral crystalline compound is exposed to a light source to undergo a specific transformation with respect to the reactive functional group (Fig. 1.9). Chiral crystals are molecular materials with no center of symmetry and glide plane; and thus, must fit into one of the 65 known chiral space groups; the most common groups being *$P2_12_12_1$, $2P_1$, and $P1$*.[28] Only a

few examples of compounds are known to crystallize in chiral space groups. The use of chiral crystals has been known for a century with the most famous and well known example of racemic sodium ammonium tartrate, which was recrystallized (below 28 ^{o}C) by Pasteur as a mixture of enantiomeric crystals that could be differentiated by their morphology and separated by hand.[29] The crystallization of achiral substrates in a chiral space group will enable asymmetric photo-transformations without any chiral source, as the chirality comes from the crystal, it is termed as *absolute asymmetric synthesis*.

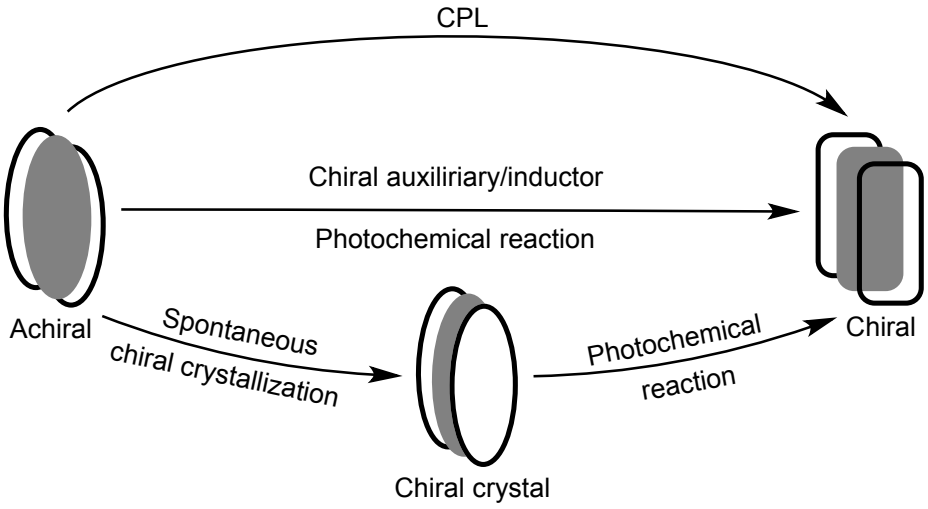

Figure 1.9: Absolute asymmetric photochemical transformation in the crystalline state.

In 1986, John R. Scheffer first reported asymmetric photochemical transformations in the crystalline state. Scheffer and co-workers have shown that samples of ethenoanthracene dicarboxylate (**22**) and methyladamantan-arylethanone (**24**) could undergo spontaneous crystallization by slowly evaporating the solvent.[29] In the case of the anthracene diester sample **22**, two dimorph crystals were grown and their identity was verified by infrared spectroscopy. The diester samples crystallized in the $P2_12_12_1$ space group and single crystals of the two dimorphs were irradiated using a Molectron UV-22 nitrogen laser (337nm, 330-mW average power). In this condition (Scheme 1.8), only the α,β-unsaturated diester chromophore (n→π* transition) was excited to undergo the famous di-π-methane rearrangement.[30] Chirally enriched dibenzosemibullvalene photoproduct (**23**) was then isolated with a specific rotation (average of ten separate irradiations) of 24.2±2.9 ^{o}.

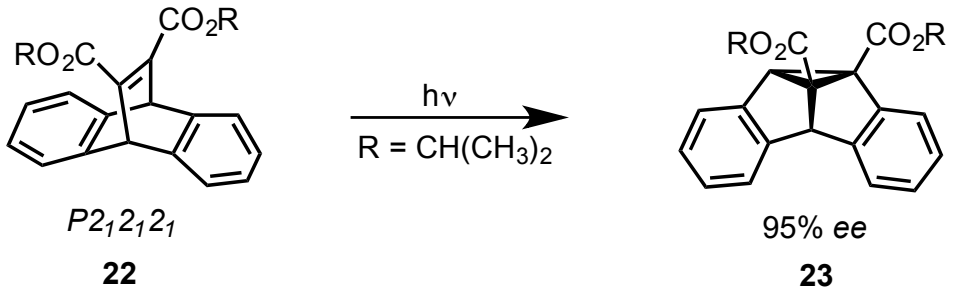

P2₁2₁2₁

22

95% *ee*

23

The di-π-methane rearrangement mechanism

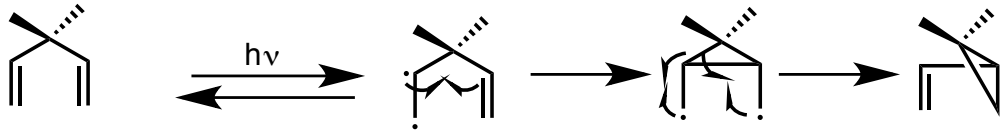

Scheme 1.8: Di-π-methane rearrangement in the solid state: Adapted from ref. 29.

The adamantyl sample also crystallized in the space group *P2₁2₁2₁* as very large prismatic crystals. Alkyl ketones are precluded to undergo Norrish/Yang type II reaction when optimal conditions are met (Scheme 1.9) (the Norrish or Norrish-Yang type II reaction will be thoroughly detailed in chapter 8). Crystals of **24** were irradiated at 8 ^{o}C to 8% conversion to yield cyclobutanol **25** as the major photoproduct with a "crude" specific rotation of -24.5 ^{o}. After workup, pure cyclobutanol was isolated in 70% yield with 80% *ee* and optical activity $[\alpha]_D$ = -21.6 ^{o}. [29]

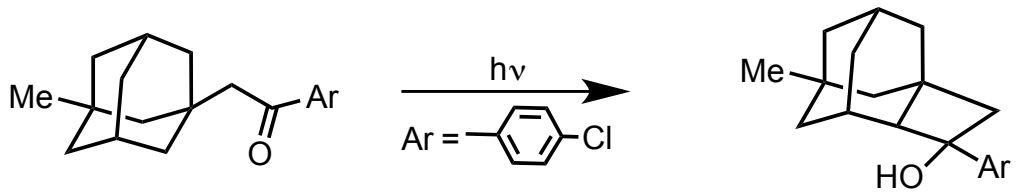

P2₁2₁2₁

24

80% *ee*

25

The Norrish/Yang type II mechanism

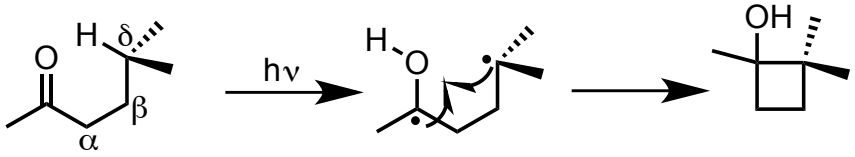

Scheme 1.9: Adapted from ref. 29.

The absolute asymmetric photochemical transformations in the crystalline state have been performed on other systems as well. In 1994, Toda and co-workers reported a 6π-photocyclization of chiral crystals of methylsuccinimide helicene derivatives (**26**) in the solid state to give optically active photocyclized product **27** (Scheme 1.10).[31]

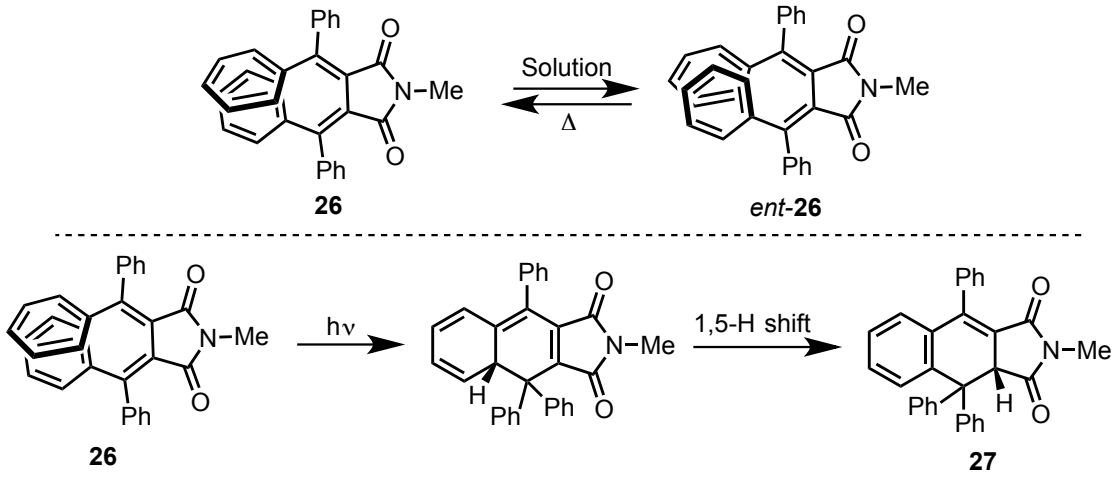

Scheme 1.10: 6π-Photocyclization of helicene derivatives in the crystalline state: Adapted from ref. 31 and from a handout by Qihui Jin, Princeton University.

Another clever approach by John Scheffer and co-workers in popularizing the concept of absolute asymmetric photochemistry in the solid-state was to devise chromophores bearing *meta*-disubstituted benzene moieties, as it was predicted by Curtin and co-workers that these systems are more likely to crystallize in noncentrosymmetric space groups than are their *ortho*- and *para*-isomers.[32] *Meta*-substituted 2-pyridones were synthesized, recrystallized and were found to be isomorphous, but crystallized in the chiral space group $P2_12_12_1$ whereas the *ortho* and *para*-substituted analogues crystallized in centrosymmetric (achiral) space groups.[33] Photochemical 4π-electrocyclization of the *meta*-substituted 2-pyridone **28** derivatives in the crystalline state afforded β-lactam photoproducts **29** with *ee* as high as 99% (Scheme 1.11).

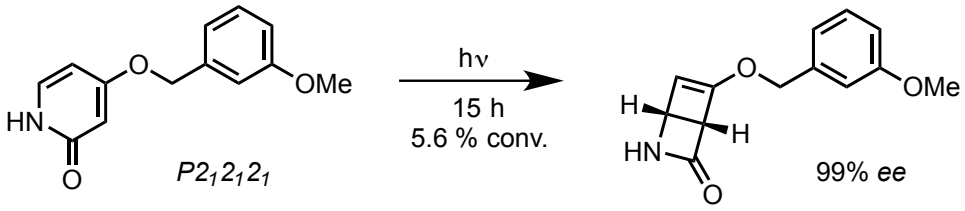

$P2_12_12_1$

28 **29**

Scheme 1.11: Intramolecular [2+2]-photocycloaddition of pyridone derivatives in the crystalline state: Adapted from ref. 33.

Other elegant transformations include intra and intermolecular [2+2] photocycloadditions. In 1993, Sakamoto and co-workers explored the intramolecular photochemical [2+2] cycloaddition of thioamide derivatives (**30**) in the solid state (Scheme 1.12). Thioamide photo-substrate was recrystallized from a hexane solution and the crystals ($P2_12_12_1$) were irradiated under N_2 through a Pyrex filter with a 500-W high-pressure Hg lamp at -45 ^oC for 12 h. After chromatographic workup, optically active thietane-fused β-lactam **31** was obtained in 70% yield with $[\alpha]_D$ = +93 ^{o} (*c* 0.1 in $CHCl_3$) and 40% *ee* (30% conv).[34]

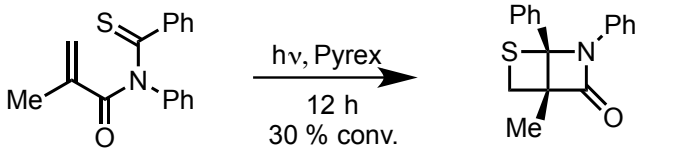

$P2_12_12_1$

30 **31**

Scheme 1.12: Intramolecular [2+2]-photocycloaddition of thioamide derivatives in the crystalline state: Adapted from ref. 34.

In the same year, they also reported an intramolecular photochemical Paternò-Büchi ([2+2] cycloaddition between a carbonyl and an alkene functional groups) of achiral acyclic imide (**32**) in the crystalline state to yield fused bicyclic oxetane moieties (**33**). Single crystals ($P2_12_12_1$) of the imide were grinded and sandwiched between two Pyrex slides and irradiated under the same conditions described above. At -78 ^oC, the solid-state irradiation yielded 89% of the oxetane moieties with 100% conversion

after 4 h of irradiation (Scheme 1.13). The *syn* photo-adduct was found to be the major product with >95% *ee* and $[\alpha]_D$ = +92 ^{o} (*c* 0.1 in $CHCl_3$).[35]

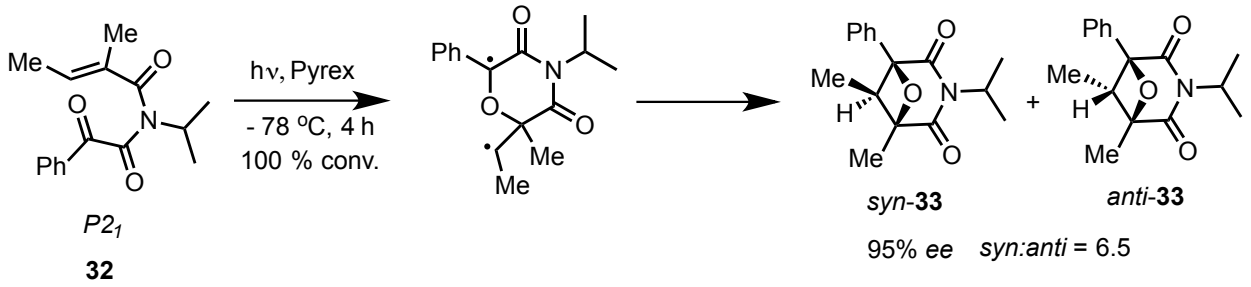

P2₁

32

syn-**33**

anti-**33**

95% *ee* *syn:anti* = 6.5

Scheme 1.13: Intramolecular Paternò-Büchi reaction involving oxoamides derivatives in the crystalline state: Adapted from ref. 35.

The intermolecular version of this transformation in the crystalline state might involve single crystals or co-crystals of chromophoric molecular reactant(s). Schmidt and co-workers were the first to investigate intermolecular [2+2] photocycloaddition of arylalkenes to generate cyclobutane scaffolds. In the early 1960s, Schmidt and co-workers successfully converted single crystal/powder of cinnamic acid (**34**) into α- and β-truxillic acid photoproducts (**35**) (Scheme 1.14).[36]

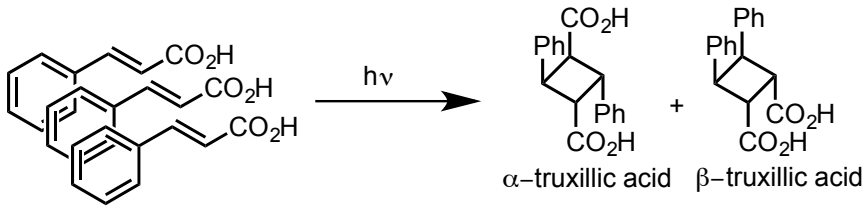

34

α−truxillic acid β−truxillic acid

35

Scheme 1.14: Intermolecular [2+2] photocycloaddition of cinnamic acid in the crystalline state: Adapted from ref. 36.

Schmidt and co-workers also reported the first hetero-dimerization ([2+2] photocycloaddition) of co-crystals (**37**) of 1-(2,6-dichlorophenyl)-4-phenyl-*trans,trans*-1,3-butadiene and its thiophene analog 1-(2,6-dichlorophenyl)-4-thienyl-*trans,trans*-1,3-butadiene. A sample containing two chromophores formed mixed crystals (polycrystalline compound) that upon irradiation gave hetero-dimers cyclobutane moieties (Scheme 1.15). The conversion to the cyclobutane photoproduct(s) (**38** and **39**) was achieved by

irradiating single mixed chiral crystals of the two alkenes in a ratio of 85:15 respectively to obtain optically active cyclobutane derivatives.[37]

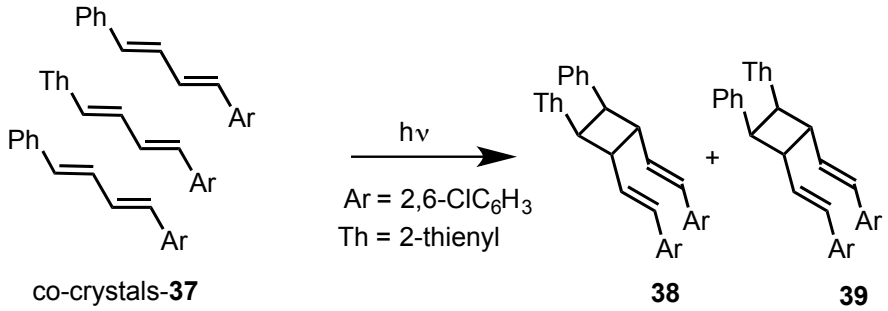

Scheme 1.15: Intermolecular [2+2] photocycloaddition of co-crystalline olefin derivatives: Adapted from ref. 37.

1.5.5. Ionic auxiliary concept in asymmetric photochemical transformations

In the mid 90's, John Scheffer and co-workers introduced the concept of ionic auxiliary for solid-state asymmetric photochemistry. With the progress made in the crystalline state transformations, they envisioned two different functional molecular entities to form co-crystals in the form of organic salts. This was termed as the ionic auxiliary approach, where carboxylic acid and amine functional groups (forming the ionic salt) were tailored through organic synthesis to serve the desired solid-state function. Apart from this functional group complementarity, Scheffer and co-workers implemented that the molecular reactant should a) be achiral in order to avoid diastereomeric resolution and b) react efficiently in the solid state to afford a chirally enriched photoproduct with one or more stereogenic centers after removal of the chiral handle. In order to test this concept, they chose to study the di-π-methane photorearrangement of a crystalline salt derived from the reaction between an ester of (*S*)-proline (**41**) and a carboxylic acid derivative (**40**) that is preset to undergo the transformation of interest.[38] Scheme 1.16 depicts the overall transformation leading to chirally enriched dibenzosemibullvalene regiomeric derivatives with 95% *ee* and 20% conversion. The ionic chiral auxiliary was removed after acidic workup treatment of the photo-sample with diazomethane. Similar strategies have been employed to carry out the photochemical Norrish/Yang type II transformation of crystalline salt of L-prolinol and adamantylacetophenone carboxylic

acid derivative.[38] Likewise the enantiomeric excess in the expected cyclized photoproduct were enhanced to up to 97% after removal of the chiral handle and treatment of the photo-sample with diazomethane.

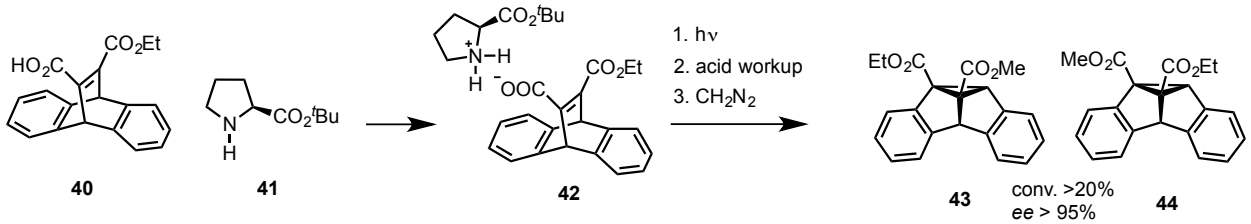

Scheme 1.16: Ionic auxiliary concept in solid-state asymmetric photochemical transformation: Adapted from ref. 38.

Absolute synthesis using chiral crystalline solids sparked fundamental research interests in asymmetric organic photochemistry. However, this growing interest faced major challenges in term of drastic reaction conditions and state-of-the-art techniques to grow single crystalline materials for photochemical transformations in the solid state. On the other hand, the longer irradiation time and the reaction temperature (in some of the cases described above) required to achieve considerable yield and enantiomeric excess prompted photo-chemists to devise alternatives to solvent-free irradiations. The first alternative was to perform photochemical transformations with nanocrystalline suspensions (solution phase). This approach not only reduced the irradiation time but also minimize the time required to grow single crystals. The second alternative was to devise chiral nano-containers *viz.* zeolites that were used as chiral inductors.[39] Nano-containers formed supramolecular templates with achiral guest chromophores; therefore, absolute asymmetric transformation would be achieved to give optically active photoproduct(s).

1.5.6. Nanocrystalline suspensions for stereoselective photochemical reactions

Nanocrystalline suspensions are precipitates of crystalline compounds in solution phase. The well known technique for the preparation of organic nanocrystals is the bottom-up approach, which is the solvent exchange method.[40] For example, a saturated solution of a target hydrophobic chromophore in acetone is dispersed into a vigorously stirred aqueous solution (Fig. 1.10), preferably water or cetyltrimethylammonim bromide (CTAB). This technique has been widely used by Garcia-Garibay and co-

workers for nanocrystallization of chromophoric achiral molecular reactants that could undergo photochemical transformation in the crystalline state.[41-43] Solid-to-solid stereoselective photodecarbonylation of diketones was scaled up by performing the same transformation with nanocrystalline suspensions. The methodology was proven even more useful for bulk scale synthesis of natural product(s).[43] Scheme 1.17 depicts the stereoselective photodecarbonylation of diketone derivatives (**45**) with retention of absolute configuration in the final photoproduct (**46**). Optically active cuperanone isomers (**49**) were synthesized using this technique.

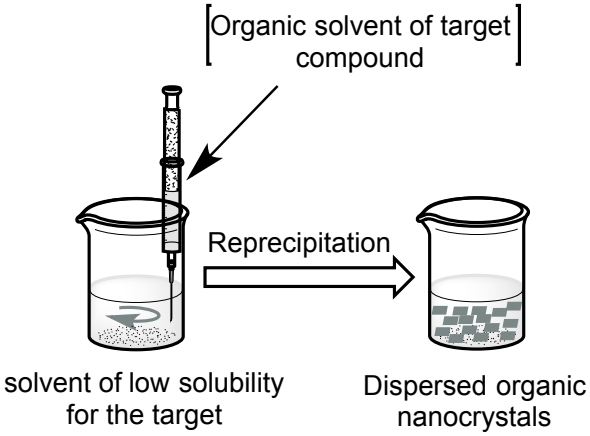

Figure 1.10: Nanocrystalization technique: Adapted from ref. 40.

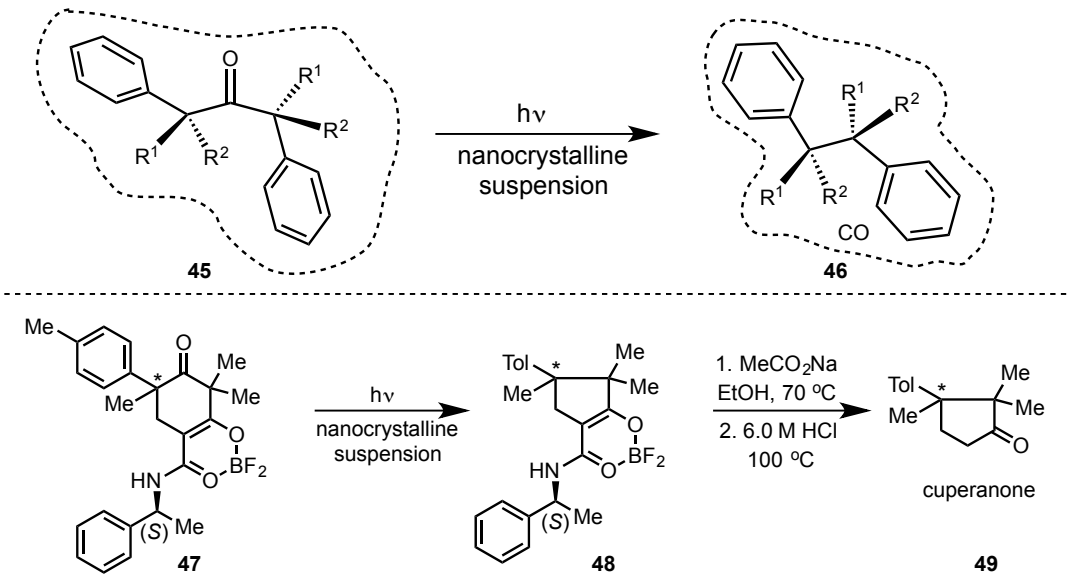

Scheme 1.17: Photodecarbonylation reaction in nanocrystalline matrix: Adapted from ref. 41 – 43.

Although scheme 1.17 illustrated a novel asymmetric synthesis of cuperanone by tethering a chiral auxiliary to the molecular reactant (which is an empirical methodology), it is important to point out that the reaction with the nanocrystalline suspension is a more cleaner and faster transformation compared to low temperature irradiations in the crystalline state. In the example reported by Garcia-Garibay and co-workers, (–)-(*S*)-(α)-methylbenzylamine (MBA) was used as chiral handle to stereochemically resolve isomers of the diketone starting material. After workup and removal of the MBA handle, optically pure isomers of (±)-cuperanone **49** were isolated with >99% *ee* and 26% yield for each pure enantiomer.[43]

1.5.7. Frozen chirality in crystals for stereospecific asymmetric photochemical transformation

As detailed in section 2.6, chiral crystals could be formed by spontaneous seeding/crystallization of achiral molecular chromophores. Various photochemical transformations have used this strategy to generate chirally enriched photoproduct(s) with varying degrees of success (low to moderate *ee*) the factors that play against an effective asymmetric transformation in the chiral crystalline lattice is the loss of the crystallinity of the reacting material during the course of the transformation i.e. the reacting system becomes achiral again due to the melting of the crystalline substrate. To retain/freeze the chirality of the crystals generated by spontaneous crystallization, Sakamoto and co-workers have designed imides (**50**) that could be frozen in the solid-state by rendering them chiral and use for chiral transfer during photochemical transformation. The systems of interest are achiral in solution, but their structural features enable them to display chirality when a given conformation is frozen in the crystalline environment. Optically pure crystals underwent Intramolecular Paternò-Büchi reaction to afford regiomeric diastereoisomeric oxetane scaffolds (**51**) with >99% *ee* at 15^{o}C (100% yield) compare to 0% *ee* at 0 ^{o}C when the system was irradiated in THF.[44]

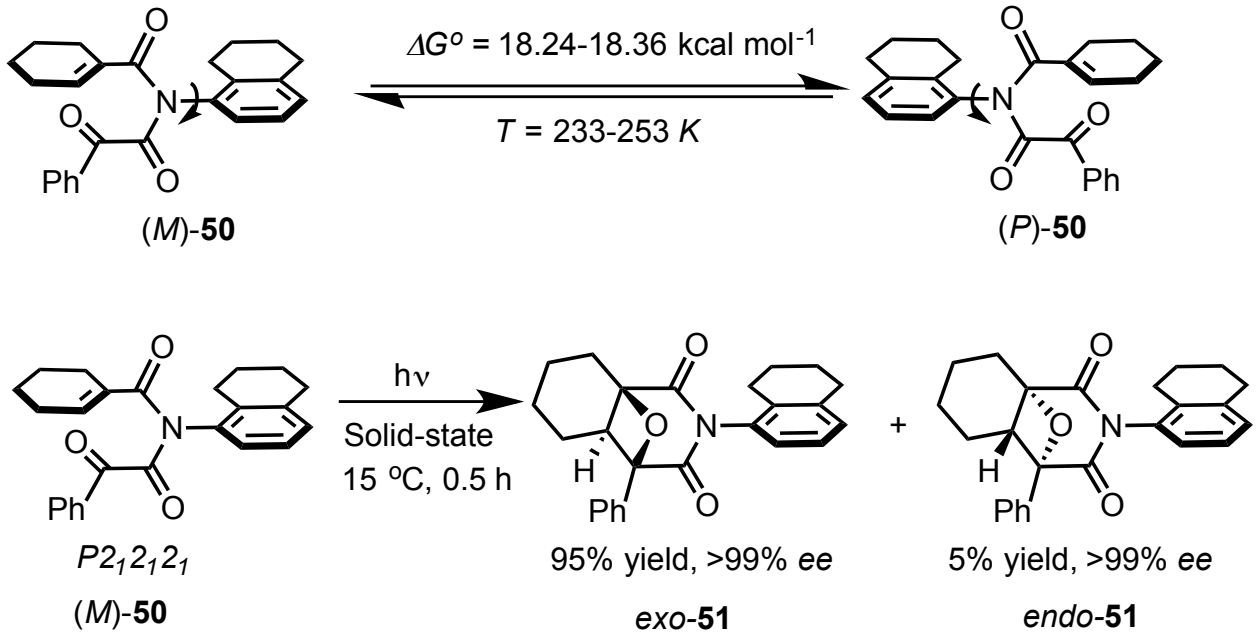

Scheme 1.18: Intramolecular Paternò-Büchi reaction involving atropisomeric oimides derivatives in the crystalline state by spontaneous crystallization: Adapted fro ref. 44 and from a handout by Qihui Jin, Princeton University.

The technique by Sakamoto and co-workers uses one of the conformational isomers during the transformation, but it lacks the prediction of which conformer will be crystallized. Clayden and Curran for example have extensively studied similar systems during *ortho*-directed aromatic substitution reactions and asymmetric radical cyclization reactions. The next section will discuss contributions from both research groups with regard to employing chiral compounds that lack stereo-centers.

1.6. Atropisomers in Asymmetric Thermal Reactions

Atropisomeric systems *viz.* axially or molecularly chiral compounds are conformational isomers that tend to slowly interconvert in solution at a *given temperature* and exist as discrete compounds. Atropisomerism is a phenomenon widespread among the biaryl classes of natural product and chiral ligands.[45] This peculiar phenomenon was first reported by Christie and Kenner during the resolution of γ-6:6'-dinitro- and 4:6:4':6'-tetranitro-diphenic acids (**52** and **53**) into their corresponding optically active components in 1922 (Scheme 1.19).[46] Since, many investigations have attempted to elucidate not only the stereodynamics and kinetic features of these systems but also to synthesize other classes of atropisomeric molecules.

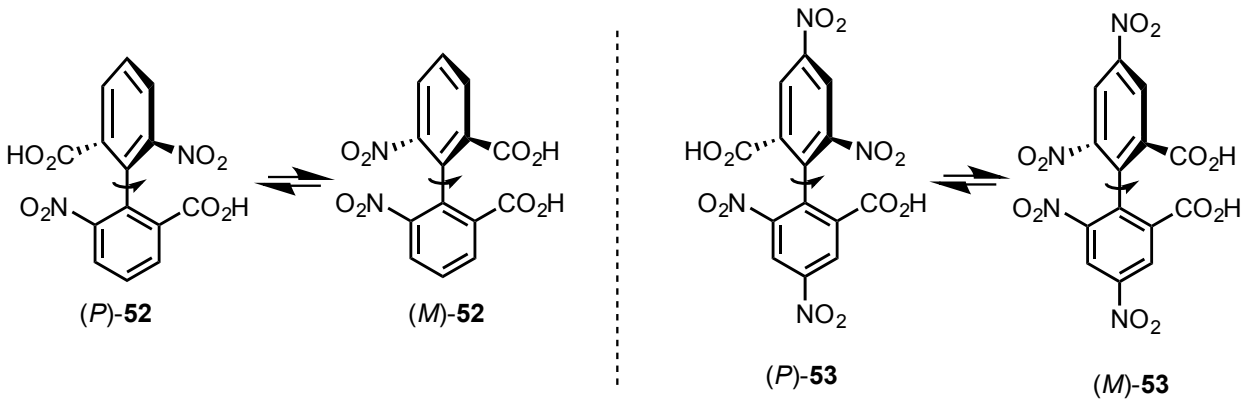

Scheme 1.19: First atropisomeric compounds reported in 1922: Adapted from ref. 46.

In the mid 90's, Clayden and Curran have respectively synthesized optically active non-biaryl atropisomers involving amides and anilides. They utilized the unique property of these classes of compounds in stereoselective/specific thermochemical transformations. A comprehensive synthetic investigation and stereodynamics study of atropisomeric compounds (acrylanilides and α-oxoamides) for photochemical transformations will be detailed in the next chapter(s).

1.6.1. Diastereoselective synthesis of non-biaryl atropisomeric derivatives of naphthamides

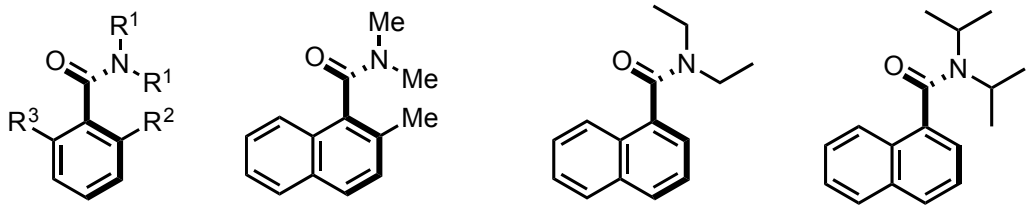

Figure 1.11: Adapted from ref. 53.

Derivatives of tertiary arylamides **54** have been extensively studied for their propensity to have slow rotation about the CO–C(aryl) bond when R^2 and $R^3 \neq$ H atom. It has been demonstrated that the amide functional group in this class of compound lies more or less perpendicular to the plane of the

aromatic ring.[47-50] Moreover, the barrier to rotation of rotamers of **54** $\Delta G^{\neq}$ could be manipulated so that the two enantiomers are resolvable. Enantiomers of compound **55** ($\Delta G^{\neq}_{rac}$ = 24.14 kcal mol^{-1} at room temperature) have been separated using HPLC on a chiral stationary phase and the half-life for racemization has been computed to be 6 h at ambient temperature. [51,52] In this picture Clayden *and co-workers* chose to investigate the atropisomeric derivatives of naphthamides **56** and **57** by functionalizing the *ortho*-position using *sec*-BuLi followed by electrophilic quench to install alkyl, alcohol or silyl groups; thereby inducing slow rotation about the CO–C(aryl) bond.

Scheme 1.20 depicts the preparation of *ortho*-methyl (**58**) and *ortho*-trimethylsilyl (**59**) atropisomeric derivatives (from achiral naphthamides **56** and **57)**, which did not show coalescence NMR signal even after heating at 160 ^{o}C in 1,2 dichlorobenzene. Furthermore, the isopropyl atropisomeric enantiomers were separable by HPLC on a chiral stationary phase (Whelk O-1 from Regis®).[53] In similar reaction conditions, addition of aldehydes to lithiated amides **56** or **57** affords atropisomeric diastereoisomers **60** bearing alcohol functional groups at the *ortho*-position, which could be separated by preparative HPLC (scheme 1.22).

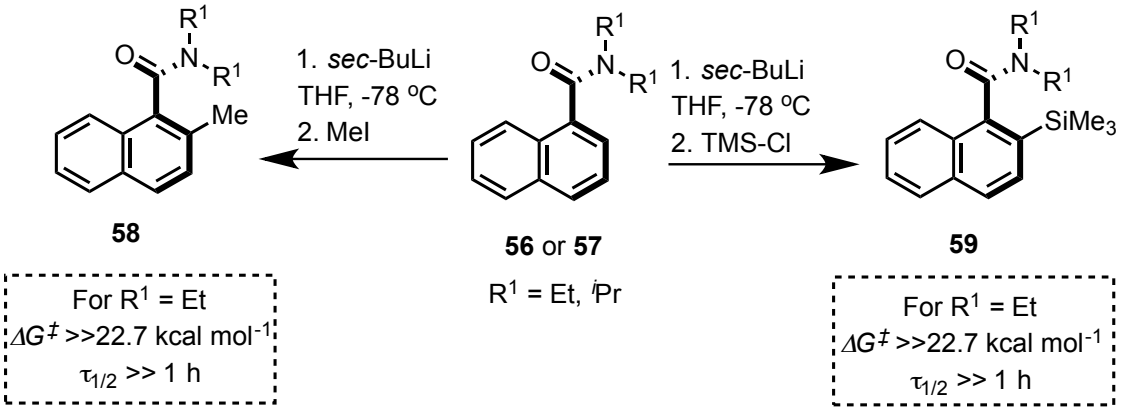

Scheme 1.20: *ortho*-Substituents inducing atropisomerism in lithiated naphthamides derivatives: Adapted from ref. 53.

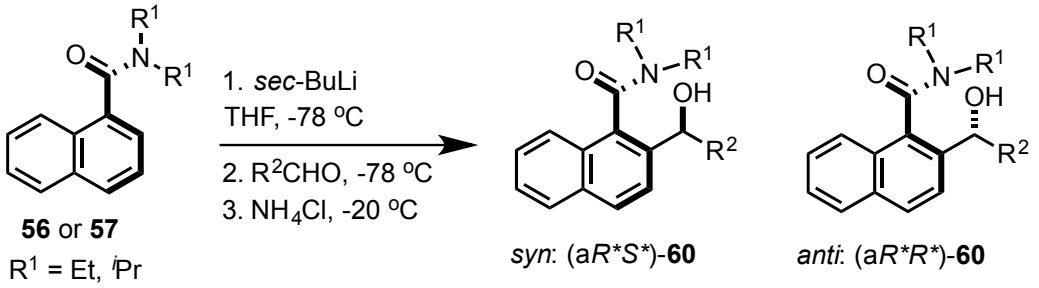

	R^1 = Et		R^1 = ^{i}Pr	
R^2	*syn:anti*	yield (%)	*syn:anti*	yield (%)
Me	77:23	67	85:15	92
Ph	51:49	85	72:28	89

Scheme 1.21: Diastereoselective preparation of atropisomeric naphthamides derivatives: Adapted from ref. 53.

The diastereoselectivity outcome of this transformation was explained by a transition state in which the aldehyde coordinates to the lithiated amides such that the oxygen atom of the aldehyde displaces one solvent molecule (THF) was primarily coordinated to the lithium atom. Also, the size of the alkyl/aryl group on the aldehyde was very crucial, due to severe steric interaction between R^1 and R^2 depending on the size of the substituents.

1.6.2. Chiral transfer in the radical cyclization of *ortho*-iodoacrylanilides

The preliminary investigations[47-50] on atropisomeric systems paved the way to utilize them as very useful scaffolds for asymmetric synthesis in thermal reactions. Beside the diastereoselective synthesis of alcohols from pro-atropisomeric lithiated amides by Clayden and co-workers, various research groups have investigated atropisomeric amides (acrylanilides) derivatives for chiral induction thermal transformations (Scheme 1.22).[54-58]

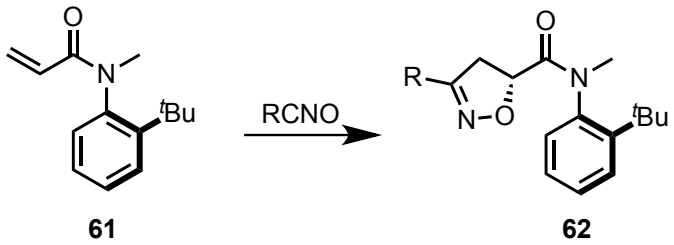

Scheme 1.22: Asymmetric induction with axially chiral *N*-acryloyl anilides by Curran and co-workers: Adapted from ref. 59.

The intramolecular stereoselective radical cyclization of derivatives of axially chiral *ortho*-iodo-*N*-acrylanilides (**63**) resulted with complete transfer of chirality (Scheme 1.23). The radical cyclization was initiated by Bu_3SnH in the presence of triethylborane and under oxygen atmosphere. The selectivity during the course of the reaction was postulated to have its origin from the aryl radical intermediate that must have a much lower barrier of rotation than the starting material, but its barrier to cyclization to give the oxindole radical species is even lower; thus, racemization at that step does not prevail leading to high selectivity in the cyclized product (Scheme 1.23).[59]

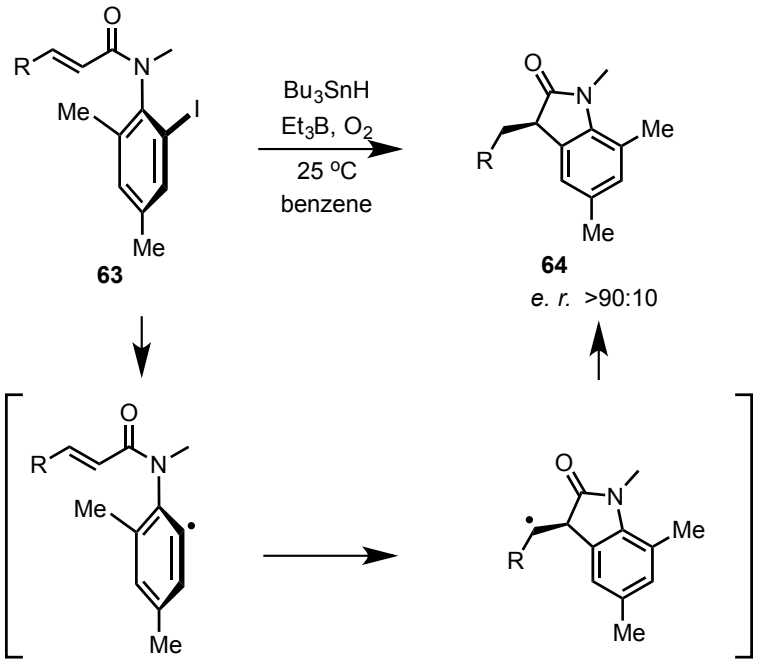

Scheme 1.23: Chirality transfer in radical cyclization of *o*-iodoacrylanilides: Adapted from ref. 59.

To elucidate the extent of axial chirality in the starting material(s) in determining the optical purity of the expected cyclized product(s), various substrates were synthesized and their stereodynamic features were measured. Curran and co-workers have also reported various synthetic routes to obtain the atropisomeric substrates. The systems of interest were prepared *via* a straightforward reaction of 2-iodo-4,6-dimethylaniline[60] and acryloyl chlorides followed by *N*-allylation as shown in scheme 1.24.

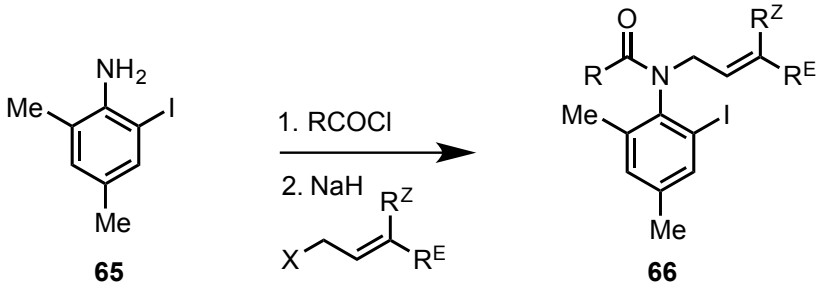

R	R^Z	R^E	$\Delta G^{\ddagger}$ (kcal/mol)
Ph	H	H	29.7
$PhCH_2$	H	H	32.6
$PhCH_2CH_2$	H	H	32.7
p-BrC_6H_4	Me	Me	30.7

Scheme 1.24: Synthesis and rotational barrier for four axially chiral anilides: Adapted from ref. 59.

After synthesis, racemic atropisomers were resolved by preparative HPLC on chiral stationary phase [(*S,S*)-Whelk-O1, 25cmX10.0 mm I.D.] using 10-40% ^{i}PrOH:hexanes as the mobile phase. The rotation barrier was measured by racemization study: optically pure atropisomers were heated at 140 ^{o}C in 9:1 hexane:^{i}PrOH and the decrease in *ee* was measured as a function of time by HPLC analysis on a chiral stationary phase. The result from the racemization study revealed that optically pure atropisomers could be conveniently manipulated at room temperature during the course of the radical cyclization reaction due to the high rotational barrier of the N-C(aryl) bond. Furthermore, addition of tin hydride to the enantioenriched atropisomers (**67**) afforded chirally enriched indoline derivative **68** with *ee* >93%. The beauty of this methodology was that during the transformation, axially chiral radical intermediates do not interconvert to each other as depicted in scheme 1.25.

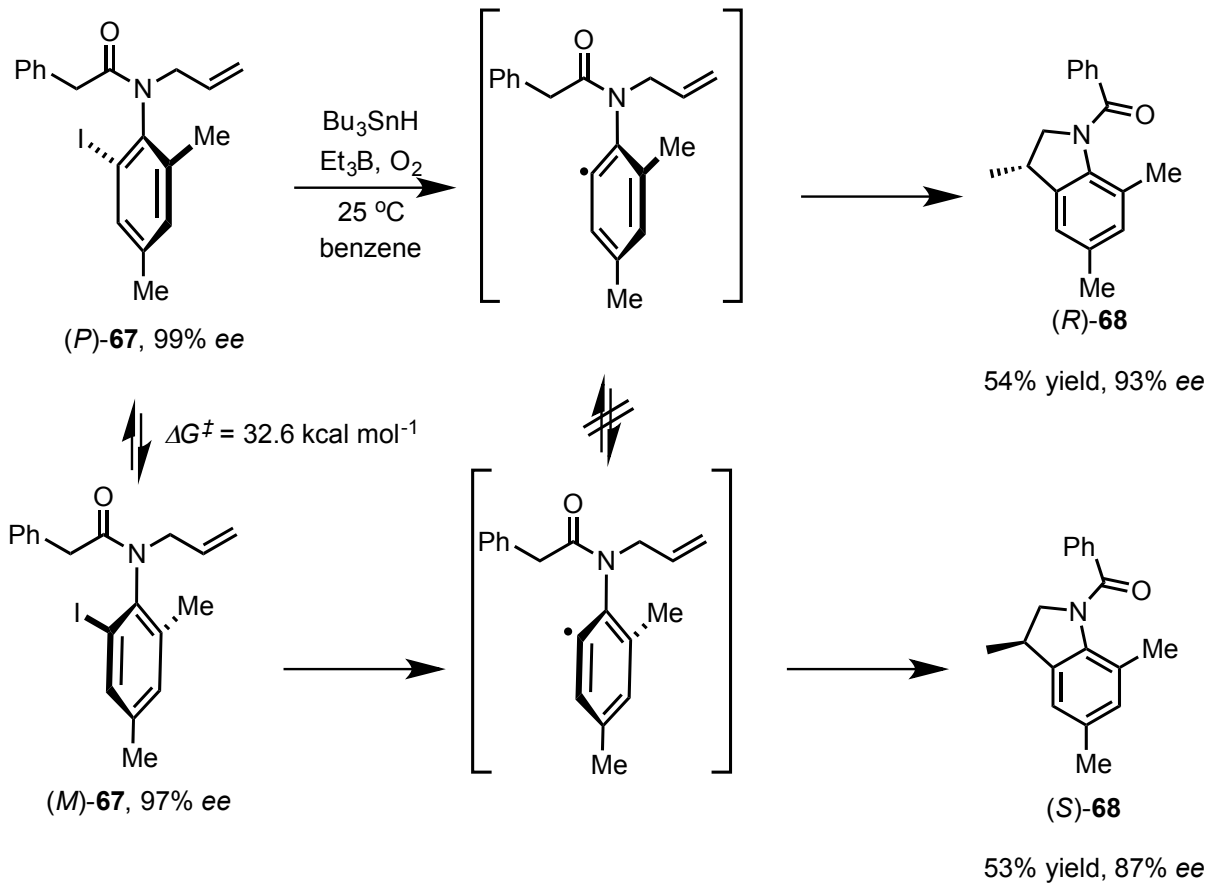

Scheme 1.25: Enantioselective synthesis of indoline amide derivative **68**: Adapted from ref. 59.

1.7. Summary and Outlook

Previously reported solid-state photochemical transformations involving frozen chirality in the solid-state by Sakamoto and co-workers and the current strategies (by Clayden and Curran) to utilize them in chiral transfer processes allowed us to envision methodologies in solution phase photochemistry in order to synthesize chirally enriched molecules and complement established thermochemical transformations. The next chapter(s) will address and detail stereospecific solution phase photochemical transformations involving non-biaryl atropisomeric compounds. Furthermore, chromatography, XRD and spectroscopy evidences/techniques will contribute to comprehensively rationalize the mechanism during the chiral transfer process in the photochemical reactions of interest.

1.8. References

(1) Wardle, B. *Principles and Applications of Photochemistry*; West Sussex, UK: Wiley, 2009.

(2) Pagni, R.; Compton, R. Is Circularly Polarized Light an Effective Reagent For Asymmetric Synthesis? *Mini-Reviews in Organic Chemistry* **2005**, *2*, 203–209.

(3) Turro, N. J. 1.; Ramamurthy, V.; Scaiano, J. C. J. C. 1. *Modern molecular photochemistry of organic molecules*; Sausalito, CA: University Science Books, 2010.

(4) March, J. 1. *Advanced organic chemistry : reactions, mechanisms, and structure*; New York, NY : Wiley, 1985.

(5) Meierhenrich, U. *Amino acids and the asymmetry of life : caught in the act of formation*; New York : Springer, 2008.

(6) Nicol, W. Beobachtungen über die in krystallisirten Mineralien enthaltenen Flüssigkeiten. *Annalen der Physik* **1828**, *89*, 510–513.

(7) Fresnel, Augustin (1819). "Memoir on the Diffraction of Light". *The Wave Theory of Light – Memoirs by Huygens, Young and Fresnel*. American Book Company. pp. 79–14.

(8) Crew, H.; Huygens, C.; Young, T.; Fresnel, A. J.; Arago, F. The wave theory of light memoirs of Huygens, Young and Fresnel, http://www.archive.org/details/wavetheoryofligh00crewrich (accessed Apr 7, 2013).

(9) Le Bel, J. A. Sur les relations qui existent entre les formulas atomiques de corps organiques et le pouvior rotatiore de leurs dissolutions. *Bull. Soc. Chim. Fr.* **1874**, *22*, 337–347.

(10) Van't Hoff, J. H. Voorstel tot uitbreiding der tegenwoordig in de scheikunde gebruikte structuur-formules in de ruimte: benevens een daarmee samenhangende opmerking omtrent het verband tusschen optisch actief vermogen en chemische constitutie van organische verbindingen. **1874**.

(11) Noorduin, W. L.; Bode, A. A. C.; van der Meijden, M.; Meekes, H.; van Etteger, A. F.; van Enckevort, W. J. P.; Christianen, P. C. M.; Kaptein, B.; Kellogg, R. M.; Rasing, T.; Vlieg, E. Complete chiral symmetry breaking of an amino acid derivative directed by circularly polarized light. *Nature Chem* **2009**, *1*, 729–732.

(12) Kuhn, W.; Braun, E. Photochemische Erzeugung optisch aktiver Stoffe. *Die Naturwissenschaften* **1929**, *17*, 227–228.

(13) Kuhn, W.; Knopf, E. Photochemische Erzeugung optisch aktiver Stoffe. *Die Naturwissenschaften* **1930**, *18*, 183–183.

(14) Kagan, H.; Moradpour, A.; Nicoud, J. F.; Balavoine, G.; Tsoucaris, G. Photochemistry with circularly polarized light. Synthesis of optically active hexahelicene. *J. Am. Chem. Soc.* **1971**, *93*, 2353–2354.

(15) Balavoine, G.; Moradpour, A.; Kagan, H. B. Preparation of chiral compounds with high optical purity by irradiation with circularly polarized light, a model reaction for the prebiotic generation of optical activity. *J. Am. Chem. Soc.* **1974**, *96*, 5152–5158.

(16) Flores, J. J.; Bonner, W. A.; Massey, G. A. Asymmetric photolysis of (RS)-leucine with circularly polarized ultraviolet light. *J. Am. Chem. Soc.* **1977**, *99*, 3622–3625.

(17) Hammond, G. S.; Cole, R. S. Asymmetric Induction during Energy Transfer. *J. Am. Chem. Soc.* **1965**.

(18) Murov, S. L.; Cole, R. S.; Hammond, G. S. Mechanisms of photochemical reactions in solution. LIV. A new mechanism of photosensitization. *J. Am. Chem. Soc.* **1968**, *90*, 2957–2958.

(19) Ouannes, C.; Beugelmans, R.; Roussi, G. Asymmetric induction during transfer of triplet energy. *J. Am. Chem. Soc.* **1973**, *95*, 8472–8474.

(20) Kagan, H. B.; Fiaud, J. C. Topics in Stereochemistry, 18. *Wiley-Interscience, New York* **1988**, 249.

(21) Horner, L.; Klaus, J. Chemie an starren Grenzflächen, 6 Photochemisch induzierte Reaktionen mit grenzflächengebundenen Sensibilisatoren. *Liebigs Ann. Chem.* **1981**, *1981*, 792–810.

(22) Inoue, Y.; Shimoyama, H.; Yamasaki, N.; Tai, A. Enantiodifferentiating Photoisomerization of 1, 2-Diphenylcyclopropane Sensitized by Chiral Aromatic Esters. *Chem. Lett.* **1991**.

(23) Inoue, Y.; Yamasaki, N.; Shimoyama, H.; Tai, A. Enantiodifferentiating cis-trans photoisomerizations of 1,2-diarylcyclopropanes and 2,3-diphenyloxirane sensitized by chiral aromatic esters. *J. Org. Chem.* **1993**, *58*, 1785–1793.

(24) Gassman, P. G.; Bottorff, K. J. Photoinduced lactonization. A useful but mechanistically complex single electron transfer process. *J. Am. Chem. Soc.* **1987**, *109*, 7547–7548.

(25) Gassman, P. G.; De Silva, S. A. Use of sterically hindered sensitizers for improved photoinduced

electron-transfer reactions. *J. Am. Chem. Soc.* **1991**, *113*, 9870–9872.

(26) Álvaro, M.; Formentín, P.; García, H.; Palomares, E.; Sabater, M. J. Chiral N-Alkyl-2,4,6-triphenylpyridiniums as Enantioselective Triplet Photosensitizers. Laser Flash Photolysis and Preparative Studies. *J. Org. Chem.* **2002**, *67*, 5184–5189.

(27) Müller, C.; Bauer, A.; Bach, T. Light-driven enantioselective organocatalysis. *Angew. Chem. Int. Ed. Engl.* **2009**, *48*, 6640–6642.

(28) Sakamoto, M. Molecular and Supramolecular Photochemistry. In *Chiral Photochemistry*; Inoue, Y.; Ramamurthy, V., Eds. Dekker, Marcel: New York; Vol. 11, pp. 415–461.

(29) Omkaram, N.; Scheffer, J. R. Use of chiral single crystals to convert achiral reactants to chiral products in high optical yield: application to the di-.pi.-methane and Norrish type II photorearrangements - Journal of the American Chemical Society (ACS Publications). *J. Am. Chem. Soc.* **1986**, *108*, 5648–5650.

(30) Zimmerman, H. E.; Schuster, D. J. The photochemical rearrangement of 4,4-diphenylcyclohexadienone. Paper i on a general theory of photochemical reactions. *J. Am. Chem. Soc.* **1961**, *83*, 4486–4488.

(31) Toda, F.; Tanaka, K. A new simple chiral helicene 3,4-bis(diphenyl-methylene)-N-methylsuccimide in its chiral crystal. A generation of chirality. *Supramolecular Chemistry* **1994**, *3*, 87–88.

(32) Curtin, D. Y.; Paul, I. C. Chemical consequences of the polar axis in organic solid-state chemistry. *Chem. Rev.* **1981**, *81*, 525–541.

(33) Wu, L.-C.; Cheer, C. J.; Olovsson, G.; Scheffer, J. R.; Trotter, J.; Wang, S.-L.; Liao, F.-L. Crystal engineering for absolute asymmetric synthesis through the use of meta.substituted aryl groups. *Tetrahedron Lett.* **1997**, *38*, 3135–3138.

(34) Sakamoto, M.; Hokari, N.; Takahashi, M.; Fujita, T.; Watanabe, S.; Iida, I.; Nishio, T. Chiral Thietane-Fused β-Lactam from an Achiral Monothioimide Using the Chiral Crystal Environment. *J. Am. Chem. Soc.* **1993**, *115*, 818.

(35) Sakamoto, M.; Takahashi, M.; Fujita, T.; Watanabe, S.; Iida, I.; Nishio, T.; Aoyama, H. Solid-state Photochemistry: “Absolute”Asymmetric Oxetane Synthesis from an Achiral Acyclic Imide Using

the Chiral Crystal Environment. *J. Org. Chem.* **1993**, *58*, 3476–3477.

(36) Schmidt, G. M. J. 385. Topochemistry. Part III. The crystal chemistry of some trans-cinnamic acids. *J. Chem. Soc.* **1964**, 2014.

(37) Elgavi, A.; Green, S. B.; Scmidt, G. M. J. Reactions in Chiral Crystals. Optically Active Heterophotodimer Formation from Chiral Single Crystals. *J. Am. Chem. Soc.* **1973**, *95*, 2058–2059.

(38) Gamlin, J. N.; Jones, R.; Leibovitch, M.; Patrick, B.; Scheffer, J. R.; Trotter, J. The Ionic Auxiliary Concept in Solid State Organic Photochemistry. *Acc. Chem. Res.* **1996**, *29*, 203–209.

(39) Sivaguru, J.; Natarajan, A.; Kaanumalle, L. S.; Shailaja, J.; Uppili, S.; Joy, A.; Ramamurthy, V. Asymmetric photoreactions within zeolites: role of confinement and alkali metal ions. *Acc. Chem. Res.* **2003**, *36*, 509–521.

(40) Kasai, H.; Nalwa, H. S.; Oikawa, H.; Okada, S.; Matsuda, H.; Minami, N.; Kakuta, A.; Ono, K.; Mukoh, A.; Nakanishi, H. A Novel Preparation Method of Organic Microcrystals. *Jpn. J. Appl. Phys.* **1992**, *31*, L1132–L1134.

(41) Veerman, M.; Resendiz, M. J. E.; Garcia-Garibay, M. A. Large-Scale Photochemical Reactions of Nanocrystalline Suspensions: A Promising Green Chemistry Method. *Org. Lett.* **2006**, *8*, 2615–2617.

(42) Resendiz, M.; Taing, J.; Garcia-Garibay, M. A. Photodecarbonylation of 1,3-Dithiophenyl Propanone: Using Nanocrystals to Overcome the Filtering Effect of Highly Absorbing Trace Impurities. *Org. Lett.* **2007**, *9*, 4351–4354.

(43) Natarajan, A.; Ng, D.; Yang, Z.; Garcia-Garibay, M. A. Parallel Syntheses of (+)- and (−)-α-Cuparenone by Radical Combination in Crystalline Solids. *Angew. Chem., Int. Ed.* **2007**, *119*, 6605–6607.

(44) Sakamoto, M.; Iwamoto, T.; Nono, N.; Ando, M.; Arai, W.; Mino, T.; Fujita, T. Memory of Chirality Generated by Spontaneous Crystallization and Asymmetric Synthesis Using the Frozen Chirality. *J. Org. Chem.* **2003**, *68*, 942–946.

(45) Eliel, E. L.; Wilen, S. H. Chirality in Molecules Devoid of Chiral Centers. *Stereochemistry of Organic Compounds* **1994**, 1119–1190.

(46) Christie, G. H.; Kenner, J. LXXI.—The molecular configurations of polynuclear aromatic compounds. Part I. The resolution of γ-6: 6′-dinitro-and 4: 6: 4′: 6′-tetranitro-diphenic acids into optically active components. *J. Chem. Soc.* **1922**, 614–620.

(47) Siddall, T. H., III; Garner, R. H. SOME STUDIES OF SLOW ROTATIONS AROUND BONDS IN AMIDES. *Can. J. Chem.* **1966**, *44*, 2387–2394.

(48) Stewart, W. E.; Siddall, T. H. Nuclear magnetic resonance studies of amides. *Chem. Rev.* **1970**, *70*, 517–551.

(49) Jennings, W. B.; Tolley, M. S. Concerning geminal nonequivalence in benzamides and thiobenzamides. *Tetrahedron Lett.* **1976**, *17*, 695–698.

(50) Berg, U.; Sandström, J. Magnetic non-equivalence in N, N-diethylbenzamides and-thiobenzamides conformation of the N-alkyl groups. *Tetrahedron Lett.* **1976**, *17*, 3197–3200.

(51) Cuyegkeng, M. A.; Mannschreck, A. Liquid Chromatography on Triacetycellulose, 14 Chromatographic Separation of Enantiomers and Barriers to Enantiomerization of Axially Chiral Aromatic Carboxamides. *Chem. Ber.* **1987**, *120*, 803–809.

(52) Pirkle, W. H.; Welch, C. J.; Zych, A. J. Chromatographic investigation of the slowly interconverting atropisomers of hindered naphthamides. *Journal of Chromatography A* **1993**, *648*, 101–109.

(53) Bowles, P.; Clayden, J.; Tomkinson, M. ScienceDirect.com - Tetrahedron Letters - Diastereoisomeric atropisomers from the addition of lithiated N,N-dialkyl-l-naphthamides to aldehydes. *Tetrahedron Letters* **1995**, *36*, 9219–9222.

(54) Curran, D. P.; Liu, W.; Chen, C. H.-T. Transfer of Chirality in Radical Cyclizations. Cyclization of o-Haloacrylanilides to Oxindoles with Transfer of Axial Chirality to a Newly Formed Stereocenter. *J. Am. Chem. Soc.* **1999**, *121*, 11012–11013.

(55) Curran, D. P.; Geib, S.; DeMello, N. Rotational features of carbon-nitrogen bonds in N-aryl maleimides. Atroposelective reactions of o-tert-butylphenylmaleimides. *Tetrahedron* **1999**, *55*, 5681–5704.

(56) Ates, A.; Curran, D. P. Synthesis of Enantioenriched Axially Chiral Anilides from Atropisomerically Enriched Tartarate Ortho-Anilides. *J. Am. Chem. Soc.* **2001**, *123*, 5130–5131.

(57) Kondru, R. K.; Hiu-Tung Chen, C.; Curran, D. P.; Beratan, D. N.; Wipf, P., * Determination of the

absolute configuration of 1,3,5,7-tetramethyl-1,3-dihydroindol-2-one by optical rotation computation. *Tetrahedron: Asymmetry* **1999**, *10*, 4143–4150.

(58) Curran, D. P.; Qi, H.; Geib, S. J.; DeMello, N. C. Atroposelective Thermal Reactions of Axially Twisted Amides and Imides. *J. Am. Chem. Soc.* **1994**, *116*, 3131–3132.

(59) Curran, D. P.; Chen, C. H. T.; Geib, S. J.; Lapierre, A. B. Asymmetric radical cyclization reactions of axially chiral N-allyl-o-iodoanilides to form enantioenriched N-acyl dihydroindoles. *Tetrahedron* **2004**, *60*, 4413–4424.

(60) Kajigaeshi, S.; Kakinami, T.; Yamasaki, H.; Fujisaki, S.; Okamoto, T. Halogenation using quaternary ammonium polyhalides. VII. Iodination of aromatic amines by use of benzyltrimethylammonium dichloroiodate(1-). *Bull. Chem. Soc. Jpn.* **1988**, *61*, 600–602.

CHAPTER 2. REGIOCHEMISTRY OF 6π-PHOTOCYCLIZATION OF ACRYLANILIDES[‡]

2.1. Introduction

Photocyclization of acrylanilides **69** (Scheme 2.1) to the corresponding 3,4-dihydroquinolin-2-ones (*cis*-**70** and *trans*-**71**) was first described by Chapman and co-workers.[1,2] Due to the interesting stereochemistry and the relavance of quinolinone moiety in natural products, various groups have employed different techniques to study the formation of the final photoproduct as well as the effect of various substituents on the reactive substrate(s). Ogata and co-workers investigated the influence of various substituents ($R^1 = R^2 = H$ or R^1 = Ph and $R^2 = H$) on the alkenyl double bond; however, the anilides of interest did not undergo photocyclization.[3] On the other hand, for other derivatives, the cyclization has been found to proceed cleanly in selected solvents presumably from the singlet state with quantum yield varying from 0.1 to 0.26.[3-6]

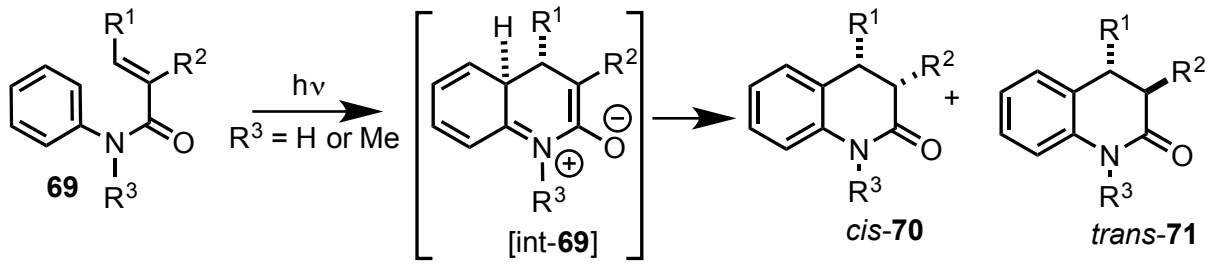

a) $R^1 = R^2 = R^3$ = Me

b) R^1, R^2 = H_2C ⌒ CH_2 and R^3 = Me

Scheme 2.1: 6π-Photocyclization of acrylanilides **69**.

Photophysical investigations showed that the singlet state of the acrylanilide substrates was not quenched by 1,3-pentadiene; and Ogata and co-worker did not observe any sensitized transformation (triplet) in the presence of triplet sensitizers such as acetophenone (E_T = 73.6 kcal/mol) or benzophenone (E_T = 68.5 kcal/mol). However, their quenching studies revealed that the

[‡] The material in this chapter was co-authored by Anoklase J.-L. Ayitou (AJA) Dr. J. Sivaguru (JS). AJA in consultation with JS synthesized all compounds and performed all experiments detailed in this chapter. AJA and JS came up with the mechanistic rationale as well as the conclusion described in this chapter.

phosphorescence emissions of acetophenone and acetone were readily quenched by the acrylianilide of interest[3] suggesting that the substrate could also undergo photocyclization from the triplet excited when required conditions are met. The reactive spin state dependent photocyclization will be detailed in chapter 4. The 6π-photocyclization of acrylanilides has been also found to proceed effectively in organized assemblies such as crystals and crystalline chiral hosts.[7-9] Recently, Bach and co-workers reported that a Kemp triacid derived host (*cf*. chapter 1. Section 1.5.3) mediates the photocyclization of acrylanilides with ~60% *ee* at -15 ^{o}C.[5]

The precedence in the 6π-photocyclization of acrylanilides prompted us to devise new molecular systems to investigate the stereochemistry of the transformation. In this regard, achiral and atropisomeric acrylanilides were synthesized based on reported procedures. (*cf.* section 2.4 for the general synthesis of the molecular reactant) Chart 2.1 shows a library of compounds that were synthesized to investigate the stereochemistry (regiochemistry) during 6π-photocyclization.

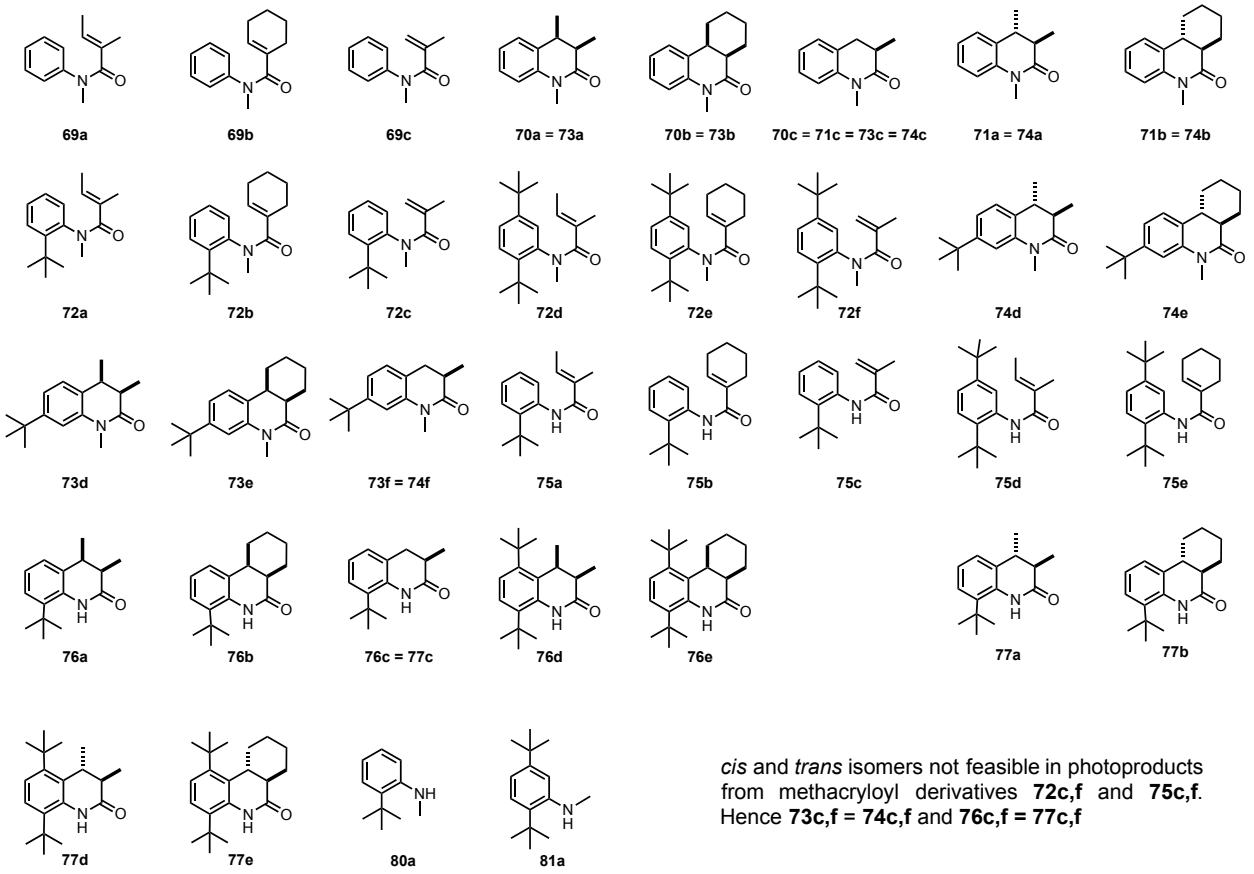

Chart 2.1: Acrylanilides molecular reactants and corresponding photoproduct(s).

2.2. Understanding Photochemical Reactivity of *o-tert*-butyl Substituted Acrylanilides

2.2.1. Interplay between the stuctural features and the mode of cyclization

Mechanistically, it was reported that the 6π-photocyclization of acrylanilides occurs via a conrotatory ring closure (Scheme 2.1) leading to a zwitterionic intermediate *int*-**69**. [3-6] In the case of acrylanilides **69**, photocyclization lead to a mixture of *cis*-**70** and *trans*-**71** 3,4-dihydroquinolin-2-ones (Scheme 2.1).[3-6] In an aprotic solvent for example, H-transfer in *int*-**69** (Scheme 2.1) occurred to a large extent via a thermally allowed intramolecular suprafacial [1,5]-H shift. On the other hand, in protic solvents or in the presence of Brønsted acids, the proton was delivered intermolecularly.[3-6] Also, the that the *cis*-**70**:*trans*-**71** ratio in the photoproduct was found to be dependent on the nature of the solvent employed.[3-6] Previously, it was indicated that the isolated yields of *cis*-**70** and *trans*-**71** (4 to 90%) depends on the substitution on the phenyl ring and the solvent employed.[10]

Based on the above observations, I decided to investigate acrylanilide systems for molecular chiral transfer in solution of atropisomeric acrylanilides and compared them to the reactivity of their achiral counterpart **69a,b**. The enantioselectivity aspect of the transformation will be comprehensively detailed in the next chapter. During the preliminary investigations, it was necessary to compare the mode of cyclization and reactivity of **72** (R^3 = Me) and **75** (R^3 = H) systems.

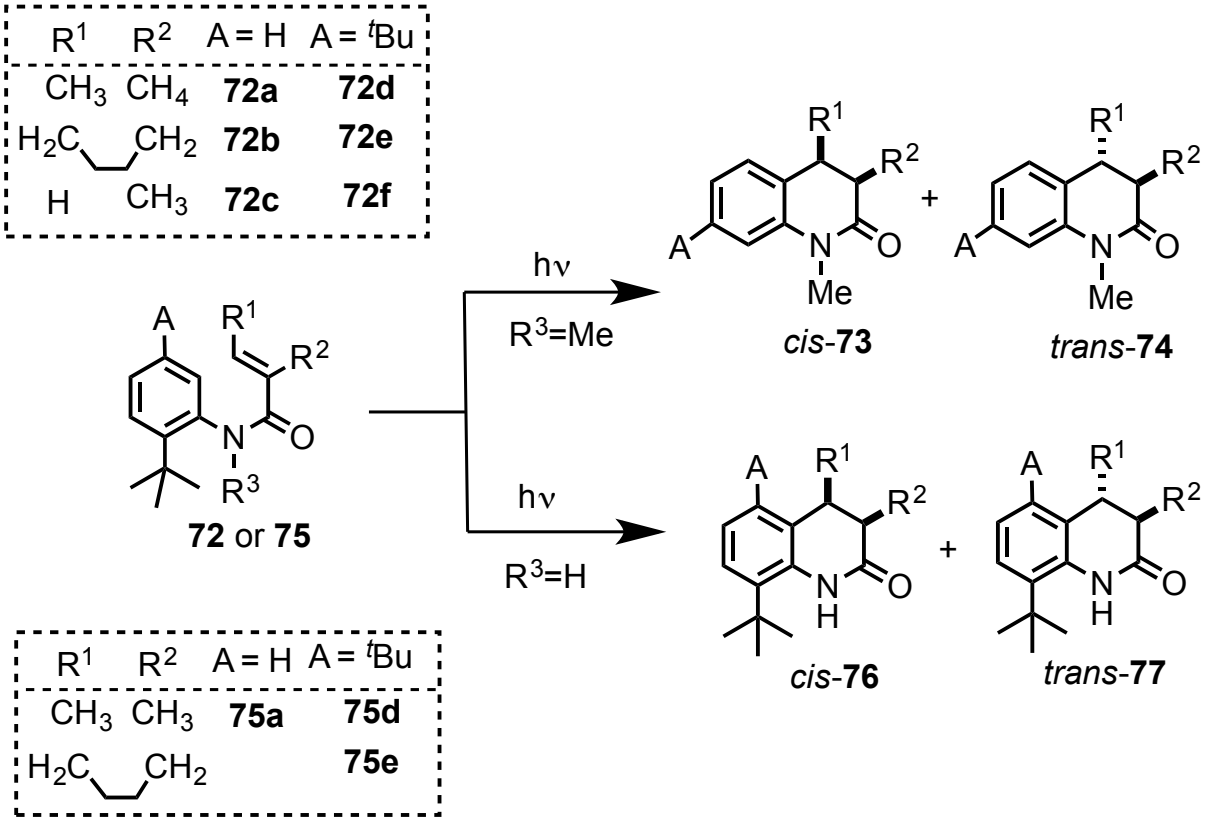

Scheme 2.2: Photocyclization of *o-tert*-butyl N-methyl acrylanilides **72** and corresponding N-H derivatives **75**.

Table 2.1: Photocyclization [a] of *N*-methyl-*o-tert*-butylacrylanilides **72**.

Entry	Substrates	*cis*-**73** : *trans*-**74** (% conversion)			
		1:2 THF-C_6H_6	MeOH	$CHCl_3$	Acetone[b]
1.	**72a**	62:38 (4)	38:62 (15)	61:39 (28)	55:45 (52)
2.	**72b**	22:78 (24)	*c*	29:71 (16)	67:33 (32)
3.	**72c**	*c*	*c*	*c*	*c*
4.	**72d**	42:58 (5)	35:65 (21)	61:39 (21)	46:54 (56)
5.	**72e**	52:48 (17)	70:30 (10)	41:59 (7)	63:37 (55)
6.	**72f** [d,e]	- (8)	- (11)	- (8)	- (58)

[a] Irradiations were performed with 450 W medium pressure Hg lamp for 5 h under a constant flow of nitrogen. Increasing the irradiation time (>5 h) resulted in higher conversion, but uncharacterized additional side products were observed. *cis:trans* ratio and conversion based on relative integration of corresponding peaks in NMR and HPLC/GC. [b] In acetone, the reaction was clean up to 5 h with conversion of -60%. Isolated yields were 49 and 51% in acetone for **72e** and **72f** respectively for 5 h irradiation. [c] Conversion was less than 5% [d] 2 h irradiation. [e] *cis* and *trans* isomers not feasible in photoproducts from **72c** and **72f**, so only conversion are reported.

Atropisomeric mixtures of *o*-*tert*-butylacrylanilides with *N*-methyl substitution **72a-f** were irradiated using a 450 W medium pressure Hg-lamp with Pyrex cutoff in various solvents (Scheme 2.2; Table 2.1).

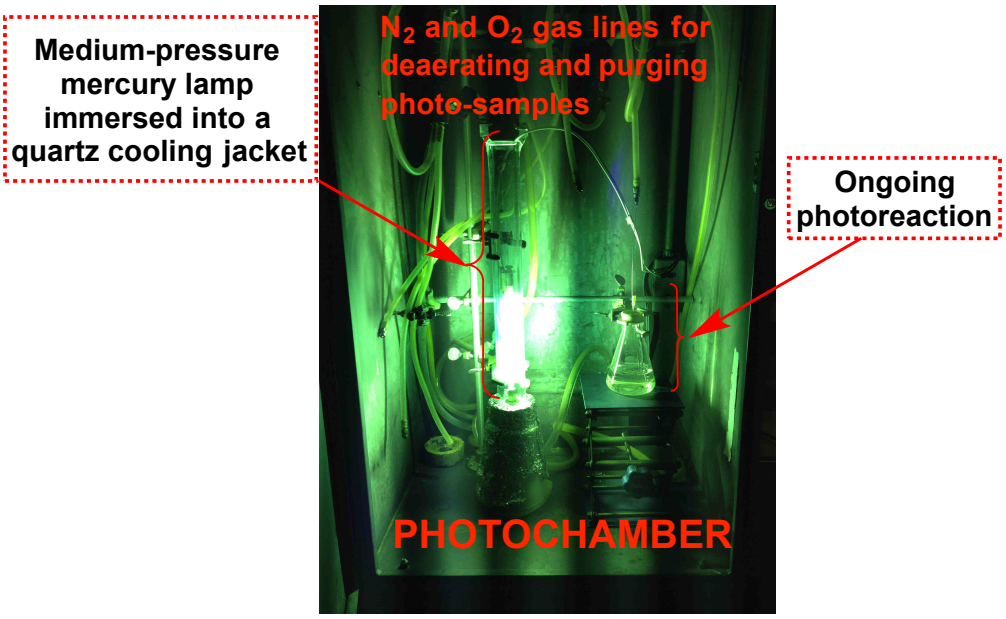

Figure 2.1: Photochamber and light source for photoreactions.

The photoproducts were characterized by NMR spectroscopy, High Resolution Mass Spectrometry (HRMS) and chromatographic (HPLC and GC) analysis that confirmed the formation of *cis*-**73** and *trans*-**74** 3,4-dihydroquinolin-2-ones without the *tert*-butyl group (Scheme 2.2) (*cf.* Section 2.4). Irradiation of the corresponding N-H derivatives **7** under identical conditions gave the cyclized products *cis*-**76** and *trans*-**77** (Scheme 2.2; Table 2.2), with the *o*-*tert*-butyl group intact on the phenyl ring (*cf.* Section 2.4). As a control study, photocyclization of the N-methyl derivative without the *o*-*tert*-butyl group (parent acrylanilide **69**) gave photoproducts *cis*-**70** and *trans*-**71** as reported in the literature. [3,5,6]

Table 2.2: Photocyclization [a,b] of unsubstituted N-Me acrylanilide **69** and *o-tert*-butylacrylanilides with N-H substitution **75.**

Entry	Substrates	*cis*-**70** *: trans*-**71** (% conversion)			
		1:2 THF- C_6H_6	MeOH	$CHCl_3$	Acetone
1.	**69a**	52:48 (16)	18:82 (68)	49:51 (72)	36:64 (>99)
2.	**69b**	11:89 (85)	83:17 (36)	41:59 (33)	14:86 (>99)
		cis-**8** *: trans*-**9** (% conv)			
3.	**75a**	72:28 (79)	80:20 (3)	70:30 (85)	*c*
4.	**75d**	82:18 (53)	*c*	90:10 (47)	*c*
				Benzene	
5.	**75e**	-	-	96:04 (61)	-

[a] Irradiations were performed with 450 W medium pressure Hg-lamp for 5 h under a constant flow of N_2. >5 h irradiation resulted in increased conversion, but uncharacterized additional side products were observed. *cis:trans* ratio and conversion based on relative integration of corresponding peaks in NMR and HPLC/GC. [b] Photocyclization of various derivatives of **1** is already reported in literature (Reference 1-4, 6-8, 10). [c] No photoproducts observed and the starting material was recovered.

The dichotomy in the mode of cyclization (N-H *vs*. N-Me) is quite unusuable i.e. the N-substitution was able to dictate the regiochemistry of cyclization on the phenyl ring. Based on the behavior of the parent **72** to acrylanilide **69** (scheme 2.1), one would expect the cyclization of occur at the unsubstituted *ortho*-position on the phenyl ring. In the N-methyl *o-tert*-butylacrylanilide **72**, the cyclization occurs at the *ortho*-carbon bearing the *tert*-butyl group, leading to *cis*-**73** and *trans*-**74**. On the other hand, in the corresponding N-H derivatives **75**, photocyclization occurs at the expected unsubstituted *ortho* carbon (similar to the parent acrylanilide **69**) leading to *cis*-**76** and *trans*-**77**. A mechanistic rationale for the difference in behavior between the N-methyl acrylanilide **72** and the corresponding N-H acrylanilide **75** became crucial for employing the system for studying molecular chiral (axial chiral) transfer during phototransformations that will be detailed in the next chapter.[11] The ratio of *cis:trans* 3,4-dihydroquinolin-2-ones in the photocyclization of *o-tert*-butyl N-methyl acrylanilides **72** was found to be dependent on the type of substrate and the solvent employed. In protic methanol, the *trans*-product **74** predominatd in the tigloyl derivatives **72a** and **72d** (Table 2.1; Entries 1 and 4), and the *cis*-isomer **73** predominated in the cyclohexyl derivative **72e** (Table 2.1; Entry 5). On the other hand, in aprotic $CHCl_3$, the *cis*-isomer predominates in the tigloyl derivatives

72a and **72d** (Table 2.1; Entries 1 and 4), and the *trans*-isomer predominates in the cyclohexyl derivative **72b** and **72e** (Table 2.1; Entries 2 and 5). This difference in the product distribution in the protic and aprotic solvents was likely reflective of the difference in intramolecular and intermolecular H-transfer pathways leading to the photoproducts. The intermolecular photocyclization process in protic solvents (methanol-*d*) was confirmed by deuterium incorporation (*cf.* Section 2.2.2). The reactivity of N-methyl derivatives **72** and the corresponding N-H derivatives **75** were similar in 1:2-THF:benzene. The *cis*-isomer predominated in both NH and N-methyl *mono-tert*-butyl tigloyl derivatives **72a** and **72a** (compare Table 2.1, Entry 1 and Table 2.2, entry 3). Similarly, the *trans*-product predominates in the corresponding *di-tert*-butyl tigloyl derivatives **72d** and **75d** (compare Table 1; Entry 4 and Table 2; entry 4). In acetone, the *cis:trans* ratio was close to 50:50 for the N-methyl tigloyl derivatives **72a** and **72d** (Table 2.1; Entries 1 and 4), whereas there was a slight preference for the *cis*-isomer for the cyclohexyl derivative **72b** and **72e** (Table 2.1; Entries 2 and 5). Conversely, there was no appreciable conversion for the NH derivatives **75**. Thus the solvent effects reflected a trend that was inherent for the individual NH derivatives **75** and the corresponding N-methyl acrylanilides **72**.

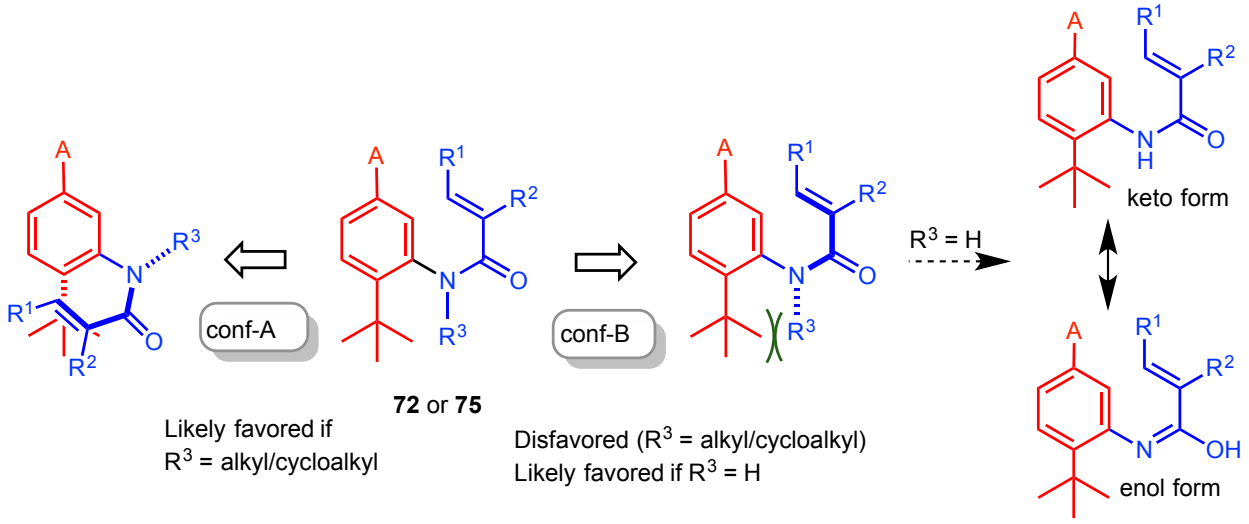

Scheme 2.3: Likely conformations of acrylanilides depending on N-alkyl/cycloalkyl or N-H substitution.

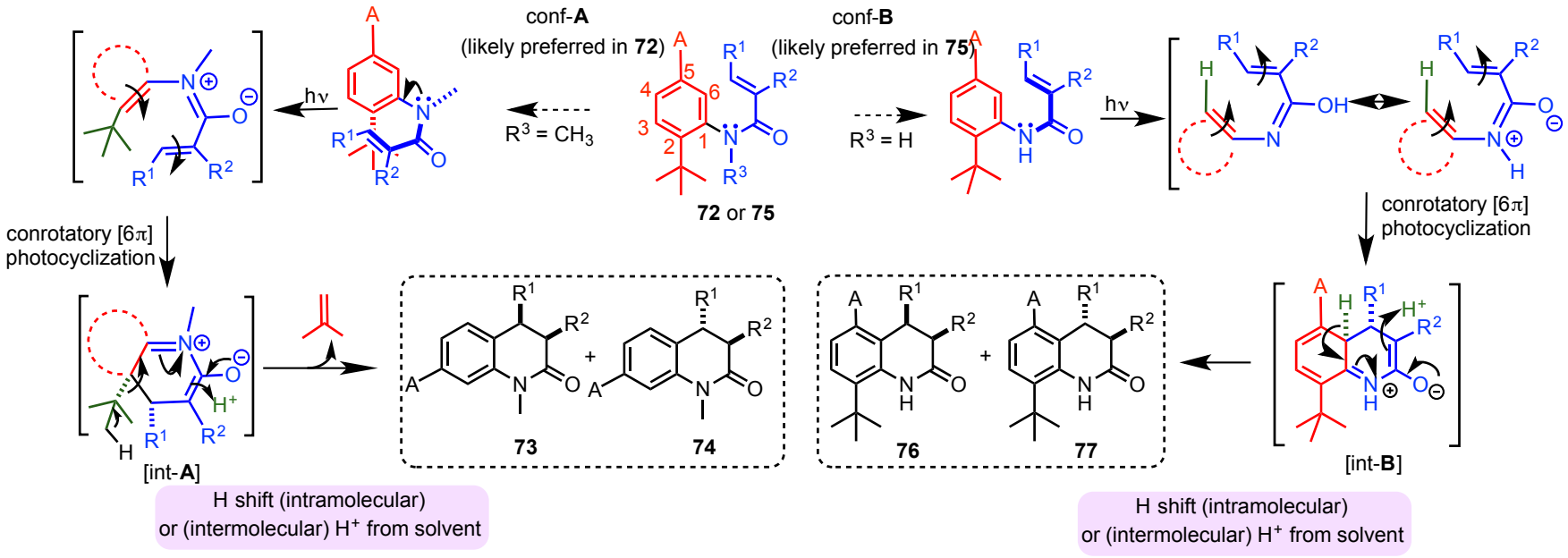

Scheme 2.4: Mechanism of photocyclization for acrylanilides **72** and **75.**

2.2.2. Deteurium incorporation experiment

Photocyclization of **72d** was performed in methanol-*d* to ascertain the intermolecular vs intramolecular [1,7]-H migration from the intermediate *int*-**A** leading to photocyclized *cis* and *trans* products.

It is well established in literature[3,5,6] that in protic solvents, the zwitterionic intermediate *int*-**69** (Scheme 2.5) from the N-Methyl substituted parent acrylanilides **69** undergoes intramolecular [1,5]-H shift and yields the *trans* product, whereas the *cis* isomer is formed by intermolecular H migration. Photocyclization of **72d** in methanol-*d* clearly showed (based on deuterium incorporation in *d*-*cis*-**73d**, Figures 2.2-blue and 2.3) that the proton is incorporated in the *cis* isomer by intermolecular hydrogen transfer to the zwitterionic intermediate *int*-**A** (Scheme 2.4, Figures 2.2 and 2.3) from the protic solvent. On the other hand, proton was delivered intramolecularly by a [1,7]-H shift leading to the *trans*-**74d** product (no deuterium incorporation in the *trans*-**74d** photoproduct (Figures 2.2 and 2.3). *trans*-**74d** and *d*-*cis*-**73d** were not separable by chromatography, hence their characterization was done as a mixture by ^{1}H NMR (Figure 2.2) and HRMS (Figure 2.3) that clearly established the formation of photoproducts by intramolecular pathway in the case of *trans* isomer and intermolecular pathway in the case of *cis* isomer.

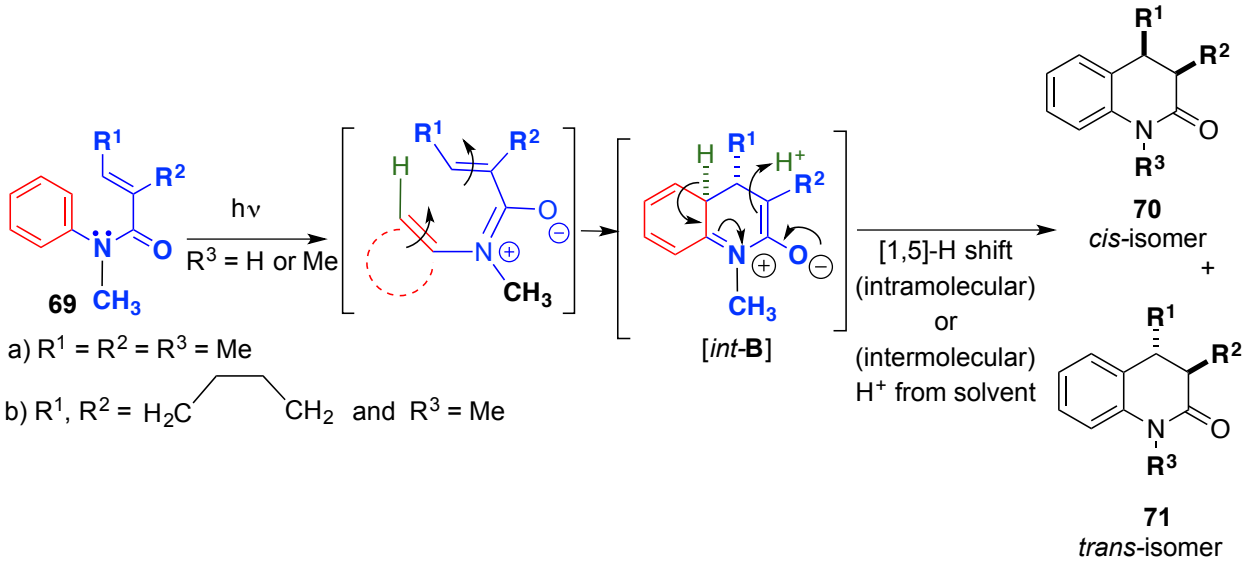

Scheme 2.5: Mechanism of photocyclization for parent acrylanilide **69.**

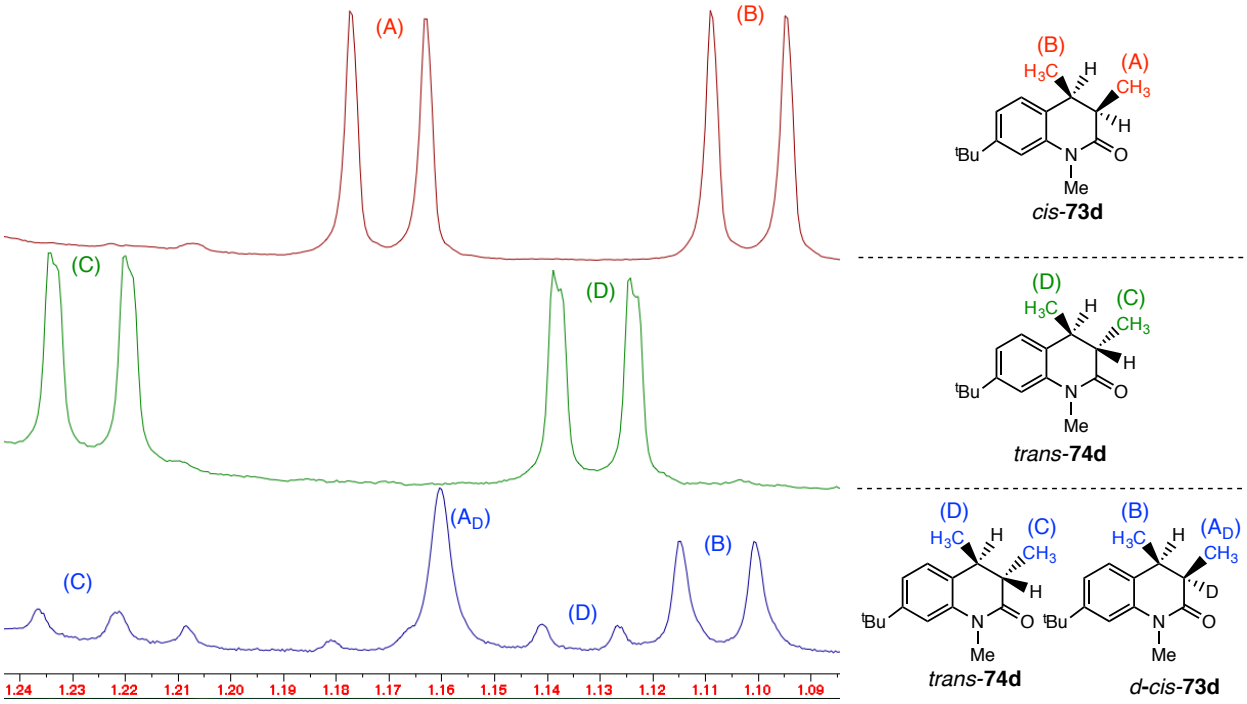

Figure 2.2: ^{1}H NMR upon photocyclization of **72d** in methanol-*d* (Blue). The methyl resonances in *cis*-**73d** (red) and *trans*-**74d** (green) are given for comparison.

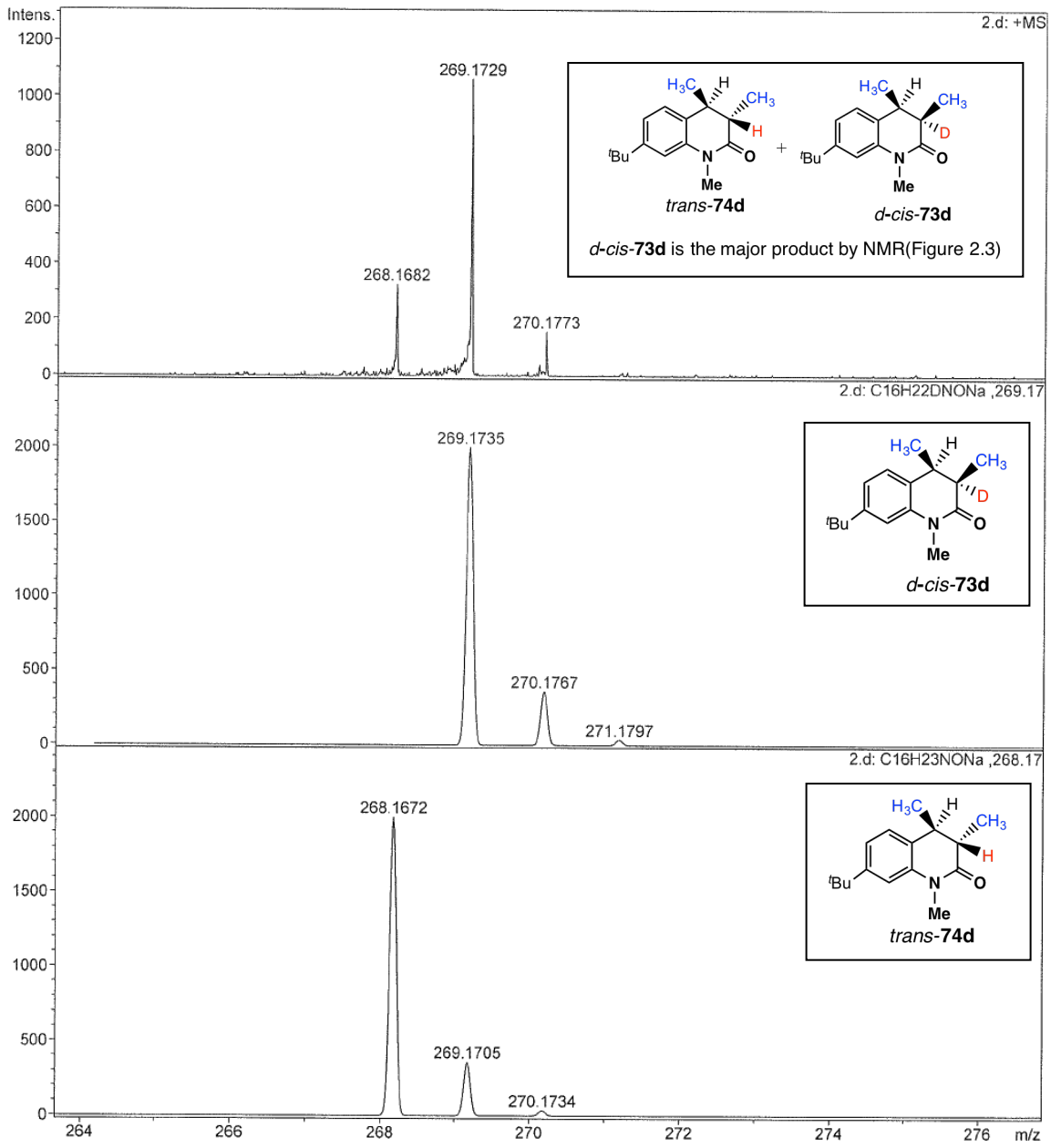

Figure 2.3: Top: HRMS-ESI of *d-cis*-**73d** and *trans*-**74d** mixture from photocyclization of **72d** in methanol-*d*; Middle: simulation of HRMS-ESI spectra for *d-cis*-**73d**; Bottom: simulation of HRMS-ESI spectra for *trans*-**73d**.

2.2.3. Single crystal XRD analysis

To enable a detailed mechanistic rationalization for the observed difference in the photocyclization between the N-Me *o-tert*-butylacrylanilides **72** and the corresponding N-H derivatives **75**, the structural parameters must be reliably known. Fortunately, the X-ray crystal structures for N-Me derivative (**72c** and **72f)** and the N-H derivative **75a** were obtained. It should be emphasized that the rigid conformation in the solid state must be utilized just as a starting point to rationalize the observed photobehavior in solution.

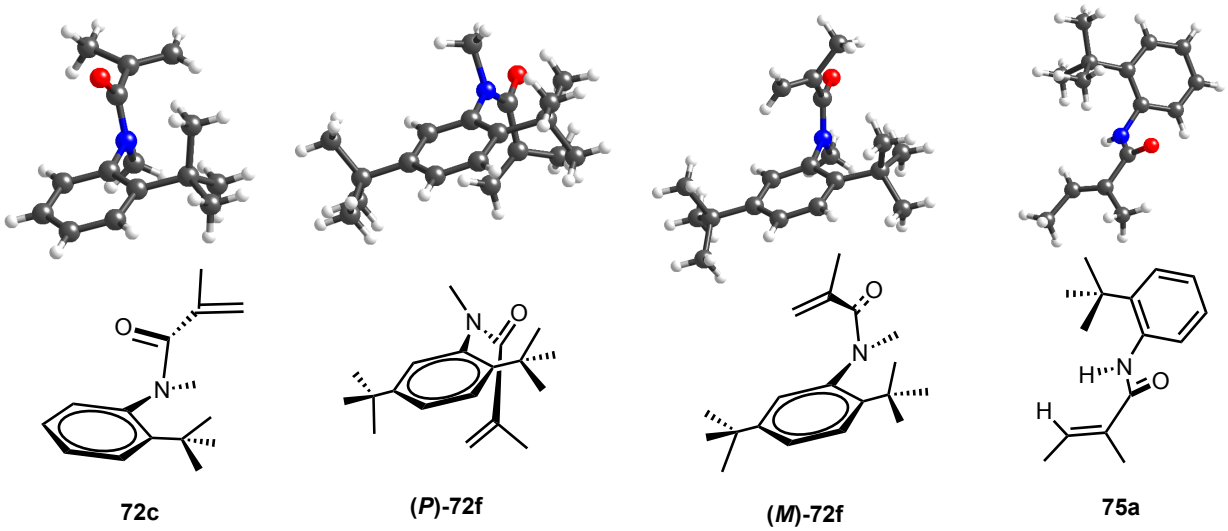

72c **(*P*)-72f** **(*M*)-72f** **75a**

Figure 2.4: X-ray crystal structures of **72c, 72f** and **75a**. Crystallizations were done in methanol (**72c**), benzene (**72f**) or pentane (**75a**).

Examination of the crystal structures of acrylanilides **72c**, **72f** and **75a** (Figure 2.4) reveals details regarding the difference in reactivity of the N-H and the N-methyl derivatives. In the case of **72f**, both the atropisomers (*P* and *M* isomers) are present in the unit cell. It is well established that in acrylanilides, the rotational feature of the amide N-CO bond generates amide *E/Z* isomers and the N-C(Aryl) bond generates *P*/*M* enantiomers (atropisomers).[12] For the mechanistic analysis, the rationale for the *P* isomer is also applicable to its enantiomeric *M* form. The amide N-CO bond favors the *E*-isomer and the planes of the aryl and the N-methyl acryloyl groups are roughly perpendicular. Additionally, there was a noticeable twist in the orientation of the methacryloyl functionality that is anticipated from prior crystal studies in literature. [12] In the case of **72c**, the crystal structure revealed

that the amide N-CO bond favors the *Z*-isomer (Figure 2.4). (Ref. 11, crystal structure of **72c** was already reported) The planes of the aryl group and the amide substituents are again roughly perpendicular, and the methacryloyl group is not in the plane of the amide. [12] For the 6π-photocyclization of the acrylanilides, the distance between the β-alkene carbon and the *ortho*-carbon on the N-phenyl ring is of relevance.

Based on the crystal structure and literature precedence, this distance must be generally less than 4 Å.[7-9,13] The distance between the β-alkene carbon and the *ortho*-carbon bearing the ^{t}Bu substituent is 5.24 Å for **72c** (*Z*-isomer) and 3.64 Å for **72f** (*E*-isomer). Similarly, the distance between the β-alkene carbon and the unsubstituted *ortho* carbon is 5.37 Å for **72c** (*Z*-isomer) and 3.34 Å for **72f** (*E*-isomer). Based on the β-alkene carbon and the *ortho*-carbon distances, the photocyclization can occur only from the amide N-CO *E*-isomer.[7-9,13] ^{1}H NMR studies and previous literature reports[12] on *o-tert*-butylacrylanilides **72** indicate that both the N-CO *Z* and *E* isomers are present at room temperature (Figures 2.8, 2.11 and 2.14 for example). The *Z/E* ratio was dependent on the nature of the solvent and the temperature. For example, in the case of **72d**, an *E*/*Z* ratio of 2.16/1 was observed in $CDCl_3$ (Figure 2.16).[12]

From a photochemical standpoint, it must be noted that *Z/E* isomers (amide N-CO isomers) might have different photophysical properties (molar absorptivity, emissive properties and reaction rates, etc.).[14,15] As both the *Z* and *E*-isomer are present in solution (based on NMR studies[12]), the photophysical properties have to be elucidated to completely understand their photoreactivity (chapter 4). For example, in **72c** both the amide N-CO *Z* and *E* isomers are observed by ^{1}H NMR spectroscopy (Figure 2.13) at room temperature (*Z*-isomer is observed exclusively below -60 ^{o}C and in the crystalline state).[12] No photoproducts were observed in the photocyclization of **72c** in methanol at 58±2 ^{o}C and in acetone at 40±2 ^{o}C (Figure 2.49). Thus, it is tempting to speculate that the low reactivity of **72c** is due to its preference for a conformation not sutiable for photocyclization in the solvents investigated (Table 2.1; entry 3) even though this speculation is based on the single crystal X-ray structure. In the current investigation, we will concentrate on product regiochemistry, and the photophysical properties will be explored subsequently (chapters 3 and 4).

2.2.4. Mechanistic rationale during 6π-photocyclization of acrylanilides

A comparison of the crystal structures of **72f** (N-Me *ortho*-*tert*-butylacrylanilides derivatives) and **75a** (N-H *ortho*-*tert*-butylacrylanilides derivatives) revealed two distinct conformations of the N-CO *E*-isomer (critical for 6π-photocyclization). Intuitively, the nitrogen substitution dictates the geometric preference in the N-CO *E*-isomer. In the case of **72**, conformation *conf*-**B** (Scheme 2.3) is likely disfavored due to severe 1,3-allylic strain between the *o*-*tert*-butyl and the N-Me groups. It is plausible that conformation *conf*-**A** (Scheme 2.3) that is observed in the crystalline state (Figure 2.4) is reflective of the diminished steric impediments between the *o*-*tert*-butyl and the N-Me groups. In the case of the N-H derivative **75**, *conf*-**B** is quite likely (based on single crystal X-ray crystallography, Figure 2.4) as it could tautomerize to the enol form to avoid steric impediments (Scheme 2.3). Presumably, the difference in the photobehavior of **72** and **75** is reflective of this difference in the conformational orientation of the N-CO *E*-isomer and the ability of the NH derivative to undergo tautomerization the enol form to minimize steric interactions.

As illustrated in scheme 2.4, 6π-photocyclization of the N-Me *o*-*tert*-butylacrylanilides **72** likely occured from *conf*-**A** resulting in a zwitterionic intermediate "*int*-**A**". Based on the structure of the photoproducts, the intermediate "*int*-**A**" subsequently undergoes either an intramolecular hydrogen shift from the *o*-*tert*-butyl substituent or an intermolecular H-transfer leading to *cis*-**73** and *trans*-**74**, with the loss of 2-methylpropene (Scheme 2.4). The intramolecular or intermolecular H-transfer depends on the solvent employed.[3-6] Photocyclization in methanol-*d* confirmed the intermolecular photocyclization process in protic solvents based on deuterium incorporation (*cf.* section 2.2, Schemes 2.4 and 2.5). On the other hand, 6π-photocyclization of the N-H derivatives **75** likely occured from *conf*-**B** or from the corresponding tautomeric form. Photocyclization likely proceeded via a zwitterionic intermediate "*int*-**B**" (Scheme 2.4) that subsequently underwent an intramolecular H shift or an intermolecular H-shift to *cis*-**76** and *trans*-**77**.[1-3,5-8,16] Thus, photocyclization of **75** is similar to the one reported[1-3,5-8,16] for the parent acrylanilides **69** without an *o*-^{t}Bu group (Scheme 2.1). Photocyclization from *conf*-**A** is expected to be slower compared to *conf*-**B** or its corresponding tautomer,[7,8,16] and is reflected in the reaction efficiency (compare conversions in Tables 2.1 and 2.2). In spite of this, the photocyclization of **72** was found to be very efficient and

clean in acetone with 50-60% conversion (Figure 2.5). This posed an important question regarding the reactive spin state involved in acetone irradiations. Control studies were carried out with **72e** in the presence of triplet quenchers (Section 2.2.5)[17,18] (oxygen, triethylamine) to ascertain the nature of the reactive spin state. Photoirradiation of **72e** was carried out (Figure 2.5) in acetone for 5 h under a) N_2 atmosphere; b) O_2 atmosphere; and c) in the presence of triethylamine under N_2 atmosphere. Photoirradiation in acetone under N_2 atmosphere resulted in ~70% conversion. Under O_2 atmosphere and in the presence of triethylamine under N_2 atmosphere, the conversion was ~6 % and ~30%. The results likely point out to a mixture of singlet and triplet spin states involved in acetone irradiation.[17,19] The triplet state is quenched under O_2 atmosphere[19] and an in the presence of triethylamine, hence its likely that the reaction proceeded only from the singlet state resulting in conversion similar to the one reported for other solvents where typical conversion was between 5-30% (Table 2.1). In the case of triethylamine, it was well established in literature that depending on the concentration of triethylamine, it could quench both the singlet and triplet spin states of acetone.[21] Detail photophysical investigations are currently in progress in our laboratory to ascertain the role of reactive spin states in different solvents. Irrespective of the nature of the reactive spin state, the *o-tert*-butyl group on the N-phenyl ring was lost during the photocyclization of **72**.

2.2.5. Photocyclization of 72e in acetone under N_2, O_2 and Et_3N to ascertain the reactive spin state

Photo-irradiation of **72e** was carried out (Figure 2.5) in acetone under a) N_2 atmosphere; b) O_2 atmosphere; and c) in the presence of Et_3N under N_2 atmosphere.

Solution of **72e** (0.1 mmol) and Et_3N (0.25 mmol) in 15 mL of acetone was irradiated for 5 h in a Pyrex tube with a 450 W Hg lamp at room temperature and under constant flow of nitrogen. The photolysate was analyzed on a HPLC (Figure 2.5 – bottom) and compared with the irradiation done under N_2 without Et_3N (Figure 2.5 – top).

Solutions of **72e** (0.1 mmol) in 15 mL of acetone was irradiated for 5 h in Pyrex tube with a 450 W Hg lamp at room temperature and under constant flow of oxygen. The photolysate was analyzed on a HPLC (Figure 2.5 – middle) and compared with the irradiation done under N_2 (Figure 2.5 – top).

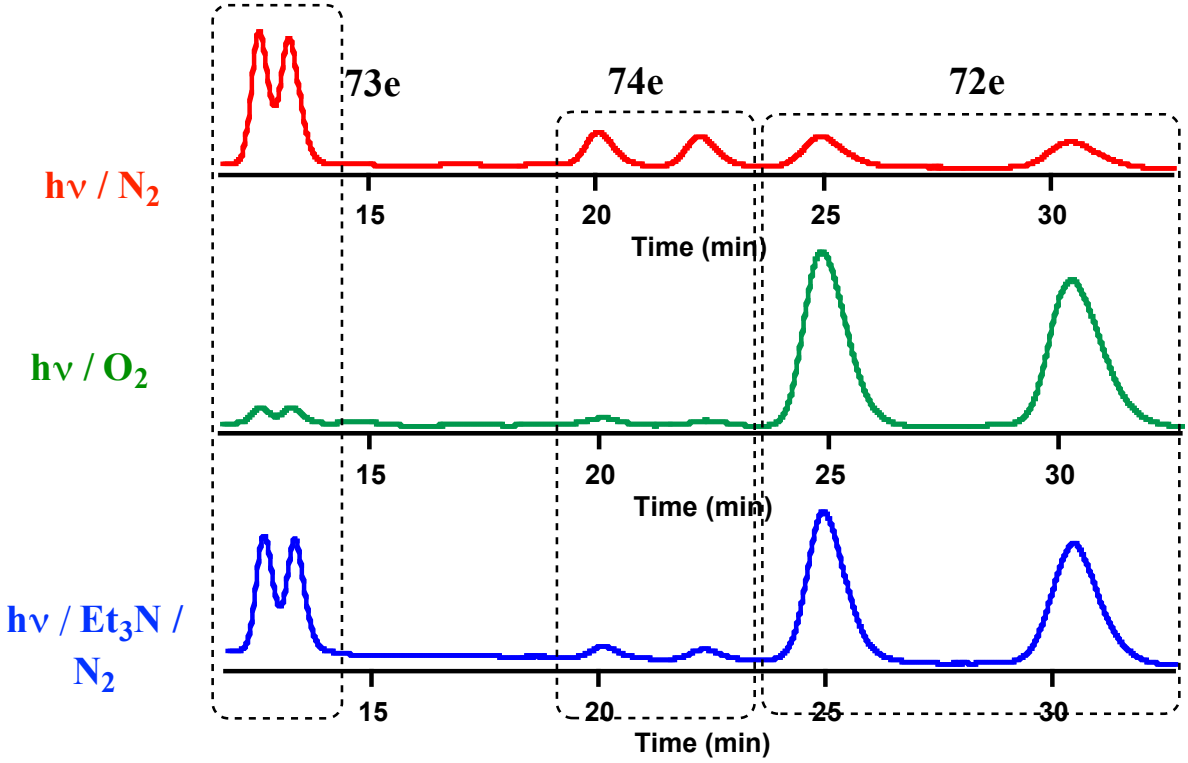

Figure 2.5: HPLC analysis after photoirradiation of **72e** in acetone under N_2 (top); O_2 (middle); under N_2 in the presence of Et_3N (bottom).

2.3. Summary and Outlook for Photocyclization of *o*-^{t}Bu-acrylanilides

This investigation established that N-methyl *o-tert*-butylacrylanilides undergo cyclization at the unexpected ortho carbon that bears the *tert*-butyl substituent. Based on product studies, the photocyclization was hypothesized to occur via a zwitterionic intermediate, which is analogous to the parent acrylanilides **69** (without an *o-tert*-butyl group). The intermediate derived from the *ortho-tert*-butyl N-Me derivatives **72** undergoes an unexpected hydrogen shift that was not observed with either the N-H derivatives **75** or **69**. Photocyclization of **72** in acetone likely involves a mixture of singlet and triplet spin states. As *o-tert*-butylacrylanilides exist as atropisomers,[12,20,21] the novel photocyclization process has opened up a platform to investigate the transfer of axial chirality (from the individual *P* and *M* isomers) to point chirality in the photoproducts.[11,18,22] This aspect of the transformation and the photophysical properties(of the systems of interest) investigations to ascertain the reaction multiplicities in various solvents will be addressed in the next chapter.

2.4. Experimental Section

2.4.1. General method

All solvents and chemicals were purchased from Alfa Aesar®, Sigma – Aldrich®, Across®, and Oakwood® Products, and were used as received without further purification. HPLC grade solvents (purchased from EMD®) were used for carrying out photoreactions. ^{1}H-NMR and ^{13}C-NMR spectra were obtained on Varian 400 MHz or 500 MHz spectrometer. Coupling constants (*J*) are reported in hertz (Hz). Standard abbreviations indicating multiplicity were used as follows: s (singlet), b (broad), d (doublet), t (triplet), q (quartet), m (multiplet), virt (virtual), and ABq (AB quartet). Electrospray Ionization Spectra were recorded on a Bruker – Daltronics® BioTof mass spectrometer in positive (ESI+) ion mode. HPLC analyses were performed on Waters® HPLC equipped with 2525 pump. Waters® 2767 sample manager was used for automated sample injection. All HPLC injections were monitored using a Waters® 2487 dual wavelength absorbance detector at 254 nm and 270 nm. Analytical and semi-prepaprative injections were perfomed on chiral stationary phase uisng (R,R) WHELK–01 columns: (25cm X 4.6 mm column for analytical injections, and 25 cm x 10mm for semi-preparative injections). Masslynx software version 4.1 was used to analyse the HPLC injections. Igor Pro® Sofware version 4.0 was used to process the chromatographic data. UV-Vis spectra were recored on a shimadzu 2501PC UV-Vis spectrometer using UV quality fluorimeter cells (with range until 190 nm) purchased from Luzchem. When necessary, the reactants and photoproducts were purified by chromatography on silica gel (Sorbent Technologies®, silica gel standard grade: Porosity 60 Å, Particle size: 230 x 400 mesh, Surface area: 500 – 600 m^2/g, Bulk density: 0.4 g/mL, pH range: 6.5 – 7.5). The Retention Factor (R*f*) values were recorded using a 30 % EtOAc-Hexanes as mobile phase (unless indicated) and on *Whatman*® flexible TLC plates (250 m layer 20 x 20 cm, UV_{254}, PE SIL G/UV).

Structure determination: Single crystal X-ray diffraction data sets were collected on a SIEMENS diffractometer with a 1K CCD area detector (graphite-monochromated Mo Ka radiation, crystals protected with Parathone-N oil). The structures were solved by direct methods and refined on F^2 using the SHELXTL V6.14 package (after absorption corrections with SADABS). Details of the data collections and refinements are given in the table 2.3.

Structure **72c**: $C_{15}H_{21}NO$, M=231.33, Monoclinic, P21/c (no.14), a = 11.120(16), b = 10.165(15), c = 12.745(18), β = 108.04(3), V = 1370 (3) $Å^3$, 298K, Z = 4, 6779 reflections measured, 2388 unique reflections (R_{int} = 0.0575) which were used in all calculations. R_1/wR_2 = 6.01/18.72, R_1/wR_2 (all) = 7.26/20.29

Structure **72f**: $C_{19}H_{29}NO$, M=287.43, Triclinic, P-1 (no.2), a = 11.073(10), b = 14.119(13), c = 14.351(13), α = 115.446(14), β = 96.908(16), γ = 107.764(15), V = 1845 (3) $Å^3$, 298K, Z = 4, 13641 reflections measured, 6418 unique reflections (R_{int} = 0.0380) which were used in all calculations. R_1/wR_2 = 8.54/25.23, R_1/wR_2 (all) = 11.61/28.64

Structure **75a**: $C_{15}H_{21}NO$, M=231.33, Tetragonal, I-4 (no.82), a = 17.588(12), c = 8.963(13), V = 2773 (5) $Å^3$, 250K, Z = 8, 7197 reflections measured, 1463 unique reflections (R_{int} = 0.0444) which were used in all calculations. R_1/wR_2 = 5.62/16.52, R_1/wR_2 (all) = 7.53/19.64

The A-errors reported for structure **72f** are regarding structural disorder in the t-butyl groups. The observed disorder is not unusual for such molecules and it has no influence on the subject of interest discussed in the paper.

Table 2.3: Crystallography parameters of **72c**, **72f**, and **75a.**

Structure	**72c**	**72f**	**75a**
Formula	$C_{15}H_{21}NO$	$C_{19}H_{29}NO$	$C_{15}H_{21}NO$
FW	231.33	287.43	231.33
space group, Z	P2(1)/c, 4	P-1, 4	I-4, 8
a [Å]	11.120(16)	11.073(10)	17.588(12)
b [Å]	10.165(15)	14.119(13)	17.588(12)
c [Å]	12.745(18)	14.351(13)	8.963(13)
α [°]	90.0	115.446(14)	90.0
β [°]	108.04(3)	96.908(16)	90.0
γ [°]	90.0	107.764(15)	90.0
V [$Å^3$]	1370(3)	1845(3)	2773(5)
ρ_{calc} [$g \cdot cm^{-3}$]	1.122	1.035	1.108
No. of measured refl.	6779	13641	7197
No. of indep. refl.	2388	6418	1463
No. of used refl.	1905	4199	1101
μ [cm^{-1}]	0.069	0.063	0.069
$2\theta_{max}$ [°]	50	50	52
R1/wR2 ($I \geq 2\sigma_1$)* [%]	6.01/18.72	8.54/25.23	5.62/16.52
R1/wR2 (all data) [%]	7.26/20.29	11.61/28.64	7.53/19.64

[*] $R1 = \Sigma||F_o| - |F_c|| / \Sigma|F_o|$, $wR2 = \{[\Sigma[(F_o)^2 - (F_c)^2]^2] / [\Sigma w(F_o^2)^2]\}^{1/2}$ for $F_o^2 > 2\sigma(F_o^2)$, $w = [\sigma^2(F_o)^2 + (AP)^2 + BP]^{-1}$ where $P = [(F_o)^2 + 2(F_c)^2] / 3$; A (B) = 0.1325 (0.24) for 4c, A (B) = 0.1185 (0.0) for 4f, A (B) = 0.1673 (0.7359) 7a.

2.4.2. General procedure for synthesis of *N*-methyl anilines 80a and 81a

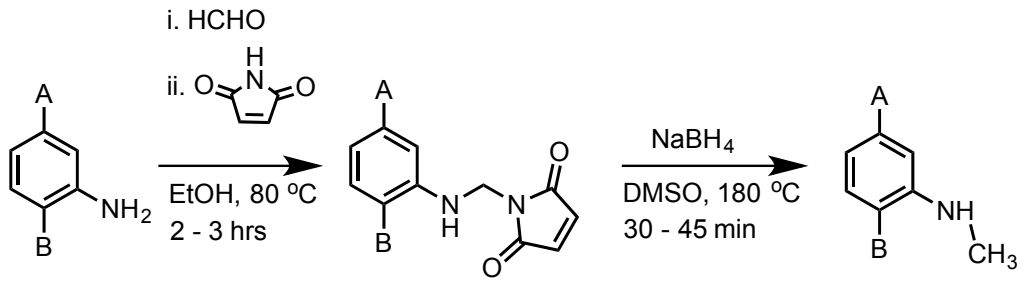

2-*tert*-butylaniline: A = H, B = ^{t}Bu
2,5-di-*tert*-butylaniline: A = B = ^{t}Bu

80a: A = H, B = ^{t}Bu
81a: A = ^{t}Bu, B = ^{t}Bu

Scheme 2.6: Synthesis of *N*-Methyl substituted anilines **80a** and **81a**.

N-Methyl anilines **80a** and **81a** were synthesized using previously reported procedures.[12] 1 equiv. of aniline (or substituted aniline) (5 g, 5.2 mL, 34 mmol) was dissolved in 15 mL of EtOH; then, 1.1 equiv. of 37.9 % formaldehyde solution (1.11g, 3 mL, 37 mmol) and 1.1 equiv. of succinimide (3.65 g, 37 mmol) were respectively added to the aniline solution. The new mixture was allowed to reflux while stirring the reaction medium. After 2 to 3 hrs of reaction time, the solution was allowed to cool to room temperature and concentrated by removing the excess of solvent by roto-evaporation. The concentrated solution was then kept aside to solidify/crystallize by adding a minimum amount (5 to 10 mL) of pentane to the reaction flask. A crystalline, powdered, or gelly succinamide functionalized aniline derivative was collected by vacuum filtration, washed several times with cold ethanol, dried and was used without further purification.

Succinamide functionalized aniline (8.85 g, 34 mmol; 1 equiv.) was dissolved in 20 mL of dry DMSO under N_2 atmosphere. While heating the reaction flask and stirring the new solution, 1.1 equiv. (1.42 g, 37 mmol) of $NaBH_4$ was slowly added to the flask. The new mixture was allowed to reflux for 45 min under extremely dry conditions. The reaction mixture was cooled and the solution was transferred to a beaker containing cold DI water (about 200 mL). The organic layer was extracted with diethyl ether (3x20 mL). The ether layer was then dried over *anh.* Na_2SO_4, filtered, and concentrated to obtain the expected *N*-Methyl substituted anilines. The purity (based on TLC, NMR, HPLC) of the synthesized compounds allowed us to employ them in subsequent reactions without further purification.

2.4.3. Characterization of *N*-methyl anilines 80a and 81a

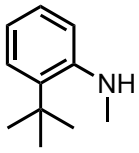

80a

***o-tert*-Butyl-*N*-methylaniline 80a**: R*f* = 0.78

^{1}H NMR (500 MHz, $CDCl_3$, δ ppm) 7.38 – 7.35 (d, *J* = 7.8, 1H), 7.30 – 7.24 (t, *J* = 7.6, 1H), 6.86 – 6.73 (m, 2H), 4.05 (bs, 1H), 3.01 (s, 3H), 1.53 (s, 9H)

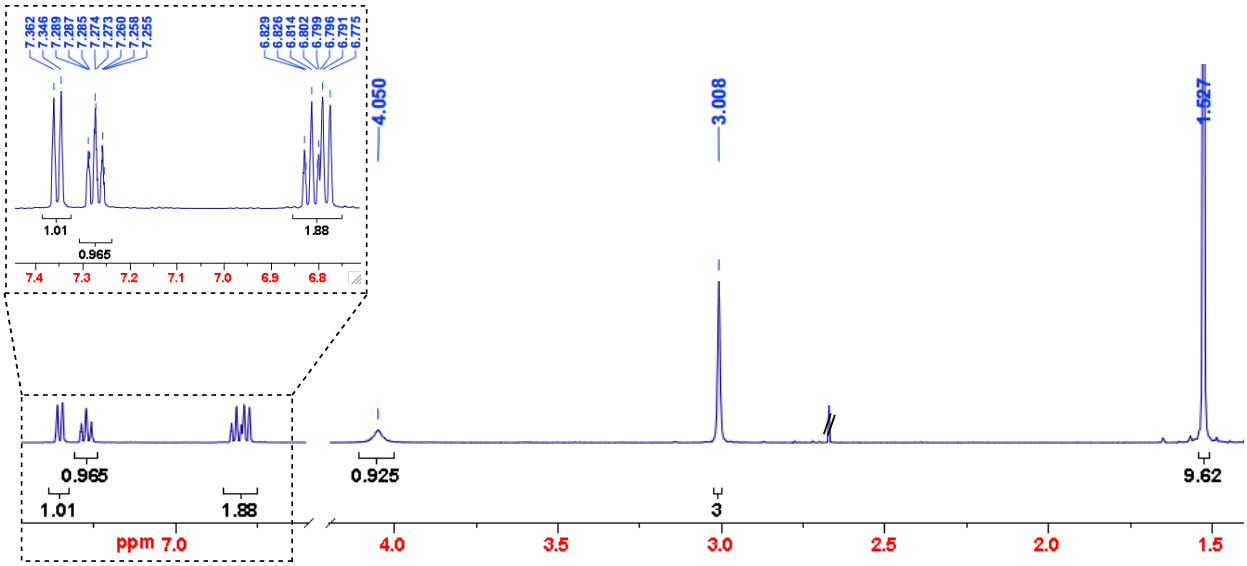

Figure 2.6: ^{1}H NMR (500 MHz, $CDCl_3$, δ ppm) spectrum for aniline **80a.**

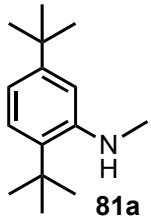

81a

2,5-di-*tert*-butyl-*N*-methylaniline 81a: R*f* = 0.89

^{1}H NMR (400 MHz, $CDCl_3$, δ ppm) 7.17 – 7.15 (d, *J* = 8, 1H), 7.00 (s, 1H), 6.77 – 6.75 (d, *J* = 8, 1H), 5.11 (bs, 1H), 2.64 (s, 3H), 1.37 (s, 9H), 1.29 (s, 9H)

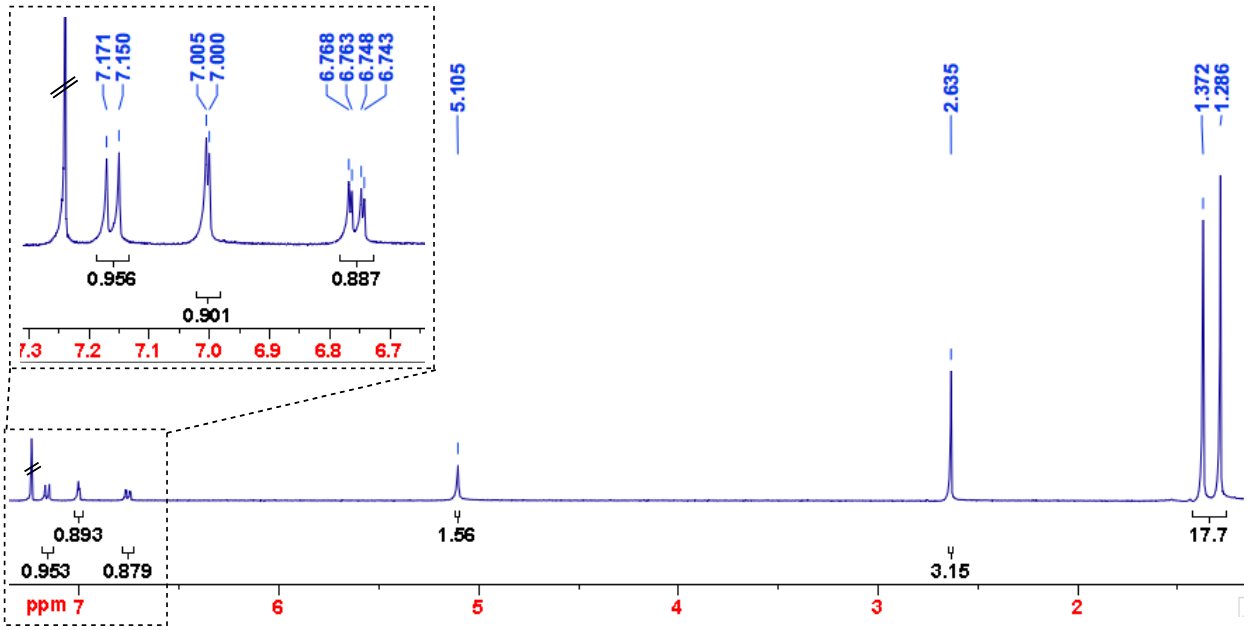

Figure 2.7: ^{1}H NMR (400 MHz, $CDCl_3$, δ ppm) spectrum for aniline **81a.**

2.4.4. General procedure for synthesis of acrylanilides 69, 72 and 75

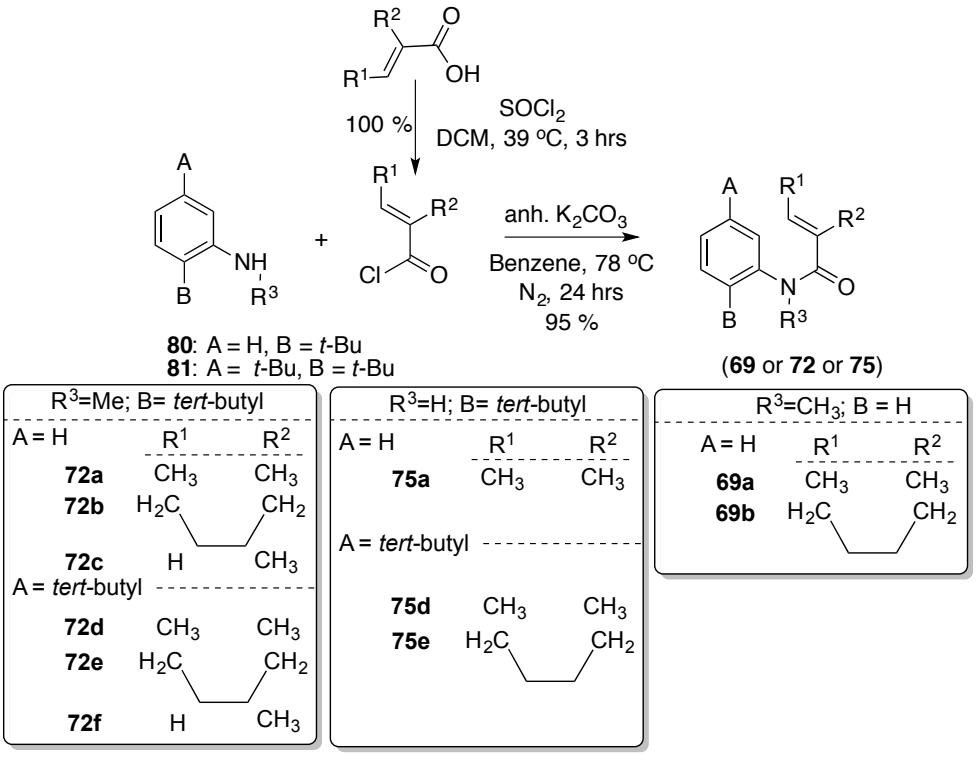

Scheme 2.7: Synthesis of acrylanilides **69**, **72** and **75**.

Acrylanilides **69**, **72** and **75** were prepared using procedures reported in literature (Scheme 2.6).[3,5,6,12] In a typical reaction, 1 equiv. of N-methyl aniline (substituted aniline for **72** and **75**) was dissolved in 20 mL of benzene. Then, the aniline solution was stirred and purged with N_2 gas; 1.5 equivalent of *anh.* K_2CO_3 was added to the reaction flask, and 1.5 equivalent of acyl (tigloyl, cyclohexyl, or methacryl) chloride (synthesized from the corresponding carboxylic acid or commercially available) was slowly added to the mixture in the flask constantly stirred and under N_2 atmosphere. The new solution was allowed to reflux (78 ^{o}C) overnight (24 hrs). After completion, the reaction was quenched (10 – 20 mL of water) and washed with water (2 x 20 mL) followed by extraction with ethyl acetate (EtOAc) (2 x 20 mL). The organic layer was then dried over *anh.* Na_2SO_4 and concentrated by rotor evaporation under reduced pressure. The expected amides were finally purified by flash chromatography on silica gel. Non-methylated amides (crystalline compounds) were recrystallized in pentane or diethyl ether.

2.4.5. Characterization of acrylanilides 69, 72 and 75

***o-tert*-Butyl acrylanilide 72a**: R*f* = 0.11

^{1}H NMR (500 MHz, $CDCl_3$, δ ppm) 7.53 – 7.46 (m, 1H), 7.32 – 7.21 (m, 1H), 7.15 (t, *J* = 7.4 Hz, 1H), 7.06 – 6.93 (m, 1H), 5.87 and 5.73 (q, 1H, minor and major conformer), 3.29 and 3.24 (s, 3H, minor and major conformer) 1.95 and 1.55 (s, 3H, α-Me minor and major conformer), 1.77 and 1.45 (d, *J* = 6.5 Hz, b-Me minor and major conformer), 1.40 and 1.37 (s, 9H, ^{t}Bu minor and major conformer).

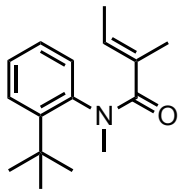

72a

HRMS-ESI ([M + Na]$^+$): Calculated: 268.1672; Observed: 268.1669; Δm = 1.1 ppm

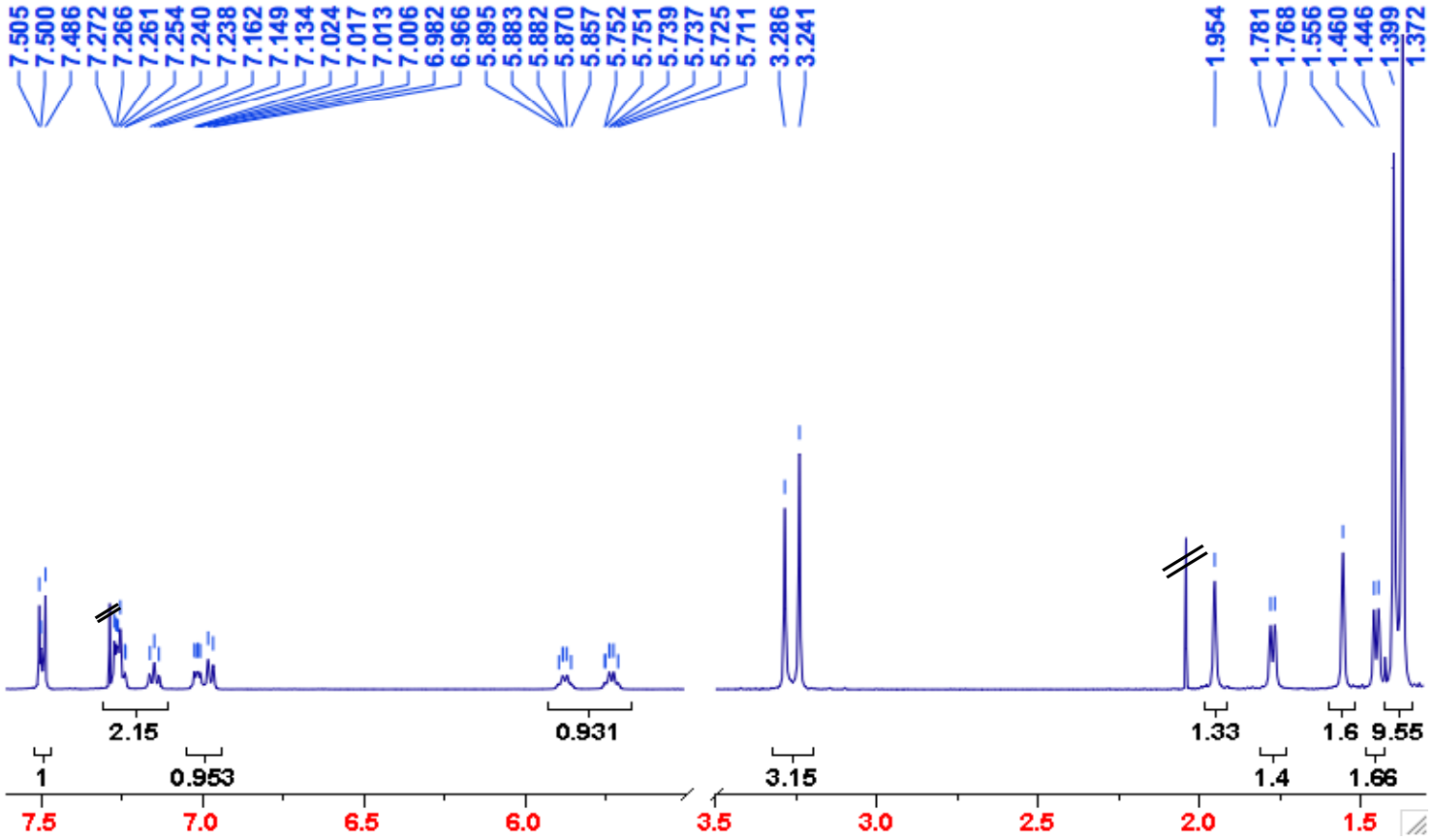

Figure 2.8: ^{1}H NMR (500 MHz, $CDCl_3$, δ ppm) spectrum for acrylanilide **72a.**

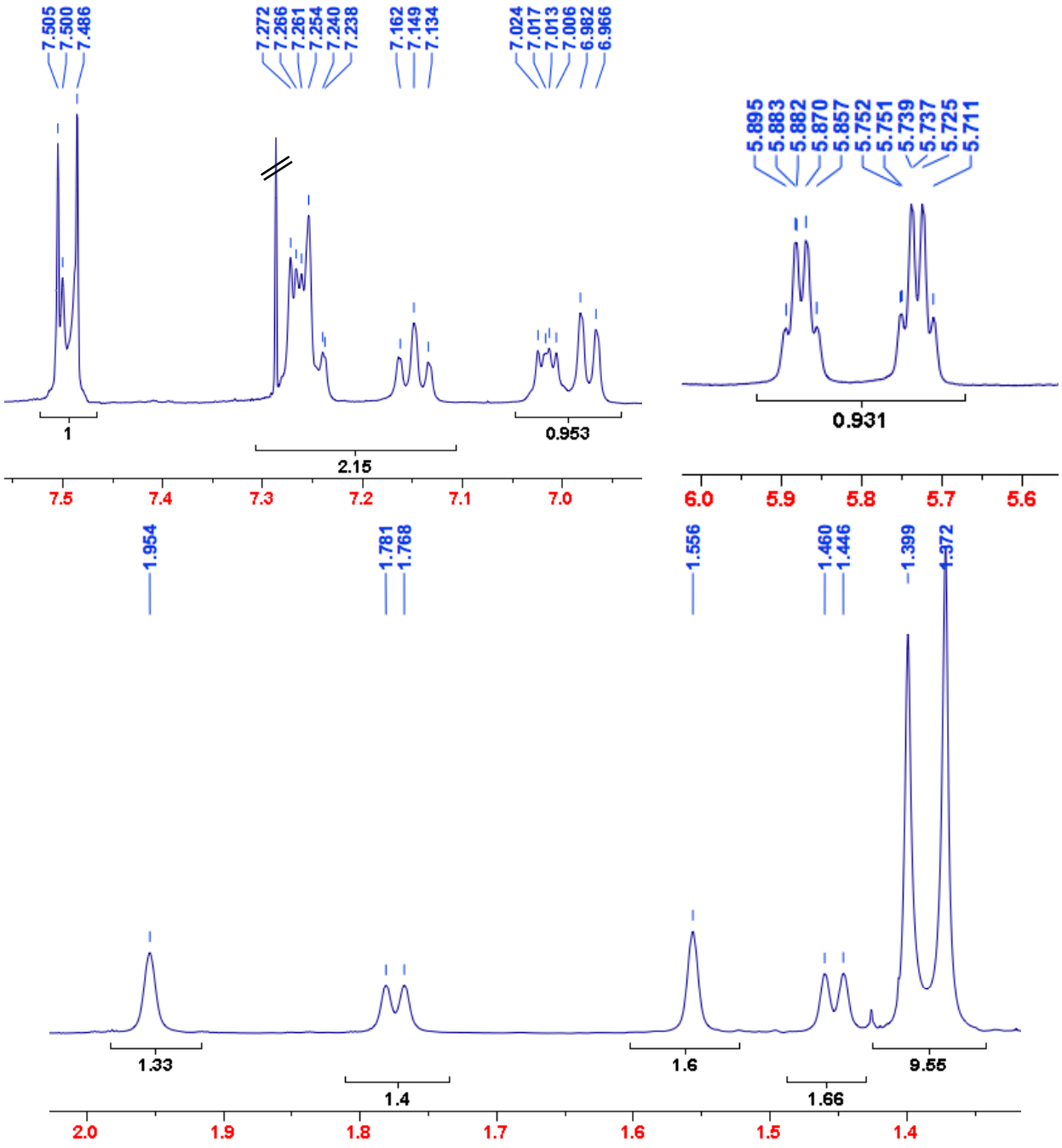

Figure 2.9: ^{1}H NMR (500 MHz, $CDCl_3$, δ ppm) spectrum for acrylanilide **72a:** Expanded regions.

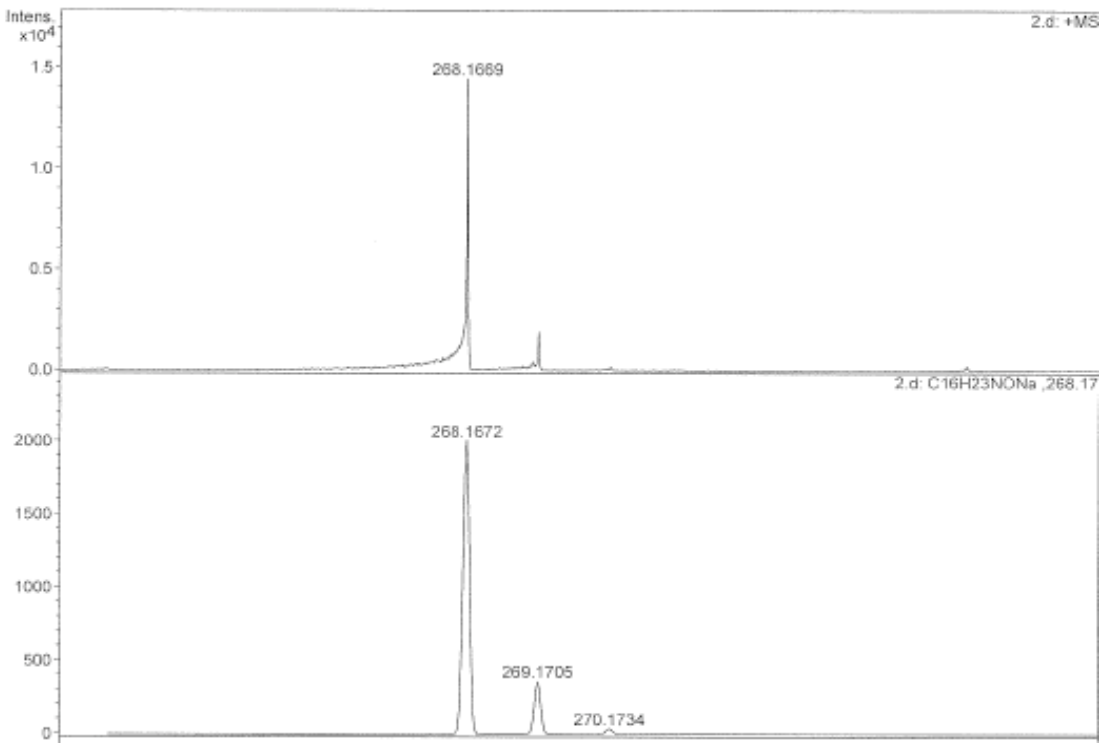

Figure 2.10: HRMS for acrylanilide **72a.**

***o-tert*-Butyl acrylanilide 72b**

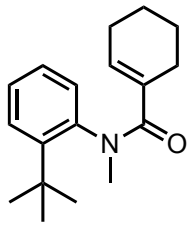

72b

^{1}H NMR (400 MHz, $CDCl_3$, δ ppm) 7.46 (d, *J* = 9.2 Hz, 1H), 7.26 – 7.17 (m, 1H), 7.10 (t, *J* = 8.4 Hz, 1H), 6.95 (m, 1H), 5.98 and 5.76 (s,1H, alkene H minor and major conformer), 3.30 and 3.22 (s, 3H, N-Me minor and major conformer), 2.44 -1.54 (m, 8H), 1.33 and 1.31 (s, 9H, ^{t}Bu minor and major conformer)

HRMS-ESI ([M + Na]$^+$): Calculated: 294.1828; Observed: 294.1825; Δm = 1 ppm

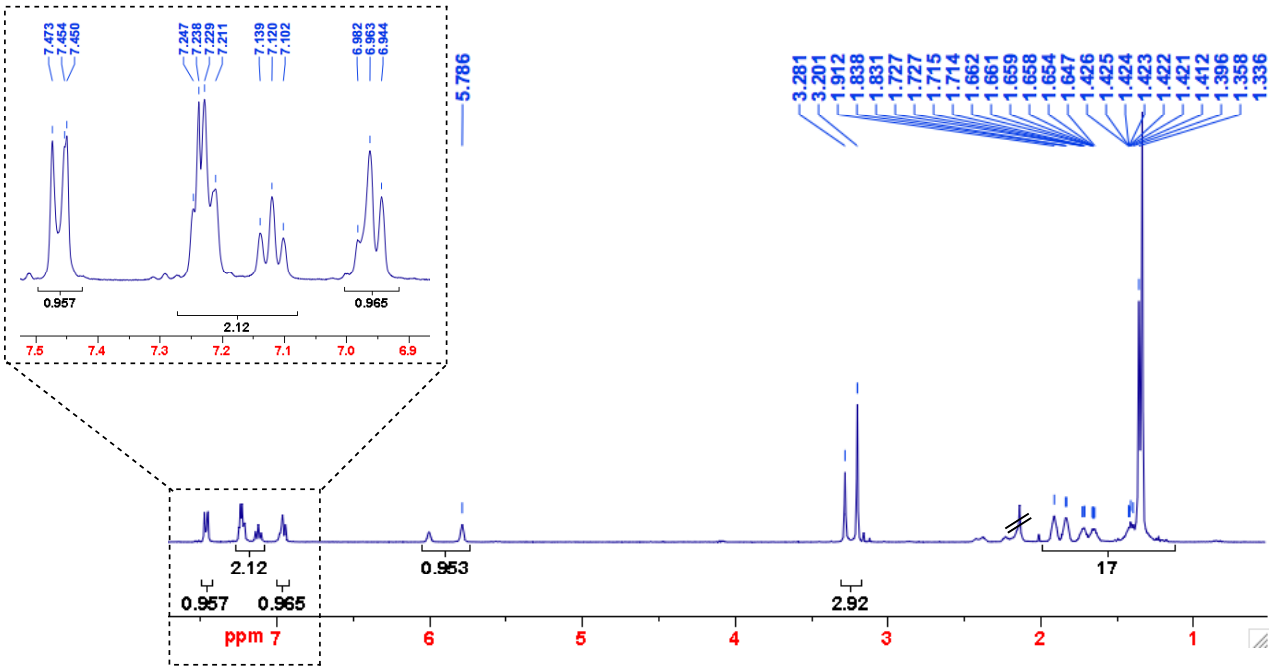

Figure 2.11: ^{1}H NMR (400 MHz, $CDCl_3$, δ ppm) spectrum for acrylanilide **72b.**

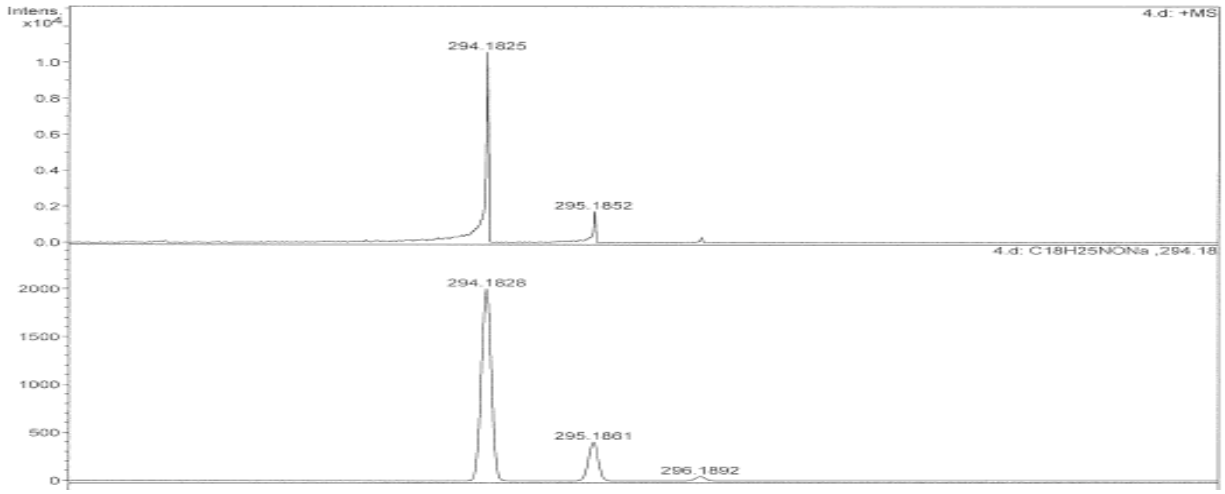

Figure 2.12: HRMS for acrylanilide **72b.**

***o-tert*-Butyl acrylanilide 72c**

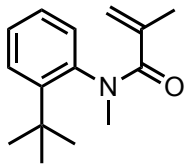

72c

^{1}H NMR (500 MHz, $CDCl_3$, δ ppm) 7.53-6.95 (Ar, 4 H), 5.29 and 5.04 (s, 1H, minor and major conformer), 5.23 and 4.87 (s, 1H, minor and major conformer), 3.30 and 3.22 (s, 3H, N-Me minor and major conformer), 2.04 and 1.76 (s, 3H, a-Me minor and major conformer), 1.37 and 1.36 (s, 9H, ^{t}Bu minor and major conformer)

HRMS-ESI ($[M + Na]^+$): Calculated: 254.1515; Observed: 254.1504; Δm = 4.3 ppm

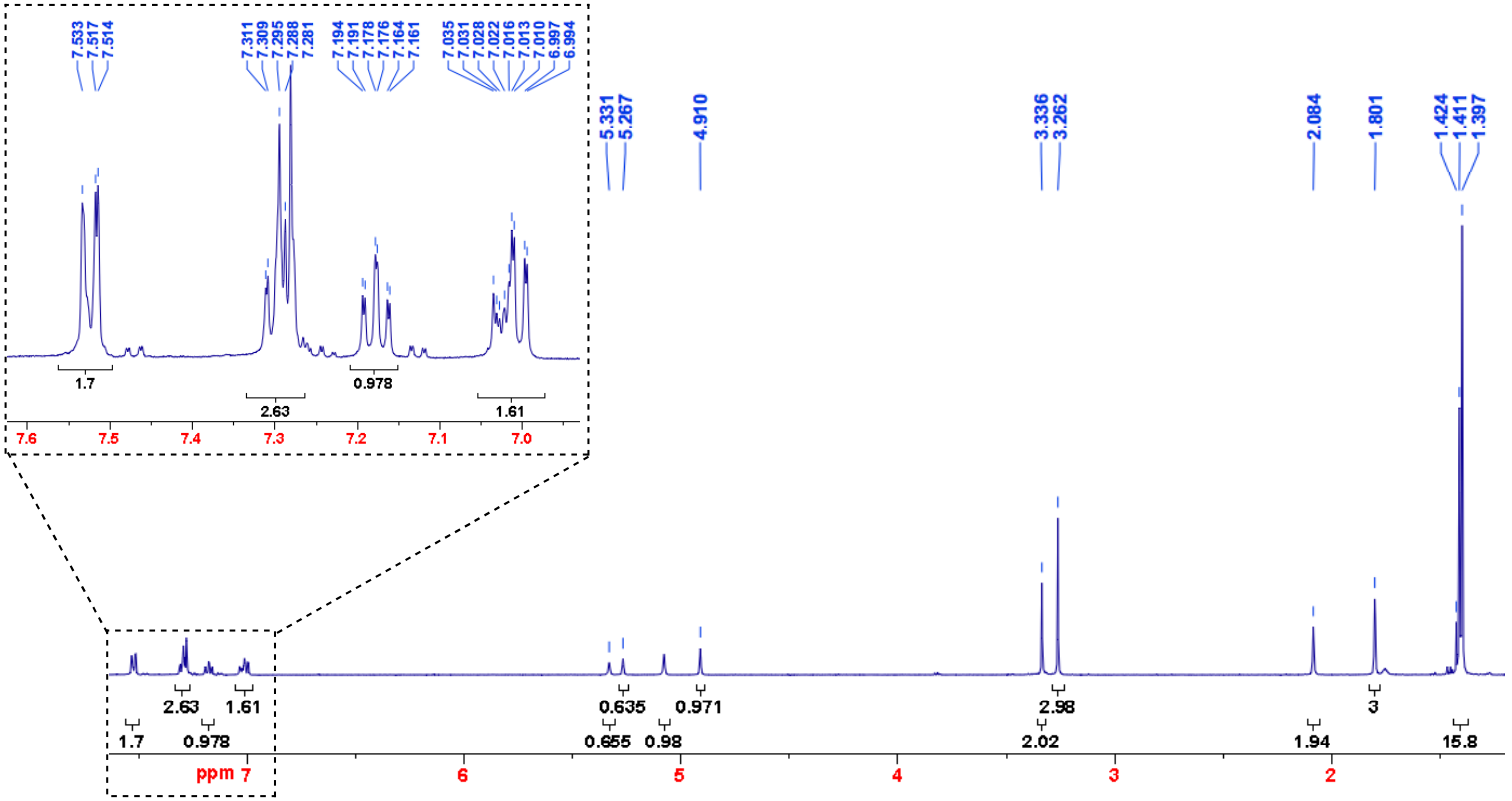

Figure 2.13: ^{1}H NMR (500 MHz, $CDCl_3$, δ ppm) spectrum for acrylanilide **72c.**

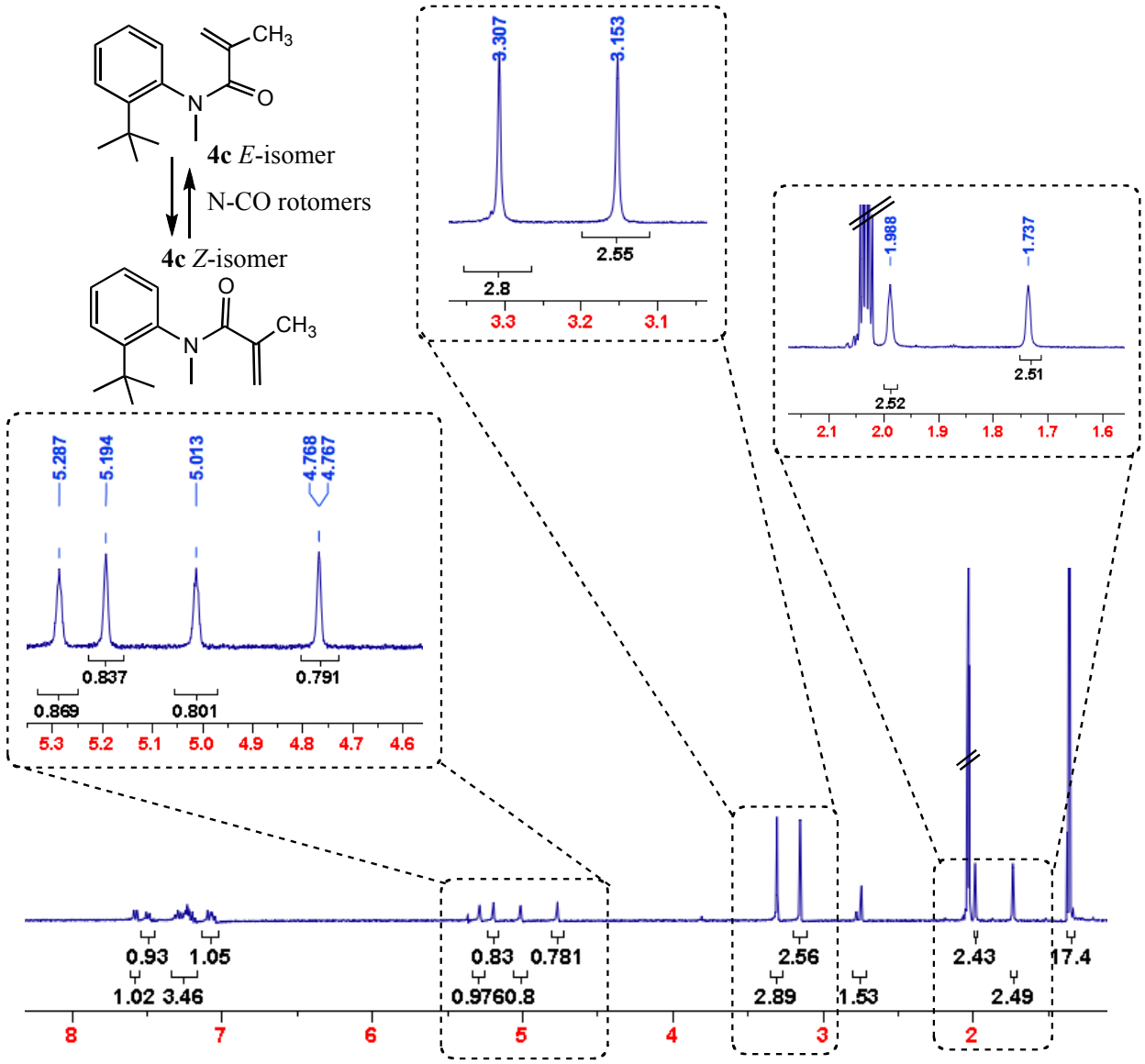

Figure 2.14: ^{1}H NMR (500 MHz, δ ppm) spectrum for acrylanilide **72c** in acetone-d_6: The *E:Z* N-CO rotamer ratio was close to 50:50. A comparison of rotamer ratio in acetone-d_6 and $CDCl_3$ shows that both *E* and *Z* isomers are present in solution.

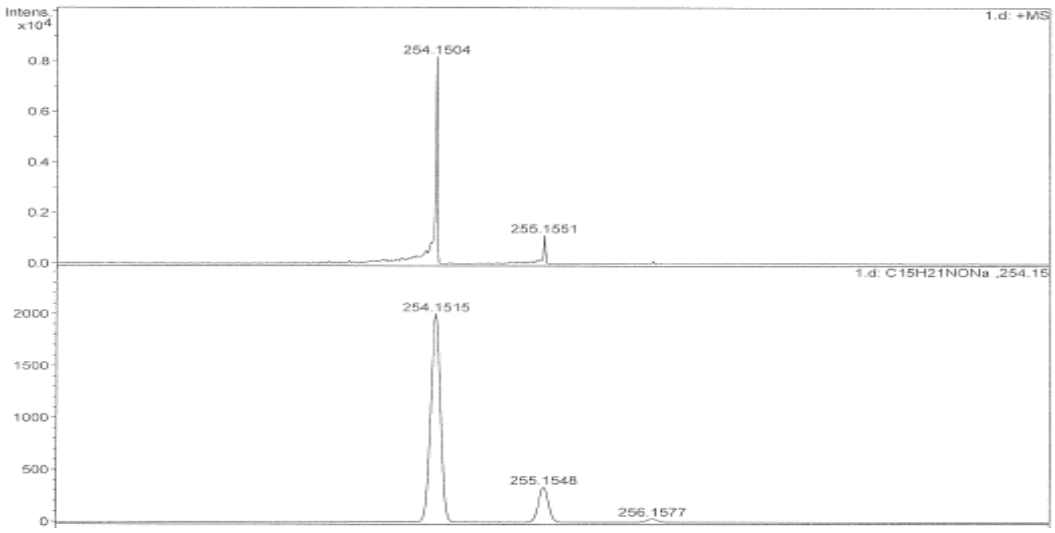

Figure 2.15: HRMS for acrylanilide **72c.**

2,5-*tert*-butyl acrylanilide 72d: R*f* = 0.59

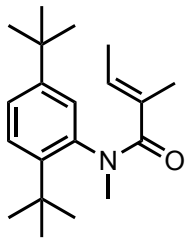

72d

Purified at 20% EtOAc/Hexanes by flash chromatography on silica gel.

^{1}H NMR (500 MHz, $CDCl_3$, δ ppm) 7.36 – 7.34 (m, 1H), 7.23 – 7.20 (m, 1H), 6.89 – 6.87 (m, 1H), 5.84 – 5.80 (q, alkene H minor conformer), 5.72 – 5.68 (q, alkene H major conformer), 3.23 (s, N-Me minor conformer), 3.19 (s, N-Me major conformer), 1.90 (s, a-Me minor conformer), 1.72 – 1.71 (d, b-Me minor conformer), 1.46 (s, a-Me major conformer), 1.39 – 1.38 (d, b-Me major conformer), 1.33 and 1.31 (^{t}Bu, 9H, minor and major conformer), 1.25 and 1.22 (^{t}Bu, 9H, minor and major conformer)

HRMS-ESI ([M + Na] $^+$): Calculated: 324.2298; Observed: 324.2296; Δm = 0.6 ppm

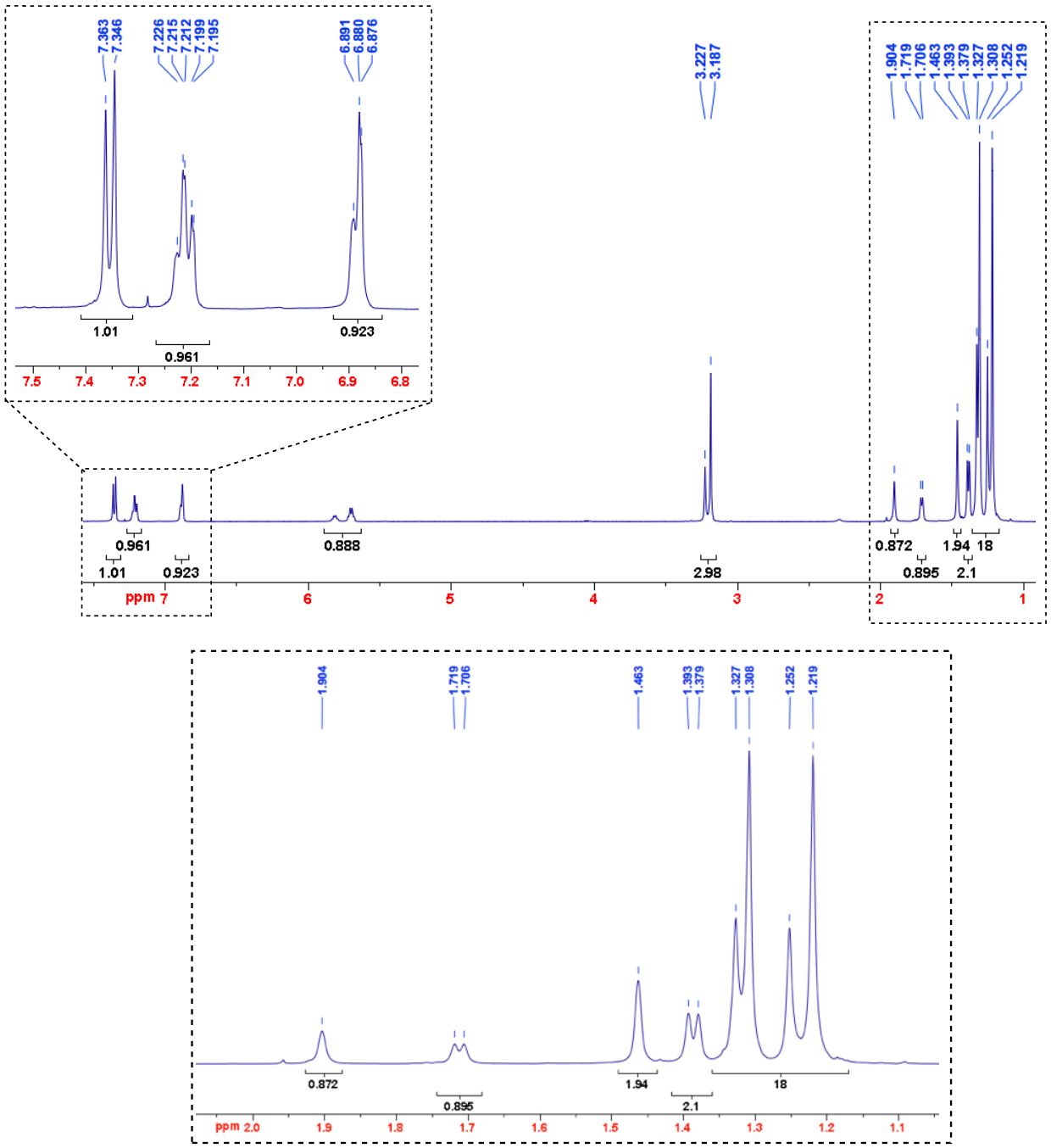

Figure 2.16: ^{1}H NMR (500 MHz, $CDCl_3$, δ ppm) spectrum for acrylanilide **72d.**

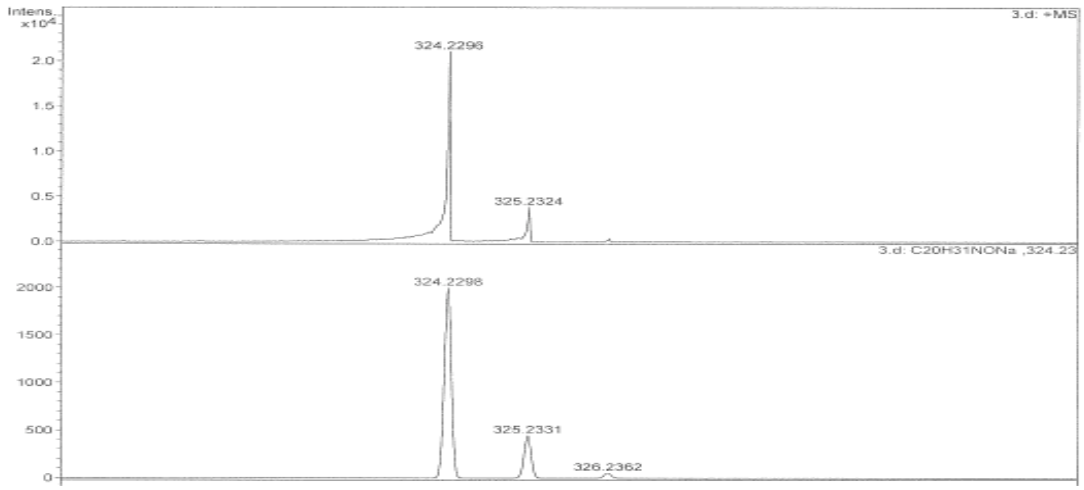

Figure 2.17: HRMS for acrylanilide **72d.**

2,5-*tert*-Butyl acrylanilide 72e: R*f* = 0.60

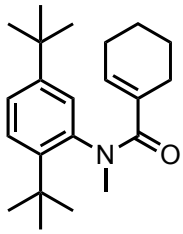

72e

Purified at 15% EtOAc/Hexanes by flash chromatography on silica gel

^{1}H NMR (400 MHz, $CDCl_3$, δ ppm) 7.41 – 7.35 (m, 1H), 7.27 – 7.20 (m, 1H), 6.92 – 6.86 (m, 1H), 6.03 – 5,96 (m, alkene H minor conformer), 5.86 – 5.79 (m, alkene H, major conformer), 3.23 (s, N-Me minor conformer), 3.15 (s, N-Me major conformer), 1.99 – 1.04 (m, 26H)

^{13}C NMR (100 MHz, $CDCl_3$ δ ppm) 172.2, 133.1, 128.3, 125.0, 40.5, 32.4, 31.3, 26.7, 25.3, 22.5 and 21.6

HRMS-ESI ([M + Na]$^{+}$): Calculated: 350.2454; Observed: 350.2461; Δm = 0.2 ppm

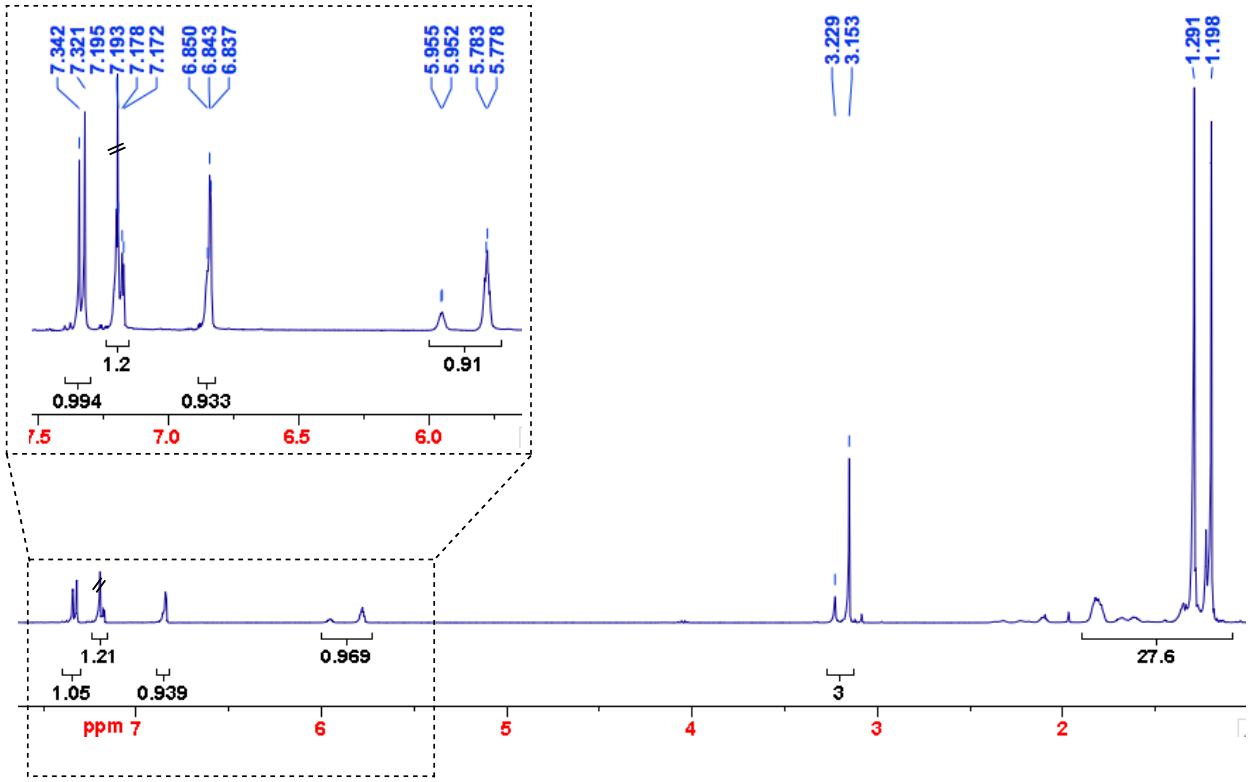

Figure 2.18: ^{1}H NMR (400 MHz, $CDCl_3$, δ ppm) spectrum for acrylanilide **72e.**

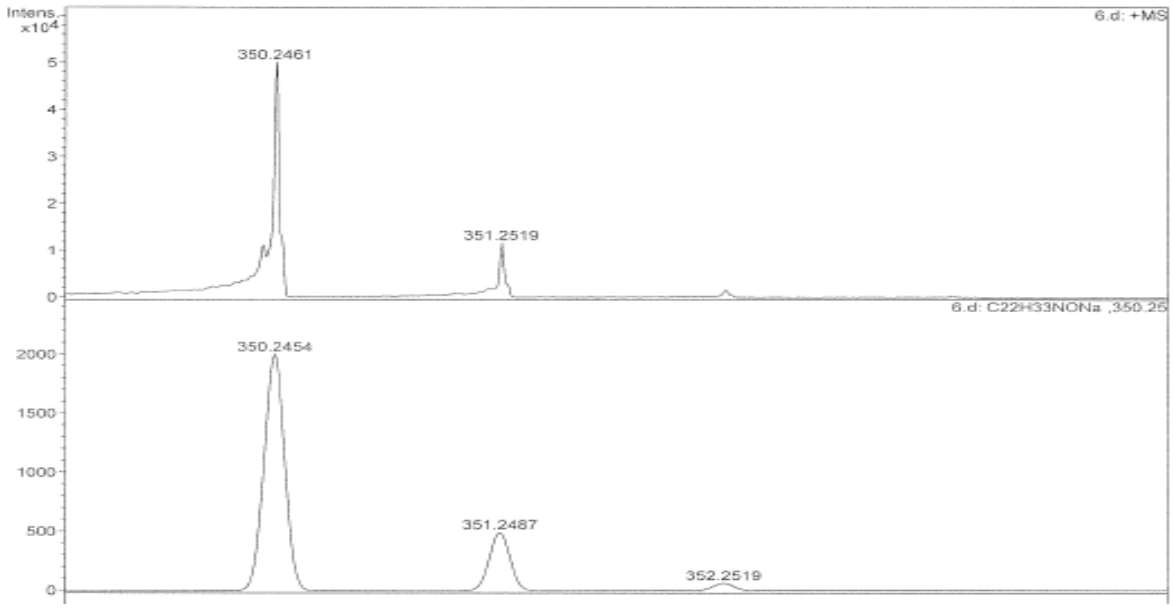

Figure 2.19: HRMS for acrylanilide **72e.**

2,5-*tert*-Butyl acrylanilide 72f: R*f* = 0.38

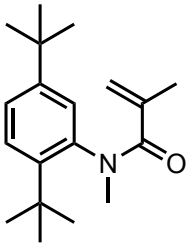

72f

Crude **72f** crystallized upon standing at room temperature after the reaction was completed.

^{1}H NMR (400 MHz, $CDCl_3$, δ ppm) 7.17 – 7.14 (d, 1H), 7.01 (s, 1H), 6.77 – 6.74 (d, 1H), 5.10 (s, 2H), 2.63 (s, 3H), 1.37 (s, 9H), 1.29 (s, 9H)

HRMS-ESI ([M + Na]$^+$): Calculated: 310.2141; Observed: 310.2126; Δm = 4.8 ppm

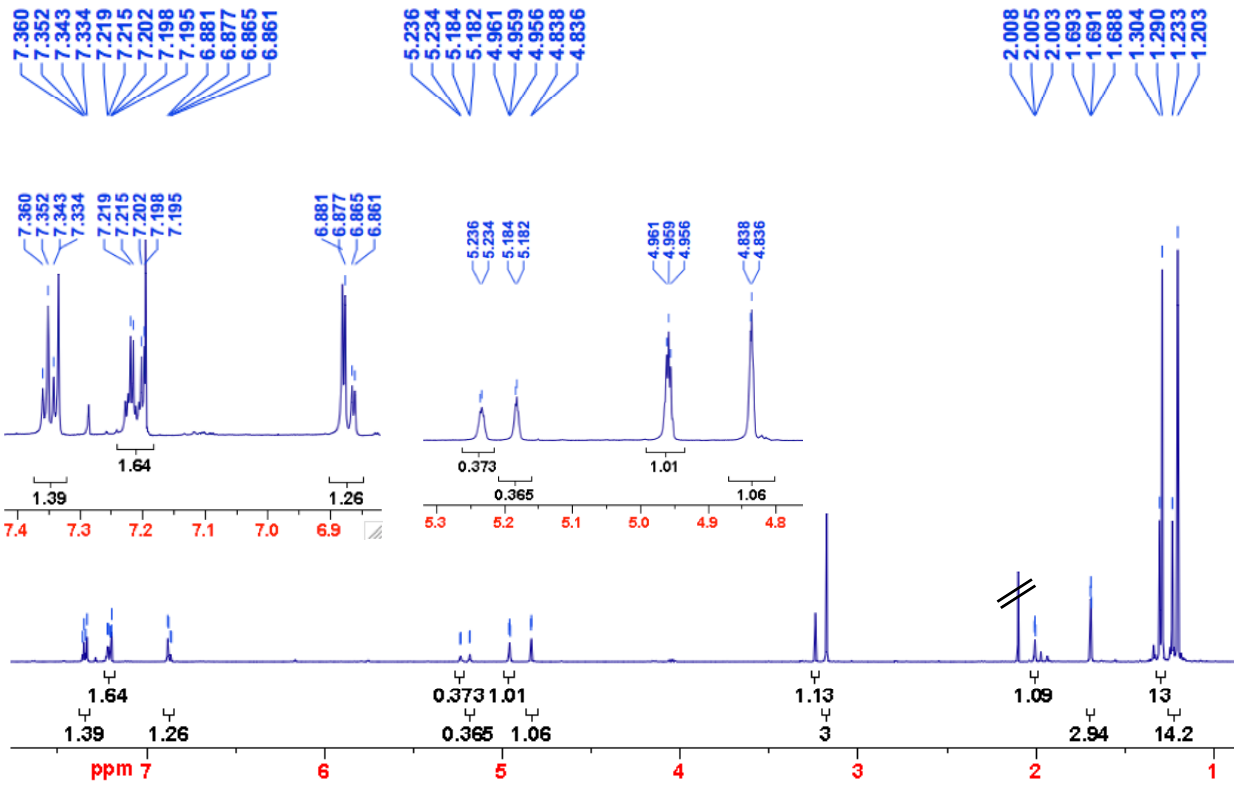

Figure 2.20: ^{1}H NMR (400 MHz, $CDCl_3$, δ ppm) spectrum for acrylanilide **72f.**

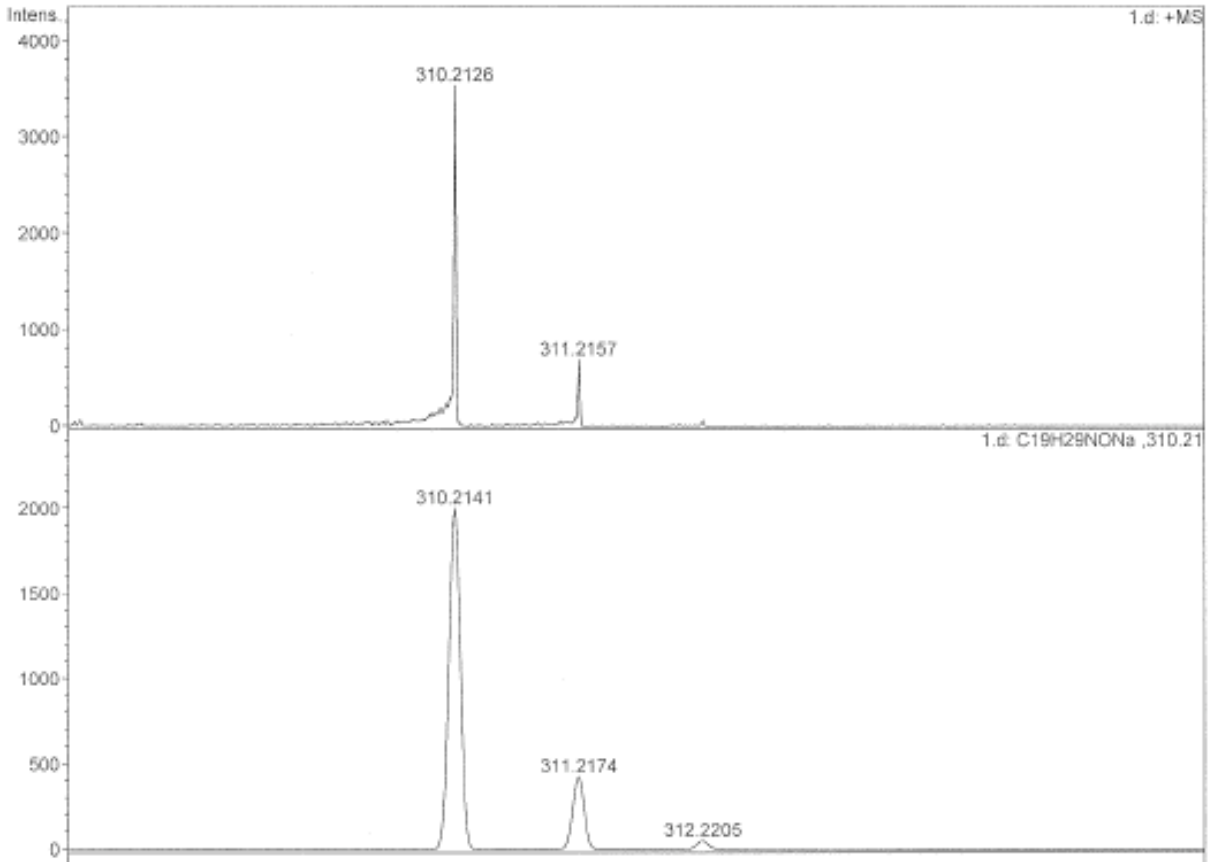

Figure 2.21: HRMS for acrylanilide **72f.**

Parent acrylanilide 69a: R*f* = 0.20

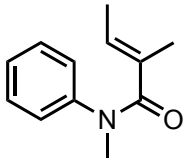

69a

69a was purified at 30 % EtOAc/Hexanes by flash chromatography on silica gel (R*f* = 0.20); pure **69a** formed white needle like crystals upon standing at ambient temperature.

^{1}H NMR (500 MHz, $CDCl_3$, δ ppm) 7.14 – 7.05 (t, 2H), 7.00 – 691 (t, 1H), 6.91 – 6.83 (d, 2H), 5.58 – 5.40 (m, 1H), 3.13 – 3.05 (virt. s, 3H). 1.40 – 1.28 (s, 3H), 1.27 – 1.17 (d, *J* = 7, 3H)

^{13}C NMR (125 MHz, $CDCl_3$, δ ppm) 173.1, 132.7, 130.3, 129.1, 126.4, 126.3, 37.72, 14.0, and 13.3

HRMS-ESI ([M + Na]$^{+}$): Calculated: 212.1046; Observed: 212.1053; Δm = 3 ppm

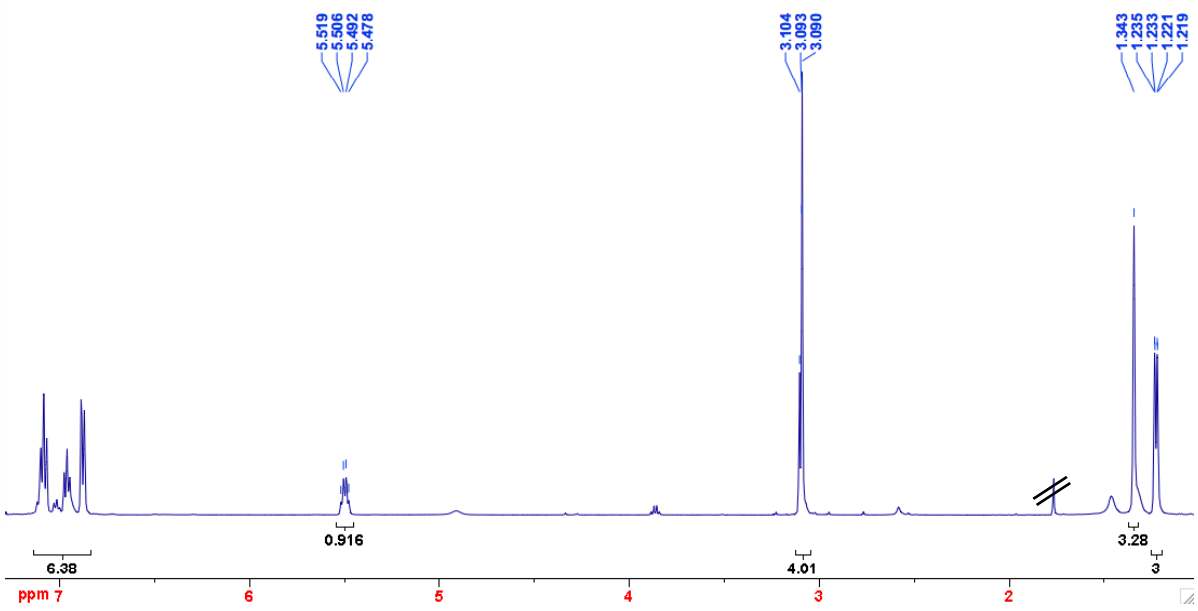

Figure 2.22: ^{1}H NMR (500 MHz, $CDCl_3$, δ ppm) spectrum for acrylanilide **69a.**

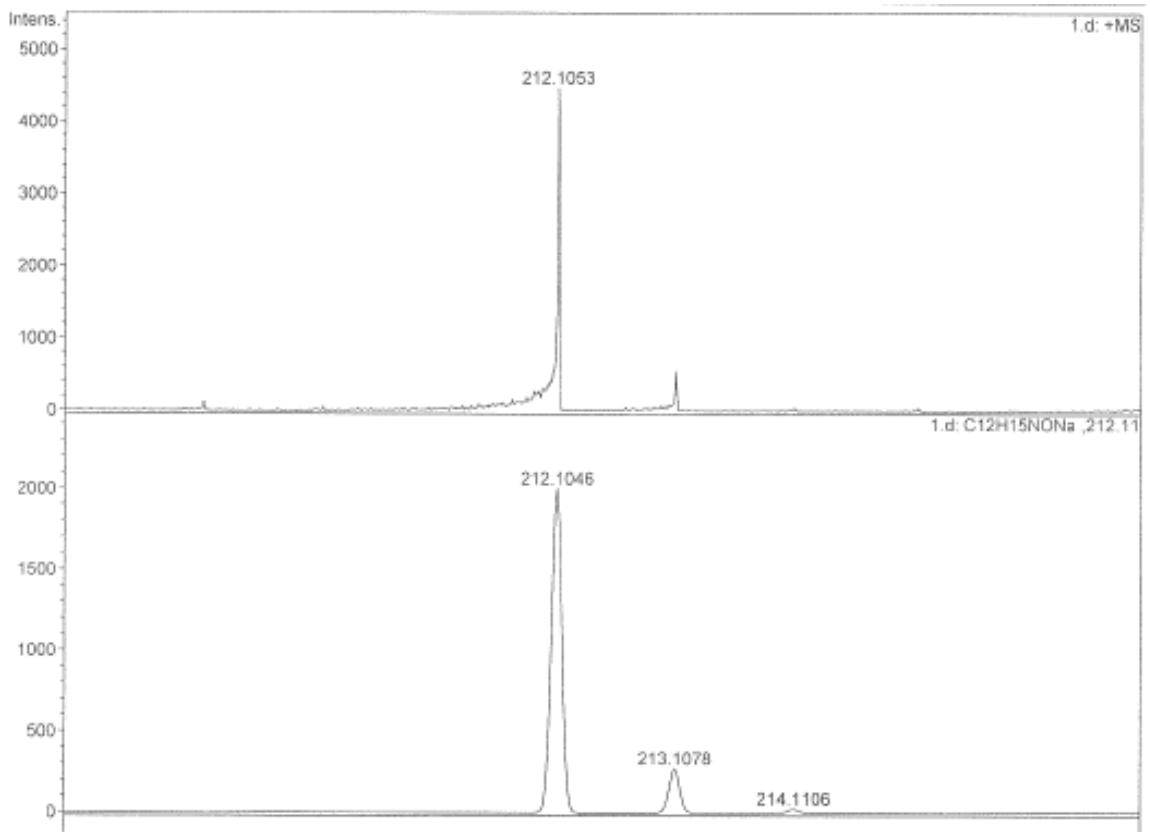

Figure 2.23: HRMS for acrylanilide **69a.**

Parent acrylanilide 69b: R*f* = 0.49

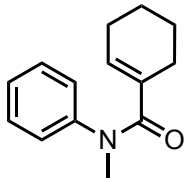

69b

69b was purified at 12 % EtOAc/Hexanes by flash chromatography on silica gel (R*f* = 0.49).

^{1}H NMR (500 MHz, $CDCl_3$, δ ppm) 7.34 – 7.28 (t, 2H), 7.23 – 7.17 (t, 1H), 7.13 – 7.08 (d, 2H), 5.83 – 5.79 (m, 1H), 3.32 (s, 3H), 1.98 – 1.82 (m, 4H), (1.47 – 1.34 (m, 4H)

HRMS-ESI ([M + Na]$^+$): Calculated: 238.1202; Observed: 238.1193; Δm = 3.8 ppm

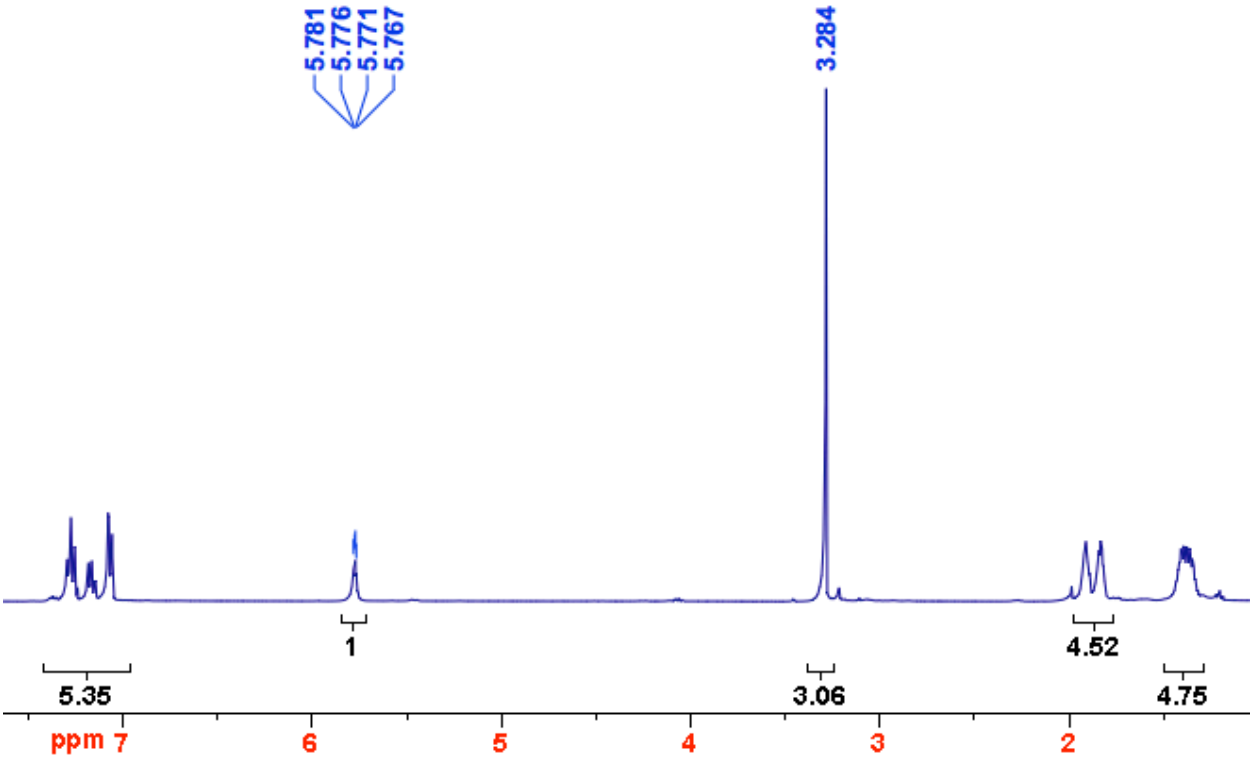

Figure 2.24: ^{1}H NMR (500 MHz, $CDCl_3$, δ ppm) spectrum for acrylanilide **69b.**

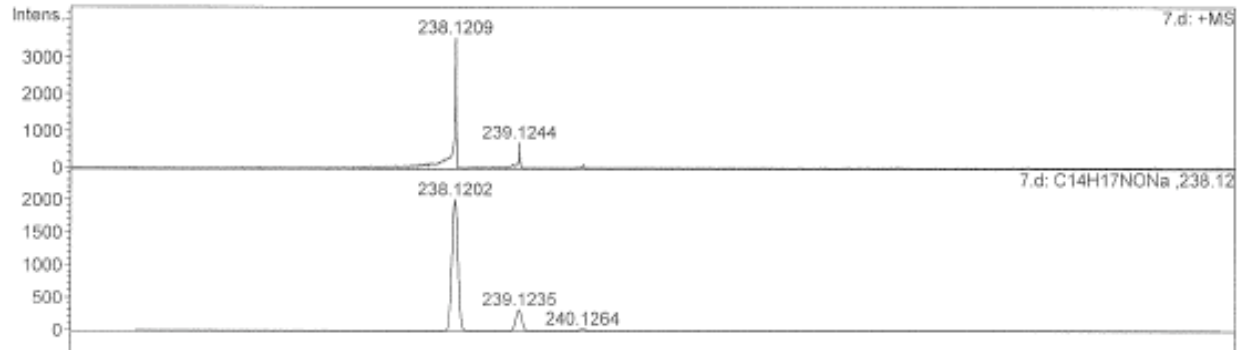

Figure 2.25: HRMS for acrylanilide **69b.**

Parent acrylanilide 69c: R*f* = 0.37

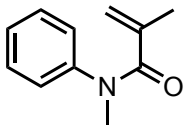

69c

The reaction leading to the formation of **69c** was totally driven to completion (conversion yield: 99 %); thus, no further purification was required. Also, **69c** upon standing at room temperature formed white needle-like crystals at room temperature (R*f* = 0.37)

^{1}H NMR (500 MHz, $CDCl_3$, δ ppm) 7.35 – 7.27 (t, 2H), 7,25 – 7.18 (t, 1H), 7.14 – 7.07 (d, 2H), 5.02 – 4.91 (d, 2H), 3.31 (s, 3H), 1.76 – 1.69 (s, 3H)

HRMS-ESI ($[M + Na]^+$): Calculated: 198.0889; Observed: 198.0889; Δm = 0 ppm

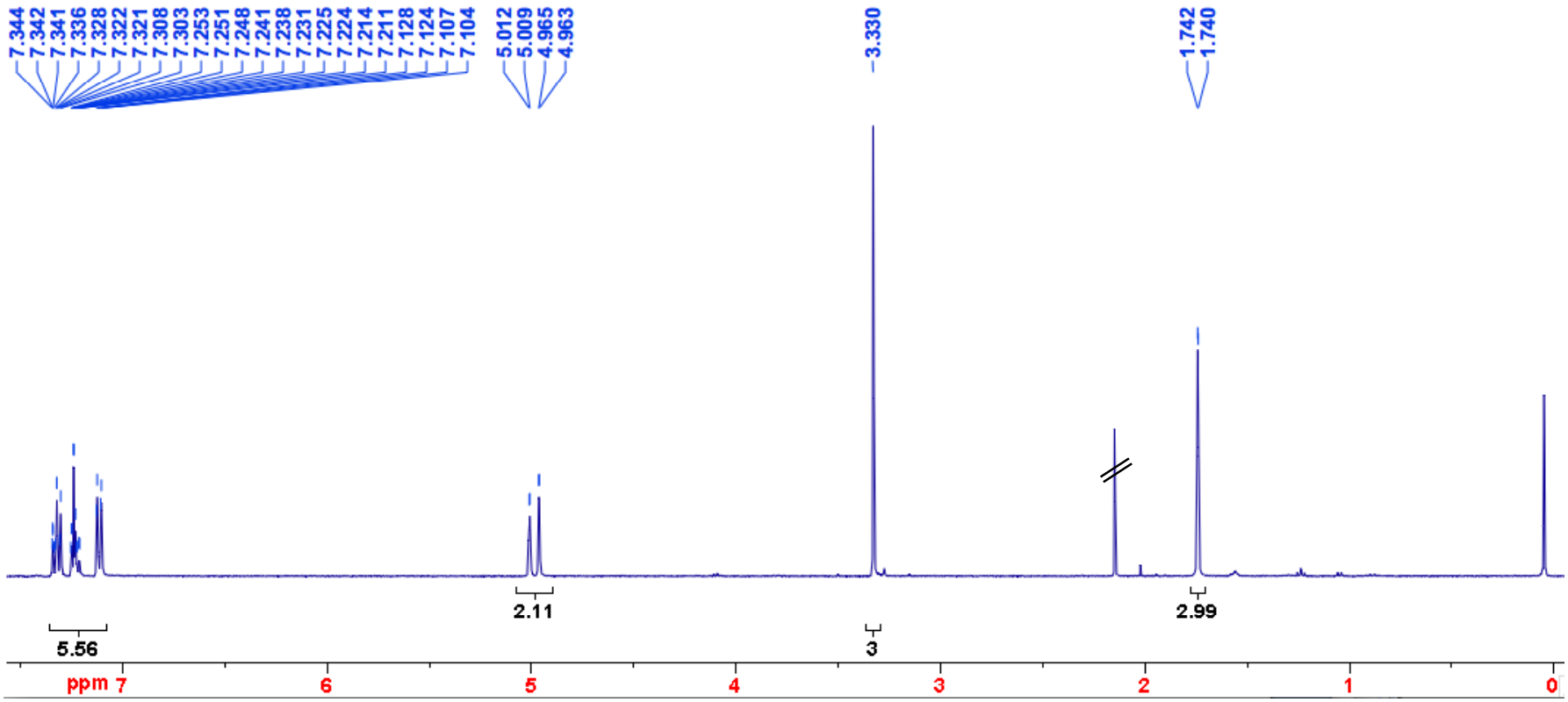

Figure 2.26: ^{1}H NMR (500 MHz, $CDCl_3$, δ ppm) spectrum for acrylanilide **69c.**

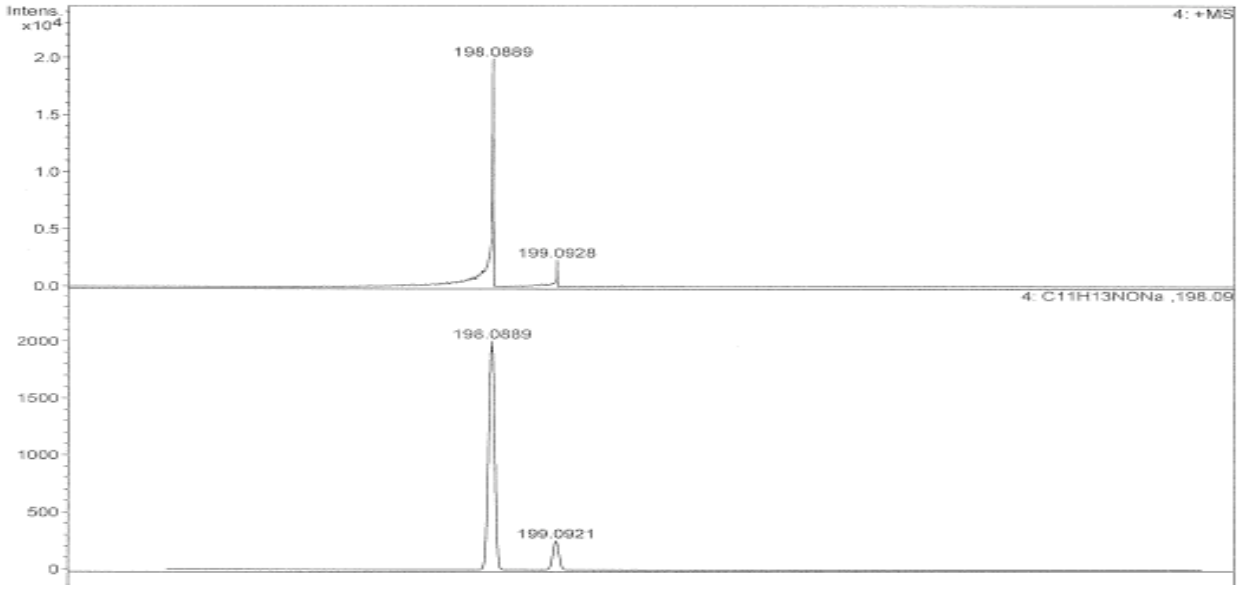

Figure 2.27: HRMS for acrylanilide **69c.**

***o-tert*-Butyl-NH acrylanilide 75a:** R*f* = 0.45

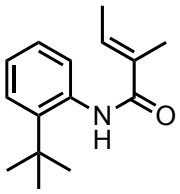

75a

^{1}H NMR (400 MHz, $CDCl_3$, δ ppm) 7.68 – 7.61 (d, *J* = 8.0, 1H), 7.44 (bs, 1H), 7.40 – 7.33 (d, *J* = 8.0, 1H), 7.26 – 7.18 (t, *J* = 7.0, 1H), 7.18 – 7.09 (t, *J* = 7.2, 1H), 6.65 – 6.54 (m, 1H), 2.01 – 1.94 (m, 3H), 1.86 – 1.78 (m, 3H), 1.40 (s, 9H)

^{13}C NMR (125 MHz, $CDCl_3$, δ ppm) 167.6, 142.5, 135.7, 132.8, 131.8, 127.9, 127.1, 126.7, 126.1, 34.8, 30.9, 14.4 and 12.9.

HRMS-ESI ([M + Na]$^{+}$): Calculated: 254.1515; Observed: 254.1512; Δm = 1.2 ppm

HPLC analysis conditions: Column: (R,R) WHELK–01; Abs. detector: 254 nm and 270 nm; Mobile phase: Hexanes: IPA = 93:07; Flow rate: 1 mL/min

Retention time (min): ~ 35.55

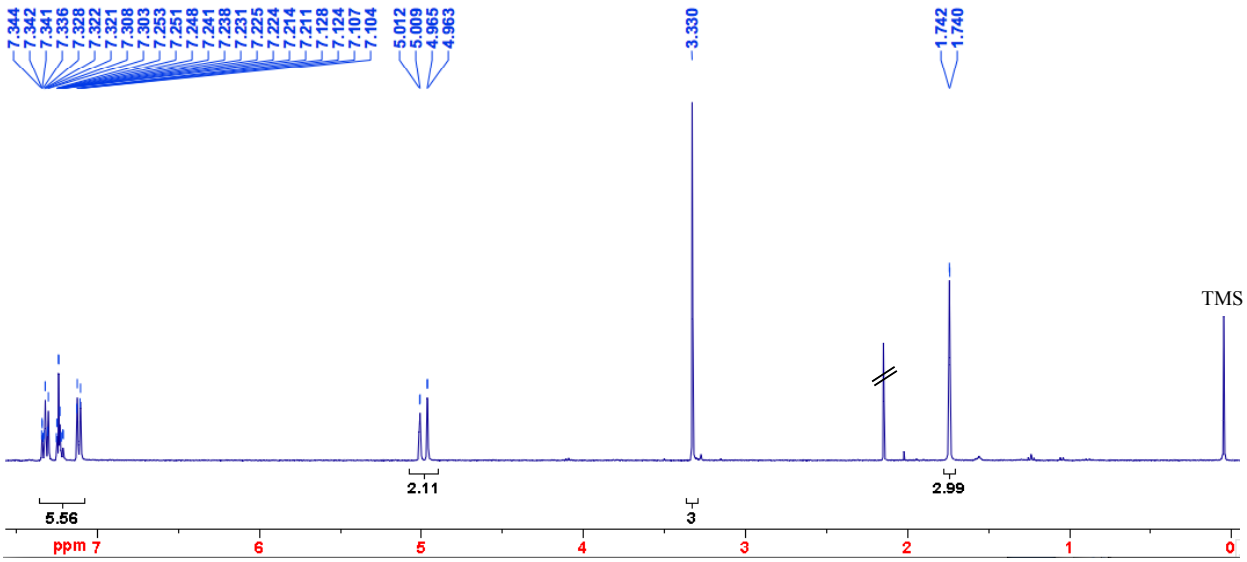

Figure 2.28: ^{1}H NMR (500 MHz, $CDCl_3$, δ ppm) spectrum for acrylanilide **75a.**

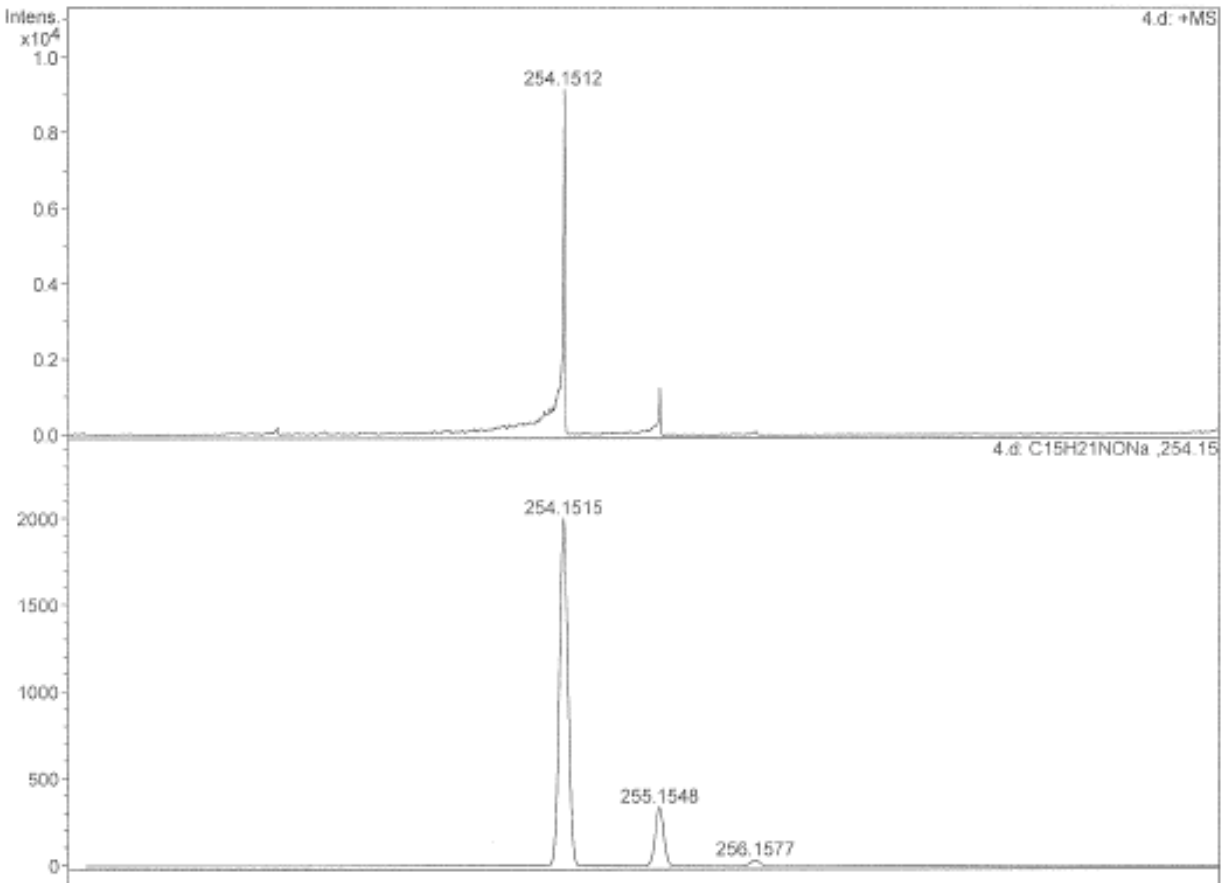

Figure 2.29: HRMS for **75a**.

***o-tert*-Butyl-NH acrylanilide 75d:** R*f* = 0.56

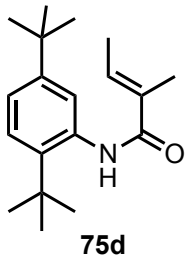

75d

^{1}H NMR (500 MHz, $CDCl_3$, δ ppm) 7.75 (Ar, 1H), 7.49 (bs, 1H), 7.57 – 7.42 (d, *J* = 8.5, 1H), 7.38 – 7.31 (d, *J* = 8.5, 1H), 6.69 – 6.59 (m, 1H), 2.01 (s, 3H), 1.90 – 1.84 (d, *J* = 7, 3H), 1.43 (s, 9H), 1.34 (s, 9H)

^{13}C NMR (125 MHz, $CDCl_3$, δ ppm) 187.8, 149.9, 139.2, 135.4, 131.7, 126.4, 124.9, 122.9, 34.6, 34.4, 31.5, 31.0, 14.4 and 12.9

HRMS-ESI ([M + Na]$^{+}$): Calculated: 310.2148; Observed: 310.2141; Δm = 2.3 ppm

HPLC analysis conditions: Column: (R,R) WHELK–01; Abs. detector: 254 nm and 270 nm**;** Mobile phase: Hexanes: IPA = 93:07; Flow rate: 1 mL/min

Retention time (min): ~13.69

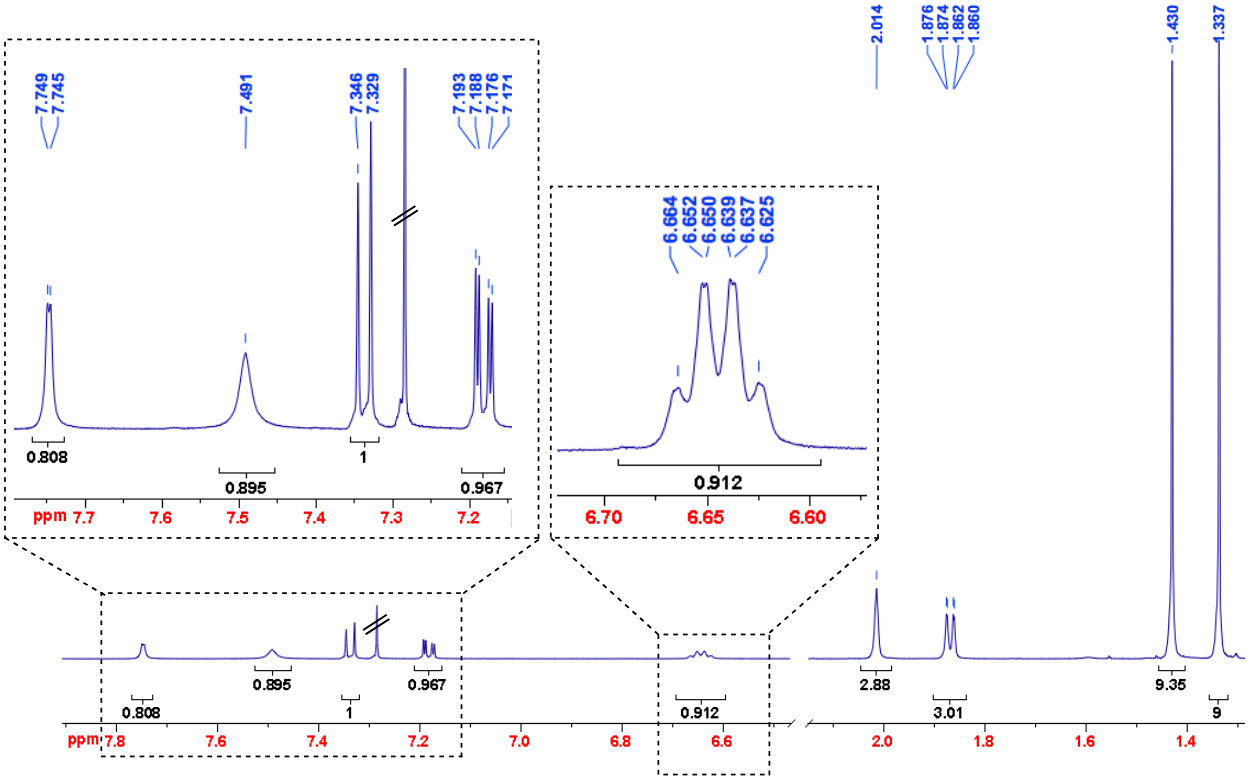

Figure 2.30: ^{1}H NMR (500 MHz, $CDCl_3$, δ ppm) spectrum for acrylanilide **75d.**

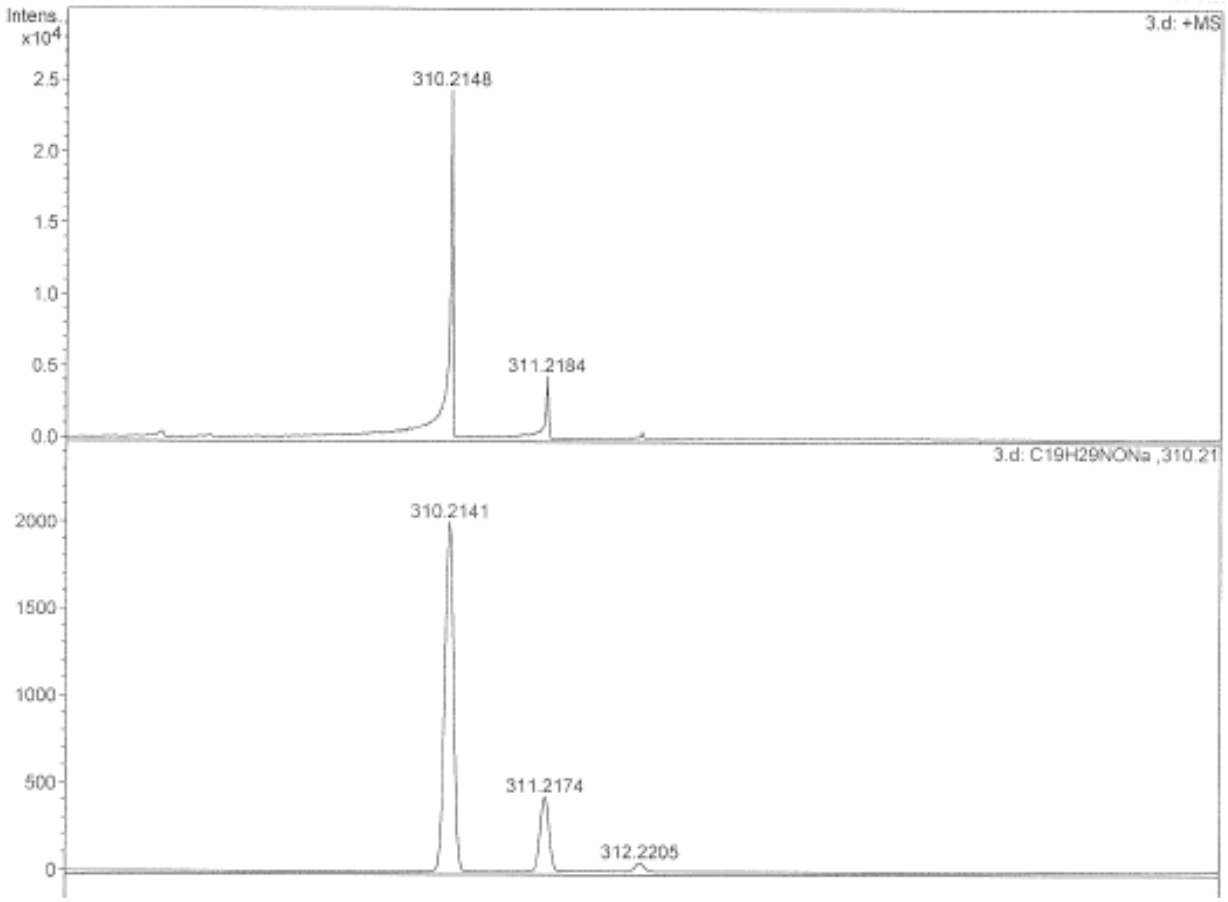

Figure 2.31: HRMS for acrylanilide **75d.**

***o-tert*-Butyl-NH acrylanilide 75e:** R*f* = 0.64

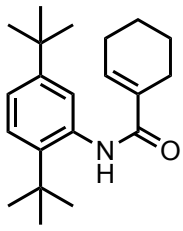

75e

^{1}H NMR (400 MHz, $CDCl_3$, δ ppm) 7.76 (Ar, 1H), 7.45 (bs, 1H), 7.36 – 7.32 (d, *J* = 6.8, 1H), 7.20 – 7.15 (d, *J* = 6.4, 1H), 6.85 (dd, 1H), 2.46 – 2.23 (m, 4H), 1.84 – 1.64 (m 4H), 1.43 (s, 9H), 1.33 (s, 9H)

HRMS-ESI ([M + Na]$^+$): Calculated: 336.2298; Observed: 336.2287, Δm = 3.3 ppm

HPLC analysis conditions: Column: (R,R) WHELK–01; Abs. detector: 254 nm and 270 nm**;** Mobile phase: Hexanes: IPA = 90:10; Flow rate: 1 mL/min

Retention time (min): ~ 13.09

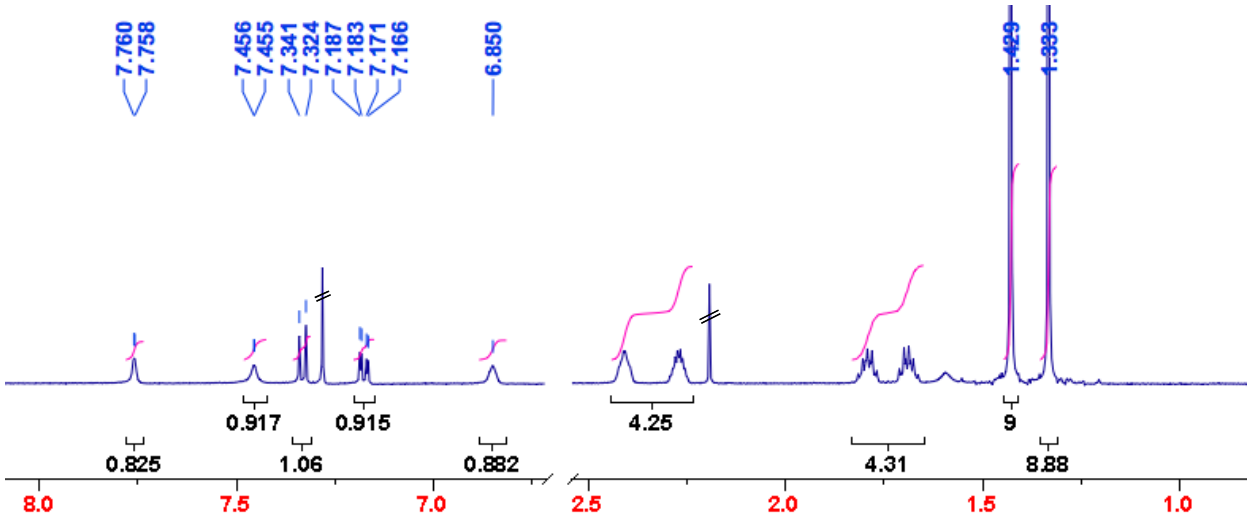

Figure 2.32: ^{1}H NMR (400 MHz, $CDCl_3$, δ ppm) spectrum for acrylanilide **75e.**

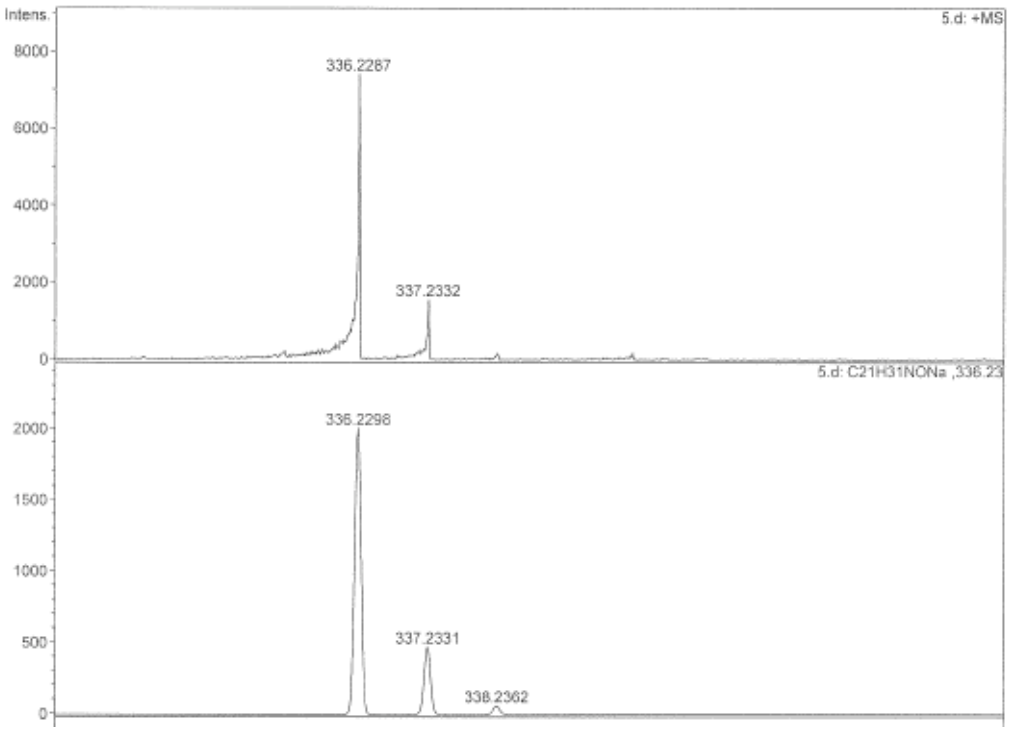

Figure 2.33: HRMS for acrylanilide **75e.**

2.4.6. General irradiationprocedure for acrylanilides 69, 72 and 75

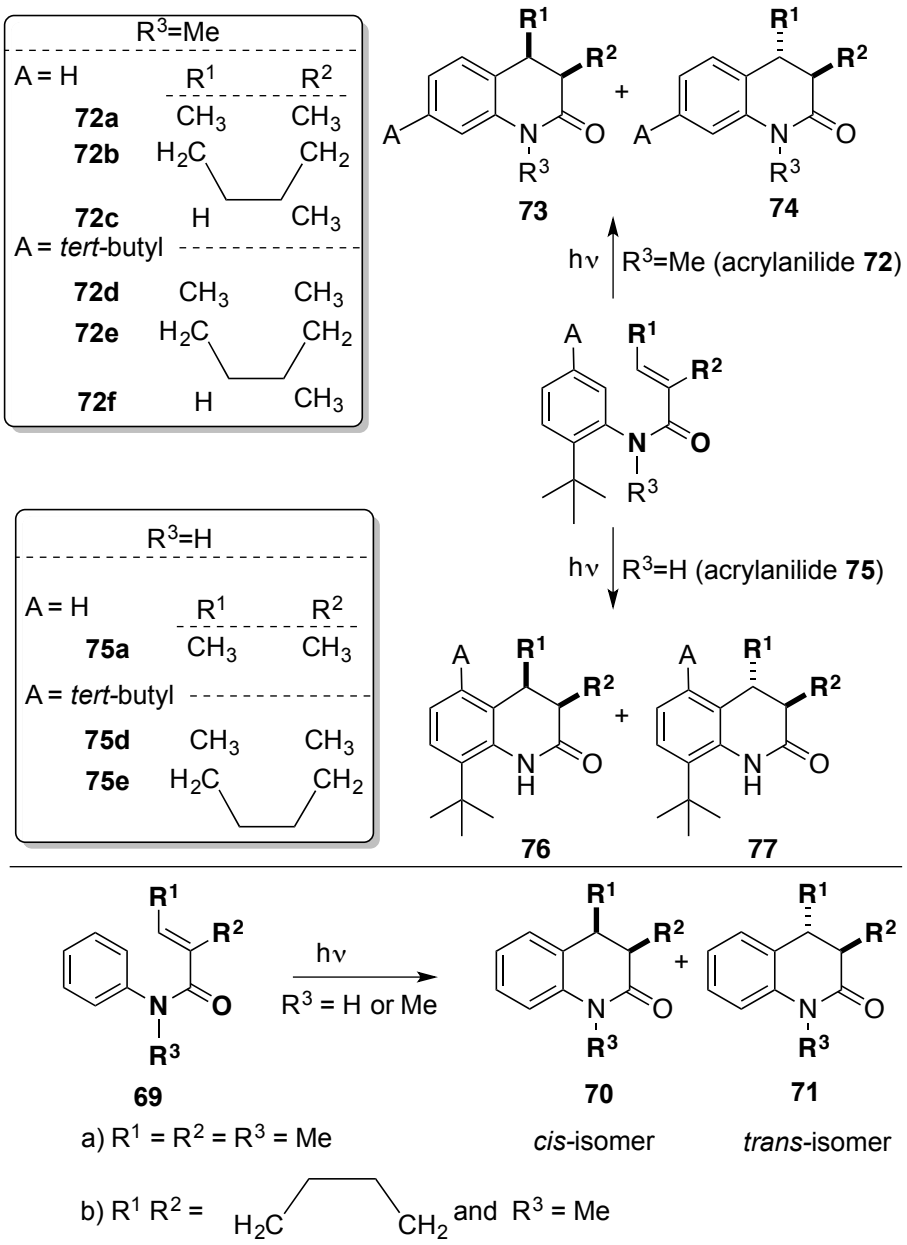

Scheme 2.8: Photoreaction of acrylanilides **69, 72** and **75.**

Solutions of acrylanilides (0.1mmol) in 15 mL of the selected solvent were irradiated for 3 - 5 h in Pyrex test tubes with a 450 W medium pressure Hg-lamp at room temperature and under constant flow of nitrogen. The reaction was monitored by TLC; after 5 h of irradiation, the solvent was removed under reduced pressure and the photoproducts were characterized by NMR spectroscopy. The *cis/trans* ratio in

the photoproducts was calculated from NMR and from chromatographic analysis (HPLC / GC) of the photolysate.

2.4.7. General characterization of photoproducts 70, 71, 73, 74, 76 and 77

***cis*-70a (= 73a)**: R*f* = 0.54

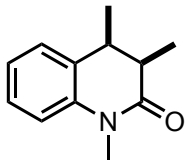

70a = **73a**

Note: The photoproducts were separated from the starting material **69a** by preparative chromatography on TLC plate (Eluting Solvent: 8 % EtOAc/Hexanes).

^{1}H NMR (500 MHz, $CDCl_3$, δ ppm) 7.29 – 7.22 (Ar, 1H), 7.19 – 7.13 (Ar, 1H), 7.07 – 7.01 (Ar, 1H), 7.00 – 6.94 (Ar, 1H), 3.36 (s, 3H), 3.02 – 2.92 (m, 1H), 2.81 – 2.71 (m, 1H), 1.21 – 1.16 (d, *J* = 7, 3H), 1.15 – 1.10 (d, *J* = 7, 3H)

HRMS-ESI ([M + Na]$^+$): Calculated: 212.1046; Observed: 212.1034; Δm = 5.7 ppm

HPLC analysis conditions: Column: (R,R) WHELK–01; Abs. detector: 254 nm and 270 nm; Mobile phase: Hexanes: IPA = 93: 07; Flow rate: 1 mL/min

Retention time (min): ~16.9 (**70a**) (*ent*-**70a** does not resolve in the condition employed)

^{1}H NMR: Aromatic hydrogen atoms (left) and α and β hydrogen atoms (right) of compound **70a** (= **73a**).

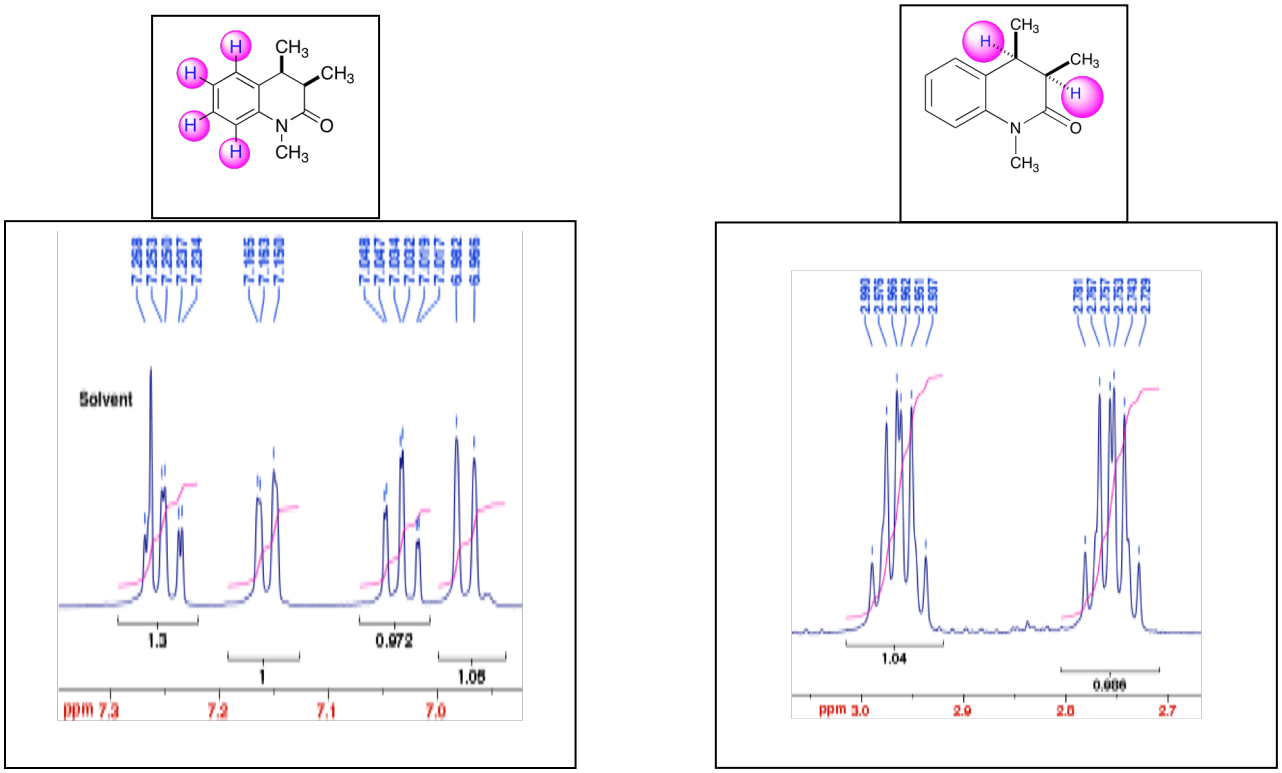

Figure 2.34: ^{1}H NMR (500 MHz, $CDCl_3$, δ ppm) expanded spectrum: for quinolinone **70a = 73a.**

***trans*-71a (= 74a):** R*f* = 0.46

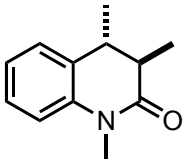

71a = 74a

Note: The *trans* photoproducts were separated from the starting material by chromatography (Eluting Solvent: 8 % EtOAc/Hexanes).

^{1}H NMR (500 MHz, $CDCl_3$, δ ppm) 7.29 – 7.23 (Ar, 1H), 7.21 – 7.16 (Ar, 1H), 7.09 – 7.02 (Ar, 1H), 7.01 – 6.97 (Ar, 1H), 3.37 (s, 3H), 2.75 – 2.67 (m, 1H), 2.59 – 2.51 (m, 1H), 1.25 – 1.21 (d, *J* = 7.5, 3H), 1.14 – 1.10 (d, *J* = 7, 3H)

HRMS-ESI ([M + Na]$^+$): Calculated: 212.1046; Observed: 212.1034; Δm = 5.7 ppm

HPLC analysis conditions: Column: (R,R) WHELK–01; Abs. detector: 254 nm and 270 nm**;** Mobile phase: Hexanes:IPA = 93:07; Flow rate: 1 mL/min

Retention time (min): ~17.5 (**71a**) and ~20.3 (*ent*-**71a**)

^{1}H NMR (Aromatic hydrogen atoms (left) and α and β hydrogen atoms (right) of compound **71a** (= **74a**).

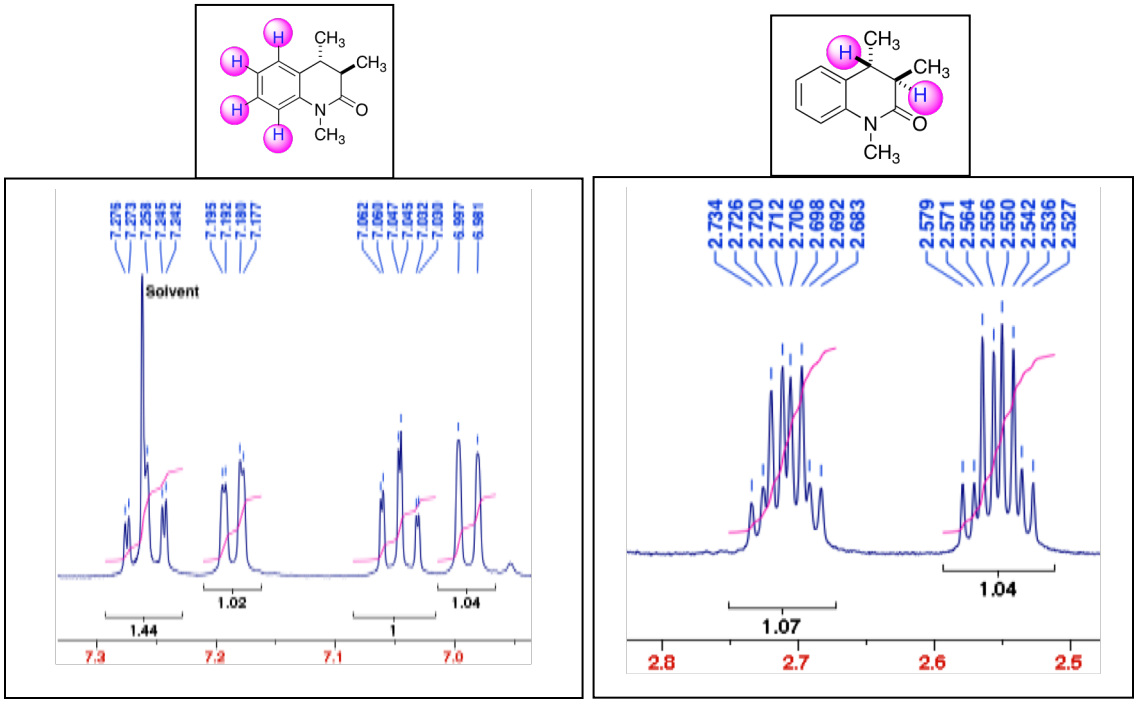

Figure 2.35: ^{1}H NMR (500 MHz, $CDCl_3$, δ ppm) expanded spectrum: for quinolinone **71a = 74a.**

***cis*-70b (= 73b):** R*f* = 0.67

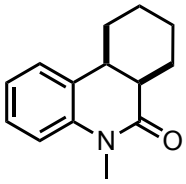

70b = 73b

^{1}H NMR (500 MHz, $CDCl_3$, δ ppm) 7.31 – 7.24 (Ar, 1H), 7.21 – 7.16 (Ar, 1H), 7.09 – 7.03 (Ar, 1 H), 7.01 – 6.97 (Ar, 1H), 3.4 (s, 3H), 2.96 – 2.87 (m, 1H), 2.86 – 2.77 (m, 1H), 1.83 – 1.14 (m, 8H)

^{13}C NMR (100 MHz, $CDCl_3$ δ ppm) 172.7, 130.8, 127.4, 124.1, 123.0, 114.7, 43.7, 37.2, 30.1, 29.0, 27.1, 25.4 and 25.3

HRMS-ESI ([M + Na]$^{+}$): Calculated: 238.1202; Observed: 238.1195; Δm = 3 ppm

HPLC analysis conditions: Column: (R,R) WHELK–01; Abs. detector: 254 nm and 270 nm**;** Mobile phase: Hexanes:IPA = 90:10; Flow rate: 1 mL/min

Retention time (min): ~14.87 (**70b**) and ~15.89 (*ent*-**70b**)

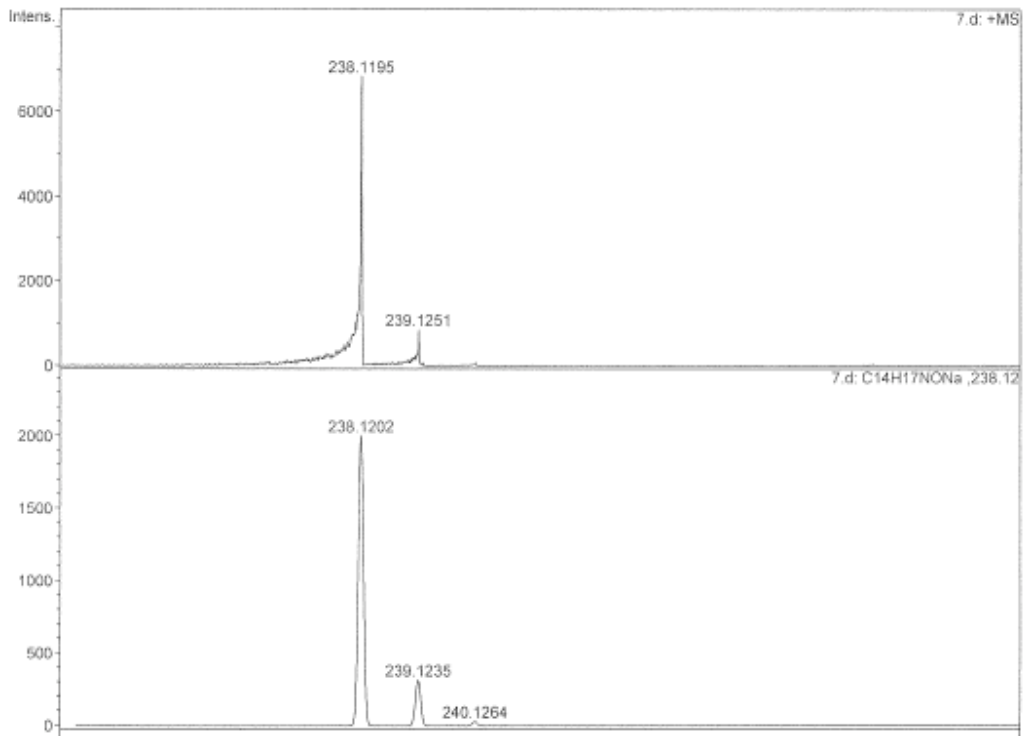

Figure 2.36: HRMS for quinolinone **70b** = **73b**.

***trans*-71b (= 74b):** R*f* = 0.63

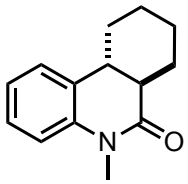

71b = **74b**

^{1}H NMR (500 MHz, $CDCl_3$, δ ppm) 7.32 – 723 (Ar, 2H), 7.12 – 7.06 (Ar, 1H), 7.03 – 7.6.97 (Ar, 1H), 3.39 (s, 3H), 2.63 – 2.53 (m, 1H), 2.52 – 2.45 (m, 1H), 2.11 – 1.84 (m, 4H), 1.48 – 1.31 (m, 4H)

^{13}C NMR (100 MHz, $CDCl_3$ δ ppm) 25.36, 25.42, 27.10, 29.00, 30.06, 37.23, 43.68, 114.65, 123.00, 124.13, 127.43, 130.77, 172.67

HRMS-ESI ([M + Na]$^{+}$): Calculated: 238.1202; Observed: 238.1195; Δm = 3 ppm

HPLC analysis conditions: Column: (R,R) WHELK–01; Abs. detector: 254 nm and 270 nm**;** Mobile phase: Hexanes:IPA = 90:10; Flow rate: 1 mL/min

Retention time (min): ~24.15 (**71b**) and ~29.52 (*ent*-**71b**)

70c (= 71c = 73c = 74c): R*f* = 0.44 (Eluting Solvent: 10 % EtOAc/Hexanes).

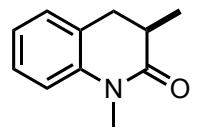

70c = 71c = 73c = 74c

cis and *trans* isomers not feasible in photoproducts from methacryloyl derivatives **69c** or **72c**. Hence **70c = 71c = 73c = 74c.**

^{1}H NMR (500 MHz, $CDCl_3$, δ ppm) 7.28 – 7.23 (Ar, 1H), 7.18 – 7.14 (Ar, 1H), 7.04 – 6.99 (Ar, 1H), 6.99 – 6.95 (Ar, 1H), 3.36 (s, 3H), 2.97 – 2.89 (m, 1H), 2.74 – 2.55 (m, 2H), 1.29 – 1.23 (d, *J* = 7, 3H)

^{13}C NMR (100 MHz, $CDCl_3$ δ ppm) 173.4, 140.6, 128.1, 127.6, 125.9, 122.9, 114.7, 35.7, 33.5, 30.0 and 15.9

HRMS-ESI ([M + Na]$^{+}$): Calculated: 198.0889; Observed: 198.0894; Δm = 2.5 ppm

HPLC analysis conditions: Column: (R,R) WHELK–01; Abs. detector: 254 nm and 270 nm**;** Mobile phase: Hexanes:IPA = 98:02; Flow rate: 1 mL/min

Retention time (min): ~34.50 (**70c**) and ~39.30 (*ent*-**70c**)

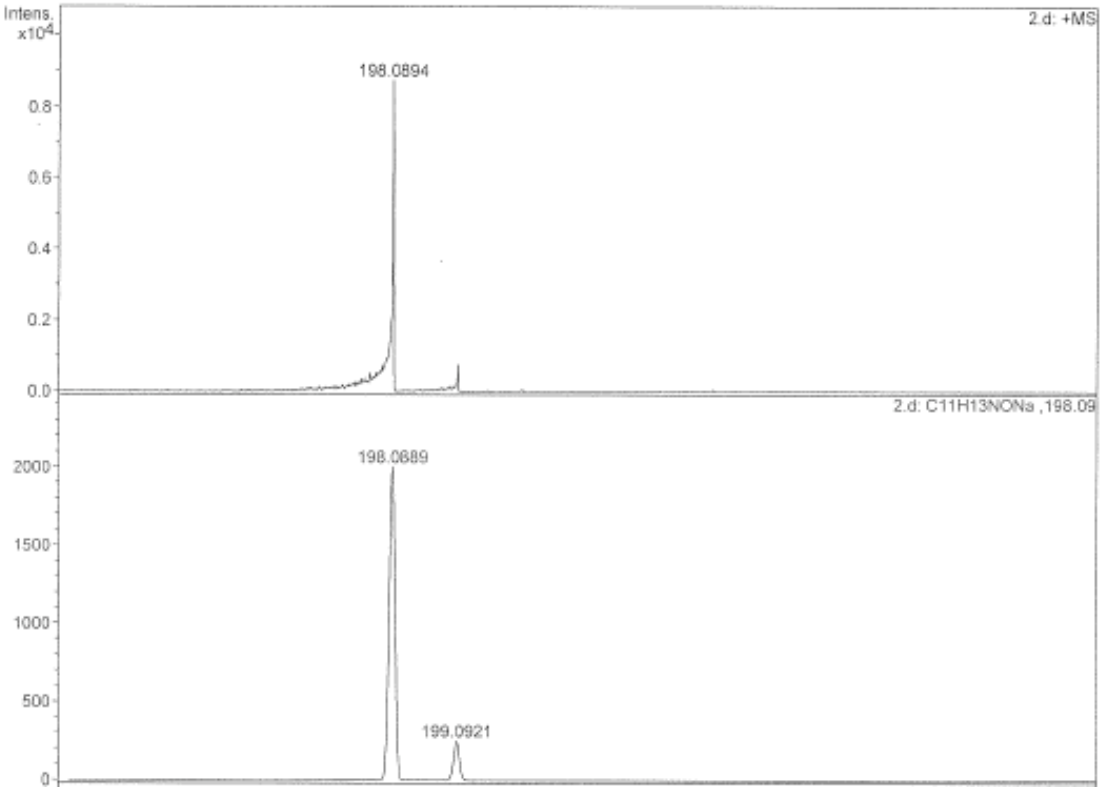

Figure 2.37: HRMS for quinolinone 70c (= 71c = 73c = 74c).

***cis*-73d:** R*f* = 0.83

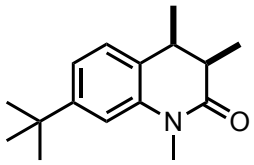

73d

^{1}H NMR (500 MHz, $CDCl_3$, δ ppm) 7.10 – 6.96 (Ar, 3H), 3.38 (s, 3H), 2.97 – 2.88 (m, 1H), 2.78 – 2.69 (m, 1H), 1.33 (s, 9H), 1.19 – 1.15 (d, *J* = 7, 3H), 1.12 – 1.08 (d, *J* = 7, 3H)

HRMS-ESI ([M + Na]$^+$): Calculated: 268.1672; Observed: 268.1683; Δm = 4.1 ppm

HPLC analysis conditions: Column: (R,R) WHELK–01; Abs. detector: 254 nm and 270 nm**;** Mobile phase: Hexanes:IPA = 93:7; Flow rate: 1mL/min

Retention time (min): ~13.25 (**73d**) (*ent*-**73d** does not resolve in the condition employed)

^{1}H NMR (Aromatic hydrogen atoms (top) and α and β hydrogen atoms (bottom) of compound **73d**.

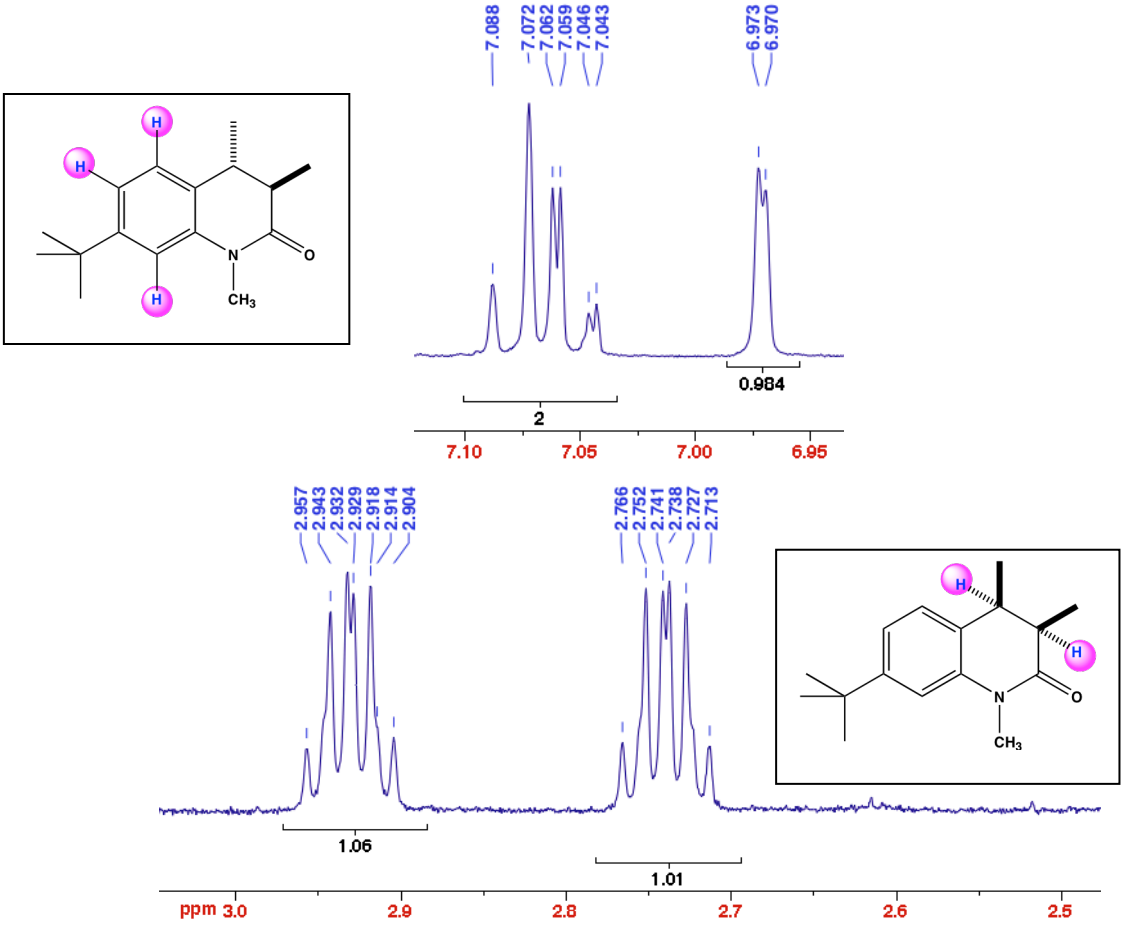

Figure 2.38: ^{1}H NMR (500 MHz, $CDCl_3$, δ ppm) expanded spectrum for quinolinone **73d.**

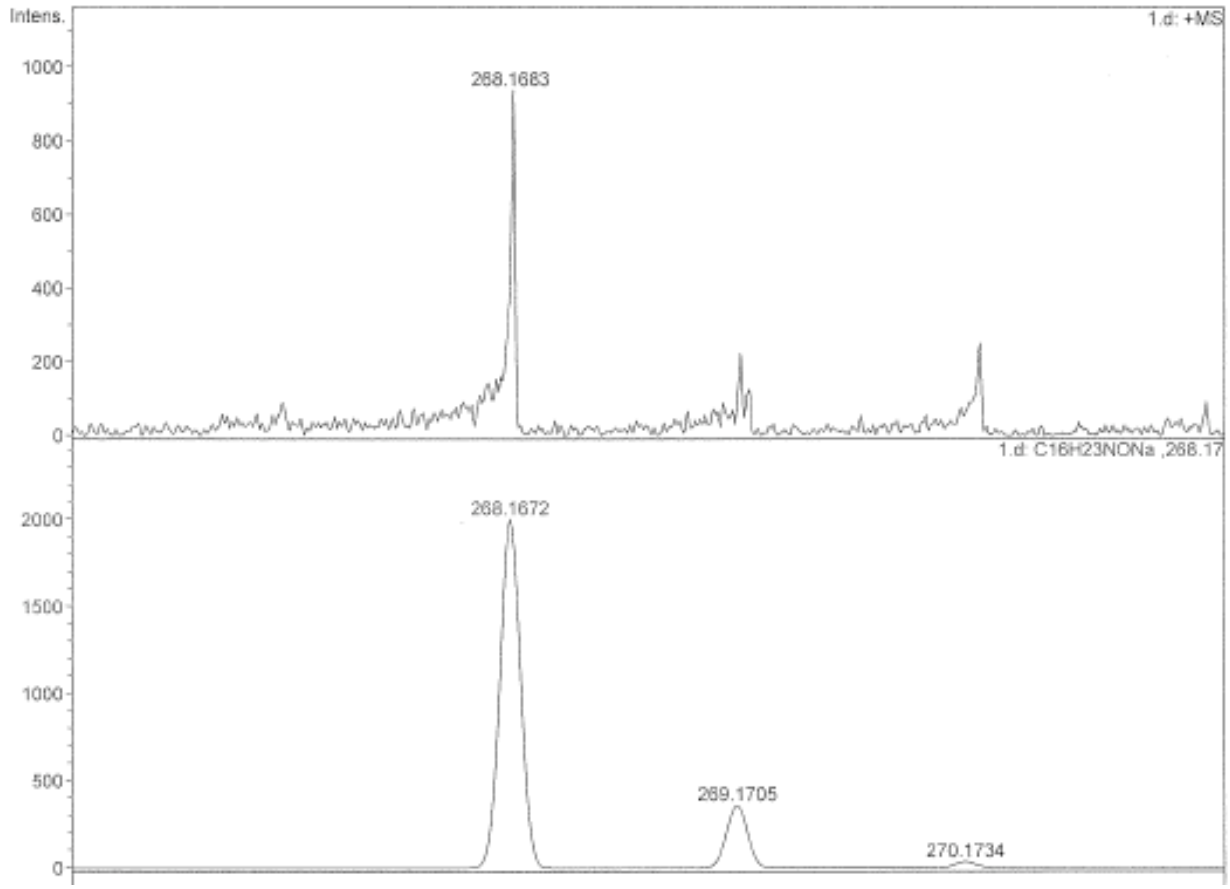

Figure 2.39: HRMS for quinolinone **73d.**

***trans*-74d:** R*f* = 0.77

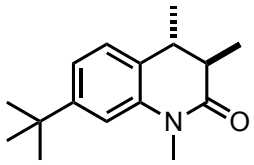

74d

^{1}H NMR (500 MHz, $CDCl_3$, δ ppm) 7.13 – 6.96 (Ar, 3H), 3.39 (s, 3H), 2.70 – 2.63 (m, 1H), 2.55 – 2.47 (m, 1H), 1.34 (s, 9H), 1.24 – 1.21 (d, *J* = 7, 3H), 1.15 – 1.11 (d, *J* = 7.5, 3H)

HRMS-ESI ([M + H]$^+$): Calculated: 268.1672; Observed: 268.1683; Δm = 4.1 ppm

HPLC analysis conditions: Column: (R,R) WHELK–01; Abs. detector: 254 nm and 270 nm**;** Mobile phase: Hexanes:IPA = 93:07; Flow rate: 1 mL/min

Retention time (min): ~15.23 (**74d**) and ~16.40 (*ent*-**74d**)

^{1}H NMR (Aromatic hydrogen atoms (top) and α and β hydrogen atoms (bottom) of compound **74d**.

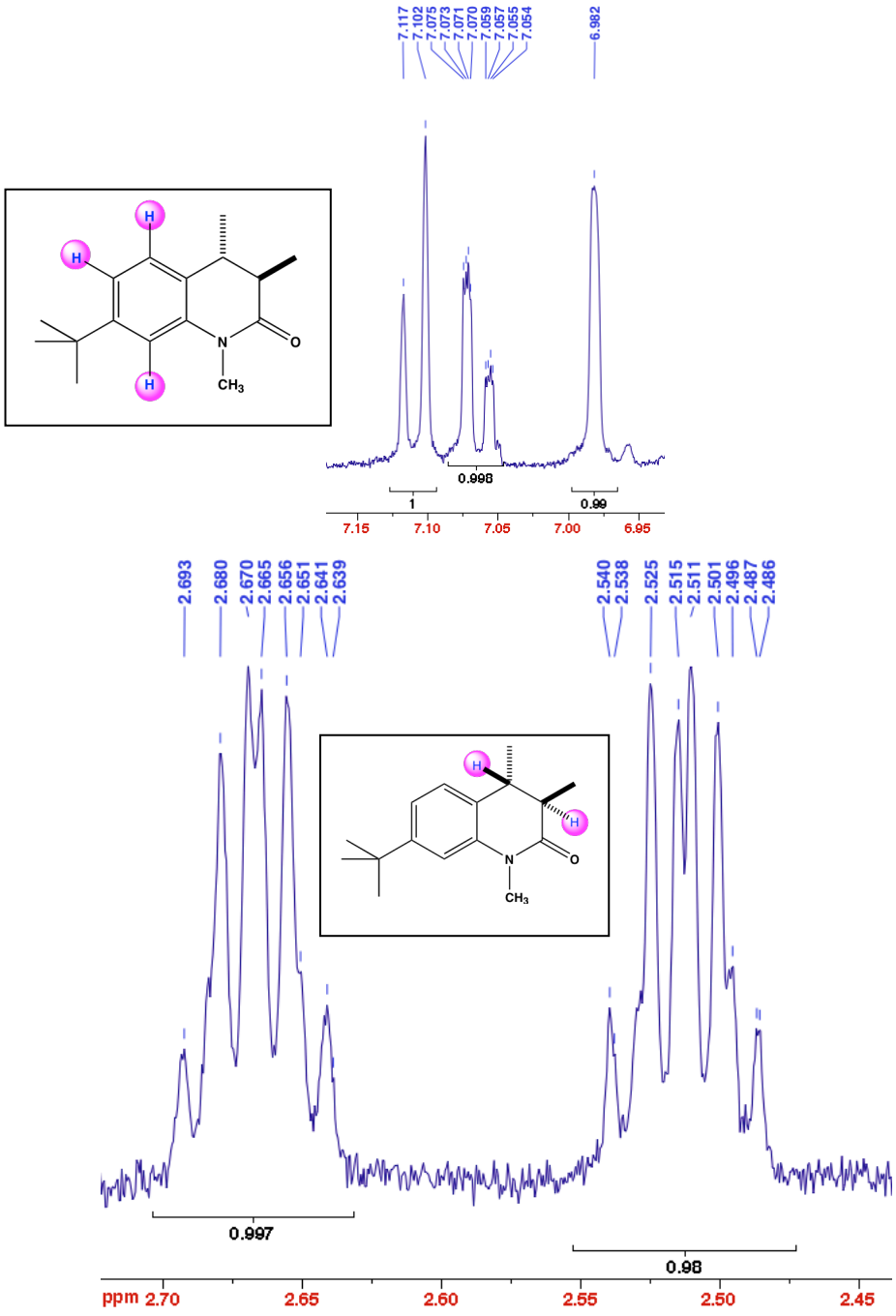

Figure 2.40: ^{1}H NMR (500 MHz, $CDCl_3$, δ ppm) expanded spectrum for quinolinone **74d.**

***cis*-73e:** R*f* = 0.66

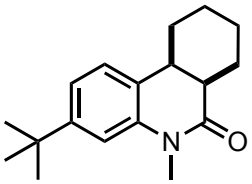

73e

^{1}H NMR (400 MHz, $CDCl_3$, δ ppm) 7.04 – 6.87 (Ar, 3H), 3.32 (s, 3H), 2.84 – 2.73 (m, 1H), 2.72 – 2.64 (q, 1H), 1.1-2.1 (m, 17H)

HRMS-ESI ([M + Na]$^+$): Calculated: 294.1828; Observed: 294.1825; Δm = 1 ppm

HPLC analysis conditions: Column: (R,R) WHELK–01; Abs. detector: 254 nm and 270 nm**;** Mobile phase: Hexanes:IPA = 90 : 10; Flow rate: 1 mL/min

Retention time (min): ~12.53 (**73e**) and ~13.39 (*ent*-**73e**)

***trans*-74e:** R*f* = 0.66

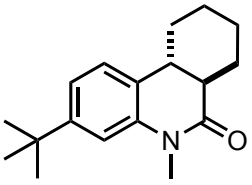

74e

As the R*f* is identical with the starting isomer the isolation to characterize by NMR was not feasible. NMR analysis was performed on the crude mixture and was analyzed by HPLC.

HRMS-ESI ([M + Na]$^+$): Calculated: 294.1828; Observed: 294.1825; Δm = 1 ppm

HPLC analysis conditions: Column: (R,R) WHELK–01; Abs. detector: 254 nm and 270 nm**;** Mobile phase: Hexanes:IPA = 90 : 10; Flow rate: 1 mL/min

Retention time (min): ~20.45 (**74e**) and ~22.74 (*ent*-**74e**)

73f (= 74f): R*f* = 0.36 (Solvent System: 10 % EtOAc/Hexanes).

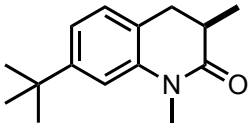

73f = 74f

cis and *trans* isomers not feasible in photoproducts from methacryloyl derivatives **72f** (and **69c**). Hence **73f = 74f.**

Purification Conditions: Compound **73f** was purified by chromatography using CombiFlash®: RediSep column: 12 g silica. Flow rate: 21 mL/min; Mobile phase: 22 % diethyl ether:*n*-pentane

^{1}H NMR (400 MHz, $CDCl_3$, δ ppm) 7.1 – 6.94 (Ar, 3H), 3.36 (s, 3H), 2.93 – 2.8 (m, 1H), 2.7 – 2.5 (m, 2H), 1.31 (s, 9H), 1.23 (d, *J* = 6.8 Hz, 3H)

^{13}C NMR (100 MHz, $CDCl_3$, δ ppm) δ 173.5, 150.8, 140.3, 127.6, 123.1, 119.7, 15.94, 111.9, 35.8, 35.0, 33.1, 31.6, 30.0

HRMS-ESI ([M + Na]$^+$): Calculated: 254.1515; Observed: 254.1523; ΔM = 3 ppm.

HPLC analysis conditions: Column: (R,R) WHELK–O1; Abs. detector: 254 nm and 270 nm**.** Mobile phase: Hexanes:IPA = 98:2; Flow rate: 1 mL/min

Retention time (min): **73f:** ~30.70 and *ent*-**73f:** ~32.07

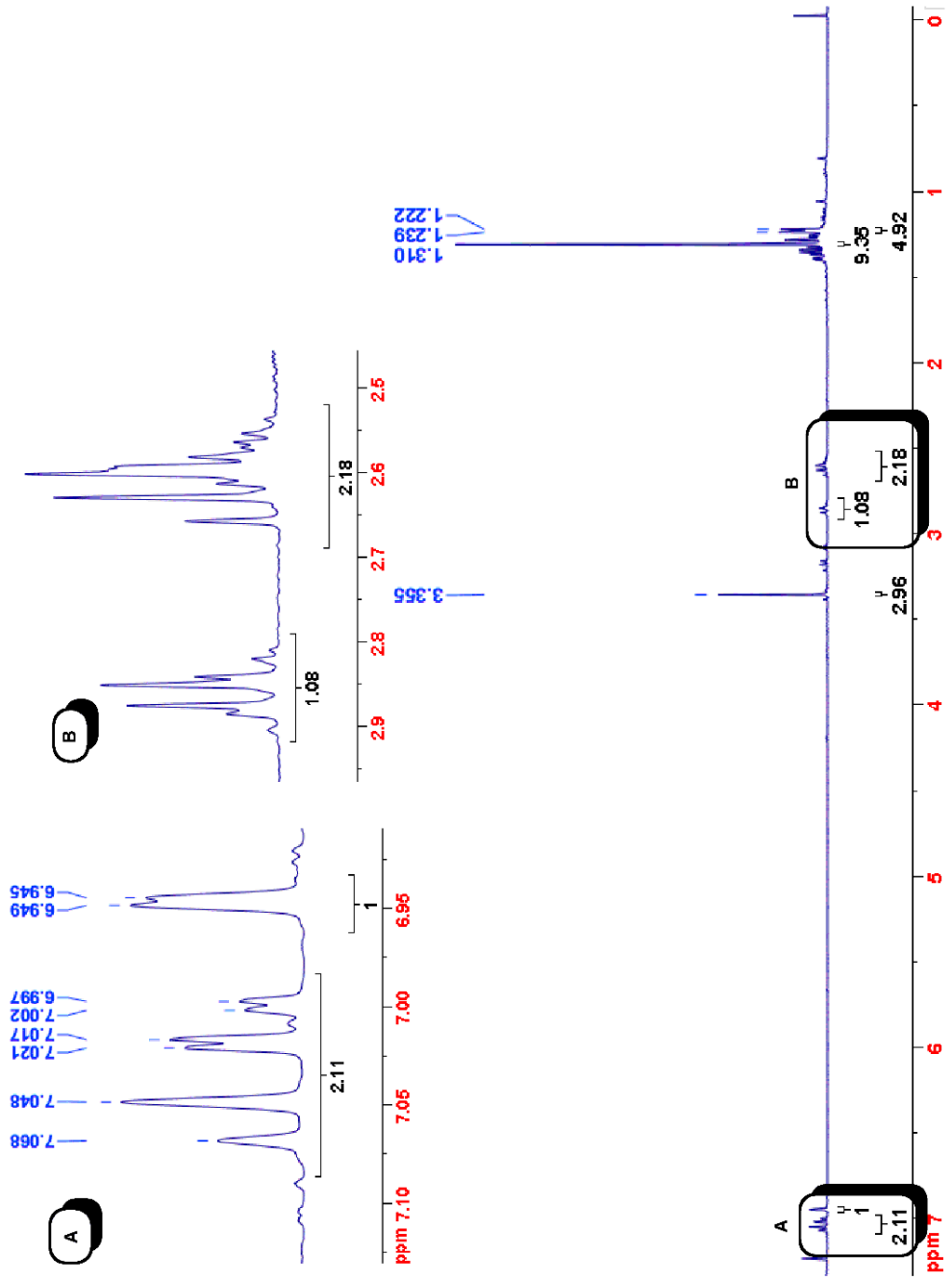

Figure 2.41: ^{1}H NMR (400 MHz, $CDCl_3$, δ ppm) spectra for quinolinone **73f** = **74f.**

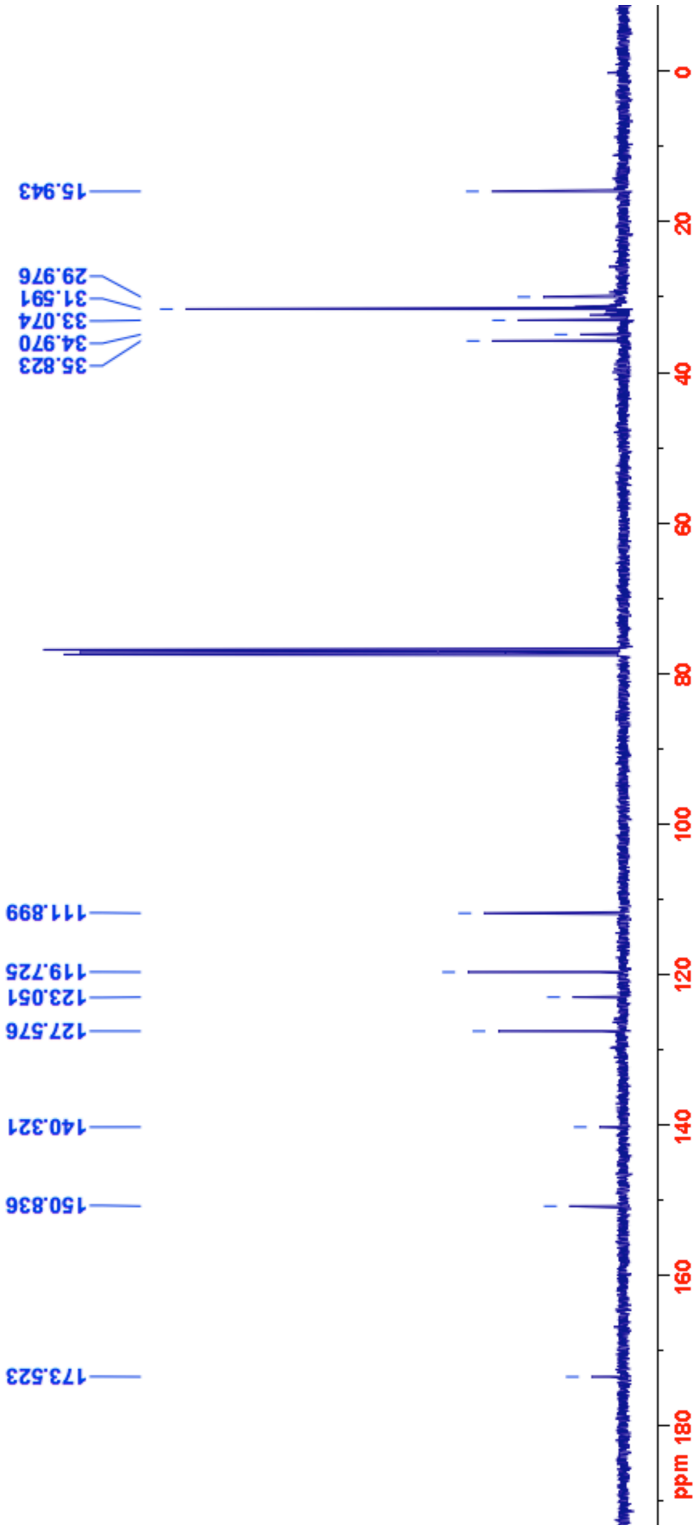

Figure 2.42: ^{13}C NMR (100 MHz, $CDCl_3$, δ ppm) spectra for quinolinone **73f = 74f.**

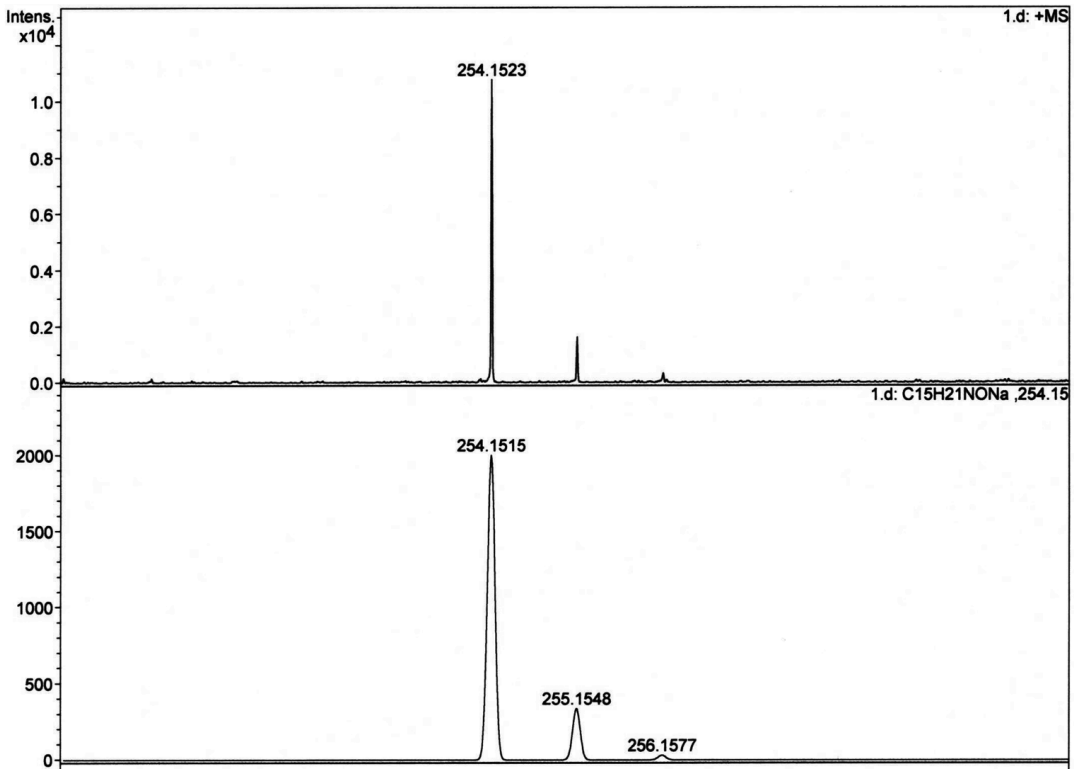

Figure 2.43: HRMS for quinolinone **73f** = **74f**.

***cis*-76a:** R*f* = 0.53

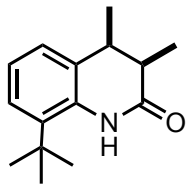

76a

^{1}H NMR (500 MHz, $CDCl_3$, δ ppm) 7.64 (bs, 1H), 7.32 – 7.20 (Ar, 1H), 7.10 – 7.04 (Ar, 1H), 7.03 – 6.94 (Ar, 1H), 3.06 – 2.94 (m, *J* = 2.5 and 7, 1H), 2.84 – 2.273 (m, *J* = 2.5 and 7, 1H), 1.45 (s, 9H), 1.27 – 1.19 (d, *J* = 7, 3H), 1.19 – 1.11 (d, *J* = 7, 3H)

^{13}C NMR (125 MHz, $CDCl_3$ δ ppm): 173.3, 135.1, 134.5, 131.9, 125.06, 125.2, 123.1, 39.1, 37.5, 34.3, 30.8, 14.9 and 11.4

HRMS-ESI ([M + Na]$^{+}$): Calculated: 254.1515; Observed: 254.1511; Δm = 1.6 ppm

HPLC analysis conditions: Column: (R,R) WHELK–01; Abs. detector: 254 nm and 270 nm**;** Mobile phase: Hexanes:IPA = 93:07; Flow rate: 1 mL/min

Retention time (min): ~8.14 (**76a**) and ~10.44 (*ent*-**76a**)

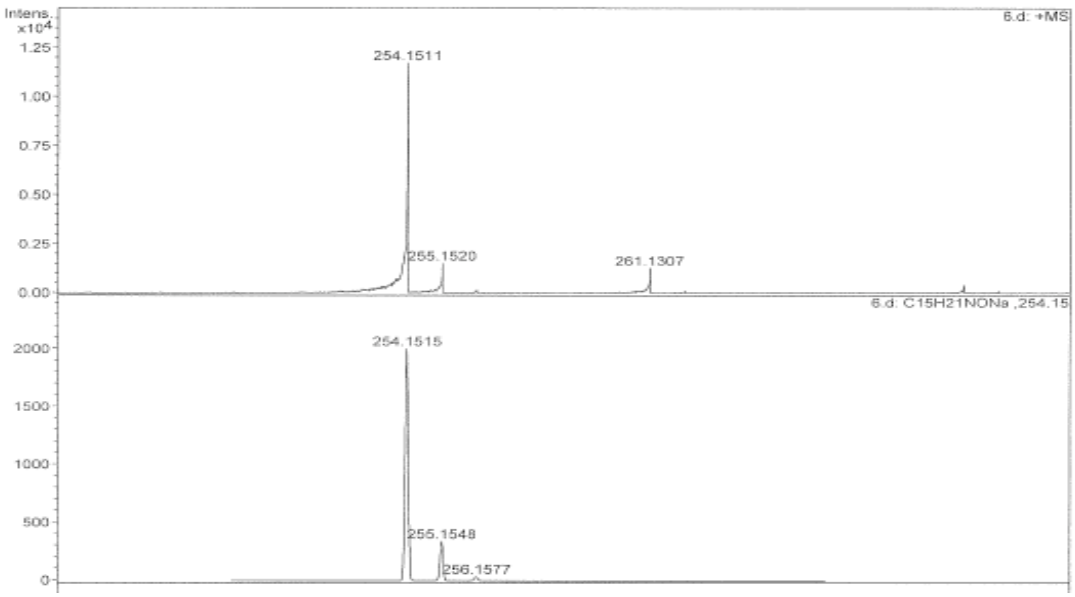

Figure 2.44: HRMS for quinolinone **76a.**

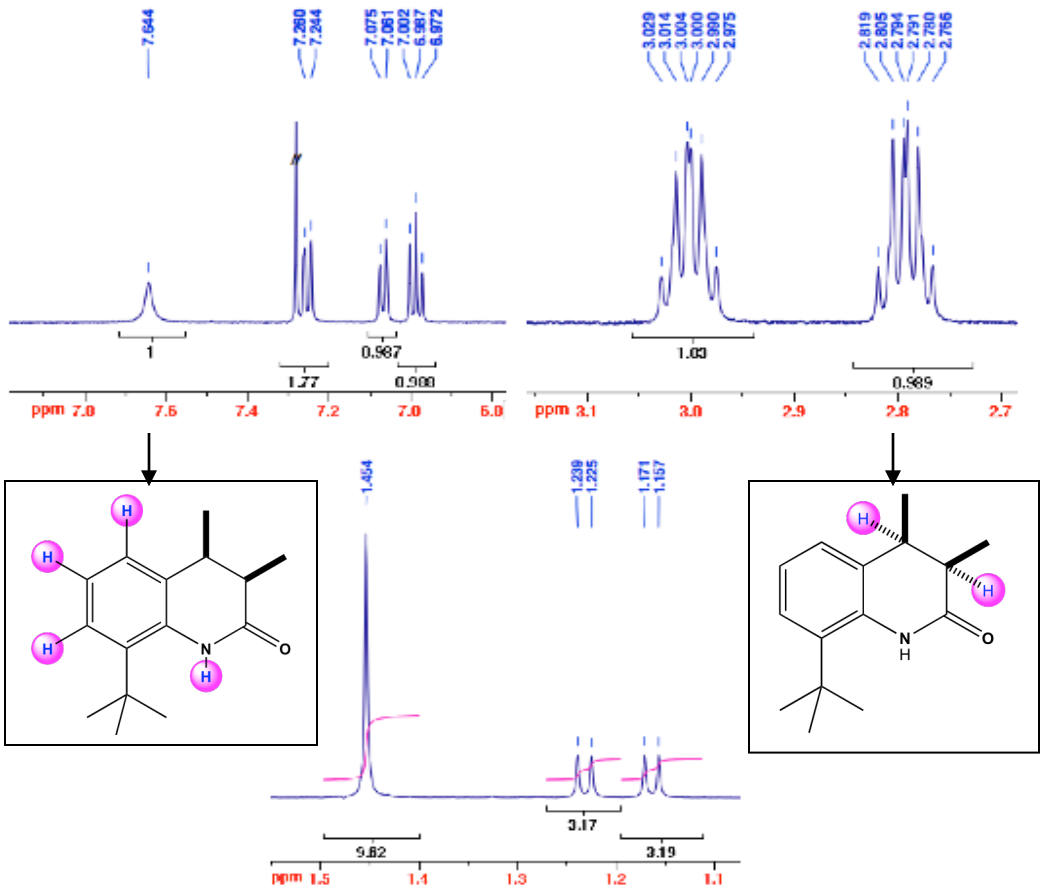

Figure 2.45: ^{1}H NMR (500 MHz, $CDCl_3$, δ ppm) expanded spectrum for quinolinone **76a.**

***trans*-77a:** R*f* = 0.46

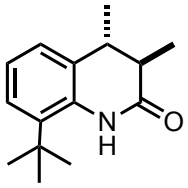

77a

^{1}H NMR (500 MHz, $CDCl_3$, δ ppm) 7.66 (bs, 1H), 7.30 – 7.21 (Ar, 1H), 7.13 – 7.06 (Ar, 1H), 7.03 – 6.95 (Ar, 1H), 2.83 – 273 (m, 1H), 2.54 – 2.43 (m, 1H), 1.45 (s, 9H), 1.30 – 1.26 (d, *J* = 7, 3H), 1.19 -1.14 (d, *J* = 7.5, 3H)

^{13}C NMR (125 MHz, $CDCl_3$ δ ppm) 173.3, 135.1, 134.5, 131.9, 125.1, 125.2, 123.1, 39.1, 37.5, 34.3, 30.8, 14.9 and 11.4

HRMS-ESI ([M + Na]$^{+}$): Calculated: 254.1515; Observed: 254.1511; Δm = 1.6 ppm

HPLC analysis conditions: Column: (R,R) WHELK–01; Abs. detector: 254 nm and 270 nm**;** Mobile phase: Hexanes:IPA = 93:07; Flow rate: 1 mL/min

Retention time (min): ~9.82 (**77a** and *ent*-**77a**)

***cis*-76d:** R*f* = 0.39

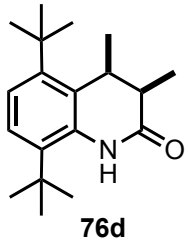

76d

^{1}H NMR (500 MHz, $CDCl_3$, δ ppm) 7.68 (bs, 1H), 7.22 – 7.08 (ABq, 2H), 3.64 – 3.48 (m, 1H), 2.65 – 2.52 (m, 1H), 1.46 (s, 18H), 1.31 – 1.26 (d, *J* = 7, 3H), 1.13 – 1.09 (d, *J* = 7.5, 3H)

HRMS-ESI ([M + Na]$^{+}$): Calculated: 310.2141; Observed: 310.2143; Δm = 0.6 ppm

HPLC analysis conditions: Column: (R,R) WHELK–01; Abs. detector: 254 nm and 270 nm**;** Mobile phase: Hexanes:IPA = 93:07; Flow rate: 1 mL/min

Retention time (min): 9.52 (**76d**) and 10.48 (*ent*-**76d**)

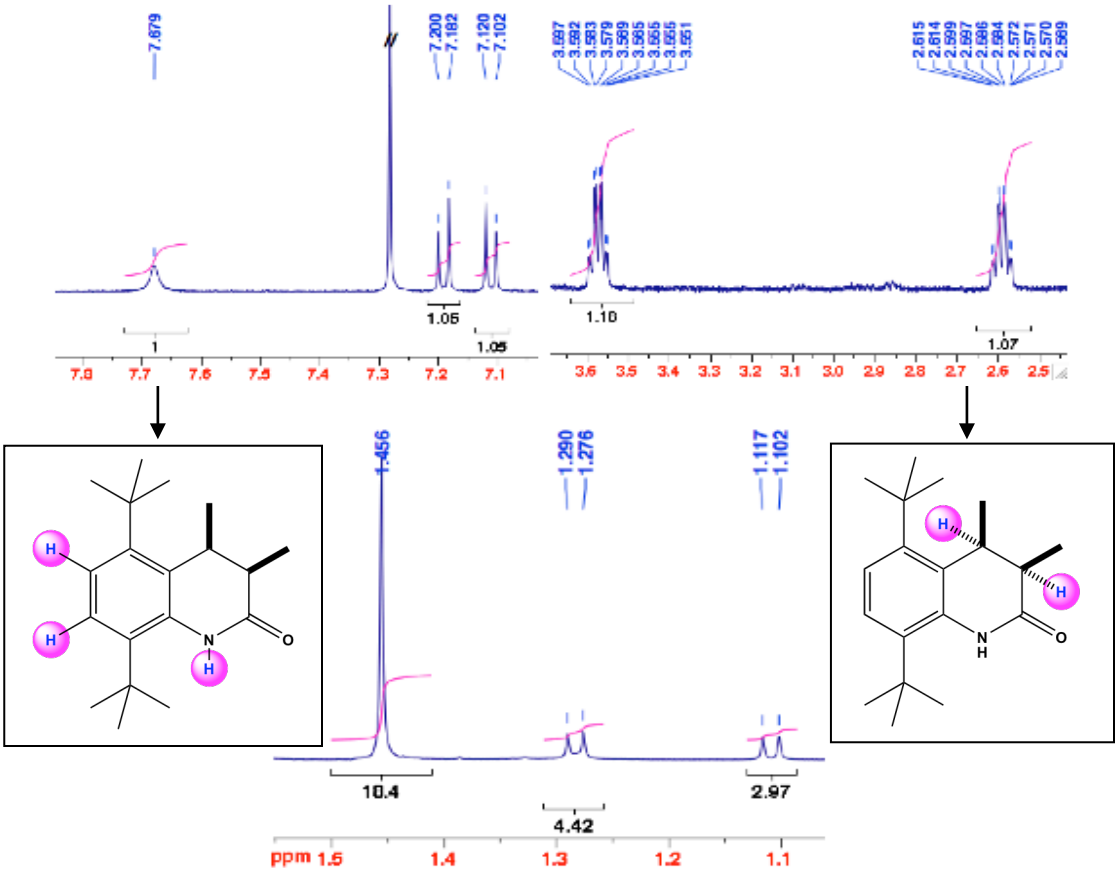

Figure 2.46: ^{1}H NMR (500 MHz, $CDCl_3$, δ ppm) expanded spectrum for quinolinone **76d.**

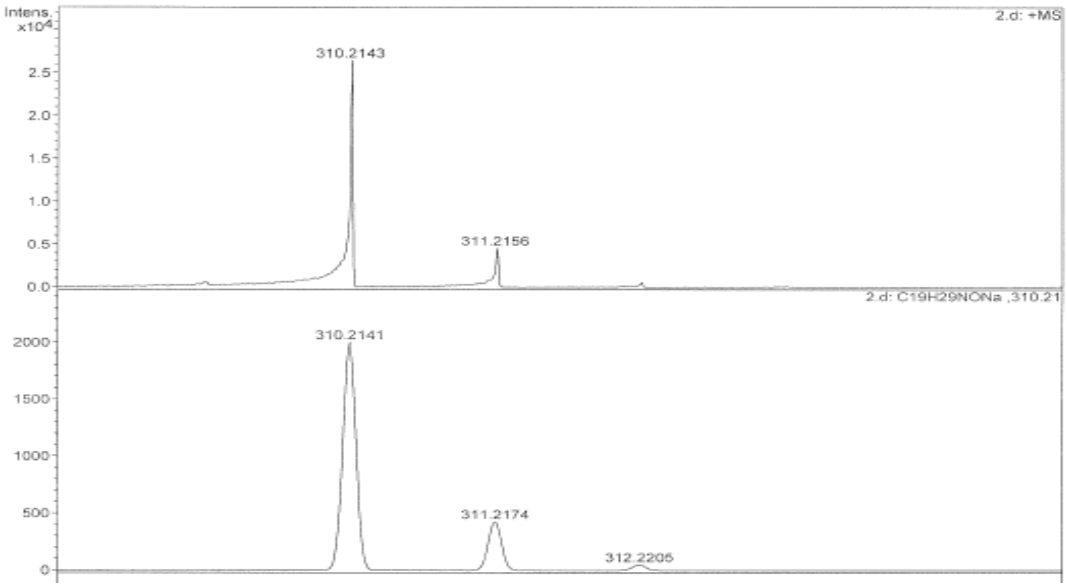

Figure 2.47: HRMS for quinolinone **76d.**

***trans*-77d:** R*f* = 0.61

The isolation of **77d** (R*f* = 0.61) by chromatography was not possible due to its close R*f* with the starting material (**75a** R*f* = 0.56) and hence NMR characterization not provided.

HRMS-ESI ([M + Na]$^+$): Calculated: 310.2141; Observed: 310.2143; Δm = 0.6 ppm

HPLC analysis conditions: Column: (R,R) WHELK–01; Abs. detector: 254 nm and 270 nm**;** Mobile phase: Hexanes:IPA = 93:07; Flow rate: 1 mL/min

Retention time (min): 10.00 (**77d** *ent*-**77d**)

Mixture of Photoproducts [*cis*-76e *and trans*-77e]

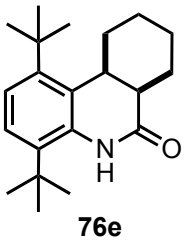

76e

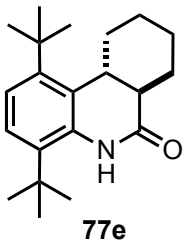

77e

cis-**76e** *and trans*- **77e** are not separable by preparative chromatography. The major photoproduct formed in benzene irradiations was assigned based on previous trends in the NMR shifts. The characterization provided below is from the mixture of isomers in comparison with the starting material (Figure 2.45). The *cis:trans* ratio was cross-verified on HPLC.

77e: ^{1}H NMR (500 MHz, $CDCl_3$, δ ppm) 7.45 (bs, 1H), 7.18 – 7.05 (ABq, 2H), 3.48- 3.41 (m, 1H), 2.76 – 2.70 (m, 1H), 1.84 -1.50 (m, 8H), 1.46 (s, 9H), 1.44 (s, 9H).

HPLC analysis conditions: Column: (R,R) WHELK–01; Abs. detector: 254 nm and 270 nm**;** Mobile phase: Hexanes:IPA = 90:10; Flow rate: 1 mL/min

Retention time (min): ~4.90 (**77e**) and 5.10 (*ent*-**77e** non-separable)

~6.37 (**76e**) and ~7.95 (*ent*-**76e**)

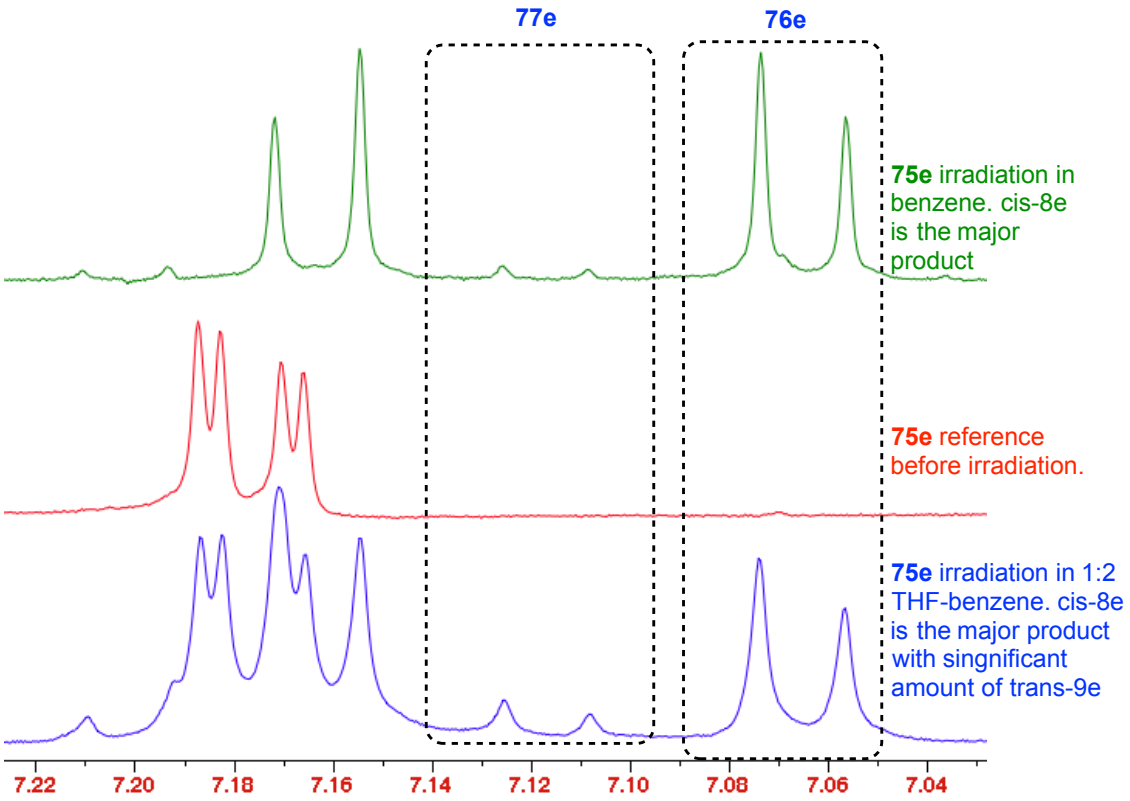

Comparision of the aromatic region in **75e** and its photoproduct irradiation mixture

Figure 2.46: ^{1}H NMR (500 MHz, $CDCl_3$, δ ppm) analysis of *cis*-**76e** and *trans*-**77e** photoproducts.

2.4.8. Verifying *cis:trans* ratio by NMR spectroscopy and HPLC analysis

In general, NMR spectroscopy analysis showed that crude reaction mixture can be employed to ascertain the *cis:trans* ratio as the *cis*-isomer resonates slightly downfield than the corresponding *trans*-isomer. For example the ratio of **73a:74a** (**70a:71a**) can be identified from the crude reaction mixture (**73a** resonate at ~3.00 and 2.76 ppm; **74**: resonate at 2.74 and 2.52). **73a** (=**70a**) and **74a** (=**71a**) can be separated by chromatography and were characterized independently as indicated before (sections 2.4.9).

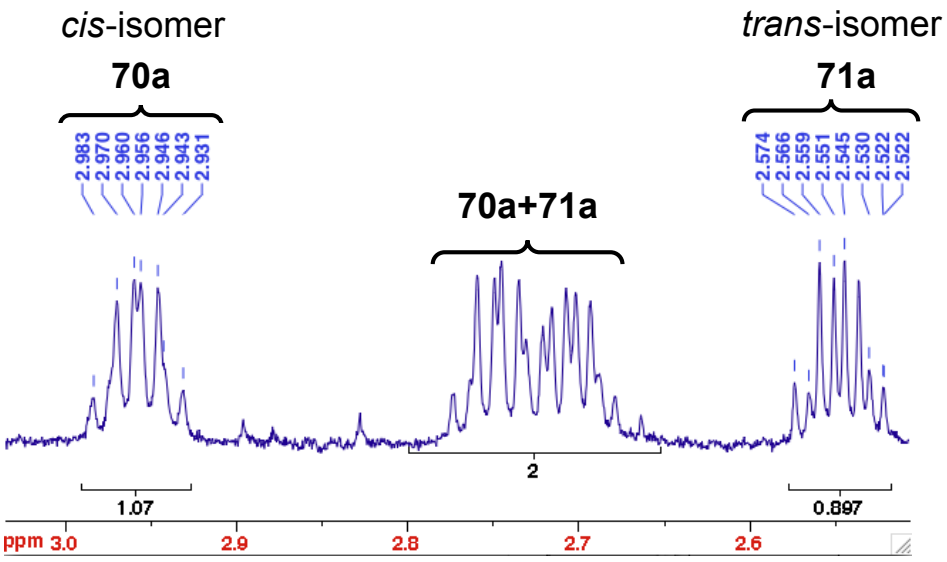

Figure 2.49: ^{1}H NMR (500 MHz, $CDCl_3$, δ ppm) analysis to determine *cis:trans* ratio: The proton resonances of the quinolinone hydrogen atoms are shown.

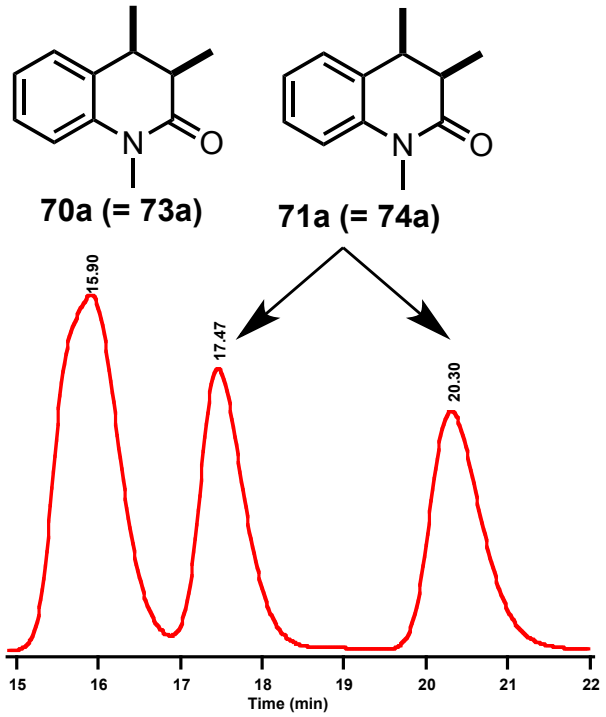

Figure 2.50: HPLC analysis to verify *cis:trans* ratio. (Note: **70a**) and *ent*-**70a** are not resolved on a chiral stationary phase HPLC separation and elutes as a single peak at ~15.9 min.

2.4.9. Product verification by independent synthesis

As photoproducts from **69a** and **72a** are identical, the products were verified by HPLC analysis that showed identical retention time. The *cis* product **73a** (**= 70a**) did not resolve under our analysis condition. On the other hand, the *trans* product **74a** (**= 71a**) was resolved with the two enantiomers having different retention time. The *cis* to *trans* ratio from HPLC analysis (Figure 2.47) correlated with ^{1}H NMR spectroscopic analysis (see section 2.4.8).

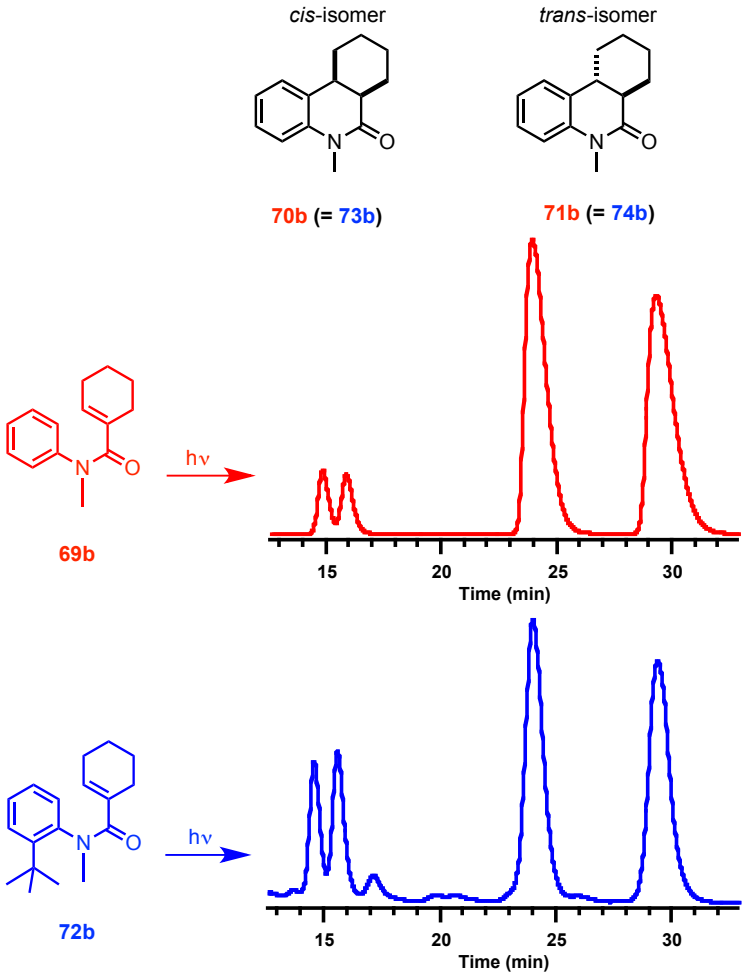

Figure 2.51: Product verification by independent synthesis.

2.4.10. Photocyclization of 72c at elevated temperature in MeOH and acetone-d_6

Photocyclization of **72c** was performed in methanol (at 58±2 ^{o}C) and in acetone (at 40±2 ^{o}C) to ascertain reactivity at elevated temperatures.

Solution of **72c** (0.01 mmol) in 1 mL of acetone-d_6 was irradiated for 4 h in a Pyrex tube with a 450 W medium pressure Hg-lamp at room temperature and at 40±2 ^{o}C under constant flow of nitrogen. The reaction was monitored by ^{1}H NMR spectroscopy that did not show any observable photoproducts.

Solution of **72c** (0.1 mmol) in 15 mL of methanol was irradiated for 5 h and 13 h in Pyrex tube with a 450 W Hg lamp at room temperature and at 58±2 ^{o}C under constant flow of nitrogen. The reaction mixture was analyzed after 5h and 13 h of irradiation time by HPLC on a chiral stationary phase and the retention times were compared with authentic sample prepared from the parent acrylanilide **69c**. No photoproducts were detected (Figure 2.49).

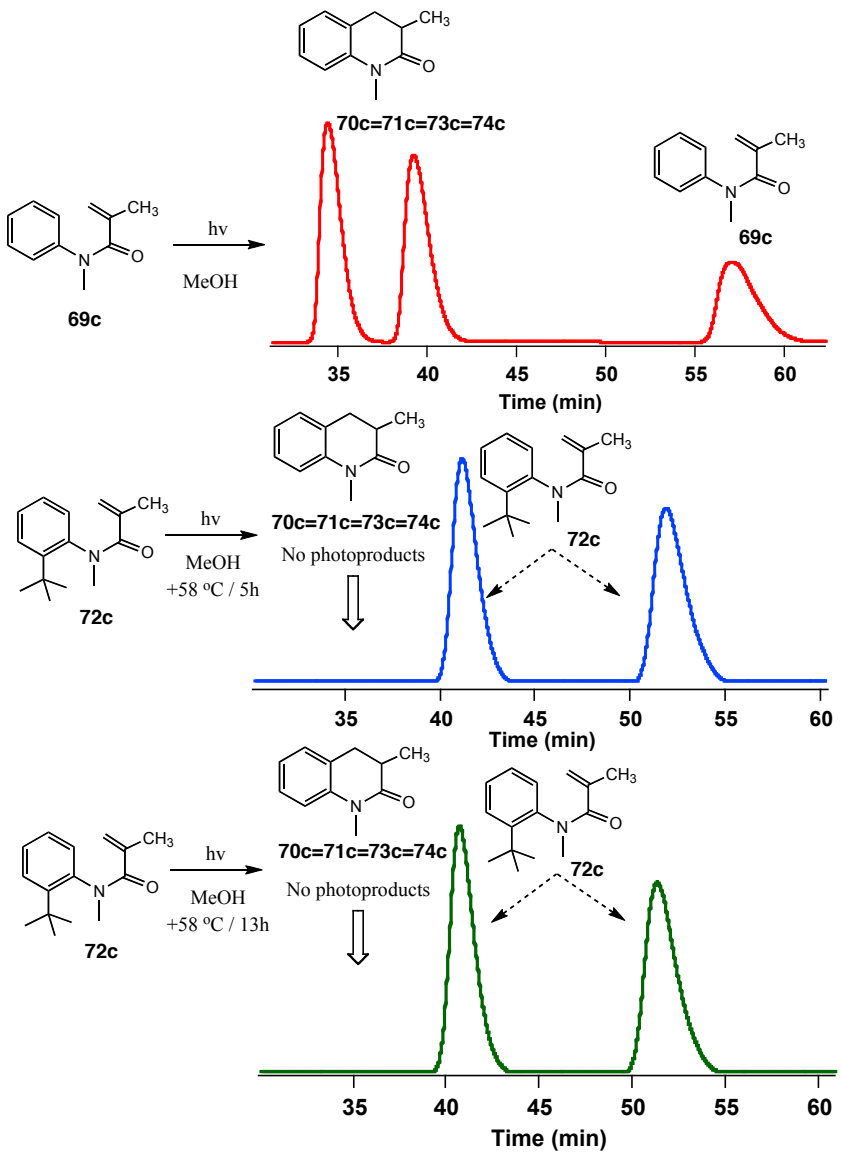

Figure 2.52: HPLC analysis after photo-irradiation of **72c** at RT (middle) and +58 ^{o}C (bottom). The authentic photoproduct form **69c** (top) is provided as reference.

2.5. References

(1) Cleveland, P. G.; Chapman, O. L. Non-oxidative photocyclization of alkyl-substituted acrylic acid anilides to dihydrocarbostyrils. *Chem. Commun.* **1967**, 1064–1065.

(2) Chapman, O. L.; Adams, W. R. Photochemical transformations. XXII. Photoisomerization of substituted acrylic acids and acrylamides to .beta.-lactones and β-lactams. *J. Am. Chem. Soc.* **1968**, *90*, 2333–2342.

(3) Ogata, Y.; Takagi, K.; Ishino, I. Photocyclization of acrylanilides. *J. Org. Chem.* **1971**, *36*, 3975–3979.

(4) Lenz, G. R. Enamide photochemistry. Stereochemistry of photocyclization of 1-ethylidene and 1-benzylidene 2-benzoyltetrahydroisoquinolines. *Journal of Organic Chemistry* **1976**, *41*, 2201–2207.

(5) Bach, T.; Grosch, B.; Strassner, T.; Herdtweck, E. Enantioselective [6pi]-photocyclization reaction of an acrylanilide mediated by a chiral host. Interplay between enantioselective ring closure and enantioselective protonation. *J. Org. Chem.* **2003**, *68*, 1107–1116.

(6) Ninomiya, I.; Yamauchi, S.; Kiguschi, T.; Shinobara, A.; Naito, T. Photocyclisation of enamides. Part V. Photocyclisation of α,β-unsaturated anilides. *J. Chem. Soc., Perkin Trans. 1.,* **1974**, 1747–1751.

(7) Toda, F.; Miyamoto, H.; Kikuchi, S.; Kuroda, R.; Nagami, F. Enantioselective Photocyclization of 2-Arylthio-3-methylcyclohexen-1-ones to Dihydrobenzothiophene Derivatives in an Inclusion Crystal with an Optically Active Host. *J. Am. Chem. Soc.* **1996**, *118*, 11315–11316.

(8) Tanaka, K.; Kakinoki, O.; Toda, F. Control of the Stereochemistry in the Photocyclisation of Acrylanilides to 3,4-Dihydroquinolin-2(1 H)-ones. Delicate Dependence on the Host Compound. *Chem. Commun.* **1992**, 1053–1054.

(9) Tanaka, K.; Toda, F. Solvent-Free Organic Synthesis. *Chem. Rev.* **2000**, *100*, 1025–1074.

(10) Ninomiya, I.; Kiguchi, T.; Yamauchi, S.; Naito, T. Photocyclisation of Enamides. Part 14 Substituent Effects in the Photocyclisation of N-α,β-Unsaturated Acylanilides. *J. Chem. Soc., Perkin Trans. 1.,* **1980**, 197–202.

(11) Ayitou, A. J.-L.; Sivaguru, J. Light-induced transfer of molecular chirality in solution:

enantiospecific photocyclization of molecularly chiral acrylanilides. *J. Am. Chem. Soc.* **2009**, *131*, 5036–5037.

(12) Curran, D. P.; Hale, G. R.; Geib, S. J.; Balog, A.; Cass, Q. B. L.; Degani, A. L. G.; Hernandes, M. Z.; Freitas, L. C. G. Rotational features of carbon-nitrogen bonds in axially chiral o-tert. butyl anilides and related molecules. Potential substrates for the “prochiral auxiliary” approach to asymmetric synthesis. *Tetrahedron: Asymmetry* **1997**, *8*, 3955–3975.

(13) Schmidt, G. M. J. Photodimerization in the solid state. *Pure Appl. Chem.* **1971**, *27*, 647–678.

(14) Havinga, E.; Schlatmann, J. L. M. A. Remarks on the specificities of the photochemical and thermal transformations in the vitamin D field. *Tetrahedron* **1961**, *16*, 146.

(15) Saltiel, J.; Tarkalanov, N.; Sears, J. D. F. Conformer-Specific Adiabatic Cis→Trans Photoisomerization of cis-1-(2-Naphthyl)-2-phenylethene. A Striking Application of the NEER Principle. *J. Am. Chem. Soc.* **1995**, *117*, 5586–5587.

(16) Tanaka, K.; Toda, F. Solvent-Free Organic Synthesis. *Chem. Rev.* **2000**, *100*, 1025–1074.

(17) Pischel, U.; Nau, W. M. Switch-Over in Photochemical Reaction Mechanism from Hydrogen Abstraction to Exciplex-Induced Quenching: Interaction of Triplet-Excited versus Singlet-Excited Acetone versus Cumyloxyl Radicals with Amines. *J. Am. Chem. Soc.* **2001**, *123*, 9727–9737.

(18) Inoue, Y. Asymmetric Photochemical Reactions in Solution. *Chem. Rev.* **1992**, *92*, 741–770.

(19) Wettack, F. S.; Renkes, G. D.; Rockley, M. G.; Turro, N. J.; Dalton, J. C. Quenching of alkyl ketone fluorescence by 1,3-dienes. *J. Am. Chem. Soc.* **1970**, *92*, 1793–1794.

(20) Curran, D. P.; Qi, H.; Geib, S. J.; DeMello, N. C. Atroposelective Thermal Reactions of Axially Twisted Amides and Imides. *J. Am. Chem. Soc.* **1994**, *116*, 3131–3132.

(21) Clayden, J. Atropisomers and near-atropisomers: achieving stereoselectivity by exploiting the conformational preferences of aromatic amides. *Chem. Commun.* **2004**, 127–135.

(22) Inoue, Y. Enantiodifferentiating photosensitized reactions. In *Chiral Photochemistry*; Inoue, Y.; Ramamurthy, V., Eds. Marcel Dekker: New York, 2004; Vol. 11, pp. 129–177.

CHAPTER 3. ENANTIOSPECIFIC 6π-PHOTOCYCLIZATION OF ATROPISOMERIC ACRYLANILIDE[§]

3.1. Introduction

In chapter 1 section 1.2, we explained the fundamental difference in asymmetric thermal and photochemical reactions leading to the formation of new stero-centres in the expected product. It is important to note that imprinting/inducing chiral information in the expected product has been proven to be successful in thermal reactions whereas, photochemical reactions have relatively fail to generate enantiopure product(s) due to the short life time of the excited molecules/intermediates and/or transition states species in the reaction of interest.[1] Nevertheless, photochemists in the last decade have employed various systems/strategies and organized assemblies[1-8] to carry out asymmetric photoreactions with varying degrees of success.

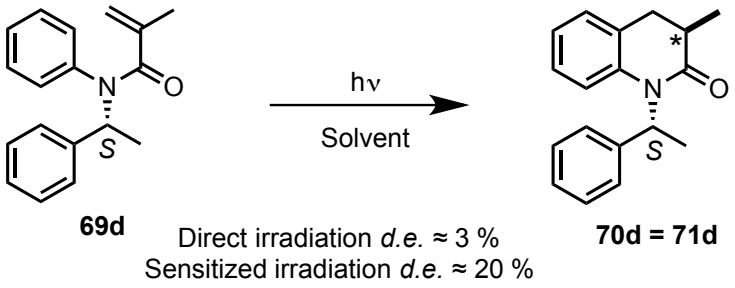

69d Direct irradiation *d.e.* ≈ 3 % **70d = 71d**
Sensitized irradiation *d.e.* ≈ 20 %

Scheme 3.1: Point chiral auxiliaries are ineffective in asymmetric photoreactions.

Conventional chiral auxiliaries employed in ground state thermal reactions are not effective to control chirality during photochemical transformations as depicted in scheme 3.1; the reason being that chiral auxiliaries could only affect the relative activation energies in the ground state. For photochemical reactions, light excitation and the chiral transfer (to the reactive species) processes may not be synchronous with respect to the energetics and the rate for each process. Thus, for asymmetric photochemical transformations in solution, it is necessary that the chiral discrimination transpire from the substrates itself in order to achieve high stereoselectivities.

[§] The material in this chapter was co-authored by Anoklase J.-L. Ayitou (AJA) Dr. J. Sivaguru (JS). AJA in consultation with JS synthesized all compounds and performed all experiments detailed in this chapter. AJA and JS came up with the mechanistic rationale as well as the conclusion described in this chapter.

Organized assemblies such as crystals on the other hand could provide a chiral environment if the substrate of interest crystallizes in one of the chiral space groups as discussed in chapter 1 section 1.5.4. But, as compounds forming crystalline materials is quite unpredictable (exacerbate the problem in addition to prolonged reaction time and loss of crystallinity that will impact the stereochemistry of the photoproduct(s) in the reaction of interest) could arise during irradiation of crystalline solids.

The strategy to obtain high stereoselectivities using axial chiral chromophores will be discussed in this chapter. Axial chirality introduces a chiral bias (Figure 3.1) in the reaction pathway, leading to high stereoselectivity in the photoproduct. It is well documented in literature that axial chirality could be transformed and transferred to the final product with very high stereospecificities in crystals. However, employing crystals has disadvantages *viz.* a) requiring the compound to be a solid with nominal melting point and getting high conversion to the product without losing the crystallinity / selectivity,[9,10] b) few reactions in the solid state are known to generate photoproduct with high conversion without loosing the selectivity. Ideally, similar methodologies of transferring axial chirality from the reactant to the product has to be developed solution phase phototransformations.[11,12]

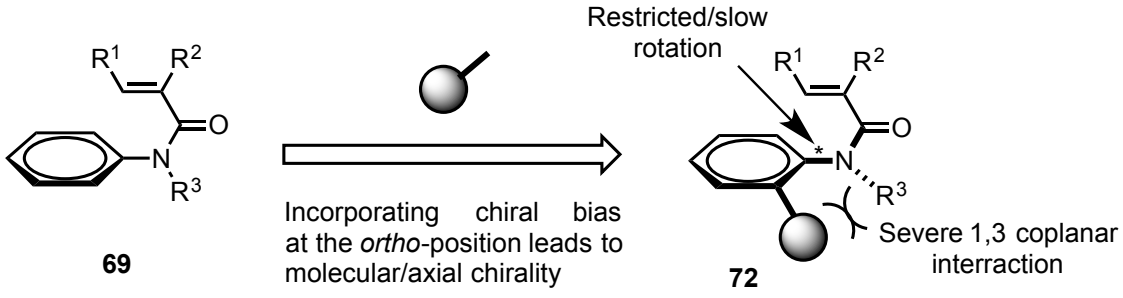

Figure 3.1: Bulky substituents could induce axial chirality: Example of acrylanilides.

The approach of using built-in constraint(s) or chiral bias within the molecular reactant leading to axial chirality stemming from axis or plane or helical could be effective to transfer the chiral information in solution phase photochemical transformation to yield chirally enriched photoproducts. The constraints that make the reactant molecularly chiral are based on the well-established concept of rotamers control via restricted bond rotation, which have been successfully employed for stereocontrol in thermal reactions (*cf.* chapter 1 section 1.6).[11,13-16] Axially chiral chromophores can be synthesized with relative ease using

established literature procedures.[11-16] So, by employing chiral rotamers that equilibrate/racemize very slowly in the ground state, it should be possible to achieve high stereoselection during phototransformations. The methodology discussed in this chapter draws inspiration from the Havinga's NEER principle (Non-Equilibrating Excited Rotamers), where conformer based product control is well documented.[17]

3.2. The Havinga's Non Equilibrating Excited Rotamers (NEER) Principle

The photochemical transformations of derivatives/precursors of vitamin D have been extensively studied by Havinga and co-workers.[18] The study has taken advantage of the single bond rotamers leading to precalciferol and tachysterol. A comprehensive study of rotational isomers (rotamers) behavior in the ground and excited states evolved into the concept of Non-Equilibrating Excited Rotamers (NEER).[17] For example, the ground state rotamers **83-A** and **83-B** can easily interconvert due to single bond rotations. Upon photolysis, interconversion from **83-A** to **83-B** and vice-versa is forbidden in the excited state, as single bonds become partial double bonds as illustrated in figure 3.2.

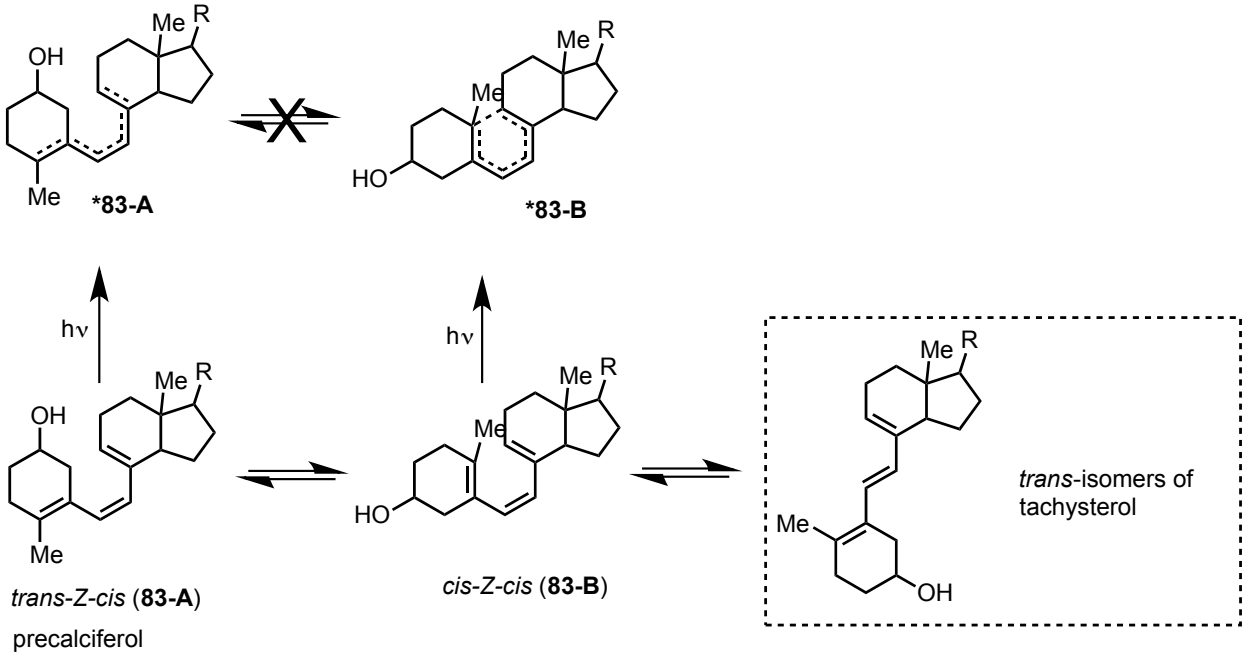

Figure 3.2: The NEER principle: the photochemical and thermal transformations of derivatives/precursors of vitamin D. (Ref. 17)

The NEER principle was able to explain the stereochemistry of the ground state rotamers but also in the product control during the phototransformation. Thus, the 6π-photocyclization of axially chiral acrylanilides was investigated as model system for the NEER principle and as a test strategy for axial to point chiral transfer. Other reasons for investigating the 6π-photocyclization of axially chiral acrylanilides were: a) acrylanilides moieties are well studied in solution and in organized media and their reactivity and product(s) upon photoreactions are well characterized;[19-22] b) it is well known that bulky *ortho*-substituents in *N*-substituted anilides (e.g. *o*-*tert*-butylanilides) are molecularly chiral due to the restricted rotation of the N-C(aryl) bond and are fairly stable temperate as illustrated in figure 3.1; and c) synthesis and chromatographic separation of these molecularly chiral chromophores are well documented in literature.[11-13,23,24]

The above aspects make the systems of interest the ideal candidates to explore/apply the NEER principle and the transfer of molecular chirality to point chirality in the photoproduct during 6π–photocyclization in solution.

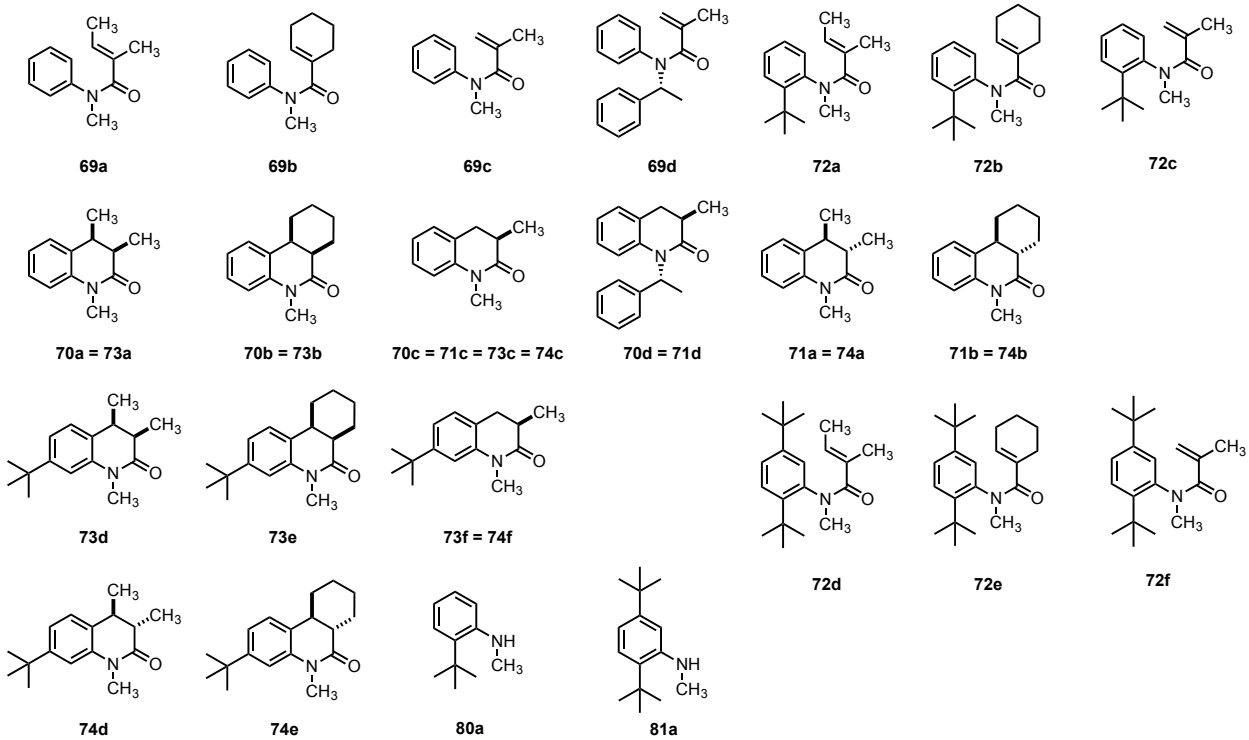

Chart 3.1: Acrylanilides molecular reactants and corresponding photoproduct(s).

3.3. Enantiospecific Photochemical Transformation of Optically Pure Atropisomeric Acrylanilides 72

Two sets of *o*-*tert*-butyl derivatives *viz.,* 2-*tert*-butylderivatives **72a-c** and 2,5-di-*tert*-butylderivatives **72d-f** were investigated. As expected[16] all the *o*-*tert*-butyl derivatives were molecularly chiral atropisomers (*P* and *M* isomers) and were characterized by NMR spectroscopy, CD spectroscopy and optical rotation (*cf.* Section 3.5). As illustrated in scheme 3.2, optically pure atropisomers (helical isomers) of **72a-f** were irradiated in various solvents using a 450 W medium pressure Hg lamp with Pyrex cutoff under constant flow of nitrogen. The conversion in acetone (~50 %) was high compared to other solvents (< 30%) for the same irradiation time (chapter 2 Table 2.1).[25] Higher irradiation time to increase the conversion resulted in a noticeable amount of side products. The products were purified by chromatography and characterized by NMR spectroscopy (*cf.* Section 3.5). HPLC analysis of the reaction mixture on a chiral stationary phase gave enantiomeric excess in the photoproducts (Table 3.1). Enantioselectivity as high as 99% was observed in photoproducts from **72a-b** and **72d-e** in the solvents investigated. Each optically pure isomers of **72** (except **72c,f**) yielded one enantiomer in the photocyclized product(s) indicating that the system is well behaved. For example, in methanol (-)-**72d** gave an ee value of 92% in *trans*-**74d** whereas the corresponding optical antipode (+)-**72d** gave the enantiomer of *trans*-**74d** with an ee value of 94% in methanol (Scheme 3.2; Table 3.1 entries 7 and 8).

Based on the mechanistic rationale detailed in the previous chapter, we postulated that the photocyclization occurs at the *ortho* carbon via "*int*-**A**" (Scheme 3.2) with removal of the *o*-*tert*-butyl substituent. This assumption is based on the observation that the enantioselectivity in the *cis*-**73** and *trans*-**74** photoproducts is identical, as the resulting zwitterionic intermediate "*int*-**A**" (Scheme 3.2) has a defined chiral center at the benzylic position. During the second step, a proton transfer (from solvent or intramolecular [1,7] H shift) occurs in a non-stereospecific fashion leading to *cis*- and *trans*-photoproducts with identical *ee* values. Fortunately, the enantiomers of both the *cis*-isomer **73** and the *trans*-isomer **74** in the case of cyclohexyl derivatives **72b** and **72e** have been separated and analyzed by polarimetry; their optical rotation values were compared with precedent findings.[26] For example, in the case of the cyclohexyl derivative **72e**, *ee* values observed for both the *cis*-**73e** and *trans*-**74e** photoproducts were

comparable (Table 3.1; entries 9 and 10). Similarly, *ee* value as high as 99% was observed for both *cis*-**73b** and *trans*-**74b** photoproducts in the photocyclization of the cyclohexyl derivative **(+)-72b** (Figure 3.2).

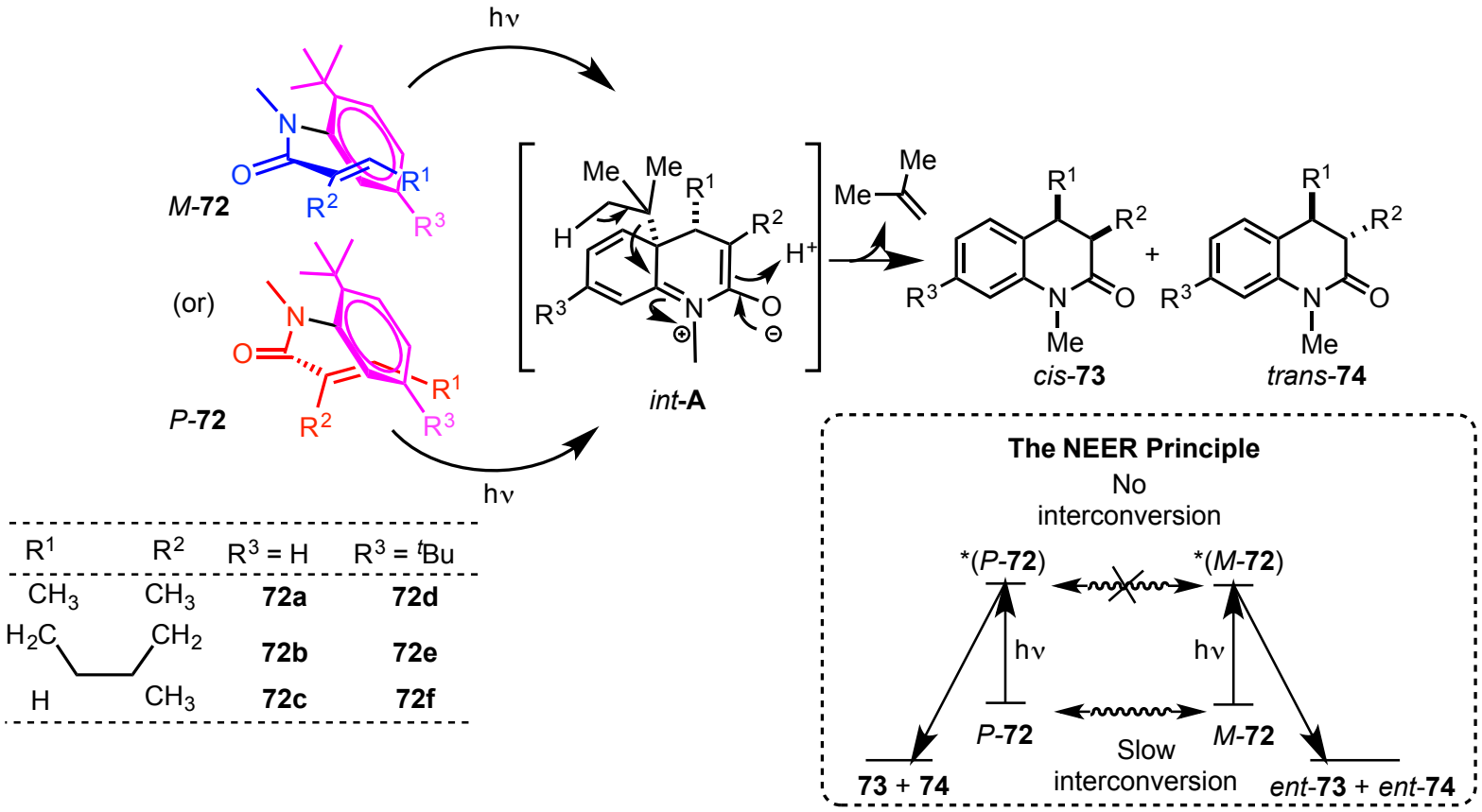

R^1	R^2	R^3 = H	R^3 = ^{t}Bu
CH_3	CH_3	**72a**	**72d**
H_2C	CH_2	**72b**	**72e**
H	CH_3	**72c**	**72f**

Scheme 3.2: Photocyclization of molecularly chiral acrylanilides **72**.

3.4. Assigning Absolute Configuration in the Photoproducts (Absolute Configuration of *cis*-73b and *trans*-74b Photoproducts)

The optical rotation values were compared with literature values [26] and the configuration were assigned based on the sign of rotation.

The HPLC peak with the retention time ~29.52 was found to have $[\alpha]_D^{23}$= -48 (*c* 0.51% in $CHCl_3$). Based on the sign of rotation and comparison of the sign of rotation from literature [26] ($[\alpha]_D^{23}$= -71, $CHCl_3$) the peak was assigned the configuration (*S, S*) (Scheme 3.3) and the corresponding enantiomer (HPLC retention time ~24.15) was assigned with (*R, R*) configuration.

Based on the mechanism, photocyclization from a given helical isomer (for example **(+)-1b**) results in identical absolute configuration at the benzylic position (10a position in the photoproduct). Thus, the absolute configuration of both the *cis*-**73b** and *trans*-**74b** photoproducts could be assigned (Scheme 3.4).

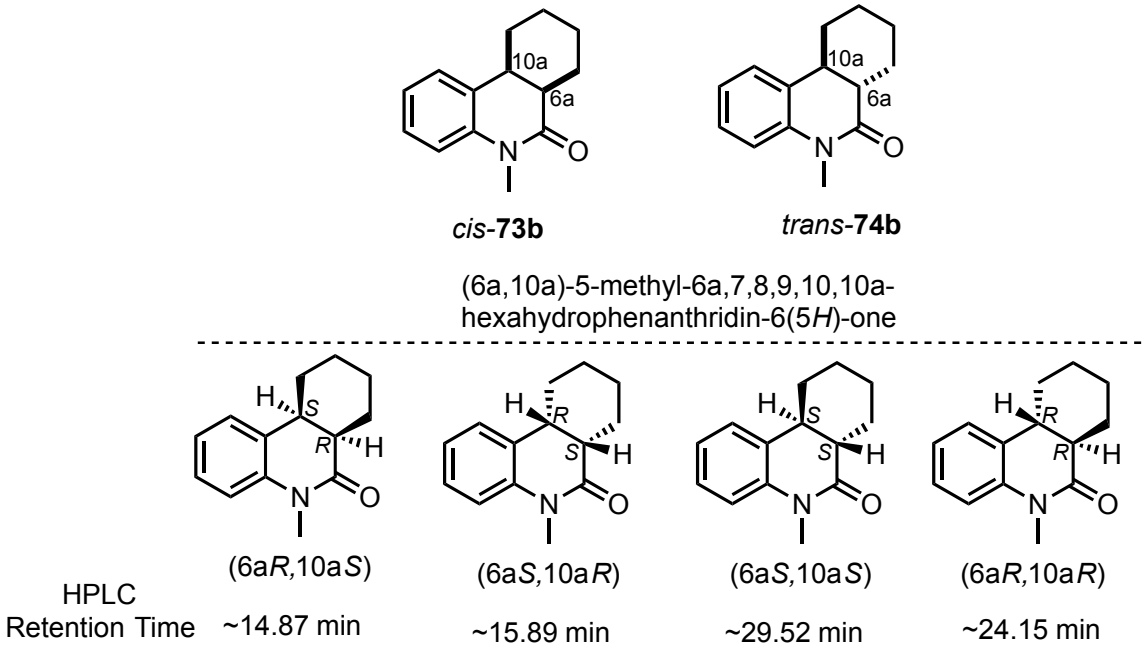

Scheme 3.3: Absolute configuration of *cis*-**73b** and *trans*-**74b** photoproducts: Absolute configurations are derived from optical rotation values reported in literature for optically pure derivatives.[26]

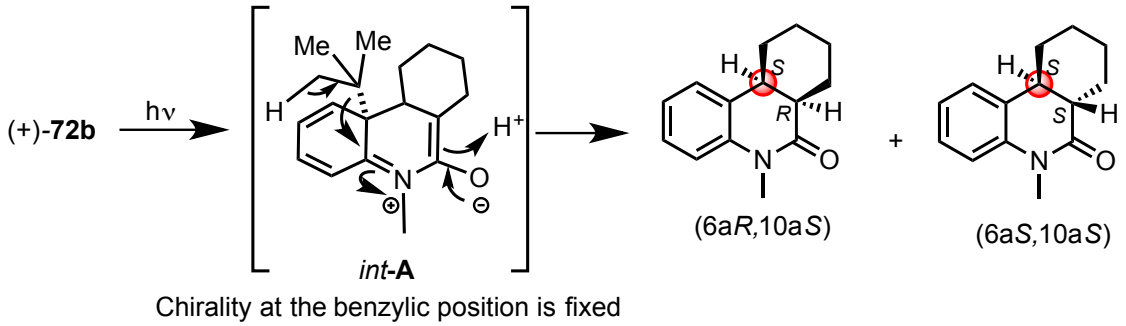

Scheme 3.4: Absolute configuration of *cis*-**73b** and *trans*-**74b** photoproducts based on the mechanism of photocyclization.

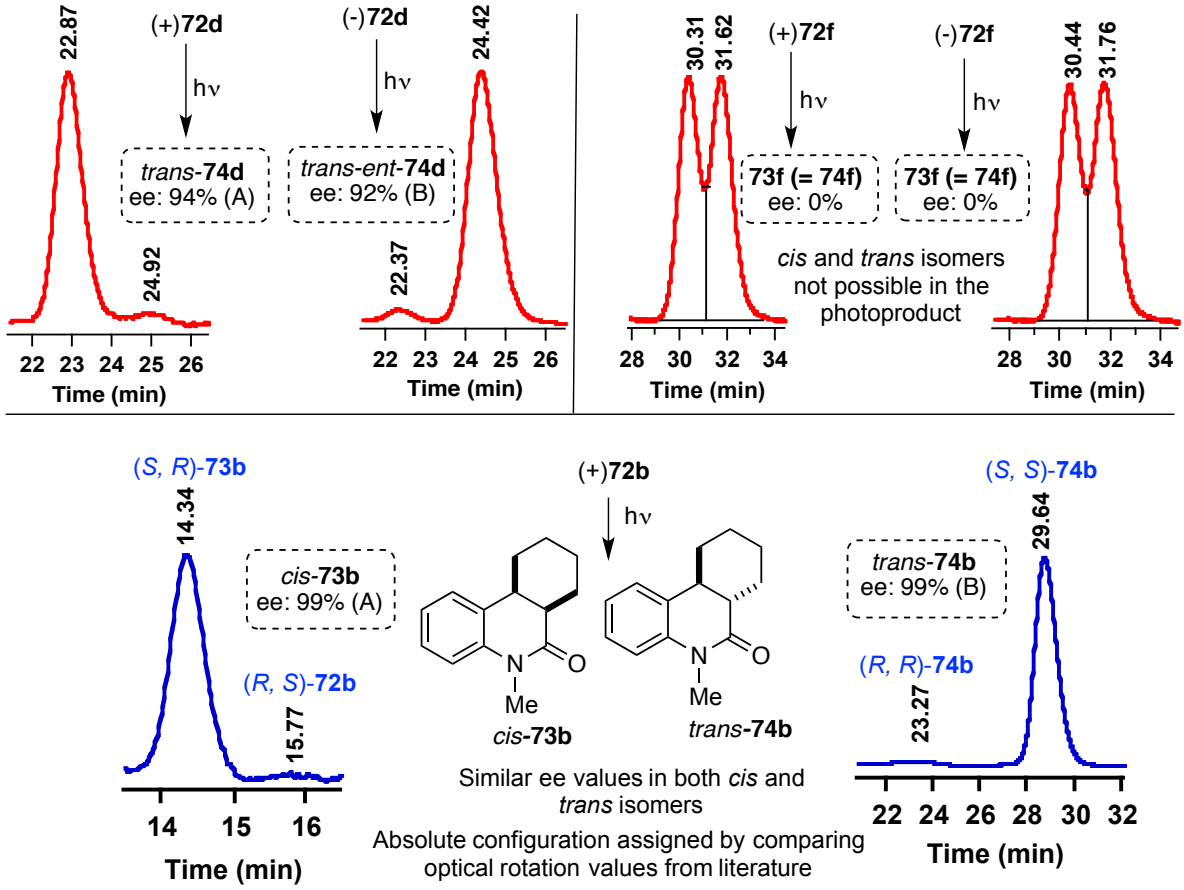

Figure 3.3: HPLC traces of photoproducts in the photocyclization of **72b,d**,**f** under direct irradiation.

Table 3.1. Enantioselective 6π-photocyclization of **72**.[a]

Entry	Substrates	MeOH		$CHCl_3$		2:1 C_6H_6/THF		Acetone	
		73	**74**	**73**	**73**	**74**	**74**	**73**	**74**
1.	**(-)72a**[b]	-	87(B)	-	-	90(B)	91(B)	-	89(B)
2.	**(+)72a**[b]	-	84(A)	-	-	94(A)	88(A)	-	95(A)
3.	**(-)-72b**[c]	85 (*R, S*)	-	92 (*R, S*)	92 (*R, S*)	-	-	80 (*R, S*)	-
4.	**(+)72b**[c]	99 (*S, R*)	99 (*S, S*)	90 (*S, R*)	92 (*S, R*)	88 (*S, S*)	95 (*S, S*)	93 (*S, R*)	94 (*S, S*)
5.	**(-)72c**[d]	0		0		0		-	
6.	**(+)72c**[d]	0		0		0		-	
7.	**(-)72d**[b]	-	92(B)	-	-	94(B)	85(B)	-	91(B)
8.	**(+)72d**[b]	-	94(A)	-	-	91(A)	99(A)	-	88(A)
9.	**(-)72e**	99(A)	99(A)	98(A)	90(A)	91(A)	99(A)	91(A)	93(A)
10.	**(+)72e**	99(B)	99(B)	91(B)	87(B)	90(B)	95(B)	90(B)	99(B)
11.	**(-)72f**[d]	0		0		0		-	
12.	**(+)72f**[d]	0		0		0		-	

[a] A and B refers to the first and second peak that elutes out on the HPLC for a given pair of enantiomers; values are average of 3 runs with ±5% error; reaction temperature 0-3 °C; For **72a-c**, (+) and (-) represents the sign of their CD signals at 240 nm in methanol. Similarly for **72d-f**, (+) and (-) represents the sign of optical rotation in $CHCl_3$. [b] *cis*-**73** enantiomers not separable on chiral stationary phase. [c]Chromatographic separation is necessary prior to HPLC analysis as HPLC retention times of *trans*-**74** photoproducts overlaps with the starting material **72**. Absolute configuration assigned based on comparison of optical rotation values from literature (Reference 26, Refer to supplementary Information for details). [d] *cis*/*trans* isomers not possible in the case of **72c,f**.

It is clear upon inspection of Table 3.1 that the β-substituent in the alkene is crucial for achieving the high enantiomeric excess under direct irradiation conditions. In solvent like methanol, higher ee value of 94% was observed for (+)-**72d** with β-CH_3 substituent, whereas the corresponding methacryloyl derivative (+)-**72f** with β-H substituent gave racemic photoproduct (Table 3.1; entries 8 and 12; Figure 3.2) as detailed in chapter 2 (*cf.* Section 2.2) the photocyclization likely occurs via a zwitterionic intermediate with a bond formation between the β-alkenylcarbon on the phenyl ring (*ortho* with the *tert*-butyl substituent): this leads to a zwitterionic intermediate "*int*-**A**". Structurally, the zwitterionic intermediate "*int*-**A**" reveals that the presence of a β-substituent in the molecular reactant is necessary in

transferring the chiral information in the reactant to point chirality at the benzylic position in the photoproduct. On the other hand, the absence of β-substituents in the reactants **72c** and **72f**, photocyclization leads to the zwitterionic intermediate "*int*-**A**" bearing an achiral benzylic carbon (-CH_2-). The second hydrogen (H) migration (step 2) is non-stereospecific resulting in racemic photoproducts. The H-migration from "*int*-**A**" can be visualized as a stepwise process that leads to an enol that subsequently tautomerize to the final product making H-migration non-stereospecific. Thus, the β-substituent in this picture may be referred as a "messenger" for the chiral transfer.

In the absence of the β-substituent (reactants **72c** and **72f**), we have shown that high stereoselectivities could be achieved by tuning the reactive spin state of the photo-substrate. This aspect of the 6π-photocyclization of molecularly chiral acrylanilides will be developed in the next chapter.

3.5. Summary and Outlook

The stereochemistry aspect of 6π-photocyclization of axially chiral acrylanilides opened up the opportunity of achieving high enantioselectivities in solution phase photochemical transformations during direct irradiation; the β-alkenyl substituent was found to be crucial for axial to point chiral transfer. This methodology of employing axially chiral chromophores that racemize very slowly in the ground state and no interconversion in the excited state leading to very high enantioselectivity in the photoproducts is an inspiration from Havinga's NEER principle (Non-Equilibrating Excited Rotamers), where stereoselectivity in product is based on the conformational differentiation of the molecular reactant is well documented.[17] Chapter 4 will address strategies to achieve high stereoselectivities in derivatives **72c,f** as they generated racemic photoproducts via direct irradiation.

3.6. Experimental Section

3.6.1. General procedure for synthesis of *N*-methyl anilines 80a and 81a

Cf. chapter 2 section 2.4.2

3.6.2. Characterization of *N*-Methyl anilines 80a and 81a

Cf. chapter 2 section 2.4.3

3.6.3. General procedure for synthesis of acrylanilides 72a-f

Cf. chapter 2 section 2.4.4

3.6.4. Characterization of acrylanilides 72a-f

For R*f* values, ^{1}H and ^{13}C NMR spectroscopy, HRMS and HPLC conditions for acrylanilides**72a-f**, *cf.* chapter 2 section 2.4.5

3.6.5. Circular dichroism spectra for 72a-c

CD Spectra of optically pure atropisomers of **72a**

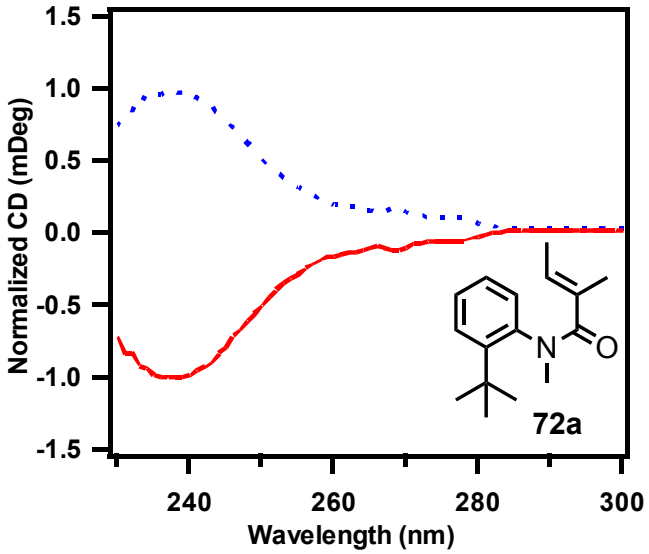

Figure 3.4: Normalized CD spectra for optically pure atropisomers of **72a.**

CD Spectra of optically pure atropisomers of **72b**

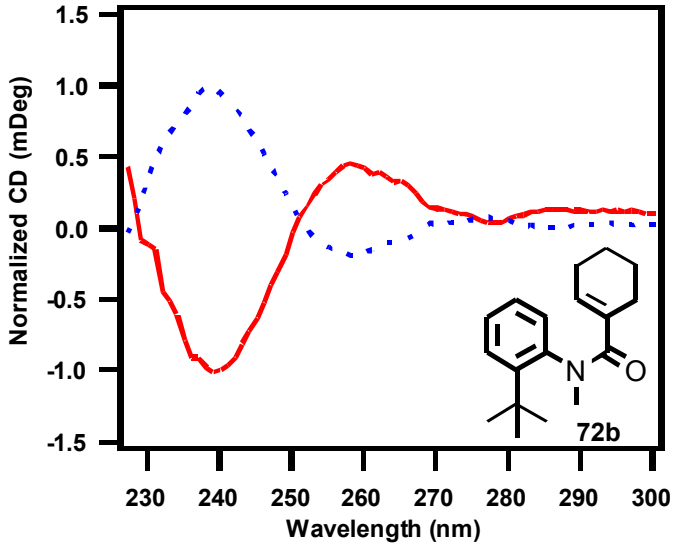

Figure 3.5: Normalized CD spectra for optically pure atropisomers of **72b.**

CD Spectra of optically pure atropisomers of **72c**

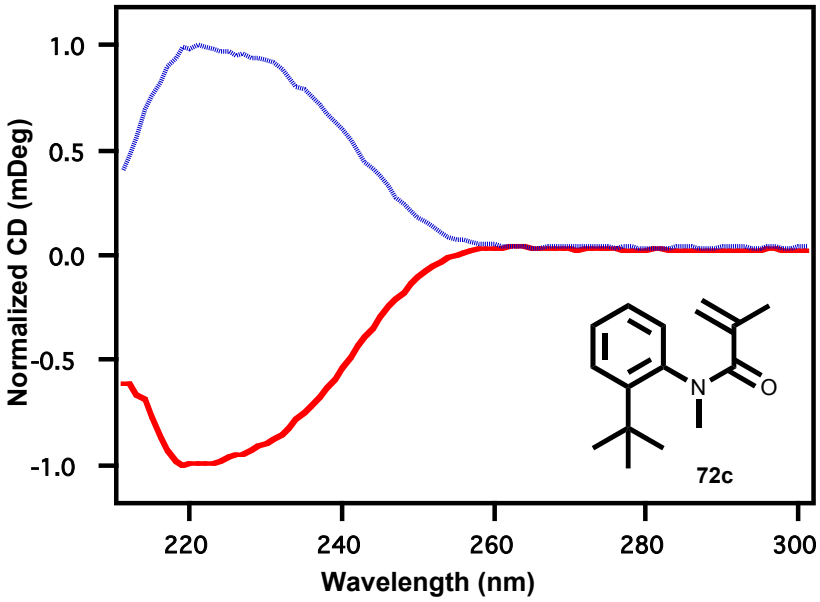

Figure 3.6: Normalized CD spectra for optically pure atropisomers of **72c.**

3.6.6. Optical rotation for 72d-f

Optical Rotation $[\alpha]_D^{28}$:

(-)-72d (*c* 0.433, $CHCl_3$) = -35 deg.

(+)-72d (*c* 0.424, $CHCl_3$) = +30 deg.

Optical Rotation $[\alpha]_D^{27}$:

(-)-72e (*c* 0.300, MeOH) = -35.67 deg.

(+)-72e (*c* 0.364, MeOH) = +35.64 deg.

Optical Rotation $[\alpha]_D^{25}$

(-)-**72f** (*c* 0.210, $CHCl_3$) = - 29.05 deg.

(+)-**72f** (*c* 0.213, $CHCl_3$) = + 25.35 deg.

3.6.7. Characterization of parent acrylanilides 69c

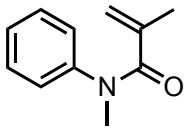

69c

The reaction that led to the formation of **69c** was totally driven to completion (conversion yield: 99 %); thus, no further purification was required. Also, **69c** upon standing formed white needle like crystals at room temperature.

R*f* = 0.37

^{1}H NMR (500 MHz, $CDCl_3$, δ ppm) 7.35 – 7.27 (t, 2H), 7,25 – 7.18 (t, 1H), 7.14 – 7.07 (d, 2H), 5.02 – 4.91 (d, 2H), 3.31 (s, 3H), 1.76 – 1.69 (s, 3H)

HRMS-ESI ($[M + Na]^+$): Calculated: 198.0889; Observed: 198.0889; Δm = 0 ppm

3.6.8. General irradiation procedures for acrylanilides 69 and 72

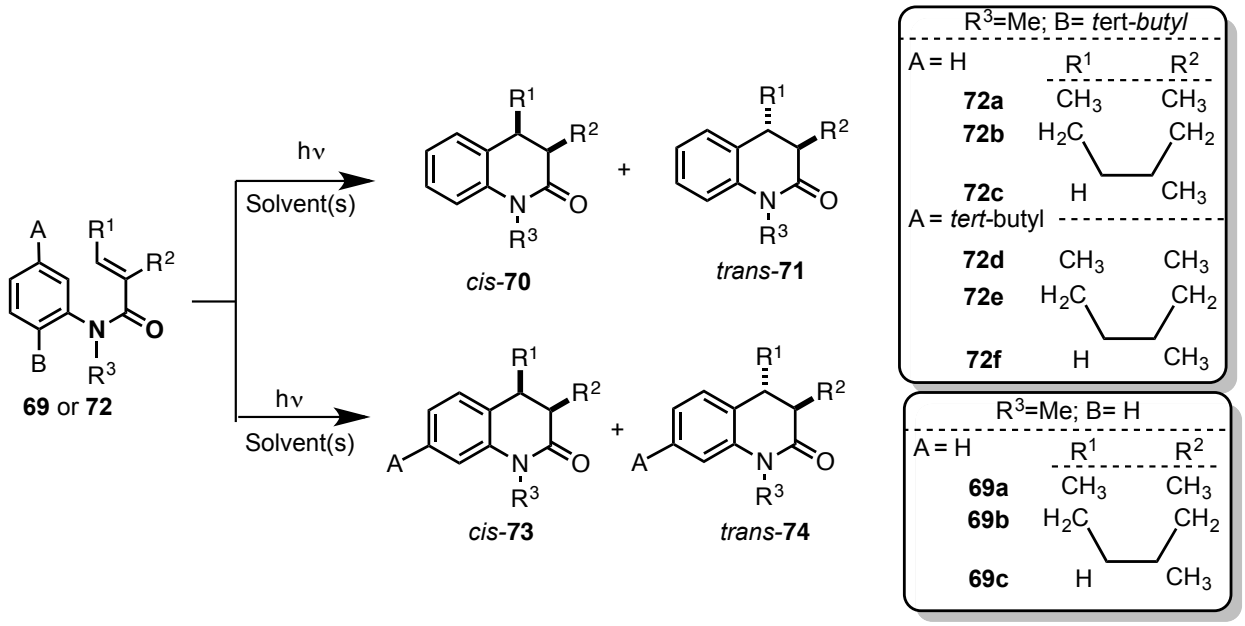

Scheme 3.5: Photo-irradiation of acrylanilides **69** and **72**.

Solutions of acrylanilides (0.1mmol) in 15 mL of the selected solvent were irradiated for 7 h in Pyrex test tubes (13 – 18 mm) with a 450 W at room temperature and under constant flow of nitrogen gas. The reaction progress was monitored by TLC, GC, HPLC and NMR spectroscopy. After irradiation, the solvent was removed by roto-evaporation under reduced pressure and the photoproducts were characterized by HPLC and NMR spectroscopy. The *ee* values in the photoproducts were determined by HPLC on chiral stationary phases.

3.6.9. Characterization of photoproducts

For quinolinones **70a-b**, **71a-c**, **73a-f** and **74a-f**, see chapter 2 section 2.4.7

3.7. References

(1) Turro, N. J. 1.; Ramamurthy, V.; Scaiano, J. C. J. C. 1. *Modern molecular photochemistry of organic molecules*; Sausalito, CA: University Science Books, 2010.

(2) Inoue, Y. Enantiodifferentiating photosensitized reactions. In *Chiral Photochemistry*; Inoue, Y.; Ramamurthy, V., Eds. Marcel Dekker: New York, 2004; Vol. 11, pp. 129–177.

(3) *Photochemistry in Organized and Constrained Media*; Ramamurthy, V. Eds. Wiley-VCH: New York, 1991.

(4) Schmidt, G. M. J. Photodimerization in the solid state. *Pure Appl. Chem.* **1971**, *27*, 647–678.

(5) Gamlin, J. N.; Jones, R.; Leibovitch, M.; Patrick, B.; Scheffer, J. R.; Trotter, J. The Ionic Auxiliary Concept in Solid State Organic Photochemistry. *Acc. Chem. Res.* **1996**, *29*, 203–209.

(6) Mori, T.; Weiss, R. G.; Inoue, Y. Mediation of Conformationally Controlled Photodecarboxylations of Chiral and Cyclic Aryl Esters by Substrate Structure, Temperature, Pressure, and Medium Constraints. *J. Am. Chem. Soc.* **2004**, *126*, 8961–8975.

(7) Bauer, A.; Westkämper, F.; Grimme, S.; Bach, T. Catalytic enantioselective reactions driven by photoinduced electron transfer. *Nature* **2005**, *436*, 1139–1140.

(8) Bach, T.; Bergmann, H.; Grosch, B.; Harms, K. Highly Enantioselective Intra- and Intermolecular [2 + 2] Photocycloaddition Reactions of 2-Quinolones Mediated by a Chiral Lactam Host: Host−Guest Interactions, Product Configuration, and the Origin of the Stereoselectivity in Solution. *J. Am. Chem. Soc.* **2002**, *124*, 7982–7990.

(9) Sakamoto, M.; Iwamoto, T.; Nono, N.; Ando, M.; Arai, W.; Mino, T.; Fujita, T. Memory of Chirality Generated by Spontaneous Crystallization and Asymmetric Synthesis Using the Frozen Chirality. *J. Org. Chem.* **2003**, *68*, 942–946.

(10) Toda, F. Solid State Organic Chemistry: Efficient Reactions, Remarkable Yields, and Stereoselectivity. *Acc. Chem. Res.* **1995**, *28*, 480–486.

(11) Bach, T.; Schr6der, J.; Harms, K. Diastereoselective Photocycloaddition of an Axial Chiral Enamide. *Tetrahedron Lett.* **1999**, *40*, 9003–9004.

(12) Müller, C.; Bach, T. Chirality Control in Photochemical Reactions:Enantioselective Formation of Complex Photoproducts in Solution. *Aust. J. Chem.* **2008**, *61*, 557–564.

(13) Curran, D. P.; Qi, H.; Geib, S. J.; DeMello, N. C. Atroposelective Thermal Reactions of Axially Twisted Amides and Imides. *J. Am. Chem. Soc.* **1994**, *116*, 3131–3132.

(14) Clayden, J. Atropisomers and near-atropisomers: achieving stereoselectivity by exploiting the conformational preferences of aromatic amides. *Chem. Commun.* **2004**, 127–135.

(15) Honda, A.; Waltz, K. M.; Carroll, P. J.; Walsh, P. J. Atropisomeric amides: Achiral ligands with chiral conformations. *Chirality* **2003**, *15*, 615–621.

(16) Curran, D. P.; Hale, G. R.; Geib, S. J.; Balog, A.; Cass, Q. B. L.; Degani, A. L. G.; Hernandes, M. Z.; Freitas, L. C. G. Rotational features of carbon-nitrogen bonds in axially chiral o-tert. butyl anilides and related molecules. Potential substrates for the “prochiral auxiliary” approach to asymmetric synthesis. *Tetrahedron: Asymmetry* **1997**, *8*, 3955–3975.

(17) Havinga, E.; Schlatmann, J. L. M. A. Remarks on the specificities of the photochemical and thermal transformations in the vitamin D field. *Tetrahedron* **1961**, *16*, 146.

(18) Havinga, E.; Schlatmann, J. L. M. A. Remarks on the specificities of the photochemical and thermal transformations in the vitamin D field. *Tetrahedron* **1961**, *16*, 146.

(19) Ogata, Y.; Takagi, K.; Ishino, I. Photocyclization of Acrylanilides. *J. Org. Chem.* **1971**, *36*, 3975–3979.

(20) Bach, T.; Grosch, B.; Strassner, T.; Herdtweck, E. Enantioselective [6π]-Photocyclization Reaction of an Acrylanilide Mediated by a Chiral Host. Interplay between Enantioselective Ring Closure and Enantioselective Protonation. *J. Org. Chem.* **2003**, *68*, 1107–1116.

(21) Toda, F.; Miyamoto, H.; Kanemoto, K. 1:1 and 2:1 Inclusion Complexes of (R,R)-(-)-trans-2,3-Bis(hydroxydiphenyl- methyl)-1,4-dioxaspiro[4.4]nonane with N-Allylfuran-2-carboxanilide Which upon Irradiation in the Solid State Give (-)- and (+)-Photocyclization Products, Respectively. *J. Org. Chem.* **1996**, *61*, 6490–6491.

(22) Tanaka, K.; Kakinoki, O.; Toda, F. Control of the Stereochemistry in the Photocyclisation of Acrylanilides to 3,4-Dihydroquinolin-2(1 H)-ones. Delicate Dependence on the Host Compound. *Chem. Commun.* **1992**, 1053–1054.

(23) Clayden, J. Atropisomers and near-atropisomers: achieving stereoselectivity by exploiting the conformational preferences of aromatic amides. *Chem. Commun.* **2004**, 127–135.

(24) Honda, A.; Waltz, K. M.; Carroll, P. J.; Walsh, P. J. Atropisomeric Amides: Achiral Ligands With Chiral Conformations. *Chirality* **2003**, *15*, 615–621.

(25) Ayitou, A. J.-L.; Ugrinov, A.; Sivaguru, J. 6pi-Photocyclization of O-tert-butylacrylanilides. N-substitution dictates the regiochemistry of cyclization. *Photochem. Photobiol. Sci.* **2009**, *8*, 751–754.

(26) Naito, T.; Tada, Y.; Ninomiya, I. Asymmetric Photocyclization of N-a,b-unsaturated Acrylanilides. *Heterocycles* **1984**, *22*, 237–240.

CHAPTER 4. REACTIVE SPIN DEPENDENT ENANTIOSPECIFIC PHOTOCYCLIZATION OF AXIALLY CHIRAL α-SUBSTITUTED ACRYLANILIDES[**]

4.1. Introduction

Phototransformations that originate from the excited state quite often involves breaking of bonds or formation of new bonds and/or migration of atom(s) or group of atoms are accompanied by major stereochemical changes within the resulting photo-product(s). In this picture, the role of excited spin states (singlet S_n or triplet T_n) dictating the stereochemistry of photochemical transformation are well documented in literature.[1-8] There are many elegant examples of reactions where reactive spin state S_1 or T_1 play significant roles in reactivities of substrates that influence the stereochemical outcome of the reaction.[4-6,9] Investigated photochemical transformations,[10-13] in this regard, have demonstrated that the regio- and diastereoselectivities in expected photoproduct(s) could be achieved in solution[14,15] and in organized assemblies.[16,17] Furthermore, the role of reactive spin states in photochemical reactions of interest leading to unique photoproduct(s) with varying enantioselectivies have been at the center of various distingished investigations.[10,11] One of the classical reports involves γ-hydrogen abstraction where transformation from the excited singlet spin state gives high enantiomeric excess whereas the triplet reactivity leads to racemic mixture of photoproducts.[10,11]

[**] The material in this chapter was co-authored by Anoklase J.-L. Ayitou (AJA) Dr. J. Sivaguru (JS). AJA in consultation with JS synthesized all compounds and performed all experiments detailed in this chapter. AJA and JS came up with the mechanistic rationale as well as the conclusion described in this chapter.

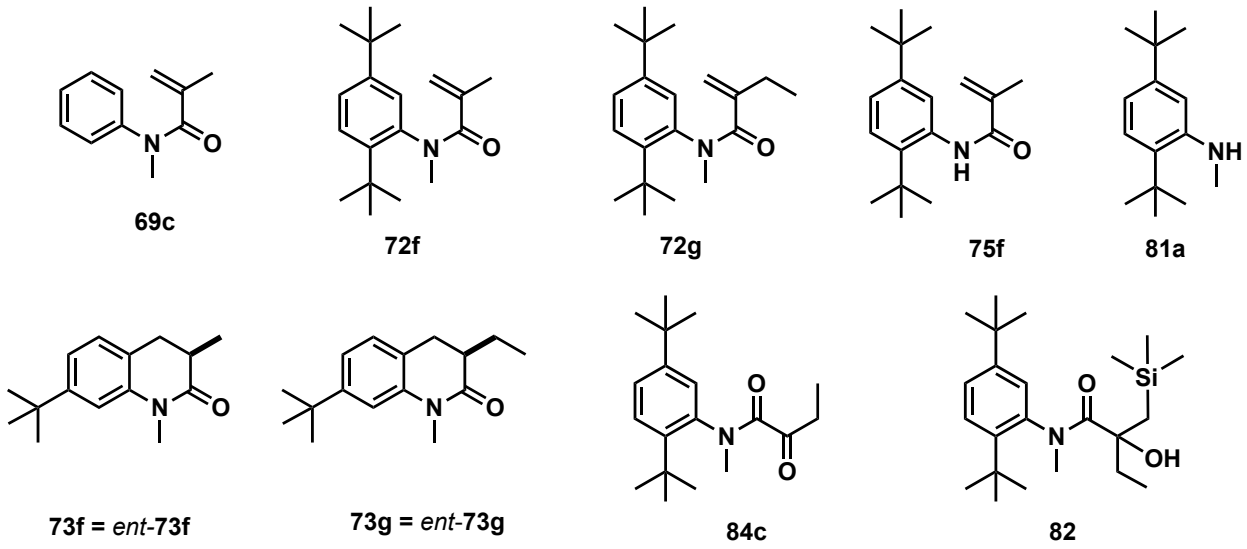

Chart 4.1: Acrylanilides molecular reactants **72f,g** and corresponding photoproduct(s).

4.2. Direct and Sensitized Irradiation of Compounds 72f,g

In chapter 3, we explained the concepts and the conditions under which the molecular reactants of interest would display axialy chirality *viz.* rotamers control due to restricted bond rotation that have been successfully employed for various chemical transformations.[18-21] We also demonstrated efficient chiral transfer from axially chiral α,β-unsaturated acrylanilides to the corresponding photoproduct(s) in solution.[22,23] In line with the previous investigation, we observed that under the same direct irradiation conditions, axially chiral acrylanilides lacking the β-subsituent (e.g. **72f**) yielded racemic mixture of the expected 3,4-dihydro-2-quinolin-2-one photoproduct. In the previous chaper (*cf.* chapter 2), we have detailed the role of the solvent employed during the irradiation on the yield of photoproduct (*cf.* chapter 2 Table 2.1). In this chapter, the photoreaction of **72f,g** was performed in solvents such as acetone (acting as both solvent and triplet sensitizer), trifluoroethanol (TFE) and methanol (MeOH), which influenced not only the reaction pathway but also the reactive spin-state (S_1 or T_1) of **73f,g** (Schemes 4.1 – 4.3).

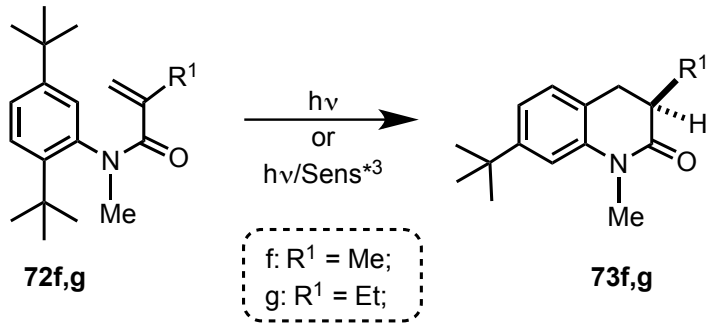

Scheme 4.1: 6π-Photocyclization of **72f,g.**

Irradiation of axially chiral α-substituted acrylanilides **72f,g** showed that the substrate(s) reactive spin state (S_1 or T_1) plays a significant role during the photocyclization leading to 3,4-dihydro-2-quinolin-2-one photoproduct **73f,g**, where the singlet reactivity (via direct irradiation in TFE or MeOH) led to a racemic product, while the corresponding triplet reactivity (via triplet sensitization in acetone) led to enantiomeric ratios (e.r. values) >95:05 in the 3,4-dihydro-2-quinolin-2-one photoproduct **73f,g** at ambient conditions (Table 4.1 Schemes 4.1 – 4.3).

Table 4.1: Enantiospecific 6π-photocyclization of **72f,g** under direct and triplet sensitized irradiations. [a-e]

Entry	Substrate [b]	Solvent	*T* (°C)	Sens. [c]	Mode	*e.r.* **73**[e]
1.	(+)**72f**	Acetone	20	Acetone	Triplet	96:04 (A)
2.		Acetone	27	Acetone	Triplet	90:10 (A)
3.		TFE	27	-	Singlet	Racemic
4.		MeOH	27	-	Singlet	Racemic
5.	(-)**72f**	Acetone	20	Acetone	Triplet	97:03 (B)
6.		Acetone	27	Acetone	Triplet	90:10 (B)
7.		TFE	27	-	Singlet	Racemic
8.		MeOH	27	-	Singlet	Racemic
9.	(+)**72g**	Acetone	20	Acetone	Triplet	97:03 (A)
10.		Acetone	27	Acetone	Triplet	90:10 (A)
11.		TFE	27	-	Singlet	Racemic
12.	(-)**72g**	Acetone	20	Acetone	Triplet	96:04 (B)
13.		Acetone	27	Acetone	Triplet	90:10 (B)
14.		TFE	27	-	Singlet	Racemic

[a] Reported values are an average of a minimum of 3 runs with ±5% error. TFE: trifluoroethanol. [b] (+) and (-) represent the signs of their CD signals at 285 nm in methylcyclohexane (MCH). [c] Sensitizer's triplet energies (E_T) for acetone: ~79 kcal•mol^{-1}. [d] Conversion calculated by ^{1}H NMR using α,α'-dichloro-*p*-xylene as internal standard. [e] A and B refers to the first and second peak that elutes out on the HPLC chiral stationary phase separation for a given pair of enantiomers.

4.3. Discussion

Observation of table 4.1 revealed that triplet sensitized irradiation of **72f,g** in acetone (serving as both solvent and sensitizer) produced chirally enriched **73f,g** with e.r. values >95:05 at ambient conditions. Optical pure isomers of **72f,g** gave enantiomers of **73f-b** respectivelly. For example, triplet sensitized irradiation of (-)-**72g** and (+)-**72g** in acetone gave e.r. values >95:05 of **73g** and *ent*-**73g** respectively (Scheme 4.2; HPLC insert). However, the irradiation of (-)-**72g** or (+)-**72g** in MeOH or TFE under identical conditions gave racemic mixture of **73f,g**. The role of the reaction temperature was also observed, as there was a minimal decrease in the e.r. values from >95:05 to 90:10 upon increasing the temperature from 20 °C to 27 °C. This is likely due to slow racemization [(slow N-C(Aryl) bond rotation] in the reactant **72f,g** at elevated temperatures.

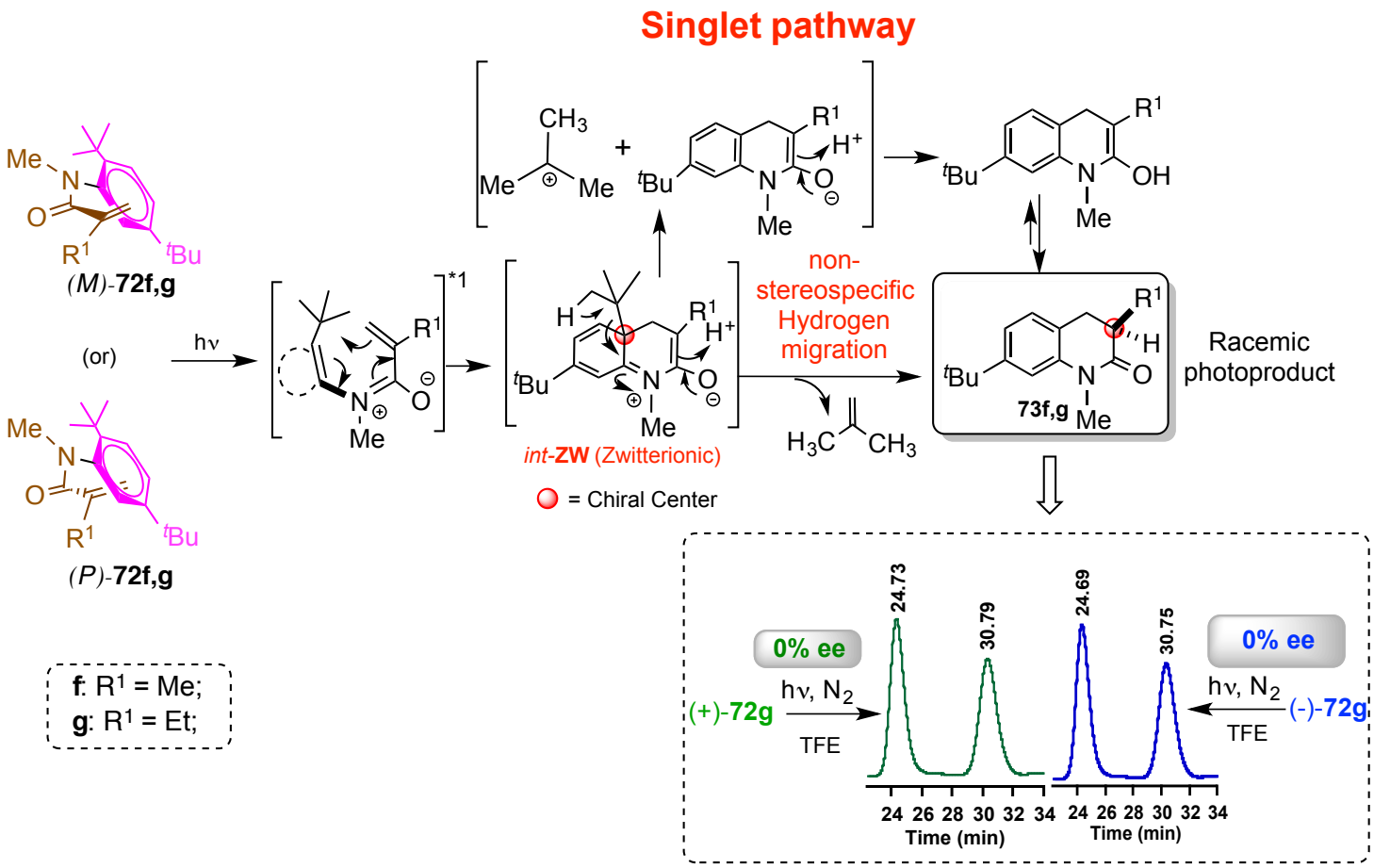

Scheme 4.2: Photocyclization of axially chiral α-substituted acrylanilides **72f,g** under direct irradiation (singlet).

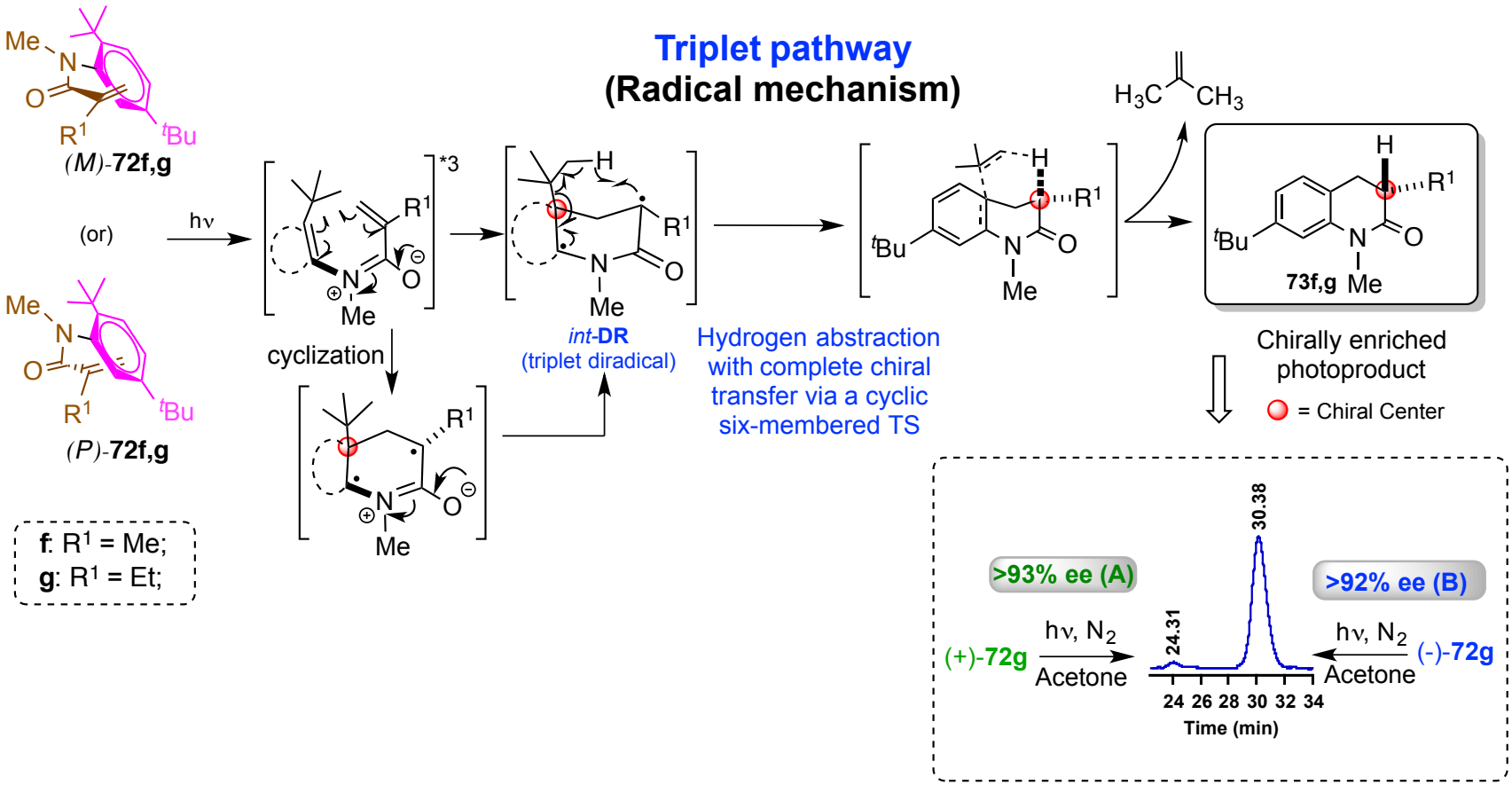

Scheme 4.3: Photocyclization of axially chiral α-substituted acrylanilides **72f,g** under sensitized irradiation conditions (triplet).

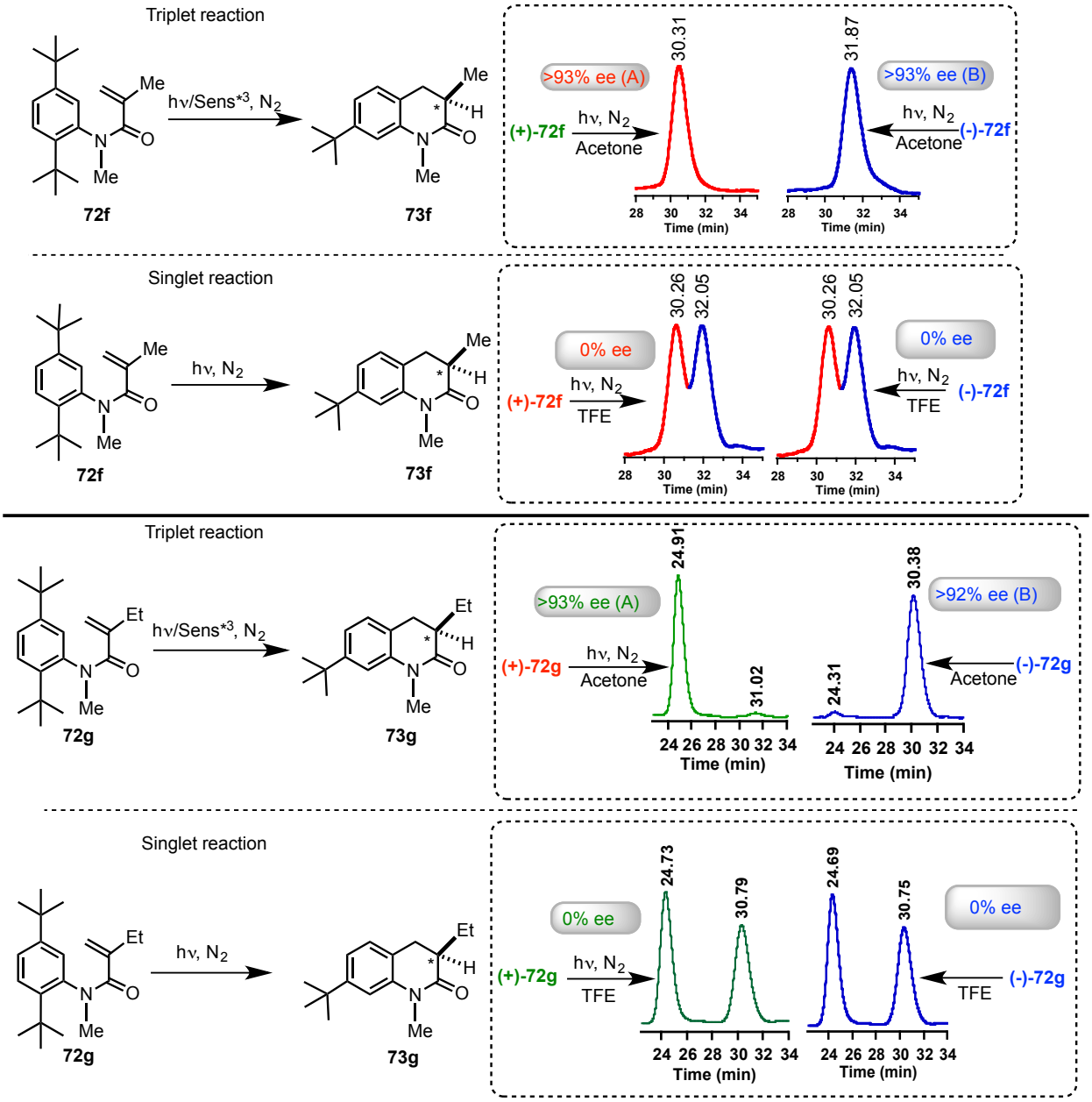

Scheme 4.4: Analysis of photoproducts **73f,g** by HPLC on chiral stationary phase.

4.4. Photophysical Investigations to Ascertain the Role of Reactive Spin States

Photophysical studies with **72f,g** showed fluorescence emission at room temperature in methylcyclohexane (MCH) (Figure 4.2-A). Interestingly, the emission (in MCH, ethanol and acetonitrile) maxima shift bathochromically upon changing the solvent from non-polar MCH to polar solvents like ethanol or acetonitrile (Figure 4.1-B). This bathochromic shift is consistent with other methacrylanlides derivatives reported in literature.[24] Furthermore, the phosphorescence profile for

72f,g was observed (Figure 4.2-A) at 77 K in MCH glass with a triplet energy (E_T) of ~77.3 kcal•mol^{-1} and a lifetime (τ_p) of ~1.58 sec as illustrated in figure 4.3. These results clearly indicate that the lowest excited singlet and triplet state for **72f,g** has a π-π^* configuration.

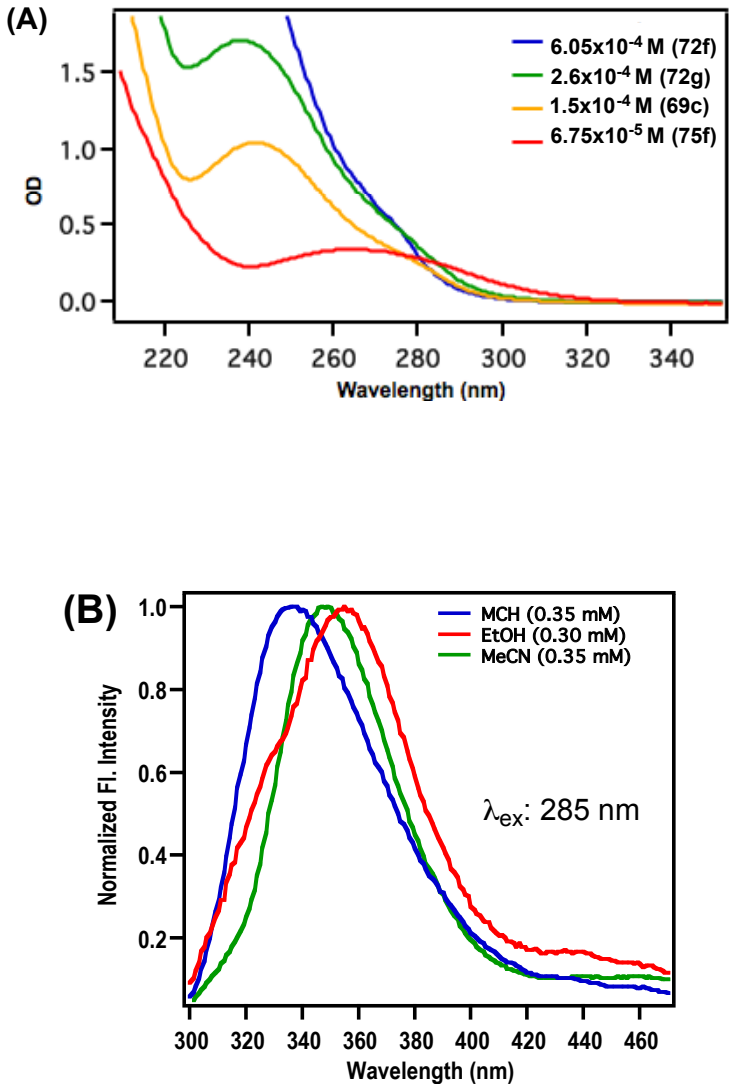

Figure 4.1: (A) UV-VIS absorption spectra of **69c, 72f,g** and **75f** in methylcyclohexane (MCH): [**72f**] = 6.05 x 10^{-4} M; [**72g**] = 2.6 x 10^{-4} M; [**69c**] = 1.5 x 10^{-4} M; and [**75f**] = 6.75 x 10^{-4} M. (B) Room temperature fluorescence spectra of **72f** in non-polar methylcyclohexane (MCH) and polar solvents acetonitrile (MeCN) and ethanol (EtOH).

Note: The following parameters were maintained during acquisition: Excitation slit-width = 1 nm; emission slit-width = 5.0 nm; Integration time = 0.1 sec; Wavelength increment = 1 nm.

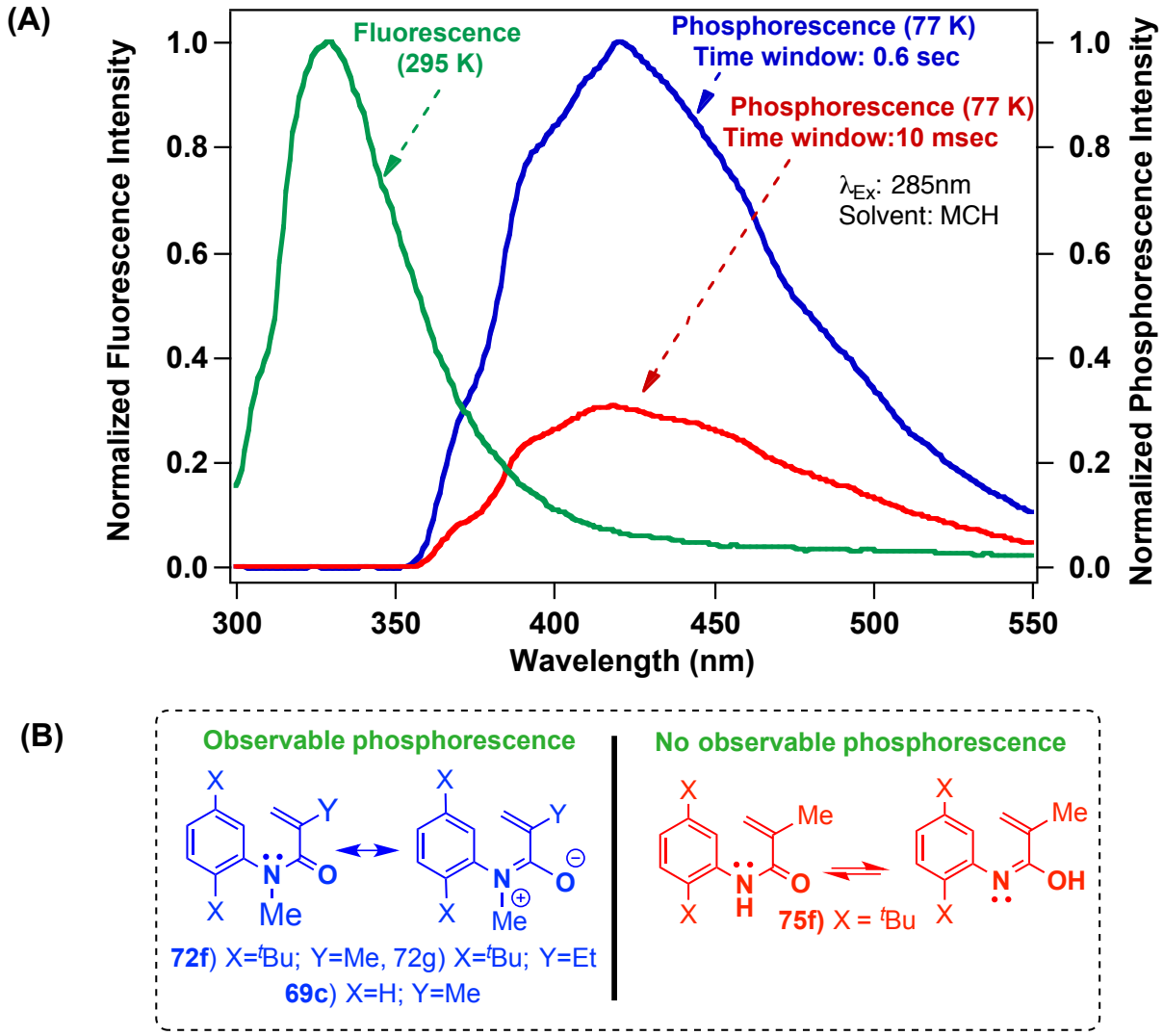

Figure 4.2: (A) Fluorescence (Green at 298 K) and Phosphorescence (Red, Blue at 77 K) of **72f** in methylcyclohexane (MCH). (B) Role of N-Methyl and N-H substitution.

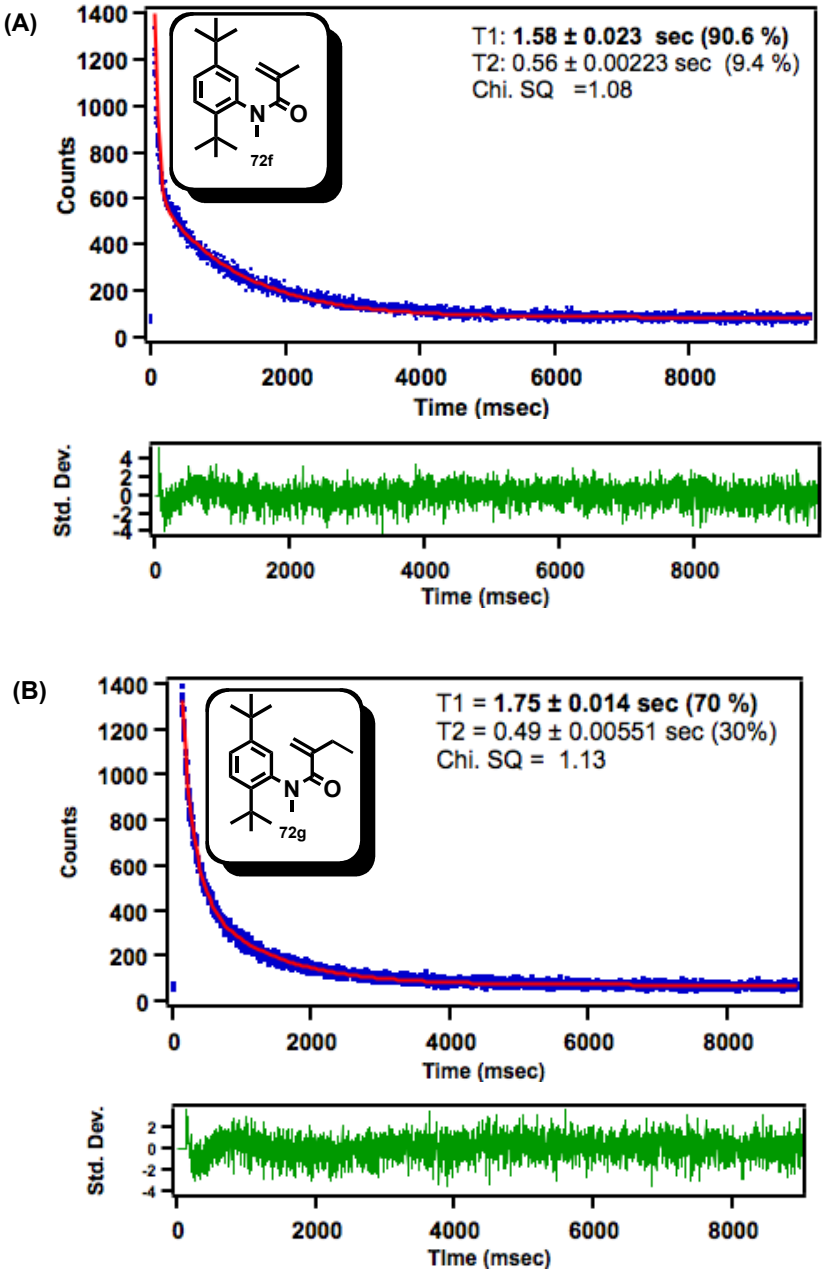

Figure 4.3: Phosphorescence decay/lifetime profiles recorded at 77 K in Methylcyclohexane (MCH): [**72f**] = 6.05 x 10^{-4} M; [**72g**] = 2.6 x 10^{-4} M. λ_{Exc} = 285 nm using a PhosLamp with a trigger pulse delay of 1%. The emission was monitored at 415 nm for **72f** and at 430 nm for **72g**. The following parameters were maintained during acquisition: Excitation slit-width = 8 nm; Emission slit-width = 8 nm Time (phosphorescence) range = 11 sec, number of sweeps = 100

Ogata and co-workers[24,25] have suggested a zwitterionic intermediate originating from the singlet π-π* (S_1 π-π*) excited-state for the 6π-photocyclization of achiral acrylanilide (N-H substituted derivative without *ortho-tert*-butyl group on the phenyl ring) (*cf.* experimental section 4.9). Furthermore, it has been

established as a paradigm[26] for photochemical reactions in recent years that a zwitterionic intermediate is likely expected for photoreactions from a π-π^* singlet excited-state [$S_1(\pi$-$\pi^*)$] whereas a diradicaloid intermediate is likely formed from the corresponding π-π^* triplet excited-state [$T_1(\pi$-$\pi^*)$].[26] In the case of **72f,g**, it is likely that the restricted N-C(Aryl) bond rotation not only induces axial chirality to the system but also enables us to access the triplet state (as phosphorescence emission was observed) at 77 K in MCH glass. We may conjecture this based on the observation in the case of achiral N-H acrylanilide (*viz., ortho-tert*-butyl N-H acrylanilide **75f**), where no phosphorescence emission was observed at 77 K: both achiral and axially chiral N-methyl derivatives (molecularly chiral **72f,g** and achiral **69c**) display observable phosphorescence at 77 K in MCH glass (Figure 4.4).

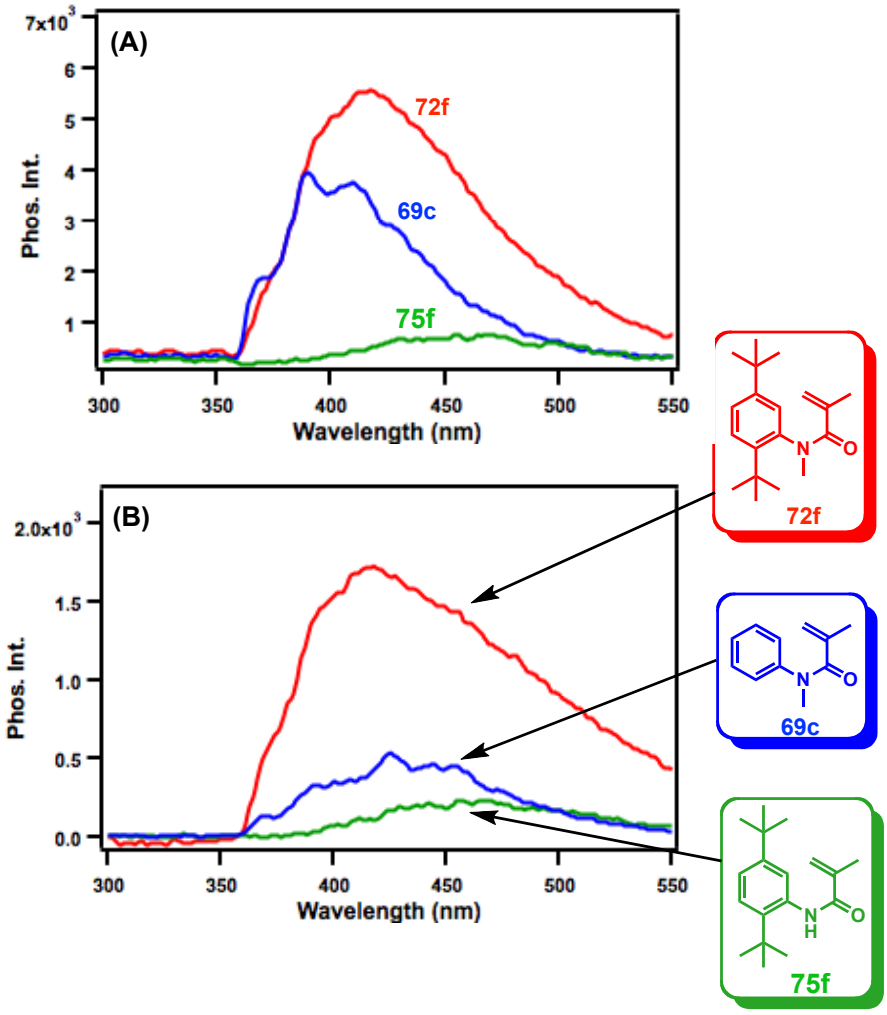

Figure 4.4: Phosphorescence emission of [**72f**] = 6.05 x 10^{-4} M; [**69c**] = 1.5 x 10^{-4} M and [**75f**] = 6.75 x 10^{-4} M in MCH at 77 K.

Note 1: *There is no emission from* ***75f*** *(N-H derivative). Only N-Me derivatives* ***69c*** *and* ***72f,g*** *showed observable phosphorescence.*

Note 2: The substrates of interest were excited at 285 nm using a pulsed Xenon lamp and monitoring the emission from 330-550 nm. The following parameters were employed during acquisition: Excitation slit-width 5 nm, emission slit-width = 8 nm. (A) Time window 1 (acquisition from 0.3 to 0.9 sec) time per flash = 1 sec; flash per count = 10, delay time = 300 msec; wavelength increments = 1 nm; sample window = 600 msec. (B) Time window 2 (acquisition from 10 to 20 msec) time per flash = 61 msec; flash per count = 10, delay time = 10 msec, wavelength increment = 1 nm; sample window = 10 msec.

From the above spectroscopic observations (Figure 4.4), it appeared that the presence of N-Me substituent is crucial to access the triplet-excited manifold. For acrylanilides, it is important to mention that enolization in the case of N-H acrylanilides (as in **75f**; Figure 4.2-B) enables them to cyclize only from the singlet-excited state, as it is oriented optimally for 6π-photocyclization. On the other hand, N-methyl derivatives (as in derivatives **69c** and **72f,g**; Figure 4.2-B), the nitrogen lone pair is part of the 6π-backbone leading to photoreactivity from the π-π* excited state. From the phosphorescence study (Figures 4.2-A and 4.3), the triplet π-π* state of **72f,g** lies at ~77 kcal•mol^{-1}; consequently, triplet energy transfer from acetone (E_T ~79 kcal•mol^{-1})[28] is quite likely. The involvement of triplet spin-state *viz.* T_1(π-π*) in the reaction pathway was ascertained by carrying out the reaction under O_2 saturated conditions that resulted in <5% conversion as illustrated in the previous chapter (chapter 2 section 2.2.5).[27] Thus 6π-photocyclization of **72f,g** could possibly occur from either the singlet (S_1) or the triplet (T_1) spin-state depending on the reaction conditions.[28]

Based on the mechanistic rationale detailed in the previous chapter,[27] it can be ascertained that the 6π-photocyclization of **72f,g** occured at the *ortho* carbon *via* the zwitterionic intermediate "*int*-**ZW**" [likely from the S_1(π-π*) excited state upon direct irradiation] (Scheme 4.2) followed by a non-stereo-specific hydrogen migration with the eventual loss of the *o*-*tert*-butyl substituent. It has been postulated that the cyclization from the S_1(π-π*) excited state goes *via* a zwitterionic intermediate (*int*-**ZW**).[24,25,29,30] The present study revealed that triplet sensitized irradiation of **72f,g** led to photocyclization from T_1(π-π*) excited state likely to a diradical (triplet diradical) intermediate "*int*-**DR**" (Scheme 4.3). In this scenario, the triplet diradical "*int*-**DR**" could subsequently abstract a hydrogen atom from *o*-*tert*-butyl substituent leading to 3,4-dihydroquinolin-2-one photoproduct **73f,g** with eventual loss of the *tert*-butyl group (as isobutene molecule). The high enantiomeric ratio (Table 4.1) in the photoproduct **73f,g** under sensitized irradiation points out to a stereospecific hydrogen abstraction via a cyclic six membered transition (Scheme 4.3) state from the triplet diradical intermediate (*int*-**DR**). It is important to highlight that the photocyclization from excited spin state S_1(π-π*) or T_1 (π-π*) not only leads to the same photoproduct *via* two different reactive intermediates and/or transition states species, but also determines the e.r. values in the photoproduct(s). Our hypothesis of

spin dependent selectivity revealed that high selectivity could be observed from the triplet spin state compound and racemic photoproduct from the corresponding singlet spin state. This observation is counter intuitive as singlet reactivity generally is highly stereospecific due to short lifetimes compared to triplet reactivity that has a longer lifetime.

4.5. Photophysical Method – Instrumentation and Technical Settings

Spectrophotometric solvents (Sigma-Aldrich®) were used where ever necessary unless or otherwise mentioned. UV quality fluorimeter cells (with range until 190 nm) were purchased from Luzchem®. Absorbance measurements were performed using a Shimadzu® UV-2501PC UV-Vis spectrophotometer. Emission spectra were recorded on a Horiba Scientific® Fluorolog 3 spectrometer (FL3-22) equipped with double-grating monochromators, dual lamp housing containing a 450-watt CW xenon lamp and a UV xenon flash lamp (FL-1040), Fluorohub/MCA/MCS electronics and R928 PMT detector. Emission and excitation spectra were corrected in all the cases for source intensity (lamp and grating) and emission spectral response (detector and grating) by standard instrument correction provided in the instrument software. Fluorescence (steady state) and phosphorescence (77 K) emission spectra were processed by FluorEssence® software. Phosphorescence lifetime measurements were performed using DAS6® V6.4 software. The goodness-of-fit was assessed by minimizing the reduced chi squared function and further judged by the symmetrical distribution of the residuals.

4.6. Monitoring Photoreaction and Conversion by ^{1}H NMR Spectroscopy

HPLC purified acrylanilide **72f,g** (3.5 mg) was dissolved in 1 ml of acetone-d_6 in a NMR tube. The sample was exposed to UV-VIS light (medium pressure Hg lamp) and the reaction was followed by ^{1}H NMR spectroscopy. Represented below is the reaction profile at different intervals for **72g**. The N-Methyl group or the *tert*-butyl group was used as NMR handle to follow the reaction.

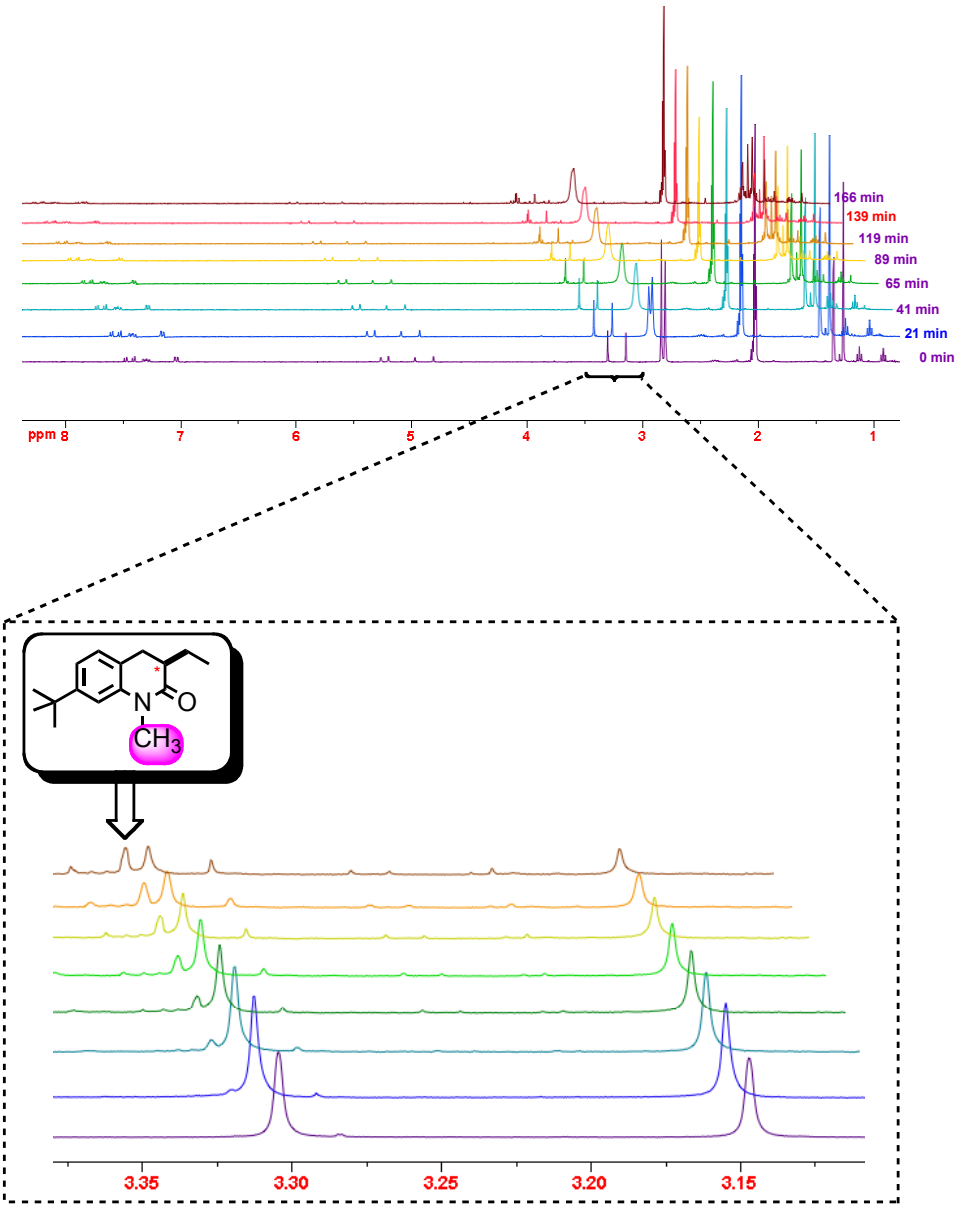

Figure 4.5: Monitoring the photoreaction of **72g** by ^{1}H NMR (400 MHz, $CDCl_3$, δ ppm) spectroscopy.

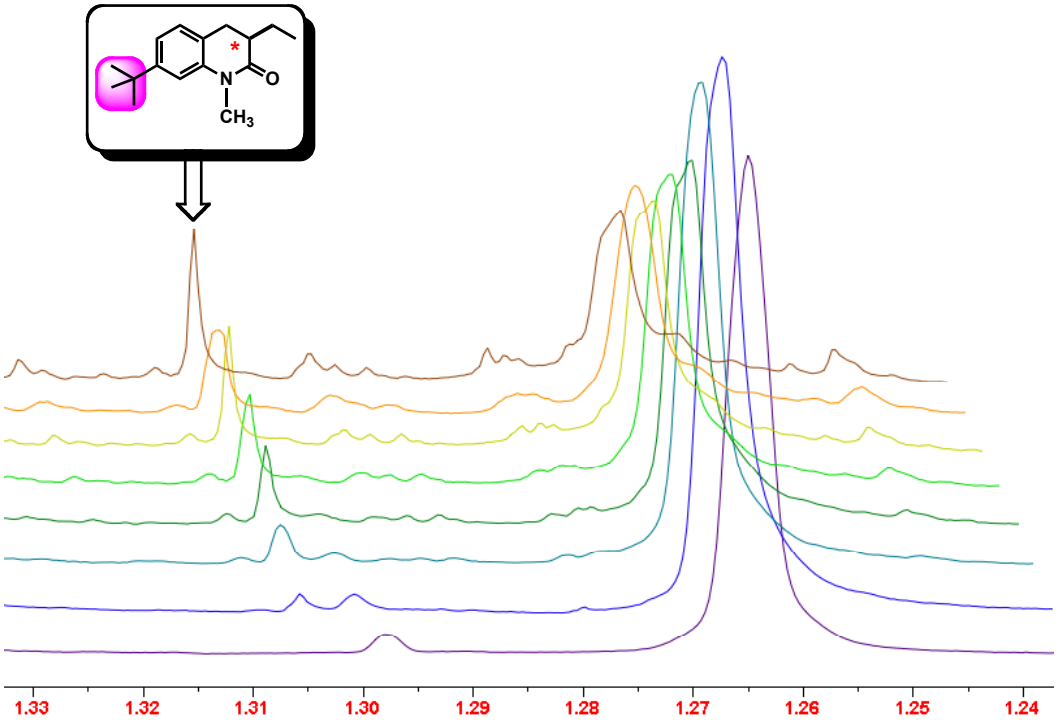

Figure 4.6: Expanded region: ^{1}H NMR (400 MHz, $CDCl_3$, δ ppm) spectra during the photoreaction of **72g**.

4.7. Absolute Photoreaction Conversion by ^{1}H NMR Spectroscopy

HPLC purified **72f,g** (3.5 mg) was dissolved in 1 ml of acetone or TFE in a 13 mm Pyrex test tube. The samples were exposed to UV-VIS light (medium pressure Hg lamp) for specified time intervals; each sample was then analyzed by ^{1}H NMR spectroscopy with α,α'-dichloro-*p*-xylene, as an internal standard.

The number of moles of analyte (product or starting material) in the NMR aliquot is given by the following equation:[31,32]

$$mol_a = mol_i \times \left(\frac{Integral(analyte)}{Integral(Int.Std.)} \right) \times \frac{N_i}{N_a}$$ **Equation 4.1**

Where N_a and N_i are the number of nuclei giving rise to the relevant analyte and standard signals respectively.[31,32]

For triplet sensitization, the conversion was ~30% for **72f,g** irradiation (90 min for **72f** and 150 min for **72g**) in acetone. Higher irradiation time resulted in higher conversion but the reactivity slowed due to decomposition products from the solvent acetone. The mass balance was >88% for all irradiations.

For singlet irradiation (in TFE or methanol) of **72f,g** the conversion was 10-20% for 6 h irradiations with >90% mass balance. Higher irradiation time led to an increase in conversion as well as formation of side-products.

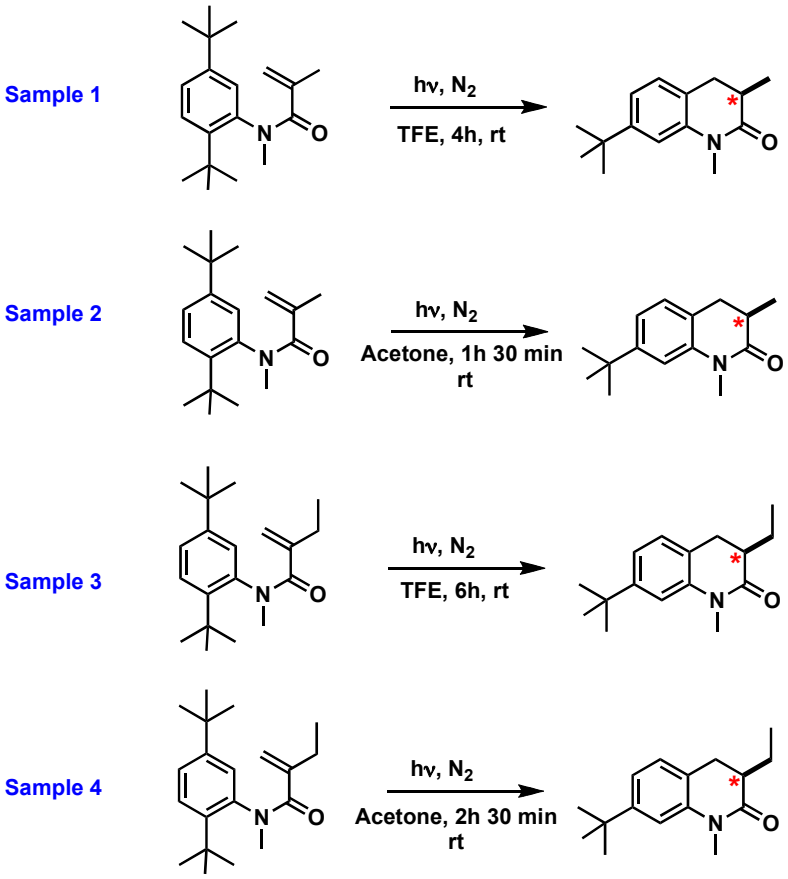

Scheme 4.5: Monitoring the photoreaction conversion by ^{1}H NMR (400 MHz, $CDCl_3$, δ ppm) spectroscopy.

The representative ^{1}H NMR traces of reactions (samples 1-4) are given below.

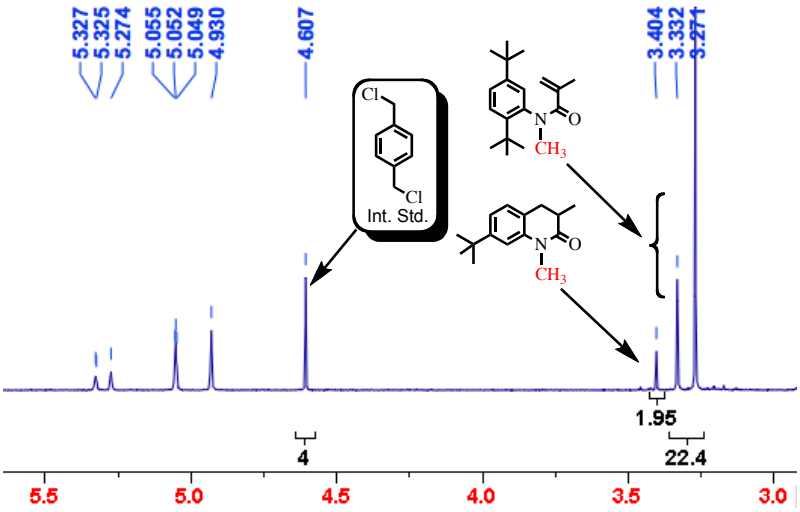

Figure 4.7: Sample 1: Photoreaction of **72f** in TFE for 4h. Expanded region for ^{1}H NMR (400 MHz, $CDCl_3$, δ ppm) spectroscopy of the crude sample from 3.0 to 5.5 ppm.

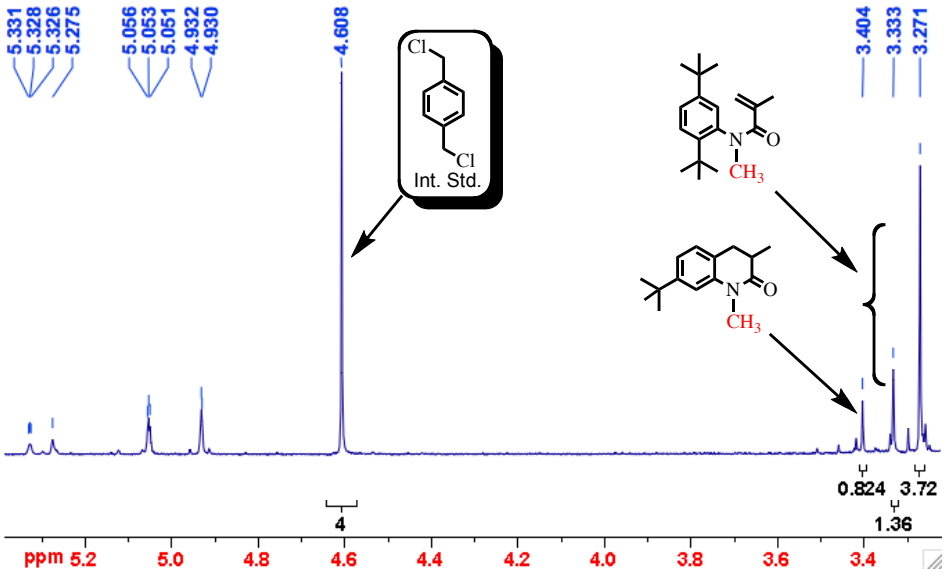

Figure 4.8: Sample 2: Photoreaction of **72f** in acetone for 1h 30 min. Expanded region for ^{1}H NMR (400 MHz, $CDCl_3$, δ ppm) spectroscopy of the crude sample from 3.0 to 5.5 ppm.

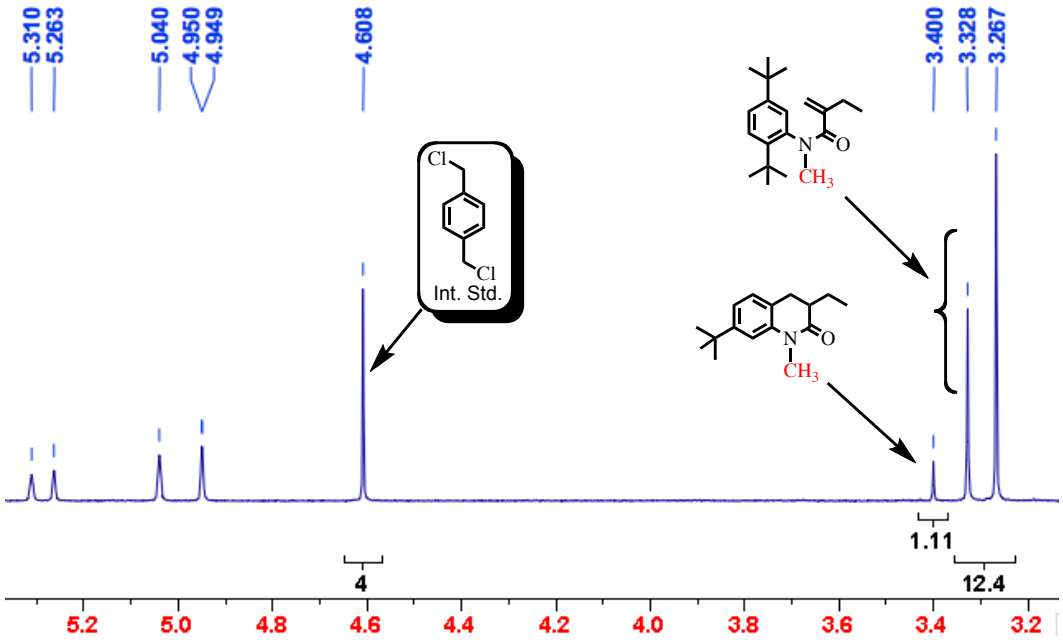

Figure 4.9: Sample 3: Photoreaction of **72g** in TFE for 6h. Expanded region for ^{1}H NMR (400 MHz, $CDCl_3$, δ ppm) spectroscopy of the crude sample from 3.0 to 5.5 ppm.

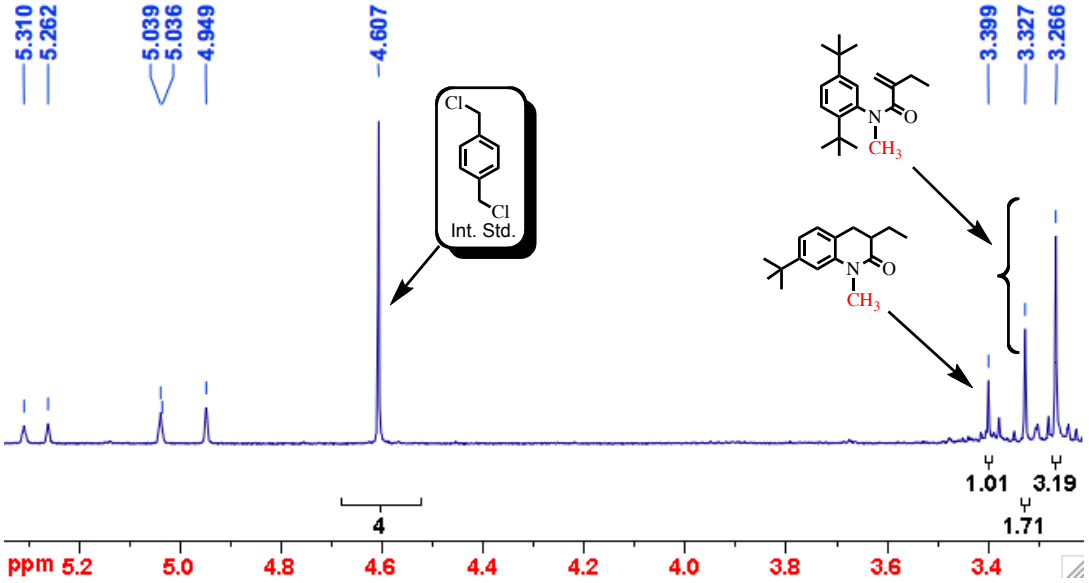

Figure 4.10: Sample 4: Photoreaction of **72g** in Acetone for 6h. Expanded region for ^{1}H NMR (400 MHz, $CDCl_3$, δ ppm) spectroscopy of the crude sample from 3.0 to 5.5 ppm.

4.8. Summary and Outlook

Exploiting axial chirality to achieve high stereoselectivities during 6π-photocyclization of acrylanilides has been detailed in the previous chapter. The current strategy revealed the role of reactive spin states in influencing the product(s) enantioselectivities during photo-transformation of α-substituted atropisomeric acrylanilides. Atropisomeric (axially chiral) acrylanilides offer rich and divergent photoreactivity that helps us to better understand mechanisms of light induced stereospecific transformations. The current investigation with α-substituted acrylanilides highlighted the role of reactive spin states in determining enantiomeric excess leading to the same photoproduct from bot singlet and triplet spin states. In the next chapter, we will highlight how the enantioselectivity of expected photoproduct could be improved by manipulating the phase of the reaction medium instead of playing with the reactive spin states of the photo-substrates.

4.9. Experimental Section

4.9.1. General method

All commercially obtained reagents/solvents were used as received; chemicals were purchased from Alfa Aesar®, Sigma – Aldrich®, Across®, TCI® America, Mallinckrodt®, and Oakwood Products®, and were used as received without further purification. Unless stated otherwise, reactions were conducted in oven-dried glassware under an atmosphere of nitrogen using anhydrous solvents; Photoreactions were performed under N_2 or O_2 atmosphere. ^{1}H NMR and ^{13}C NMR spectra were recorded on Varian 400 MHz (100 MHz) and on 500 MHz (125 MHz) spectrometers. Data for ^{1}H NMR spectra are reported relative to residual deuterated solvent signals, and are reported as follows: chemical shift (δ ppm), multiplicity, coupling constant (Hz) and integration. Coupling constants (*J*) were reported in hertz (Hz). Standard abbreviations indicating multiplicity were used as follows: b (broad), s (singlet), d (doublet), t (triplet), q (quartet), m (multiplet), virt (virtual), and ABq (AB quartet). Data for ^{13}C NMR spectra are reported relative to residual deuterated solvent signals. High-resolution mass spectra (HRMS) were recorded on a Bruker – Daltronics® BioTof mass spectrometer in positive (ESI+) ion mode. HPLC analyses were performed on Waters® HPLC equipped with 2525 pump. Waters® 2767 sample manager was used for automated sample injection. All HPLC injections were

monitored using a Waters® 2487 dual wavelength absorbance detector at 254 nm and 270 nm. Analytical and semi-preparative injections were perfomed on chiral stationary phase using Regis® PIRKLE COVALENT (R,R) WHELK–O1 10/100 FEC columns‡. Masslynx software version 4.1 was used to analyse/process the HPLC injections. Igor Pro® Software version 4.0 was used to generate graphics of the chromatographic data. When necessary, the reactants and photoproducts were purified by chromatography: CombiFlash and/or on silica gel (Sorbent Technologies®, silica gel standard grade: Porosity 60 Å, Particle size: 230 x 400 mesh, Surface area: 500 – 600 m^2/g, Bulk density: 0.4 g/mL, pH range: 6.5 – 7.5). The Retention Factor (R*f*) values were recorded using a 20 % EtOAc-Hexanes as mobile phase (unless indicated) on SORBENT TECHNOLOGIES® Silica Gel TLC plates (200 mm thickness w/ UV_{254}). Optical activity values were recorded on JASCO® DIP – 370 digital polarimeter. CD spectra were recorded on JASCO® - 710 digital CD spectrometer.

‡ Regis® PIRKLE COVALENT (R,R) WHELK–O1 10/100 FEC columns: 25cm X 4.6 mm column for analytical injections, and 25 cm x 10.0 mm for semi-preparative injections.

4.9.2. Photophysical method

Spectrophotometric solvents (Sigma-Aldrich®) were used where ever necessary unless or otherwise mentioned. UV quality fluorimeter cells (with range until 190 nm) were purchased from Luzchem. Absorbance measurements were performed using a Shimadzu® UV-2501PC UV-Vis spectrophotometer. Emission spectra were recorded on a Horiba Scientific® Fluorolog 3 spectrometer (FL3-22) equipped with double-grating monochromators, dual lamp housing containing a 450-watt CW xenon lamp and a UV xenon flash lamp (FL-1040), Fluorohub/MCA/MCS electronics and R928 PMT detector. Emission and excitation spectra were corrected in all the cases for source intensity (lamp and grating) and emission spectral response (detector and grating) by standard instrument correction provided in the instrument software. Fluorescence (steady state) and phosphorescence (77 K) emission spectra were processed by FluorEssence® software. Phosphorescence lifetime measurements were performed using DAS6® V6.4 software. The goodness-of-fit was assessed by minimizing the reduced chi squared function and further judged by the symmetrical distribution of the residuals.

4.9.3. Procedure for synthesis and characterization of 81a, 69c and 72f

Cf. chapter 2 sections 2.4.2 and chapter 3 section 3.6.7

4.9.4. Synthesis and characterization of 82 and 84c

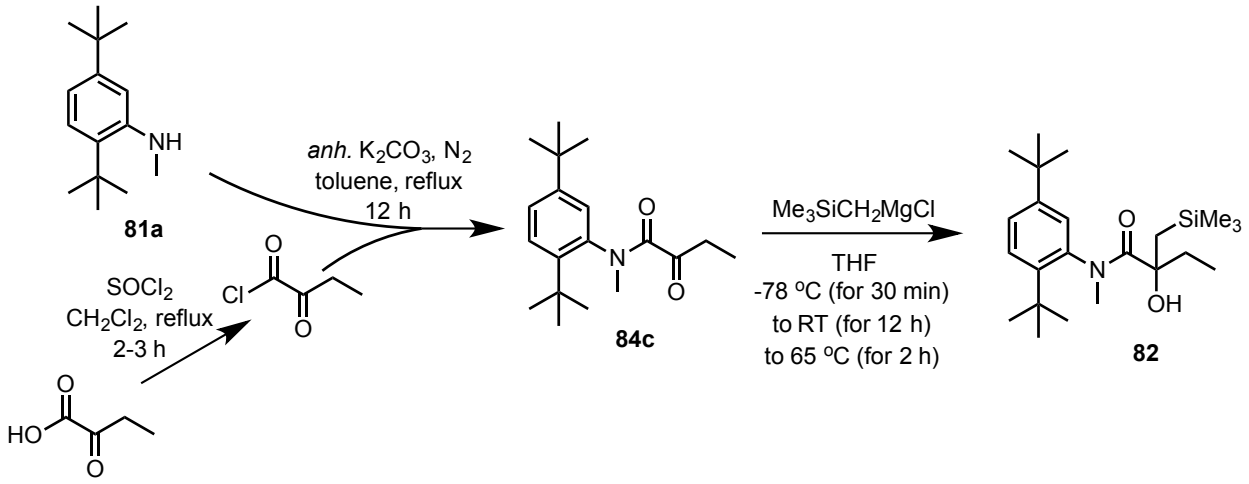

Scheme 4.6: Synthesis of **82** and **84c**.

α-Oxoamide **84c:** 2-ketobutyric acid (2.09 g) was dissolved in 10 mL of dry chloroform (CH_2Cl_2); while the solution was kept under N_2 atmosphere, thionyl chloride (excess) was slowly added to the flask, and the new mixture was allowed to reflux for 2 to3 h. The excess of CH_2Cl_2 and thionyl chloride was removed by roto-evaporation, and the acyl chloride was used in the subsequent step without further purification.

In a clean round-bottom flask, 2,5-di-*tert*-butyl-*N*-methylaniline **81a** (3.35 g) was dissolved in 20 mL of toluene and *anh.* K_2CO_3 (1.5 equiv.) was added to the solution. The new mixture was vigorously stirred and kept under N_2 atmosphere. 2-ketobutyric acid chloride (prepared as detailed above) was slowly added to the aniline reaction flask. The new mixture was allowed to reflux overnight (~12 h). The expected oxoamide **84c** was isolated from the reaction mixture and was purified by chromatography using CombiFlash®.

Purification conditions: (CombiFlash®) 24 g silica, flow rate: 25 mL/min. Mobile phase: 16 % EtOAc – Hexanes. The overall yield: ~ 95 %.

^{1}H NMR (500 MHz, $CDCl_3$, δ ppm) 7.5 – 6.85 (Ar, 3H, major and minor conformers), 3.26 & 3.25 (s, 3 H, major and minor conformers), 2.97 – 2.82 (m, 1H, major and minor conformers), 2.58 – 2.48 (m, 1H, major and minor conformers), 1.43 & 1.41 (s, 9 H, major and minor conformers), 1.29 & 1.28 (s, 9 H, major and minor conformers), 1.27 & 0.92 (t, *J* = 6 Hz, 3H, major and minor conformers).

^{13}C NMR (125 MHz, $CDCl_3$, δ ppm) δ for both *s-cis* and *s-trans* conformers (major and minor conformers) are observed for all carbon atoms.

HRMS-ESI ($[M + Na]^+$): Calculated: 326.2091; Observed: 326.2089; ∆m = 0.88 ppm.

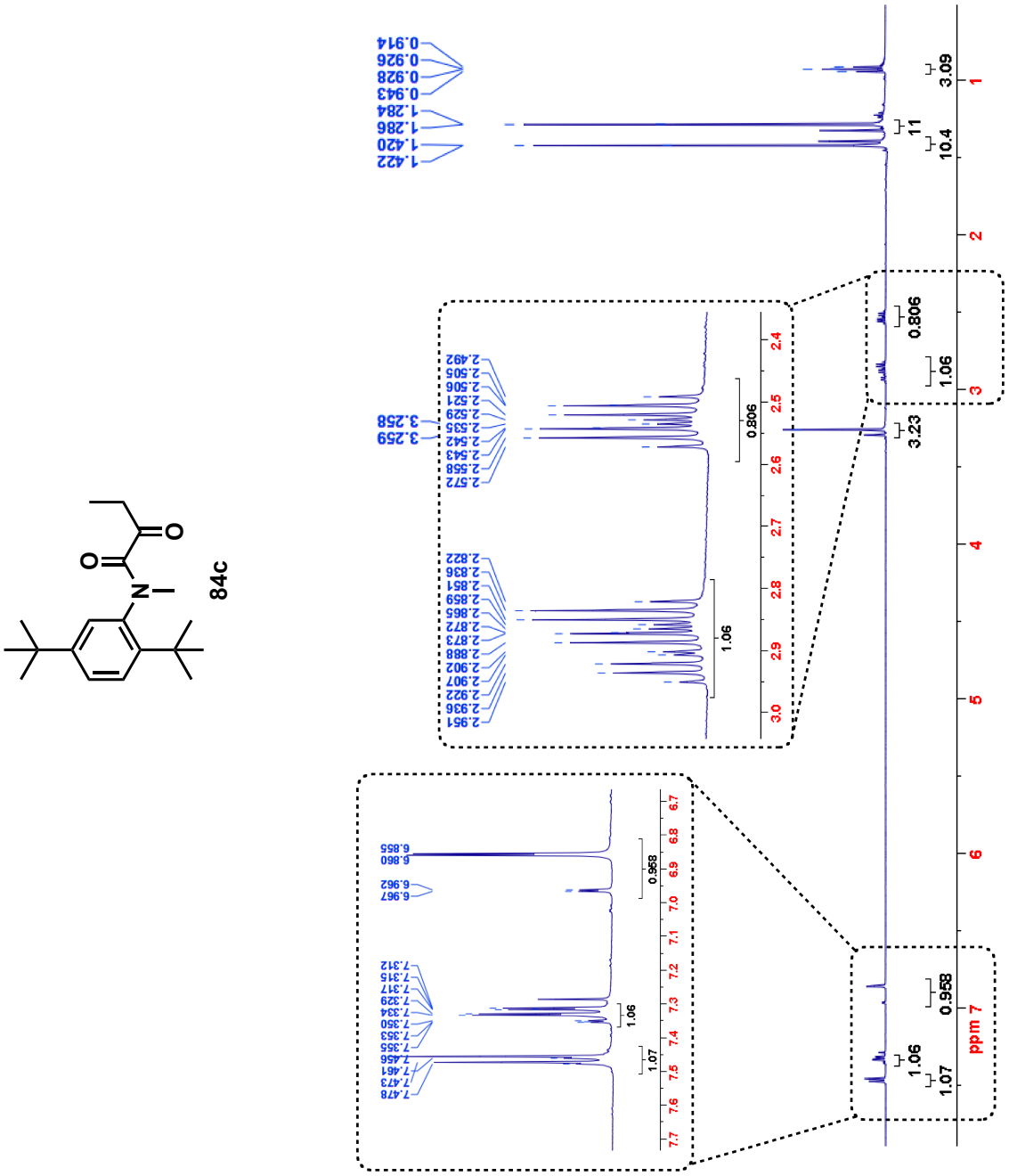

Figure 4.11: ^{1}H NMR (500 MHz, $CDCl_3$, δ ppm) spectrum for oxoamide **84c.**

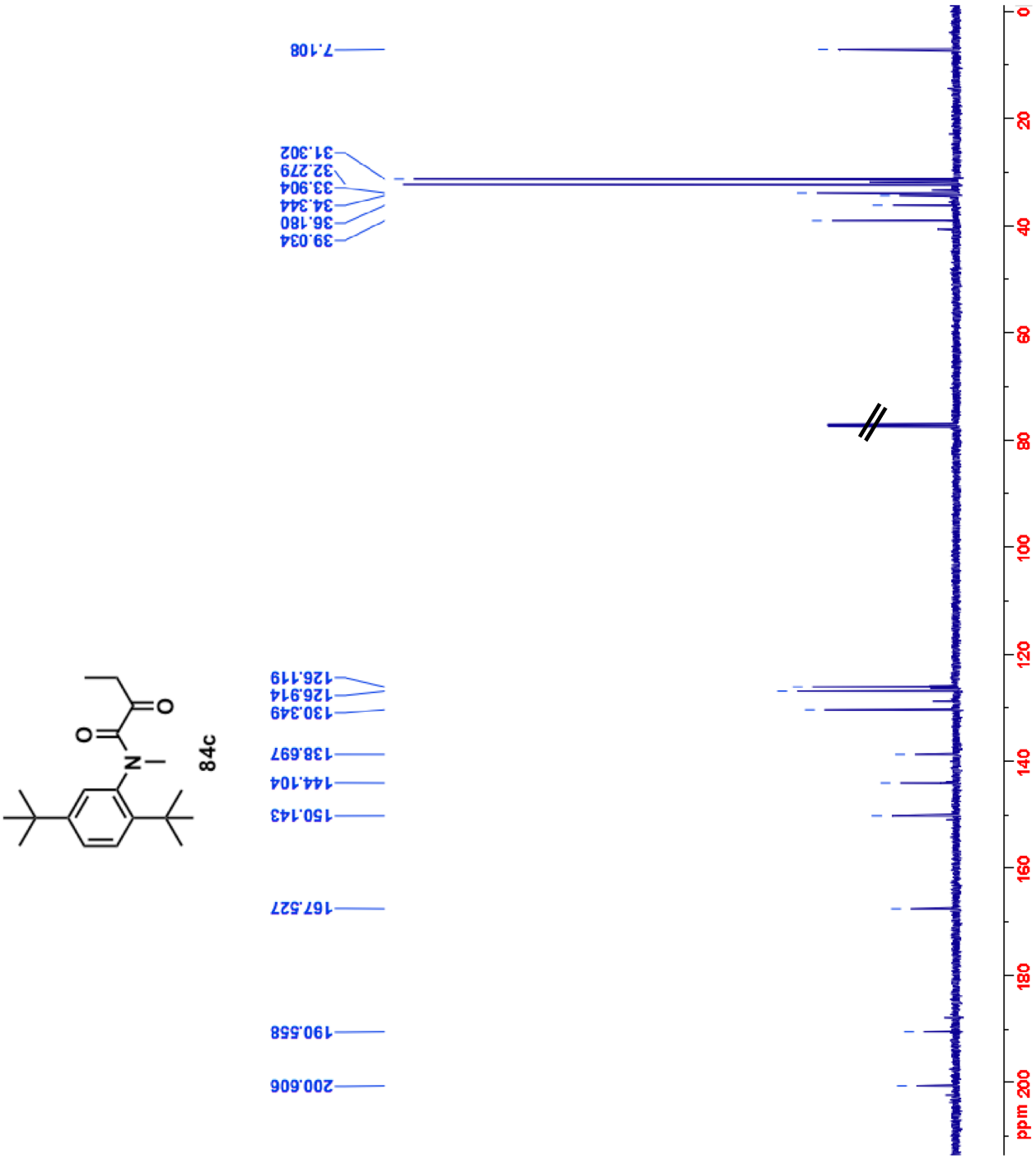

Figure 4.12: ^{13}C NMR (125 MHz, $CDCl_3$, δ ppm) spectrum for oxoamide **84c.**

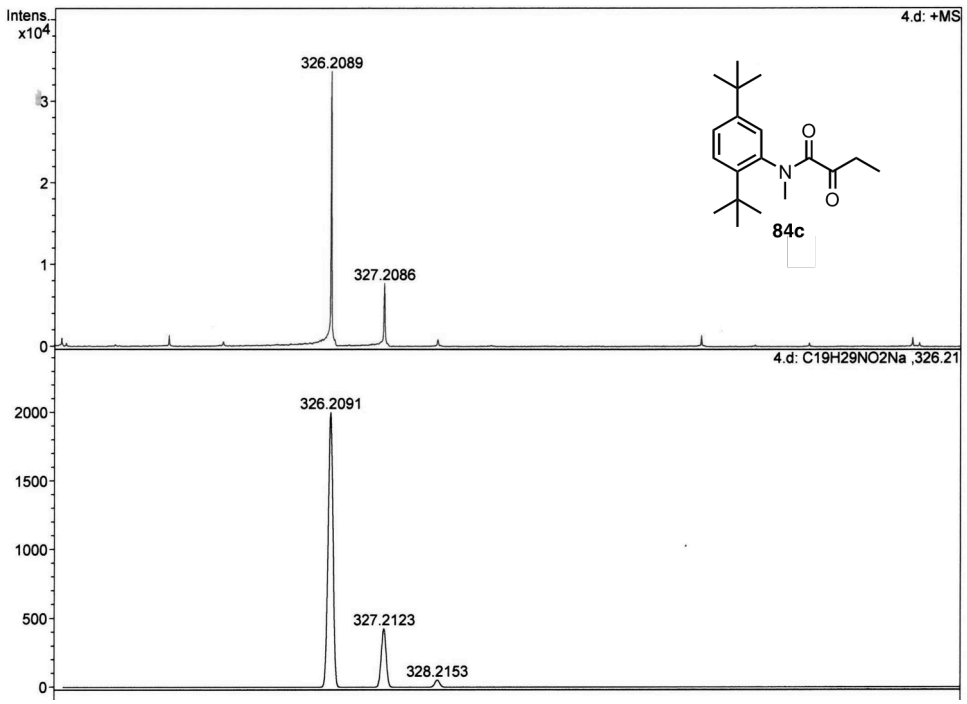

Figure 4.13: HRMS for oxoamide **84c**.

Silanol **82**: Silanol **82** was prepared according to a procedure reported in literature.[33] Oxoamide **6** was dissolved in a minimum of dry tetrahydrofuran (THF); the solution was cooled to -78 ^{o}C and kept at that temperature for 20 min. Me_3SiCH_2MgCl (5 equiv.) was added to the reaction flask; The new mixture was stirred for 30 min at -78 ^{o}C, then for 12 h at room temperature, and finally for 2 h at 65 ^{o}C. Silanol **82** was not isolated, but was observed by HRMS analysis of the reaction mixture, which showed complete consumption of the starting oxoamide **84c.** A major molecular ion peak at 414.2816 ($M + Na^+$) was observed indicating the formation of the expected compound **82**. Silanol **82** was used in the subsequent step without further purification.

HRMS-ESI ([M + Na]$^+$): Calculated: 414.2799; Observed: 414.2816; Δm = 4 ppm

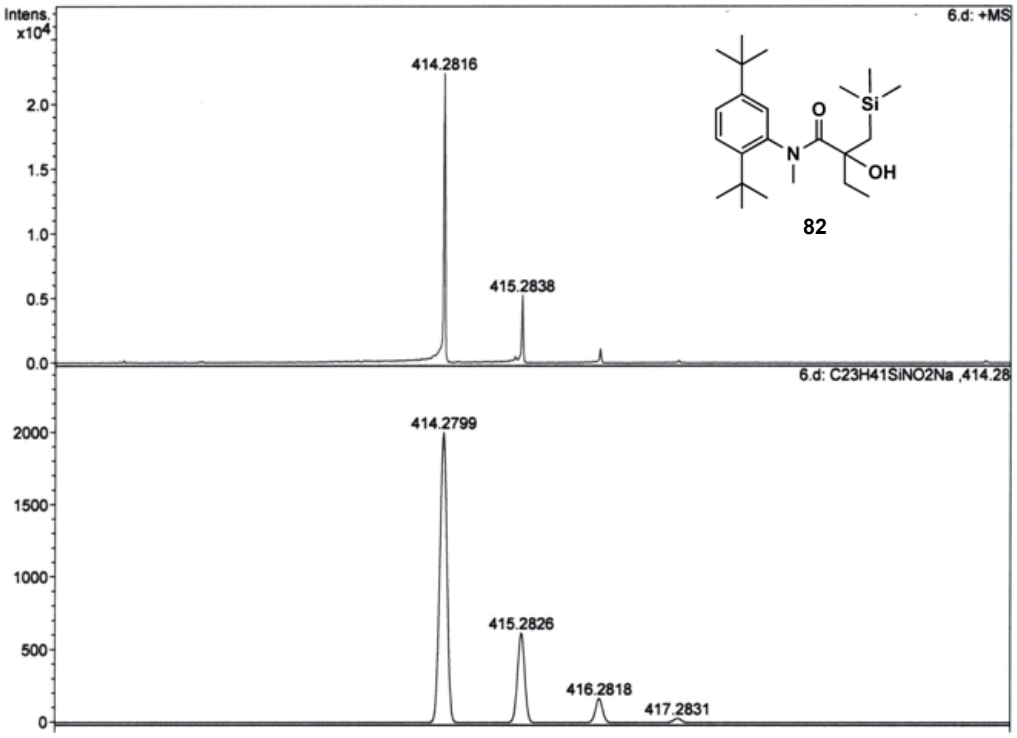

Figure 4.14: HRMS for silanol **82.**

4.9.5. Procedure for synthesis and characterization of acrylanilide 72g

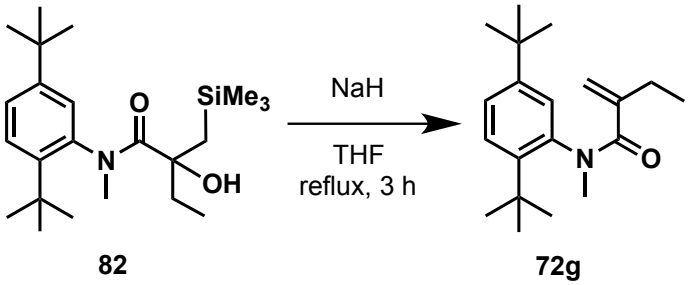

Scheme 4.7: Synthesis of acrylanilide **72g.**

Silanol **82** was dissolved in a minimum (~ 20 mL) of THF and NaH (excess) was added to the solution. The mixture was constantly stirred and allowed to reflux for 3 h. After, the reaction mixture was slowly quenched with deionized (DI) water (while the flask was immersed into an ice bath). The insoluble by-product was filtered on celite. The recovered filtrate was washed with DI water, and the expected

crude **72g** was extracted with ethyl acetate (EtOAc) (3 x 20 mL). The combined organic fractions was concentrated and purified by CombiFlash®.

Purification conditions: Silica gel (24 g) at 18 % EtOAc – Hexanes with a flow rate of 25 mL/min.

^{1}H NMR (400 MHz, $CDCl_3$, δ ppm) 7.43–6.86 (Ar, 3H, contribution from major and minor conformers), 5.05 – 4.85 & 5.3 – 5.15 (2H, major and minor conformers, olefinic H), 3.28 & 3.22 (s, 3H, major and minor conformers, *N*-CH_3), 2.28 – 1.96 & 2.54 – 2.32 (m, 2H, major and minor conformers, α-CH_2), 1.35 & 1.34(s, 9H, minor and major conformers, ^{t}Bu), 1.27 & 1.24 (s, 9H, minor and major conformers, ^{t}Bu), 1.16 & 0.93 (t, *J* = 7.2 Hz, 3H, major and minor conformers, α-CH_2-CH_3).

HRMS-ESI ([M + Na]$^+$): Calculated: 324.2298; Observed: 324.2285; Δm = 4 ppm.

HPLC analysis conditions: Column: (R,R) WHELK–O1; Abs. detector: 254 nm and 270 nm**;** mobile phase: Hexanes:IPA = 98:2; Flow rate: 1 mL/min**.**

Retention time (min): **Peak A:** ~ 36.75**; Peak B:** ~ 45.47

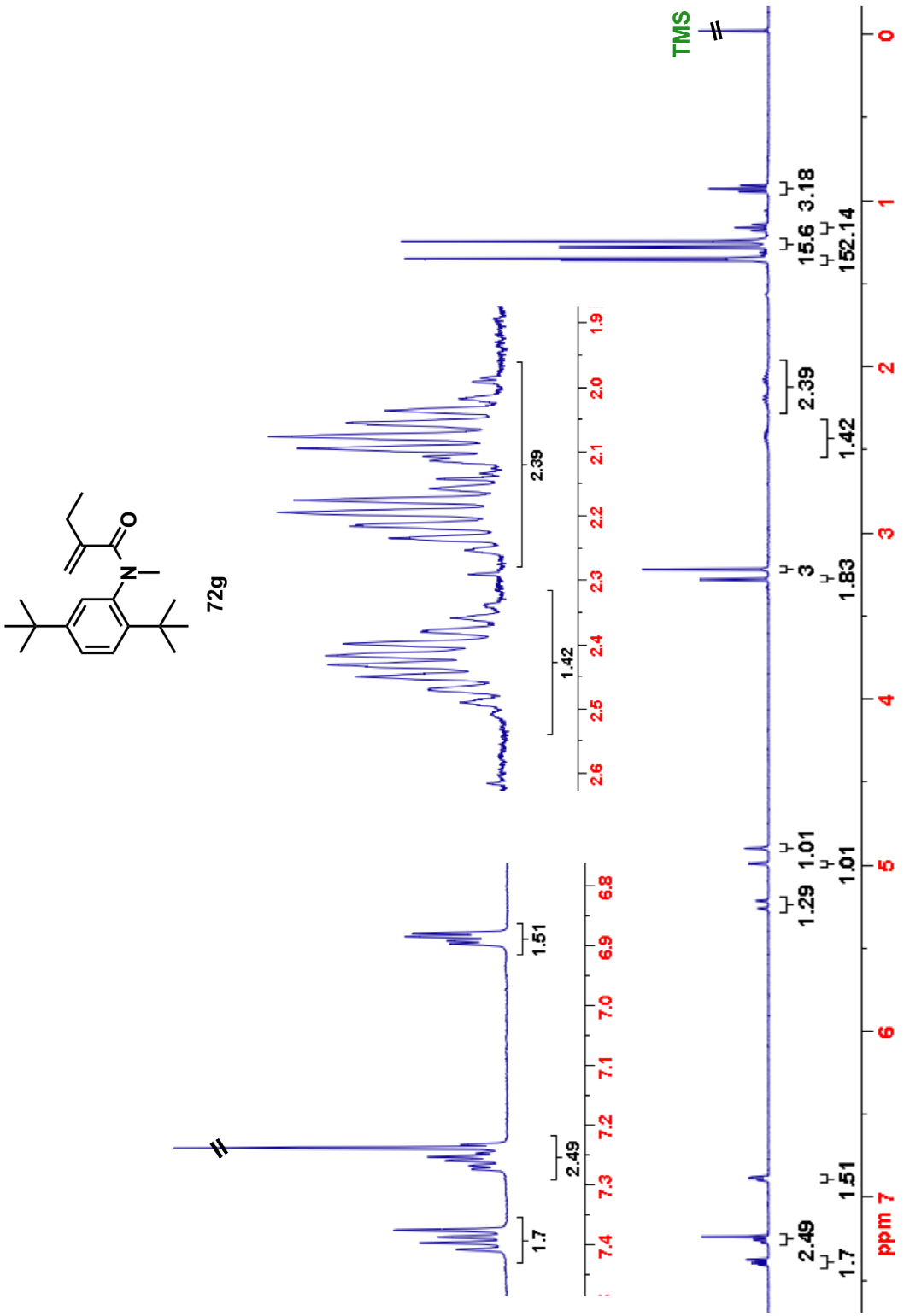

Figure 4.15: ^{1}H NMR (400 MHz, $CDCl_3$, δ ppm) of acrylanilide **72g.**

^{13}C NMR (100 MHz, $CDCl_3$, δ ppm) δ for both *s-cis* and *s-trans* conformers (major and minor conformers) are observed for all carbon atoms.

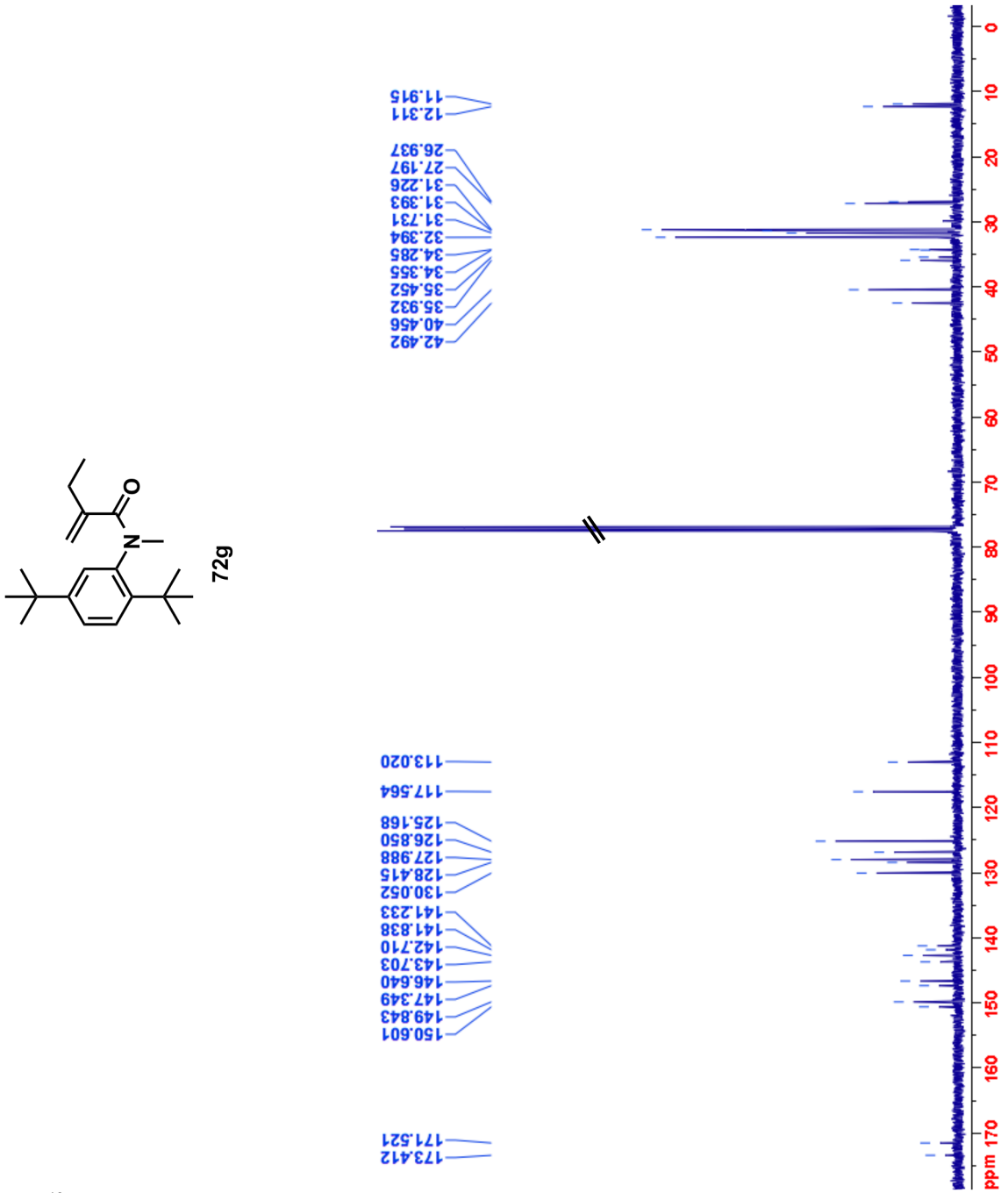

Figure 4.16: ^{13}C NMR (100 MHz, $CDCl_3$, δ ppm) of acrylanilide **72g.**

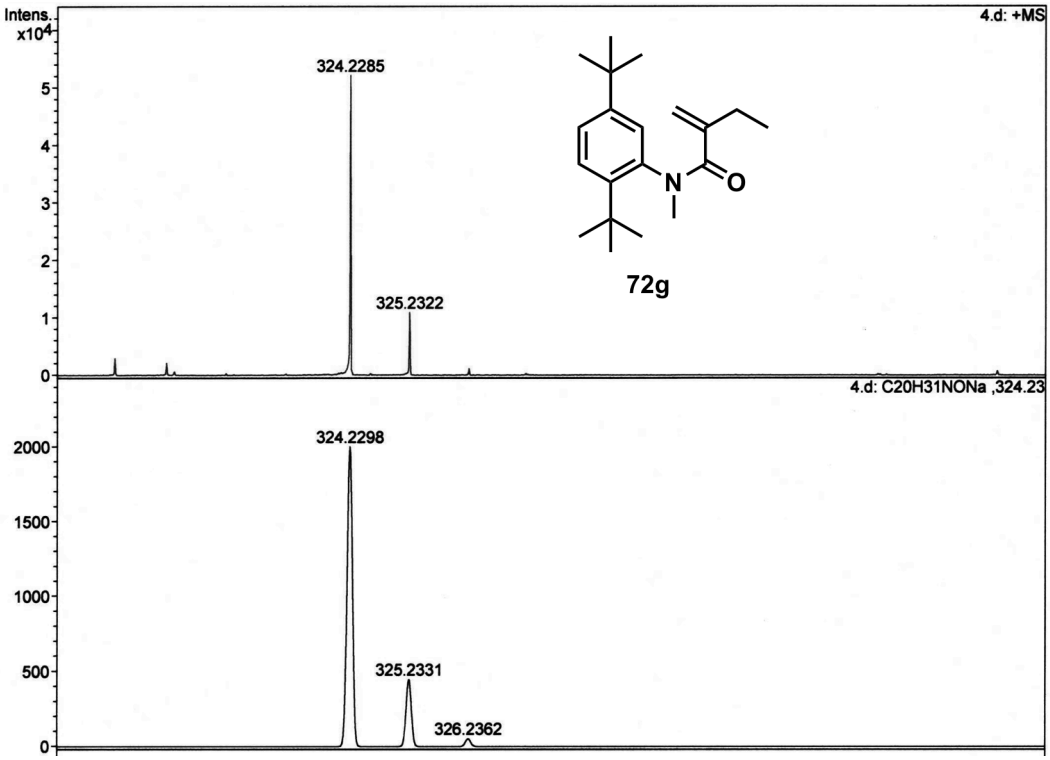

Figure 4.17: HRMS for acrylanilide **72g.**

4.9.6. Procedure for synthesis and characterization of acrylanilide 75f

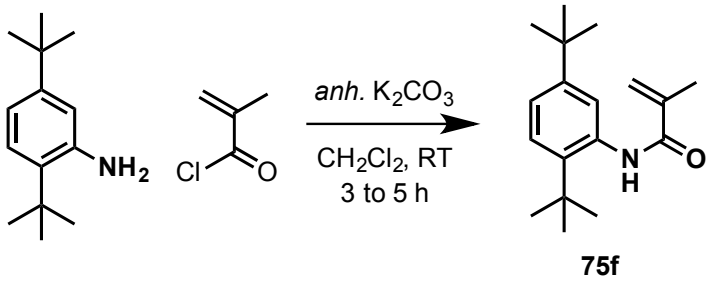

75f

Scheme 4.8: Synthesis of acrylanilide **75f.**

.

Acrylanilide **75f** was prepared using procedures reported in literature.[19,24,34,35] In a typical reaction, commercially available 2,5-di-*tert*-butylaniline (1 equiv.) was dissolved in 20 mL of CH_2Cl_2. The aniline solution was then stirred and purged with N_2; *anh.* K_2CO_3 (1.5 equiv.) and methacryloyl chloride (1.5 equiv.) were respectively and slowly added to the solution with continuous stirring. The new solution was allowed to react at room temperature for 3 – 5 h. After, the reaction was quenched with DI water, and

the crude expected product **75f** was extracted from the aqueous fraction with chloroform (3 x 20 mL). The organic fraction was concentrated by roto-evaporation; and **75f** was purified by recrystallization in *n*-pentane.

^{1}H NMR (500 MHz, $CDCl_3$, δ ppm) 7.80 (s, 1H), 7.63 – 7.62 (b s, N-H), 7.36 – 7.33 (d, 1H), 7.21 – 7.18 (dd, 1H), 5.88 (s, 1H), 5.51 (s, 1H), 2.13 (s, 3H), 1.44 (s, 9H), 1.35 (s, 9H)

^{13}C NMR [125 MHz, DMSO (Temp. = 45 ^{o}C), δ ppm] 167.9, 149.3, 144.4, 136.3, 128.9, 127.1, 124.4, 120.3, 35.1, 34.5, 31.7, 31.6, 19.4, 19.4

(**Note**: To observe the amide carbonyl resonance, the solvent was changed from $CDCl_3$ to DMSO-d_6 and the NMR was recorded at 45 ^{o}C).

HRMS-ESI ([M + Na]$^{+}$): Calculated: 296.1985; Observed: 296.1972; Δm = 4.3 ppm.

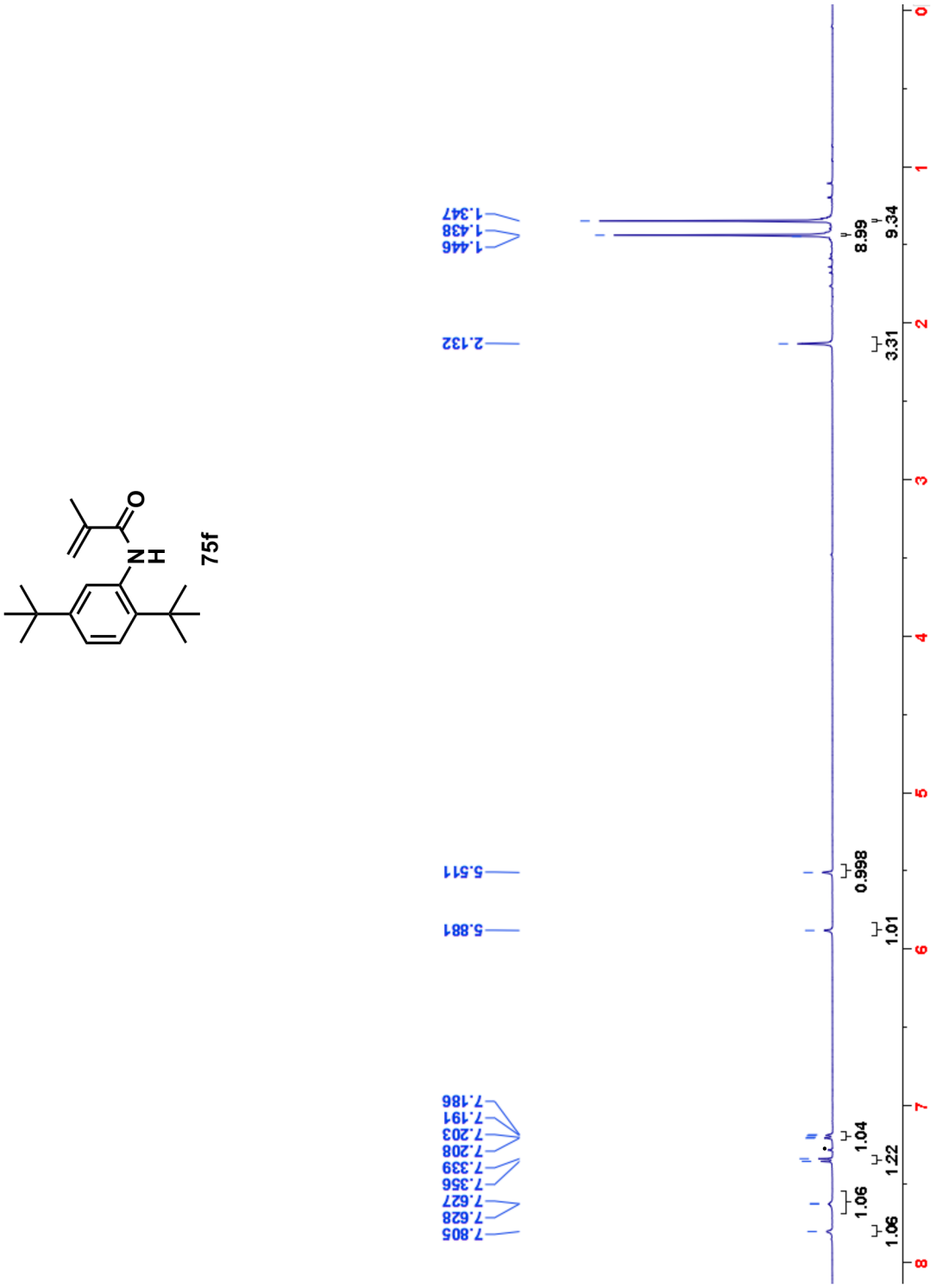

(*=Solvent)

Figure 4.18: ^{1}H NMR (500 MHz, $CDCl_3$, δ ppm) spectrum for acrylanilide **75f.**

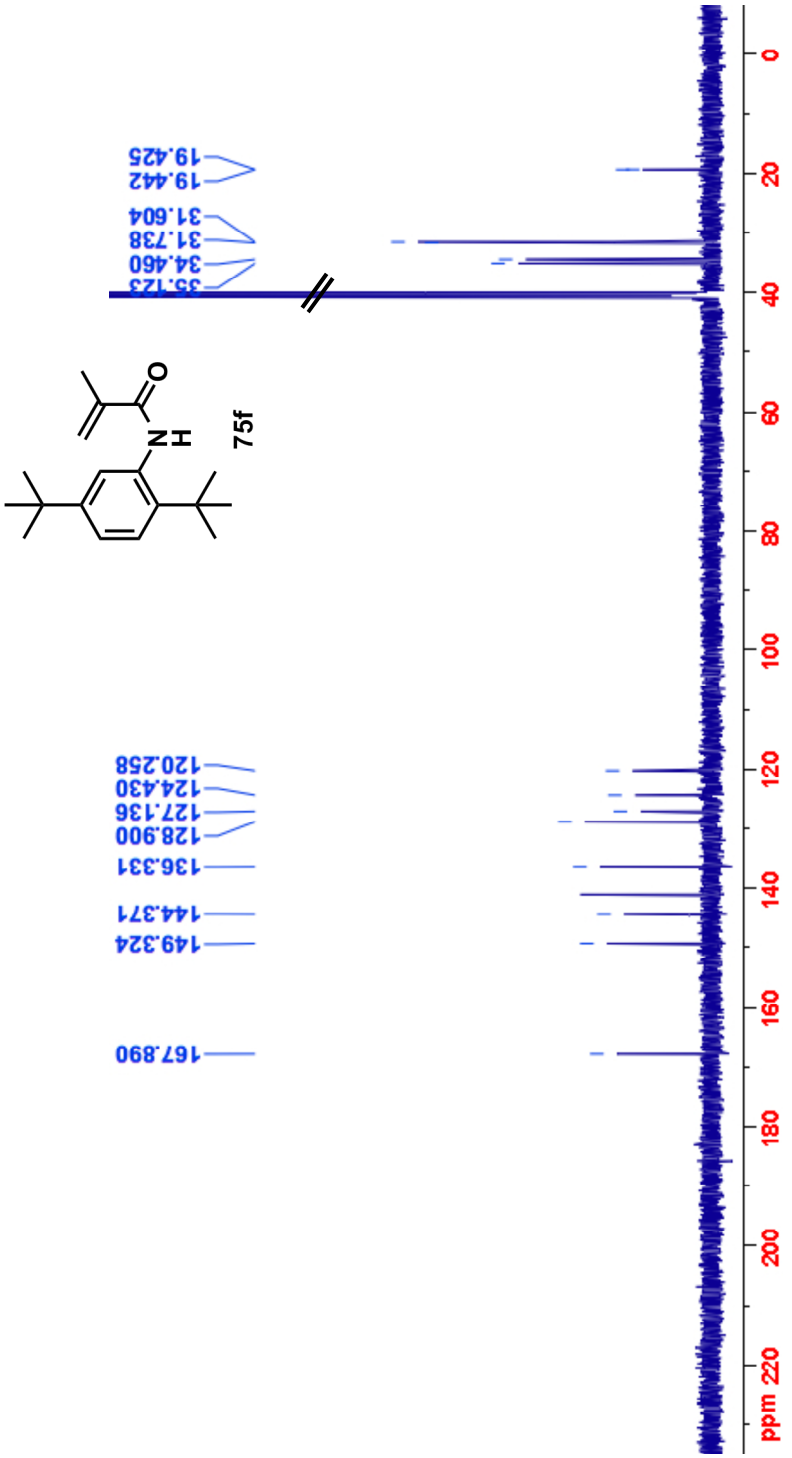

Figure 4.19: ^{13}C NMR (125 MHz, $CDCl_3$, δ ppm) spectrum for acrylanilide **75f.**

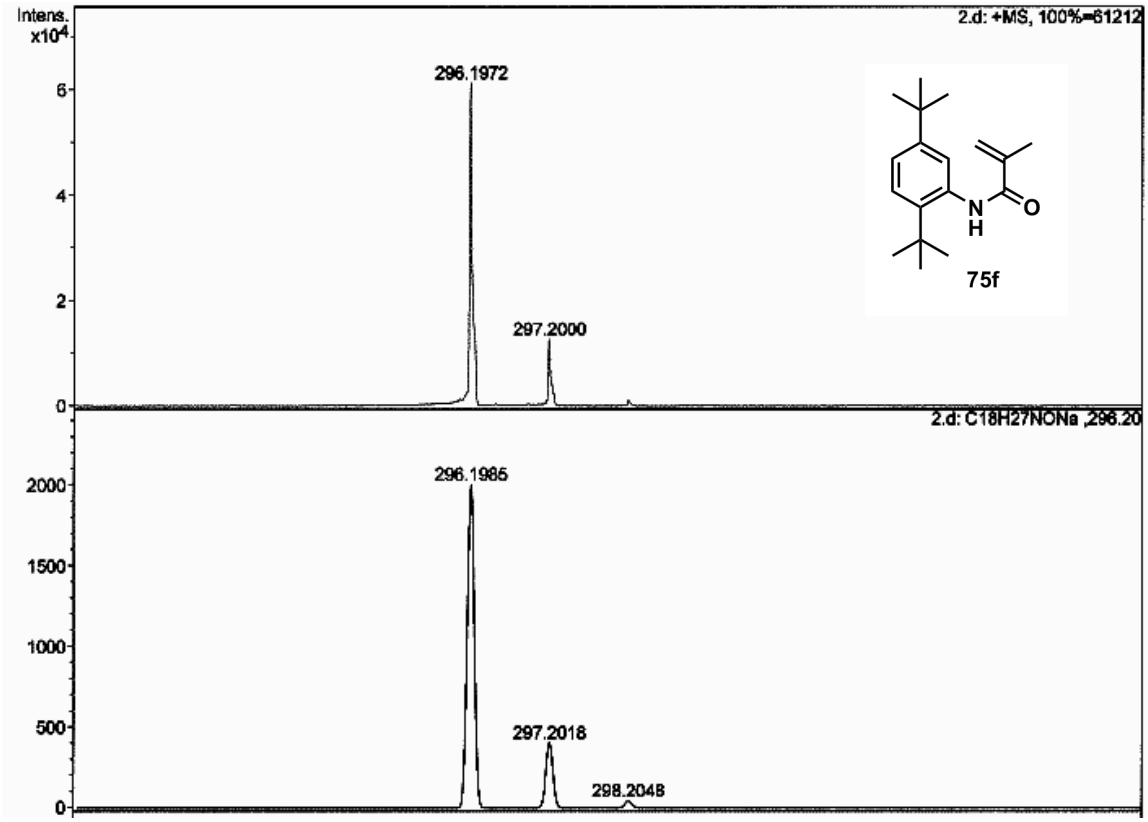

Figure 4.20: HRMS for acrylanilide **75f.**

4.9.7. Circular dichroism spectroscopy and optical rotation for 72f,g

Optically pure isomers of **72f,g** were separated by HPLC and dissolved in spectrophotometric grade methylcyclohexane (MCH) for CD experiments and $CHCl_3$ for polarimetry experiments.

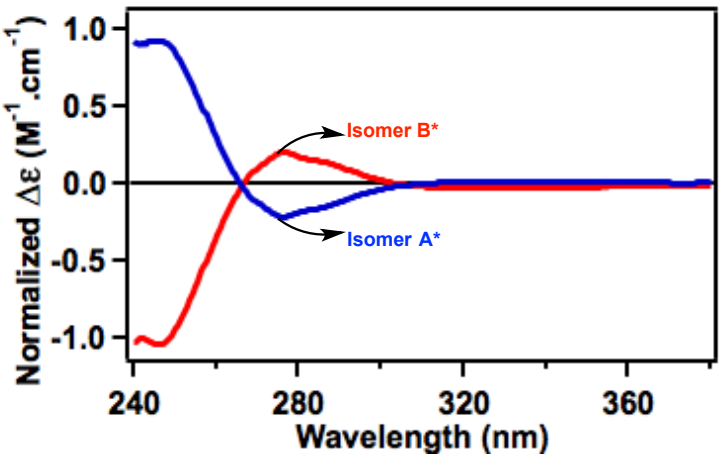

Figure 4.21: CD spectra for acrylanilide **72f** in MCH: $[\mathbf{72f}]_A$ = 1.25 mM; $[\mathbf{72f}]_B$ = 1.04 mM; path length = 1 cm.

Optical Rotation $[\alpha]_D^{25}$

Peak A (**72f**) = - 29.05 (*c* 0.210 %, $CHCl_3$),

Peak B: (**72f**) = + 25.35 (*c* 0.213 %, $CHCl_3$)

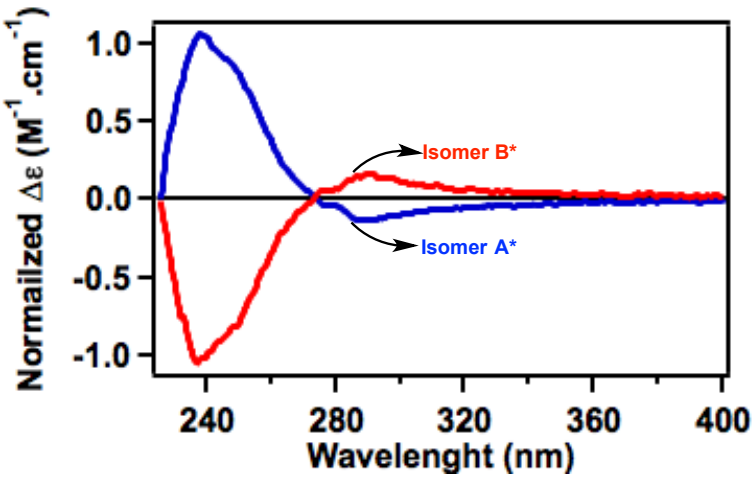

Figure 4.22: CD spectra for acrylanilide **72g** in MCH: $[\mathbf{72g}]_A$ = 4.64 x 10^{-4} M; $[\mathbf{72g}]_B$ = 5.97 x 10^{-4} M; path length = 1 cm

Note 1: *peak A and B refers to the first and second peak respectively that elute from the HPLC chiral stationary phase analysis/separation.*

Note 2: (-) and (+) are assigned based on the sign of CD spectra at 285 nm to the optically pure isomers peak A and peak B that elute from the HPLC chiral stationary phase analysis/separation. In the present case (with **72f,g**), peak A was assigned as the (-) isomer and peak B was assigned as the (+) isomer based on the sign of the Cotton effect.

4.9.8. General irradiation procedures and characterization of photoproducts

HPLC purified/optically pure samples of **72f,g** (3.5 mg/mL) in acetone or 2,2,2-trifluoroethanol (TFE) or in methanol (MeOH) in 13 mm Pyrex tube were deaerated with N_2 for 15 min and irradiated at room temperature (27±1 ^{o}C) or at 20 ^{o}C for specified time intervals. The samples were kept under a N_2 atmosphere during the course of the irradiation. After irradiation, the samples were concentrated and analyzed by spectroscopy and chromatography.

Photoproduct **73f** = *ent*-**73f**: *cf.* chapter 2 section 2.4.7

Photoproduct **73g =** *ent*-**73g**

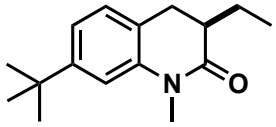

73g = *ent*-**73g**

Purification Conditions: Compound **73g** was purified by chromatography using CombiFlash®: RediSep column: 12 g silica**.** Flow rate: 21 mL/min**.** Mobile phase: 22 % diethyl ether:*n*-pentane

^{1}H NMR (400 MHz, $CDCl_3$, δ ppm) 7.08 – 6.93 (Ar, 3H), 3.35 (s, 3H), 2.95 – 2.89 (m, 1H), 2.67 – 2.60 (m, 1H), 2.46 – 2.37 (m, 1H), 1.89 – 1.77 (m, 1H), 1.48 – 1.36 (m, 1H), 1.30 (s, 9H), 0.96 (t, *J* = 7.2 Hz, 3H)

^{13}C NMR (100 MHz, $CDCl_3$, δ ppm) 173.0, 150.8, 140.2, 127.8, 122.8, 119.7, 111.8, 42.5, 35.0, 31.6, 29.9, 29.8, 22.9, 11.8

HRMS-ESI ($[M + H]^+$): Calculated: 246.1852; Observed: 246.1852; ΔM = 0 ppm.

HPLC analysis conditions: Column: (R,R) WHELK–01; Abs. detector: 254 nm and 270 nm**;** mobile phase: Hexanes:IPA = 98:2; Flow rate: 1 mL/min

Retention time (min): **73g:** ~27.05 and *ent*-**73g:** ~33.37

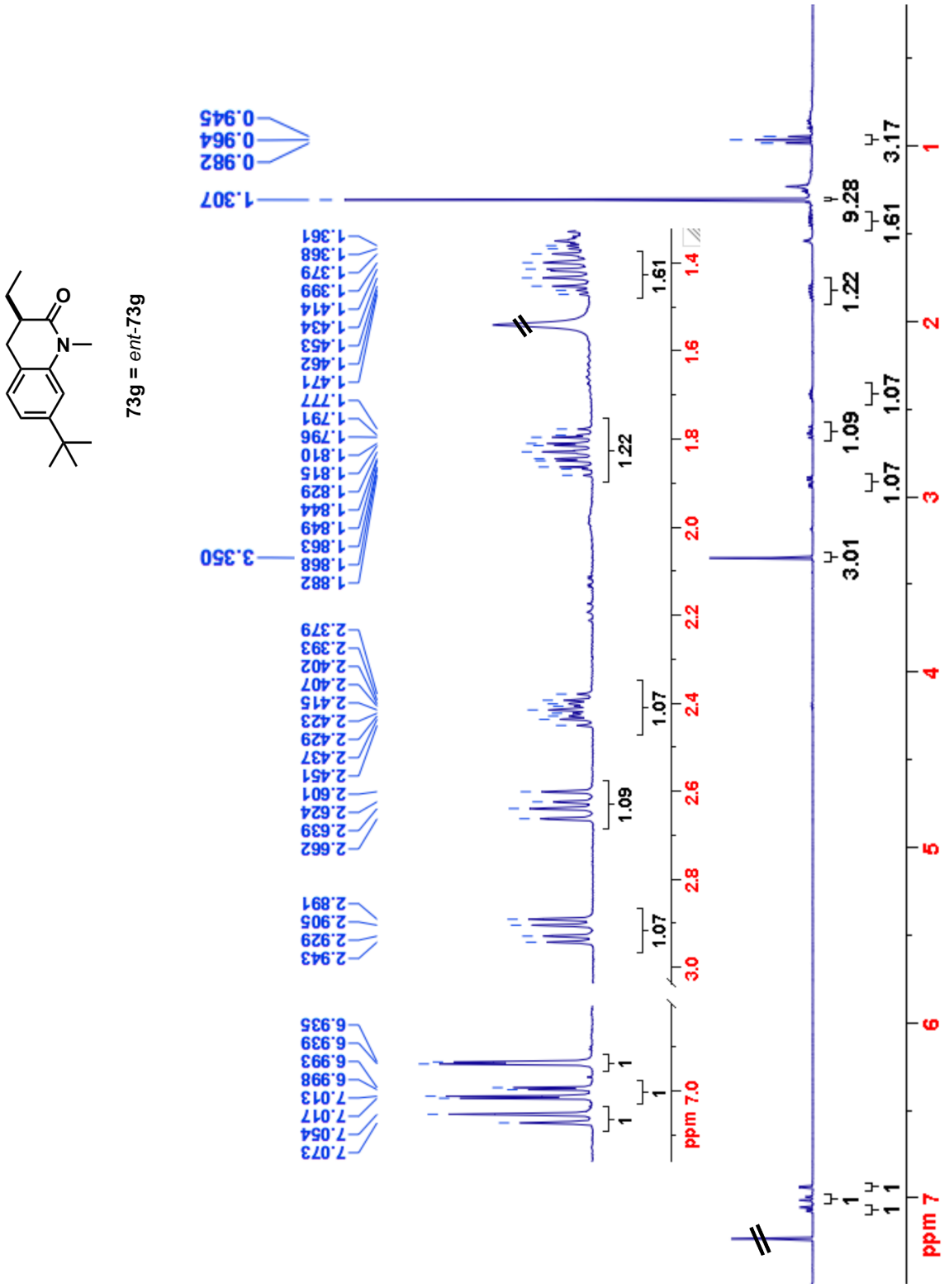

Figure 4.23: ^{1}H NMR (400 MHz, $CDCl_3$, δ ppm) spectrum for photoproduct **73g** = *ent*-**73g.**

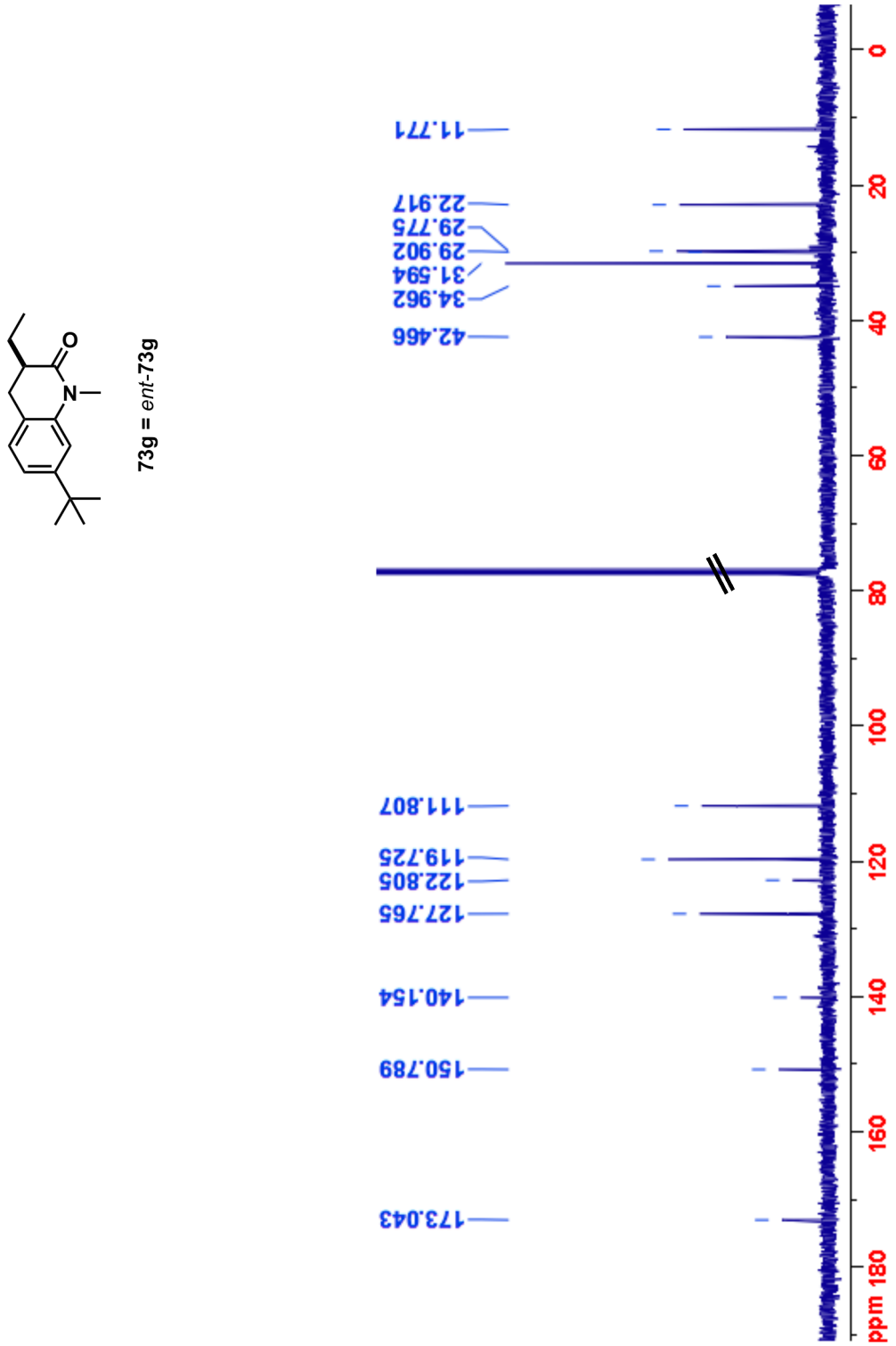

Figure 4.24: ^{13}C NMR (100 MHz, $CDCl_3$, δ ppm) spectrum for photoproduct **73g** = *ent*-**73g.**

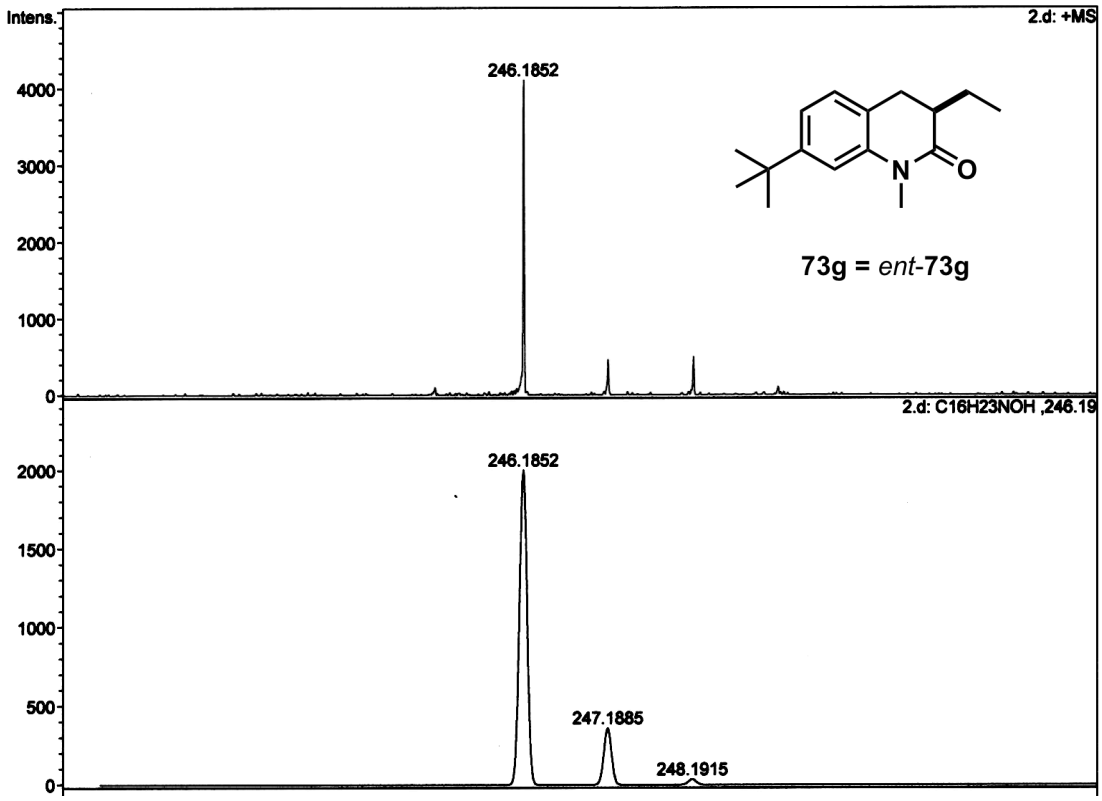

Figure 4.25: HRMS for photoproduct **73g** = *ent*-**73g.**

4.10. References

(1) Turro, N. J. Molecular Photochemistry. *Chem. Eng. News* **1967**, *45*, 84.

(2) Quinkert, G. En Route to Multisurface Chemistry. *Angew. Chem., Int. Ed.* **1975**, *14*, 790–800.

(3) Hammond, G. S.; Saltiel, J.; Lamola, A. A.; Turro, N. J.; Bradshaw, J. S.; Cowan, D. O.; Counsell, R. C.; Vogt, V.; Dalton, C. Mechanisms of Photochemical Reactions in Solution. XXII.1 Photochemical cis-trans Isomerization. *J. Am. Chem. Soc.* **1964**, *86*, 3197–3217.

(4) Hixson, S. S.; Mariano, P. S.; Zimmerman, H. E. Di-π-methane and oxa-di-π-methane rearrangements. *Chem. Rev.* **1973**, *73*, 531–551.

(5) Plattner, D. A. Interspin Crossing and Reactivity. *Angew. Chem., Int. Ed.* **1999**, *38*, 82–86.

(6) Zimmerman, H. E.; Epling, G. A. Mechanistic and exploratory organic photochemistry. LV. Geometric control of multiplicity in the di-.pi.-methane rearrangement. *J. Am. Chem. Soc.* **1970**, *92*, 1411–1412.

(7) Zimmerman, H. E.; Schuster, D. I. A New Approach to Mechanistic Organic Photochemistry. IV. Photochemical Rearrangements of 4,4-Diphenylcyclohexadienone. *J. Am. Chem. Soc.* **1962**, *84*, 4527–4540.

(8) Zimmerman, H. E.; Schuster, D. J. The photochemical rearrangement of 4,4-diphenylcyclohexadienone. Paper i on a general theory of photochemical reactions. *J. Am. Chem. Soc.* **1961**, *83*, 4486–4488.

(9) Adam, W.; Fragale, G.; Klapstein, D.; Nau, W. M.; Wirz, J. Phosphorescence and Transient Absorption of Azoalkane Triplet States. *J. Am. Chem. Soc.* **1995**, *117*, 12578–12592.

(10) Giese, B.; Wettstein, P.; Stähelin, C.; Barbosa, F.; Neuburger, M.; Zehnder, M.; Wessig, P. Memory of Chirality in Photochemistry. *Angew. Chem. Int. Ed.* **1999**, *38*, 2586–2587.

(11) Griesbeck, A. G.; Kramer, W.; Lex, J. Diastereo- and Enantioselective Synthesis of Pyrrolo[1,4]benzodiazepines through Decarboxylative Photocyclization. *Angew. Chem. Int. Ed.* **2001**, *40*, 577–579.

(12) Sakamoto, M.; Kawanishi, H.; Mino, T.; Fujita, T. Asymmetric synthesis of β-lactams using chiral-memory effect on photochemical γ-hydrogen abstraction by thiocarbonyl group. *Chem. Commun.* **2008**, 2132–2133.

(13) Sivaguru, J.; Shichi, T.; Ramamurthy, V. Reactive-state spin-dependent diastereoselective photoisomerization of trans,trans-2,3-diphenylcyclopropane-1- carboxylic acid derivatives included in zeolites. *Org. Lett.* **2002**, *4*, 4221–4224.

(14) Rau, H. Asymmetric photochemistry in solution. *Chem. Rev.* **1983**, *83*, 535–547.

(15) Inoue, Y. Enantiodifferentiating photosensitized reactions. In *Chiral Photochemistry*; Inoue, Y.; Ramamurthy, V., Eds. Marcel Dekker: New York, 2004; Vol. 11, pp. 129–177.

(16) Ramamurthy, V. Photoprocesses of Organic Molecules included in Zeolites. In *Photochemistry in Organized and Constrained Media*; Ramamurthy, V., Ed. Wiley-VCH: New York, 1991; pp. 429–493.

(17) Mori, T.; Inoue, Y.; Weiss, R. G. Enhanced Photodecarboxylation of an Aryl Ester in Polyethylene Films. *Org. Lett.* **2003**, *5*, 4661–4664.

(18) Curran, D. P.; Qi, H.; Geib, S. J.; DeMello, N. C. Atroposelective Thermal Reactions of Axially Twisted Amides and Imides. *J. Am. Chem. Soc.* **1994**, *116*, 3131–3132.

(19) Curran, D. P.; Hale, G. R.; Geib, S. J.; Balog, A.; Cass, Q. B. L.; Degani, A. L. G.; Hernandes, M. Z.; Freitas, L. C. G. Rotational features of carbon-nitrogen bonds in axially chiral o-tert. butyl anilides and related molecules. Potential substrates for the “prochiral auxiliary” approach to asymmetric synthesis. *Tetrahedron: Asymmetry* **1997**, *8*, 3955–3975.

(20) Clayden, J. Atropisomers and near-atropisomers: achieving stereoselectivity by exploiting the conformational preferences of aromatic amides. *Chem. Commun.* **2004**, 127–135.

(21) Honda, A.; Waltz, K. M.; Carroll, P. J.; Walsh, P. J. Atropisomeric amides: Achiral ligands with chiral conformations. *Chirality* **2003**, *15*, 615–621.

(22) Ayitou, A. J.-L.; Jesuraj, J.; Barooah, N.; Ugrinov, A.; Sivaguru, J. Enantiospecific Photochemical Norrish/Yang Type II Reaction of Non-biaryl Atropchiral α-Oxoamides In Solution – Axial to Point Chirality Transfer. *J. Am. Chem. Soc.* **2009**, *131*, 11314–11315.

(23) Ayitou, A. J.-L.; Sivaguru, J. Light-induced transfer of molecular chirality in solution: enantiospecific photocyclization of molecularly chiral acrylanilides. *J. Am. Chem. Soc.* **2009**, *131*, 5036–5037.

(24) Ogata, Y.; Takagi, K.; Ishino, I. Photocyclization of Acrylanilides. *J. Org. Chem.* **1971**, *36*, 3975–

3979.

(25) Ninomiya, I.; Yamauchi, S.; Kiguschi, T.; Shinobara, A.; Naito, T. Photocyclisation of enamides. Part V. Photocyclisation of α,β-unsaturated anilides. *J. Chem. Soc., Perkin Trans. 1.,* **1974**, 1747–1751.

(26) Turro, N. J. 1.; Ramamurthy, V.; Scaiano, J. C. J. C. 1. *Modern molecular photochemistry of organic molecules*; Sausalito, CA. : University Science Books, 2010.

(27) Ayitou, A. J.-L.; Ugrinov, A.; Sivaguru, J. 6π-Photocyclization of O-tert-butylacrylanilides. N-substitution dictates the regiochemistry of cyclization. *Photochem. & Photobio. Sc.* **2009**, *8*, 751–754.

(28) Lapouyade, R.; Manigand, C.; Nourmamod, A. Photocyclization of 2-vinylbiphenyls: stereochemistry of the triplet state cyclization. *Can. J. Chem.* **1985**, *63*, 2192–2196.

(29) Chapman, O. L.; Adams, W. R. Photochemical transformations. XXII. Photoisomerization of substituted acrylic acids and acrylamides to .beta.-lactones and .beta.-lactams. *J. Am. Chem. Soc.* **1968**, *90*, 2333–2342.

(30) Bach, T.; Grosch, B.; Strassner, T.; Herdtweck, E. Enantioselective [6π]-Photocyclization Reaction of an Acrylanilide Mediated by a Chiral Host. Interplay between Enantioselective Ring Closure and Enantioselective Protonation. *J. Org. Chem.* **2003**, *68*, 1107–1116.

(31) Peterson, J. 1H NMR analysis of mixtures using internal standards: A quantitative experiment for the instrumental analysis laboratory. *J. Chem. Educ.* **1992**, *69*, 843.

(32) Wallace, T. Quantitative analysis of a mixture by NMR spectroscopy. *J. Chem. Educ.* **1984**, *61*, 1074.

(33) Rossiter, S. A convenient synthesis of 3-methyleneoxindoles: cytotoxic metabolites of indole-3-acetic acids. *Tetrahedron Lett.* **2002**, *43*, 4671–4673.

(34) Kadin, S. B. Monomethylation of aromatic amines via sodium borohydride mediated carbon-nitrogen bond cleavage. *J. Org. Chem.* **1973**, *38*, 1348–1350.

(35) Ninomiya, I.; Yamauchi, S.; Kiguschi, T.; Shinobara, A.; Naito, T. Photocyclisation of enamides. Part V. Photocyclisation of α,β-unsaturated anilides. *J. Chem. Soc., Perkin Trans. 1.,* **1974**, 1747–1751.

CHAPTER 5. CRYSTALLINE CONFINEMENT DEPENDENT ENANTIOSPECIFIC 6π-PHOTOCYCLIZATION OF ATROPISOMERIC α-SUBSTITUTED ACRYLANILIDES[§]

5.1. Introduction

In 1918, Kohschütter first advanced the concept of chemical transformations in the solid/crystalline state occurring with minimum atomic and molecular.[1] Following this, Scmidt and co-workers in 1960 introduced the concept of topochemical reactivity in the solid, which led to the recent resurgence of the field.[2-4] In recent years, it has been shown that the stereochemistry of product(s) resulting from many photochemical reactions could be tailored by performing the transformations of interest in the crystalline confinement (*cf.* chapter 1 section 1.5.4).[5-9] Although the use of crystalline confinement was one of the elegant methodologies to achieve/control high stereoselectivity in photochemical transformation, it has been challenging to have a complete control during the formation of new stereo-centers within the expected photoproduct(s).[10,11] There are classical examples that have taken advantage of the physical properties *viz*. chirality offer by the crystalline environment to perform absolute asymmetric photochemical synthesis.[5,7,12] An elegant strategy in this regard is the chiral ionic auxiliary approach introduced by Scheffer and co-workers as detailed in the first chapter.[5] In the continuation of achieving highly enantioselective photochemical transformations in solution using axially chiral chromophores, we explained in the previous chapter how the reactive spin states could be successfully manipulated to achieve high stereoselectivity in the transformation of interest. In the current study, we investigated the influence of the phase of the reaction medium during 6π-photocyclization of axially chiral α-substituted acrylanilides on the stereochemistry of the expected 3,4-dihydro-2-quinolin-2-

[§] The material in this chapter was co-authored by Anoklase J.-L. Ayitou (AJA), Nandini Vallavoju (NV), Dr. Angel Ugrinov (AU) and Dr. J. Sivaguru (JS). AJA in consultation with JS synthesized all compounds and performed all experiments detailed in this chapter. NV helped characterizing the compounds and analyzing photoreaction samples. AU performed the XRD analyses and solved x-ray crystals structures for all the compounds. AJA and JS came up with the mechanistic rationale of the reaction as well as the conclusion described in this chapter.

one photoproduct(s). This strategy of employing crystalline environment to control stereochemistry is attractive as it involves solvent-free reaction conditions.

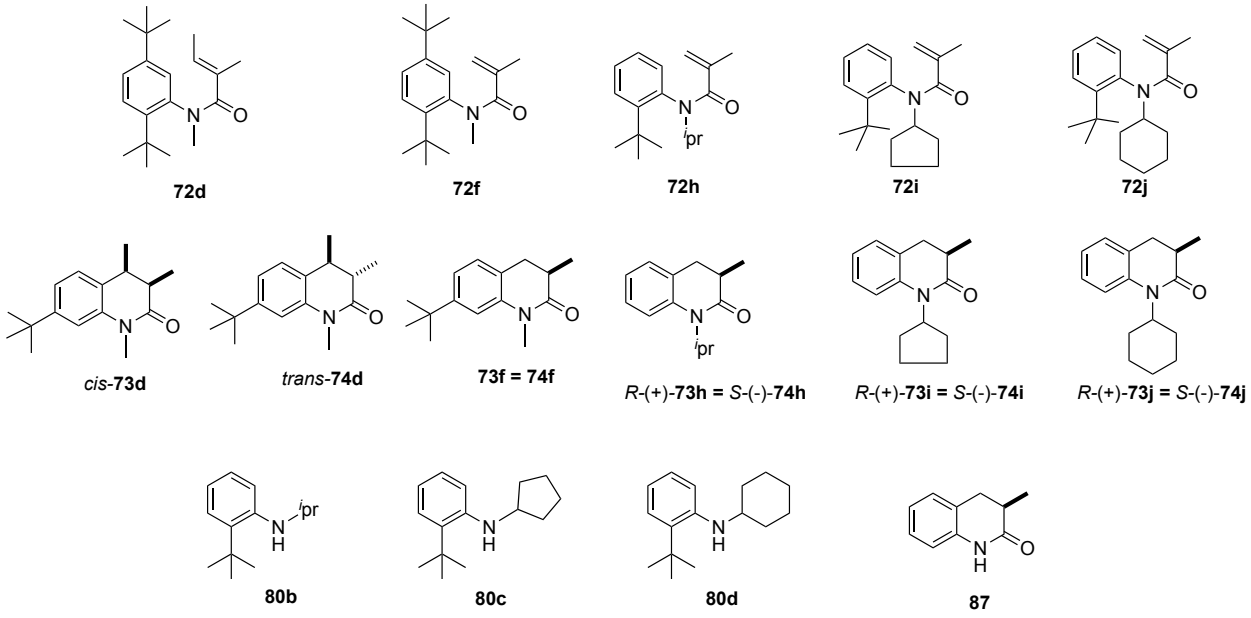

Chart 5.1: Crystalline acrylanilides molecular reactants and corresponding photoproduct(s).

From the library of axially chiral acrylanilides (Chart 5.1), compounds **72h-j** were found to be crystalline materials. Irradiation of compound **72h-j** in solution phase and solid state was investigated: the overall findings are discussed the next section.

5.2. Discussion

In chapters 3, we demonstrated that axially chiral α,β-unsaturated acrylanilides (e.g. **72d**) could be effectively employed during 6π-photocyclization in solution via direct irradiation to achieve high enantioselectivity in the photoproduct(s). We also observed the important role of the β-substitution to achieve high enantioselectivity in the photoproduct (Scheme 5.1).[13] While acrylanilide **72d** gave chirally enriched photoproducts *cis*-**78c** and *trans*-**74d**, the α-substituted acrylanilide **72f** gave racemic photoproduct **73f** as shown in figure 5.1. This dichotomy was further detailed in chapter 4, where we shed

light on the reactive spin states of the systems of interest to achieve high selectivity in the photoproduct upon triplet sensitized irradiation of atropisomeric α-substituted acrylanilides.

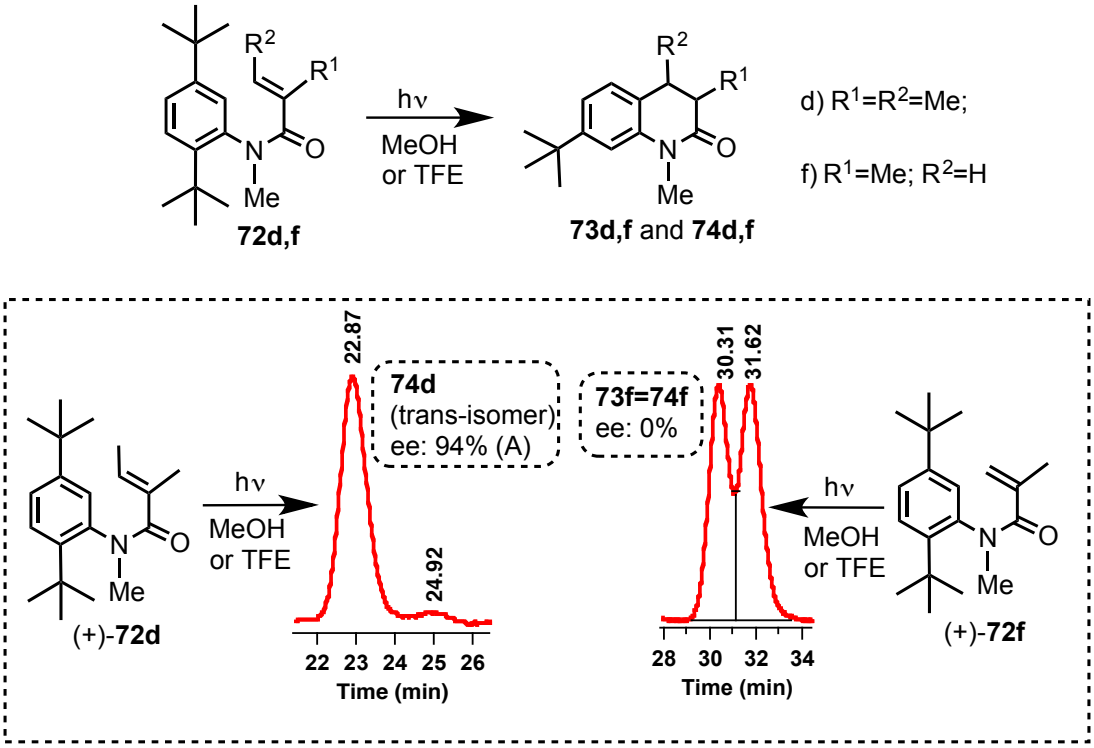

Scheme 5.1: Enantioselectivity during 6π-photocyclization of acrylanilides **72d,f:** Role of the β-substitution.

During 6π-photocyclization study of non-biaryl atropisomeric acrylanilides[14,15] **72**, I found that **72h-j** could be employed in the crystalline state and wished to compare the findings with direct and triplet sensitized irradiation from previously reported results (chapter 3 & 4) in order to test the dual role of axial chirality and the effect of crystalline confinement in determining the enantioselectivity in the expected 3,4-difydroquinolin-2-one photoproducts **73** and **74.**

5.2.1. Structural features from XRD

Compounds **72h-j** were employed as crystalline solids during 6π-photocyclization. Individual isomers of **72h-j** were separated by HPLC on a chiral stationary phase (*cf.* experimental section 5.5) and recrystallized to obtain single crystals for XRD analysis. Observation of their structural features in the

crystalline lattice showed that the β-alkenyl carbon was at an optimum distance from the *ortho* carbon on the phenyl ring in the crystalline state (Figures 5.1, 5.2 and Table 5.1).[16,17]

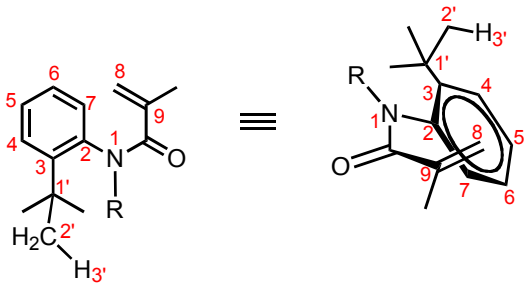

Table 5.1: Structural features for acrylanilides **72h-j:** Interatomic distances.

Compounds	R	$d[C_8 - C_3]$ (Å)	$d[C_8 - C_7]$ (Å)	$d[C_8 - H_{3'}]$ (Å)
P-**72j**	cyH	3.630	3.362	2.856
M-**72j**	cyH	3.628	3.359	2.860
72i	cyP	3.983	3.338	2.994
72h	^{i}pr	3.502	3.328	2.766

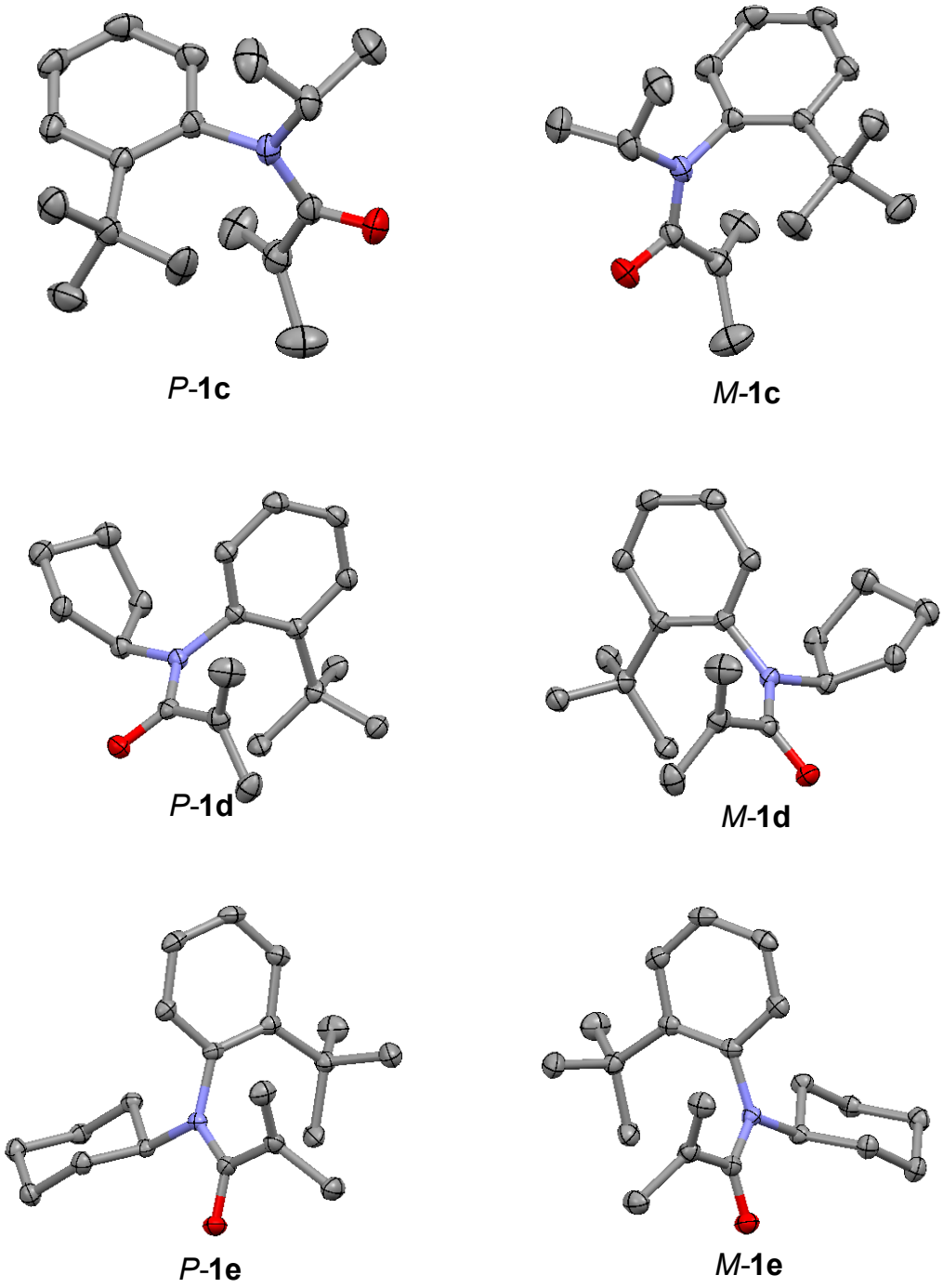

Figure 5.1: X-ray crystal structures for individual atropisomers for acrylanilides **72h-j.**

Note: X-ray crystallographic data (CCDC #: CCDC 810246 - 810249) are available from the Cambridge database as a cif file. See DOI: 10.1039/b000000x/

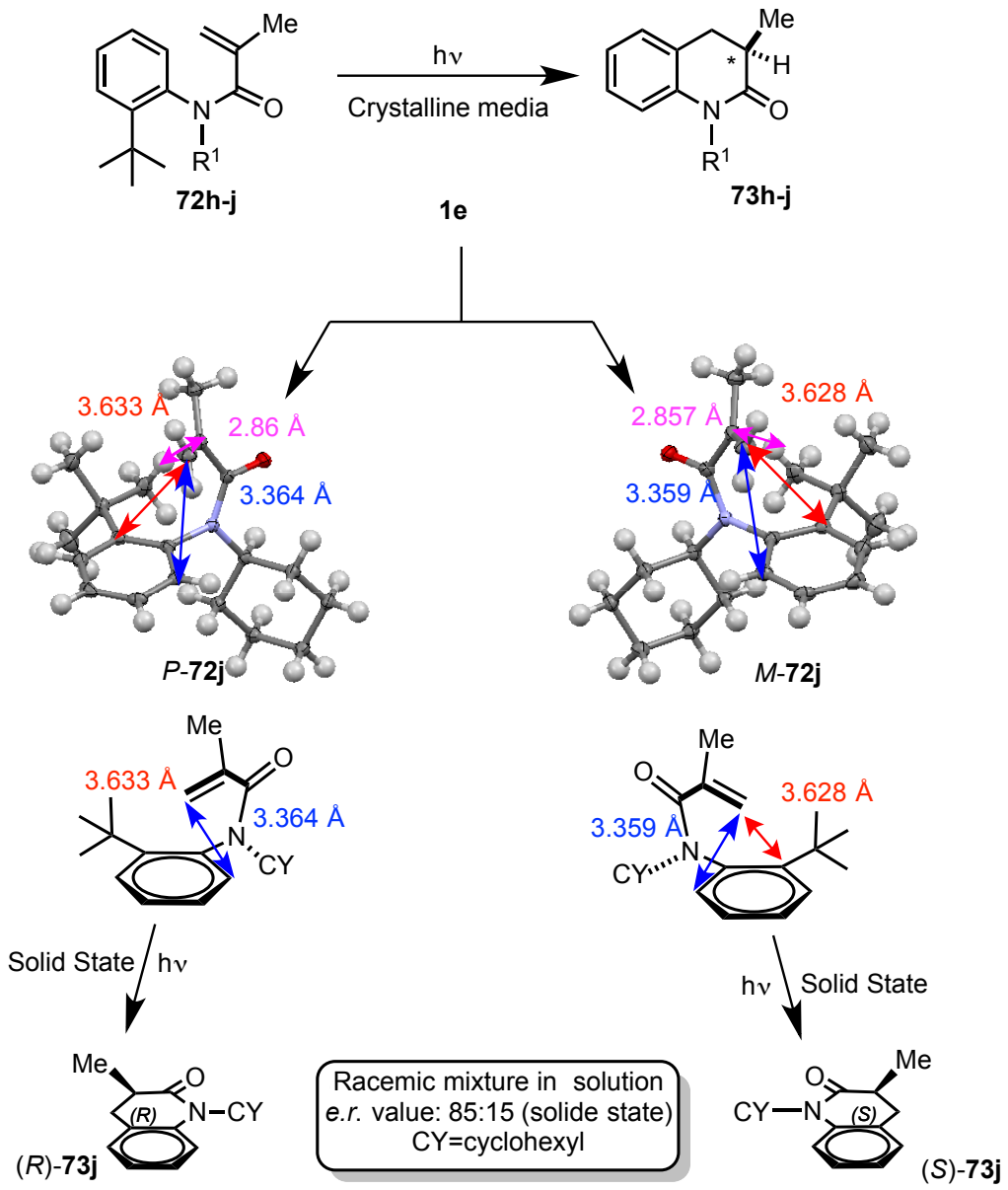

Figure 5.2: Enantiospecific 6π-photocyclization of molecularly chiral acrylanilides **72h-j** in the solid state: Photoreaction of **72j** is presented as a representative example.

5.2.2. Photoreactions conditions and results

In the previous chapter, we detailed the role of β-alkenyl substituent as a "messenger" in transferring the axial chirality in the reactant to point chirality in the photoproduct(s) during direct irradiation.[18] In the absence of β-alkenyl substituent (α-substituted acrylanilides), photocyclization under direct irradiation conditions led to a racemic mixture of photoproduct in solution. [18] After separation and recrystallization of individual atropisomers of **72h-j,** photochemical reaction was performed in the solid-state to determine the influence of the crystalline environment on the stereochemical course of the reaction. Optically pure *P* and *M* isomers of **72h-j** were crystallized on the walls of Pyrex test tubes. The Pyrex test tubes were mounted on a merry-go-around and irradiated using 450 W medium pressure Hg lamp. I also noticed that during the course of the irradiation, the crystals melted resulting in a gluey mass that was dissolved in ethyl acetate. The expected 3,4-dihydro-2-quinolin-2-one photoproduct **73h-j** (and **74h-j**) (Scheme 5.2) was isolated and purified by chromatography. Also the conversion to photoproducts **73h-j** (and **74h-j**) depended on the quality of crystal and the time of irradiation based the observed reaction characteristic. In the case of **72h**, for example, 52% conversion with >98% mass balance was observed after 72 h of irradiation. Individual photoproducts were characterized by NMR spectroscopy, polarimetry and HRMS (*cf.* experimental section 5.5). The absolute configuration for photoproducts **73h-j (and 74h-j)** were determine by independent synthesis. The optical rotation values of the optically pure isomers (synthesized by independent route) and the isomers obtained in the actual photoreactions were compared by polarimetry and by HPLC analysis on a chiral stationary phase (Table 5.3 and Scheme 5.3-5.5).

Table 5.2: Result 6π-photocyclization of **72h-j**.

Entry	Substrates	Optical rotation in **72h-j**	**72h-j**[e] (Abs. configuration)	Media	e. r. in **73h-j** (and **74h-j**) (abs. configuration) [f]
1.	**72h**	(+)		Solid state	85 (*R*) : 15 (*S*)
2.		(-)		Solid state	13 (*R*) : 87 (*S*)
3.		(+)		MeOH	Racemic
4.		(-)		MeOH	Racemic
5.	**72i**	(+)	*P*	Solid state	85 (*R*) : 15 (*S*)
6.		(-)	*M*	Solid state	14 (*R*) : 86 (*S*)
7.		(+)	*P*	MeOH	Racemic
8.		(-)	*M*	MeOH	Racemic
9.	**72j**	(+)		Solid state	85 (*R*) : 15 (*S*)
10.		(-)		Solid state	14 (*R*) : 86 (*S*)
11.		(+)		MeOH	Racemic
12.		(-)		MeOH	Racemic

[a] Reported values are an average of 3 trials with ±2% error. (+) and (-) represent the signs of their CD signals at 250 nm in methanol (MeOH); all irradiation were done for using a medium pressure Hg lamp. [b] The mass balance was >97%. [c] The photoproduct yield was >95% based on the recovered unreacted starting material using ^{1}H NMR with α,α'-dichloro-*p*-xylene as internal standard. [d] MeOH = methanol used as solvent. [e] Absolute configuration determined by single crystal XRD after HPLC separation of the individual atropisomers by chiral stationary phase. [f] The enantiomers were separated on HPLC using chiral stationary phase to compute the *e.r.* values; absolute configuration obtained from independent synthesis and compared $[\alpha]_D$ with literature values.[19]

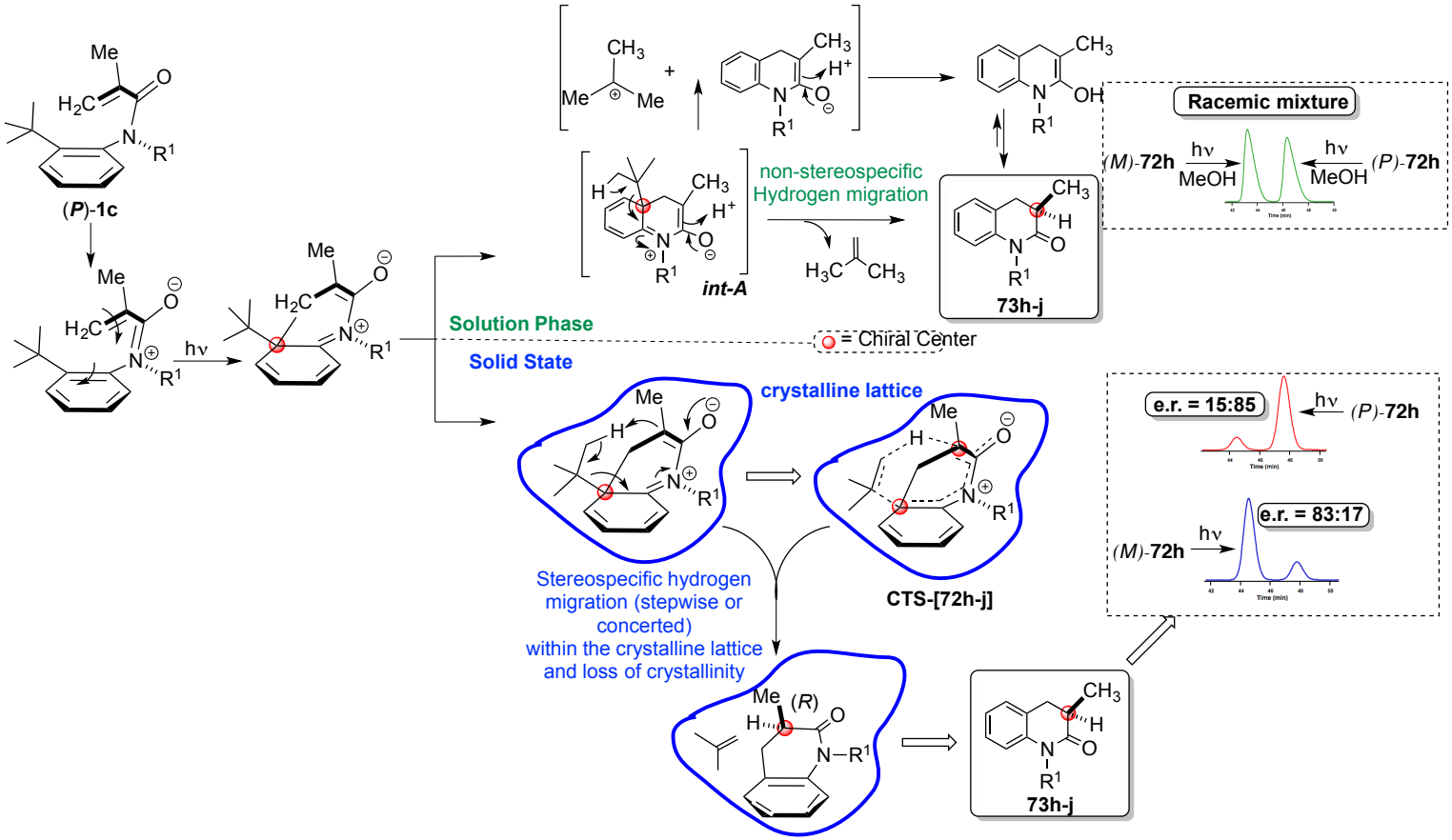

Scheme 5.2: Mechanistic analysis of 6π-photocyclization of acrylanilides **72h-j** in solution (top) and in the solid state (bottom).

5.2.3. Mechanistic rationale during 6π-photocyclization of acrylanilides 72h-j in the solid state

The mechanistic rationale in solution irradiation (Scheme 5.2-top) was comprehensively explained in chapters 3 and 4. Direct irradiation of atropisomeric α-substituted acrylanilides led to a zwitterionic intermediate "***int-A***". From the zwitterionic intermediate "***int-A***", a non-stereospecific H-migration occurs followed by re-aromatization leading to 3,4-dihydro-2-quinolin-2-one photoproduct **73h-j** (and **73h-j**), with removal of the *o-tert*-butyl group. When the photocyclization of **72h-j** occurred in the crystalline state, an enantiomeric ratio (e.r) of 85:15 was observed in the photoproducts **73h-j** (and **74h-j**) (Table 5.3). The high e.r. values in the crystalline state likely points to a stereospecific hydrogen migration in the second step (Scheme 5.2-bottom).

From the analysis of the crystal structures it is important to note that the β-alkenyl carbon is within optimal distance to both the *ortho* carbons on the phenyl ring (Table 5.1, Figures 5.2 and 5.3).[17,20] For example in the case of **73h**, the distance between the β-alkenyl carbon and the *ortho* carbon bearing the *tert*-butyl group is ~3.6 Å and the distance between the β-alkenyl carbon and the unsubstituted *ortho* carbon is ~3.4 Å. We have seen in chapter 2 that the severe 1,3-allylic strain ($A^{1,3}$-strain) between the N-alkyl and the *o-tert*-butyl group dictates the photocyclization to occur at the substituted *ortho* carbon so that the intramolecular strain could be released in the final photoproduct(s). As the *o-tert*-butyl H-atom is at ~2.8 Å from the α-alkenyl carbon (Table 5.1 and Figure 5.3), a stereospecific H-migration in the zwitterionic intermediate "***int-A***" through a cyclic 6-membered transition state **CTS-[72h-j]** is likely in the crystalline state leading to photoproduct **73h-j** (and **74h-j**) and 1-propene (Scheme 5.2-bottom). This rationale was further confirmed by independent investigation, as *P*-**72h-j** produced the *R* enantiomer and *M*-**72h-j** generated the *S* enantiomer in the photoproduct **73h-j** (and **74h-j**) as expected and envisioned in the crystalline lattice**.** From the independent synthesis of the enantiomeric photoproducts was deciphered the absolute configuration of the photoproduct **73h-j** (and **74h-j**) confirming the mechanistic conjecture (Scheme 5.3). As shown in Scheme 5.6, crystalline irradiation of the optically pure *P* isomer of **72j** gave the *R*-**73j** isomer photoproduct major enantiomer and the optically pure *M* isomer of **72j** gave the *S*-**74j** isomer photoproduct major enantiomer. Finally, the less than 100% enantioselectivity in the photoproduct is likely due to the loss of crystallinity during the course of the phototransformation resulting in an *e.r.* value of 85:15.

5.3. Independent Synthesis

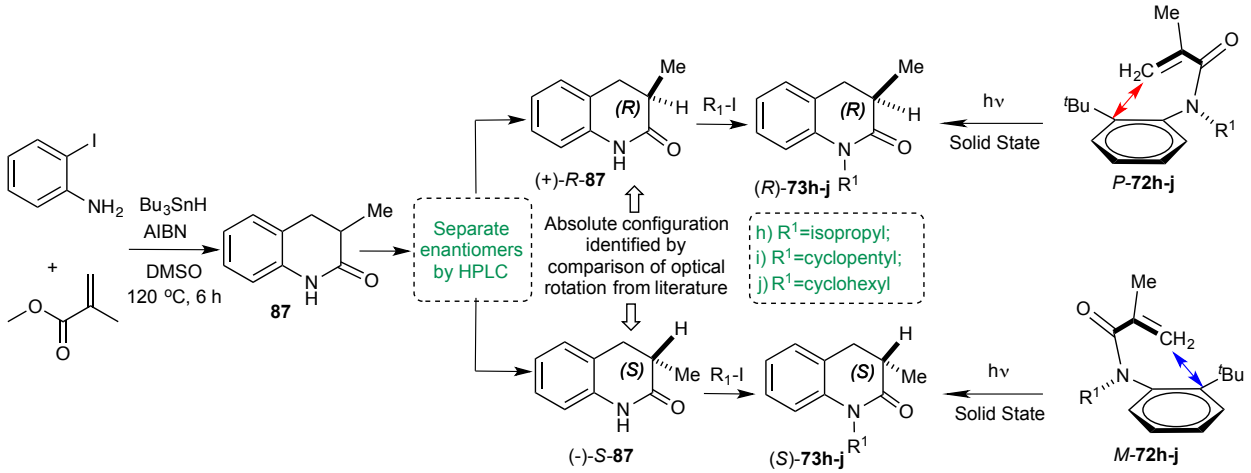

Scheme 5.3: Photoproduct **73h-j** (and **74h-j**) were synthesized independently according to reported procedures.[21]

Note: Optical rotation values in literature were compared for compounds **73h-j** (and **74h-j**) to determine the absolute configuration.[19]

(*R*)-**73h** or (*S*)-**74h:** Optically pure enantiomers of **87** were dissolved in a minimum of dry THF. 3 equiv. of NaH was added to the solution followed by addition of 2-iodopropane; the reaction was monitored by TLC for 48 h. After, the reaction was quenched with water and the corresponding optically pure isomers of **73h** was dissolved in ethyl acetate (EtOAc) and purified by chromatography with 15 % EtOAc:Hexanes as mobile phase.

(*R*)-**73i** or (*S*)-**74i:** Optically pure enantiomers of **87** were dissolved in a minimum of DMSO. Two pellets of KOH were added to the solution followed by addition of iodocyclopentane; the solution was heated at 48 ^{o}C; the reaction was monitored by TLC for 48 h. After the reaction was quenched with water, the expected optically pure isomers of **73i** were isolated with diethyl ether and purified by chromatography using 15 % EtOAc:Hexanes as mobile phase.

(*R*)-**73j** or (*S*)-**74j:** Optically pure enantiomers of **87** were separately dissolved in a minimum of DMSO. Two pellets of KOH were added to the solution followed by addition of iodocyclohexane; the

solution was heated at 48°C and the reaction was monitored by TLC for 48 h. After the reaction was quenched with water, the expected optically pure isomers of **73j** were isolated with diethyl ether and purified by chromatography using 15 % EtOAc:Hexanes as mobile phase.

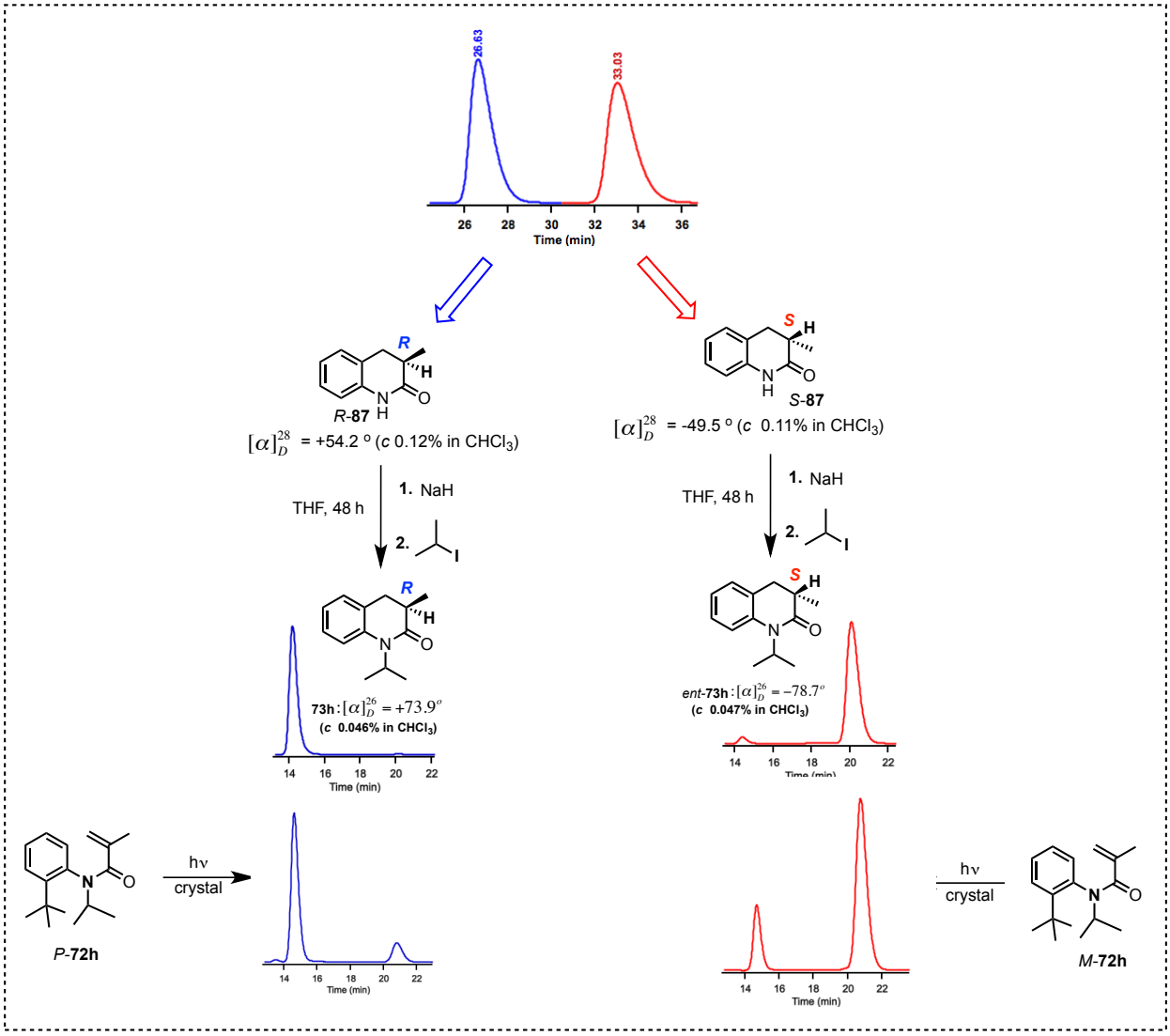

Scheme 5.4*:* Independent synthesis of enantiomers of **73h** followed by polarimetry and assignment of absolute configuration.

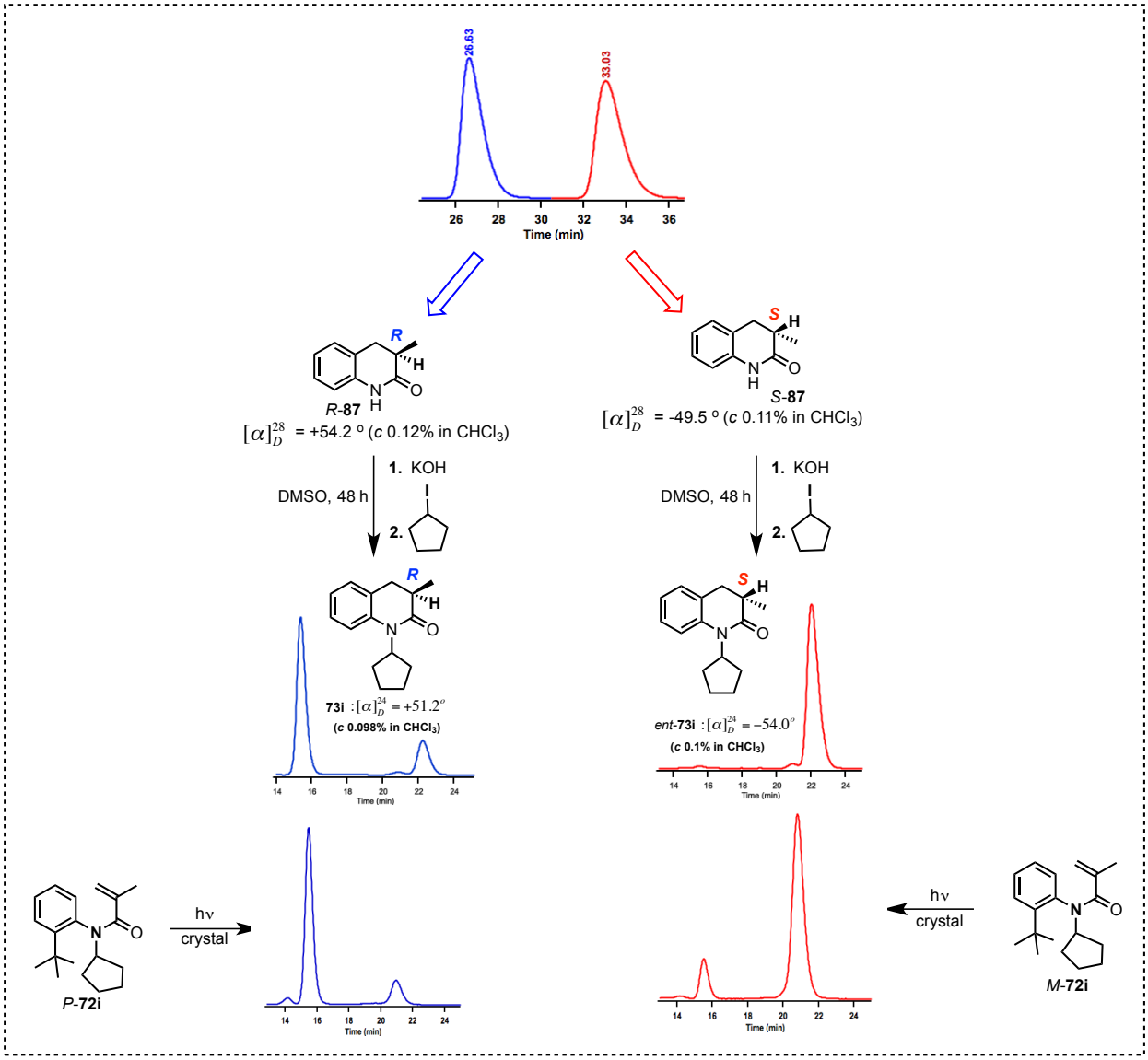

Scheme 5.5: Independent synthesis of enantiomers of **73i** followed by polarimetry and assignment of absolute configuration.

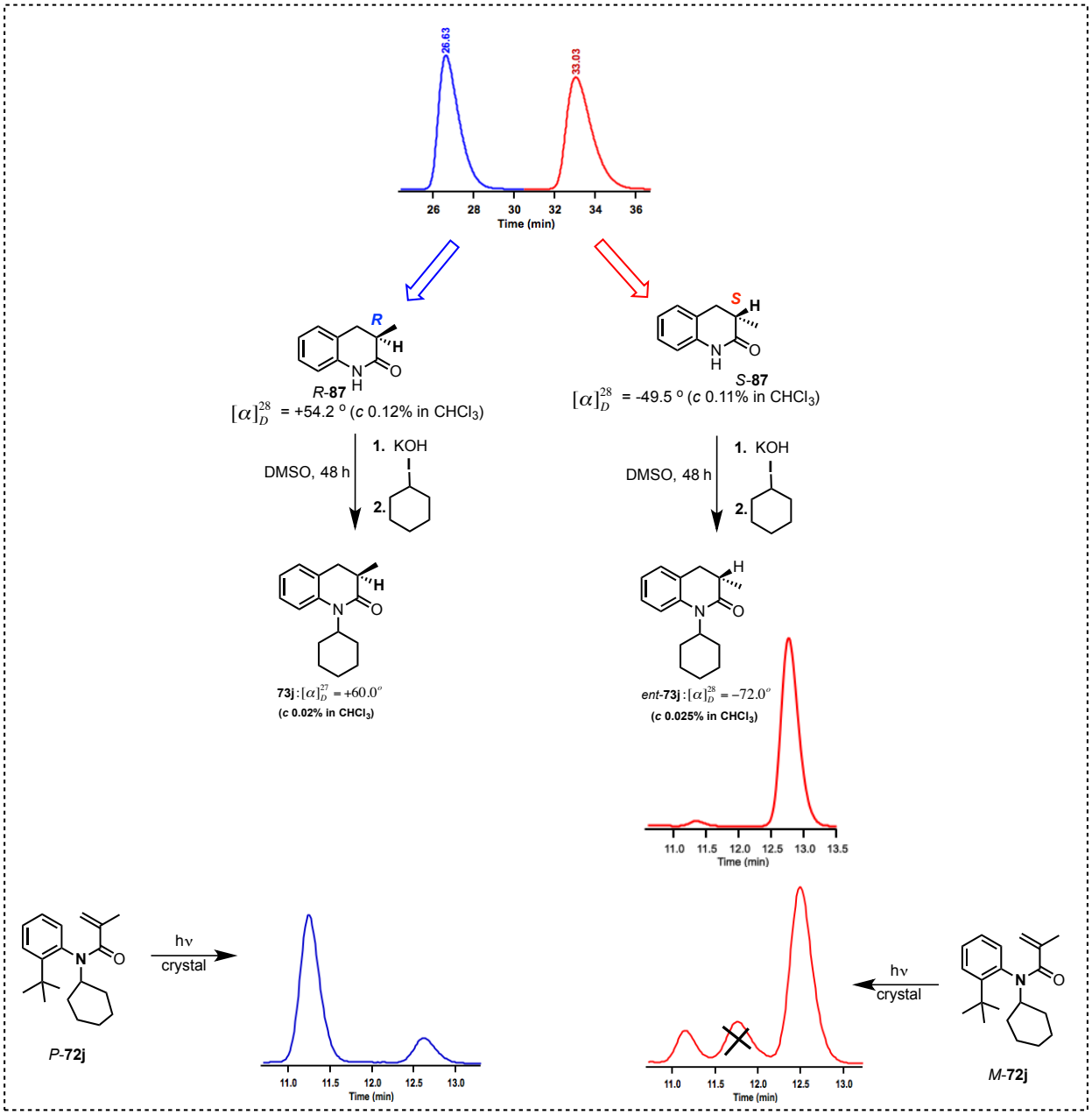

Scheme 5.6: Independent synthesis of enantiomers of **73j** followed by polarimetry and assignment of absolute configuration.

5.4. Summary and Outlook

The enantiospecific 6π-photocyclization of atropisomeric acrylanilides in the crystalline lattice demonstrated that reaction media would offer a powerful and complementary strategy to achieve high stereoselectivity during chemical transformations. Based on crystallographic and chromatographic analyses, the mechanistic rationale and the stereochemical course of reaction of axially chiral atropisomeric α-substituted acrylanilides **72h-j** to 3,4-dihydro-2-quinolin-2-one photoproduct **73h-j** was deciphered. The high *ee* values in the photoproduct opens up new avenues to achieve high selectivity with atropisomeric acrylanilides by direct irradiation.

5.5. Experimental Section

5.5.1. General method

All commercially obtained reagents/solvents were used as received; chemicals were purchased from Alfa Aesar®, Sigma – Aldrich®, Across®, TCI® America, Mallinckrodt®, and Oakwood Products®, and were used as received without further purification. Unless stated otherwise, reactions were conducted in oven-dried glassware under an atmosphere of nitrogen using anhydrous solvents. ^{1}H NMR and ^{13}C NMR spectra were recorded on Varian 400 MHz and 100 MHz spectrometers respectively. Data for ^{1}H NMR spectra are reported relative to deuterated solvent signals, and are reported as follows: chemical shift (δ ppm), multiplicity, coupling constant (Hz) and integration. Coupling constants (*J*) were reported in hertz (Hz). Standard abbreviations indicating multiplicity were used as follows: br (broad), s (singlet), d (doublet), t (triplet), q (quartet), m (multiplet), virt (virtual), and ABq (AB quartet). Data for ^{13}C NMR spectra are reported in terms of chemical shift. Electro spray Ionization Spectra(High Resolution Mass Spectrometry) were recorded on a Bruker – Daltronics® BioTof mass spectrometer in positive (ESI+) ion mode. HPLC analyses were performed on Waters® HPLC equipped with 2525 pump. Waters® 2767 sample manager was used for automated sample injection. All HPLC injections were monitored using a Waters® 2487 dual wavelength absorbance detector at 254, and 270 nm. Analytical and semi-preparative injections were performed on chiral stationary phase using various columns*. Masslynx software version 4.1 was used to analyze/process the HPLC injections. Igor Pro® Software version 6.0 was used to process the chromatographic data. When necessary, the reactants and photoproducts were purified by

chromatography: CombiFlash and/or on silica gel (Sorbent Technologies®, silica gel standard grade: Porosity 60 Å, Particle size: 230 x 400 mesh, Surface area: 500 – 600 m^2/g, Bulk density: 0.4 g/mL, pH range: 6.5 – 7.5). *The Retention Factor (Rf) values were recorded using a 20 % EtOAc-Hexanes as mobile phase (unless indicated) and on SORBENT TECHNOLOGIES® Silica Gel TLC plates (200 mm thickness w/ UV_{254}).* Optical activity values were recorded on JASCO® DIP – 370 digital polarimeter. CD spectra were recorded on JASCO® - 710 digital CD spectrometer.

* Regis® PIRKLE COVALENT (R,R) WHELK–O1 10/100 FEC columns: 25cm X 4.6 mm column for analytical injections, and 25 cm x 10.0 mm for semi-preparative injections

* CHIRALPAK® AD-H: 25cm X 4.6 mm column for analytical injections, and 25 cm x 10.0 mm for semi-preparative injections

* CHIRALPAK ® IC: 25cm X 4.6 mm column for analytical injections, and 25 cm x 10.0 mm for semi-preparative injections

5.5.2. Structure determination

Single crystal X-ray diffraction data of compound **72h** was collected on a SIEMENS diffractometer with a 1K CCD area detector (graphite-monochromated Mo Kα-radiation). The structures were solved by direct methods and refined on *F*2 using the SHELXTL V6.14 package (after absorption corrections with SADABS).

Single crystal X-ray diffraction data sets of **72i**, *M*-**72j** and *P*-**72j** were collected on a Bruker Apex Duo diffractometer with a Apex 2 CCD area detector. Cu radiation was used for all 3 data sets. The structures were process with Apex 2 v2010.9-1 software package (SAINT v. 7.68A, XSHELL v. 6.3.1). Direct method was used to solve the structures after multi-scan absorption corrections. Details of all four data collections and refinements are given in the table below.

Table 5.3: X-ray crystallography parameters.

	72h	**72i**	***M*-72j**	***P*-72j**
Formula	$C_{17}H_{25}NO$	$C_{19}H_{27}NO$	$C_{20}H_{29}NO$	$C_{20}H_{29}NO$
FW	259.38	285.42	299.44	299.44
cryst. size [mm]	.22 x .40 x .58	.06 x .09 x .011	.09 x .13 x .16	.09 x .13 x .16
cryst. system	Monoclinic	Monoclinic	Orthorhombic	Orthorhombic
Space Group, Z	C_c, 4	$P2_1/c$, 4	$P2_12_12_1$, 4	$P2_12_12_1$, 4
a [Å]	8.7219(13)	11.2894(3)	8.7688(10)	8.7698(5)
b [Å]	14.862(2)	8.7386(2)	11.3647(14)	11.3683(7)
c [Å]	12.6513(18)	17.1678(4)	17.512(2)	17.5191(10)
α [Å]	90	90	90	90
ß [Å]	99.836(4)	105.623(1)	90	90
γ [Å]	90	90	90	90
V [$Å^3$]	1615.8(4)	1631.09(7)	1745.2(4)	1746.61(18)
ρ_{calc} [g/cm^3]	1.066	1.162	1.140	1.139
μ [cm^{-1}]	0.065	0.540	.526	.525
F(000)	568	624	656	656
no of measured refl.	6999	21695	13484	11331
no of indep. refl.	3366	2899	3004	3080
no of refl. (I ≥ 2σ)	2910	2788	2953	3033
Resolution [Å]	.78	.83	.84	.84
R1/wR2 (I ≥ 2σ)[a] [%]	4.16/11.34	3.60/9.11	2.61/7.01	2.53/6.51
R1/wR2 (all data) [%]	4.97/12.15	3.71/9.20	2.66/7.05	2.59/6.56

[a]] $R1 = \Sigma||F_O| - |F_C|| / \Sigma|F_O|$, $wR2 = \{[\Sigma[(F_O)^2 – (F_C)^2]^2] / [\Sigma w(F_O^2)^2]\}^{1/2}$ for $F_O^2 > 2\sigma(F_O^2)$, $w = [\sigma^2(F_O)^2 + (AP)^2 + BP]^{-1}$ where $P = [(F_O)^2 + 2(F_C)^2] / 3$; Compound **72h**: A (B) = 0.0782 (0.1202), **72i**: A (B) = 0.0437 (0.6553), ***M*-72j**: A (B) = 0.0466 (0.2206), ***P*-72j**: A (B) = 0.0323 (0.2778)

5.5.3. Synthesis of anilines 80b-d

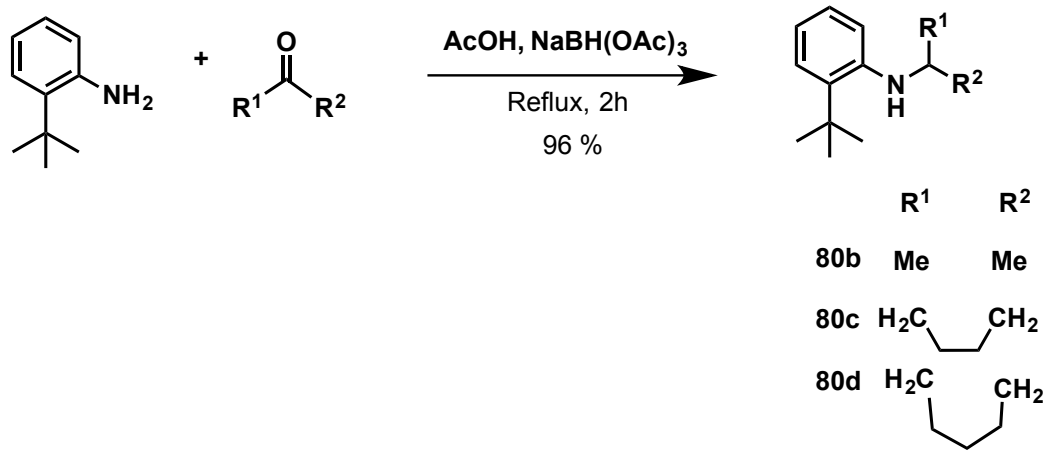

Scheme 5.7: Synthesis of N-alkyl-2-tert-butylaniline **80b-d.**

In a tandem reaction, commercially available *o-tert*-butylaniline (1 equiv., 1g, 6.7 mmol), 1.1 equiv. of acetic acid (AcOH), and 2 equiv. of sodium triacetoxyborohydride ($NaBH(OAc)_3$) were mixed in 8 mL of ketone (acetone, cyclopentanone and cyclohexanone). The new reaction mixture was allowed to reflux with stirring. After 2 h, the excess of ketone solvent was removed by roto-evaporation under reduced pressure. The residue was then washed with 3x20 mL of saturated $NaHCO_3$ solution. The expected aniline **80b-d** was extracted with EtOAc, and the combined organic fraction was dried over *anh.* Na_2SO_4, filtered, and concentrated to obtain the expected N-alkyl aniline **80b-d** (98 % conversion for all of the substrates). The expected compound(s) may be used in a subsequent reaction without further purification. **80b-d** were purified by flash chromatograph over silica gel using CombiFlash®: 12 g silica; flow rate: 22 mL/min, solvent system: 2 – 5% EtOAc : Hexanes

5.5.4. Characterization of amines 80b-d

***ortho-tert*-Butyl-*N*-isopropylaniline 80b**

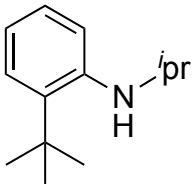

80b

^{1}H NMR (400 MHz, $CDCl_3$, δ ppm) 7.28 – 7.22 (dd, *J* = 8, 4 Hz, 1H), 7.16 – 7.08 (m, 1H), 6.74 – 6.6 (m, 2H), 4.0 – 3.6 (br m, 2H), 1.4 (s, 9H), 1.3 – 1.27 (d, *J* = 4Hz, 6H)

^{13}C NMR (100 MHz, $CDCl_3$, δ ppm) 145.7, 133.1, 127.3, 126.5, 116.54, 112.4, 44.5, 34.3, 30.2, 23.4

HRMS-ESI ($M+H^+$): Calculated: 192.1747; Observed: 192.1750; Δm = 1.6 ppm

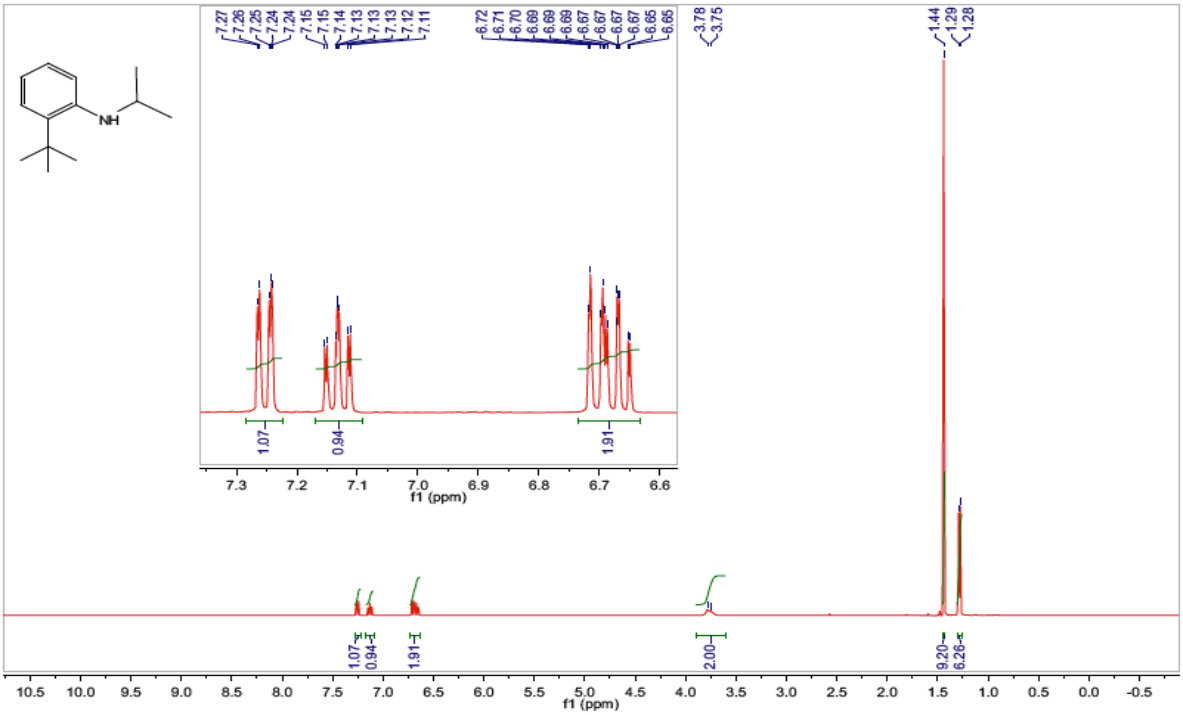

Figure 5.3: ^{1}H NMR (400 MHz, $CDCl_3$, δ ppm) spectrum for aniline **80b.**

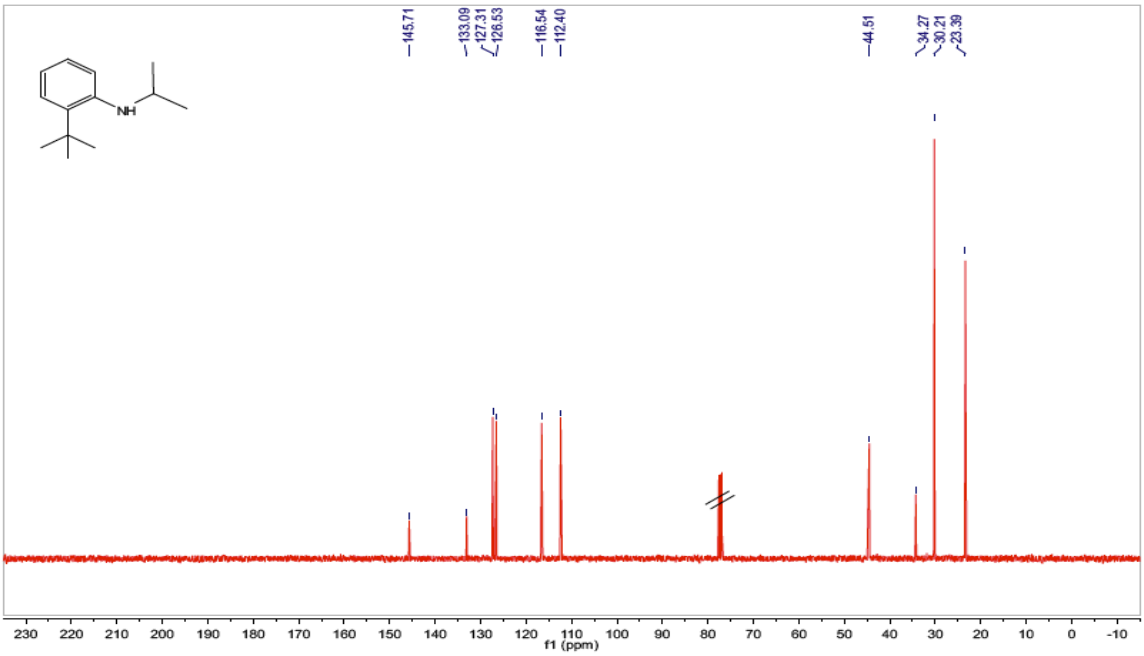

Figure 5.4: ^{13}C NMR (100 MHz, $CDCl_3$, δ ppm) spectrum for aniline **80b.**

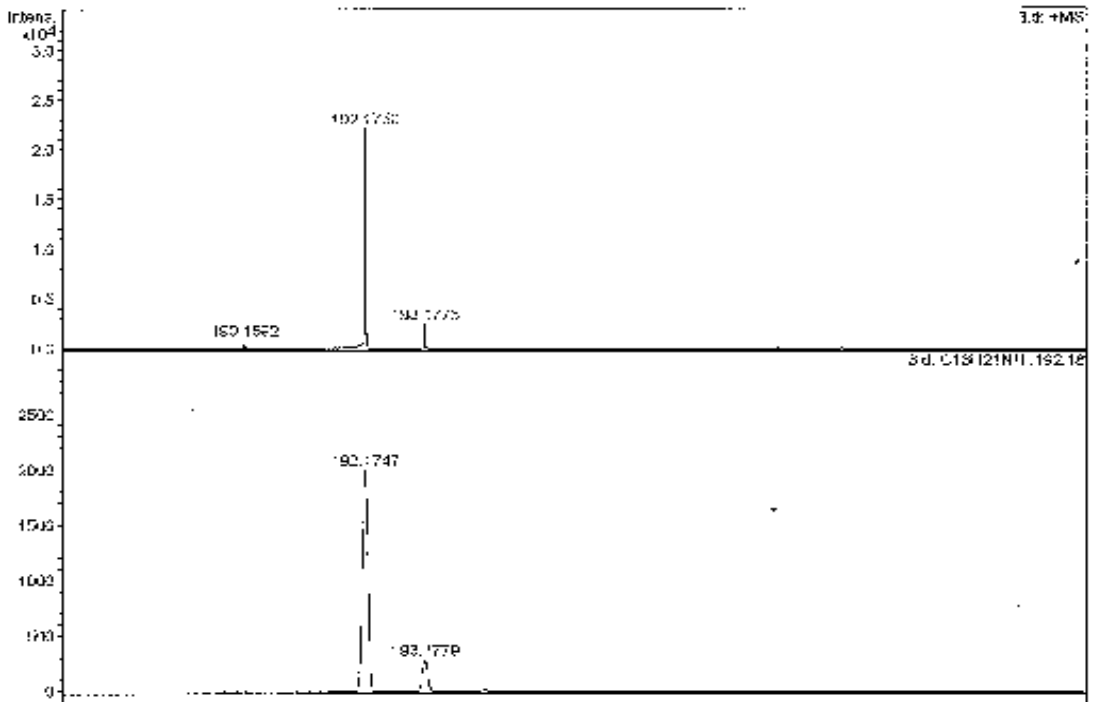

Figure 5.5: HRMS for aniline **80b**.

***ortho-tert*-Butyl-*N*-cyclopentylaniline 80c**

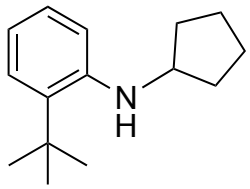

80c

^{1}H NMR (400 MHz, $CDCl_3$, δ ppm) 7.25 – 7.18 (d, *J* = 8Hz, 1H), 7.14 – 7.08 (t, *J* = 16, 8Hz, 1H), 6.73 – 6.59 (m, 2H), 4.0 – 3.85 (br m, 2H), 2.07 – 1.50 (m, 8H), 1.40 (s, 9H)

^{13}C NMR (100 MHz, $CDCl_3$, δ ppm) 146.1, 133.1, 127.2, 126.35, 116.5, 112.5, 54.9, 34.3, 34.0, 30.1, 24.3

HRMS-ESI ($M+H^+$): Calculated: 218.1903; Observed: 218.1903; Δm = 0 ppm

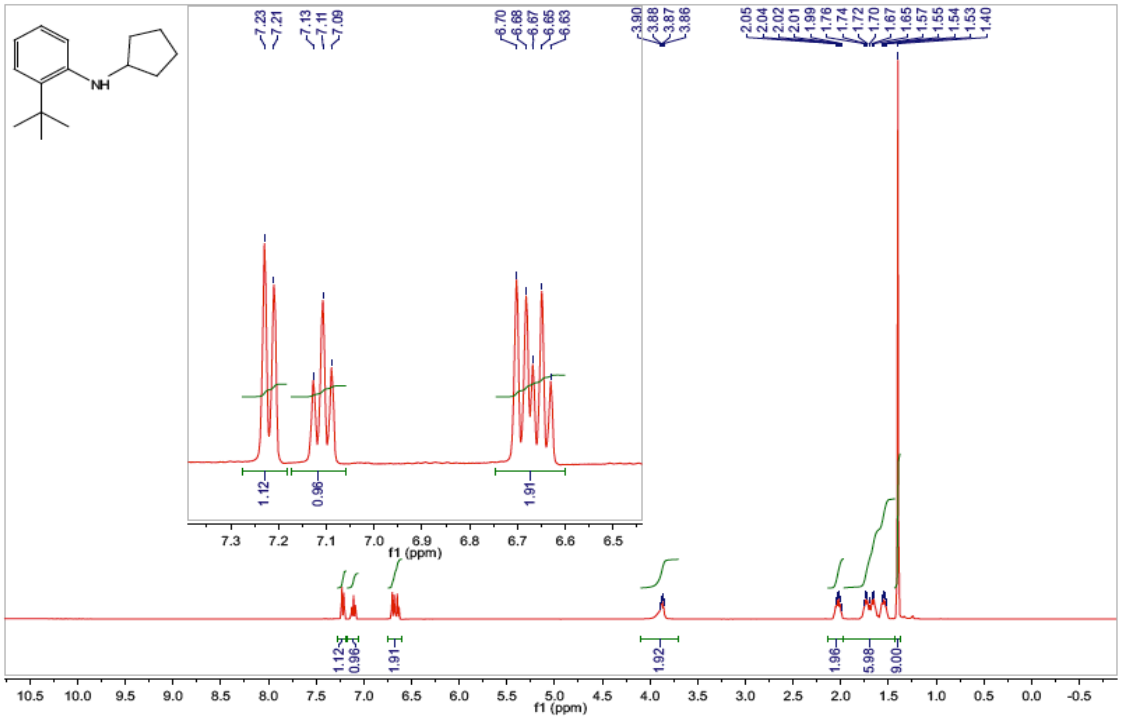

Figure 5.6: ^{1}H NMR (400 MHz, $CDCl_3$, δ ppm) spectrum for aniline **80c.**

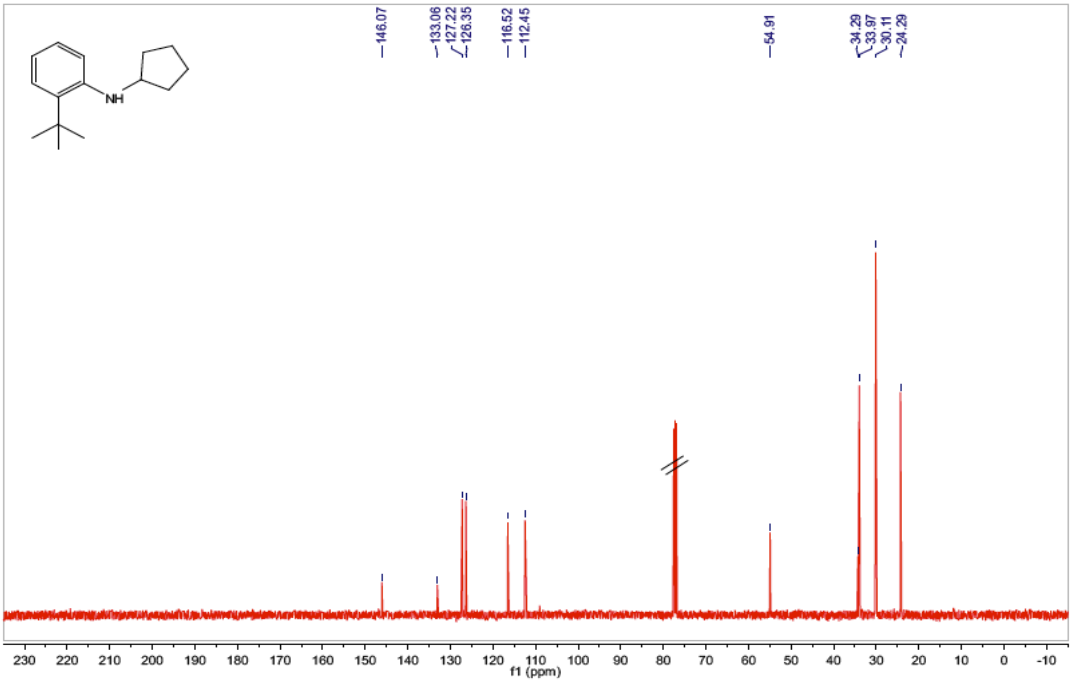

Figure 5.7: ^{13}C NMR (100 MHz, $CDCl_3$, δ ppm) spectrum for aniline **80c.**

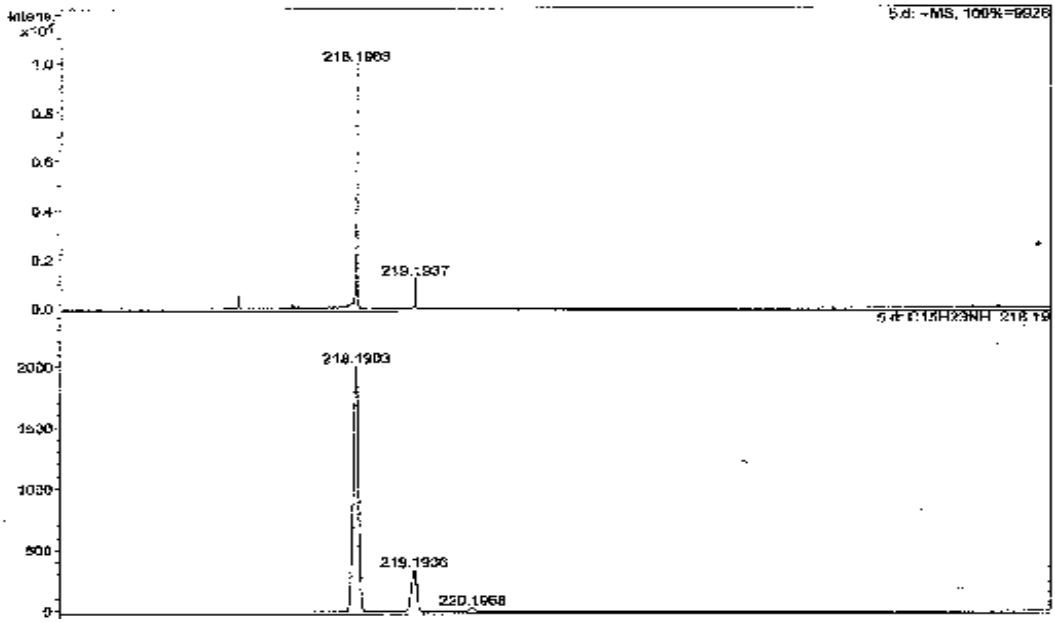

Figure 5.8: HRMS for aniline **80c**.

***ortho-tert*-Butyl-*N*-cyclohexylaniline 80d**

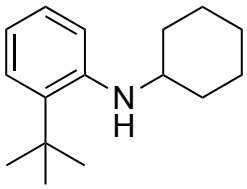

80d

^{1}H NMR (400 MHz, $CDCl_3$, δ ppm) 7.24 – 7.19 (dd, *J* = 8, 4Hz, 1H), 7.11 – 7.04 (m, 1H), 6.7 – 6.58 (m, 2H), 3.9 – 3.75 (d, 1H), 3.45 – 3.32 (m, 1H), 2.2 – 1.1 (m, 19H)

^{13}C NMR (100 MHz, $CDCl_3$, δ ppm) 145.5, 132.8, 127.3, 126.6, 116.3, 112.1, 51.8, 34.3, 33.6, 30.2, 26.3, 25.1

HRMS-ESI [$(M+Na)^+$]: Calculated: 232.2060; Observed: 232.2064; Δm = 1.7 ppm

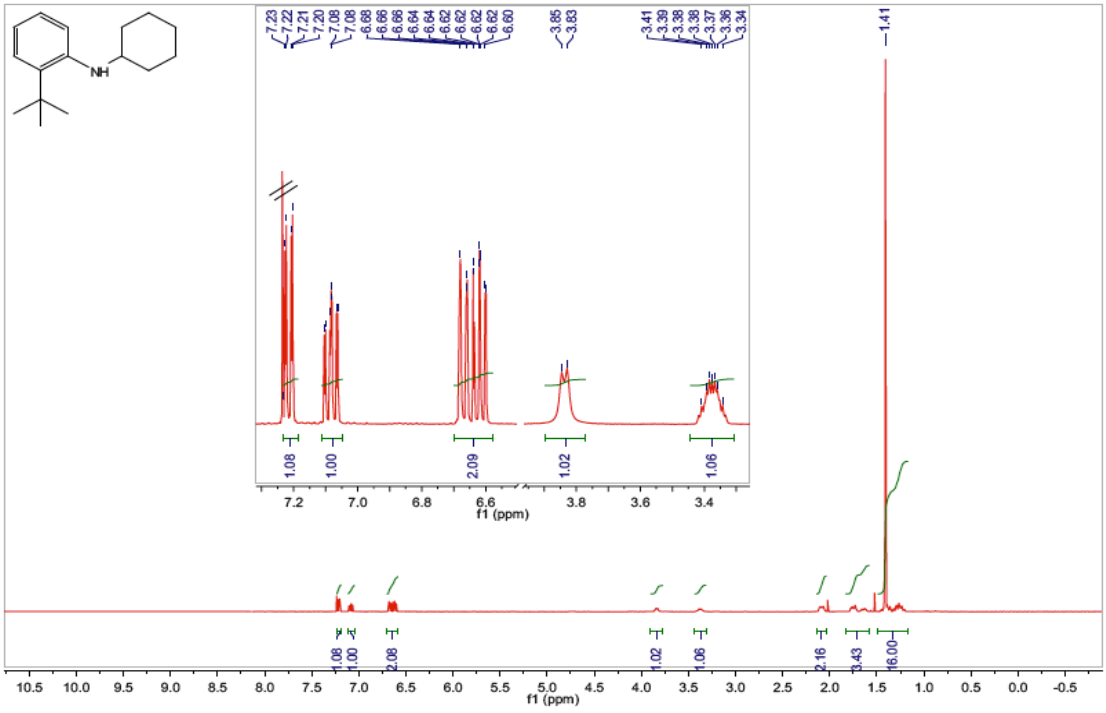

Figure 5.9: ^{1}H NMR (400 MHz, $CDCl_3$, δ ppm) spectrum for aniline **80d.**

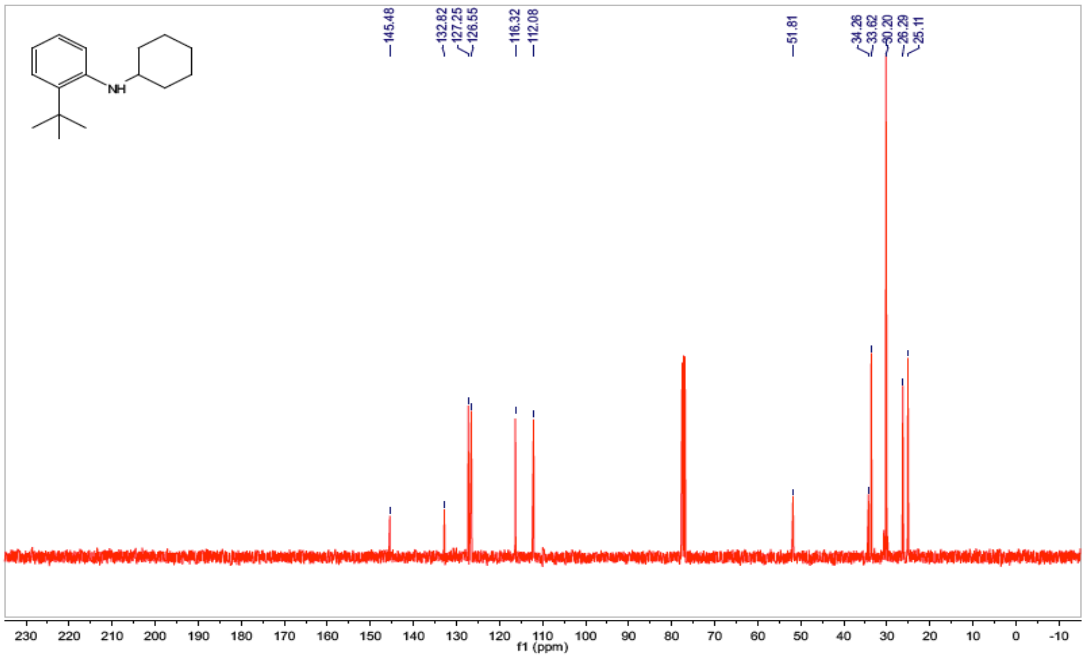

Figure 5.10: ^{13}C NMR (100 MHz, $CDCl_3$, δ ppm) spectrum for aniline **80d.**

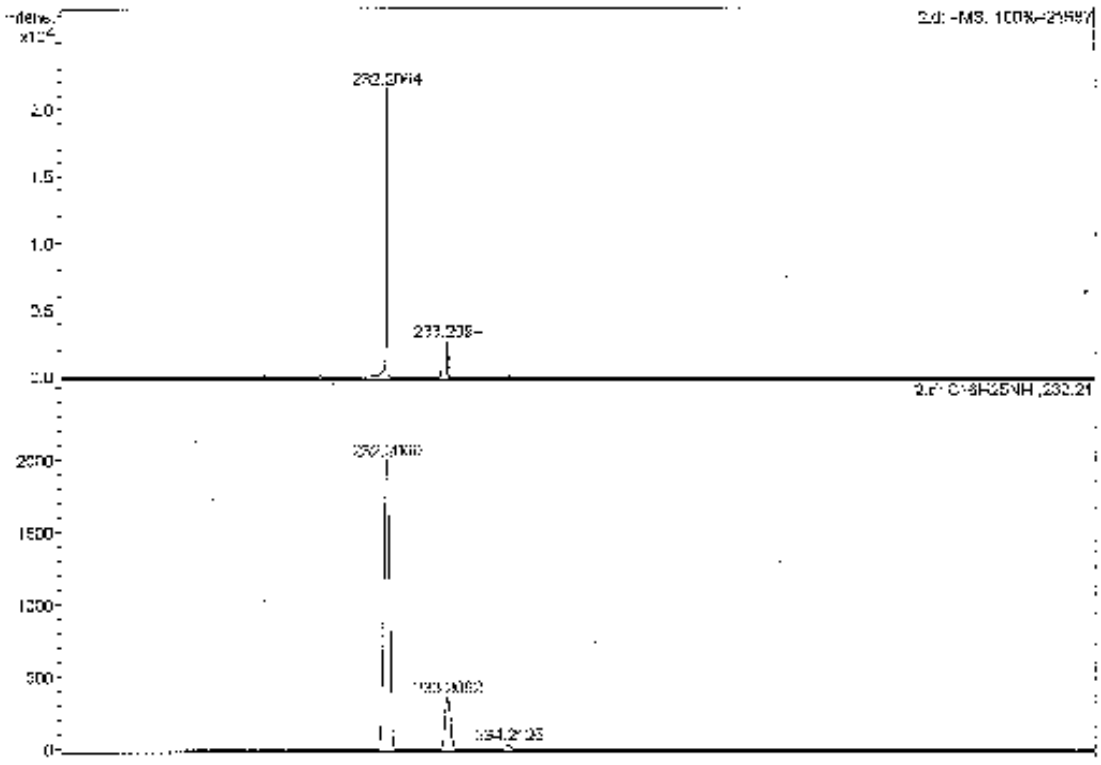

Figure 5.11: HRMS for aniline **80d**.

5.5.5. Synthesis of acrylanilides 72h-j

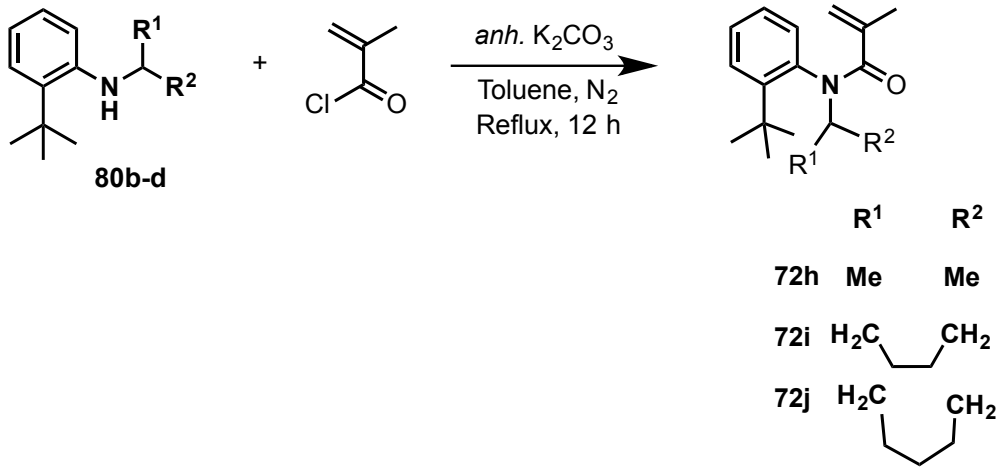

Scheme 5.8: Synthesis of acrylanilides **72h-j.**

Acrylanilides **72h-j** were prepared using procedures reported in literature. [22] In a typical reaction, freshly synthesized aniline **80b-d** (1 equiv.) was dissolved in 20 mL of toluene. The aniline solution was then stirred and purged with N_2 gas. *Anh.* K_2CO_3 (1.2 equiv.) and methacryloyl chloride (1.5 equiv.) were respectively and slowly added to the solution with continuous stirring. The new solution was allowed to reflux (100 ^oC) overnight (12 h). After, the reaction was quenched with 10 – 20 mL of DI water followed by extraction of the organic layer with EtOAc (2 x 20 mL). The organic layer was then dried over *anh.* Na_2SO_4 and concentrated by roto-evaporation. The expected anilide was finally purified by chromatography (using CombiFlash®): 12 g silica; flow rate: 22 mL/min, solvent system: 15% EtOAc : Hexanes.

5.5.6. Characterization of acrylanilides 72h-j

Acrylanilide 72h

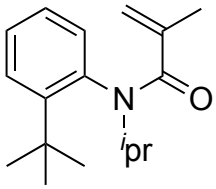

72h

^{1}H NMR (400 MHz, $CDCl_3$, δ ppm) 7.55 – 7.42 (d, *J* = 8Hz, 1H), 7.30 – 7.20 (m, 1H), 7.15 – 7.0 (m, 2H), 5.24 – 4.84 (Olefinic H, minor & major conformers, s, 2H), 5.01 (s, 1H), 4.84 (s, 1H), 4.55 – 4.40 (m, 1H), 2.07 & 1.72 (acryl CH_3, minor & major

conformers, s, 3H), 1.45 – 1.4 (d, *J* = 4Hz, 3H), 1.30 (s, 9H), 0.9 – 0.84 (d, *J* = 8Hz, 3H)

^{13}C NMR (100 MHz, $CDCl_3$, δ ppm) 170.2, 147.3, 141.6, 136.9, 132.6, 131.2, 128.2, 125.7, 121.0, 49.7, 36.6, 32.8, 22.5, 21.4, 20.1

HRMS-ESI (M+Na^+): Calculated: 282.1828; Observed: 282.1823; Δm = 1.8 ppm

Polarimetry*:* $[\alpha]^{27}_{D}$

72h: (*c* 0.03 in $CHCl_3$) = +120.0 deg.

ent-**72h**: (*c* 0.03 in $CHCl_3$) = –126.7 deg

HPLC Conditions: Column: (R,R) WHELK–01 for analysis and AD-H for separation;

Abs. detector: 254 nm and 270 nm**;** mobile phase: Hexanes:IPA = 98:2

Flow rate: 1 mL/min (Analysis), and 2.5 mL/min (separation)

Retention time (min): (+)-**72h:** ~31.3, (-)-**72h:** ~43.8

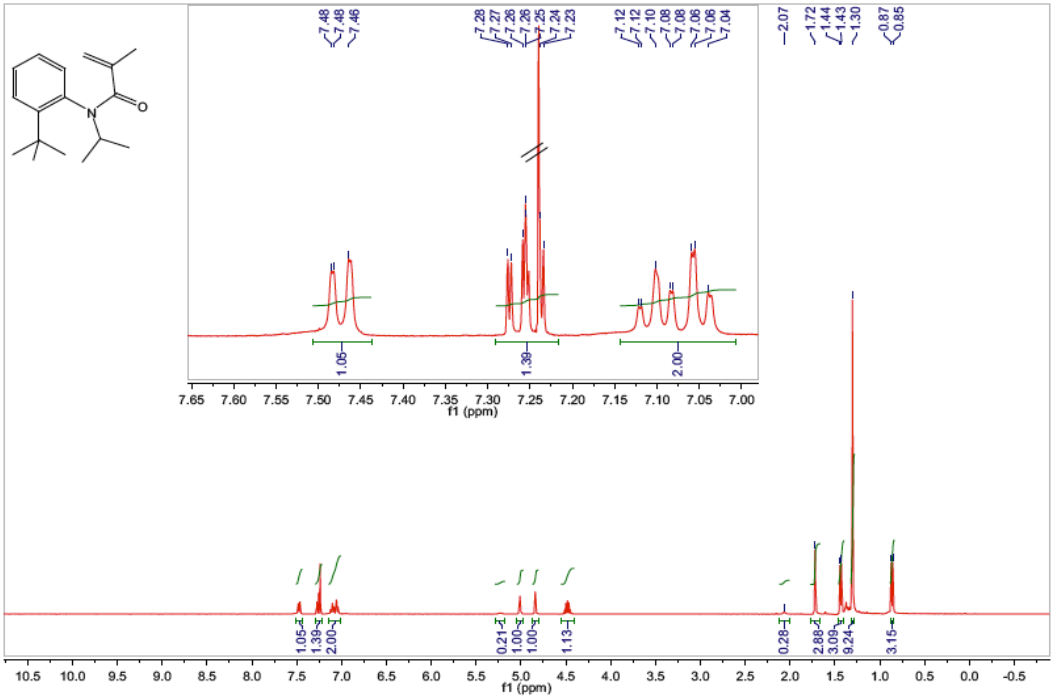

Figure 5.12: ^{1}H NMR (400 MHz, $CDCl_3$, δ ppm) spectrum for acrylanilide **72h.**

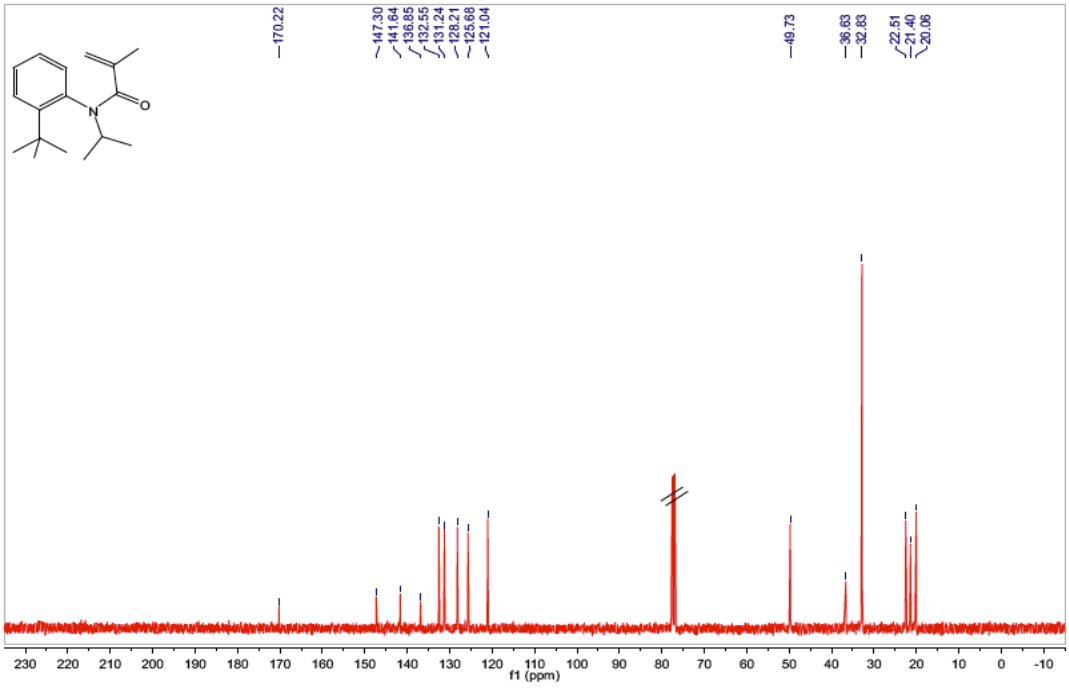

Figure 5.13: ^{13}C NMR (100 MHz, $CDCl_3$, δ ppm) spectrum for acrylanilide **72h.**

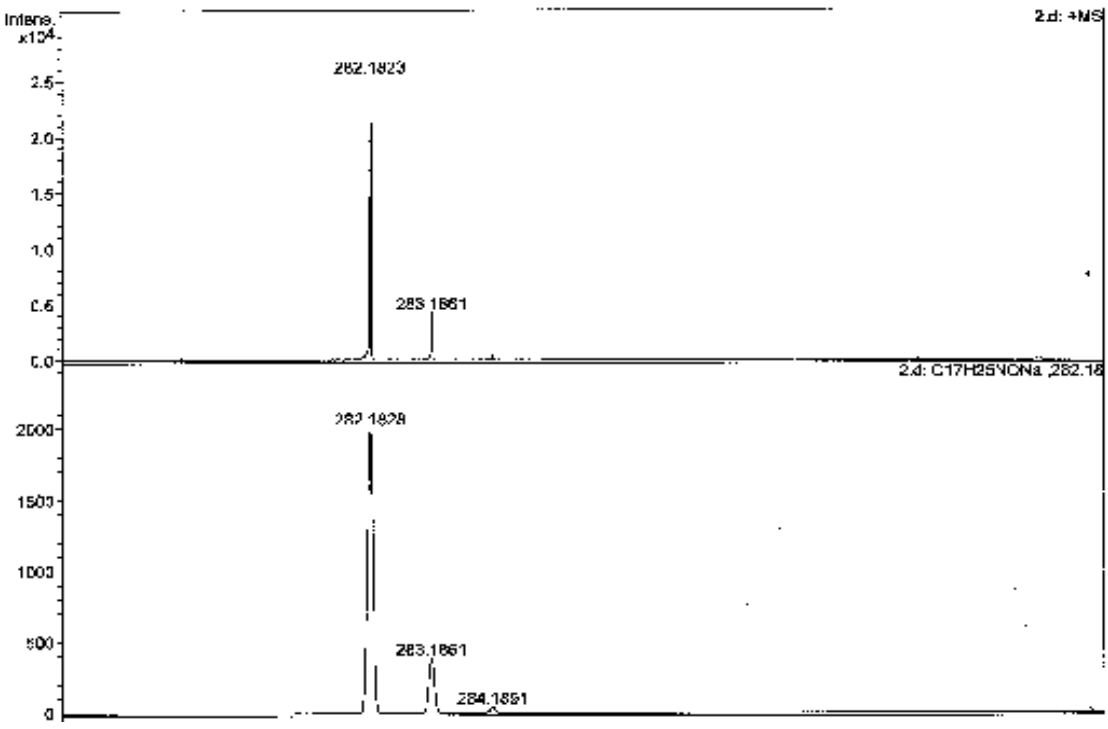

Figure 5.14: HRMS for acrylanilide **72h.**

CD Spectroscopy:

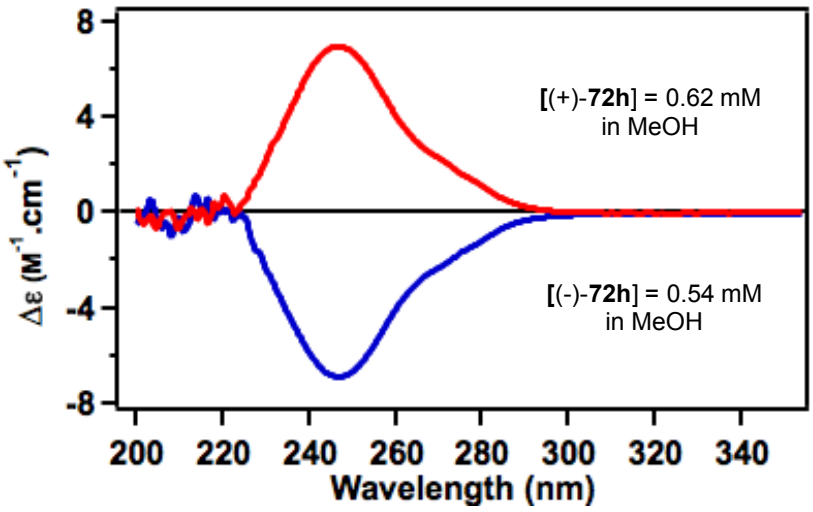

Figure 5.15: CD spectra for acrylanilide individual optically pure isomers of **72h.**

Acrylanilide 72i

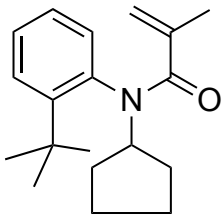

72i

^{1}H NMR (400 MHz, $CDCl_3$, δ ppm) 7.52 – 6.9 (Ar, major and minor conformers, 4H), 5.18 (br s, olefinic H, minor conformer), 4.93 (s, 1H), 4.76 (s, 1H), 4.45 – 4.30 (m, 1 H), 4.11 – 4.0 (m, Me_2CH, minor conformer), 2.5 – 1.0 (major and minor conformers, 26H)

^{13}C NMR (100 MHz, $CDCl_3$, δ ppm) 170.7, 147.1, 141.6, 138.0, 132.6, 131.0, 128.3, 126.0, 120.1, 61.3, 36.6, 32.7, 32.4, 32.1, 29.2, 24.4, 24.0, 21.7

HRMS-ESI (M+Na$^+$): Calculated: 308.1985; Observed: 308.1980; Δm = 1.6 ppm

Polarimetry*:* $[\alpha]^{27}_{D}$

72i: (*c* 0.04 in $CHCl_3$) = +80.0 deg.

ent-**72i**: (*c* 0.04 in $CHCl_3$) = –82.5 deg.

HPLC Conditions: Column: (R,R) WHELK–01 for analysis and AD-H for separation;

Abs. detector: 254 nm and 270 nm; mobile phase: Hexanes:IPA = 98:2;

Flow rate: 1 mL/min (Analysis), and 2.5 mL/min (separation)

Retention time (min): (+)-**72i:** ~47.6, (-)-**72i:** ~67.7

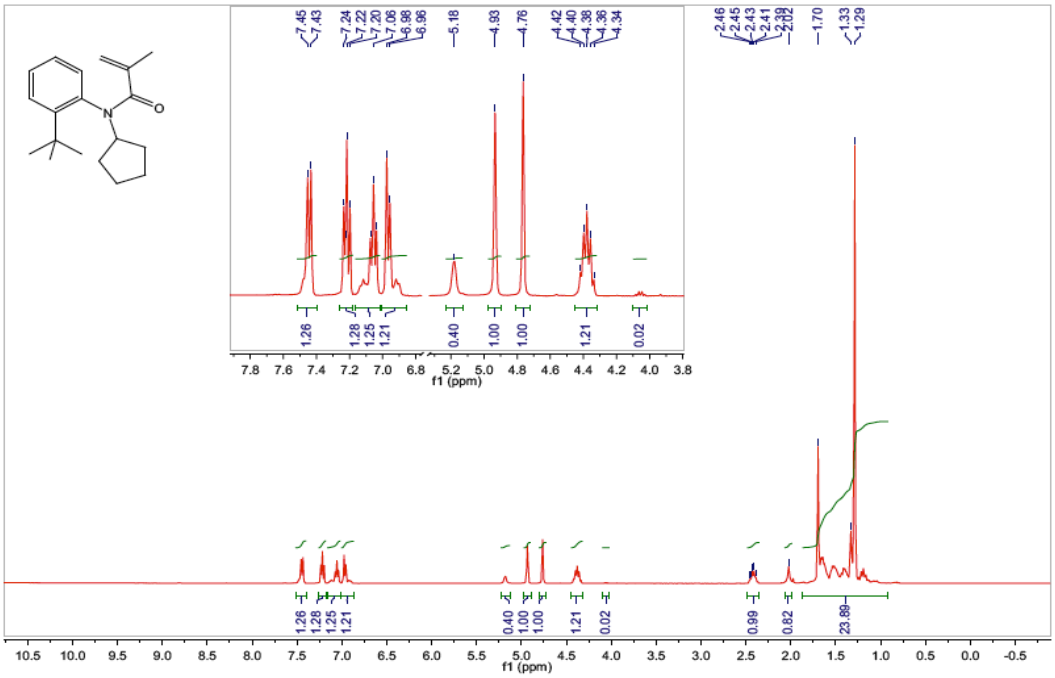

Figure 5.16: ^{1}H NMR (400 MHz, $CDCl_3$, δ ppm) spectrum for acrylanilide **72i.**

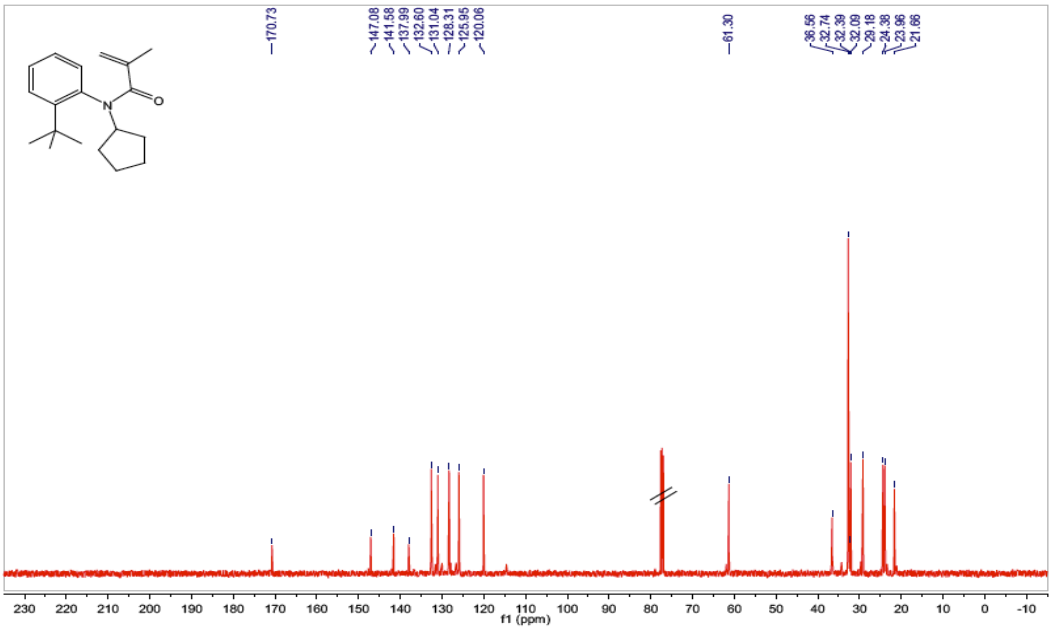

Figure 5.17: ^{13}C NMR (100 MHz, $CDCl_3$, δ ppm) spectrum for acrylanilide **72i.**

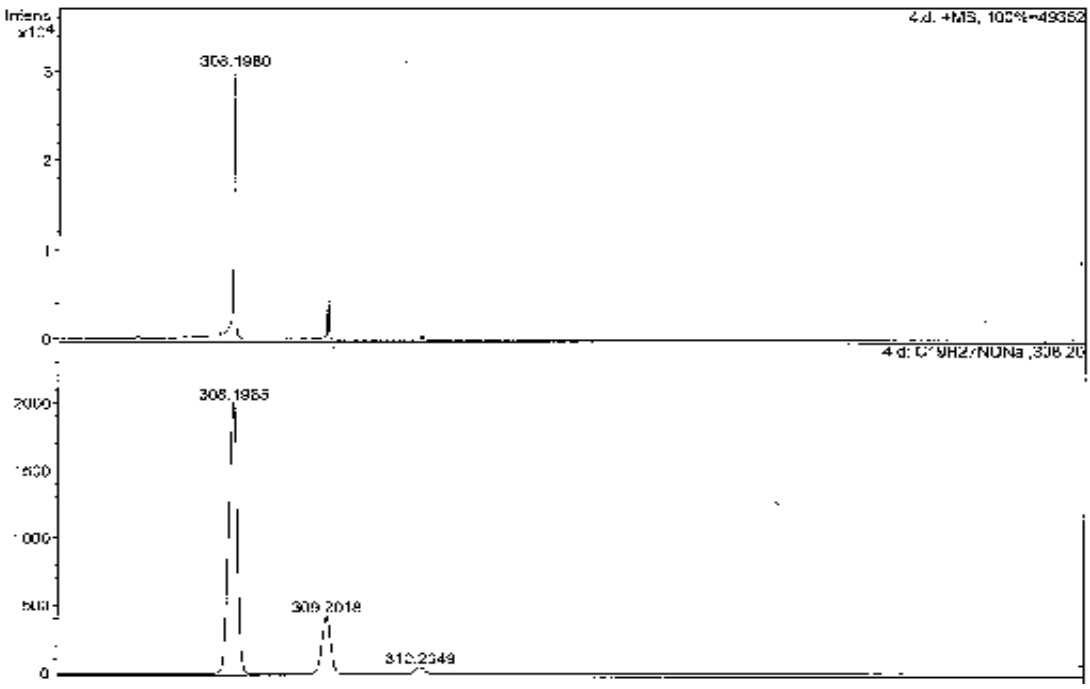

Figure 5.18: HRMS for acrylanilide **72i.**

CD Spectroscopy:

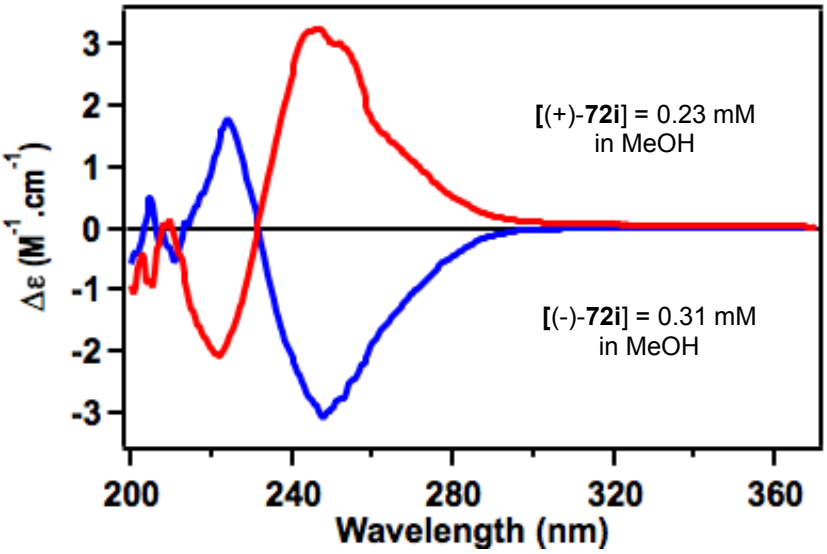

Figure 5.19: CD spectra for acrylanilide individual optically pure isomers of **72i.**

Acrylanilide 72j

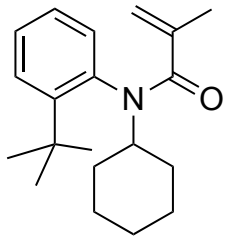

72j

^{1}H NMR (400 MHz, $CDCl_3$, δ ppm) 7.5 – 7.0 (Ar, major and minor conformers, 4H), 5.20 (br s, Olefinic H, minor conformer), 4.98 (s, 1H), 4.82 (s, 1H), 4.15 – 3.9 (m, 1H), 2.6 – 0.6 (major and minor conformers, 27H)

^{13}C NMR (100 MHz, $CDCl_3$, δ ppm) 167.0, 147.4, 141.6, 136.9, 132.7, 131.1, 128.1, 125.6, 121.0, 58.2, 36.6, 33.2, 32.9, 32.6, 31.0, 26.3, 26.2, 26.0, 21.4

HRMS-ESI ($M+Na^+$): Calculated: 322.2141; Observed: 322.2153; Δm = 3.7 ppm

Polarimetry*:* $[\alpha]^{27}_{D}$

72j: (*c* 0.0052 in MeOH) = +163.5 deg.

ent-**72j**: (*c* 0.051 in MeOH) = –164.7 deg.

HPLC Conditions: Column: CHIRALPAK® IC for analysis and AD-H for separation;

Abs. detector: 254 nm and 270 nm; mobile phase: Hexanes:IPA = 98:2;

Flow rate: 1 mL/min (Analysis), and 2.5 mL/min (separation)

Retention time (min): (+)-**72j:** ~28.00, (-)-**72j:** ~32.47

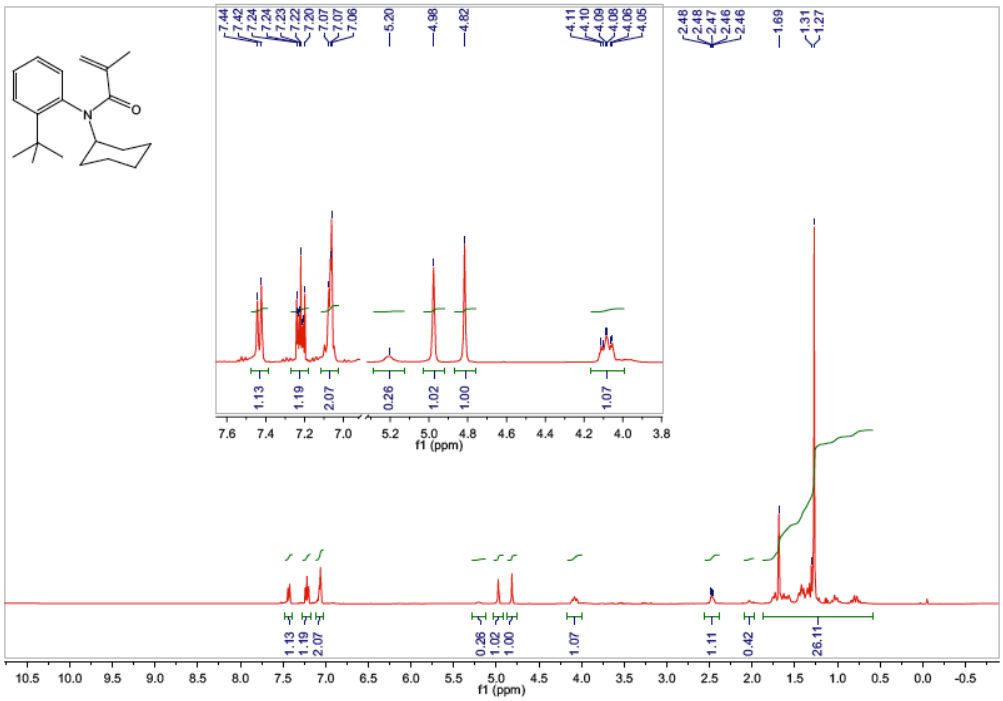

Figure 5.20: ^{1}H NMR (400 MHz, $CDCl_3$, δ ppm) spectrum for acrylanilide **72j.**

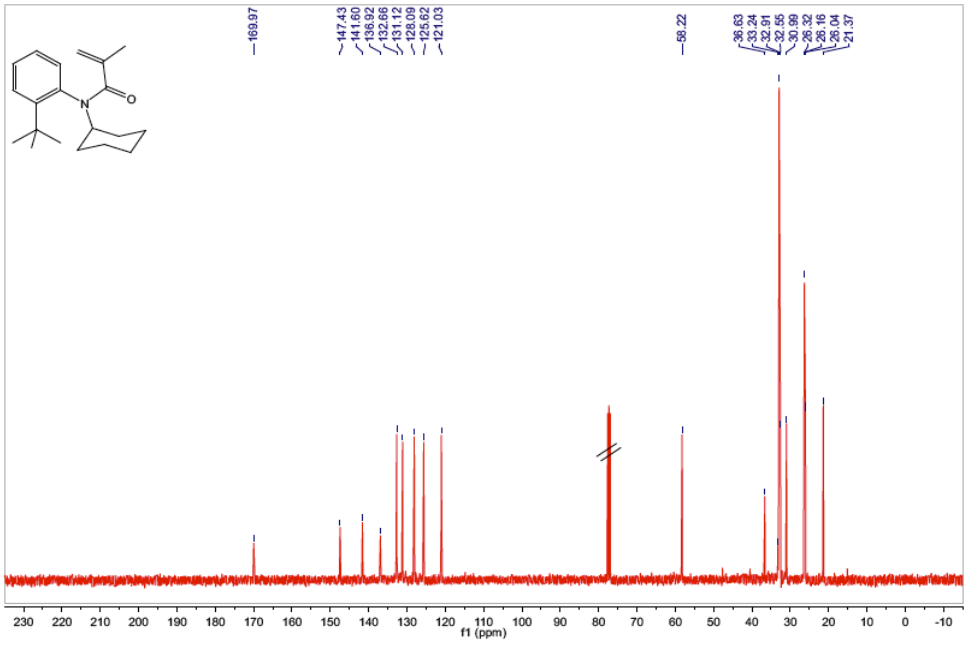

Figure 5.21: ^{13}C NMR (100 MHz, $CDCl_3$, δ ppm) spectrum for acrylanilide **72j.**

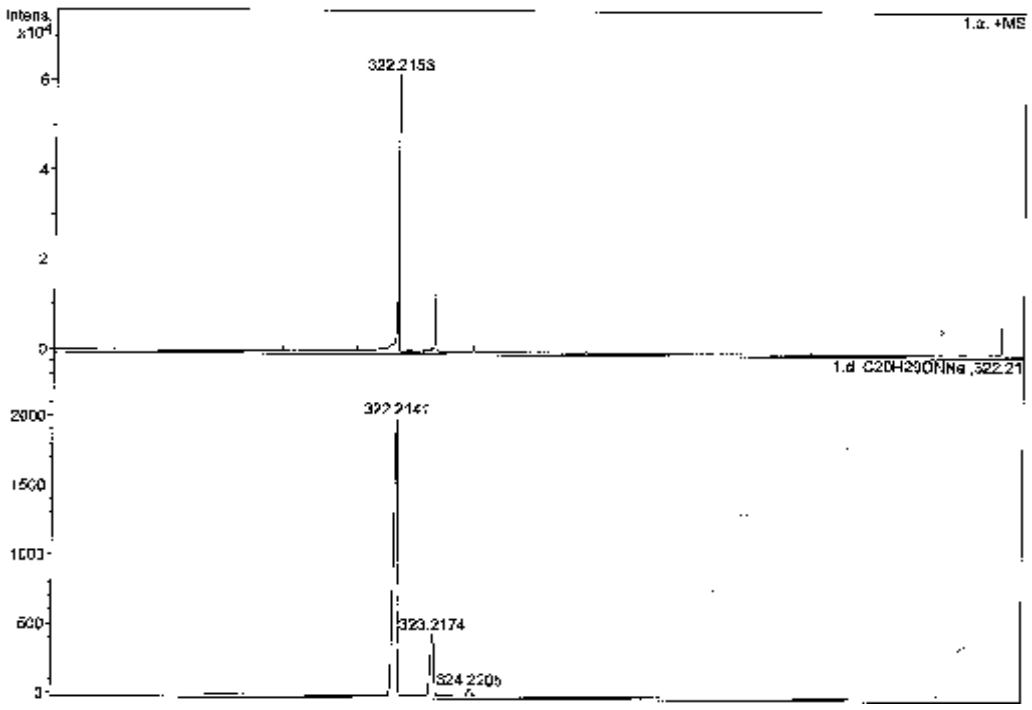

Figure 5.22: HRMS for acrylanilide **72j.**

CD Spectroscopy:

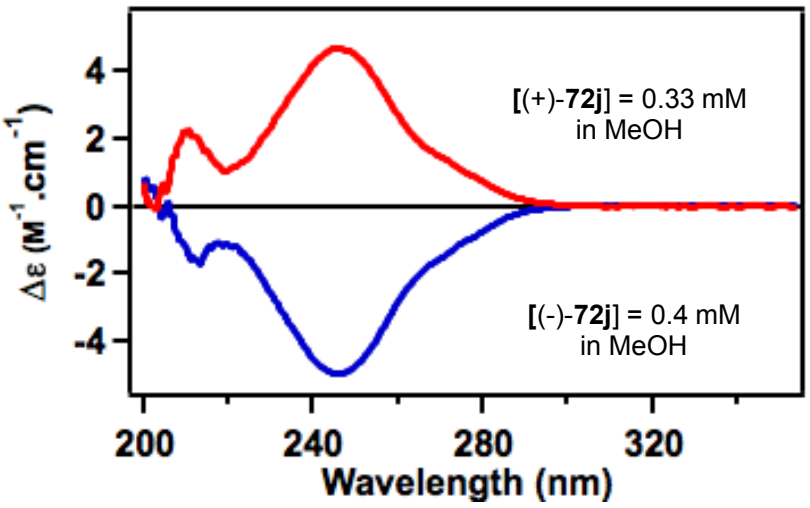

Figure 5.23: CD spectra for acrylanilide individual optically pure isomers of **1e.**

5.5.7. Photo-irradiation procedures for acrylanilides 72h-j

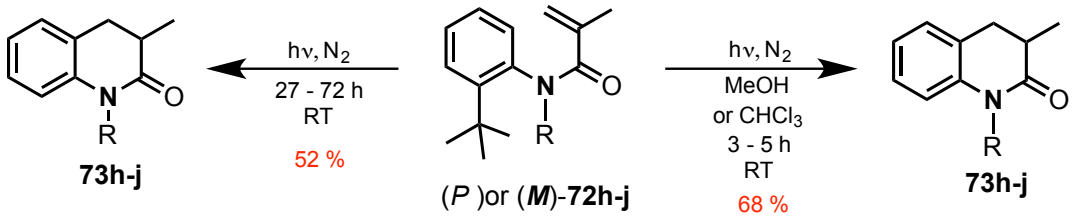

Scheme 5.9: solvent-free reaction conversion: R = ^{i}pr, time = 70 h
Reaction in MeOH: R = cyclopentyl, time = 5 h

Solvent-free photoreaction: Optically pure isomers of **72h-j** were separated (using HPLC) and recrystallized overnight inside a 13 mm Pyrex test tube. The test tube was mounted on a merry-go-around, and was then exposed to a medium pressure Hg lamp at room temperature (26 ± 2 ^{o}C) for 27 – 72 h. During the course of the reaction, the conversion of the crystals to the corresponding product was perceptible by the formation of a brownish glue-like substance. After, the crystals+brownish substance was dissolved in a minimum of chloroform ($CHCl_3$), and chromatographed to obtain the expected photoproduct.

Note: *The amount of isolated photoproduct(s) depends on the quality of the crystals, the irradiation time, and the temperature of the reaction environment.*

Photoreaction in Solution (MeOH, $CHCl_3$): Optically pure isomers of **72h-j** were separated (using HPLC) and dissolved in MeOH/$CHCl_3$ (1mg/mL). The solutions were deaerated with N_2 gas, and exposed to a medium pressure Hg lamp at room temperature (26 ± 2 ^{o}C) for 3 – 5 h. After, the solvent was either removed by purging air through the solution for HPLC analysis (on chiral stationary phase) or chromatographed in order to isolate the expected photoproduct(s) for spectroscopy/spectrometry analysis.

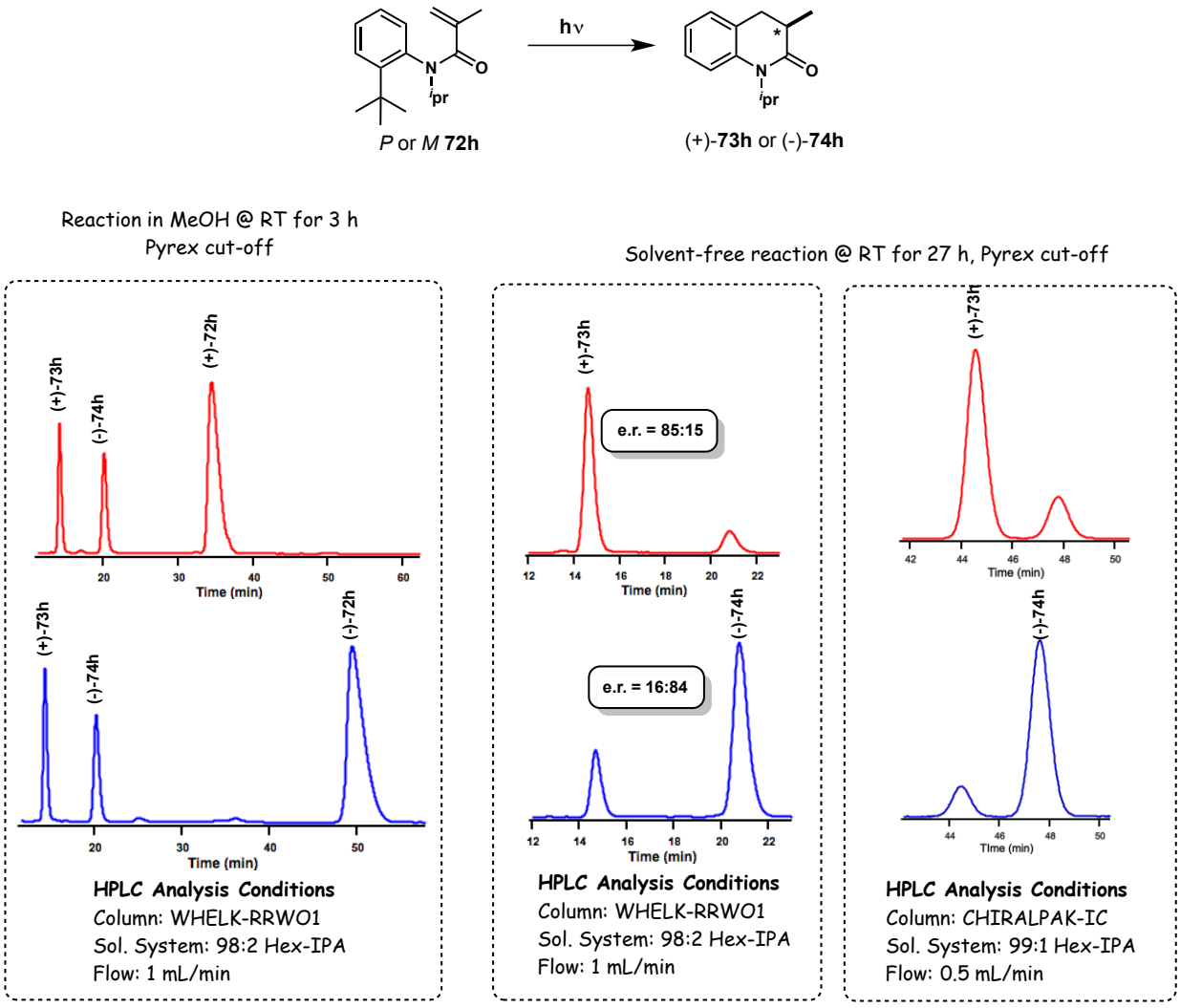

Scheme 5.10: HPLC traces comparison of solvent-free reaction and irradiation in MeOH.

Note: *The enantiomer of 2c were injected in two different chiral stationary phases viz. WHELK-RRWO1 and CHIRALPAK IC to verify the enantiomeric ratios.*

5.5.8. Characterization for quinolinone 73h-j = 74h-j

Quinolinone *R*-(+)-**73h** = *S*-(-)-**74h**

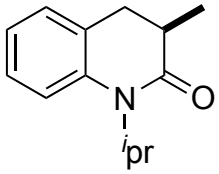

R-(+)-**73h** = *S*-(-)-**74h**

Purification Conditions: CombiFlash®: 12 g silica; flow rate: 20 mL/min; Solvent system: 6 % EtOAc: Hexanes

^{1}H NMR (400 MHz, $CDCl_3$, δ ppm) 7.21 – 7.14 (t, *J* = 16, 8 Hz, 1H), 7.15 – 7.05 (m, 2H), 7.0 – 6.92 (t, *J* = 16, 8 Hz, 1H), 4.71 – 4.57 (m, 1H), 2.85 –

2.74 (dd, *J* = 16, 4Hz, 1H), 2.65 – 2.55 (virt t, 1H), 2.54 – 2.4 (m, 1H), 1.53 – 1.46 (virt dd, 6H), 1.2 – 1.17 (d, *J* = 4 Hz, 3H)

^{13}C NMR (100 MHz, $CDCl_3$, δ ppm) 173.9, 140.3, 128.1, 128.0, 127.1, 122.9, 116.3, 48.8, 37.0, 33.9, 20.9, 19.9, 15.5

HRMS-ESI [$(M+Na)^+$]: Calculated: 226.1202; Observed: 226.1200; Δm = 0.9 ppm

Polarimetry*:* $[\alpha]^{26}_{D}$

73h: (*c* 0.046 in $CHCl_3$) = +73.9 deg.

74h: (*c* 0.047 in $CHCl_3$) = –78.7 deg.

HPLC Analysis Conditions: Column: (R,R) WHELK–01; Abs. detector: 254 nm and 270 nm; mobile phase: Hexanes:IPA = 98:2; Flow rate: 1 mL/min

Retention time (min): *R*-(+)-**73h:** ~14.1**,** *S*-(-)-**74h:** ~19.8

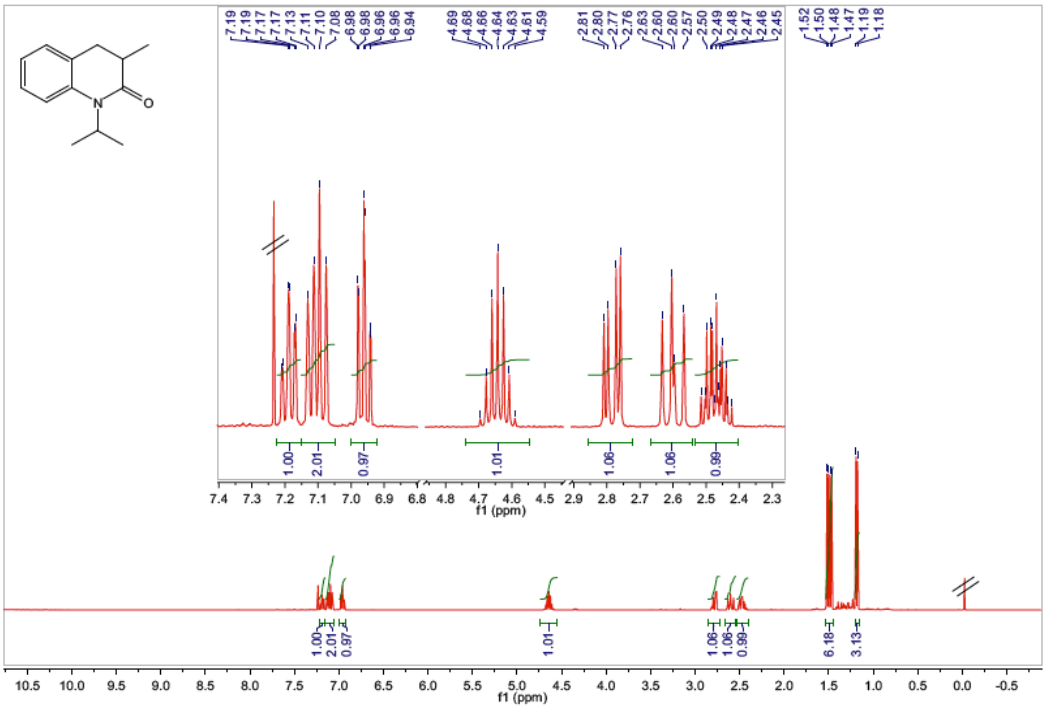

Figure 5.24: ^{1}H NMR (400 MHz, $CDCl_3$, δ ppm) spectrum for quinolinone **73h=74h.**

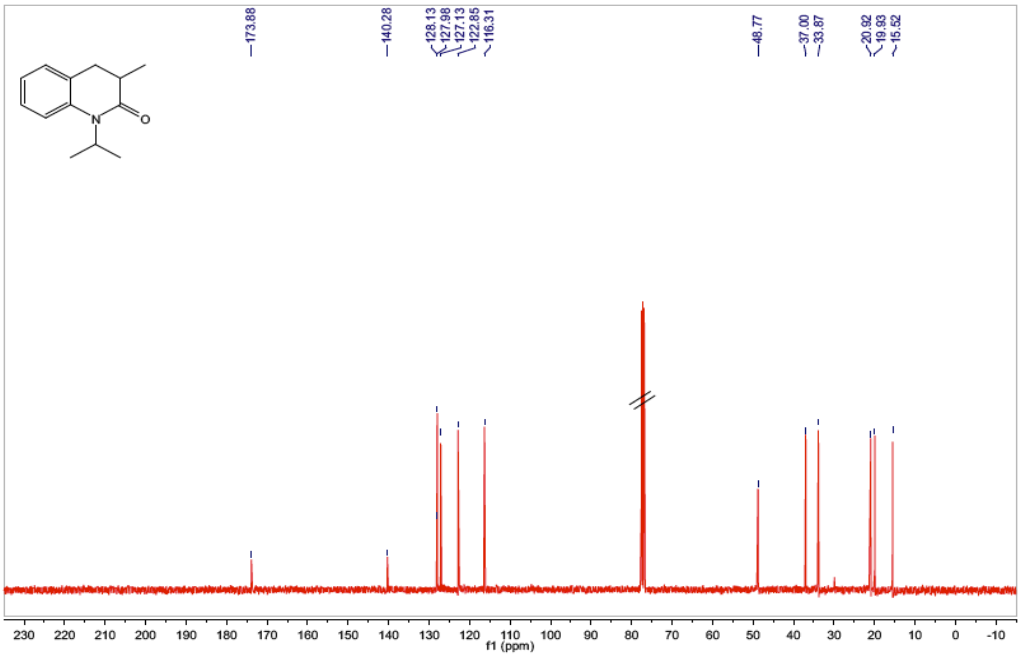

Figure 5.25: ^{13}C NMR (100 MHz, $CDCl_3$, δ ppm) spectrum for quinolinone **73h=74h.**

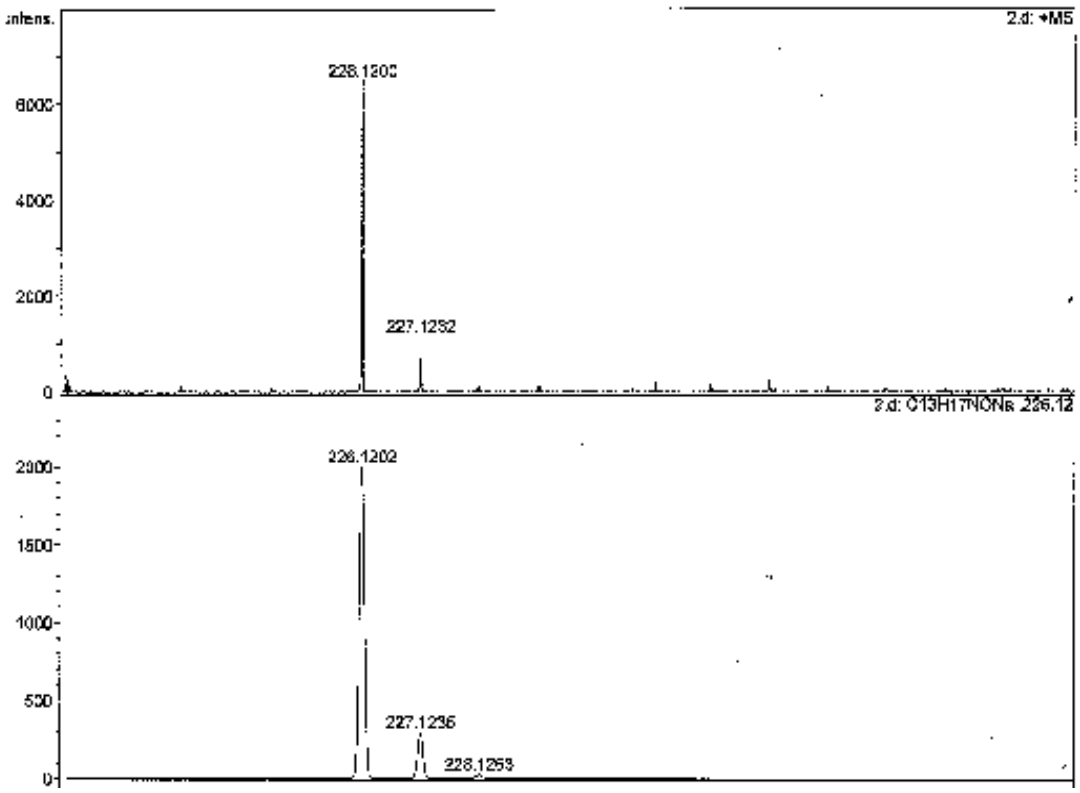

Figure 5.26: HRMS for quinolinone **73h=74h.**

Quinolinone *R*-(+)-**73i** = *S*-(-)-**74i**

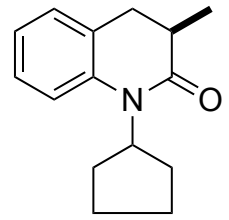

R-(+)-**73i** = *S*-(-)-**74i**

Purification Conditions: CombiFlash®: 12 g silica; flow rate: 20 mL/min; Solvent system: 12 % EtOAc: Hexanes

^{1}H NMR (400 MHz, $CDCl_3$, δ ppm) 7.21 – 7.15 (virt t, *J* = 8, 4Hz, 1H), 7.15 – 7.09 (d, *J* = 8Hz, 1H), 7.08 – 7.01 (d, 8Hz, 1H), 7.0 – 6.93 (t, *J* = 16, 8Hz, 1H), 4.73 – 4.56 (m, 1H), 2.85 – 2.74 (dd, *J* = 16, 8Hz, 1H), 2.68 – 2.55 (virt t, 1H), 2.54 – 2.4 (m, 1H), 2.3 – 1.5 (m, 9H), 1.22 – 1.16 (d, *J* = 8Hz, 3H)

^{13}C NMR (100 MHz, $CDCl_3$, δ ppm) 173.8, 140.8, 128.0, 127.9, 127.2, 122.8, 116.3, 58.0, 37.1, 33.7, 29.3, 28.8, 26.0, 25.8, 15.6

HRMS-ESI [$(M+Na)^+$]: Calculated: 252.1359; Observed: 252.1369; Δm = 4 ppm

Polarimetry*:* $[\alpha]^{24}_D$

73i: (*c* 0.098 in $CHCl_3$) = +51.2 deg.

74i: (*c* 0.1 in $CHCl_3$) = –54.0 deg.

HPLC Analysis Conditions*:* Column: (R,R) WHELK–01; Abs. detector: 254 nm and 270 nm; mobile phase: Hexanes:IPA = 98:2; Flow rate: 1 mL/min

Retention time (min): *R*-(+)-**73i:** ~14.8**,** *S*-(-)-**74i:** ~20.00

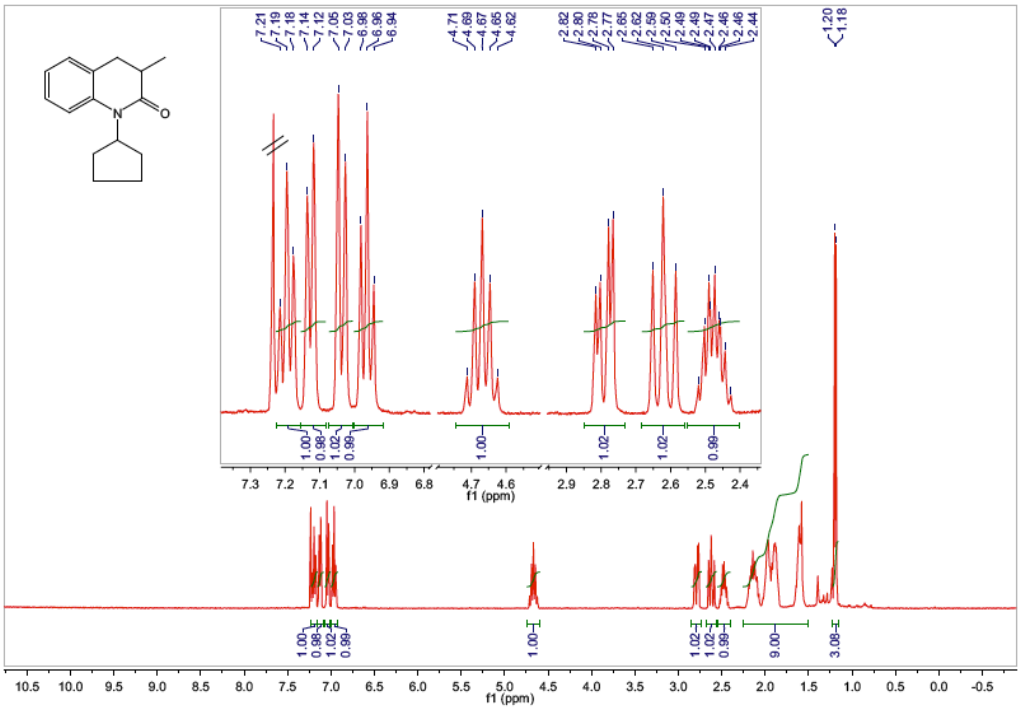

Figure 5.27: ^{1}H NMR (400 MHz, $CDCl_3$, δ ppm) spectrum for quinolinone **73i=74hi.**

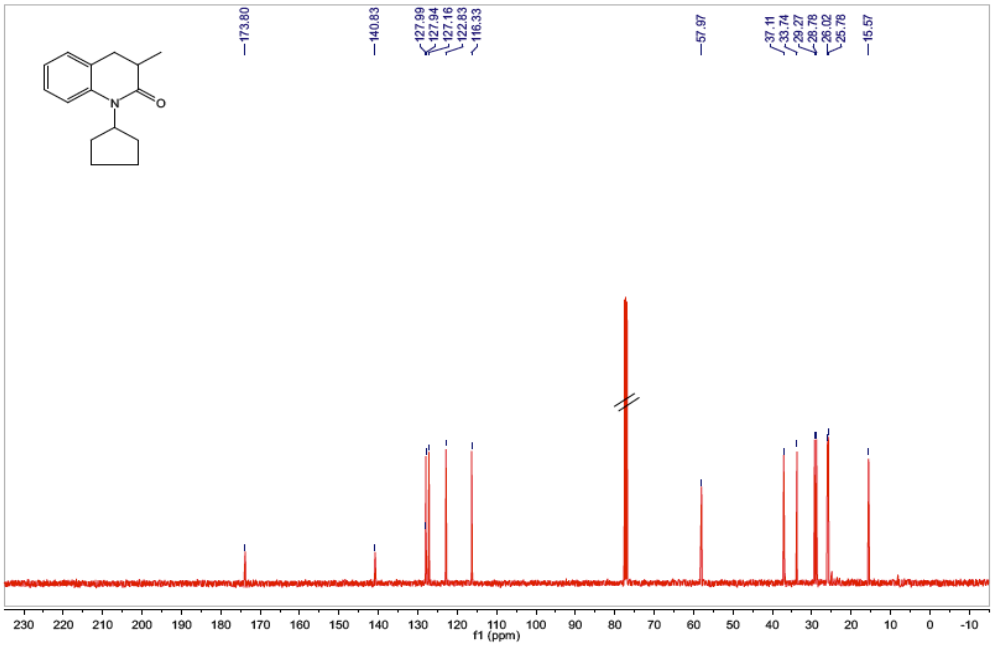

Figure 5.28: ^{13}C NMR (100 MHz, $CDCl_3$, δ ppm) spectrum for quinolinone **73i=74i.**

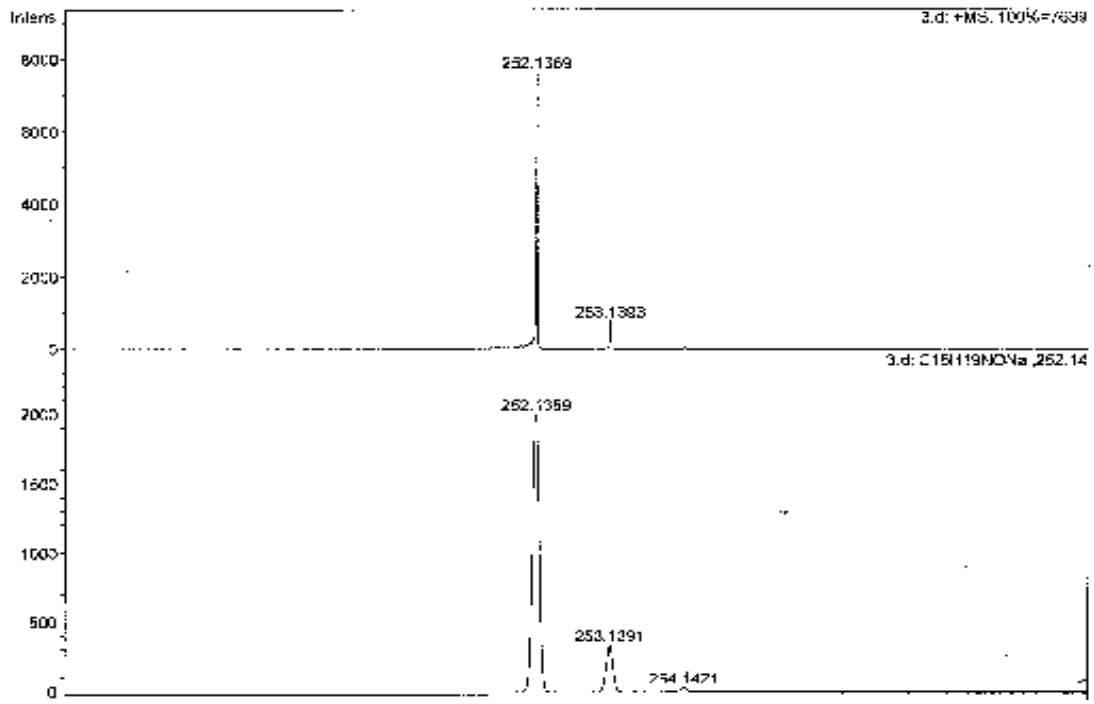

Figure 5.29: HRMS for quinolinone **73i=74i.**

Quinolinone *R*-(+)-**73j** = *S*-(-)-**74j**

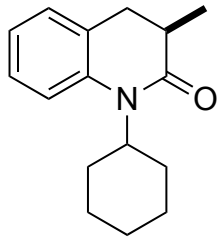

R-(+)-**73j =** *S*-(-)-**74j**

Purification Conditions: CombiFlash®: 12 g silica; flow rate: 20 mL/min; Solvent system: 9 % EtOAc: Hexanes

^{1}H NMR (400 MHz, $CDCl_3$, δ ppm) 7.25 – 7.2 (virt t, 1H), 7.2 – 7.12 (m, 2H), 7.04 – 6.95 (virt t, 1H), 4.18 – 4.05 (m, 1H), 2.85 – 2.76 (dd, *J* = 12, 4Hz, 1H), 2.7 – 2.6 (virt t, 1H), 2.55 – 2.45 (m, 1H), 2.45 – 2.31 (m, 2H), 2.0 – 1.2 (m, 13H)

^{13}C NMR (100 MHz, $CDCl_3$, δ ppm) 174.1, 140.9, 128.4, 127.9, 127.2, 122.9, 116.6, 58.6, 37.2, 34.0, 30.5, 29.7, 27.0, 26.8, 25.8, 15.6

HRMS-ESI [$(M+Na)^+$]: Calculated: 266.1515; Observed: 266.1518; Δm = 1.1 ppm

Polarimetry*:* $[\alpha]^{27}_D$

73j: (*c* 0.02 in $CHCl_3$) = +60.0 deg.

74j: (*c* 0.02 in $CHCl_3$) = –72.0 deg.

HPLC Analysis Conditions: Column: CHIRALPAK® IC; Abs. detector: 254 nm and 270 nm; mobile phase: Hexanes:IPA = 98:2; Flow rate: 1 mL/min

Retention time (min): *R*-(+)-**73j:** ~11.35**,** *S*-(-)-**74j:** ~12.82

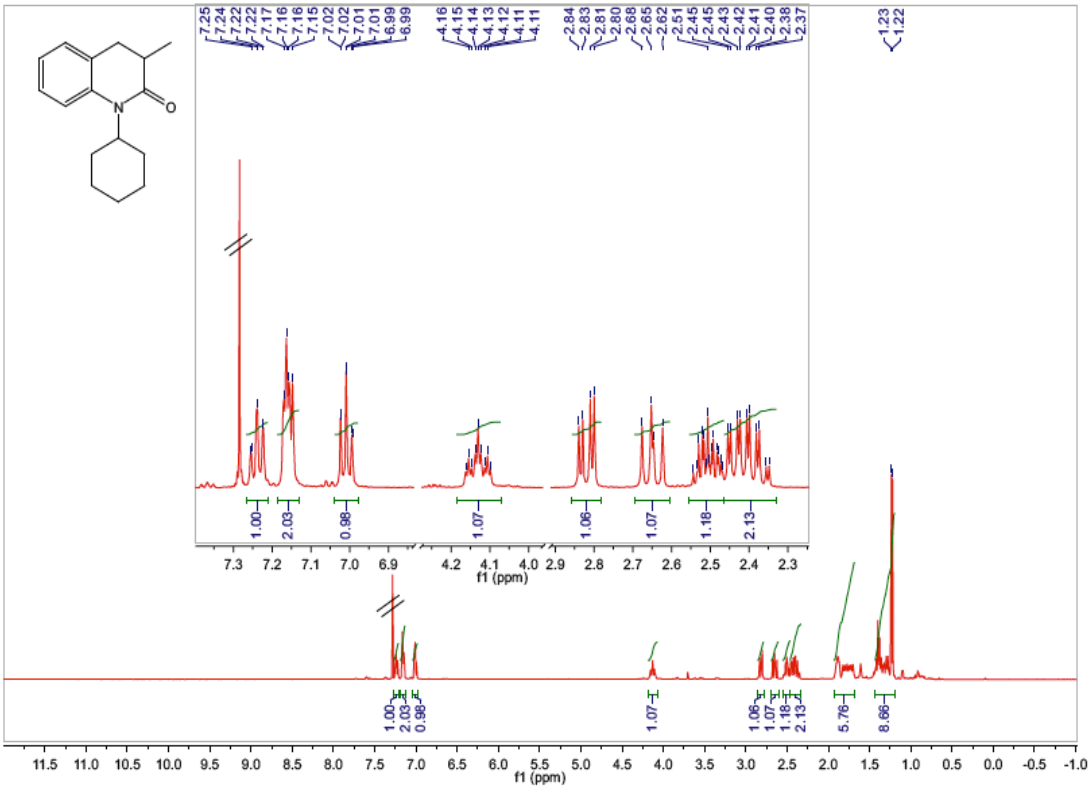

Figure 5.30: ^{1}H NMR (400 MHz, $CDCl_3$, δ ppm) spectrum for quinolinone **73j=74j.**

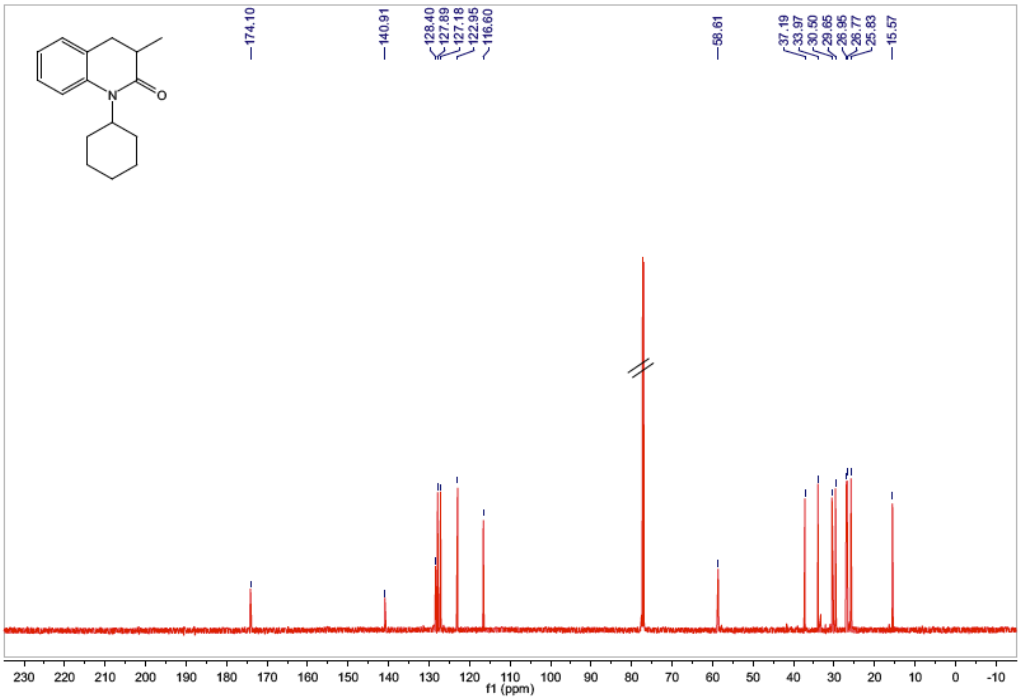

Figure 5.31: ^{13}C NMR (100 MHz, $CDCl_3$, δ ppm) spectrum for quinolinone **73j=74j.**

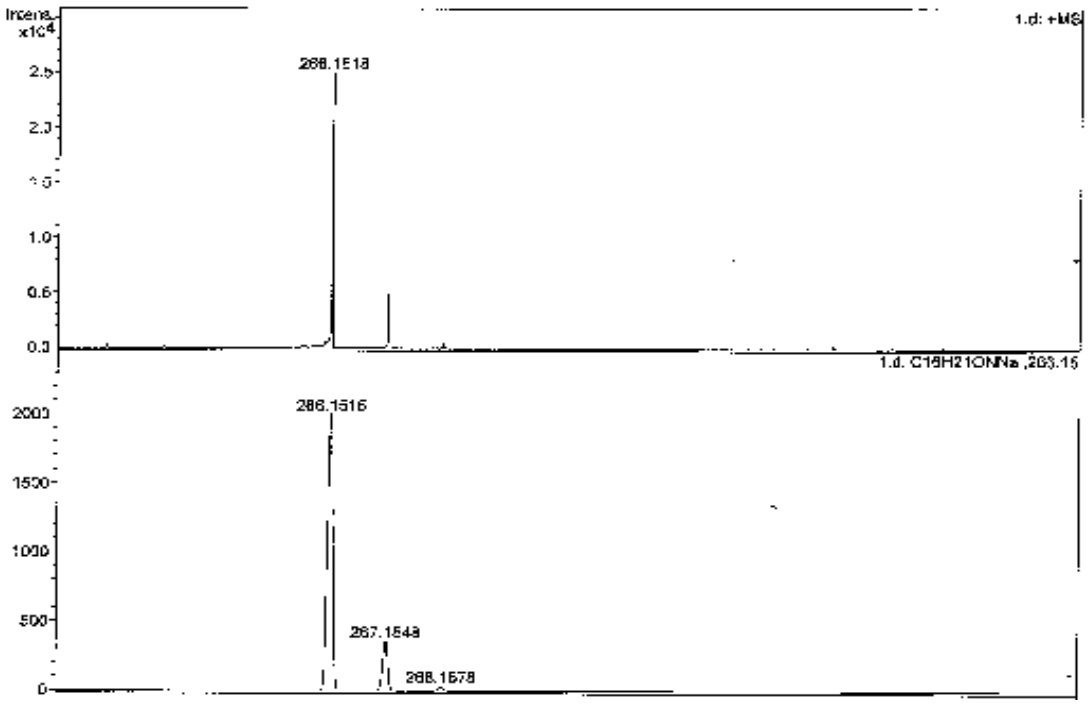

Figure 5.32: HRMS for quinolinone **73j=74j.**

5.5.9. Absolute conversion for photocyclization by ^{1}H NMR

Substrate **72h** was recrystallized in a 13 mm Pyrex tube and irradiated (450 W medium pressure Hg lamp) for 70 h at room temperature. The sample was then dissolved in 1 mL of $CDCl_3$ and analyzed by ^{1}H NMR spectroscopy with α,α'-dichloro-*para*-xylene, as an internal standard.

The number of moles of analyte (product or starting material) in the NMR aliquot is given by the following equation:[4,5]

$$mol_a = mol_i \times \left(\frac{Integral(analyte)}{Integral(Int.Std.)} \right) \times \frac{N_i}{N_a}$$

Equation 5.1

Where N_a and N_i are the number of nuclei giving rise to the relevant analyte and standard signals respectively.

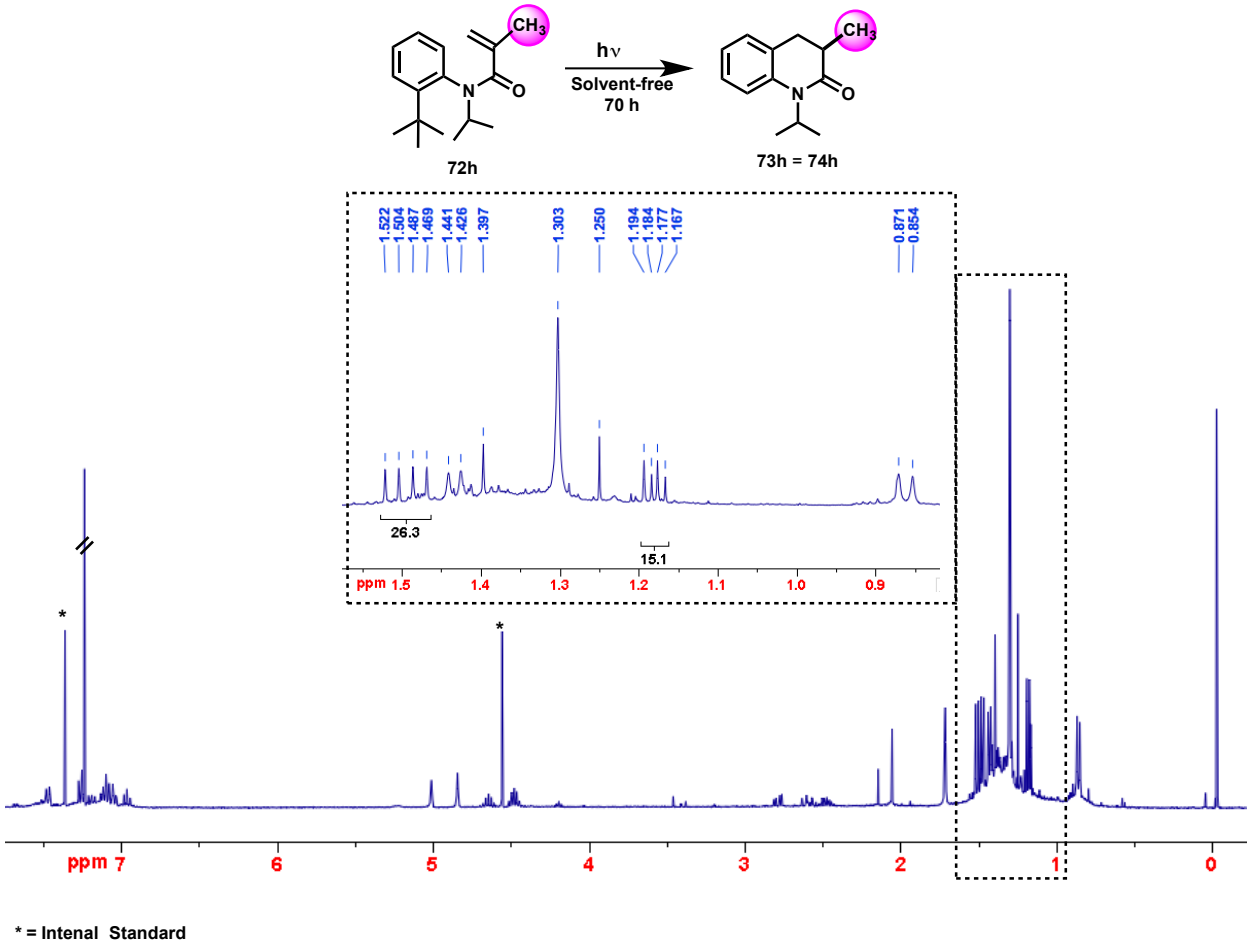

Figure 5.33: ^{1}H NMR (400 MHz, $CDCl_3$, δ ppm) for the conversion **72h** to **73h=74h:** Monitoring α-CH_3 group.

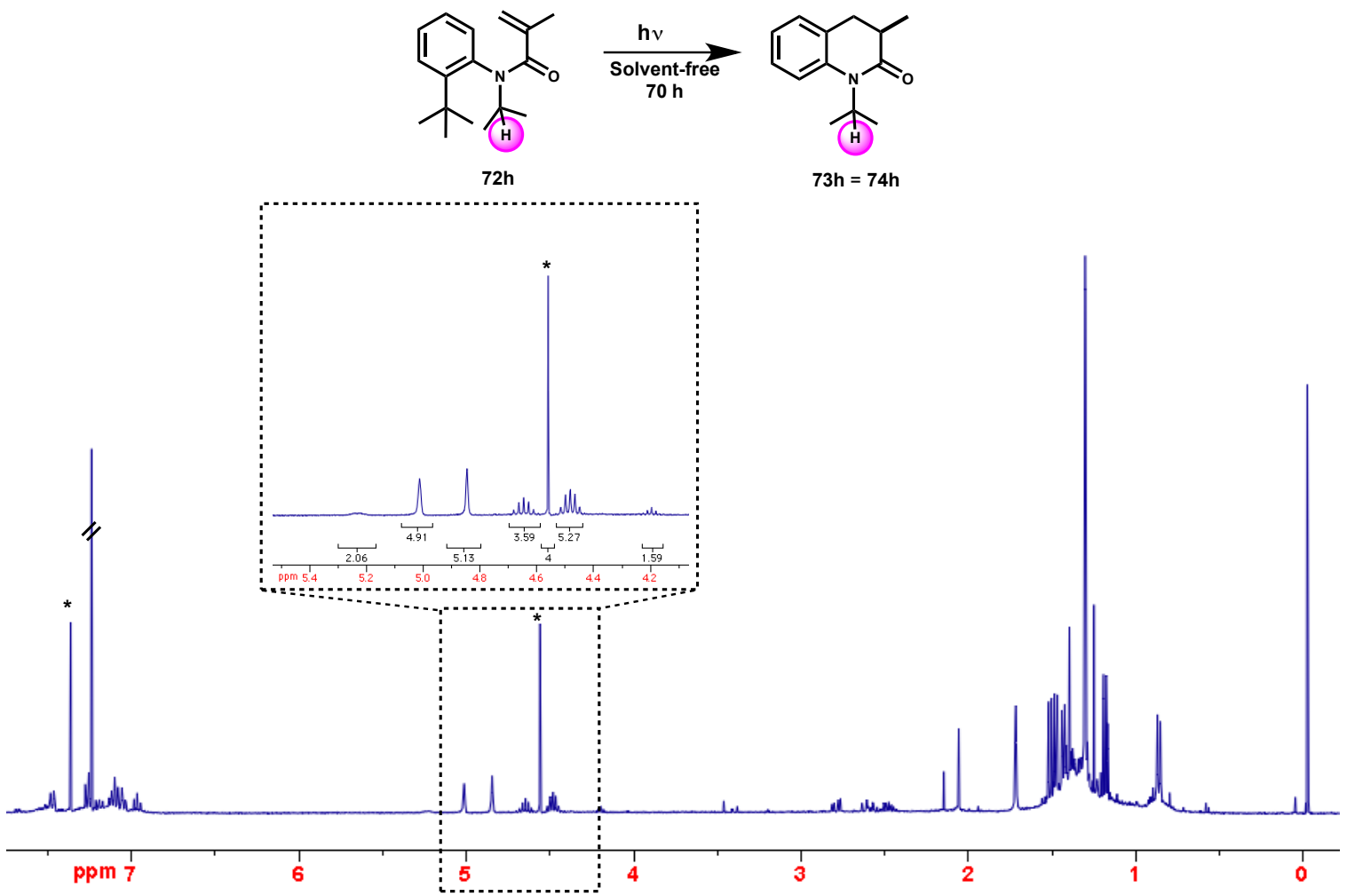

*** = Intenal Standard**

Figure 5.34: ^{1}H NMR (400 MHz, $CDCl_3$, δ ppm) for the conversion **72h** to **73h=74h:** Monitoring ^{i}Pr-H atom.

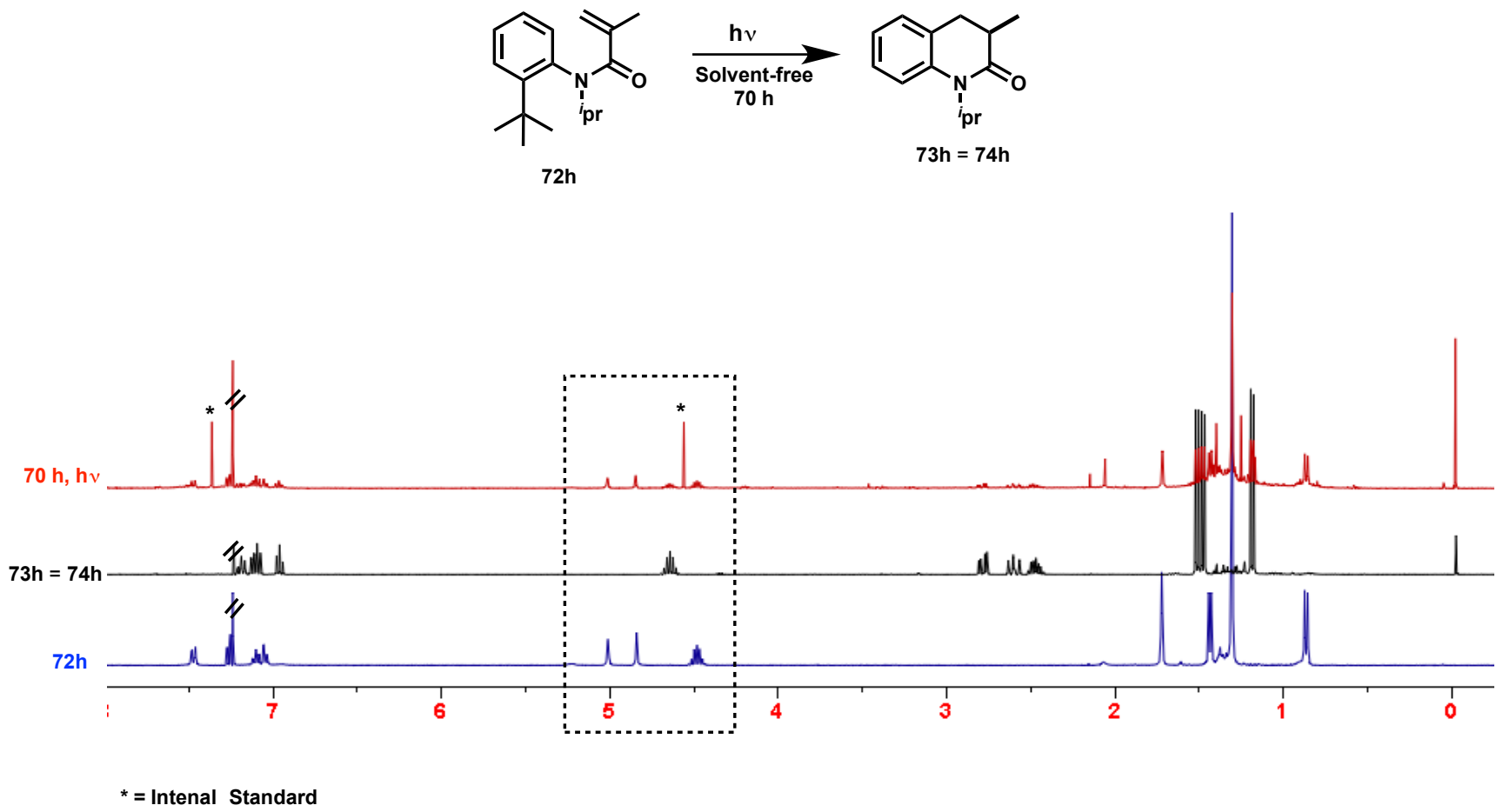

Figure 5.35: ^{1}H NMR (400 MHz, $CDCl_3$, δ ppm) comparison for the conversion **72h** to **73h=74h.**

72h: initial mass is 8.5 mg.

72h: concentration in 1 mL of $CDCl_3$ is 3.93×10^{-2} M (3.93×10^{-5} mol)

Internal Standard concentration in 1 mL of $CDCl_3$ is 3.37×10^{-3} M (3.37×10^{-6} mol)

$$mol_{73h} = 3.37 \times 10^{-6} \times \left(\frac{3.59}{4}\right) \times \frac{4}{1} = 1.21 \times 10^{-5}\, mol$$

$$mol_{72h} = 3.37 \times 10^{-6} \times \left(\frac{6.77}{4}\right) \times \frac{4}{1} = 2.31 \times 10^{-5}\, mol$$

Equation 5.2

$Mass_{73h}$ = 2.46 mg

$Mass_{72h}$ = 6 mg

Absolute conversion is 52 %

Mass balance = 89.6%

5.5.10. Synthesis of quinolinone 87 (*cf.* Scheme 5.3)

Synthesis of **87** was done using a procedure reported by Zhou and co-workers[23] In a typical reaction, 2-iodoaniline (1 equiv., 1 g, 4.57 mmol) was dissolved in 15 mL of DMSO. To the reaction mixture, methyl methacrylate (4 equiv., 1.95 mL, 18.26 mmol), AIBN (4 equiv., 3 g, 18.26 mmol), and Bu_3SnH (1.5 equiv., 1.82 mL, 6.85 mmol) were slowly added. The mixture was heated at 140 ^{o}C with stirring. After 6 h, the reaction mixture was cooled to room temperature and quenched with 15 mL of DI water. The organic phase was extracted with 3 x 15 mL of EtOAc; the combined organic fraction was washed with brine solution and dried over *anh*. Na_2SO_4. The expected product crude **87** was concentrated by roto-evaporation and purified by flash chromatography using CombiFlash®: 12 g silica (RediSep Column); flow rate: 22 mL/min; Solvent system: 28 % EtOAc: Hexanes.

5.5.11. Characterization of quinolinone 87

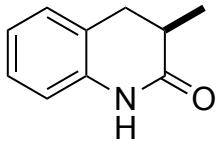

87

^{1}H NMR (400 MHz, $CDCl_3$, δ ppm) 8.5 – 8.1 (br s, 1H), 7.22 – 7.15 (m, 2H), 7.03 – 6.98 (t, *J* = 8Hz, 1H), 6.83 – 6.77 (d, *J* = 12 Hz, 1H), 3.05 – 2.98 (dd, *J* = 12, 4 Hz, 1H), 2.8 – 2.63 (m, 2H), 1.35 – 1.3 (d, *J* = 4 Hz, 3H)

^{13}C NMR (100 MHz, $CDCl_3$, δ ppm) 187.9, 137.4, 128.3, 127.7, 123.9, 123.2, 115.3, 35.2, 33.7, 15.6

HRMS-ESI [$(M+Na)^+$]: Calculated: 184.0733; Observed: 184.0732; Δm = 0.5 ppm

HPLC Analysis Conditions: Column: (R,R) WHELK–01; Abs. detector: 254 nm and 270 nm; mobile phase: Hexanes:IPA = 98:2; flow rate: 1 mL/min for analysis and 4 mL/min for separation; retention time (min): *R*-(+)-**87:** ~26.6 and *S*-(-)-**87:** ~33.03

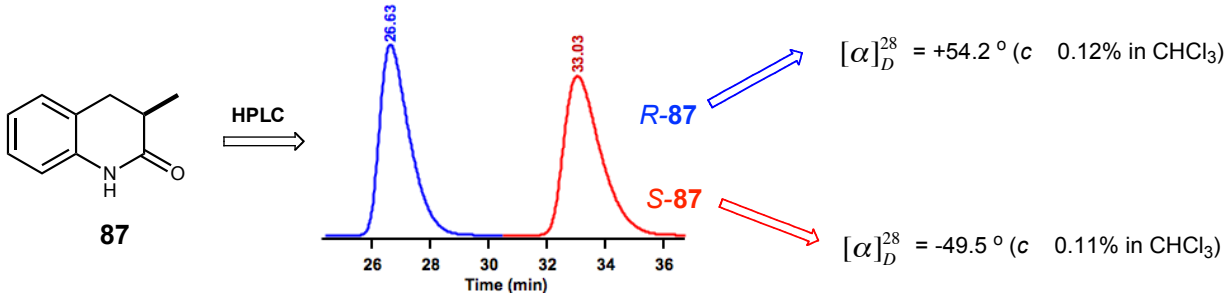

Figure 5.36: HPLC analysis and separation of quinolinone **87** into its isomers.

Quinolinone **87** was separated into its enantiomers by HPLC; each fraction was analyzed by polarimetry. The sign of the optical rotation of individual isomers with known absolute configuration are reported.[7] Comparison of optical rotation values gave the absolute configuration in the synthesized 3,4-dihydroquinolinone **73h-j** and **74h-j.**

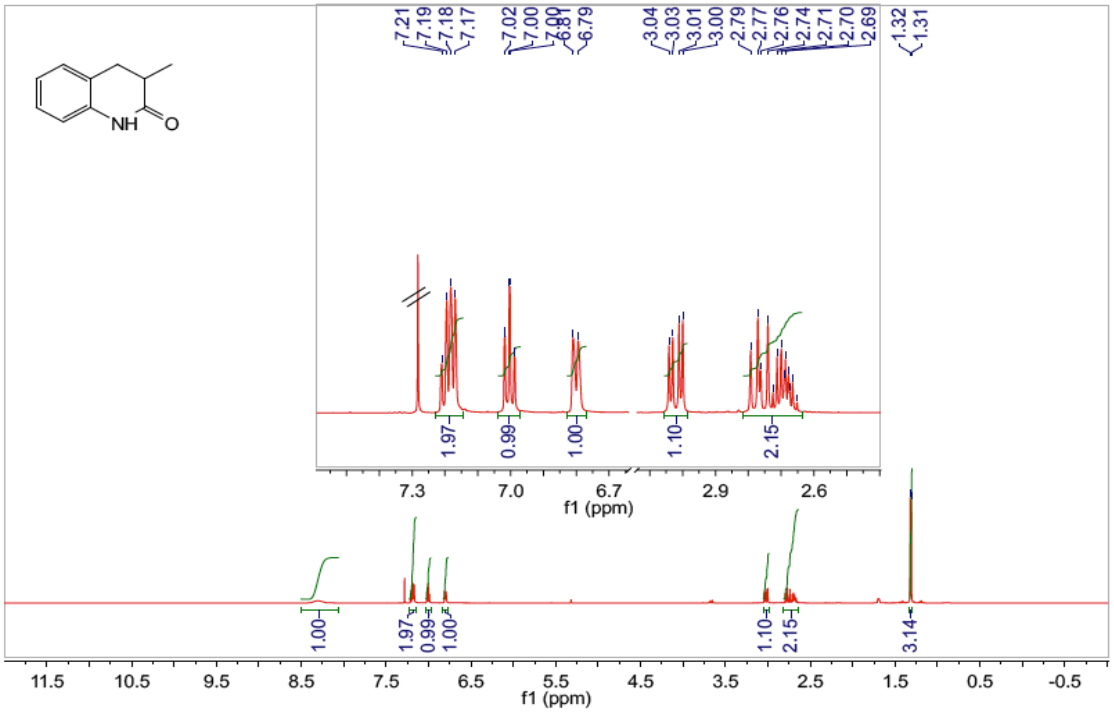

Figure 5.37: ^{1}H NMR (400 MHz, $CDCl_3$, δ ppm) spectrum for quinolinone **87.**

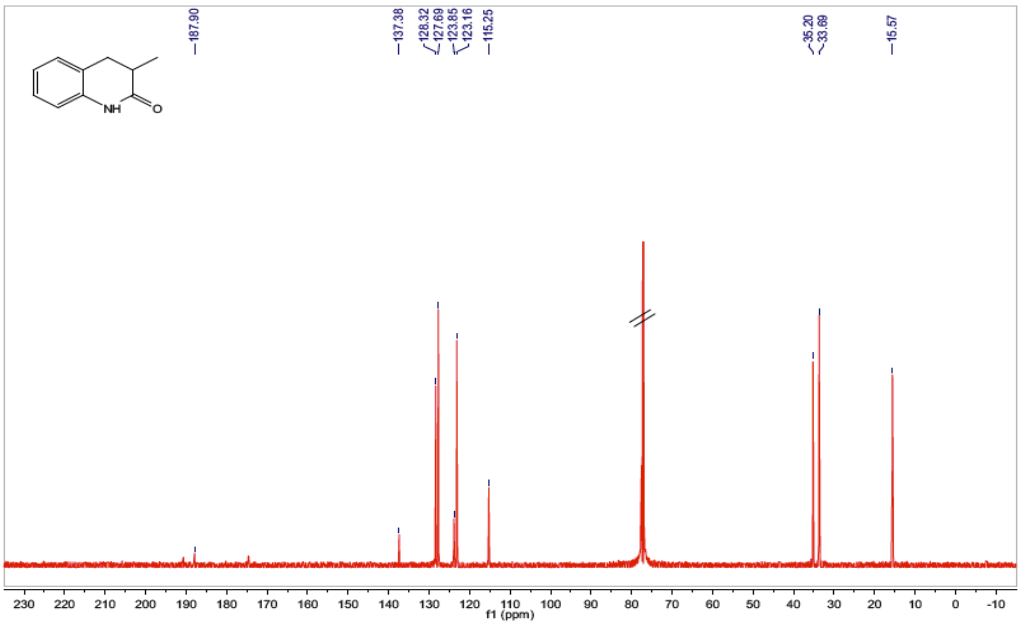

Figure 5.38: ^{13}C NMR (100 MHz, $CDCl_3$, δ ppm) spectrum for quinolinone **87.**

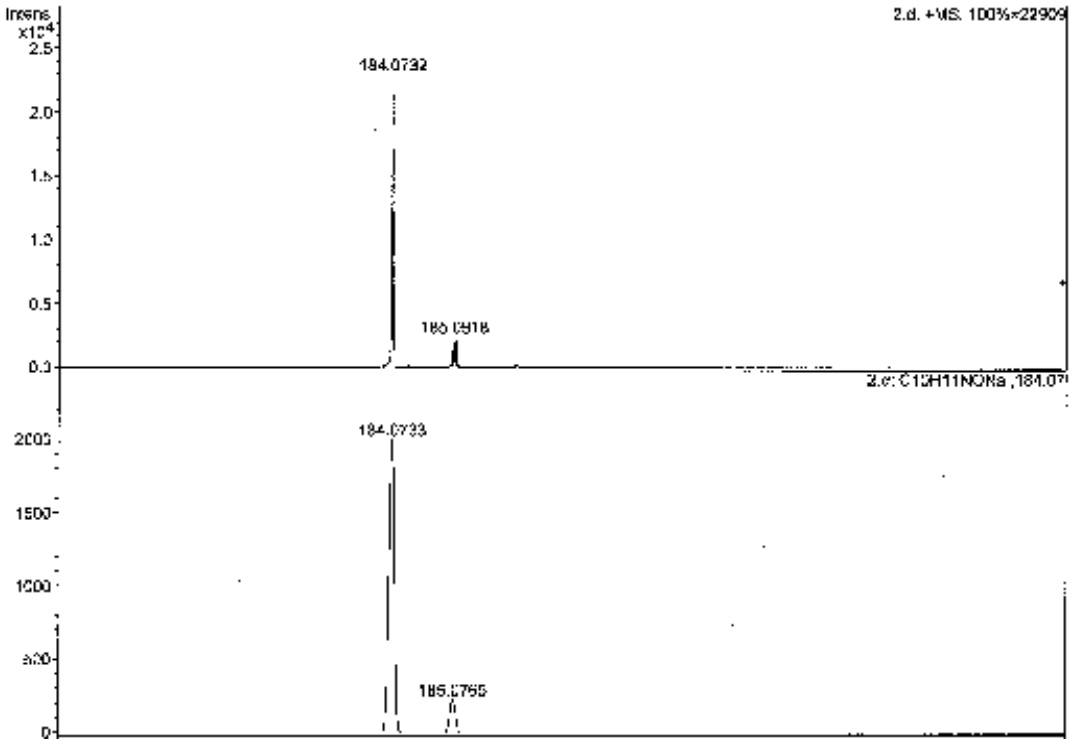

Figure 5.39: HRMS for quinolinone **87.**

5.6. References

(1) Kohlschütter, V.; Haenni, P. Zur Kenntnis des Graphitischen Kohlenstoffs und der Graphitsäure. *Anorg. Allg. Chem.* **1918**, *105*, 121–144.

(2) Cohen, M. D.; Schmidt, G. M. J. Topochemistry. Part I. A survey. *J. Chem. Soc.* **1964**, 1996.

(3) Judith Bregman, K. O. G. M. J. S. F. I. S. Topochemistry. Part IV. The crystal chemistry of some cis-cinnamic acids. *J. Chem. Soc.* **1964**, 2021.

(4) Schmidt, G. M. J. 385. Topochemistry. Part III. The crystal chemistry of some trans-cinnamic acids. *J. Chem. Soc.* **1964**, 2014.

(5) Gamlin, J. N.; Jones, R.; Leibovitch, M.; Patrick, B.; Scheffer, J. R.; Trotter, J. The Ionic Auxiliary Concept in Solid State Organic Photochemistry. *Acc. Chem. Res.* **1996**, *29*, 203–209.

(6) Garcia-Garibay, M. A. Engineering Carbene Rearrangements in Crystals: From Molecular Information to Solid-State Reactivity. *Acc. Chem. Res.* **2003**, *36*, 491–498.

(7) Toda, F. Solid State Organic Chemistry: Efficient Reactions, Remarkable Yields, and Stereoselectivity. *Acc. Chem. Res.* **1995**, *28*, 480–486.

(8) MacGillivray, L. R. Organic Synthesis in the Solid State via Hydrogen-Bond-Driven Self-Assembly. *J. Org. Chem.* **2008**, *73*, 3311–3317.

(9) Ramamurthy, V.; Venkatesan, K. Photochemical reactions of organic crystals. *Chem. Rev.* **1987**, *87*, 433–481.

(10) Veerman, M.; Resendiz, M. J. E.; Garcia-Garibay, M. A. Large-Scale Photochemical Reactions of Nanocrystalline Suspensions: A Promising Green Chemistry Method. *Org. Lett.* **2006**, *8*, 2615–2617.

(11) Dunitz, J. D. Are crystal structures predictable? *Chem. Commun.* **2003**, 545–548.

(12) Sakamoto, M.; Iwamoto, T.; Nono, N.; Ando, M.; Arai, W.; Mino, T.; Fujita, T. Memory of Chirality Generated by Spontaneous Crystallization and Asymmetric Synthesis Using the Frozen Chirality. *J. Org. Chem.* **2003**, *68*, 942–946.

(13) Ayitou, A. J.-L.; Sivaguru, J. Light-induced transfer of molecular chirality in solution: enantiospecific photocyclization of molecularly chiral acrylanilides. *J. Am. Chem. Soc.* **2009**, *131*, 5036–5037.

(14) Ogata, Y.; Takagi, K.; Ishino, I. Photocyclization of acrylanilides. *J. Org. Chem.* **1971**, *36*, 3975–3979.

(15) Bach, T.; Grosch, B.; Strassner, T.; Herdtweck, E. Enantioselective [6π]-Photocyclization Reaction of an Acrylanilide Mediated by a Chiral Host. Interplay between Enantioselective Ring Closure and Enantioselective Protonation. *J. Org. Chem.* **2003**, *68*, 1107–1116.

(16) Tanaka, K.; Kakinoki, O.; Toda, F. Control of the Stereochemistry in the Photocyclisation of Acrylanilides to 3,4-Dihydroquinolin-2(1 H)-ones. Delicate Dependence on the Host Compound. *Chem. Commun.* **1992**, 1053–1054.

(17) Ohba, S.; Hosomi, H.; Tanaka, K.; Miyamoto, H.; Toda, F. Enantioselective Photocyclization of Acrylanilides and N-Ethyl-N-methylbenzoylformamide in Inclusion Crystals with (R,R)-(-)-[trans]-2,3-Bis(.ALPHA.-hydroxydiphenylmethyl)-1,4-dioxaspiro-[4.4]nonane and -[4.5]decane. Mechanistic Study Based on X-Ray Crystal Structure Analyses. *Bull. Chem. Soc. Jpn.* **2000**, *73*, 2075–2085.

(18) Ayitou, A.; Pemberton, B. C.; Kumarasamy, E.; Vallavoju, N.; Sivaguru, J. Fun with photons: selective light induced reactions in solution and in water soluble nano-containers. *Chimia (Aarau)* **2011**, *65*, 202–209.

(19) Naito, T.; Tada, Y.; Ninomiya, I. Asymmetric Photocyclization of α,β-unsaturated Acrylanilides. *Heterocycles* **1984**, *22*, 237–240.

(20) Tanaka, K.; Kakinoki, O.; Toda, F. Control of the Stereochemistry in the Photocyclisation of Acrylanilides to 3,4-Dihydroquinolin-2(1 H)-ones. Delicate Dependence on the Host Compound. *Chem. Commun.* **1992**, 1053–1054.

(21) Johnstone, R. A. W.; Rose, M. E. A rapid, simple, and mild procedure for alkylation of phenols, alcohols, amides and acids. *Tetrahedron* **1979**, *35*, 2169–2173.

(22) Curran, D. P.; Hale, G. R.; Geib, S. J.; Balog, A.; Cass, Q. B. Rotational features of carbon-nitrogen bonds in axially chiral *o-tert*-butyl anilides and related molecules. Potential substrates for the “prochiral auxiliary” approach to asymmetric synthesis. *Tetrahedron: Asymmetry* **1997**, *8* (23), 3955–3575.

(23) Zhou, W.; Zhang, L.; Jiao, N. The tandem reaction combining radical and ionic processes: an

efficient approach to substituted 3,4-dihydroquinolin-2-ones. *Tetrahedron* **2009**, *65*, 1982–1987.

CHAPTER 6. MANIPULATING ATROPISOMERIC CHROMOPHORES UNDER ELEVATED PRESSURE FOR PHOTOREACTION[**]

6.1. Introduction

The abundance of single stereoisomer of biomolecules in nature is the essence of life on earth. Therefore, controlling the formation or the synthesis of enantiopure essential molecules is of great importance. Albeit the early attempt to make chiral molecules, in recent years, chemists have focused their attention on controlling chirality during synthetic chemical transformations by employing chiral auxiliaries/inductors. For this purpose, one of the systems that has gained considerable attention in recent years for the development of novel and effective asymmetric synthetic protocols[1] are atropisomeric compounds that have the propensity to slowly racemization at a given temperature with respect to their structural features.[2-9] Yet, it is challenging to effectively employ atropisomeric scaffolds near room temperatures, as the global absolute configuration or the chiral information of the system of interest may be destroyed revealing an obstacle to employ these systems for chemical transformations that require high reaction temperatures.[10] Thus, it is will be challenging to use atropisomeric scaffolds at high temperatures for asymmetric transformations.

It is has been demonstrated that the racemization of left- and right-handed structural forms of atropisomeric compounds could be manipulated under the influence of external stimuli like temperature that could influence the extent of hindered single bond rotation.[11] Single bong rotation in atropisomeric compounds makes them stereochemically unstable at high temperature compared to their point chiral (chiral center defined on a tetrahedral carbon or other atom).[9] Thus, finding the structural features and external factors characteristics[12-17] that influence the racemization process in atropisomeric scaffolds is indispensable for understanding the stereochemical impact of atropisomeric compounds on asymmetric

[**] The material in this chapter was co-authored by Anoklase J.-L. Ayitou (AJA), Dr. Gaku Fukuhara (GF), Elango Kumarassamy (EK), Dr. Yoshihisa Inoue (YI) and Dr. J. Sivaguru (JS). AJA in consultation with JS synthesized all compounds and performed all experiments with the help of GF and EK. GF provided technical guidance for the elevated pressure study. EK performed experiments with axially chiral 2-pyridones, which are not described in this chapter. AJA and JS came up with the mechanistic rationale of the reaction as well as the conclusion described in this chapter. YI provided advice in explaining the role of elevated pressure in stabilizing axially chiral chromophores.

chemical transformations.[9] Pressure, volume and temperature constitute a trio of parameters that have been empirically exploited to study the dynamics of natural phenomena.[18-25] Because temperature could influence the racemization of atropisomeric compounds, we will demonstrate in this chapter how to counter the effect of high temperature during racemization of the systems of interest by applying elevated pressure to the systems under study. Thus, for isochoric processes, pressure and temperature could be varied to compute thermodynamic and kinetic parameters.[24,25]

In the previous chapters, the enantiospecific 6π-photocyclization in solution using non-biaryl acrylanilides compounds was detailed.[26,27] Similarly, other photochemical transformations namely γH-abstraction[28,29] and 4π-photochemical ring closure have been previously reported from our research group[30,31]. In these studies, we have shown that effective chiral transfer is dependent on the reaction temperature.[26-30] To evaluate the potential of axially chiral chromophores for reactions requiring elevated temperatures, I investigated the effect of pressure as well, as pressure and temperature proportionally affect one another when the volume is kept constant. [24,25] In this chapter, I will detail transfer of chirality during photochemical transformations (Scheme 6.1) under elevated pressure. Results from the study indicated that elevated pressure could be successfully employed to suppress the intrinsic racemization of non-biaryl atropisomeric chromophores. Consequently, higher enantiomeric excess (*ee*) values in expected photoproducts were achieved. As illustrated in scheme 6.1, elevated pressure investigations have been done with atropisomeric α-oxoamide **84a** and acrylanilides **72h,j,k.**

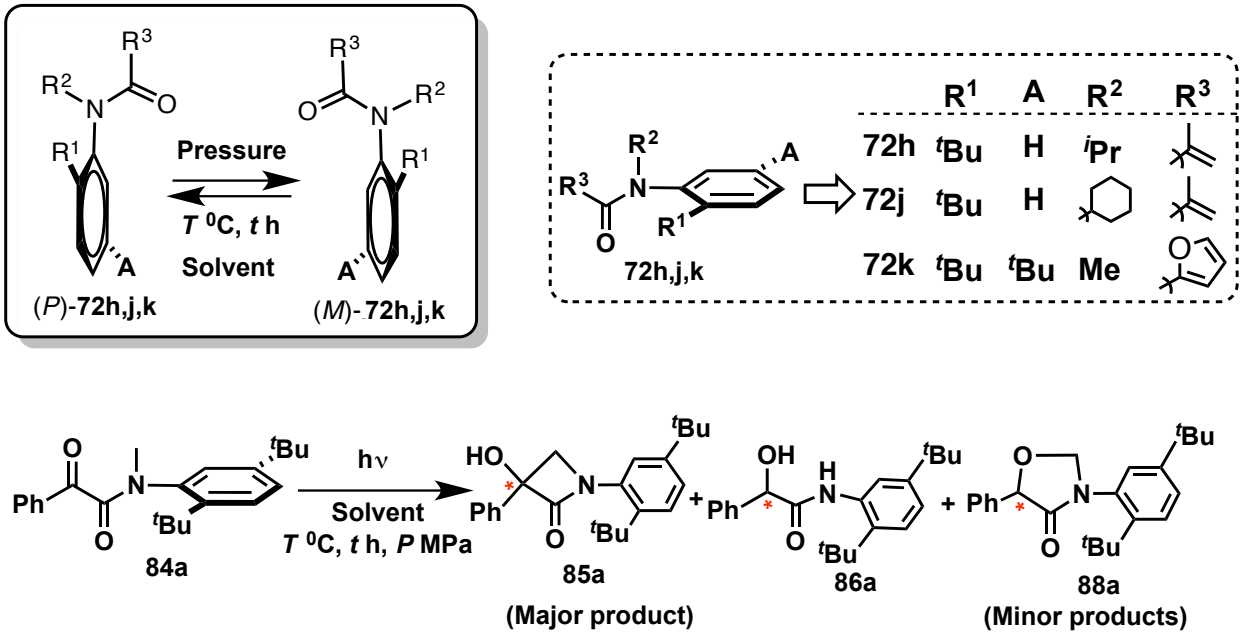

Scheme 6.1: Optically pure atropisomeric compounds **84a** and **72h,j,k** evaluated for racemization and enantiospecific photochemical transformation under elevated pressure.

6.2. Results and Discussion

Synthesis of compounds **72h,j** was reported in the previous chapter (*cf.* chapter 5); and the synthesis of compound **72k** and **84a** will be detailed in the experimental section.[26-30] Optically pure samples of **84a** and **72h,j,k** where analysed by HPLC on a chiral stationary phase. Optical rotation value and the sign of Cotton effect (circular dichroism signature) for each sample were recorded. Photochemical transformation at high pressures and racemization kinetics of optically pure isomers of **84a** and **72h,j,k** were investigated in spectrophotometric grade solvents at a given temperature and pressure in a custom-built high-pressure vessel (Figure 6.1).[24,25] The high-pressure device is fitted with three optical windows made of sapphire or diamond with an effective aperture of 9 mm or 3 mm i.d., respectively. The window materials were sapphire for photoirradiation, UV-Vis and fluorescence spectroscopy and birefringence-free diamond for circular dichroism (CD) spectroscopy. A quartz inner cell with an inside dimension of 3 mm (W) × 2 mm (D) × 7 mm (H) was connected to a short flexible Teflon tube to adjust for the volume change under pressure. This quartz cell was filled with a sample solution of a known concentration. The top end of the Teflon tube was stoppered, and the whole cell was placed inside the pressure vessel. The vessel was fixed in the sample chamber of the spectrometer with a set

hydrostatic pressure and temperature. Optically pure samples of **84a** were irradiated using a fiber optics cable delivering light from a xenon light source equipped with a 300±10 nm band-pass filter.

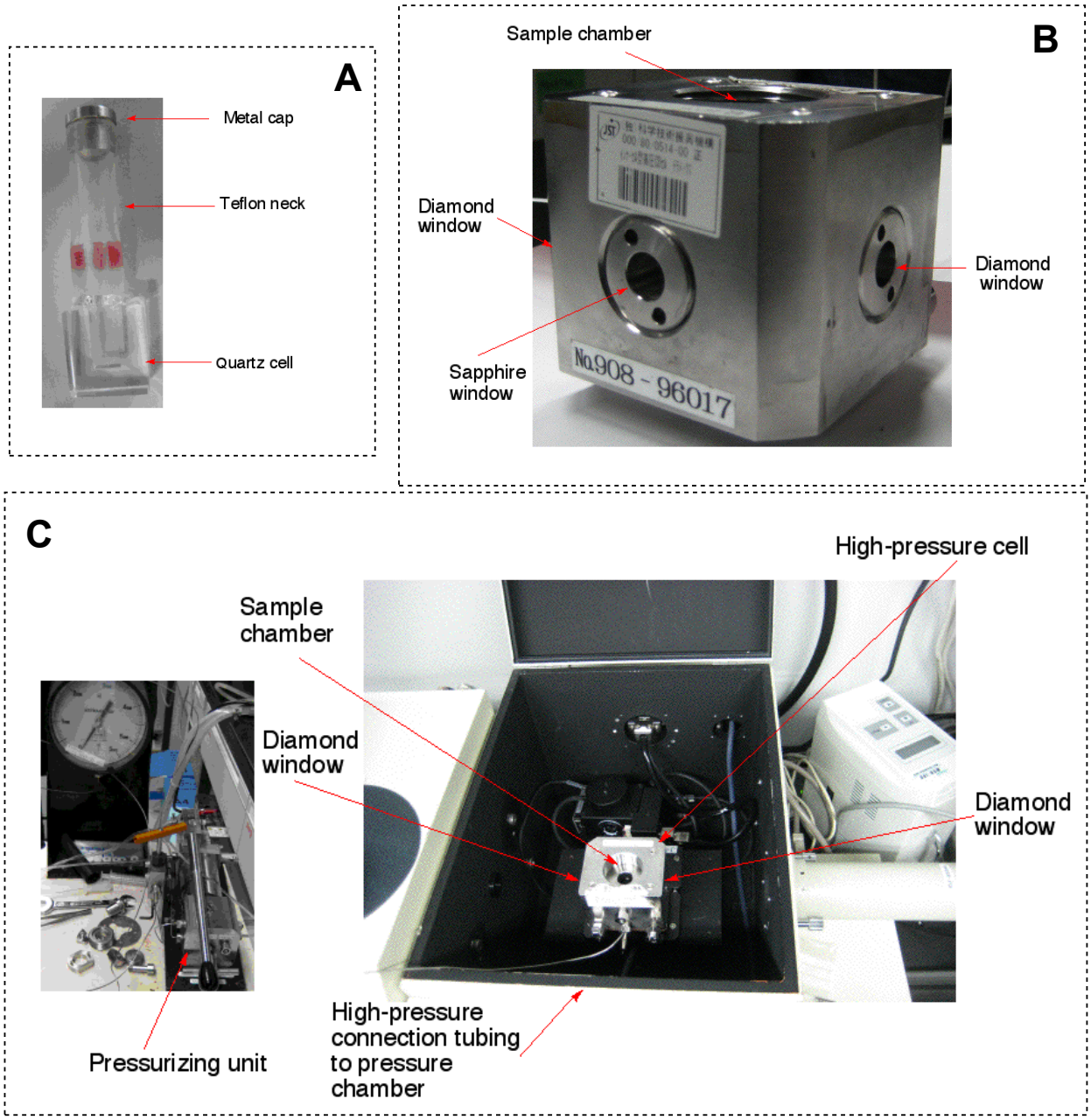

Figure 6.1: A: Custom designed quartz cell for high-pressure experiments; B: Custom designed high-pressure vessel; C: High-pressure setup in a CD spectrometer.

The temperature dependent enantiospecific photochemical Norrish-Yang cyclization of optically pure atropisomers of α-oxoamides **84a** was previously reported and will de detailed in chapter 8[28] (Scheme 6.1). Thus, this system was selected to investigate the effect of elevated pressures on

photochemical transformations while keeping the samples at high reaction temperatures (70 ^{o}C) as illustrated in scheme 6.1.

Photoreaction of optically pure samples of **84a** was investigated in acetonitrile at 70 $^{\circ}$C at different pressures (0.1 MPa to 100 MPa; Table 6.1). It has been previously reported that photoirradiation of **84a** in chloroform gave **85a** as the exclusive photoproduct. Due to the low boiling point of chloroform, acetonitrile was selected for high temperature irradiation for this investigation. Thus, photoreaction with **84a** generated 3 different photoproducts **85a, 86a** and **88a**. In acetonitrile at 0.1 MPa and 70 $^{\circ}$C, photoirradiation of **84a** gave the β-lactam **85a** as the major photoproduct (**85a**:**86a**:**88a** was 70:28:2). The *ee* values of the photoproduct(s) were verified by HPLC analysis on a chiral stationary phase. At 70 $^{\circ}$C at 0.1 MPa the *ee* value of the photoproducts **84a** was 16% (Table 6.1). On the other hand photoirradiation at 20 MPa of **84a** gave an *ee* value of 30% in the corresponding photoproduct **85a** (Table 6.1). Thus, photoirradiation under elevated pressure helped achieving higher *ee* in the expected photoproduct(s) as shown in table 6.1.

Table 6.1: Enantiospecific photochemical reaction of α-oxoamides **84a** at different pressures in acetonitrile at 70 ^{o}C.[a]

Entry	Substrates [b]	*t* (h)	% *ee* (photoproduct **85a** and *ent*-**85a**)[c]	
			0.1 MPa	20 MPa
1	(-)-**84a**	2	17 (A)	29 (A)
2	(+)-**84a**	2	16 (B)	30 (B)

[a] All irradiations were carried out within a pressure cell that is equipped with a sapphire window using an optical fiber carrying a light source from a xenon lamp with 300±10 nm band pass filter from an Asahi spectra 302 Max power supply unit. The values are an average of two runs. Reported values carry a 20% error due to experimental limitations of handling samples at elevated pressures and temperature in the pressure cell. [b] (+) and (-) denotes the sign of optical rotation of the reactant. [c] A and B refers to the elution order of enantiomers during HPLC analysis on a chiral stationary phase.

Inspection of table 6.1 shows that moderate increase of pressure from 0.1 MPa to 20 MPa affects the *ee* value of photoproduct **85a**. It is likely that, at elevated pressures, the rate of racemization of optically pure atropisomers of **84a** is slow even if the samples are kept at higher temperature. To prove

this observation, racemization study of optically pure atropisomeric α-oxoamide **84a** and acrylanilides **72h,j,k** at elevated temperatures was investigated to ascertain if the effect of pressure on inhibition/suppression of the racemization of atropisomeric compounds was a general phenomenon. Moreover, the rates of racemization for optically pure atropisomeric α-oxoamide **84a** and acrylanilides **72h,j,k** were evaluated.

6.2.1. Racemization kinetics of atropisomeric 84a and 72h,j,k

For a qualitative discussion of pressure effects on racemization it is critical to calculate the activation volume $\Delta V^{\ddagger}_{rac}$ for the racemization processes.[32] The activation volume is the difference in the partial molar volume of the transition state and the sum of the partial volumes of the reactant(s) undergoing the transformation at a given temperature and pressure. The value of activation volume is obtained at equilibrium when the substrate's internal force equalizes the applied pressure. As the rate constant depends on both temperature and pressure, at any given temperature *T*, the effect of pressure *P*, on the racemization rate constant k_{rac} is given by equations 6.1 and 6.4. [24,25]

$$\Delta V^{\ddagger}_{\mathrm{rac}} = -RT(\partial \ln k_{\mathrm{rac}} / \partial P)_T \qquad \textbf{Equation 6.1}$$

$$(\ln k_{\mathrm{rac}})_T = -(\Delta V^{\ddagger}_{\mathrm{rac}} / RT)P + \mathrm{C} \qquad \textbf{Equation 6.2}$$

$$\ln[[P]_0/([P]_0 - \mathrm{x})] = \ln [([P]+ [M])/([P] - [M])] = k_{\mathrm{rac}} t \qquad \textbf{Equation 6.3}$$

$$\tau_{1/2} = \ln 2/k_{\mathrm{rac}} \qquad \textbf{Equation 6.4}$$

$$(\ln k_{\mathrm{rac}} / T) = \Delta S^{\ddagger}_{\mathrm{rac}} / R - \Delta H^{\ddagger}_{\mathrm{rac}} / RT + \ln(k_B / h) \qquad \textbf{Equation 6.5}$$

Where k_{rac} = racemization rate constant; $\tau_{1/2}$ is the half-life of racemization; *T* is the temperature in Kelvin, *P* is the pressure in MPa, *R* is the gas constant (8.314 cm^3 MPa K^{-1} mol^{-1}), C is a constant, $[P]_0$ is the initial concentration of the *P*-isomer; x = [P_0 – *([P],[M])*]. *([P],[M])* represents the concentration of racemate at time *t*, k_B = Boltzmann constant; *h* = Planck constant. A point to note is that enantiomerization being microscopic phenomenon and racemization being a macroscopic phenomenon, it is critical to appreciate the relation that exist between the two processes i.e., k_{rac}=2*k_{enant}, with k_{enant} being the rate constant of enantiomerization.[9]

Racemization studies of optically pure isomers of **84a** and **72h,j,k** were performed by circular dichroism (CD) spectroscopy in spectrophotometric grade solvents at a given temperature and pressure in a custom-built high-pressure vessel (Figure 6.1).[24,25] To correlate the effect of pressure, temperature and volume on the racemization process, two sets of experiments were carried out.

6.2.2. Racemization study at normal pressure (0.1 MPa)

In the first set of experiments (Figures 6.2 – 6.8 and Table 6.2), the pressure was kept constant at 0.1 MPa and the temperature was varied to ascertain the racemization rate constant (k_{rac}), activation free energy of racemization ($\Delta G^{\ddagger}_{rac}$), activation enthalpy ($\Delta H^{\ddagger}_{rac}$), and activation entropy ($\Delta S^{\ddagger}_{rac}$).

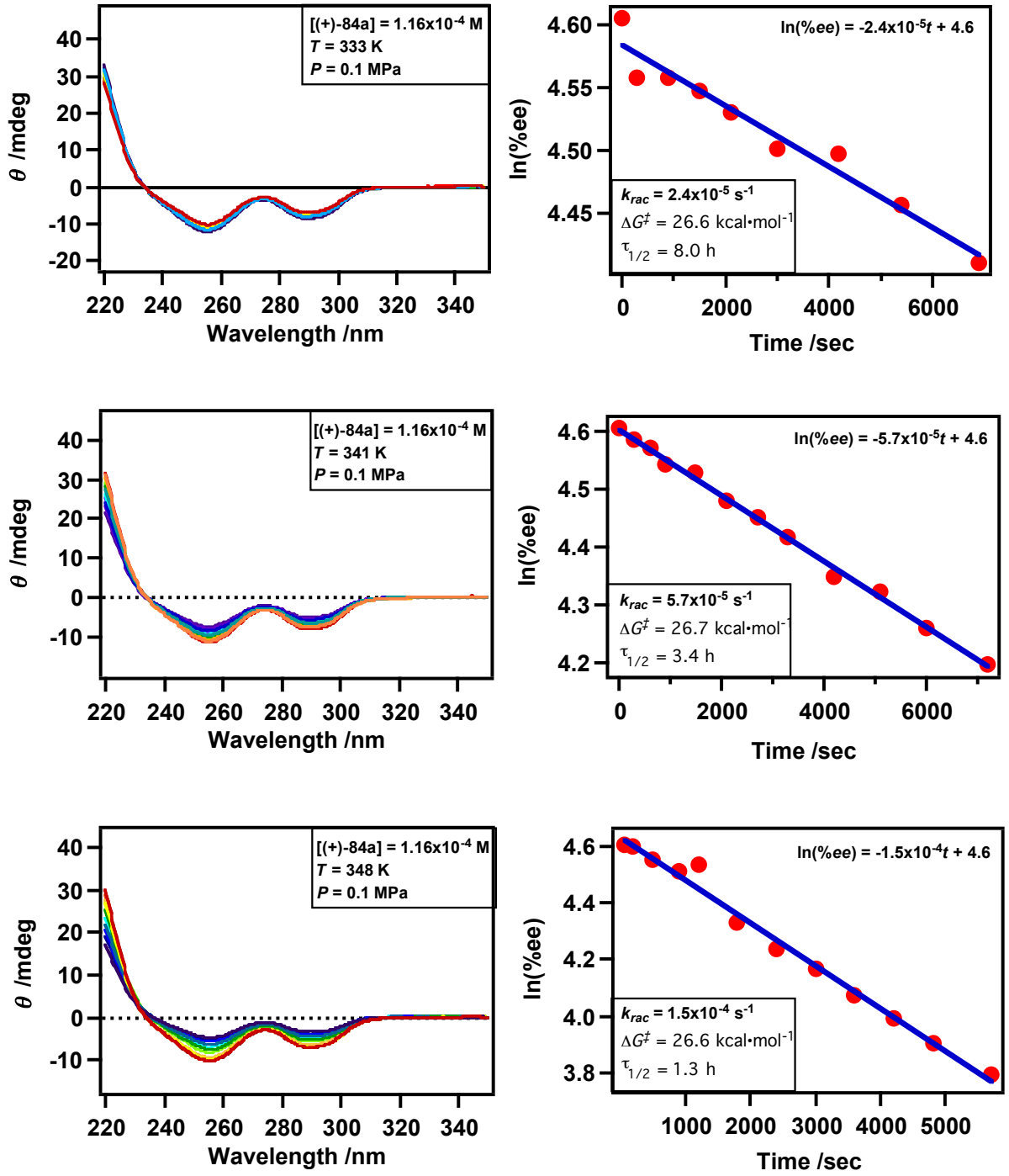

Figure 6.2: Racemization kinetic study at various temperature in MeCN for compound **84a:** Pressure = 0.1 MPa; Temperature: top 333K, middle 341 K, bottom 348 K.

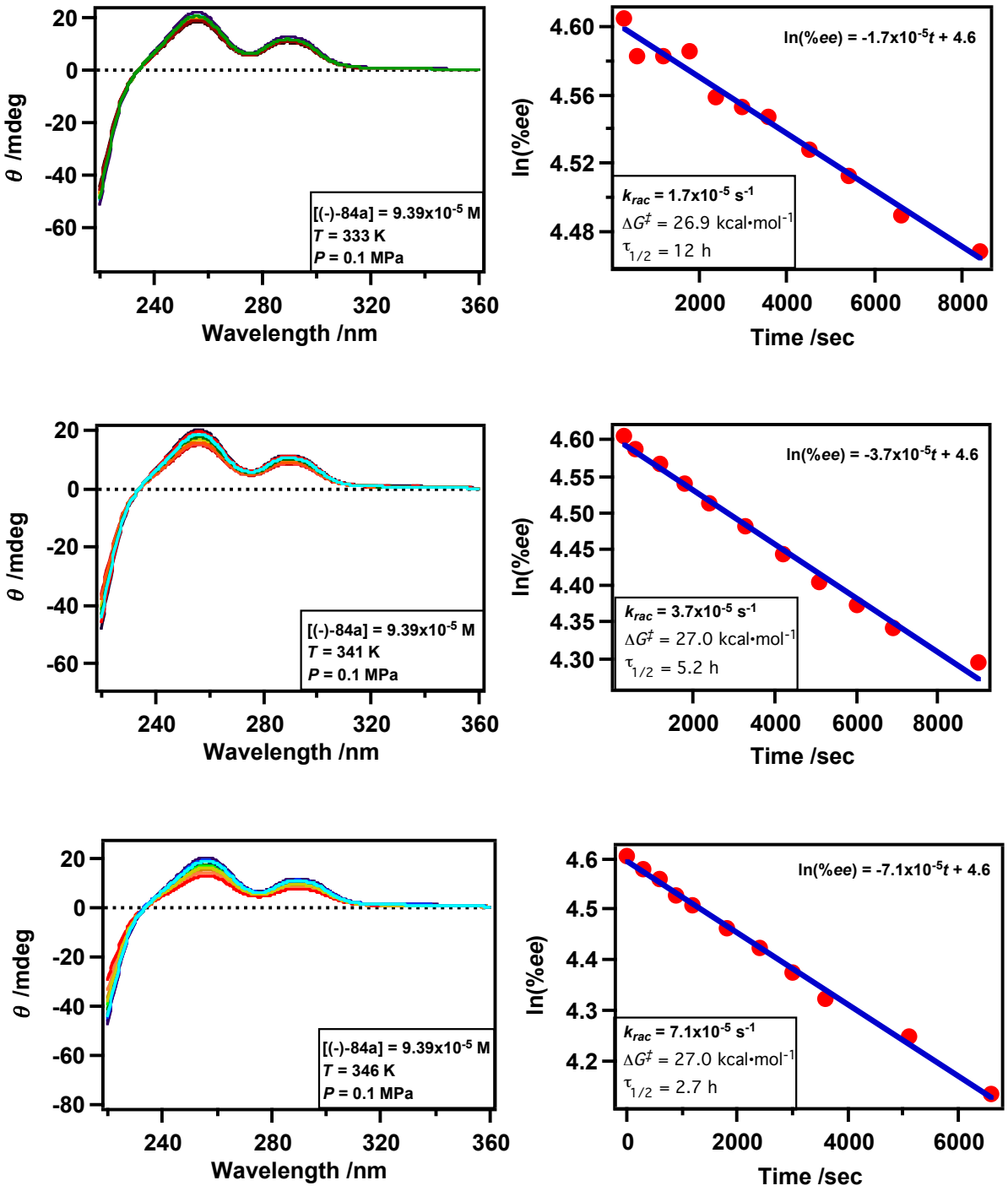

Figure 6.3: Racemization kinetic study at various temperature in EtOH for compound **84a**: Pressure = 0.1 MPa; Temperature: top 333K, middle 341 K, bottom 346 K.

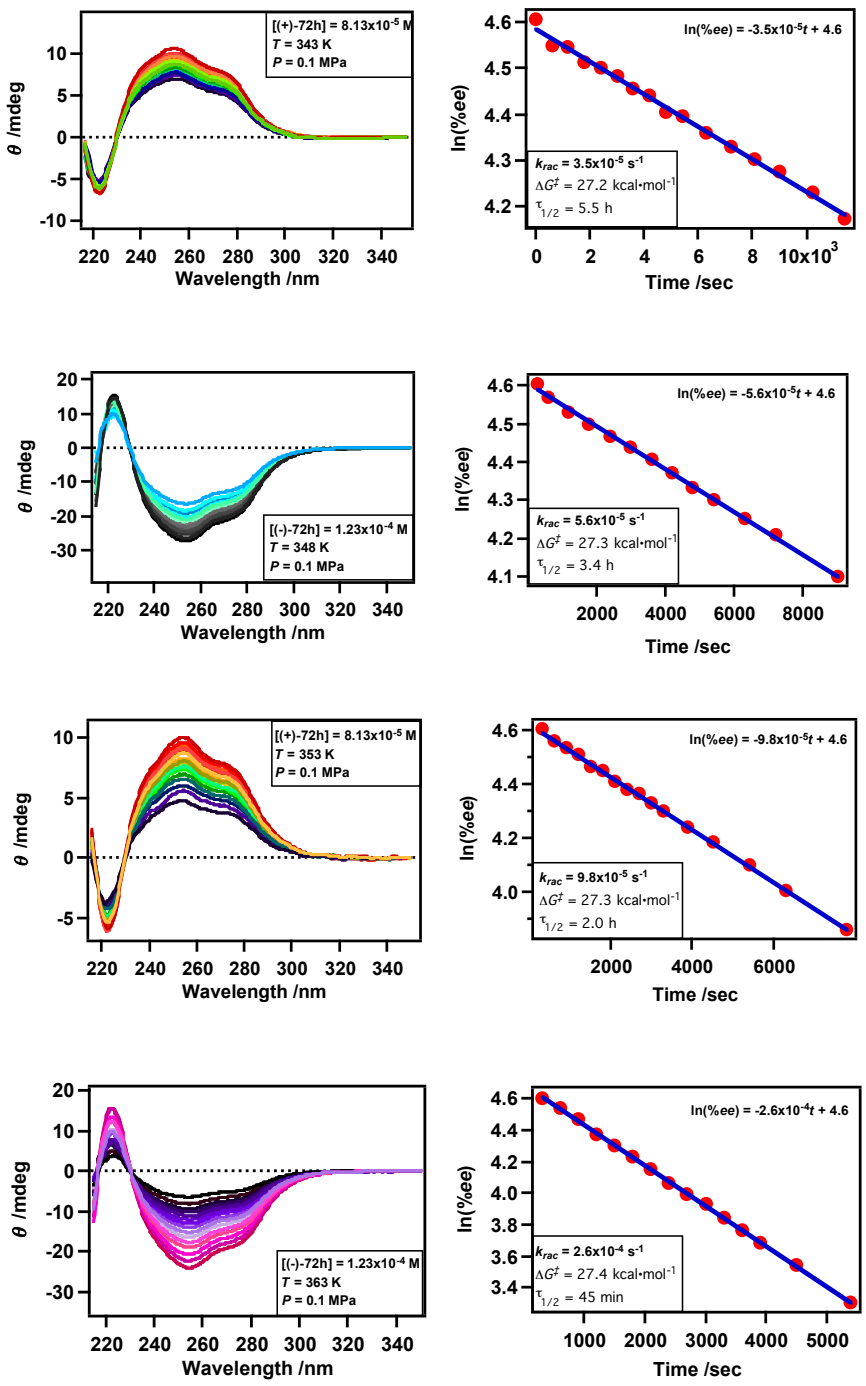

Figure 6.4: Racemization kinetic study at various temperature in methylcyclohexane (MCH) for compound **72h**: Pressure = 0.1 MPa. Temperature: top 343K, middle 353 K, bottom 363 K.

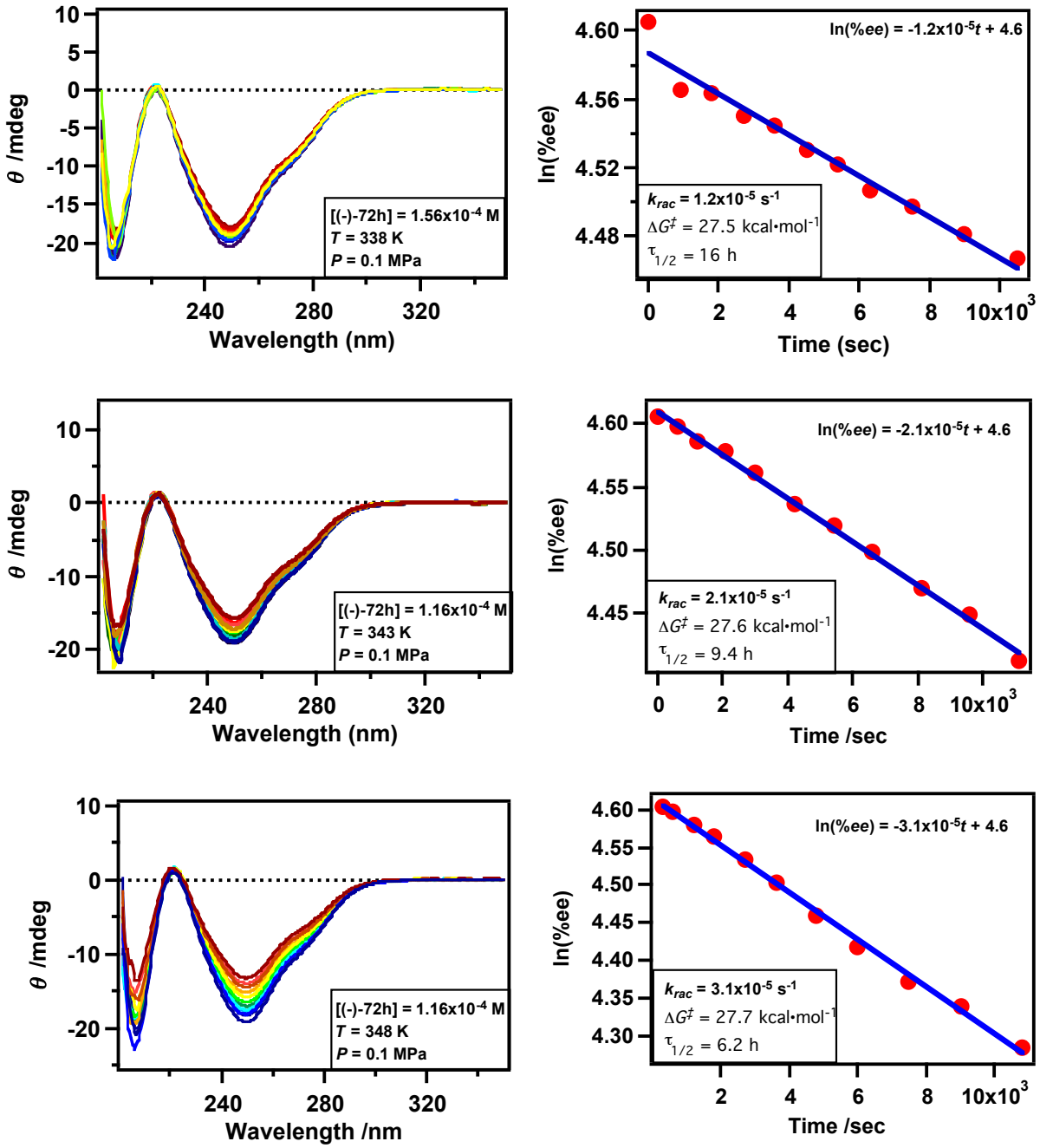

Figure 6.5: Racemization kinetic study at various temperature in MeCN for compound **72h:** Pressure = 0.1 MPa. Temperature: top 338 K, middle 343 K, bottom 348 K.

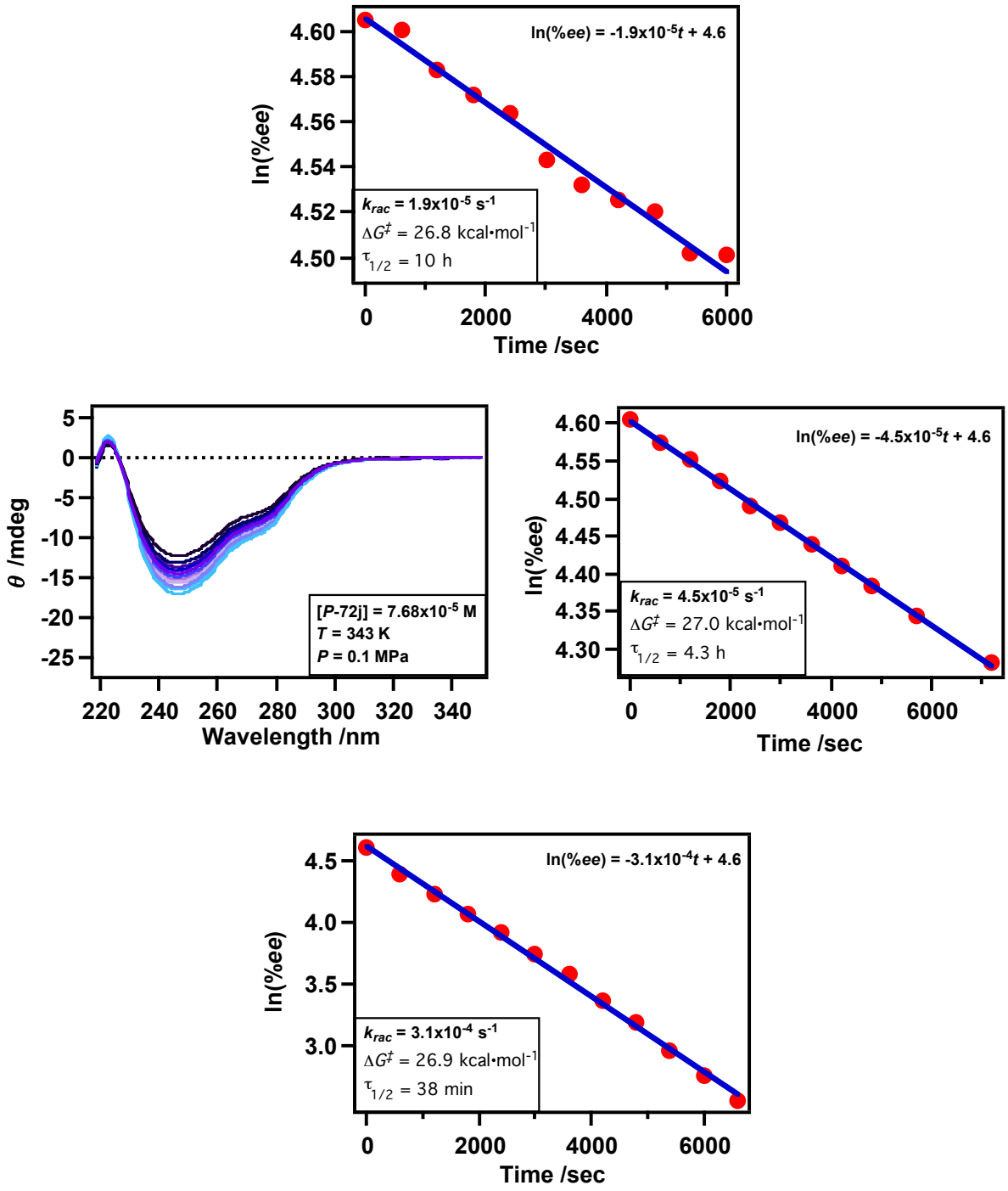

Figure 6.6: Racemization kinetic study at various temperature in MCH for compound **72j:** Pressure = 0.1 MPa; Temperature: top 333 K, middle 343 K, bottom 358 K.

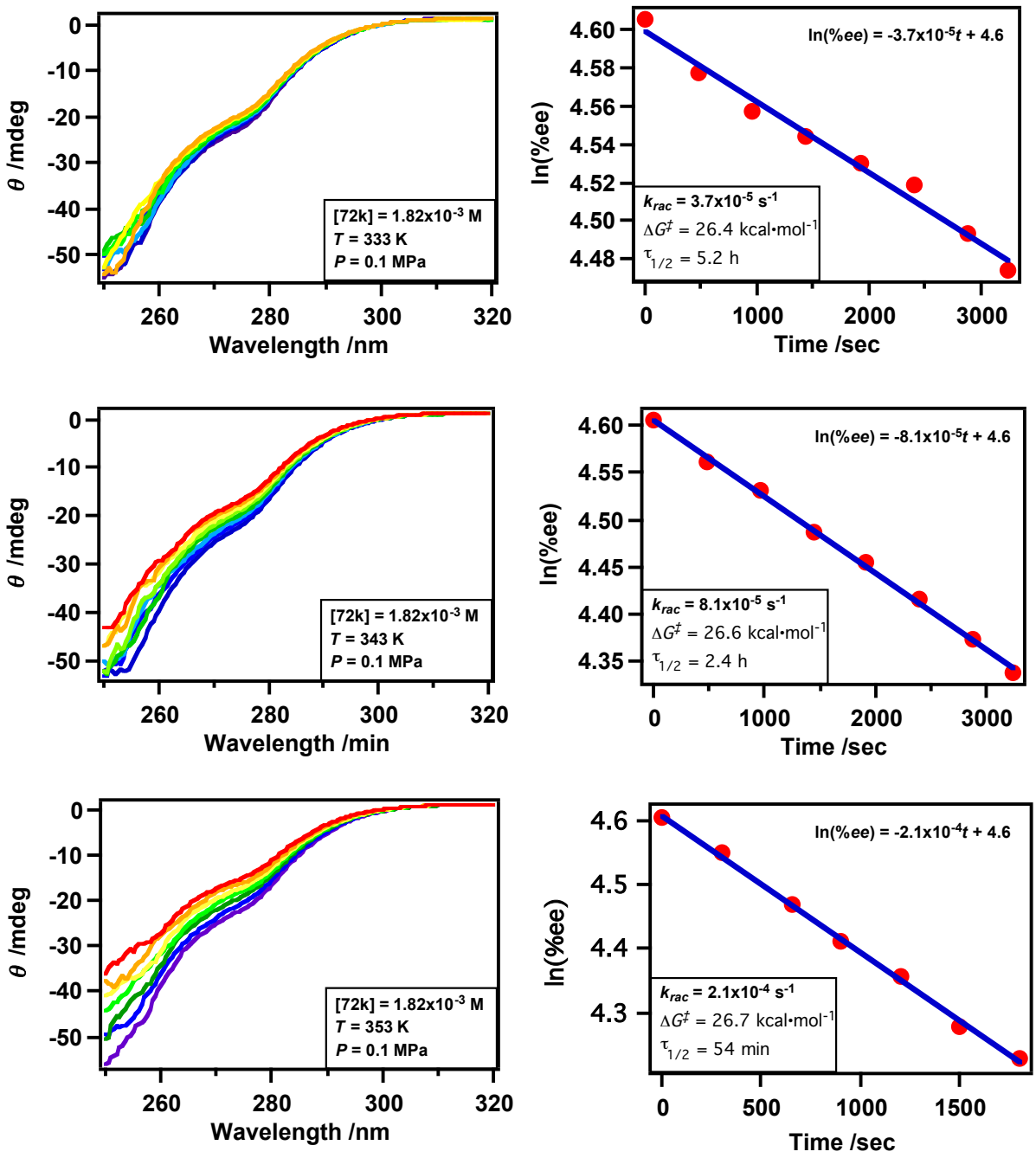

Figure 6.7: Racemization kinetic study at various temperature in MCH for compound **72k**: Pressure = 0.1 MPa; Temperature: top 333 K, middle 343 K, bottom 353 K.

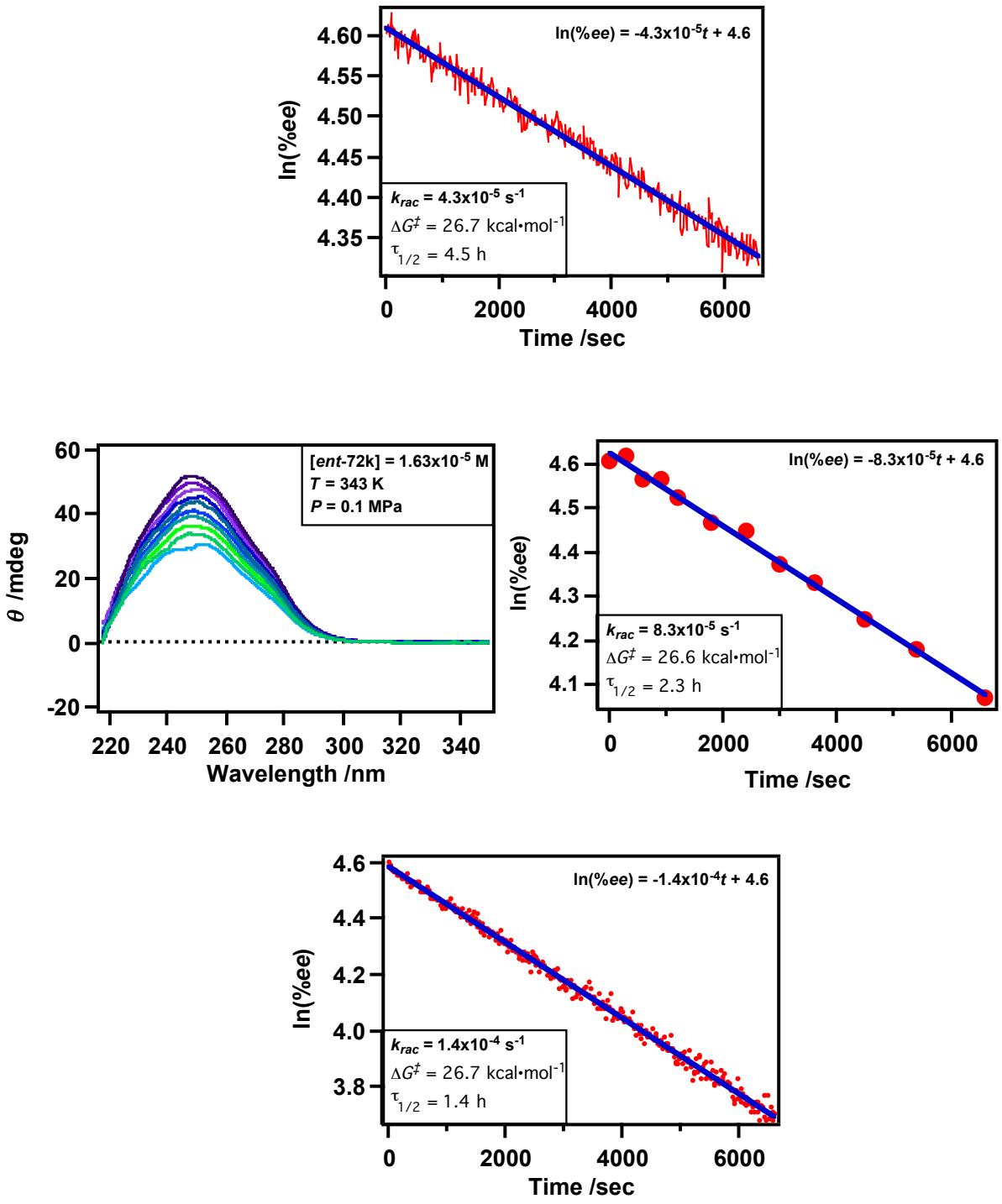

Figure 6.8: Racemization kinetic study at various temperature in MeCN for compound **72k**: Pressure = 0.1 MPa; Temperature: top 338 K, middle 343 K, bottom 348 K.

Table 6.2: Eyring parameters at different temperature and various solvents: Racemization parameters for optically pure atropisomers **84a** and **72h,j,k** at 0.1 MPa.

Entry	T (K)	Substrates / Solvent [a]	k_{rac} (s^{-1}) [b]	$\Delta G^{\ddagger}_{rac}$ ($kcal \cdot mol^{-1}$) [b]	$\tau_{1/2}$ (h) [b]
1	333	**84a** / MeCN	2.4×10^{-5}	26.6	8.0
2	341		5.7×10^{-5}	26.7	3.4
3	348		1.5×10^{-4}	26.6	1.3
4	333	**84a** / EtOH	1.7×10^{-5}	26.9	12
5	341		3.7×10^{-5}	27.0	5.2
6	346		7.1×10^{-5}	27.0	2.7
7	343	**72h** / MCH	3.5×10^{-5}	27.2	5.5
8	348		5.6×10^{-5}	27.3	3.4
9	353		9.8×10^{-5}	27.3	2.0
10	363		2.6×10^{-4}	27.4	45 m[c]
11	338	**72h** / MeCN	1.2×10^{-5}	27.5	16
12	343		2.1×10^{-5}	27.6	9.4
13	348		3.1×10^{-5}	27.7	6.2
14	333	**72j** / MCH	1.9×10^{-5}	26.8	10
15	343		4.5×10^{-5}	27.0	4.3
16	358		3.1×10^{-4}	26.9	38 m[c]
17	338	**72k** / MeCN	4.3×10^{-5}	26.7	4.5
18	343		8.3×10^{-5}	26.6	2.3
19	348		1.4×10^{-4}	26.7	1.4
20	333	**72k** / MCH	3.7×10^{-5}	26.4	5.2
21	343		8.1×10^{-5}	26.6	2.4
22	353		2.1×10^{-4}	26.7	54 m[c]

[a] The samples concentration [**84a**]: 1.16x10-4 M in MeCN, 9.39x10-5 M in EtOH; [**72h**]: 8.13x10-5 M in MCH, 1.2x10-5 M in MeCN; [**72j**]: 1.86x10-5 M in MCH; [**72k**]: 2.27x10-4 M in MCH, 1.63x10-5 M in MeCN;. [b] krac ,$\tau_{1/2}$ and $\Delta G^{\ddagger}_{rac}$ value omputed from the equations 6.4 and 6.5. [c] $\tau_{1/2}$ value in minutes.

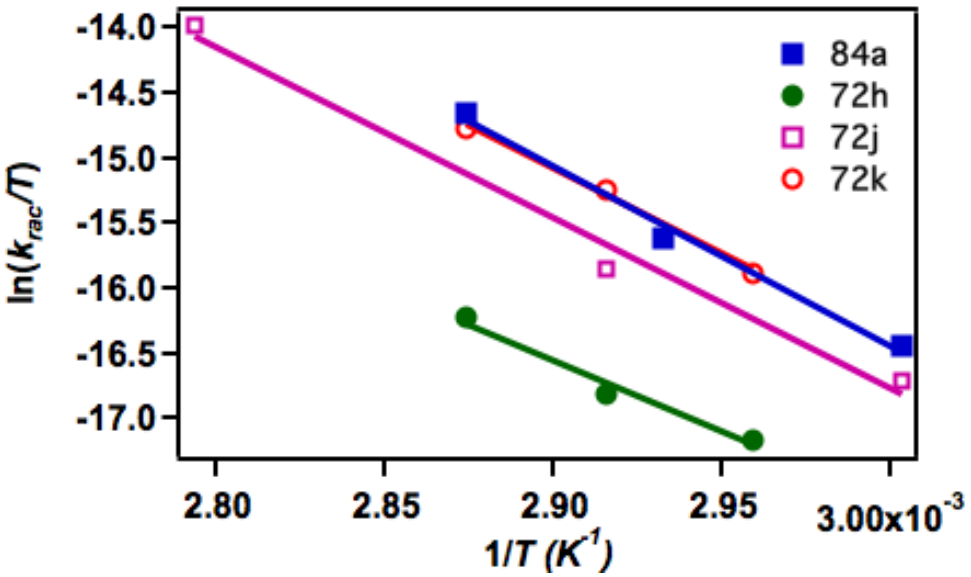

Figure 6.9: Eyring plots for racemization of substrates **84a** and **72h,j,k** at 0.1 MPa.

6.2.3. Racemization study under elevated pressure

In this experiment, the temperature was kept constant and the pressure was varied to compute the activation volume ($\Delta V^{\ddagger}_{rac}$), the racemization rate constant (k_{rac}) and the activation energy for racemization ($\Delta G^{\ddagger}_{rac}$). The racemization of optically pure non-biaryl atropisomeric compounds was monitored by CD spectroscopy at elevated temperatures at different pressures (Tables 6.3 and 6.4). To study the influence of solvent on the racemization process, racemization studies were carried out in different solvents. Thought, at pressures as high as 50 MPa some of the solutions became cloudy indicating that under high pressure, the systems of interest precipitated/crystallized. Thus, the applied pressure greatly affected the solubility of the compounds under study and physical interactions that were prevalent between the solute and the solvent. For solubility purposes, other solvents may not be suitable for the current study, as micro-crystallization may occur. So, to enhance the racemization rate the study was performed at elevated temperatures with pressure varying from 0.1 MPa to 20 MPa. CD measurements on the pressurized samples (10 MPa and 20 MPa) were recorded at 343 K (Table 6.3).

Taking the example of (*P*)-**72h** at 343 K, a decrease in the ellipticity (θ) of the CD spectra was observed at a pressure of 0.1 MPa while the decrease in the θ value was minimal at an elevated pressure of 20 MPa. The k_{rac} value was 3.5 x 10^{-5} s^{-1} with a $\tau_{1/2}$ value of 5.5 h (Table 6.2, entry 7) at a pressure of

0.1 MPa in methylcyclohexane (MCH). Increasing the pressure to a moderate 10 MPa at 343 K, the k_{rac} value was 2.1 x 10^{-5} s^{-1} with a $\tau_{1/2}$ value of 9.0 h (Table 6.3, entry 2). The half-life increased with a mere increase of pressure from 0.1 MPa to 10 MPa. In the case of **84a**, there was a minimal change in $\tau_{1/2}$ values upon varying the solvent from acetonitrile (MeCN) to ethanol (EtOH) ($\tau_{1/2}$: 3.4 h in MeCN; $\tau_{1/2}$: 5.2 h in EtOH at 341 K; Table 6.2, entries 2 and 5 respectively). This observation could implied that the solvent polarity and the ability for intermolecular interactions *viz.* H-bonding with the solvent employed could affect the racemization rates in axially chiral α-oxoamides.

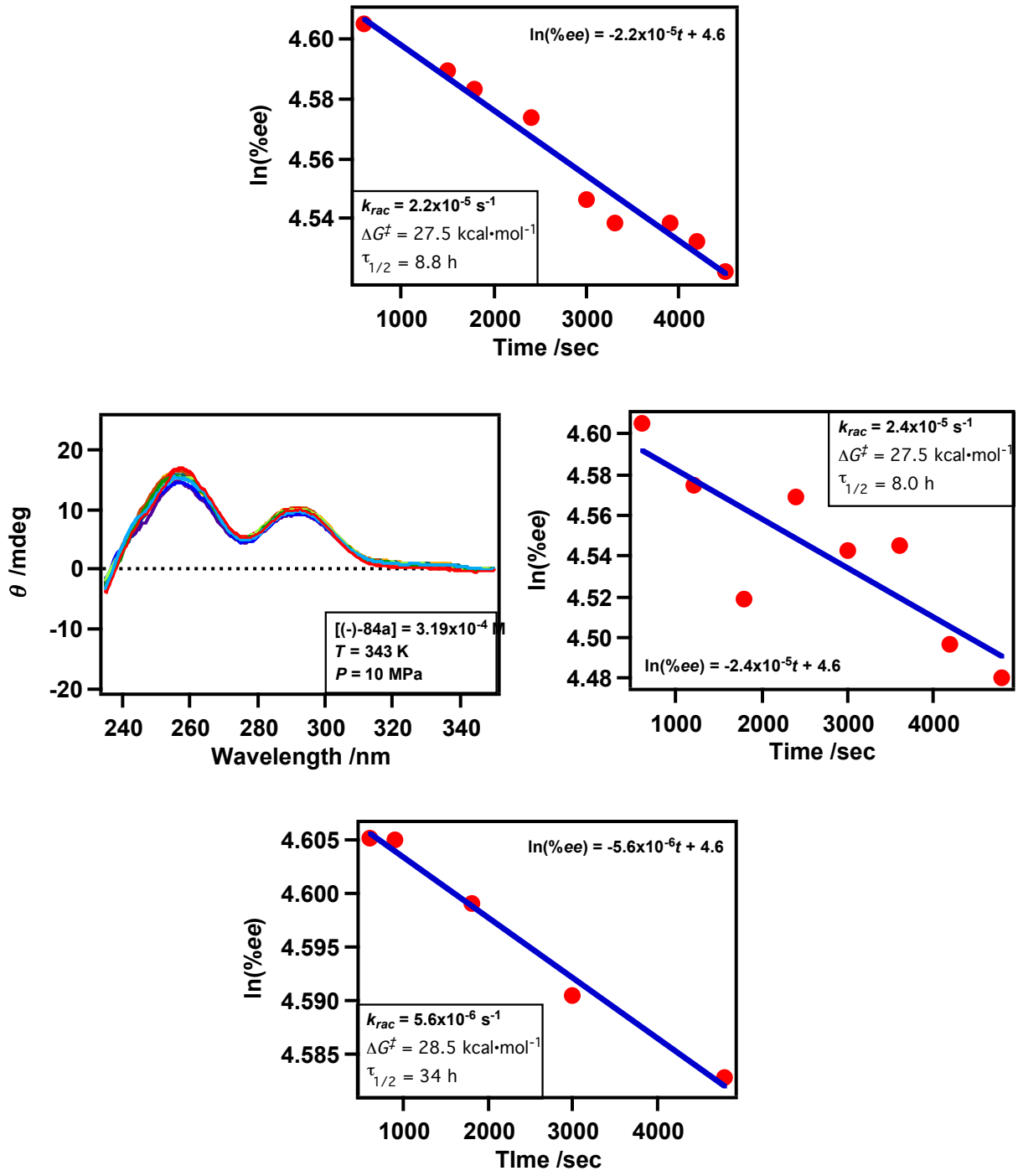

Figure 6.10: Racemization kinetic study at various pressure in EtOH for compound **84a**: Temperature = 343 K; Pressure: top 5 MPa, middle 10 MPa, bottom 25 MPa.

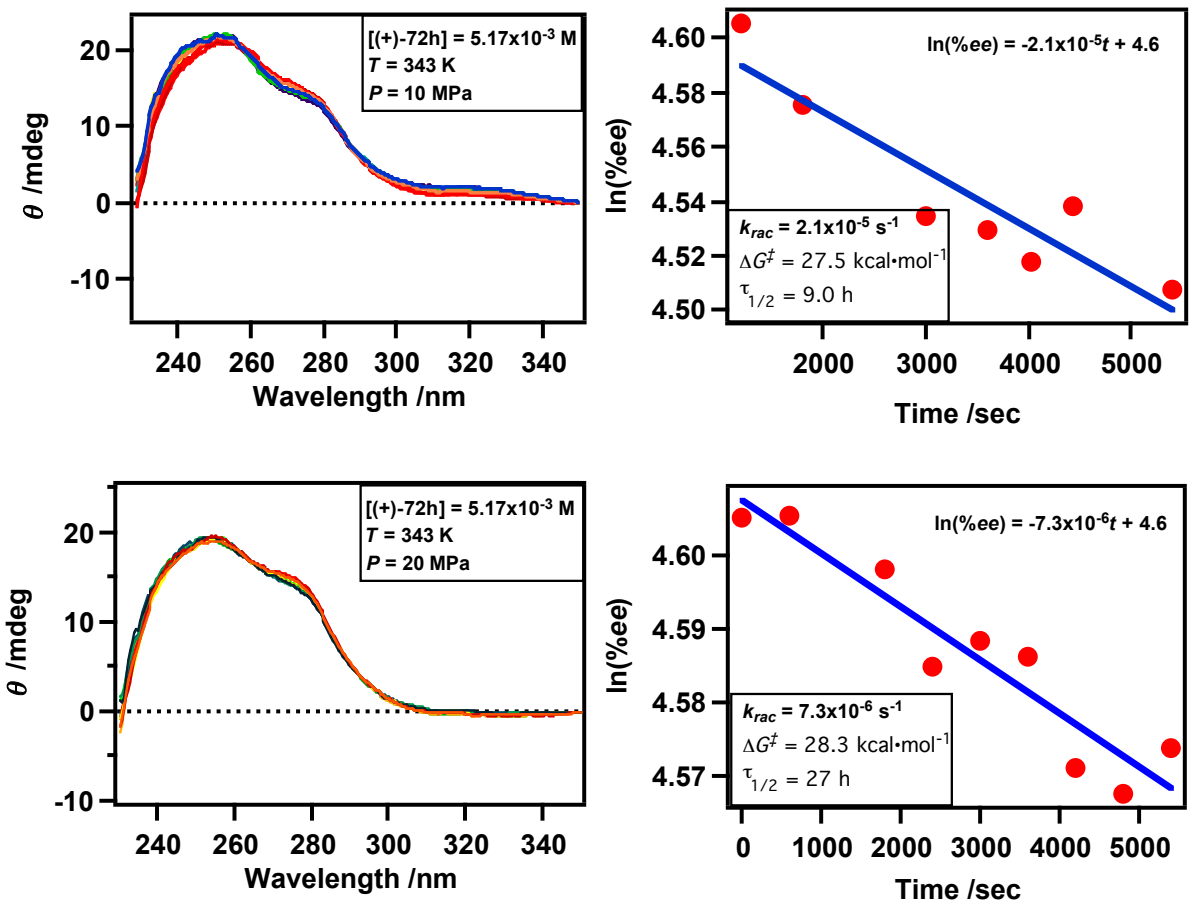

Figure 6.11: Racemization kinetic study at various pressure in MCH for compound **72h**: Temperature = 343 K; Pressure: top 10 MPa, bottom 20 MPa.

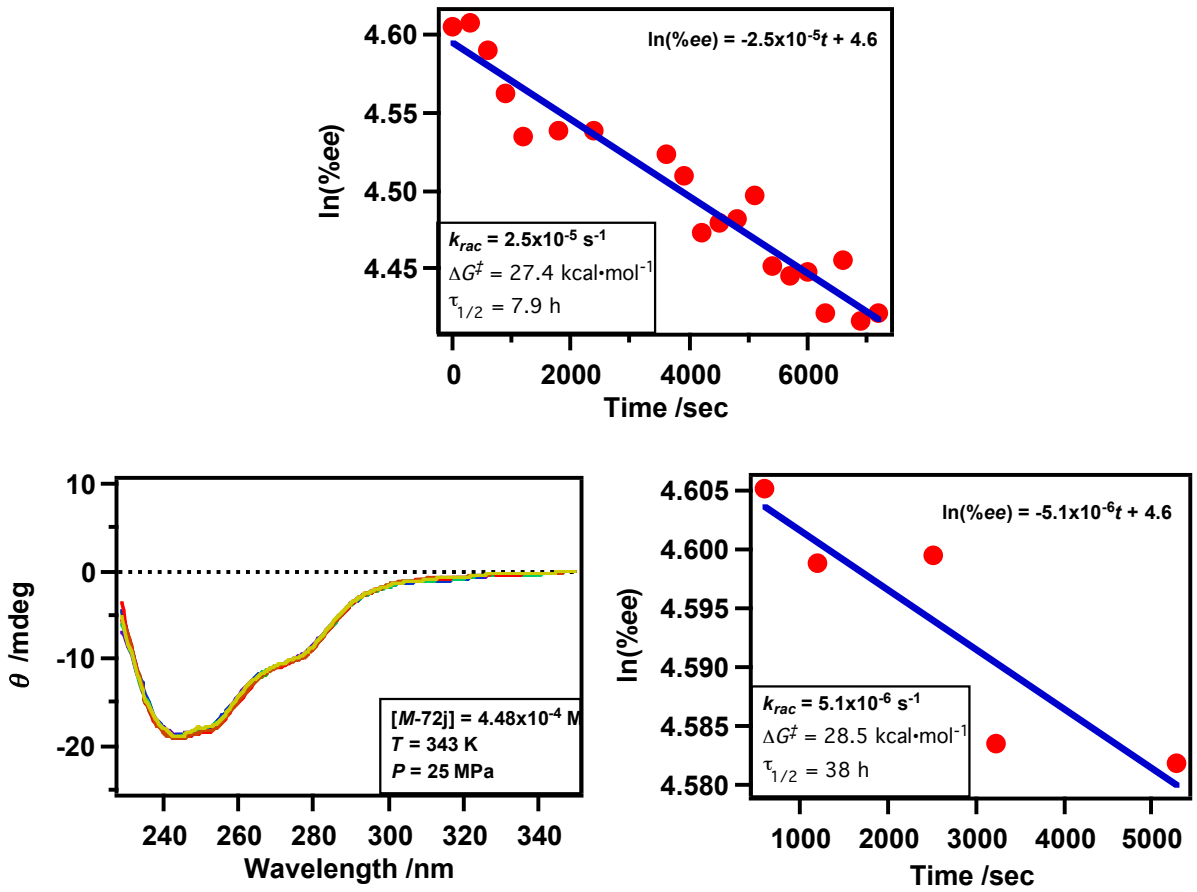

Figure 6.12: Racemization kinetic study at various pressure in MCH for compound **72j**: Temperature = 343 K; Pressure: top 10 MPa, bottom 25 MPa.

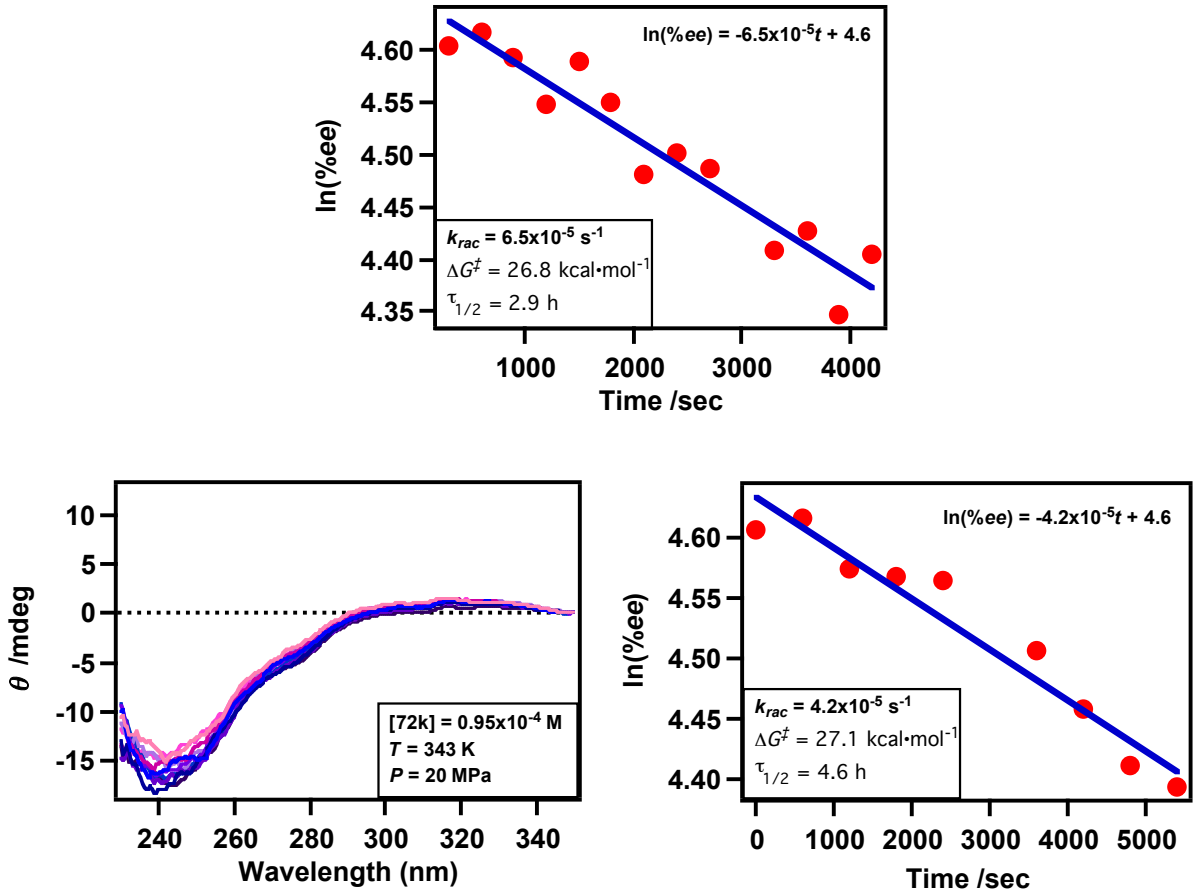

Figure 6.13: Racemization kinetic study at various pressure in MeCN for compound **72k**: Temperature = 343 K; Pressure: top 10 MPa, bottom 20 MPa.

Table 6.3: Racemization rate constants and activation energy of optically pure atropisomers **84a** and **72h,j,k** under normal and elevated pressures at 343 K.[a]

Entry	Substrates / Solvent	0.1 MPa			10 MPa			20 MPa		
		k_{rac} (s^{-1})	$\Delta G^{\ddagger}$ (kcal·mol^{-1})	$\tau_{1/2}$ (h)	k_{rac} (s^{-1})	$\Delta G^{\ddagger}$ (kcal·mol^{-1})	$\tau_{1/2}$ (h)	k_{rac} (s^{-1})	$\Delta G^{\ddagger}$ (kcal·mol^{-1})	$\tau_{1/2}$ (h)
1	**84a** / EtOH[c,d]	3.7×10^{-5}	27.0	5.2[c]	2.4×10^{-5}	27.5	8.0	5.6×10^{-6}	28.5	34[b]
3	**72h /** MCH	3.5×10^{-5}	27.2	5.5	2.1×10^{-5}	27.5	9.0	7.3×10^{-6}	28.3	27
4	**72j** / MCH	4.5×10^{-5}	27.0	4.3	2.5×10^{-5}	27.4	7.9	5.1×10^{-6}	28.5	38[b]
5	**72k** / MCH	8.1×10^{-5}	26.6	2.4	6.5×10^{-5}	26.8	2.9	4.2×10^{-5}	27.1	4.6

[a] CD spectra monitored at 260 for **84a** and 250 nm for **72h,j,k**,. Reported values carry a 10% error. [b] Pressure maintained at 25 MPa. [c] For **84a** in EtOH, at 0.1 MPa, the temperature was 341 K. [d] For **84a** in EtOH, at 5 MPa, k_{rac} =2.2x10^{-5} s^{-1} with a $\tau_{1/2}$ of 8.8 h and $\Delta G^{\ddagger}_{rac}$ = 27.5. [e] Pressure maintained at 12 MPa. [f] Due to experimental limitations, values at higher pressure were not reported.

For the study under elevated pressure, the activation enthalpy ($\Delta H^{\ddagger}_{rac}$) and activation entropy ($\Delta S^{\ddagger}_{rac}$) were computed using the Eyring plot (Eq. 6.5) for compounds **84a** and **72h,j,k** (Table 6.3; Figures 6.10 – 6.13). The racemization at normal pressure showed negative $\Delta S^{\ddagger}_{rac}$ and positive $\Delta H^{\ddagger}_{rac}$. The negative $\Delta S^{\ddagger}_{rac}$ is consistent with the fact that the racemization of non-biaryl atropisomers is entropically not favourable due to the restricted bond rotation that most often involves steric interactions. A point to be noted is the magnitude of $\Delta S^{\ddagger}_{rac}$ values. This observation could be explained by the fact that steric hindrance impedes free rotation of the N-C(aryl) bond rotation in **84a** and **72h,j,k**. The N-C(aryl) bond rotation has to overcome the steric impediments that are due to interactions with alkyl/cycloalkyl substituent(s) and the *ortho*-substituent group on the phenyl ring. While an increase in the temperature enhanced the racemization rates of non-biaryl atropisomers, an increase in the pressure had the opposite effect. Comparison of Tables 6.2 and 6.3 shows that at a given temperature the racemization rate constants are lower at elevated pressures with a trend *viz.,* faster racemization at normal pressure (0.1 MPa) and slow racemization rates at elevated pressures (5-20 MPa). This influence of pressure on the racemization rates was reflected by an increase in the $\Delta G^{\ddagger}_{rac}$ values as well as in the $\tau_{1/2}$ values of racemization.

6.2.4. Activation volumes for racemization

As change in the pressure translates with variation of the molar volume of the systems under study and thus changes (activation parameters) during chemical transformations (racemization in the present case). Analysis of equations 6.1 – 6.2 indicated that at a given temperature, the processes that occur through a transition state with negative differential activation volume would be accelerated under elevated pressures, while transition state(s) with positive differential activation volume will be decelerated. For example, in the case of cycloadditions and condensation reactions that showed rate acceleration at elevated pressures, a decrease in partial molar volume in the transition state along the reaction coordinate was postulated for the enhanced chemical reactivity.[33-35] In compounds **84a** and **72h,j,k** (Table 6.4), the activation volume was positive for the racemization process, i.e. the partial molar volume in the transition state increased considerably when compared to the partial molar volume of the optically pure atropisomeric reactant(s).

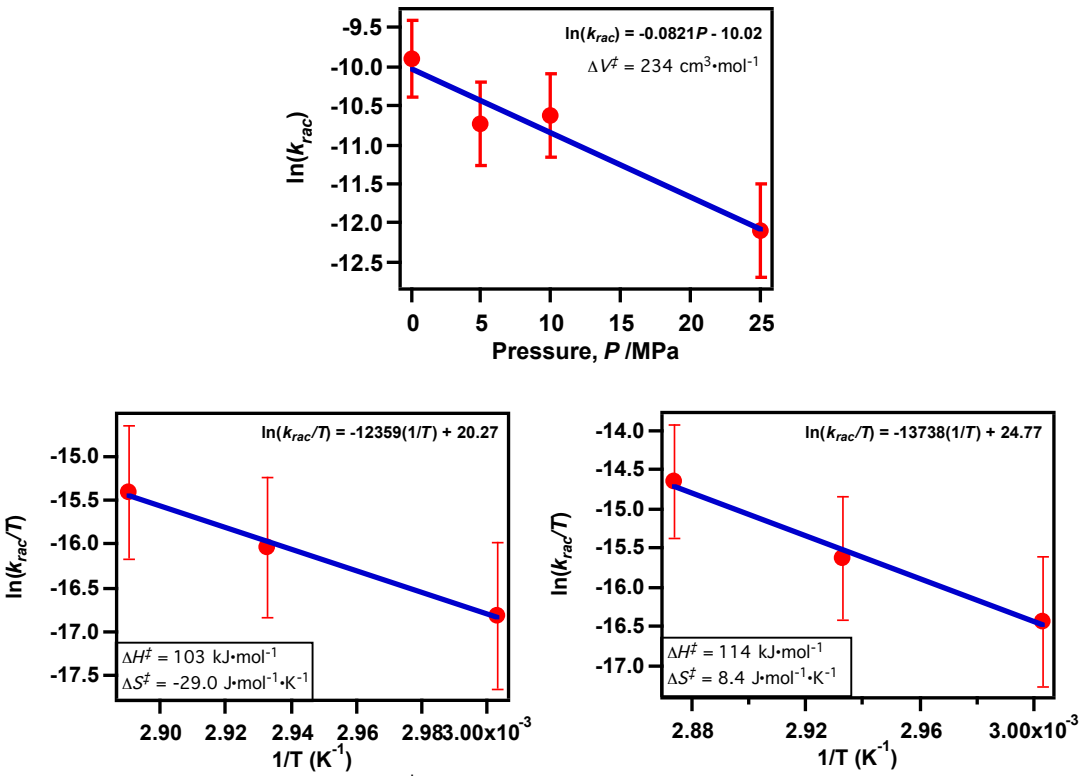

Figure 6.14: Top: Activation volume ($\Delta V^{\ddagger}_{rac}$) for racemization of **84a** in EtOH; bottom: Activation enthalpy ($\Delta H^{\ddagger}$) and activation entropy ($\Delta S^{\ddagger}$) for racemization of **84a** in EtOH (left) and MeCN (right).

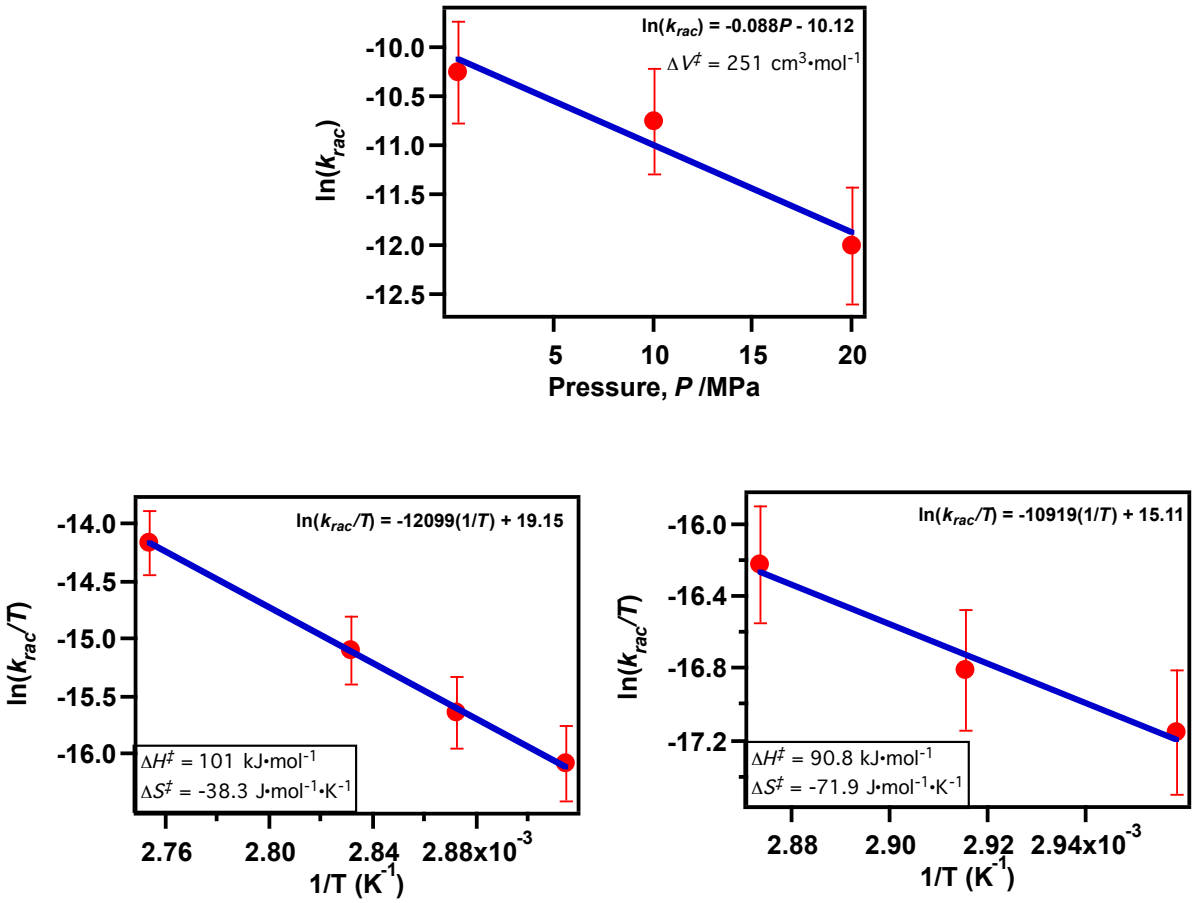

Figure 6.15: Top: Activation volume ($\Delta V^{\ddagger}_{rac}$) for racemization of **72h** in MCH; bottom: Activation enthalpy ($\Delta H^{\ddagger}$) and activation entropy ($\Delta S^{\ddagger}$) for racemization of **72h** in MCH (left) and MeCN (right).

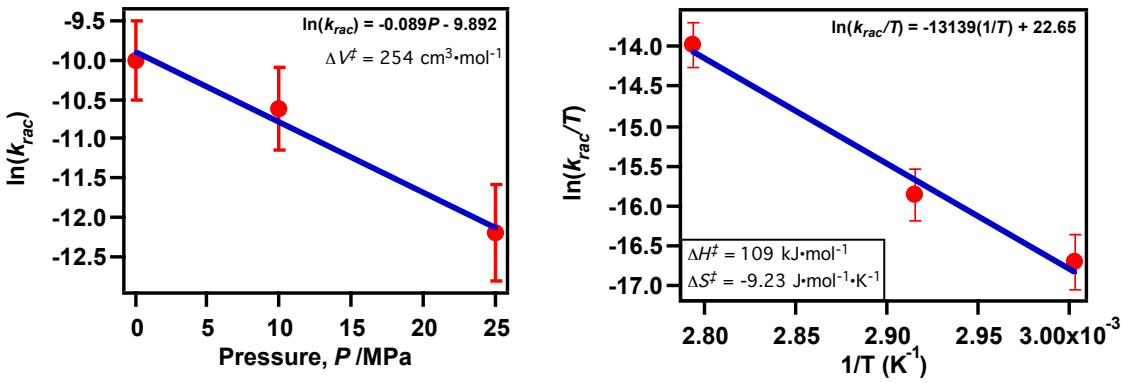

Figure 6.16: Left: Activation volume ($\Delta V^{\ddagger}_{rac}$) for racemization of **72j** in MCH; left: Activation enthalpy ($\Delta H^{\ddagger}$) and activation entropy ($\Delta S^{\ddagger}$) for racemization of **72j** in MCH.

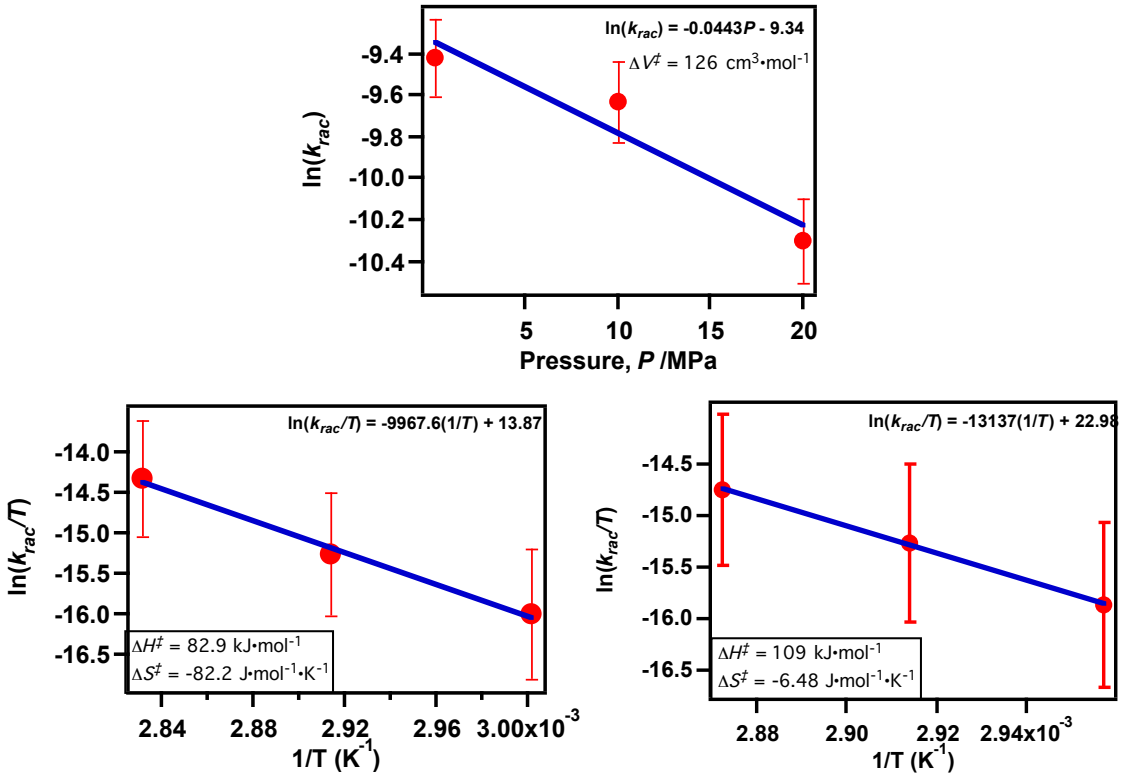

Figure 6.17: Top: Activation volume ($\Delta V^{\ddagger}_{rac}$) for racemization of **72k** in MCH; bottom: Activation enthalpy ($\Delta H^{\ddagger}$) and activation entropy ($\Delta S^{\ddagger}$) for racemization of **72k** in MCH (left) and MeCN (right).

Analysis of figures 6.14 – 6.17 showed that the change in $\Delta V^{\ddagger}_{rac}$ is a reflection of the structure features of the compounds employed for the racemization study. In the systems under study, the hindered rotation around the N-C(aryl) bond is due to steric bulk offered by the *ortho-tert*-butyl substituent on the *N*-phenyl group. Thus, during racemization i.e. the rotation of the N-C(aryl) bond in compounds **84a** and **72h,j,k**, the system has to expand effectively to accommodate the bulky *ortho-tert*-butyl substituent. A closer look at the activation volume ($\Delta V^{\ddagger}_{rac}$) in table 6.4 (~120-250 $cm^3.mol^{-1}$) ascertained a trend in not only the molecular weight of the systems under study but also a correlation to the activation entropy values ($\Delta S^{\ddagger}_{rac}$). In order to verify this observation, one must take into account the solvent cluster surrounding the atropisomeric molecules. At normal pressure, the solvent shell surrounding the systems of interest is expected to be loose (van der Waals forces). At elevated pressures, the solvent shell will be packed closely such that the molecular conformation becomes “frozen”. Racemization due to rotation of N-C(aryl) bond is unlikely, due to tight molecular packing at elevated pressures; and the bond rotation is likely hindered resulting in the observed slow racemization. In addition, the N-C(aryl) bond rotation has to be accompanied by a change in the arrangement of the "solvent cluster" surrounding the molecule during the racemization process. This is reflected in the $\Delta V^{\ddagger}_{rac}$ values (Table 6.4).

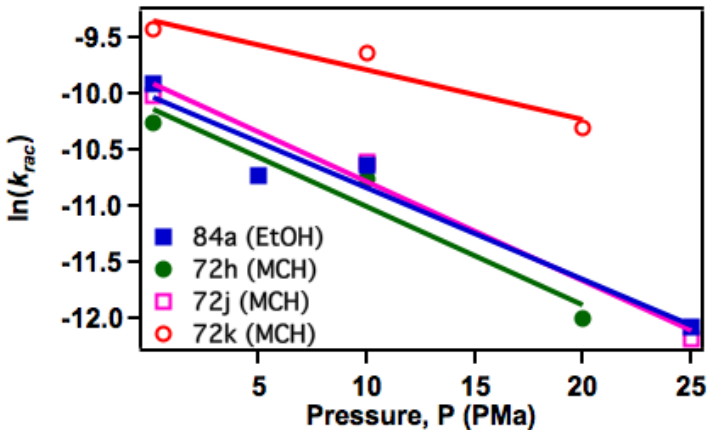

Figure 6.18: Pressure dependence of racemization to ascertain the activation volume for **84a** and **72h,j,k** at 343 K. The solvents utilized for a given compound is provided in the insert.

Table 6.4: Activation enthalpy ($\Delta H^{\ddagger}$), activation entropy ($\Delta S^{\ddagger}$) And activation volume ($\Delta V^{\ddagger}$) for racemization of optically pure **84a** and **72h,j,k**.

Entry	Compounds / Solvent	$\Delta S^{\ddagger\,a}$ ($J \cdot mol^{-1} \cdot K^{-1}$)	$\Delta H^{\ddagger\,a}$ ($kJ \cdot mol^{-1}$)	$\Delta V^{\ddagger\,b}$ at 343 K ($cm^3 \cdot mol^{-1}$)
1	**84a** / EtOH	- 29.0	103	234
3	**72h** / MCH	- 38.3	101	251
4	**72j** / MCH	- 9.23	109	254
5	**72k** / MCH	- 82.2	82.9	126

[a] computed from the Eq. 6.5. [b] computed from the Eq.6.6.

6.3. Summary and Outlook

Asymmetric photochemical transformations involving atropisomeric compounds could be achieved with high stereoselectivity in the resulting photoproduct(s). However, as high temperature could greatly affect the intrinsic racemization of atropisomeric systems, employing elevated pressure would be an elegant approach to control the rate of racemization and achieve high stereoselectivities. This strategy of employing pressure may be extended to other non-biaryl compounds for asymmetric transformations at elevated temperatures with minimal racemization. Thus, as non-biaryl atropisomers are potential ligands for asymmetric synthesis, either slow racemization or frozen chiral configuration obtained at moderate pressures opens up avenues to employ them for reactions requiring high temperatures.

6.4. Experimental Section

6.4.1. General method

All commercially obtained reagents/solvents were used as received; chemicals were purchased from Alfa Aesar®, Sigma – Aldrich®, Acros®, TCI America®, Mallinckrodt®, and Oakwood® Products, and were used as received without further purification. For spectroscopic measurements, spectrophotometric grade solvents were used. Unless stated otherwise, reactions were conducted in oven-dried glassware under nitrogen atmosphere. The starting materials were structurally characterized by ^{1}H NMR and ^{13}C NMR spectra on Varian 400 MHz (100 MHz for ^{13}C) or on 500 MHz (125 MHz for ^{13}C) spectrometers and were consistent with literature reported procedures. Data for ^{1}H-NMR are reported as chemical shift (δ

ppm) with the corresponding integration values. Coupling constants (*J*) are reported in hertz (Hz). Standard abbreviations indicating multiplicity were used as follows: s (singlet), b (broad), d (doublet), t (triplet), q (quartet), m (multiplet) and virt (virtual). Data for ^{13}C-NMR spectra are reported in terms of chemical shift (δ ppm). High-resolution mass spectrum data in Electrospray Ionization mode were recorded on a Bruker – Daltronics® BioTof mass spectrometer in positive (ESI+) ion mode. HPLC analyses were performed on Waters® HPLC equipped with 2525 pump. Waters® 2767 sample manager was used for automated sample injection. All HPLC injections were monitored using a Waters® 2487 dual wavelength absorbance detector at 220, 254 and 270 nm. Analytical and semi-preparative injections were performed on chiral stationary phase using various columns as indicated below.

i) Regis® PIRKLE COVALENT (*R*,*R*) WHELK–01

   a) 25 cm x 4.6 mm column for analytical injections.

   b) 25 cm x 10 mm column for semi-preparative injections.

ii) CHIRALPAK® AD-H

   a) 0.46 cm x 15 cm column for analytical injections.

   b) 10 mm x 25 cm column for semi-preparative injections.

iii) CHIRALPACK® IC

   a) 0.46 cm x 25 cm column for analytical injections.

   b) 10 mm x 25 cm column for semi-preparative injections

Masslynx software version 4.1 was used to monitor/analyze the HPLC injections and to process HPLC traces. Igor Pro® Software version 6.0 was used to process the HPLC graphics. UV-Vis spectra were recorded on Shimadzu 2501PC UV-Vis spectrometer using UV quality fluorimeter cells (with range until 190 nm) purchased from Luzchem. Optical activity values were recorded on JASCO® DIP – 370 digital polarimeter or JASCO® DIP – 200 digital polarimeter. When necessary, the compounds were purified by combiflash equipped with dual wavelength UV-Vis absorbance detector (Teledyn ISCO) using hexanes : EtOAc as the mobile phase and Redisep® cartridge filled with silica (Teledyne ISCO) as stationary phase. In some cases, compounds were purified by column chromatography on silica gel

(Sorbent Technologies®, silica gel standard grade: porosity 60 Å, particle size: 230 x 400 mesh, surface area: 500 – 600 m^2/g, bulk density: 0.4 g/mL, pH range: 6.5 – 7.5).

6.4.2. Synthesis of α-oxoamide 84a

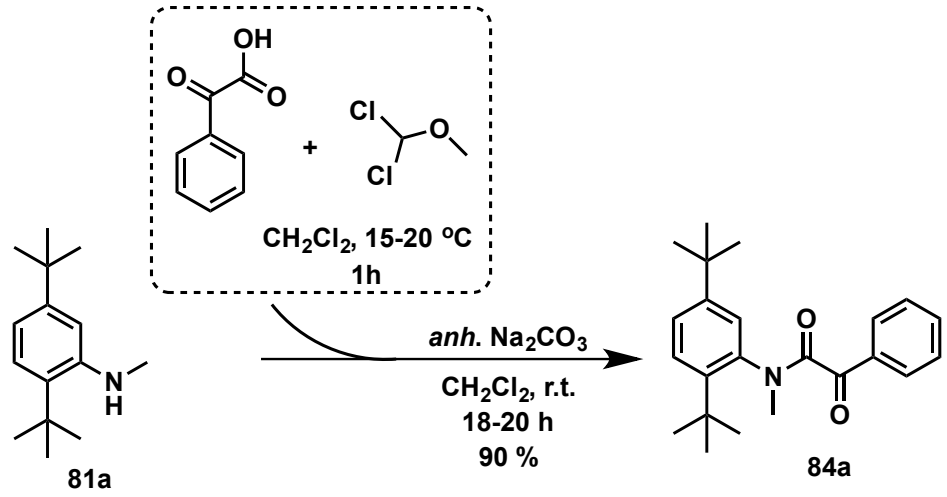

Scheme 6.2: Synthesis of α-oxoamides **84a**.

Benzoyl formyl chloride was prepared in situ, and used in the synthesis of α-oxoamides **84a**. In a 25 mL round bottom flask, 1.25 equiv. (0.912 g, 6 mmol) of benzoyl formic acid was dissolved in 5 mL of dichloromethane (CH_2Cl_2); then, 1.35 equiv. of dichloromethyl methyl ether (0.59 mL, 6.5 mmol) was added drop wise to the reaction flask under N_2 atmosphere. The mixture was stirred at 15 – 20 °C for 1 h to yield a quantitative amount of benzoyl formyl chloride that used in situ.

In a round-bottom-flask, benzoyl formyl chloride (1.2 equiv.) N_2 under atmosphere was dissolved in 20 mL of CH_2Cl_2. After, 10 equiv. of *anh*. Na_2CO_3 was added to the acid chloride solution, the mixture was stirred followed by the addition of 2,5-di-*tert*-butyl-*N*-methylaniline **81a** in CH_2Cl_2. The reaction mixture was stirred at 20-23 °C overnight (for 18-20 h). After completion, the reaction was quenched with 20 mL of DI water and the expected crude compound was extracted with CH_2Cl_2 (2 x 30 mL). The organic layer was then dried over *anh*. Na_2SO_4 and concentrated under reduced pressure in a rotatory evaporator. The expected α-oxoamides **84a** was finally purified by flash chromatography on silica gel: Isolated yield >90 %.

6.4.3. Characterization of α-oxoamide 84a

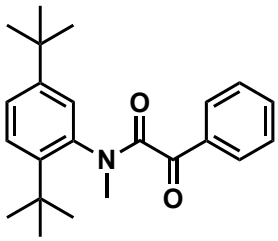

84a

Purification conditions: 84a was purified by flash chromatography on silica gel: Solvent system: 8 – 10% EtOAc:Hexanes. R*f* = 0.5 (20 % EtOAc-Hexanes). **84a** was further recrystallized in 5% benzene-Hexanes.

X-ray crystallography parameter: *Cf.* chapter 8

^{1}H NMR (400 MHz, $CDCl_3$, δ ppm) 7.85 – 6.63 (Ar, 8H), 3.35 and 3.23 (s, 3H, N-CH_3, major and minor conformers), 1.45 and 1.43 (s, 9H, major and minor conformers), 1.32 and 0.87 (9H, major and minor conformers)

^{13}C NMR (100.5 MHz, CDCl3, δ ppm) 190.8, 167.3, 149.7, 144.6, 137.5, 134.4, 134.1, 130.5, 130.0, 129.5, 129.3, 128.8, 128.1, 126.3, 38.4, 36.3, 33.9, 32.3, 31.9, 31.4, 30.7

HRMS-ESI [$(M + Na)^+$]: Calculated: 374.2091; Observed: 374.2074; Δm = 4.5 ppm

HPLC analysis conditions: For both analytical and preparative injections

Column: (R,R) WHELK–01; Abs. detector: 254 nm and 270 nm

Mobile phase: Hexanes: IPA = 90:10

Flow rate: 1 mL/min (Analytical), and 4.5 mL/min (Preparative).

Retention times (min): ~14.20 [(-)-**84a**] and ~19.70 [(+)-**84a**]

Optical Rotation $[\alpha]_D^{28}$:

HPLC peak retention time at ~14.20 min, (-)-**84a** (*c* 0.1, $CHCl_3$) = -70

HPLC peak retention time at ~19.70 min, (+)-**84a** (*c* 0.1, $CHCl_3$) = +78

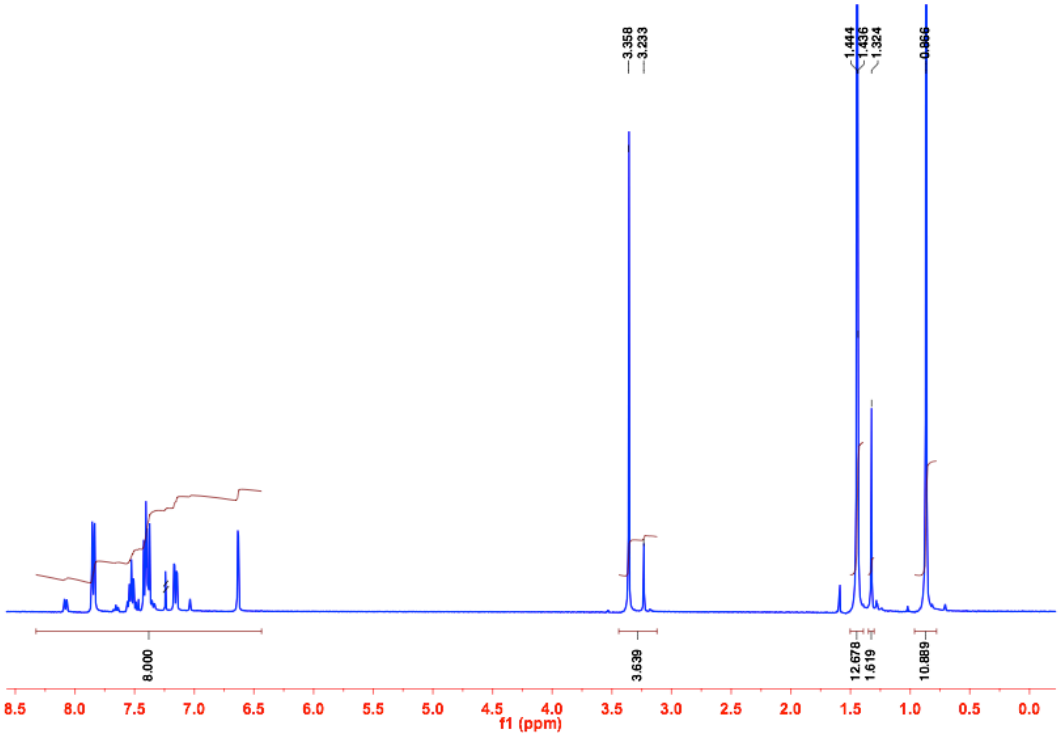

Figure 6.19: ^{1}H NMR (400 MHz, $CDCl_3$, δ ppm) spectrum for α-oxoamide **84a**.

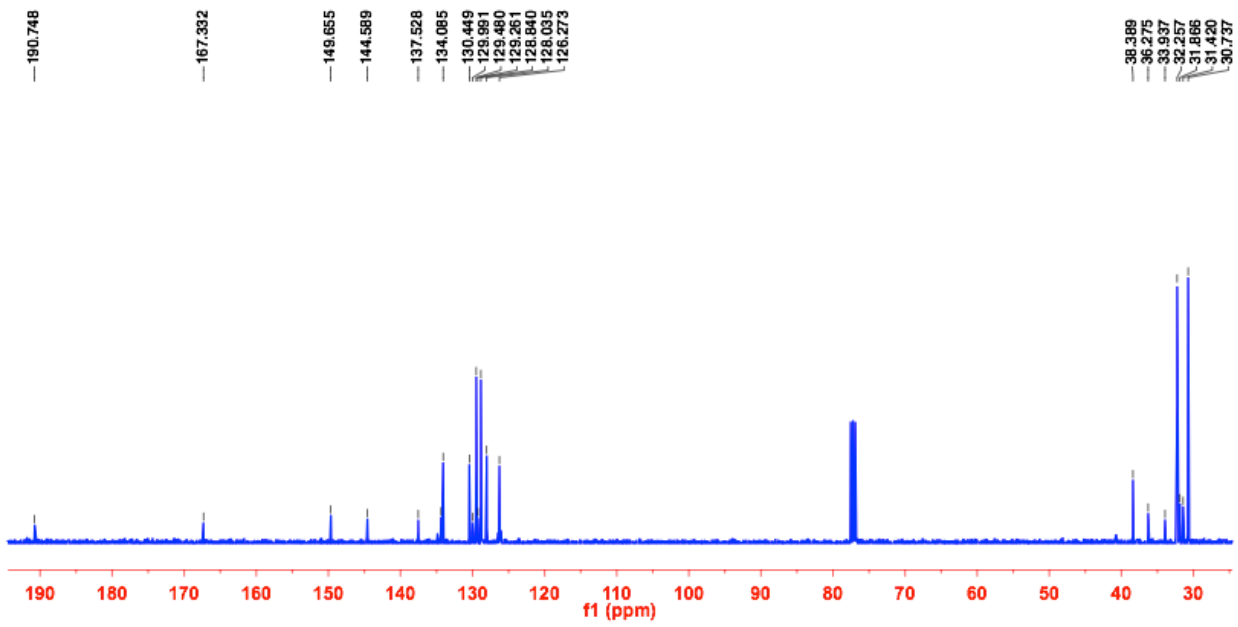

Figure 6.20: ^{13}C NMR (100 MHz, $CDCl_3$, δ ppm) spectrum for α-oxoamide **84a**.

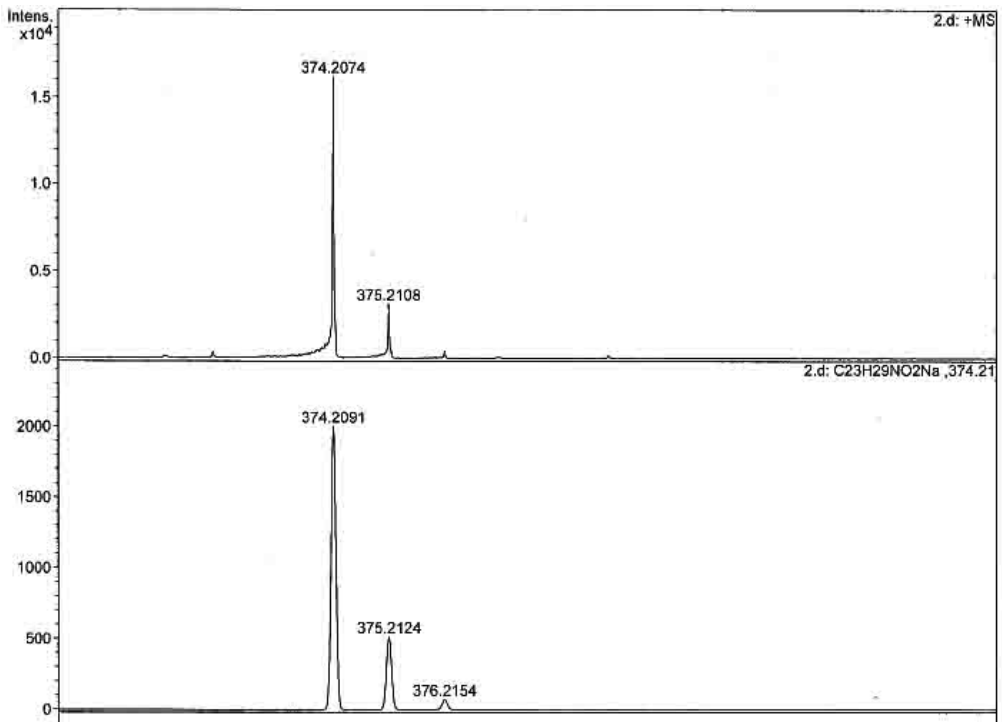

Figure 6.21: HRMS for α-oxoamide **84a**.

6.4.4. Synthesis of acrylanilide 72k

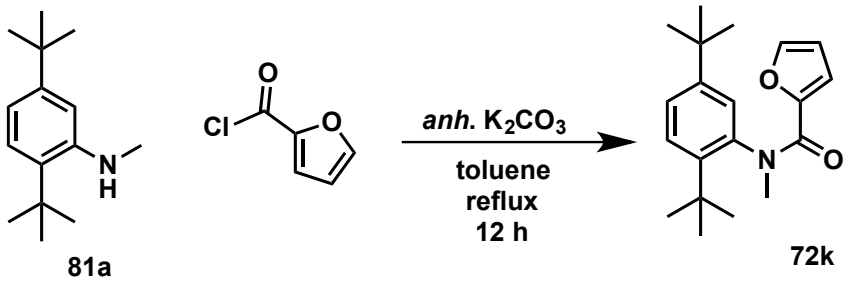

Scheme 6.3: Synthesis of acrylanilide **72k**.

Acrylanilide **72k** was prepared using procedures reported in chapters 2 and 3.

6.4.5. Characterization of acrylanilide 72k

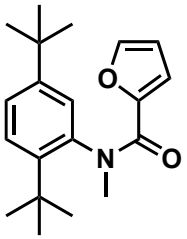

72k

Purification conditions: The expected anilide **72k** was purified by chromatography (using CombiFlash®): 12 g silica; flow rate: 21-22 mL/min, solvent system: EtOAc : Hexanes.

^{1}H NMR (400 MHz, $CDCl_3$, δ ppm) 7.48 – 7.43 (Ar, 1H), 7.39 – 7.31 (Ar, 2H), 7.04 – 6.98 (Ar, 1H), 6.13 – 6.08 (q, 1H), 5.22 – 5.17 (q, 1H), 3.34 (s, 3H), 1.25 – 1.23 (d, 18H)

^{13}C NMR (100 MHz, $CDCl_3$, δ ppm) 160.1, 151.0, 147.5, 144.5, 143.9, 141.2, 129.5, 128.0, 125.9, 116.3, 111.1, 40.2, 35.8, 34.4, 32.1, 31.3

HRMS-ESI [(M+ Na)$^+$]: Calculated: 336.1934; Observed: 336.1924; Δm = 2.9 ppm

HPLC Conditions: Column: CHIRALPAK® AD-H for Analysis and separation;

Abs. detector: 254 nm and 270 nm**;** mobile phase: Hexanes:IPA = 98:2;

Flow rate: 1 mL/min (Analysis), and 2.5 mL/min (separation)

Retention time (min): A-**72k:** ~12.12, B-**72k:** ~17.24 (separation/preparative)

Note: Isomer A & B respectively refer to the first and second peak that elute out of the HPLC chiral stationary phase during analysis/separation. The designation A & B can also be substituted with (+) and (-) to mention the sign of the CD signal of optically pure samples of **72k** at wavelength 250 nm.

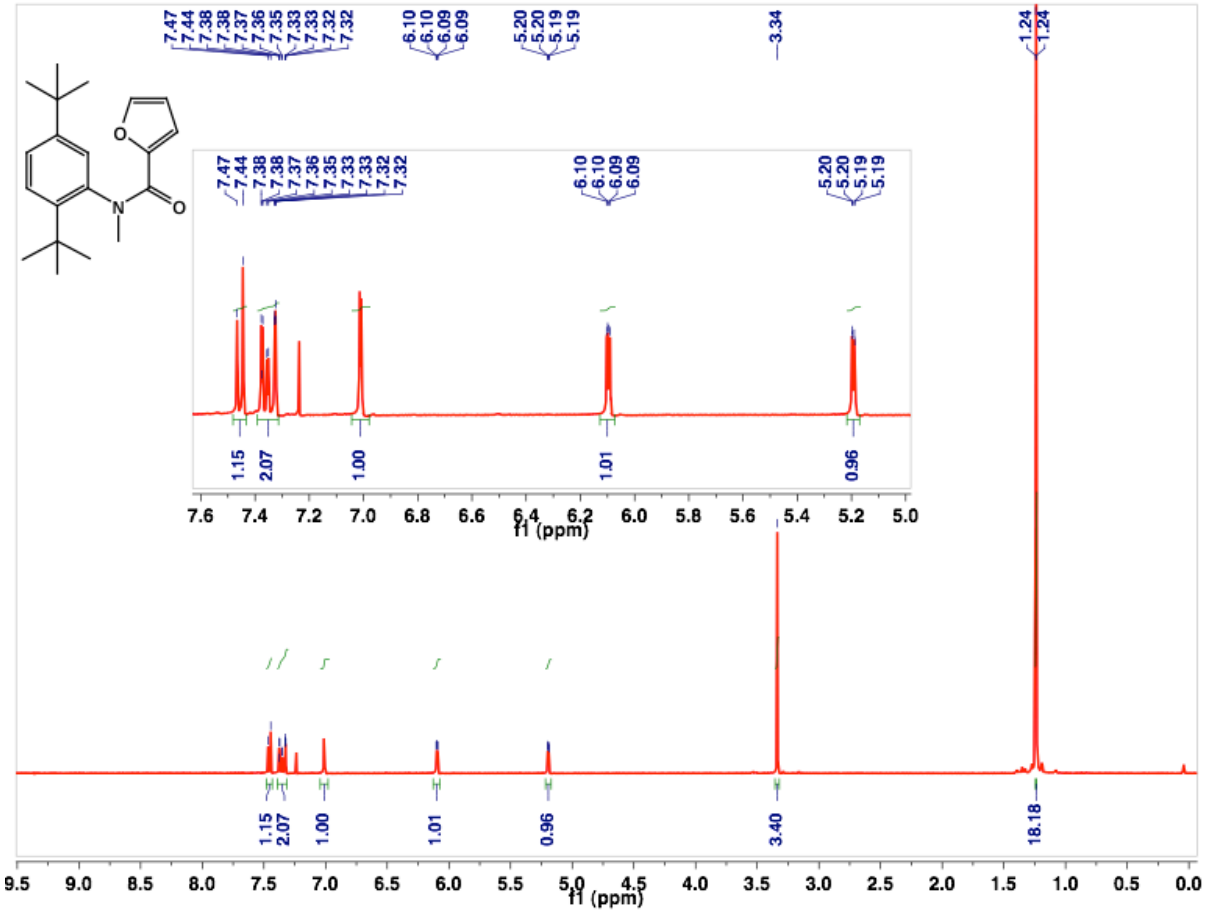

Figure 6.22: ^{1}H NMR (400 MHz, $CDCl_3$, δ ppm) spectrum for acrylanilide **72k.**

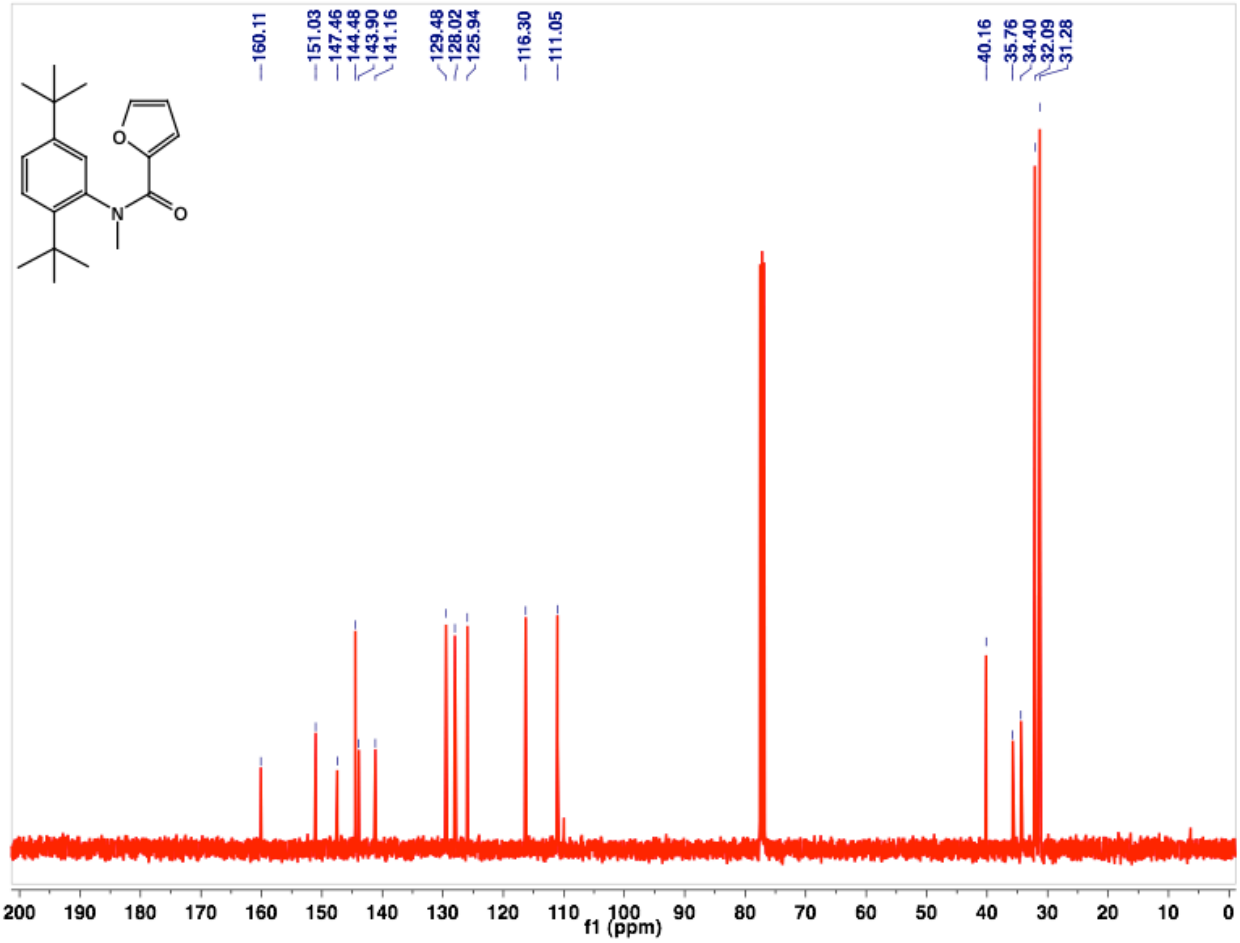

Figure 6.23: ^{13}C NMR (100 MHz, $CDCl_3$, δ ppm) spectrum for acrylanilide **72k.**

6.4.6. Irradiation procedure under elevated pressure

The photochemical reactions under elevated pressure were performed as follow: compounds 1a-e were dissolved in dry acetonitrile ([**84a**] = 11.5 mM, and [**72h**] = 11.5 mM, [**72j**] = 10 mM) and transferred into a custom designed quartz cell (Figure 6.1-A); the cell is then placed in a high-pressure vessel that is equipped with a sapphire window. The irradiations were carried out using an optical fiber carrying a light source from a Xenon lamp with 300±10 nm band pass filter from Asashi® spectra 302 Max power supply unit.

6.4.7. Characterization of β-lactam photoproducts 85a

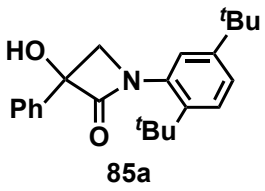

85a

Photoproduct **85a** was isolated by chromatography: Solvent system: 20% EtOAc-Hexanes. R*f* = 0.3 (20% EtOAc-Hexanes)

^{1}H NMR (500 MHz, $CDCl_3$, δ ppm) 7.77 – 7.13 (Ar, 7H), 4.1 – 3.9 (ABq, 2H), 3.3 – 3.0 (bs, 1H), 1.36 (s, 9H), 1.30 (s, 9H)

^{13}C NMR (125 MHz, CDCl3, δ ppm) 167.0, 150.6, 145.8, 138.5, 134.8, 129.2, 127.5, 126.8, 126.4, 126.3, 85.5, 62.2, 35.0, 31.5, 31.4

HRMS-ESI [(M + Na)$^{+}$]: Calculated: 374.2099; Observed: 374.2091; Δm = 2.1 ppm

HPLC analysis conditions: Column: CHIRALPACK IC; Abs. detector: 220 nm and 254 nm**; m**obile phase: Hexanes: IPA = 92.4:7.6; Flow rate: 0.5 mL/min

Retention times (min): ~11.90 (**85a**) and ~15.90 (*ent*-**85a)**

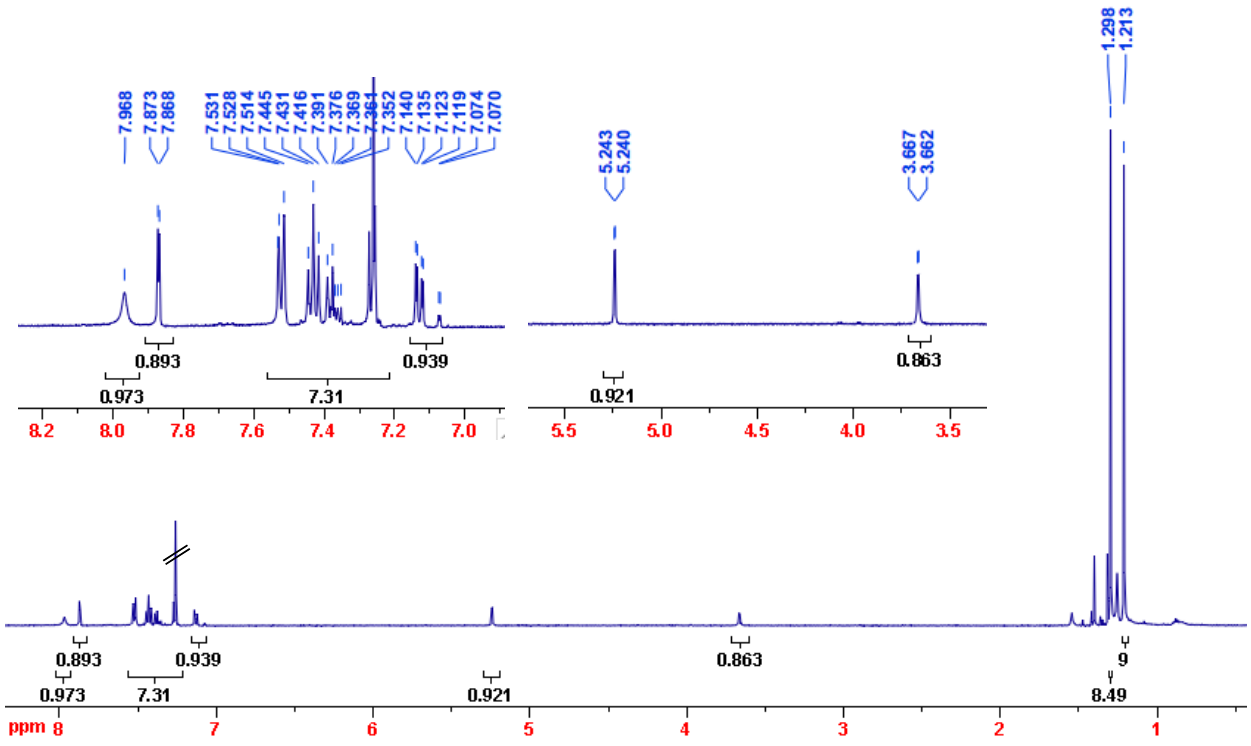

Figure 6.24: ^{1}H NMR (500 MHz, $CDCl_3$, δ ppm) spectrum for β-lactam **85a.**

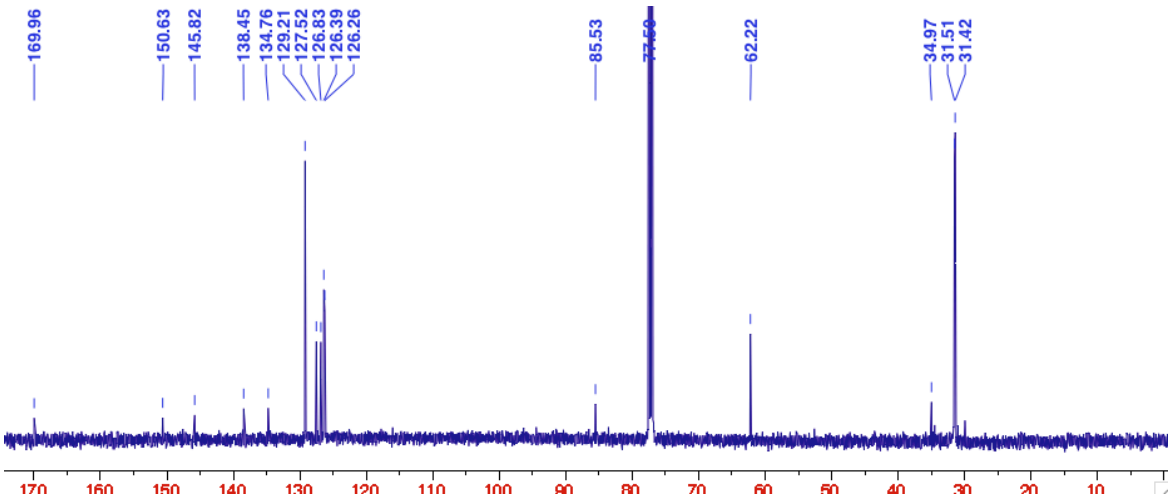

Figure 6.25: ^{13}C NMR (125 MHz, $CDCl_3$, δ ppm) spectrum for β-lactam **85a.**

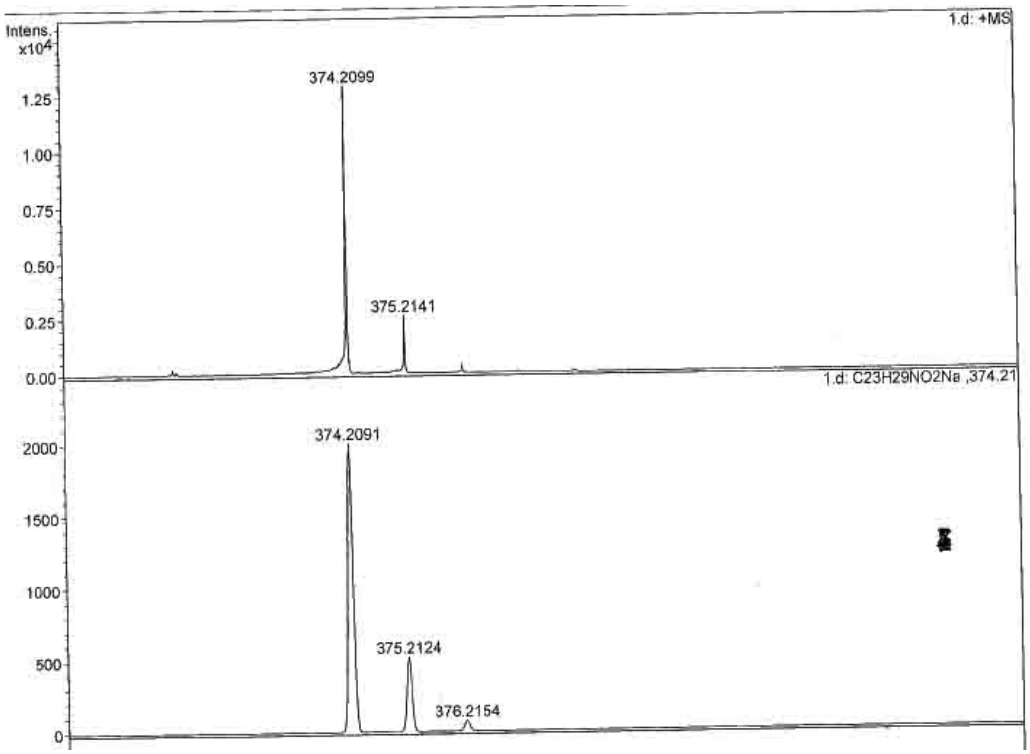

Figure 6.26: HRMS for β-lactam **85a.**

6.5. References

(1) Miyashita, A.; Yasuda, A.; Takaya, H.; Toriumi, K.; T Ito; Souchi, T.; Noyori, R. Synthesis of 2,2“-bis(diphenylphosphino)-1,1-”binaphthyl (BINAP), an atropisomeric chiral bis(triaryl)phosphine, and its use in the rhodium(I)-catalyzed asymmetric hydrogenation of .alpha.-(acylamino)acrylic acids. *J. Am. Chem. Soc.* **1980**, *102*, 7932–7934.

(2) Curran, D. P.; Qi, H.; Geib, S. J.; DeMello, N. C. Atroposelective Thermal Reactions of Axially Twisted Amides and Imides. *J. Am. Chem. Soc.* **1994**, *116*, 3131–3132.

(3) Curran, D. P.; Hale, G. R.; Geib, S. J.; Balog, A.; Cass, Q. B. L.; Degani, A. L. G.; Hernandes, M. Z.; Freitas, L. C. G. Rotational features of carbon-nitrogen bonds in axially chiral o-tert. butyl anilides and related molecules. Potential substrates for the “prochiral auxiliary” approach to asymmetric synthesis. *Tetrahedron: Asymmetry* **1997**, *8*, 3955–3975.

(4) Clayden, J. Atropisomers and near-atropisomers: achieving stereoselectivity by exploiting the conformational preferences of aromatic amides. *Chem. Commun.* **2004**, 127–135.

(5) Adler, T.; Bonjoch, J.; Clayden, J.; Font-Bardia, M.; Pickworth, M.; Solans, X.; Sole, D.; Vallverdu, L. Slow interconversion of enantiomeric conformers or atropisomers of anilide and urea derivatives of 2-substituted anilines. *Org. Biomol. Chem.* **2005**, *3*, 3173–3183.

(6) Clayden, J.; Moran, W. J.; Edwards, P. J.; LaPlante, S. R. The Challenge of Atropisomerism in Drug Discovery. *Angew. Chem. Int. Ed. Engl.* **2009**, *48*, 6398–6401.

(7) Berens, U.; Brown, J. M.; Long, J.; Selke, R. Synthesis and resolution of 2,2“-bis-diphenylphosphino [3,3”]biindolyl ; a new atropisomeric ligand for transition metal catalysis. *Tetrahedron: Asymmetry* **1996**, *7*, 285–292.

(8) Agranat, I.; Cohen, S.; Isaksson, R.; Sandstroem, J.; Suissa, M. R. Static and dynamic stereochemistry of a chiral, doubly bridged 9,10-diphenylanthracene from a stereospecific polycyclic aromatic dicarbonyl coupling. *J. Org. Chem.* **1990**, *55*, 4943–4950.

(9) Wolf, C. *Dynamic Stereochemistry of Chiral Compounds. Principles and Applications*; RSC publishing: Cambridge, UK, 2008.

(10) Shindo, M.; Koga, K.; Tomioka, K. A catalytic method for asymmetric nucleophilic aromatic substitution giving binaphthyls. *J. Am. Chem. Soc.* **1992**, *114*, 8732–8733.

(11) Gustafson, J. L.; Lim, D.; Miller, S. J. Dynamic Kinetic Resolution of Biaryl Atropisomers via Peptide-Catalyzed Asymmetric Bromination. *Science* **2010**, *328*, 1251–1255.

(12) Trapp, O. Unified Equation for Access to Rate Constants of First-Order Reactions in Dynamic and On-Column Reaction Chromatography. *Anal. Chem.* **2006**, *78*, 189–198.

(13) Maier, F.; Trapp, O. Effects of the Stationary Phase and the Solvent on the Stereodynamics of biphep Ligands Quantified by Dynamic Three-Column HPLC. *Angew. Chem., Int. Ed.* **2012**, *51*, 2985–2988.

(14) Trapp, O. Fast and precise access to enantiomerization rate constants in dynamic chromatography. *Chirality* **2006**, *18*, 489–497.

(15) Trapp, O.; Sahraoui, L.; Hofstadt, W.; Könen, W. The stereodynamics of 1,2-dipropyldiaziridines. *Chirality* **2009**, NA–NA.

(16) Trapp, O.; Schoetz, G.; Schurig, V. Determination of enantiomerization barriers by dynamic and stopped-flow chromatographic methods. *Chirality* **2001**, *13*, 403–414.

(17) Kalinowski, H. O.; Kessler, H. Topics in Stereochemistry. In *Topics in Stereochemistry*; Eliel, E. L.; Allinger, N. L., Eds. Wiley: New York, 1973; Vol. 7, pp. 295–383.

(18) Choi, M. C. K.; Chan, S. S.; Matsumoto, K. Catalytic Asymmetric Synthesis of (S)-Acetophenone Cyanohydrin under High Pressure. *Tetrahedron Lett.* **1997**, *38*, 6669–6672.

(19) Hazen, R. M.; Boctor, N.; Brandes, J. A.; Cody, G. D.; Hemley, R. J.; Sharma, A.; Yoder, H. S., Jr High pressure and the origin of life. *J. Phys.: Condens. Matter.* **2002**, *14*, 11489–11494.

(20) Jannasch, H. W.; Wirsen, C. O.; Taylor, C. D. Deep-Sea Bacteria: Isolation in the Absence of Decompression. *Science* **1982**, *216*, 1315–1317.

(21) Michels, P. C.; Clark, D. S. Pressure-enhanced activity and stability of a hyperthermophilic protease from a deep-sea methanogen. *Appl. Environ. Microbiol.* **1997**, *63*, 3985–3991.

(22) Rietveld, I. B.; Barrio, M.; Tamarit, J.-L.; Do, B.; Céolin, R. Enantiomer Resolution by Pressure Increase: Inferences from Experimental and Topological Results for the Binary Enantiomer System (R)- and (S)-Mandelic Acid. *J. Phys. Chem. B* **2011**, *115*, 14698–14703.

(23) Sharma, A.; Scott, J. H.; Cody, G. D.; Fogel, M. L.; Hazen, R. M.; Hemley, R. J.; Huntress, W. T. Microbial Activity at Gigapascal Pressures. *Science* **2002**, *295*, 1514–1516.

(24) Inoue, Y.; Matsushima, E.; Wada, T. Pressure and Temperature Control of Product Chirality in Asymmetric Photochemistry. Enantiodifferentiating Photoisomerization of Cyclooctene Sensitized by Chiral Benzenepolycarboxylates. *J. Am. Chem. Soc.* **1998**, *120*, 10687–10696.

(25) Kaneda, M.; Nakamura, A.; Asaoka, S.; Ikeda, H.; Mori, T.; Wada, T.; Inoue, Y. Pressure control of enantiodifferentiating photoisomerization of cyclooctenes sensitized by chiral benzenepolycarboxylates. The origin of discontinuous pressure dependence of the optical yield. *Org. Biomol. Chem.* **2003**, *1*, 4435–4440.

(26) Ayitou, A. J. L.; J, S. Light-Induced Transfer of Molecular Chirality in Solution: Enantiospecific Photocyclization of Molecularly Chiral Acrylanilides. *J. Amer. Chem. Soc.* **2009**, *131*, 5036–5037.

(27) Ayitou, A. J.-L.; Sivaguru, J. Reactive spin state dependent enantiospecific photocyclization of axially chiral α-substituted acrylanilides. *Chem. Commun.* **2011**, *47*, 2568–2570.

(28) Ayitou, A. J.-L.; Jesuraj, J.; Barooah, N.; Ugrinov, A.; Sivaguru, J. Enantiospecific Photochemical Norrish/Yang Type II Reaction of Non-biaryl Atropchiral α-Oxoamides In Solution – Axial to Point Chirality Transfer. *J. Am. Chem. Soc.* **2009**, *131*, 11314–11315.

(29) Jesuraj, J. L.; Sivaguru, J. Photochemical type II reaction of atropchiral benzoylformamides to point chiral oxazolidin-4-ones. Axial chiral memory leading to enantiomeric resolution of photoproducts. *Chem. Commun.* **2010**, *46*, 4791–4793.

(30) Kumarasamy, E.; Jesuraj, J. L.; Omlid, J. N.; Ugrinov, A.; Sivaguru, J. Light-Induced Enantiospecific 4π- Ring Closure of Axially Chiral 2-Pyridones: Enthalpic and Entropic Effects Promoted by H-Bonding. *J. Am. Chem. Soc.* **2011**, *133*, 17106–17109.

(31) Kumarasamy, E. Enantiospecific 4π-Photocycloaddition of Atropisomeric Pyridones, North Dakota State University: Fargo.

(32) Lawrance, G. A.; Stranks, D. R. Volumes of activation for intramolecular racemization mechanisms. High-pressure racemization of bipyridyl, phenanthroline and oxalato complexes of chromium(III) in solution. *Inorg. Chem.* **1977**, *16*, 929–935.

(33) Trost, B. M.; Parquette, J. R.; Marquart, A. L. Effect of High Pressure on a Transition-Metal-Catalyzed Cycloaddition. *J. Am. Chem. Soc.* **1995**, *117*, 3284–3285.

(34) Matsumoto, K.; Kim, J. C.; Hayashi, N.; Jenner, G. High pressure mediated three component

Strecker synthesis of α-aminonitriles from ketones, aromatic amines and trimethylsilyl cyanide. *Tetrahedron Lett.* **2002**, *43*, 9167–9169.

(35) Kuster, C. J. T.; Scheeren, H. W. High-Pressure Promoted Cycloadditions for Application in Combinatorial Chemistry. In *High Pressure Chemistry*; Wiley-VCH Verlag GmbH, 2007; pp. 284–304.

CHAPTER 7. ENATIOSPECIFIC 6π-PHOTOCYCLICATION MEDIATED BY METAL IONS: LEWIS ACIDS VS. HEAVY ATOMS[††]

7.1. Introduction

Knowing and/or manipulating the interactions of metal ions with chemical species is of great importance. Depending on the physico-chemical properties of the metal ions, these interactions can involve covalence, cation-π, cation-lone pair etc… interactions. Over the years, chemists have cleverly exploited non-bonding interactions for example between metal ion and chemical compounds to design systems for molecular recognition and to tailor chemical reactivities.[1,2]

In light induced processes, metal ions have been used for manipulating the photophysics of organometallic compounds. Metals ions have also been exploited to alter the excited state photoreactivity of organic molecules.[3-14] In the previous chapters, we discussed the excited spin state dependent enantiospecific 6π-photocyclization of atropisomeric acrylanilides **72** leading to the corresponding 3,4-dihydro-2-quinolin-2-one photoproduct(s) *cis*-**73** and *trans*-**74** (Scheme 7.1). In chapters 3, 4 and 5, the 6π-photocyclization of α,β-substituted acrylanilide **72d** in solution generated enantiopure photoproduct *cis*-**73d** and *trans*-**74d** (Scheme 7.1) whereas α-substituted acrylanilide **72f** lacking a substitution at the β-position gave a racemic mixture of the corresponding photoproduct **73** = **74** (Scheme 7.1). In the continued effort to achieve high stereoselectivity during 6π-photocyclization of α-substituted acrylanilide **72f** in solution, the influence of alkali metal ions during light induced conrotatory 6π-ring closure of optically pure samples of **72f**, **72g** and **72i** was evaluated. The prelimirary findings of this study indicated that depending on the type of metal ions, there is a possibility to have different types of reaction mechanism with varying enantioselectivity in **73f,g,i** (and **74f,g,i**). As, the current study is still being explored by Clay and co-workers[15], this chapter will only detail the preliminary observation of 6π-photocyclization in the presence of alkali metal ions.

---

†† The material in this chapter was co-authored by Anoklase J.-L. Ayitou (AJA), Anthony Clay (AC), and Dr. J. Sivaguru (JS). AJA in consultation with JS synthesized all compounds and performed all experiments detailed in this chapter. AC helped with synthesizing the compounds described in this chapter and will be performing complementary and supplementary experiments. AJA and JS came up with the mechanistic rationale of the reactions as well as the conclusion described in this chapter.

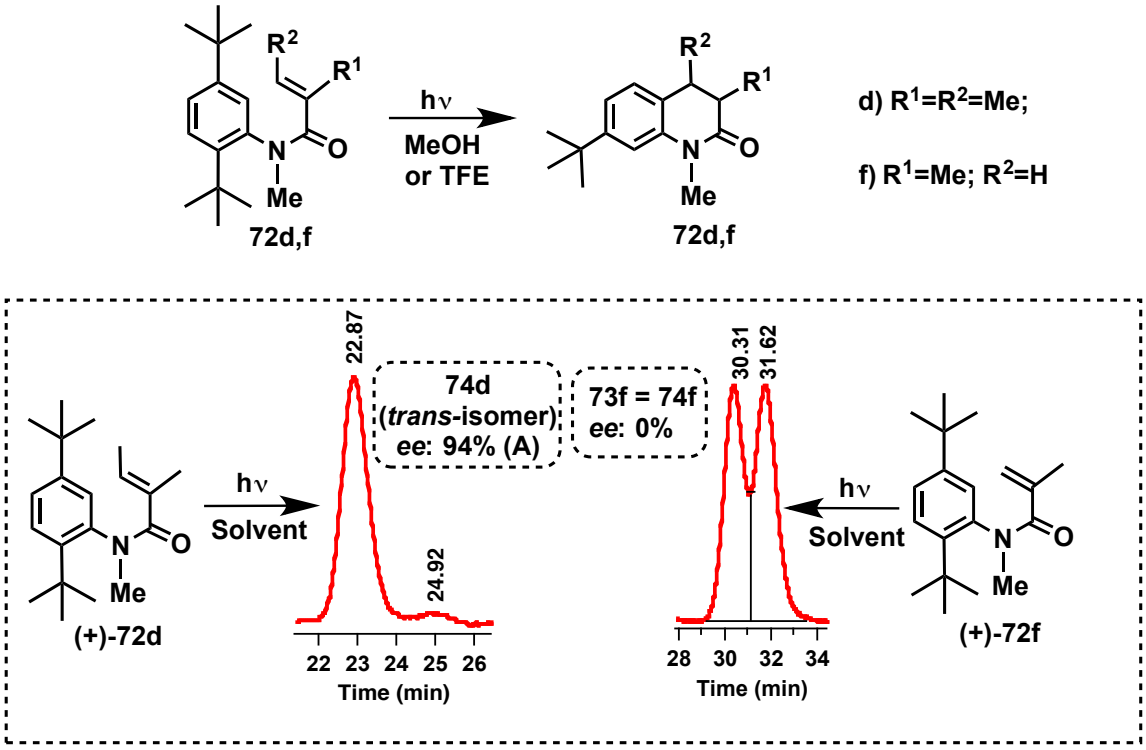

Scheme 7.1: 6π-photocyclization of acrylanilides **72.**

7.2. Procedure for Photoreaction of 72f,g,i in the Presence of Alkali Metal Additives

Optically pure isomers of **72f,g,i** were dissolved in trifluoroethanol (TFE) in the absence or in the presence of various alkali metal ions (NaF, KF, CsF and CsOH,) and irradiated in Pyrex test tubes using 450 W medium pressure Hg lamp. The expected 3,4-dihydro-2-quinolin-2-one photoproducts **73f,g,i** (and **74f,g,i**) were observed as the major product. Product(s) characterization (by NMR spectroscopy, polarimetry and HRMS) was reported in chapters 2 – 4. The *ee* values in **73f,g,i** (and **74f,g,i**) was ascertained by HPLC analysis of the reaction mixture on a chiral stationary phase.

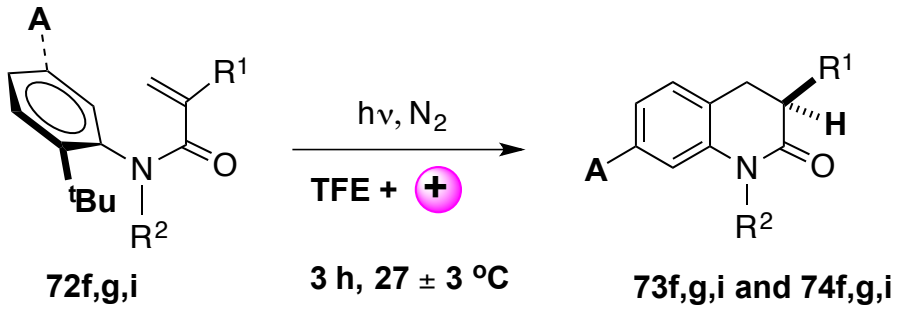

f: R^1 **= Me;** R^2 **= Me;** A **=** ^{t}**Bu;**
g: R^1 **= Et;** R^2 **= Me;** A **=** ^{t}**Bu;**
i: R^1 **= Me;** R^2 **= CP;** A **= H;**

+ = alkali metal cation

Scheme 7.2: 6π-photocyclization of acrylanilides **72f,g,i** in the presence of metal ions.

Table 7.1: Enantioselectivity in photoproducts **73f,g,i** (and **74f,g,i**) 6π-photocyclization of acrylanilides **72f,g,i** in the presence of metal ions under direct irradiation. [a,b]

Entry	Cmpd.	% *ee* values in the presence and absence of additives below [c]						
		No additives	CsF	CsOH	KF	KF/ 3 Å MS	NaF / 3 Å MS	3 Å MS
1.	**(-)-72f**	0	>90 (B)	-	>80 (B)		>90 (B)	>90 (B)
2.	**(+)-72f**	0	>90 (A)	-	>80 (A)		>80 (A)	>80 (A)
3.	**(-)-72g**	0	84 (B)	78 (B)	74 (B)	88 (B)	80 (B)	92 (B)
4.	**(+)-72g**	0	78 (A)	82 (A)	74 (A)	84 (A)	-	-
5.	**(-)-72i**	0	89 (A)	-	64 (A)	93 (A)	86 (A)	74 (A)
6.	**(+)-72i**	0	82 (B)	-	56 (B)	87 (B)	80 (B)	66 (B)

[a] (+) and (-) represent the signs of optical rotation in methylcyclohexane (MCH). [b] Solvent used for irradiation is trifluoroethanol (TFE). [c] A and B refer to the first and second peak that elutes out on the HPLC chiral stationary phase separation for a given pair of enantiomers. The conversion by ^{1}H NMR spectroscopy in all samples was kept between 10 – 20%. Though, the conversion in the presence of the cations we employed was less than 10% (7 – 10%) to ascertain the true ee values in the presence of cations as the photoproduct can also bind competitively in the presence of alkali metals.

7.3. Results and Discussion

The HPLC analysis results after photoreaction and isolation/purification of the photoproducts **73f,g,i** (and **74f,g,i**) were tabulated in table 7.1. Inspection of table 7.1 shows that direct irradiation of substituted acrylanilides **72f,g,i** in TFE gave racemic mixture of the photoproducts **73f,g,i** (and **74f,g,i**). On the other hand, in the presence of both low molecular weight (light) and heavy molecular weight (heavy) alkali metal cations, high *ee* values (ee >95%) was observed in the photoproduct (Figure 7.1).

7.5.1 Photophysical experiments

To understand the effect of alkali metal cations, it was necessary to explore the photophysics (fluorescence and phosphorescence emission measurements) of the systems of interest in the presence of additives of alkali metal cations. Photophysical measurements involving acrylanilide **72l** at room temperature and at 77 K as a transparent glass respectively both in the presence and absence of alkali metal ions and a halogen atom (heavy element) (Figure 7.2) was done. Preliminary fluorescence

emission and lifetime measurements for **72f** both in the presence and absence of alkali metal ions showed not significant change upon addition of metal cationic additives (Figure 7.1). Fluorescence lifetime measurements at room temperature showed two distinct decays with comparable contributions (Figure 7.2 and Table 7.2). Presumably, the contributing decay lifetimes were due to the N-CO *E* and *Z* rotamers of **72f**. The *E* and *Z* rotamers were also readily characterized by ^{1}H NMR spectroscopy; the contribution of the *E* and *Z* rotamers did not change appreciably upon addition of alkali metal cations (Figure 7.4). In addition, the phosphorescence lifetime measurements for **72f** showed a lifetime ~1.6 s in methylcyclohexane (MCH) glass matrix at 77 K which is indicative of a π-π^* excited state (*cf.* chapter 4 section 4.4). Moreover, for **72l** in the presence of bromine as heavy atom (Br from 1,2-dibromoethane), there was a noticeable decrease in fluorescence emission intensity whereas the phosphorescence emission intensity in MCH glass matrix at 77k was increased (Figure 7.3) indicating that the system has well behaved in term of *heavy atom effect*: in the presence of heavy cations/atoms, there is an enhanced intersystem crossing (ISC) from the singlet excited state to the triplet excited state for the systems under study.

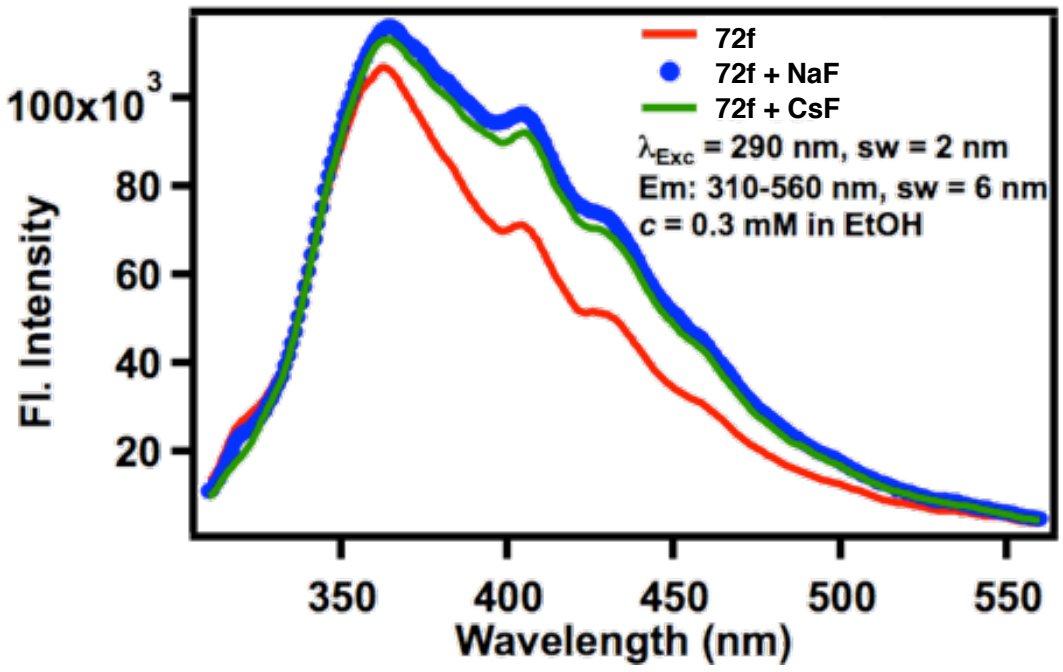

Figure 7.1: Fluorescence emission profile of **72f** in ethanol at room temperature: No major change of the emission upon addition of metal cationic additives.

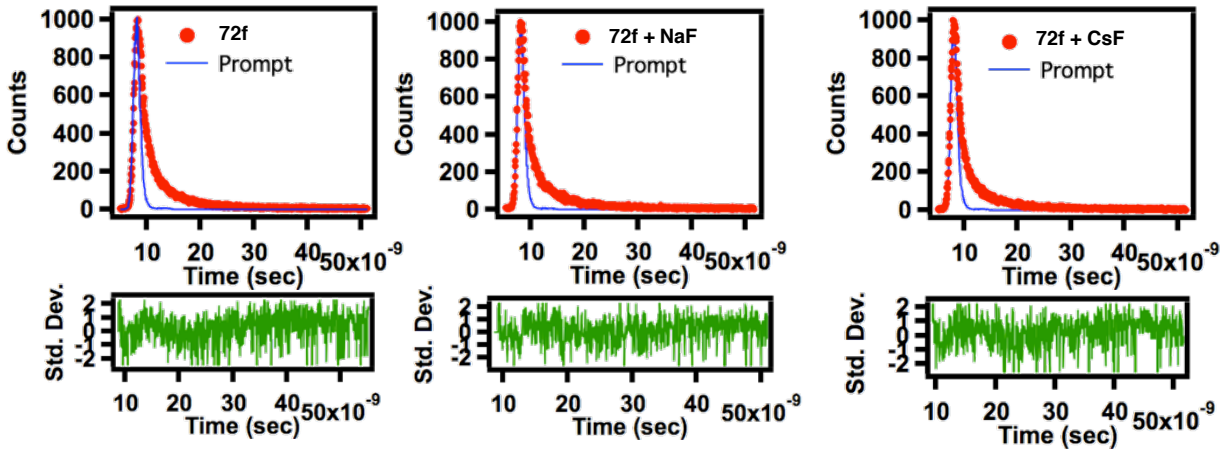

Figure 7.2: Fluorescence decay monitored at 330 nm (sw = 6 nm).
Excitation source: NanoLED 290 nm, sw = 6 nm, 1 MHz repetition rate

Delay = 80 nsec and Time range of 200 nsec

Table 7.2: Fluorescence lifetime fitting results.[a]

Cmpd. + Cation[b]	Decay monitored at 330 nm	
	τ_1 (nsec) [%]	τ_2 (nsec) [%]
72f	1.5 [46]	6.9 [54]
72f + NaF	1.7 [45]	8.4 [55]
72f + CsF	1.6 [41]	7.8 [59]

[a] The decay was monitored at 330 nm (sw = 6 nm) using NanoLED 290 nm, sw = 6 nm, 1 MHz repetition rate as excitation source: Delay = 80 nsec and Time range of 200 nsec. [b] [**72f**] = 0.3 mM in ethanol.

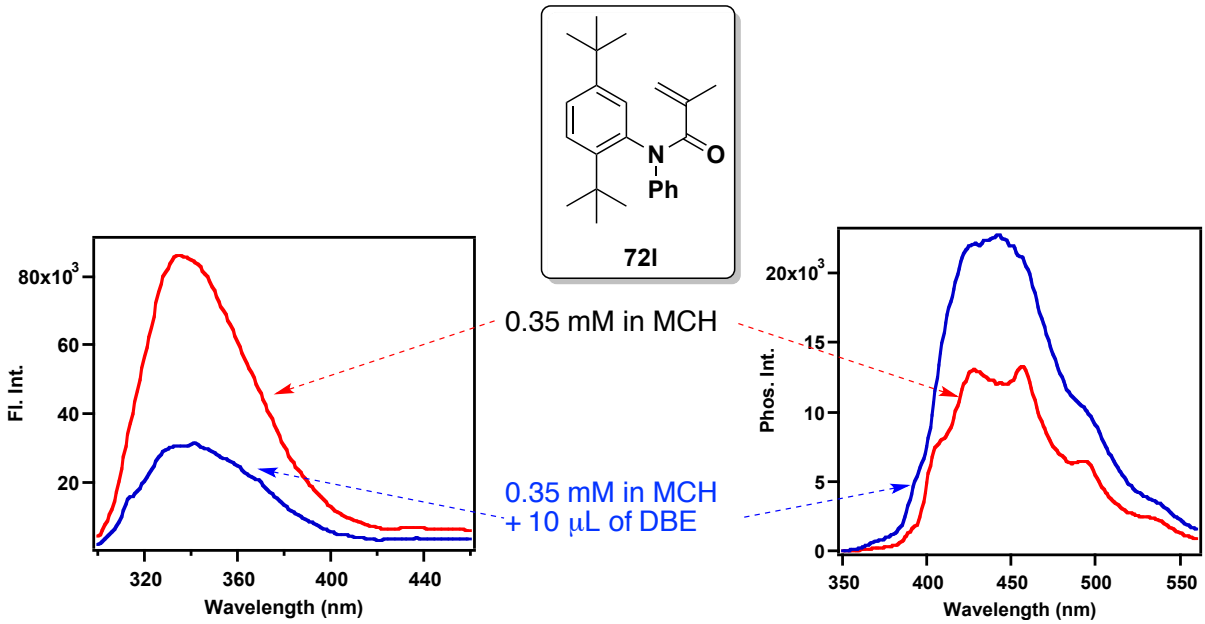

Figure 7.3: Fluorescence and phosphorescence emission spectra for **72l** in the presence of 1,2-dibromoethane (DBE).

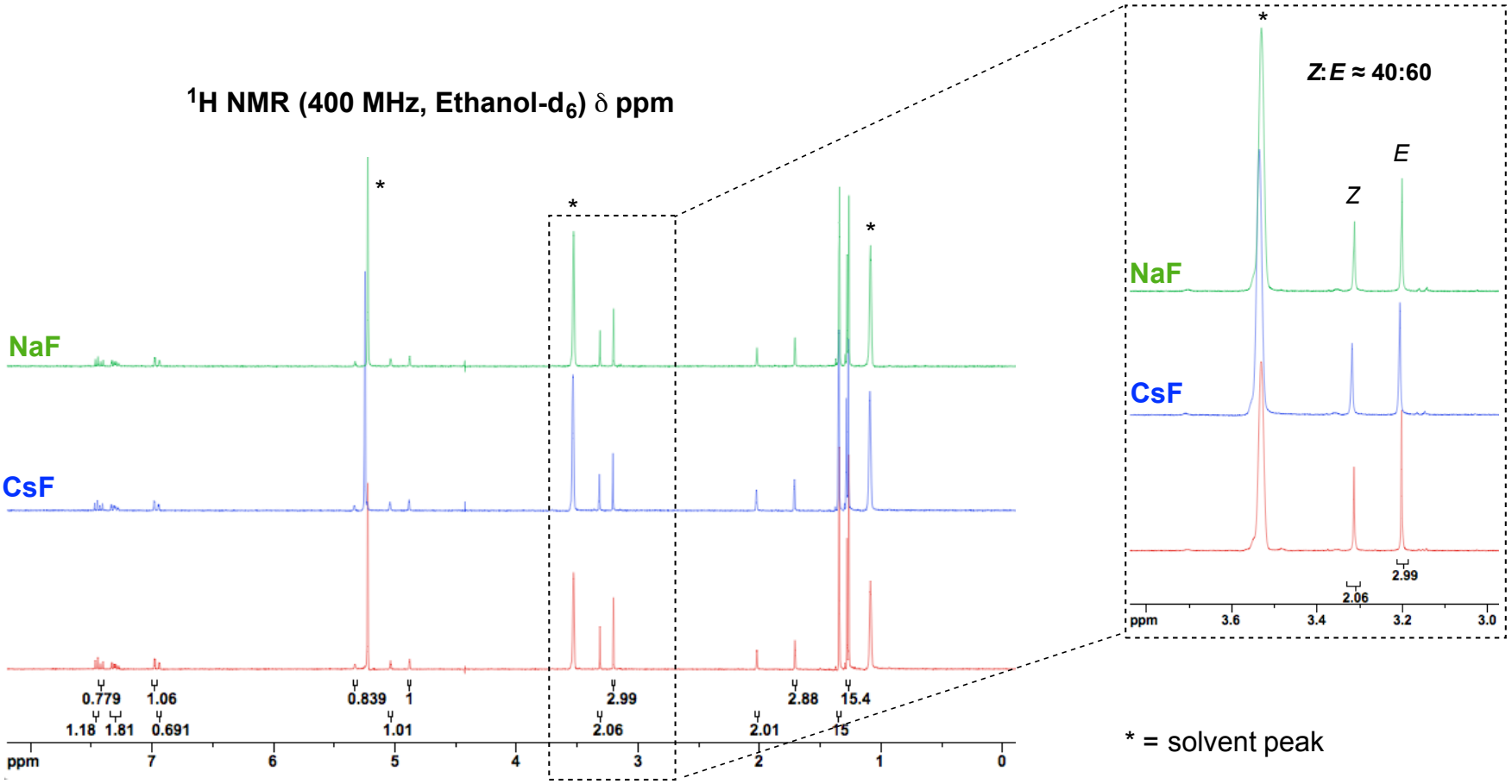

Figure 7.4: ^{1}H NMR (400 MHz, ethanol-d$_6$, δ ppm) spectra for acrylanilide **72f** in the presence and absence of Cs^+ and Na^+ additives showing no change in the ratio *Z*:*E* (inset).

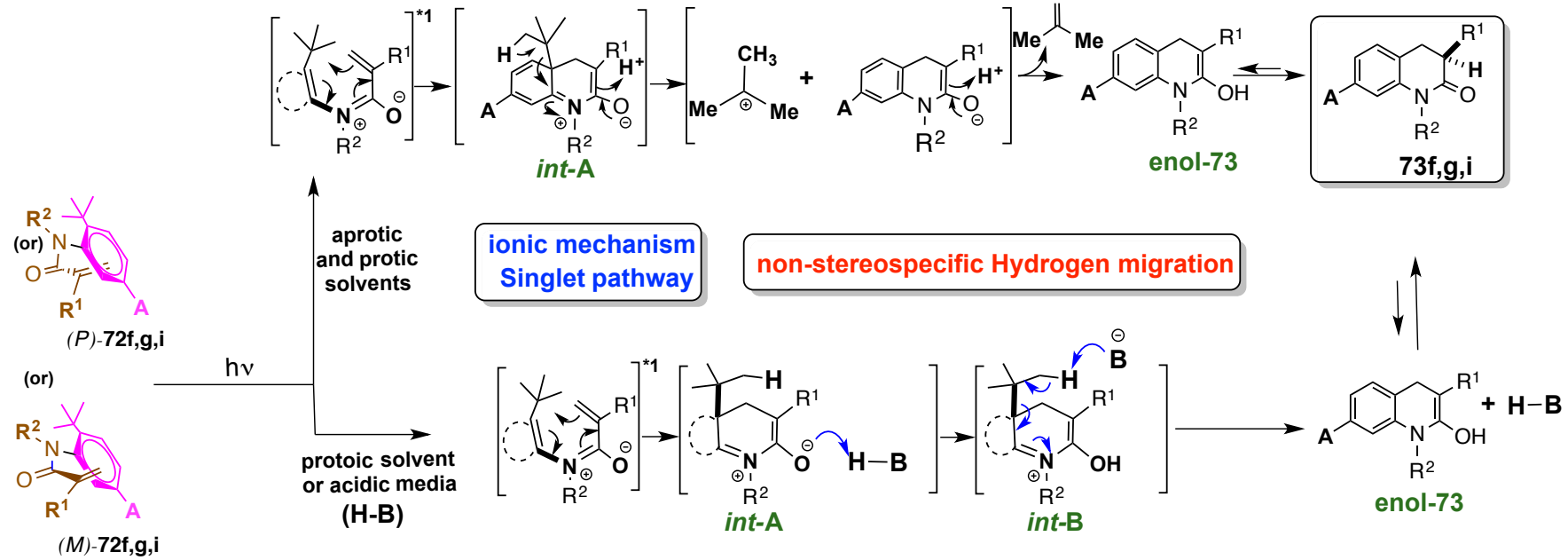

f: R^1 **= Me;** R^2 **= Me;** A = ^{t}**Bu;**
g: R^1 **= Et;** R^2 **= Me;** A = ^{t}**Bu;**
i: R^1 **= Me;** R^2 **= CP;** A **= H;**

Scheme 7.3: 6π-Photocyclization of **72f,g,i** in the absence of metal ions depicting singlet pathway.

In the previous chapters, a 'con' rotatory 6π-ring closure of the systems under study leading to a zwitterionic intermediate "*int*-**A**" (Scheme 7.3) was proposed. Depending on the type of solvent and availability of proton source, this zwitterionic intermediate "*int*-A" undergoes H-migration followed by re-aromatization leading to 3,4-dihydro-2-quinolin-2-one **73f,g,i**, with the eventual loss of the *o*-*tert*-butyl substituent as isobutene. The racemic nature of photoproducts **73f,g,i** upon direct irradiation in solution points to a non-stereospecific H-migration from the zwitterionic intermediate likely via "enol-**73**" that tautomerize to the photoproduct **73f,g,i**. Based on the results upon direct irradation in the presence of alkali metal ions, two distinct mechanisms can be envisionned. In the presence of alkali metal cations of low atomic number (or low atomic weight), the reactivity was likely dictated by the Lewis acidity of the cations, while in the presence of heavy metal cations, As the photocyclization occurs from the singlet π-π* excited state [S_1(π-π*)] upon direct irradiation, the formation of a zwitterionic intermediate (*int*-**A**) is expected. In the presence of a light alkali metal ion, the photocyclization by direct irradiation will lead to the alkali metal ion bound enolate-**73** (Scheme 7.4).

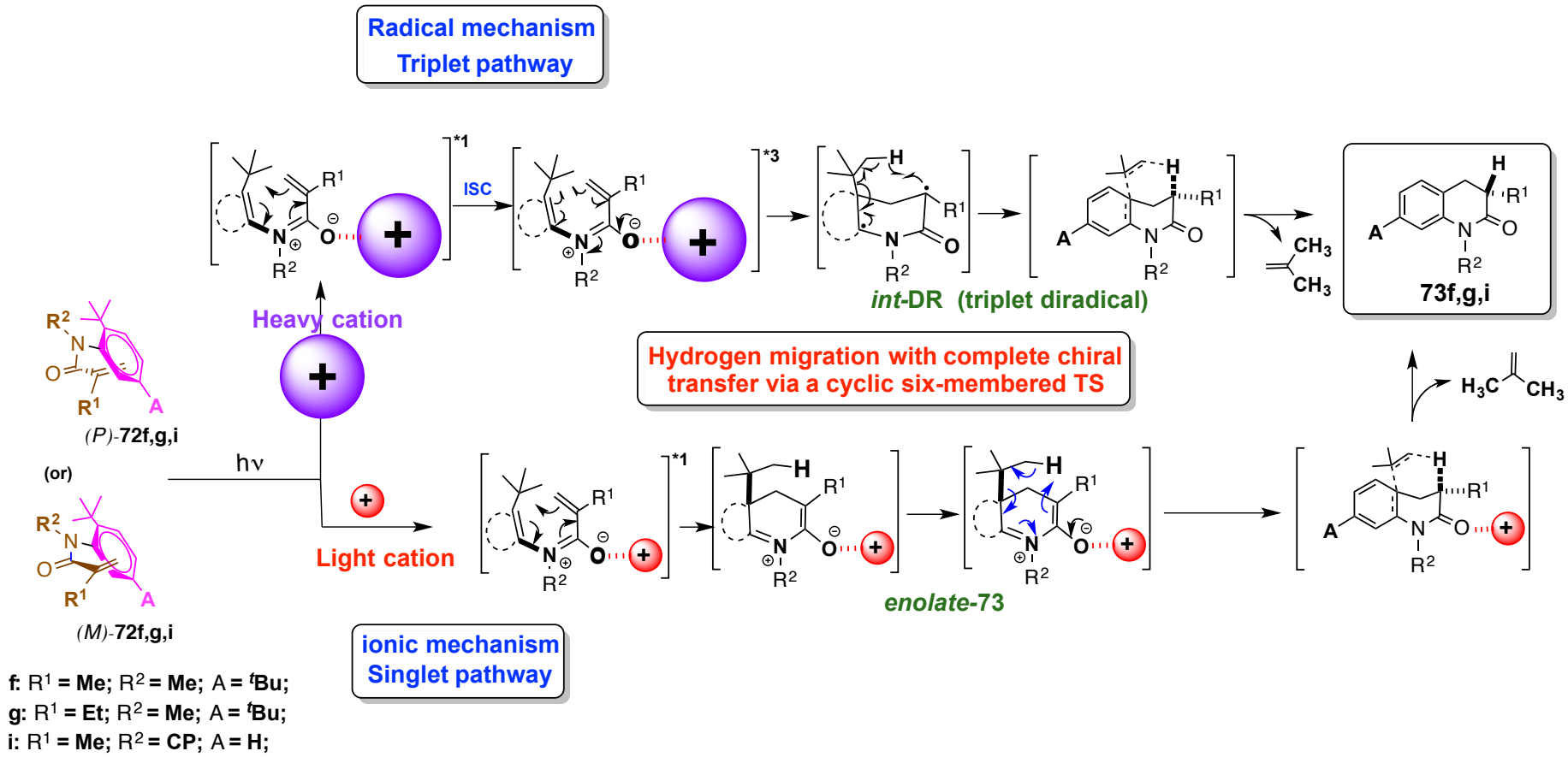

Scheme 7.4: 6π-Photocyclization of **72f,g,i** in the presence of metal ions depicting singlet and triplet mechanisms.

As illustrated in table 7.1, the expected photoproduct(s) were obtained with high enantioselectivity during transformations involving metal ions. The H-migration from alkali metal ion bound enolate-**73** is highly stereospecific. This presumably points to the Lewis acidity of the alkali metal ions. To verify this hypothesis, it may be necessary to carry out control studied with BF_3•OEt_2 (BF_3 being one the best Lewis acids). Unfortunately, due to time constrain, this investigation was not performed; however, a colleague student is currently working on complementary experiments that will give a comprehensive rationale of the current findings.[15] During the study, it was noticed that the presence of water influence the extent of selectivity in the photoproduct as water can bind strongly to Lewis acids there by preventing the formation of the cation bound enolate-**73**. The best option to carry out the reaction with dry solvent/samples was to use molecular sieves. Photochemical reactions with **72f,g,i** in the presence of 3 Å molecular sieves (3 Å MS) without having added any other metal ion was done. Suprisingly, there was a moderate enantioselectivity in the photoproduct **73f,g,i**. The conclusion form this observation was that the cations (Na+/K+) present on the surface of the 3 Å MS may be responsible for the observed selectivity as they can bind effectively to the enolate. More detailed findings will be provided upon completion of complementary investigations.

In the presence of heavy metal ions, photocyclization involving **72f,g,i** presumably occurs via a radical mechanism (Scheme 7.4). This conjecture is based on the π-π*excited state of **72** responsible for photocyclization. As the singlet-triplet gap in a π-π* excited state is large, the presence of heavy metal ions likely facilitates the inter-system crossing leading to triplet π-π* [T_1(π-π*)] excited state. Based on photochemical reactivity paradigm[16], 'con' rotatory 6π-ring closure from the T_1(π-π*) excited state will lead to triplet diradical intermediate ''*int*-**DR**'' (Scheme 7.4; bottom) that subsequently abstracts a hydrogen atom from the *ortho*-*tert*-butyl substituent leading to 3,4-dihydroquinolin-2-one photoproduct **73f,g,i**. The enantioselectivity (Table 7.1) in the photoproduct **73f,g,i** points out to a stereospecific hydrogen abstraction via a cyclic six membered transition (Scheme 7.4; bottom) state from the triplet diradical intermediate (*int*-**DR**).

7.4. Preliminary Conclusion

The preliminary results from this study point out to a combination of mechanisms during the photocyclization process in the presence of alkali metal ions. With low-molecular weight alkali metal ions, the stereospecificity is dictated by the Lewis acid character and with heavy-molecular weight alkali metal ions the reaction occurs via a radical mechanism presumably due to the intersystem crossing route facilitated by *heavy atom effect*. For alkali metals ions with intermediate molecular weight, it is presumed that a combination of mechanisms will rationalize the observed stereospecificity.

7.5. Experimental Section

All compounds except **72l** and **81b** have been reported and their characterizations are illustrated in the previous chapters.

7.5.1 Photophydical method

Spectrophotometric solvents (Sigma-Aldrich®) were used where ever necessary unless or otherwise mentioned. UV quality fluorimeter cells (with range until 190 nm) were purchased from Luzchem®. Emission spectra were recorded on a Horiba Scientific® Fluorolog 3 spectrometer (FL3-22) equipped with double-grating monochromators, dual lamp housing containing a 450-watt CW xenon lamp and a UV xenon flash lamp (FL-1040), Fluorohub/MCA/MCS electronics and R928 PMT detector. Emission and excitation spectra were corrected in all the cases for source intensity (lamp and grating) and emission spectral response (detector and grating) by standard instrument correction provided in the instrument software. Fluorescence (steady state) and phosphorescence (77 K) emission spectra were processed by FluorEssence® IgorPro® v.6 software.

7.5.2 Synthesis of aniline 81b and 72l

Compound **81b** was synthesized according to previously reported procedures.[17]

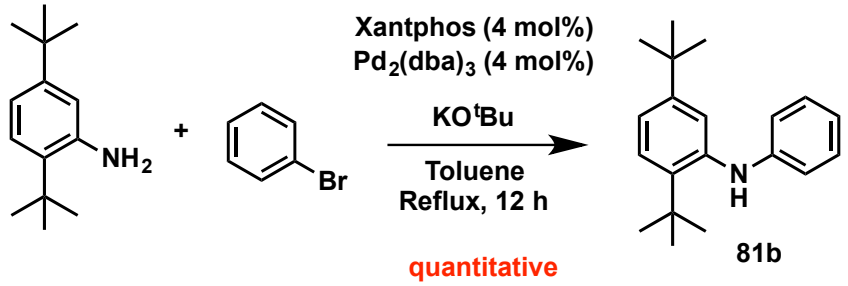

Scheme 7.5: Synthesis of *N*-phenyl aniline **81b**.

Commercially available 2,5-di-*tert*-butylaniline (1g, 1.2 equiv.) was dissolved in a minimum of toluene, followed by addition of bromobenzene (1 equiv.). Then, 4 mol% of Xantphos (113 mg) and $Pd_2(dba)_3$ (179 mg) were added to the aniline solution. KO^tBu (1.4 equiv.) was finally added to the reaction mixture. The new mixture was refluxed for 12 h. The expected *N*-phenyl aniline **81b** was isolated and purified by chromatography using Combiflash® with silica gel (40 g) and 5 % EtOAc:Hexanes as mobile phase and at a flow rate of 21 mL/min.

7.5.3 Characterization of N-phenyl aniline 81b

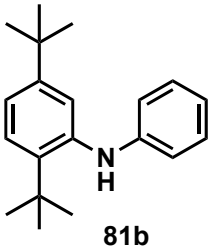

81b

^{1}H NMR (400 MHz, $CDCl_3$, δ ppm) 7.35 – 7.32 (Ar, 2H), 7.21 – 7.17 (Ar, 2H), 7.10 – 7.07 (Ar, 1H), 6.80 – 6.77 (Ar, 3H), 5.42 (bs, 1H), 1.40 (s, 9H), 1.27 (s, 9H)

^{13}C NMR (100 MHz, $CDCl_3$, δ ppm) 150.0, 146.4, 140.7, 140.4, 129.5, 129.0, 127.5, 127.4, 126.9, 123.9, 121.0, 118.9, 115.4, 34.7, 34.5, 31.4, 30.9

HRMS-ESI [(M+H$^+$)]: Calculated: 226.1590; Observed: 226.1596; Δm = 2.6 ppm

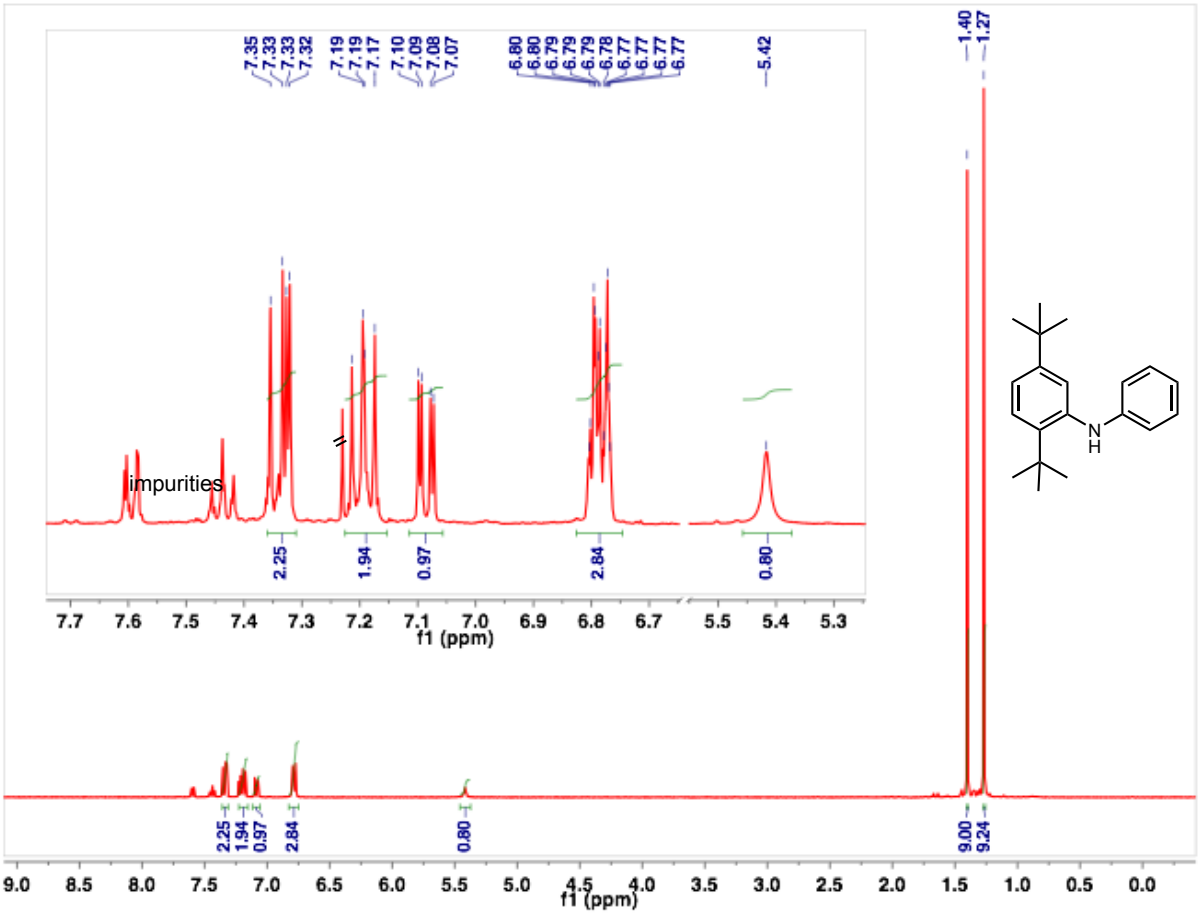

Figure 7.5: ^{1}H NMR (400 MHz, $CDCl_3$, δ ppm) spectrum for aniline **81b.**

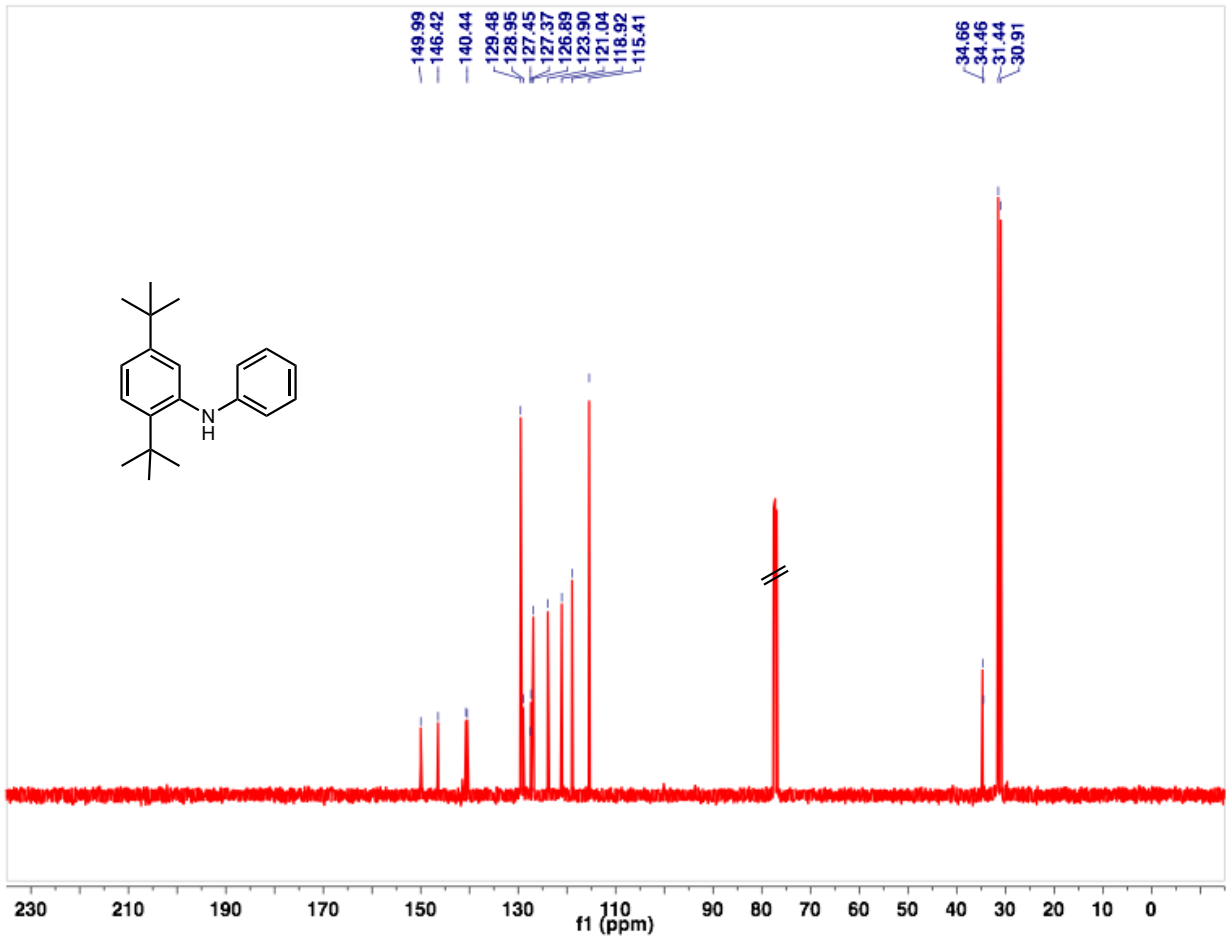

Figure 7.6: ^{13}C NMR (100 MHz, $CDCl_3$, δ ppm) spectrum for aniline **81b.**

7.5.4 Synthesis of acrylanilide 72l

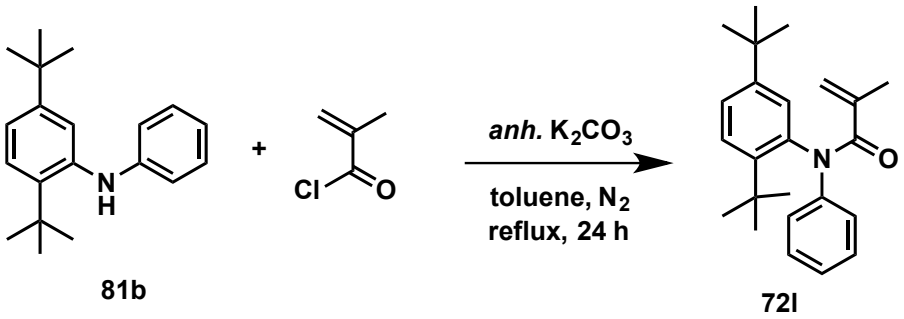

81b **72l**

Scheme 7.6: Synthesis of *N*-phenyl acrylanilide **72l**.

Compounds **72l** was synthesized according to reported procedures in the previous chapters (*cf.* chapater 2, 3 and 4). In a typical reaction, 1 equiv. of *N*-phenyl aniline **81b** was dissolved in a minimum of toluene followed by addition of 1.5 equiv. of *anhy.* K_2CO_3. The aniline solution was continuously stirred and kept under N_2 atm. Then, 1.2 equiv. of metacryloyl chloride was slowly added to the reaction mixture. The new mixture was allowed to reflux overnight. After reaction, the solution was quenched with DI water, and the expected compounds were extracted from the aqueous layer by 2 x 20 mL EtOAc. Compounds **3** was purified by chromatography using Combiflash® with silica gel (24 g) and 5 % EtOAc:Hexanes as mobile phase and at a flow rate of 19 mL/min.

7.5.5 Characterization of N-phenyl acrylanilide 72l

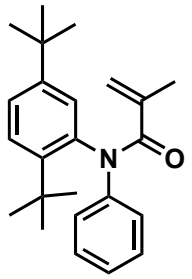

72l

^{1}H NMR (400 MHz, $CDCl_3$, δ ppm) 7.46 – 7.44 (Ar, 1H), 7.30 – 7.22 (Ar, 3H), 7.14 – 7.07 (Ar, 3H), 6.97 (virt d, 1H), 5.24 – 5.16 (br d, 2H), 1.89 (s, major conformer, 3H), 1.71 (s, minor conformer), 1.40 (s, minor conformer), 1.30 (s, minor conformer), 1.26 – 1.23 (br s, 18H)

^{13}C NMR (100 MHz, $CDCl_3$, δ ppm) 149.90, 128.61, 125.23, 125.19, 123.17, 122.77, 35.82, 34.31, 31.85, 31.42, 31.29, 30.74, 29.58, 25.38, 23.91

HRMS-ESI [($M+H^+$)]: Calculated: 372.2298; Observed: 372.2311; Δm = 3.5 ppm

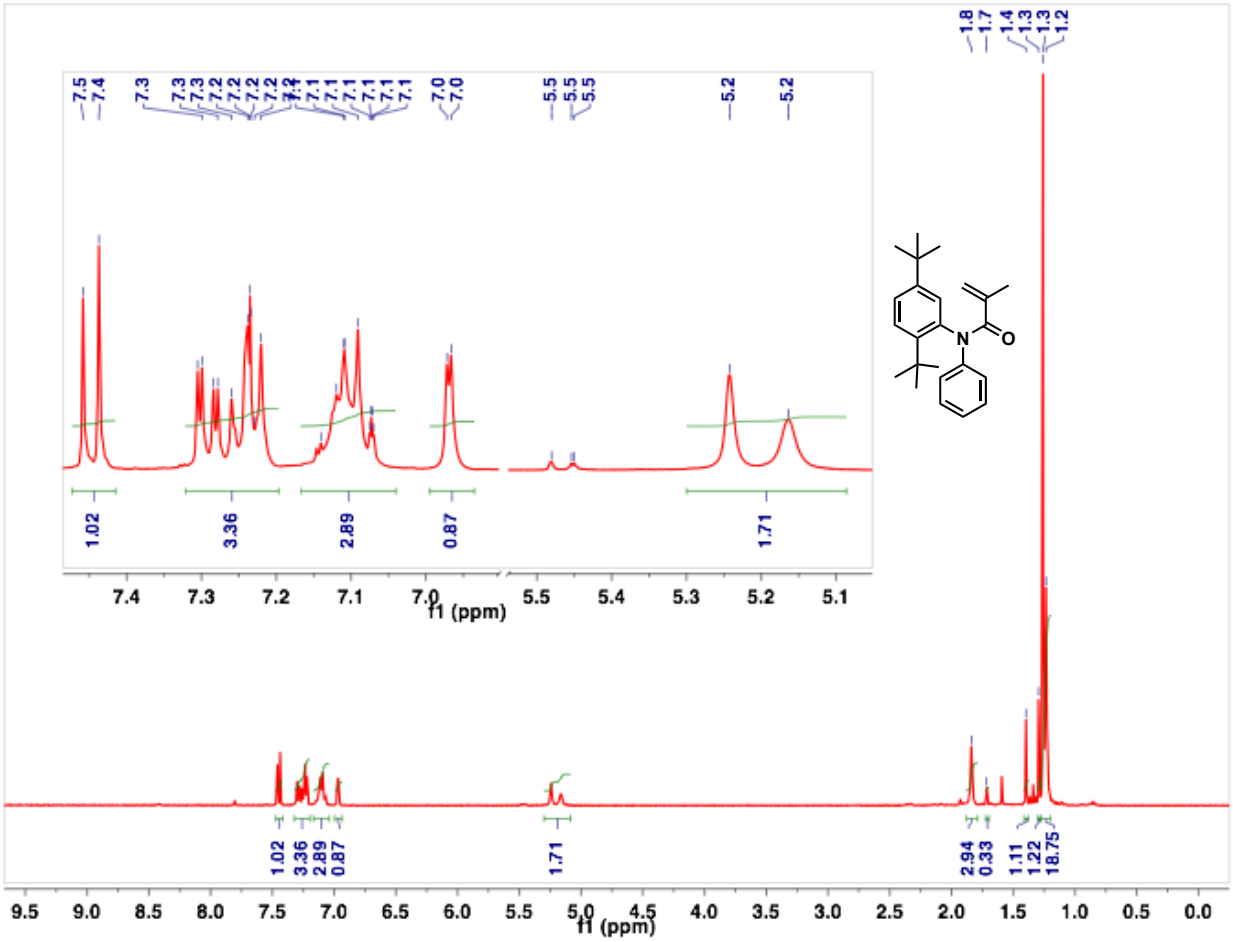

Figure 7.7: ^{1}H NMR (400 MHz, $CDCl_3$, δ ppm) spectrum for acrylanilide **72l.**

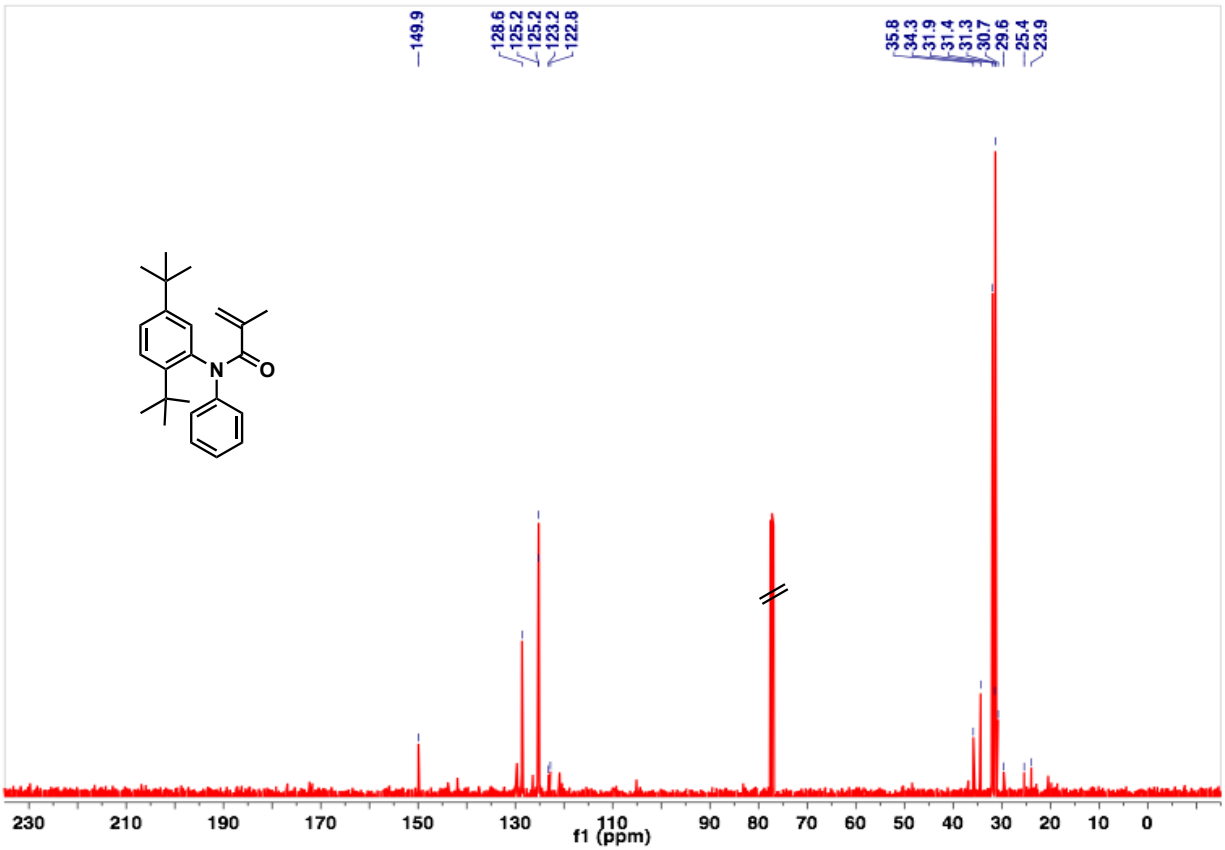

Figure 7.8: ^{13}C NMR (100 MHz, $CDCl_3$, δ ppm) spectrum for acrylanilide **72l.**

7.5.6 Photo-irradiation conditions

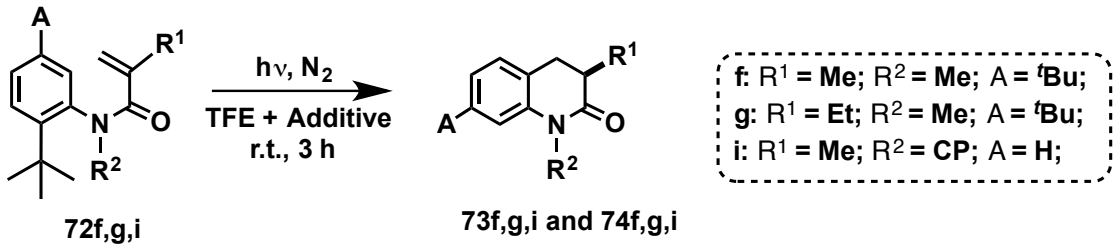

72f,g,i **73f,g,i and 74f,g,i**

Scheme 7.7: Irradiation of acrylanilides **72f,g,i** in the presence of alkali metal additives.

Optically pure samples of **72f,g,i** (2 mg/mL) were dissolved in spectrophotometric grade TFE (dried with 3Å molecular sieves) and saturated with additives NaF, KF, CsF or $CsOH•H_2O$. The samples were then deaerated for 15 min by bubbling N_2 through the solution and irradiated (450 W medium pressure Hg lamp) for 3 h in Pyrex test-tubes. After, the solvent was removed by roto-evaporation under reduced pressure. Excess of the additives was removed by washing the irradiated

samples with a few drops of DI water. The expected crude photolysates were extracted with chloroform; the samples were further concentrated and analyzed by HPLC on a chiral stationary phase.

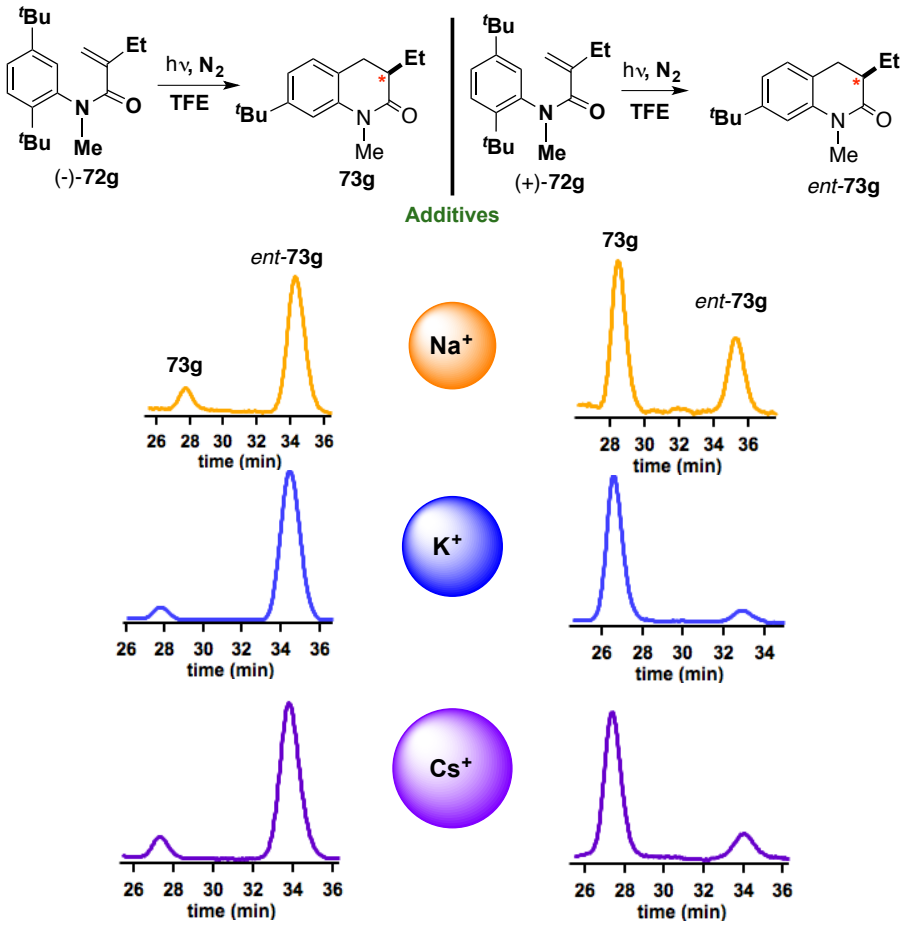

Figure 7.9: HPLC traces and enantioselectivity for photoproducts **73g** and the corresponding enantiomer *ent*-**73g**.

7.6. References

(1) Anslyn, E. V. 1.; Dougherty, D. A. 1. *Modern physical organic chemistry*; Sausalito, CA : University Science, 2006.

(2) Ma, J. C.; Dougherty, D. A. The Cation−π Interaction. *Chem. Rev.* **1997**, *97*, 1303–1324.

(3) Ramamurthy, V.; Caspar, J. V.; Corbin, D. R.; Eaton, D. F. Modification of photochemical reactivity by zeolites: location of guests within faujasites by heavy-atom-induced phosphorescence. *J. Photochem. Photobiol., A* **1989**, *50*, 157–161.

(4) Ramamurthy, V. Photochemical and photophysical studies within zeolites. *Chimia (Aarau)* **1992**, *46*, 358–376.

(5) Ramamurthy, V.; Caspar, J. V. Photophysical studies of organic molecules included within zeolites. *Mol. Cryst. Liq. Cryst. Sci. Technol., Sect. A* **1992**, *211*, 211–226.

(6) Ramamurthy, V.; Caspar, J. V.; Eaton, D. F.; Kuo, E. W.; Corbin, D. R. Heavy-atom-induced phosphorescence of aromatics and olefins included within zeolites. *J. Am. Chem. Soc.* **1992**, *114*, 3882–3892.

(7) Borecka, B.; Gudmundsdottir, A. D.; Olovsson, G.; Ramamurthy, V.; Scheffer, J. R.; Trotter, J. An Ionic Heavy-Atom Effect in the Solid State Photochemistry of a Œ≤,Œ≥-Unsaturated Ketone. *J. Am. Chem. Soc.* **1994**, *116*, 10322–10323.

(8) Ramamurthy, V. Organic Guests within Zeolites: Xenon as a Photophysical Probe. *J. Am. Chem. Soc.* **1994**, *116*, 1345–1351.

(9) Clayden, J.; Warren, S. Stereocontrol in Organic Synthesis Using the Diphenylphosphoryl Group. *Angew. Chem. Int. Ed. Engl.* **1996**, *35*, 241–270.

(10) Pitchumani, K.; Warrier, M.; Ramamurthy, V.; Scheffer, J. R. Novel approaches towards the generation of excited triplets of organic guest molecules with zeolites. *Chem. Commun. (Cambridge)* **1998**, 1197–1198.

(11) Ramamurthy, V. Controlling photochemical reactions via confinement: zeolites. *J. Photochem. Photobiol., C* **2000**, *1*, 145–166.

(12) Gu, W.; Warrier, M.; Schoon, B.; Ramamurthy, V.; Weiss, R. G. Understanding the Influence of Active (Zeolite) and Passive (Polyethylene) Reaction Cages on Photo-Claisen Rearrangements

of Aryl Benzyl Ethers. *Langmuir* **2000**, *16*, 6977–6981.

(13) Warrier, M.; Turro, N. J.; Ramamurthy, V. Heavy cation effect on intersystem crossing between triplet and singlet phenylacyl and benzyl geminate radical pairs within zeolites. *Tetrahedron Lett.* **2000**, *41*, 7163–7167.

(14) Pitchumani, K.; Warrier, M.; Kaanumalle, L. S.; Ramamurthy, V. Triplet photochemistry within zeolites through heavy atom effect, sensitization and light atom effect. *Tetrahedron* **2003**, *59*, 5763–5772.

(15) Clay, A. Stereospecific 6π-Photocyclization of Axially Chiral Acrylanilides with Labile Chiral Bias Groups, North Dakota State University: Fargo.

(16) Turro, N. J. 1.; Ramamurthy, V.; Scaiano, J. C. J. C. 1. *Modern molecular photochemistry of organic molecules*; Sausalito, CA: University Science Books, 2010.

(17) Wolfe, J. P.; Tomori, H.; Sadighi, J. P.; Yin, J.; Buchwald, S. L. Simple, Efficient Catalyst System for the Palladium-Catalyzed Amination of Aryl Chlorides, Bromides, and Triflates. *J. Org. Chem.* **2000**, *65*, 1158–1174.

CHAPTER 8. OTHER PHOTO-TRANSFORMATIONS INVOLVING AXIALLY CHIRAL CHROMOPHORE: γ-H-ABSTRACTION WITH α-OXOAMIDES[‡‡]

8.1. Introduction

Axial chirality stemming from chromophoric molecular reactants has been proven to be effective for asymmetric photochemical transformations as detailed in the previous chapters with 6π-photocyclization, as a model system, involving atropisomeric acrylanilides **72.** In order to broaden the impact and usefulness of axial chirality to induce enantioselectivity in products derived from photochemical transformations, the photochemical Norrish cyclization of α-oxoamides **84a,b** was explored. Previous chapters detailed that *N*-alkyl substituted acrylanilides with bulky *ortho*-substituents in the phenyl ring (*o-tert*-butyl) are axially chiral due to the hindered N-C(Aryl) bond rotation. Based on the above observations and considering precedent reports from literature,[1,2] α-oxoamides **84a,b** with *o-tert*-butyl-substituent on the N-phenyl ring and tested if they would be axially chiral due to restricted N-C(Aryl) bond rotation. α-Oxoamides **84a,b** with *o-tert*-butyl-substitution in the *N*-phenyl were synthesized and found to be axially chiral (*P* and *M* isomers). The individual *P* and *M* isomers were easily isolable by HPLC on a chiral stationary phase and were characterized by NMR spectroscopy, CD spectroscopy, optical rotation, HRMS and single crystal XRD. Racemization kinetic studies showed that optically pure α-oxoamides **84a,b** were stable at room temperature and could be stored at 0 ^{o}C for months without racemization. The rotation barrier $\Delta G^{\ddagger}$ at +50 ^{o}C was found to be ~27 kcal/mol. Optically pure axially chiral **84a,b** were investigated for axial to point chirality transfer during γ-hydrogen abstraction[3-7] leading to expected photoproducts **85, 86** and **88** (Scheme 8.1).

The photoproducts are expected to be a mixture of enantiomers as the N-C(Aryl) bond is expected to rotate freely due to the reduced C-N-C bond angle.[8] Photo-irradiation of optically pure atropisomers of **84a,b** (Scheme 8.1) was preformed using a 450 W medium pressure Hg

---

‡‡ The material in this chapter was co-authored by Anoklase J.-L. Ayitou (AJA), Dr. Josepha Jesuraj (JJ), Dr. Niloptal Baroah (NB), Dr Angel Ugrinov (AU) and Dr. J. Sivaguru (JS). AJA in consultation with JS synthesized all compounds and performed all experiments with the help of JJ and NB. JJ performed experiments with compound **84b**, which complemented the initial works done by AJA with compound **84a**. AU recorded the x-ray crystallography data and solved structures for all compound. AJA and JS came up with the mechanistic rationale of the reaction as well as the conclusion described in this chapter.

lamp with Pyrex cutoff and a cooling jacket under constant flow of nitrogen at various temperatures (+40 to -40 ^{o}C).

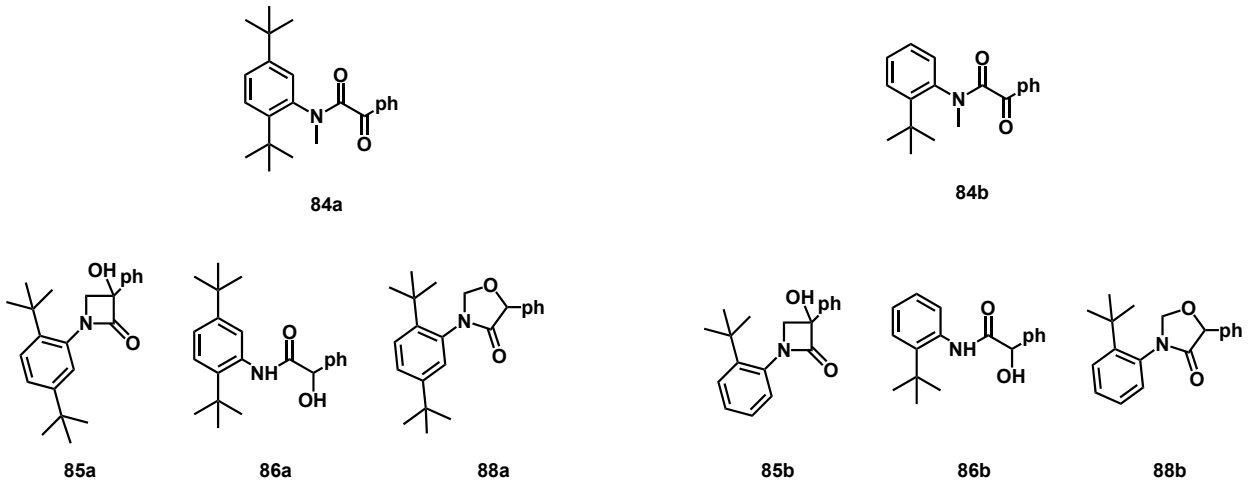

Chart 8.1: Axially chiral α-oxoamides and corresponding photoproduct(s).

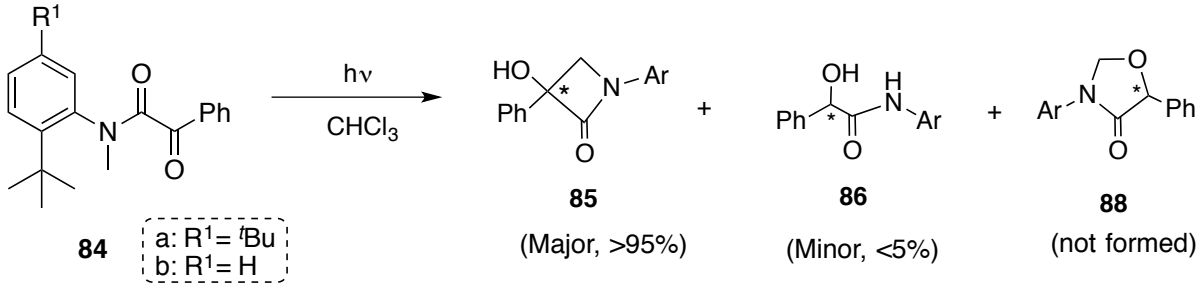

Scheme 8.1: γ-Hydrogen abstraction involving axially chiral **84a,b**.

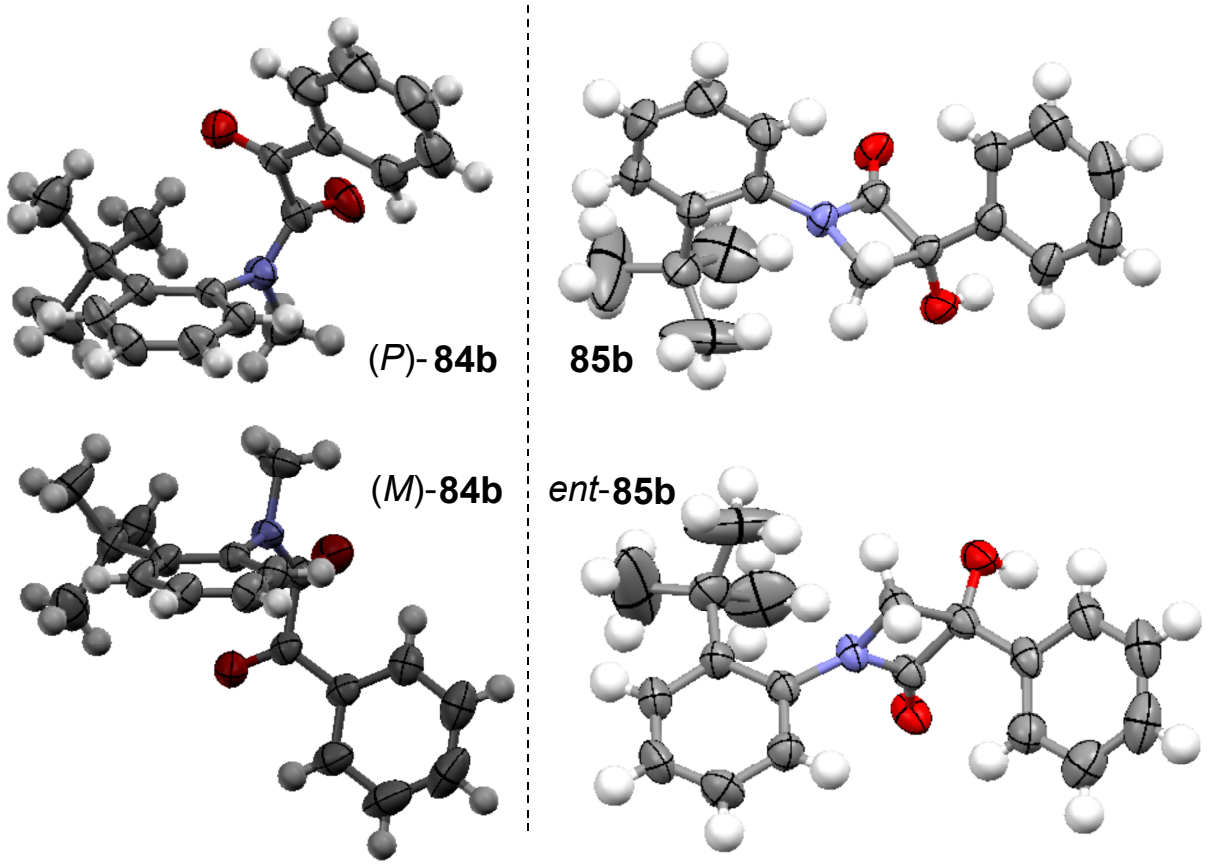

Figure 8.1: X-ray crystal structures for **84b** and corresponding β-lactam photoproduct **85b** and *ent*-**85b.**

Note: The CCDC deposition numbers for structures **84a,b** and **85b** are CCDC 734106 – 734108 respectively.

8.2. Results and Discussion

8.2.1. Racemization kinetics

Racemization of optically pure non-biaryl atropisomeric α-oxoamides was followed at 50 ^{o}C HPLC on a chiral stationary phase (Figure 8.2). The activation energy (Table 8.1) for racemization was computed from equations below.[9]

$$k = \kappa\left(\frac{k_B T}{h}\right) e^{-\Delta G^{\neq}/RT}$$

Equation 8.1

$$\Delta G^{\neq} = -RT \ln\left(\frac{hk}{\kappa h T k_B}\right)$$

Equation 8.2

Where k is the rate constant for racemization, k_B the Boltzmann's constant, h is the Planck's constant, R is the ideal gas constant, T is the temperature of the system under study and κ = 1.

Let us assume that R_0 is the initial concentration of the (*P*)-rotamer of **84a,b** S_0 is the initial concentration of the corresponding optical antipode: $x = R_0 - P,M$ (concentration of the racemate at time t); and k_{rac} is the rate constant of racemization (and $k_{rac} = 2k_{enant}$, k_{enant} is the rate constant of enantiomerization)

Then,

$$\ln\left(\frac{R_0}{R_0 - x}\right) = k_{rac} t$$

Equation 8.3

The half-life of racemization, $\tau_{1/2}$, can be calculated using the rate constant of racemization k_{rac} (assuming $S_0 = 0$ at $t = 0$).

$$\ln\left(\frac{x_{eq}}{x_{eq} - x}\right) = \ln\left(\frac{R_0}{2[P] - R_0}\right) = \ln\left(\frac{P+M}{P-M}\right) = k_{rac} t$$

Equation 8.4

Note: $R_0 = [P] + [M]$

At 50% ee, the equation becomes:

$$\tau_{1/2} = \frac{\ln 2}{k_{rac}}$$

Equation 8.5

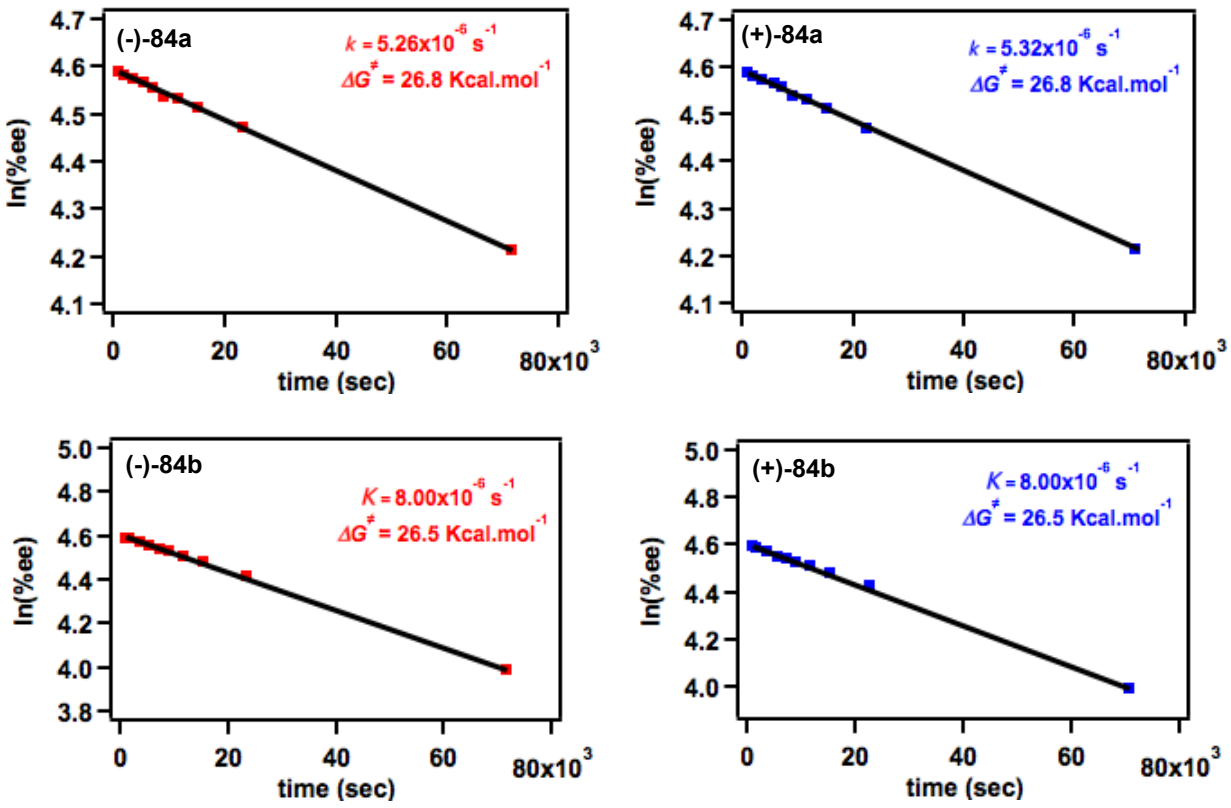

Figure 8.2: Racemization kinetics of optically pure non-biaryl atropisomeric α-oxoamides **84a,b**.

Table 8.1: Activation energy and half-life for racemization of optically pure non-biaryl atropisomeric α-oxoamides **84a,b**.

α-Oxoamides racemization (or enantiomerization) kinetics at 50 °C in iso-propanol				
Substrates	$\Delta G^{\ddagger}$(kcal•mol^{-1})	k_{rac} (sec^{-1})	k_{enant} (sec^{-1})	$\tau_{1/2}$ [day(s)]
(-)-**84a**	26.8	5.26x10^{-7}	2.63x10^{-7}	1.5
(+)-**84a**	26.8	5.32x10^{-7}	2.66x10^{-7}	1.5
(-)-**84b**	26.5	8.0x10^{-6}	4.0x10^{-6}	1
(+)-**84b**	26.5	8.0x10^{-6}	4.0x10^{-6}	1

8.2.2. Kinetics for photoreaction for α-oxoamides 84a,b

Photochemical reaction involving **84a,b** was found to be clean and efficient with >95 % conversion after 3 hours of irradiation at 30 ^{o}C (Figures 8.3 and 8.4).

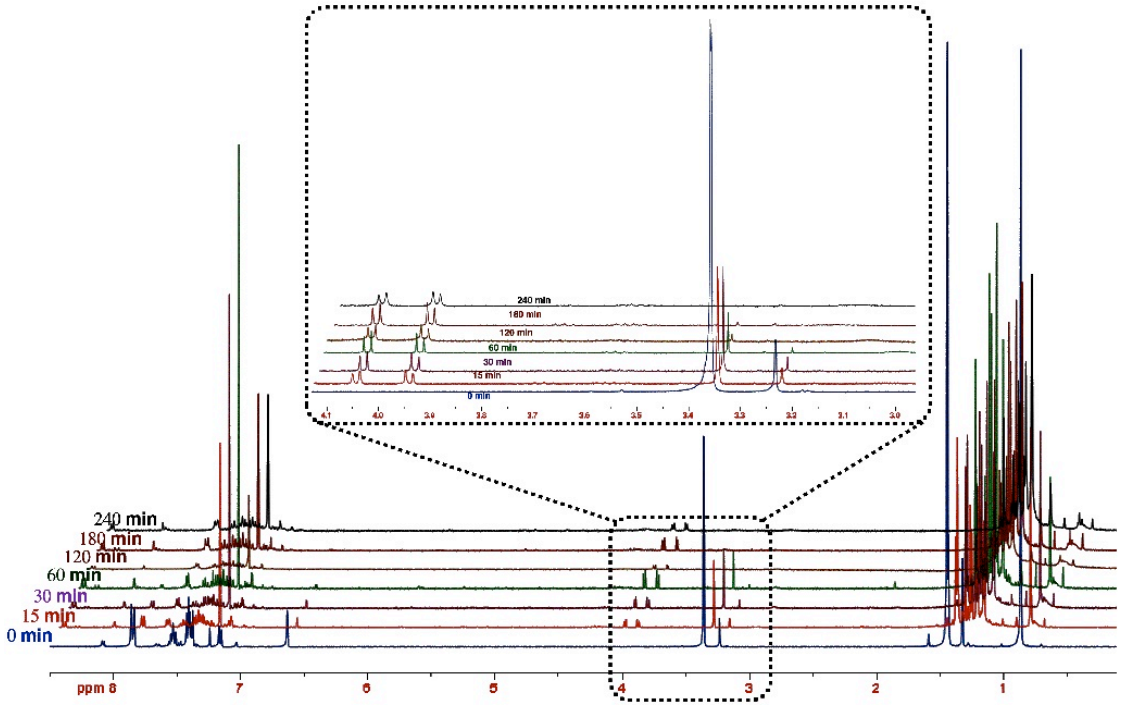

Figure 8.3: Time dependent irradiation followed by ^{1}H NMR (400 MHz, $CDCl_3$, δ ppm) spectroscopy in the case of oxoamides **84a.**

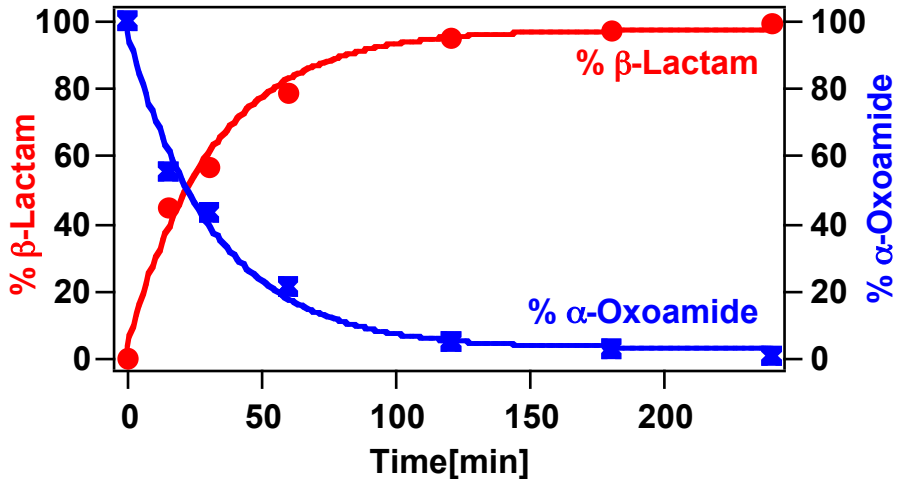

Figure 8.4: Plot highlighting the % formation of β-lactam **85a** (Red) and disappearance of the reactant α-oxoamide **84a** (Blue) upon various irradiation times at room temperature.

At low temperatures, the photoreaction of **84a,b** was slow and longer irradiation times were necessary to achieve higher conversions. After irradiation, the photoproducts were purified by chromatography and characterized by NMR spectroscopy, CD spectroscopy, optical rotation and single crystal XRD. HPLC analysis of the photoproducts on a chiral stationary phase gave the enantiomeric ratio (e.r.) in the β-lactam **85a,b** (Table 8.2). Optically pure **84a,b** gave enantiopure β-lactam **85a,b** as expected. Additionally, the e.r. values in **85a,b** were found to be dependent on the reaction temperature. For example, in the case of **84a**, e.r. values increased (with the same enantiomer) from ~74:26 to ~90:10 upon changing the temperature from +40 ^{o}C to -40 ^{o}C.

Table 8.2: Enantiomeric ratios and activation parameters ($\Delta\Delta H^{\ddagger}$ and $\Delta\Delta S^{\ddagger}$) for g-Hydrogen abstraction of **84a,b** in chloroform ($CHCl_3$). [a-c]

Entry	Time (min)	T (^{o}C)	(-)-**84a**	(+)-**84a**	(-)-**84b**	(+)-**84b**
1.	30	40	74 : 26 (A)	26 : 74 (B)	70 : 30 (A)	30 : 70 (B)
2.	30	30	76 : 24 (A)	23 : 77 (B)	72 : 28 (A)	27 : 73 (B)
3.	30	20	79 : 21 (A)	21 : 79 (B)	74 : 26 (A)	25 : 75 (B)
4.	30	10	82 : 18 (A)	18 : 82 (B)	78 : 22 (A)	22 : 78 (B)
5.	60	0	85 : 15 (A)	15 : 85 (B)	81 : 19 (A)	20 : 80 (B)
6.	120	- 20	89 : 11 (A)	11 : 89 (B)	84 : 16 (A)	15 : 85 (B)
7.	360	- 40	90 : 10 (A)	11 : 89 (B)	86 : 14 (A)	14 : 86 (B)
8.	$\Delta\Delta H^{\ddagger}$ (Kcal/mol)		-2.11	2.14	-1.80	1.60
9.	$\Delta\Delta S^{\ddagger}$ (cal/mol/K)		-4.50	4.65	-3.93	3.26

[a] Values are an average of 3 runs (±2% error). [b] A and B refers to the first and second peak that elutes in the HPLC on a chiral stationary phase. [c] $\Delta\Delta H^{\ddagger}$, $\Delta\Delta S^{\ddagger}$ were computed from Eyring plots (Eq. 8.6 and 8.7).

Eyring plots to compute differential activation parameters for the photochemical γ-H abstraction of α-oxoamides **84a,b**.

$\frac{k_R}{k_S} = \frac{[R]}{[S]}$, and $\%ee = \frac{[R]-[S]}{[R]+[S]} \times 100$, this implies: $\%ee = \frac{\frac{k_R}{k_S}[S]-[S]}{\frac{k_R}{k_S}[S]+[S]} \times 100 = \%ee = \frac{\frac{k_R}{k_S}-1}{\frac{k_R}{k_S}+1} \times 100$

$$\%ee\left(\frac{k_R}{k_S}+1\right) = \left(\frac{k_R}{k_S}-1\right) \times 100$$

$\%ee\left(\frac{k_R}{k_S}\right) + \%ee = 100\left(\frac{k_R}{k_S}\right) - 100$; this gives $\left(\frac{k_R}{k_S}\right)(100 - \%ee) = (100 + \%ee)$

Hence,

$$\ln\left(\frac{k_R}{k_S}\right) = \ln\left(\frac{100+\%ee}{100-\%ee}\right) \qquad \textbf{Equation 8.6}$$

Also,

$$\ln\left(\frac{k_R}{k_S}\right) = \ln(k_R) - \ln(k_S) = \frac{-\Delta G^{\neq}_R}{RT} - \frac{-\Delta G^{\neq}_S}{RT}$$

as $\Delta G^{\neq} = \Delta H^{\neq} - T\Delta S^{\neq}$

Hence,

$$\ln\left(\frac{k_R}{k_S}\right) = \frac{\Delta\Delta S^{\neq}_{R-S}}{R} - \frac{\Delta\Delta H^{\neq}_{R-S}}{RT} \qquad \textbf{Equation 8.7}$$

The differential activation parameters ($\Delta\Delta H^{\ddagger}$ and $\Delta\Delta S^{\ddagger}$) were computed using Eyring plots (Eq. 8.6 and 8.7 and Fig. 8.5). The enantioselectivity ($\Delta\Delta G^{\ddagger}$) depended on both $\Delta\Delta H^{\ddagger}$ and $\Delta\Delta S^{\ddagger}$. The magnitude and more importantly the signs of $\Delta\Delta H^{\ddagger}$ and $\Delta\Delta S^{\ddagger}$ helped explain the effect of temperature on e.r. ratios (Figure 8.5 has the values for $\Delta\Delta H^{\ddagger}$ and $\Delta\Delta S^{\ddagger}$). Since the ($\Delta\Delta H^{\ddagger}$/RT) term is proportional to the reciprocal temperature (Eq. 8.7), the $\ln(k_R/k_S)$, i.e., $\Delta\Delta G^{\ddagger}$ value is determined mostly by the enthalpic contribution at low temperatures; however, as the temperature increases, the relative contribution from the ($\Delta\Delta S^{\ddagger}$/R) term increases and contributes substantially to $\ln(k_R/k_S)$ value at higher temperatures. As

both $\Delta\Delta H^{\ddagger}$ and $\Delta\Delta S^{\ddagger}$ have the same sign, the decrease in temperature enhances the same isomer as the magnitude of $\Delta\Delta G^{\ddagger}$ increases (Eq. 8.7). Hence the enantioselectivity (e.r. values) should increase upon lowering the temperature as observed. The opposite signs with similar magnitude of $\Delta\Delta H^{\ddagger}$ and $\Delta\Delta S^{\ddagger}$ for a given pair of axially chiral (*P* and *M*) α-oxoamides **84a,b** are reflected in the optical antipodes of the enhanced β-lactam **85a,b**. The activation parameters and its influence on enantioselectivity in **85a,b** were indicative of conformational factors playing a pivotal role in the reaction pathway.

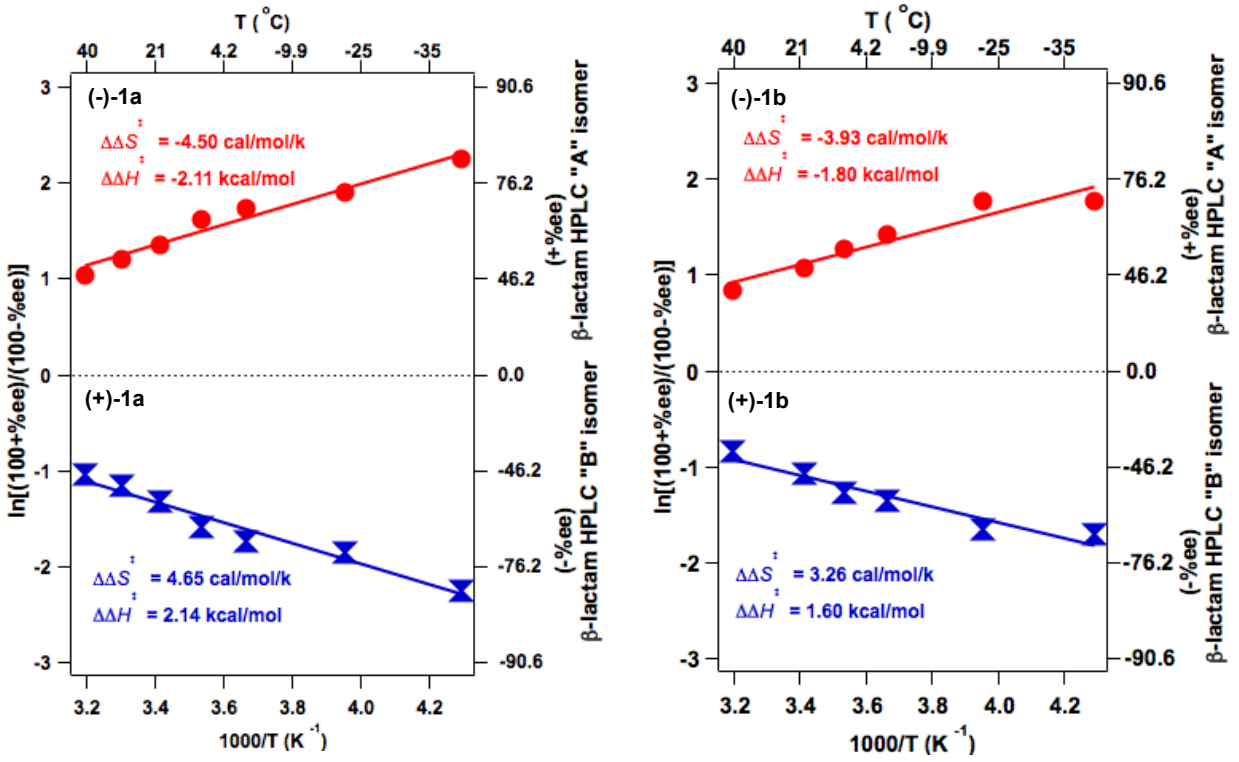

Figure 8.5: Differential activation parameters for the photochemical γ-hydrogen abstraction involving α-oxoamides **84a,b**.

8.2.3. Mechanistic rationale

NMR analysis of **84a,b** (pure *P* or *M*) showed that both *E* and *Z* N-CO rotamers exist in solution as seen in reported amides.[1,2,10] Analysis of the crystal structures of **84a,b** shows the two carbonyl groups to form an angle of 90°. The free N-CO rotation in solution presumably enables **84a,b** to undergo a smooth photochemical γ-hydrogen abstraction as defined by Scheffer and co-workers.[11] The mechanistic rationale of photoreaction in α-oxoamides involves a net hydrogen transfer to the photoexcited carbonyl

group either by direct hydrogen abstraction or in a sequential two-steps process *viz.* single electron transfer (SET) followed by proton transfer (Scheme 8.2).[5] Although γ-hydrogen abstraction may occur in aromatic ketones via the n-π* triplet state,[4] photochemical γ-hydrogen abstraction in α-oxoamides is presumed to be mediated by the electron transfer pathway even if the lowest triplet excited state of the ketone is the otherwise unreactive π-π* state.[5] The torsion angle O=C-C_α-N_β could be positive or negative with respect to axial chirality (*P* or *M*) in **84a,b**. This then leads to the possibility of γ-hydrogen abstraction from one face of the carbonyl resulting in the 1,4-diradical (*rad*-**84** or *ent-rad*-**84**).

In general, the stereochemistry of the β-lactam photoproduct **85a,b** is dictated by the mode of ring closure of the 1,4-diradical intermediate, i.e., which face of the benzylic radical center adds to the γ-carbon radical. As, the 1,4-diradical is free to rotate in solution and that there is a competition between bonds rotation and new bonds formation in the 1,4-diradical, it is likely that the extent of chiral induction in the photoproducts translates with bonds rotation vs. bonds formation. In other words, the rate of interconversion between the two diradicals (*rad*-**84** and *ent-rad*-**84**) and the rate of ring closure leading to the β-lactam photoproduct **85a,b**, imparts a dynamic nature in the system as ascertained by the differential activation parameters ($\Delta\Delta H^{\ddagger}$ and $\Delta\Delta S^{\ddagger}$). Presumably, by lowering the temperature, the rate of interconversion between the two 1,4-diradicals (*rad*-**84** and *ent-rad*-**84**) is lowered with respect to the rate of ring closure leading to the β-lactam **85a,b**, resulting in high enantioselectivity (e.r values).

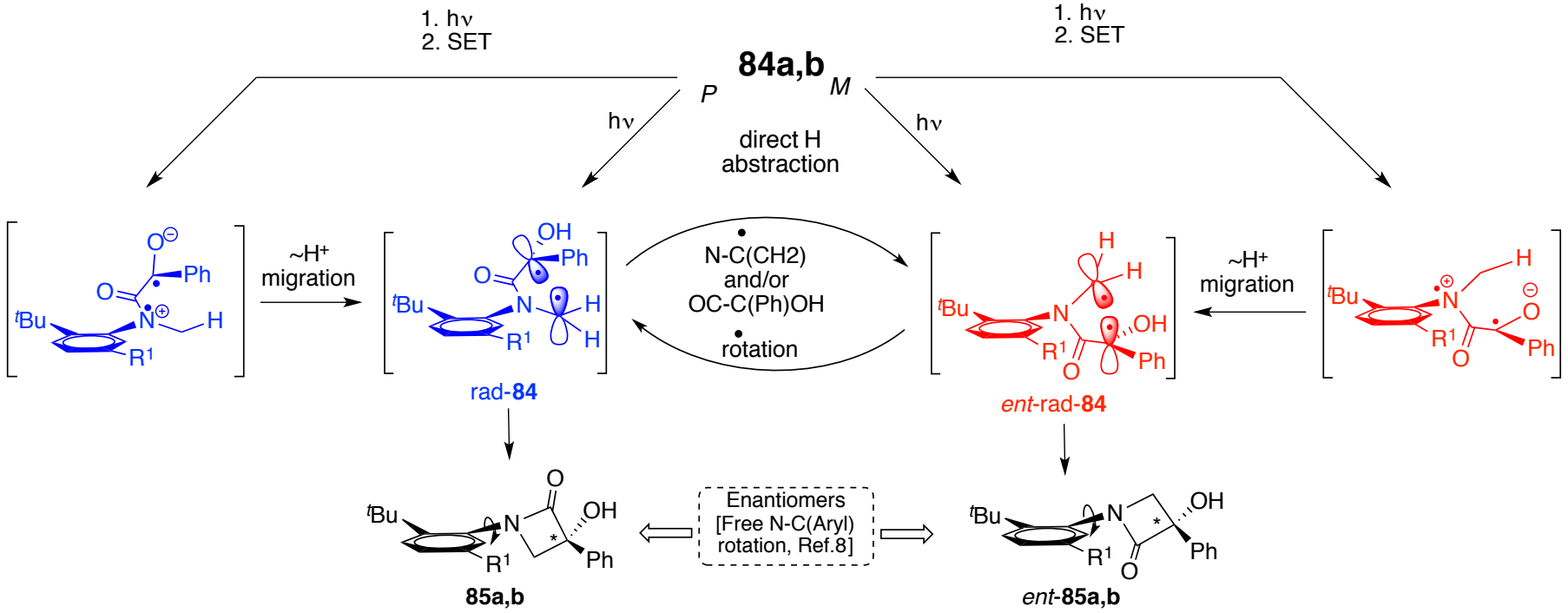

Scheme 8.2: Mechanistic rational in γ-Hydrogen abstraction involving axially chiral **84a,b.**

The slow rotation of bonds at low temperature help in a smooth and efficient transfer of axial chirality leading to high enantioselectivity in **85a,b**. This conjecture can be ascertained based on indirect evidence from activation energy for racemization ($\Delta G^{\ddagger}$). Table 8.2 shows that molecular constraints prevent bond rotation in **84a** (k = 5.26x10^{-7} s^{-1}) compared to **84b** (k = 8.0x10^{-6} s^{-1}) with respect to rate of racemization. This is reflected in the slower rate of racemization resulting in more efficient chiral transfer in **84a** than in **84b**. As shown in table 8.2, the selectivity in the di-*tert*-butyl derivative **84a** is slightly higher than the corresponding mono-*tert*-butyl derivative **84b;** this is a direct consequence of the explanation given above.

8.3. Summary and Outlook

Asymmetric photochemical transformation involving α-oxoamides **84a,b** demonstrated a broader usefulness of the transfer of chirality using atropisomeric chromophores. Thus, enantiopure molecular scaffolds could be synthesized via photochemical methods by irradiation of axially chiral chromophores that equilibrate very slowly in the ground state, whereas no interconversion would be possible in the excited state: This is a direct implication of the Havinga's NEER principle.[12] The γ-hydrogen abstraction presents a second methodology in the quest for developing a general strategy for chiral induction during photochemical transformations in solution phase.

8.4. Experimental Section

8.4.1. General method

All commercially obtained reagents/solvents were used as received; chemicals were purchased from Alfa Aesar®, Sigma – Aldrich®, Across®, TCI® America, Mallinckrodt®, and Oakwood® Products, and were used as received without further purification. Unless stated otherwise, reactions were conducted in oven-dried glassware under nitrogen atmosphere. ^{1}H NMR and ^{13}C NMR spectra were recorded on Varian 400 MHz (100 MHz for ^{13}C) and on 500 MHz (125 MHz for ^{13}C) spectrometers. Data for ^{1}H NMR are reported as chemical shift (δ ppm) with the corresponding integration values. Coupling constants (*J*) are reported in hertz (Hz). Standard abbreviations indicating multiplicity were used as follows: s (singlet), b (broad), d (doublet), t (triplet), q (quartet), m (multiplet), virt (virtual), and ABq (AB quartet). Data for ^{13}C

NMR spectra are reported in terms of chemical shift (δ ppm). Electrospray Ionization Spectra were recorded on a Bruker – Daltronics® BioTof mass spectrometer in positive (ESI+) ion mode. HPLC analyses were performed on Waters® HPLC equipped with 2525 pump. Waters® 2767 sample manager was used for automated sample injection. All HPLC injections were monitored using a Waters® 2487 dual wavelength absorbance detector at 220, 254, and 270 nm. Analytical and semi-preparative injections were performed on chiral stationary phase using various columns as indicted in the below.

iv) Regis® PIRKLE COVALENT (R,R) WHELK–01

a) 25 cm x 4.6 mm column for analytical injections.

b) 25 cm x 10 mm column for semi-preparative injections.

v) CHIRACEL® OD-H

a) 0.46 cm x 25 cm column for analytical injections.

b) 0.46 cm x 25 cm column for semi-preparative injections.

vi) CHIRALPACK® IC:

a) 0.46 cm x 25 cm column for analytical injections.

vii) CHIRALPAK® AD-H

a) 0.46 cm x 25 cm column for analytical injections.

b) 0.46 cm x 25 cm column for semi-preparative injections.

Masslynx software version 4.1 was used to analyze the HPLC injections. Igor Pro® Software version 4.0 was used to process the chromatographic data. UV-Vis spectra were recorded on a Shimadzu 2501PC UV-Vis spectrometer using UV quality fluorimeter cells (with range until 190 nm) purchased from Luzchem. Optical activity values were recorded on JASCO® DIP – 370 digital polarimeter. CD spectra were recorded on Applied Photophysics® spectrometer. When necessary, the reactants and photoproducts were purified by chromatography on silica gel (Sorbent Technologies®, silica gel standard grade: Porosity 60 Å, Particle size: 230 x 400 mesh, Surface area: 500 – 600 m^2/g, Bulk density: 0.4 g/mL, pH range: 6.5 – 7.5). The Retention Factor (R*f*) values were recorded using a 20 % EtOAc-Hexanes as mobile phase (unless indicated) and on SORBENT TECHNOLOGIES® Silica Gel TLC plates (200 mm thickness w/UV_{254}).

8.4.2. Structure determination

Single crystal X-ray diffraction data sets were collected on a SIEMENS diffractometer with a 1K CCD area detector (graphite-monochromated Mo Ka radiation). The structures were solved by direct methods and refined on *F*2 using the SHELXTL V6.14 package (after absorption corrections with SADABS). The CCDC deposition numbers for structures **84a,b** and **85b** are CCDC 734106 – 734108 respectively.

Structure **84a**: $C_{23}H_{29}NO_2$, M = 351.47, Monoclinic, P2(1)/n (no 14), a = 9.6015(16) Å, 12.896(2) Å, 16.782(3) Å, β = 92.290(3)°, V = 2076.4(6) Å^3, Z= 4, room temperature, 13476 reflections measures, 4979 unique reflections (R_{int} = 0.0288) which were used in all calculations R_1/wR_2 = 5.51/16.36%, R_1/wR_2 (all) = 7.86/18.17%.

Structure **84b**: $C_{19}H_{21}NO_2$, M = 295.37, Monoclinic, P2(1)/n (no 14), a = 9.857(10) Å, 15.906(16) Å, 10.917(11) Å, β = 104.238 (19)°, V = 1659(3) Å^3, Z= 4, room temperature, 8655 reflections measures, 3134 unique reflections (R_{int} = 0.0373) which were used in all calculations R_1/wR_2 = 6.90/19.13%, R_1/wR_2 (all) = 9.79/22.52%.

Structure **85b**: $C_{19}H_{21}NO_2$, M = 295.37, Monoclinic, P2(1)/n (no 14), a = 8.747(5) Å, 21.195(13) Å, 9.869(6) Å, β = 114.920(12)°, V = 1659.30(18) Å^3, Z= 4, room temperature, 15549 reflections measures, 3956 unique reflections (R_{int} = 0.0500) which were used in all calculations R_1/wR_2 = 6.80/21.37%, R_1/wR_2 (all) = 10.79/24.81%.

*The A-errors reported for structure **85b** are regarding structural disorder in the t-butyl groups. The observed disorder is not unusual for such molecules.*

8.4.3. Synthesis of α-oxoamides 84a,b

α-Oxoamides **84a,b** were synthesized based on the procedure reported in chapter 6.

The comprehensive characterization for compound **84a** can be retrieved in chapter 6 section 6.4.2.

8.4.4. Characterization of α-oxoamides 84b

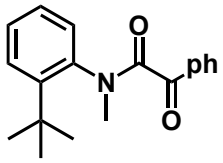

84b

84b was purified by flash chromatography on silica gel: Solvent polarity: 8 – 10% EtOAc-Hexanes. R*f* = 0.35 (20 % EtOAc-Hexanes)

Then, **84b** was further recrystallized in 5% benzene-Hexanes

X-ray crystallography: See figure 8.1

^{1}H NMR (400 MHz, $CDCl_3$, δ ppm) 8.1 – 6.7 (Ar, 9H), 3.35 and 3.25 (s, 3H, N-CH_3, major and minor conformers), 1.45 and 1.44 (s, 9H, minor and major conformers)

^{13}C NMR (100 MHz, $CDCl_3$, δ ppm) Note: each peak appears with its corresponding rotamer!

HRMS-ESI [$(M + Na)^+$]: Calculated: 318.1465; Observed: 318.1450; Δm = 4.7 ppm

HPLC analysis conditions: For both analytical and preparative injections

Column: OD-H; Abs. detector: 254 nm and 270 nm

Mobile phase: Hexanes: IPA = 97:03

Flow rate: 1 mL/min (Analytical), and 4.5 mL/min (Preparative).

Retention times (min): ~7.90 [(-)-**8ab**] and ~10.34 [(+)-**84b**]

Optical Rotation $[\alpha]_D^{28}$:

HPLC peak retention time at ~7.90 min, (-)-**84b** (*c* 0.1, $CHCl_3$) = -134 deg.

HPLC peak retention time at ~10.34 min, (+)-**84b** (*c* 0.1, $CHCl_3$) = +132 deg.

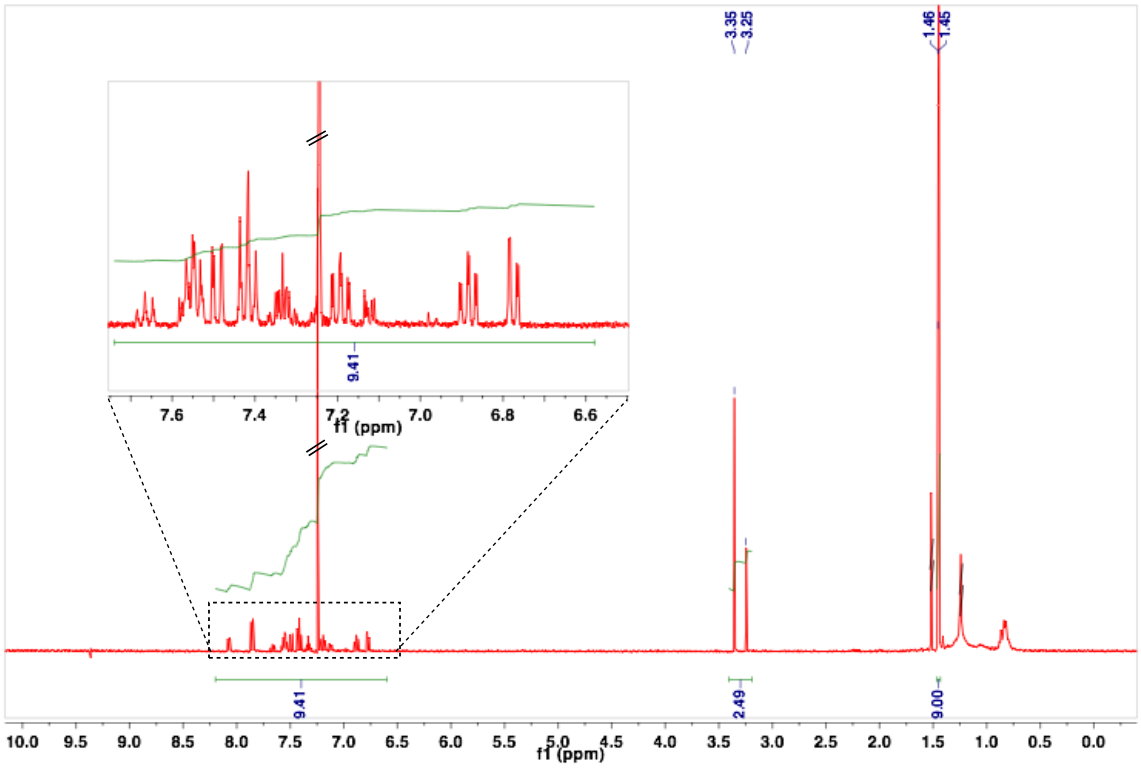

Figure 8.6: ^{1}H NMR (400 MHz, $CDCl_3$, δ ppm) spectrum for oxoamide **84b**.

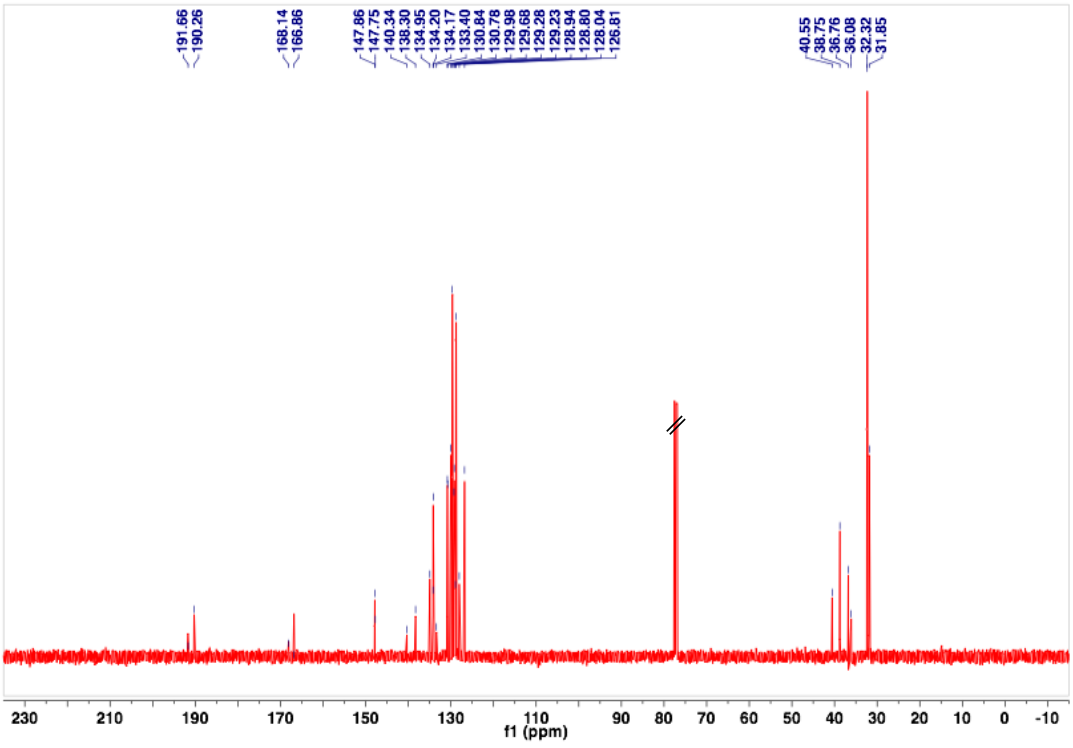

Figure 8.7: ^{13}C NMR (100 MHz, $CDCl_3$, δ ppm) spectrum for oxoamide **85b**.

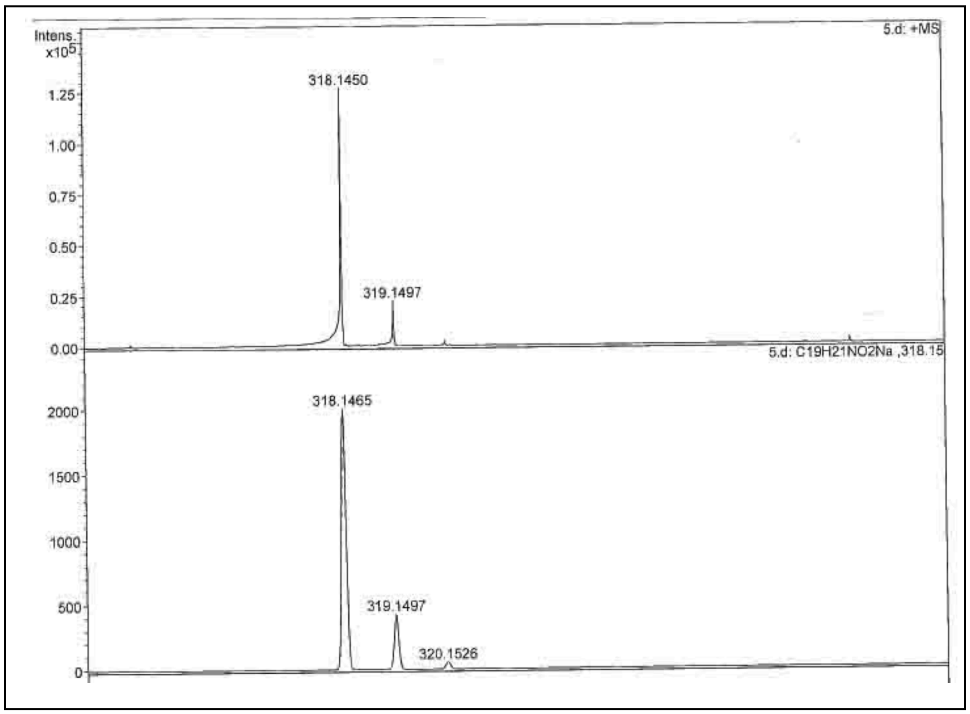

Figure 8.8: HRMS for oxoamide **84b**.

CD Spectroscopy:

c = 0.1% in Methanol

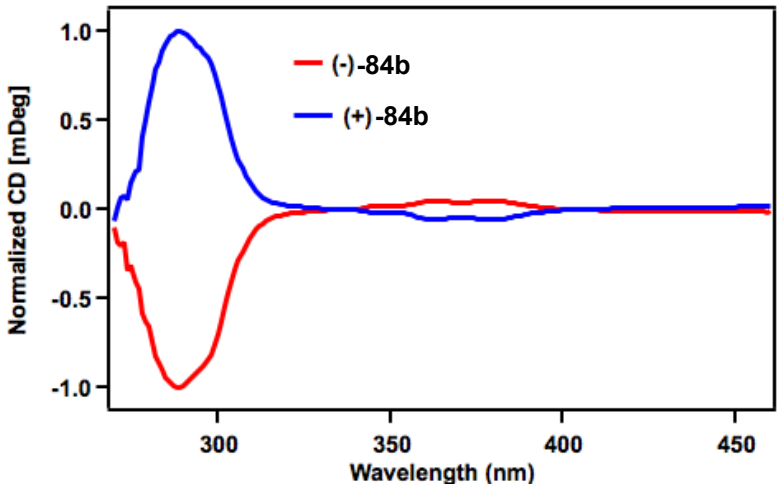

Figure 8.9: CD spectra for optically pure isomers for oxoamide **84b**.

8.4.5. Photoreaction procedure for α-oxoamides 84a,b

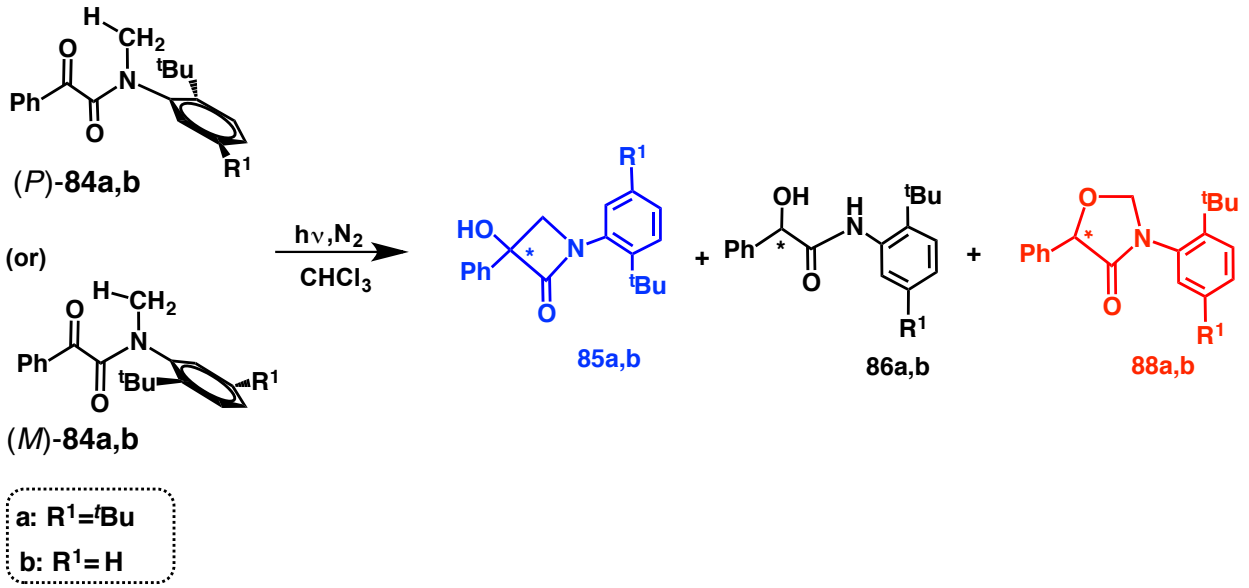

Scheme 8.3: General irradiation procedure for α-oxoamides **84a,b**.

Optically pure *P* or *M* isomer of α-oxoamides **84a,b** (2.5 mM of **84a**, and 3.4 mM for **84b**) in $CHCl_3$ was irradiated for a given time interval in Pyrex tube with a 450 W high pressure mercury lamp, at various temperatures and under constant flow of nitrogen. The reaction was monitored by ^1H NMR spectroscopy. After irradiation, the solvent was removed under reduced pressure and the photoproducts were isolated by chromatography and characterized by NMR spectroscopy, mass spectrometry, and by HPLC. HPLC analysis of the photolysate on chiral stationary phases gave the optical purity of the photoproducts.

8.4.6. Characterization of photoproducts 85a,b and 86a,b

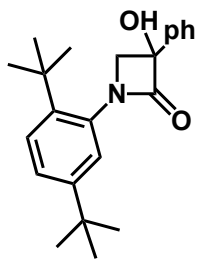

85a

β-lactam **85a** (*cf.* chapter 6 section 6.4.7)

Photoproducts **85a** were isolated by chromatography.

Solvent system: 20% EtOAc-Hexanes. R*f* = 0.3 (20% EtOAc-Hexanes)

^1H NMR (500 MHz, $CDCl_3$, δ ppm) 7.77 – 7.13 (Ar, 7H), 4.1 – 3.9 (ABq, 2H), 3.3 – 3.0 (bs, 1H), 1.36 (s, 9H), 1.30 (s, 9H)

^{13}C NMR (125 MHz, CDCl3, δ ppm) 167.0, 150.6, 145.8, 138.5, 134.8, 129.21, 127.5, 126.8, 126.4, 126.3, 85.5, 62.2, 35.0, 31.5, 31.4

HRMS-ESI [(M + Na)$^+$]: Calculated: 374.2099; Observed: 374.2091 Δm = 2.1 ppm

HPLC analysis conditions: Column: CHIRALPACK IC; Abs. detector: 220 nm and 254 nm**;** Mobile phase: Hexanes: IPA = 92.4:7.6; Flow rate: 0.5 mL/min

Retention times (min): ~11.90 (**85a**) and ~15.90 (*ent*-**85a)**

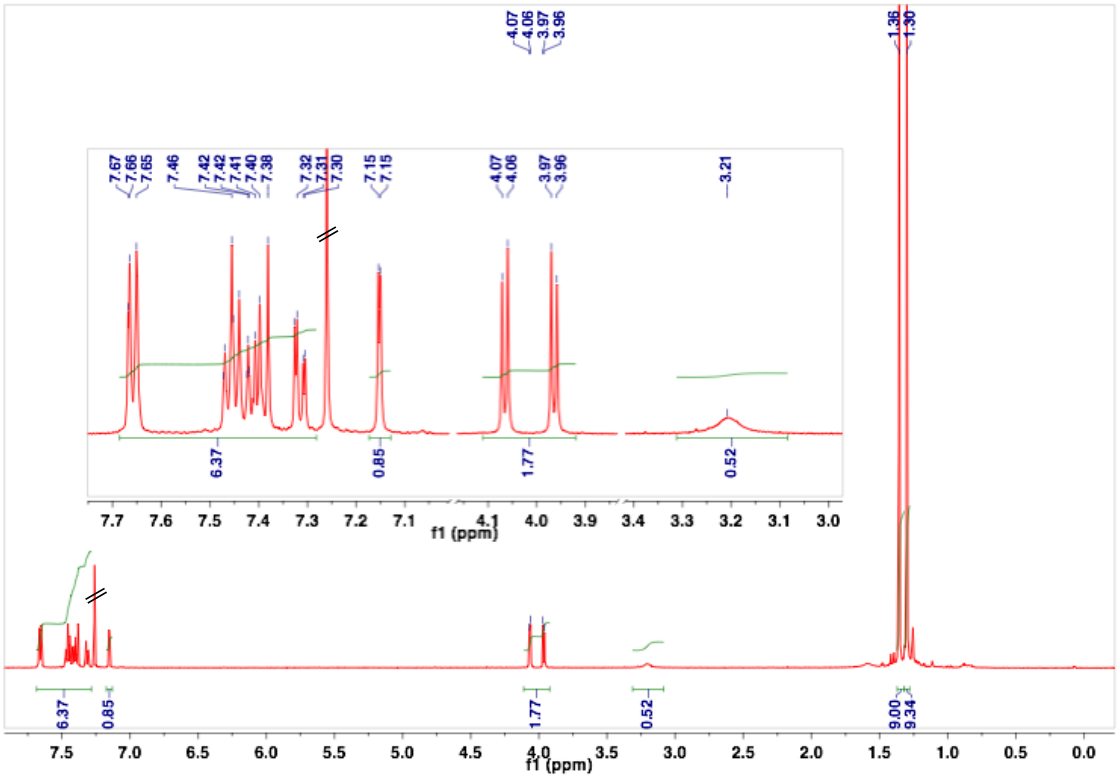

Figure 8.10: ^{1}H NMR (500 MHz, $CDCl_3$, δ ppm) spectrum for β-lactam **85a**.

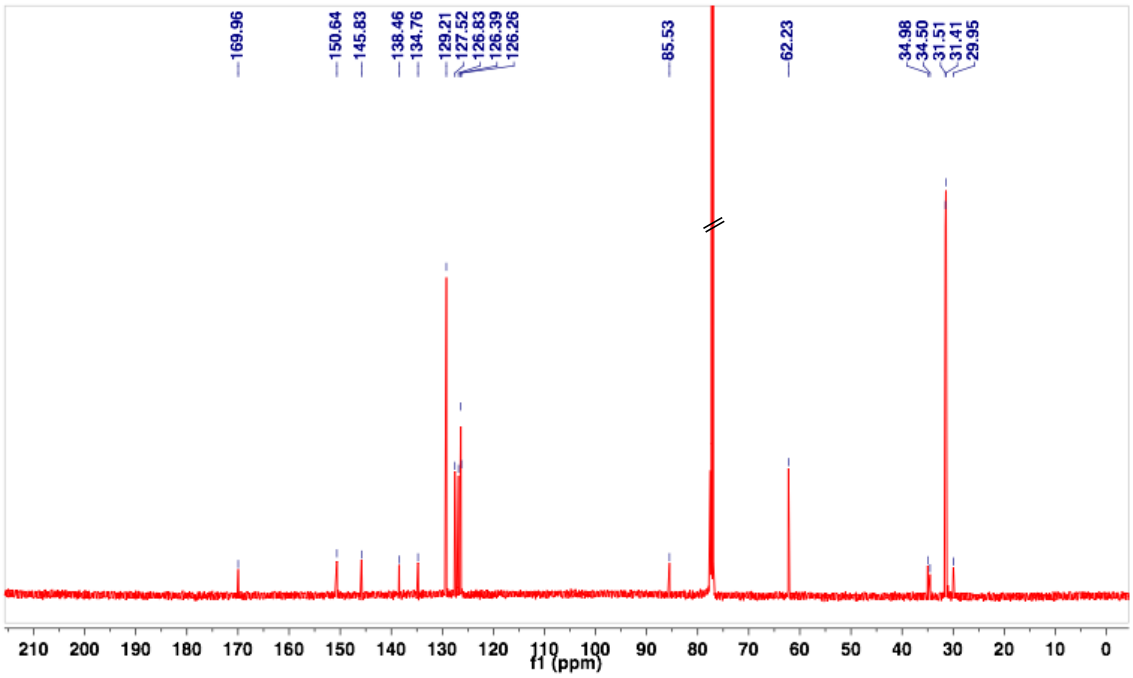

Figure 8.11: ^{13}C NMR (125 MHz, $CDCl_3$, δ ppm) spectrum for β-lactam **85a**.

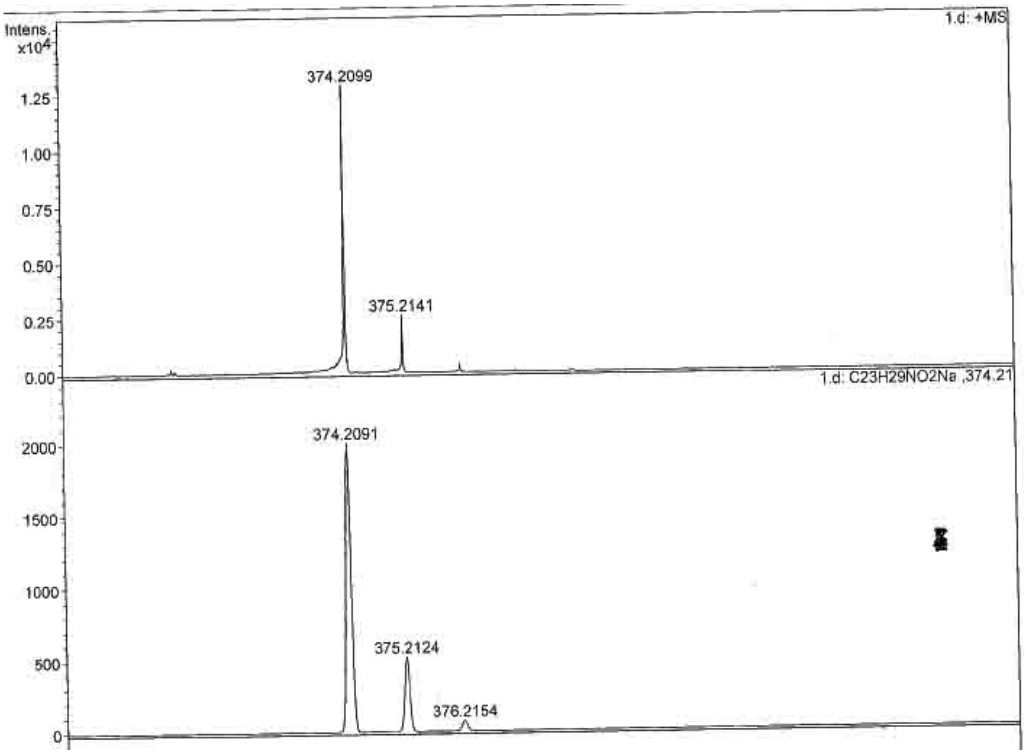

Figure 8.12: HRMS for β-lactam **85a**.

Mandelamide derivative 86a

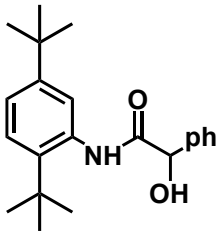

86a

Photoproducts **86a** were isolated by chromatography: Solvent system: 20% EtOAc-Hexanes. R*f* = 0.6 (20% EtOAc-Hexanes)

^{1}H NMR (500 MHz, $CDCl_3$, δ ppm) 8.1 (bs, 1H), 8 – 7 (Ar, 8 H), 5.26 – 5.23 (virt. d, *J* = 1.5, 1H), 3.7 – 3.6 (virt. d, *J* = 2.5, 1H), 1.3 (s, 9H), 1.2 (s, 9H)

^{13}C NMR (100 MHz, CDCl3, δ ppm) 169.9, 150.0, 139.1, 138.2, 134.6, 129.3, 129.2,127.3, 126.8, 126.4, 122.8, 75.1, 34.0, 31.5, 31.4, 30.6

HRMS-ESI [(M + Na)$^{+}$]: Calculated: 362.2095; Observed: 362.2091; Δm = 1.1 ppm

HPLC analysis conditions: Column: CHIRALPACK IC; Abs. detector: 220 nm and 254 nm**;** mobile phase: Hexanes: IPA = 92.4:7.6; Flow rate: 0.5 mL/min

Retention times (min): ~10.80 (**86a**) and ~13.98 (*ent*-**86a**)

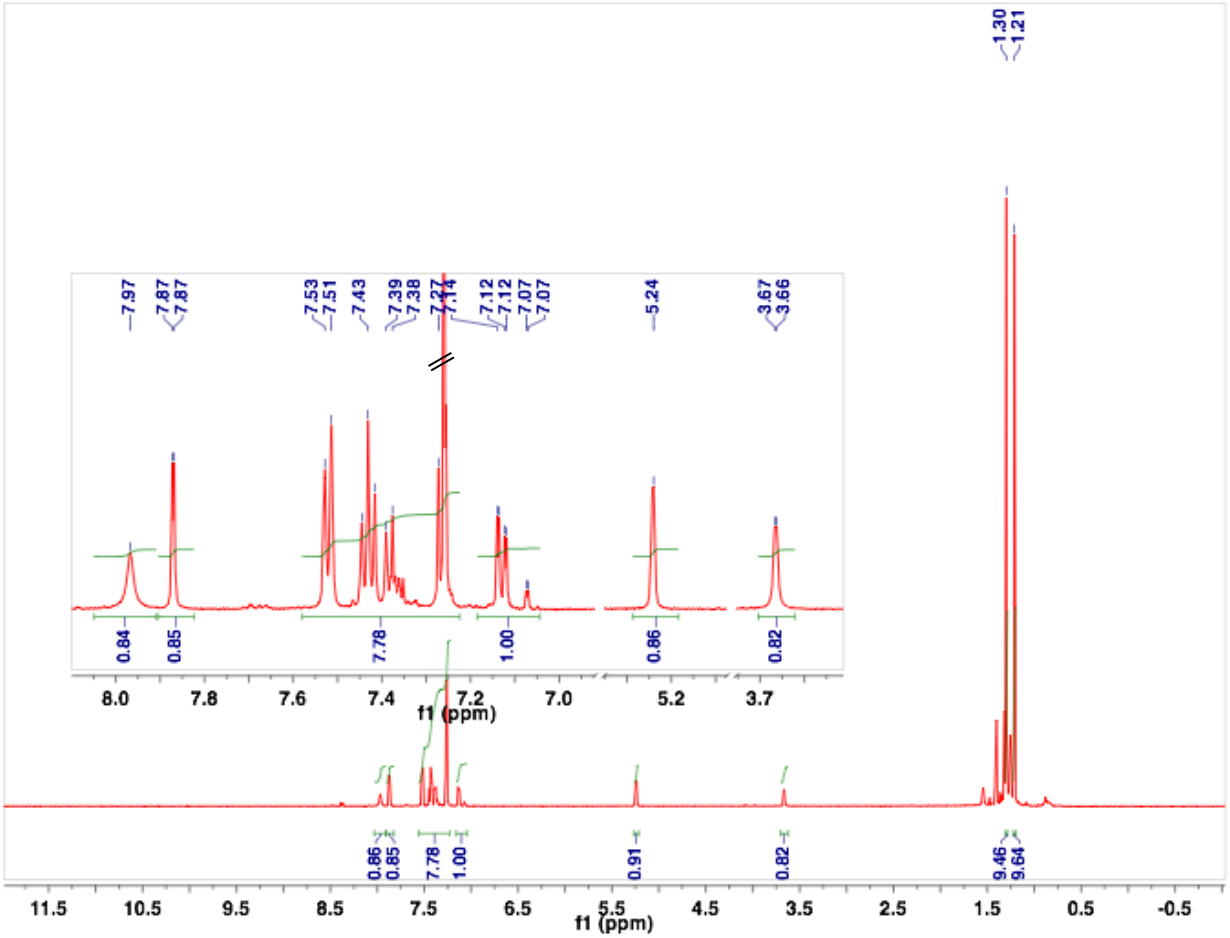

Figure 8.13: ^{1}H NMR (500 MHz, $CDCl_3$, δ ppm) spectrum for mandelamide **86a**.

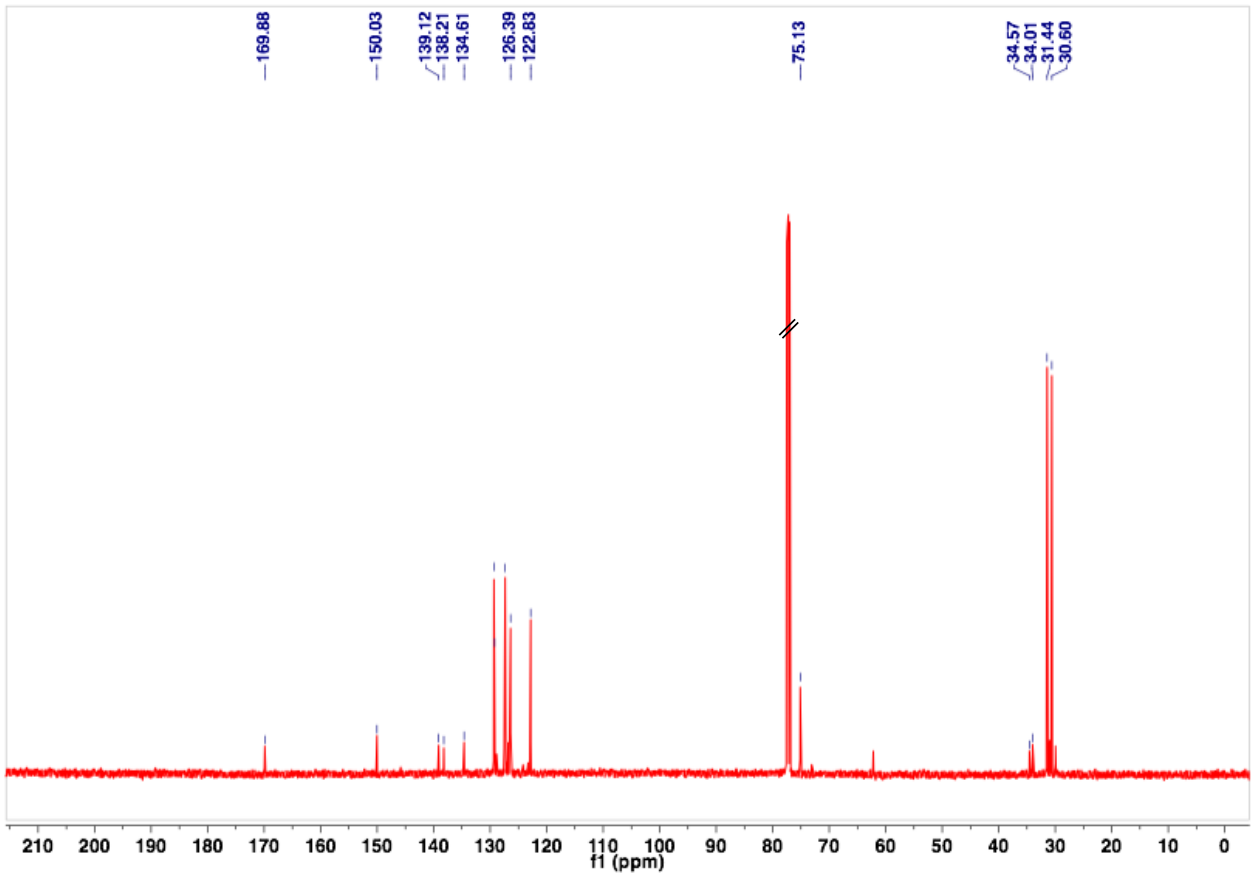

Figure 8.14: ^{13}C NMR (100 MHz, $CDCl_3$, δ ppm) spectrum for mandelamide **86a**.

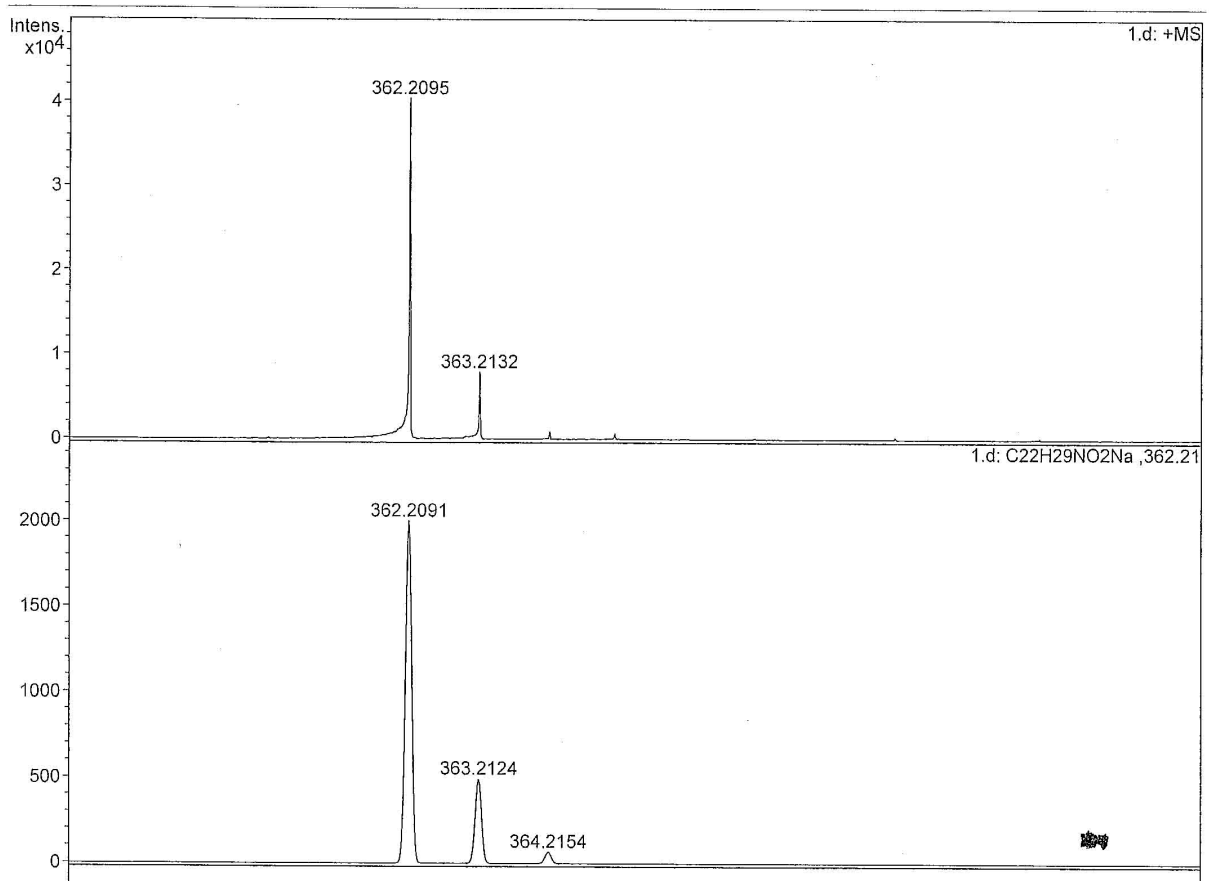

Figure 8.15: HRMS for mandelamide **86a**.

β-Lactam **85b:** R*f* = 0.3 (20% EtOAc-Hexanes)

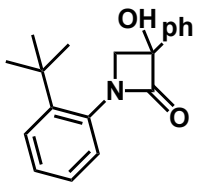

85b

Photoproducts **85b** were isolated by chromatography: Solvent system: 20% EtOAc-Hexanes**.**

X-ray crystallography: see figure 8.1

^{1}H NMR (400 MHz, $CDCl_3$, δ ppm) 7.65 – 7.15 (Ar, 9H), 4.7 – 3.92 (ABq, 2H), 3.91 – 3.65 (bs, 1H), 1.36 (s, 9H)

^{13}C NMR (100 MHz, CDCl3, δ ppm) 171.0, 149.0, 138.4, 135.3, 130.4, 129.2, 129.1, 129.0, 127.7, 127.6, 126.3, 85.6, 62.7, 35.4, 31.5

HRMS-ESI [$(M + Na)^+$]: Calculated: 318.1450; Observed: 318.1465; Δm = 5.8 ppm

HPLC analysis conditions: Column: CHIRALPACK IC; Abs. detector: 220 nm and 254 nm**;** mobile phase: Hexanes: IPA = 92.4:7.6; Flow rate: 0.5 mL/min

Retention times (min): ~ 22.67 (**85b**) and ~27.07 (*ent*-**85b)**

Optical Rotation $[\alpha]_D^{28}$:

HPLC peak retention time at ~22.67 (**85b**) (*c* 0.1, CH_3OH) = +31 deg.

HPLC peak retention time at ~ 27.07 (*ent*-**85b)** (*c* 0.1, CH_3OH) = -26 deg.

CD Spectroscopy:

For optically pure samples of **85b**: *c* = 0.1%, methanol

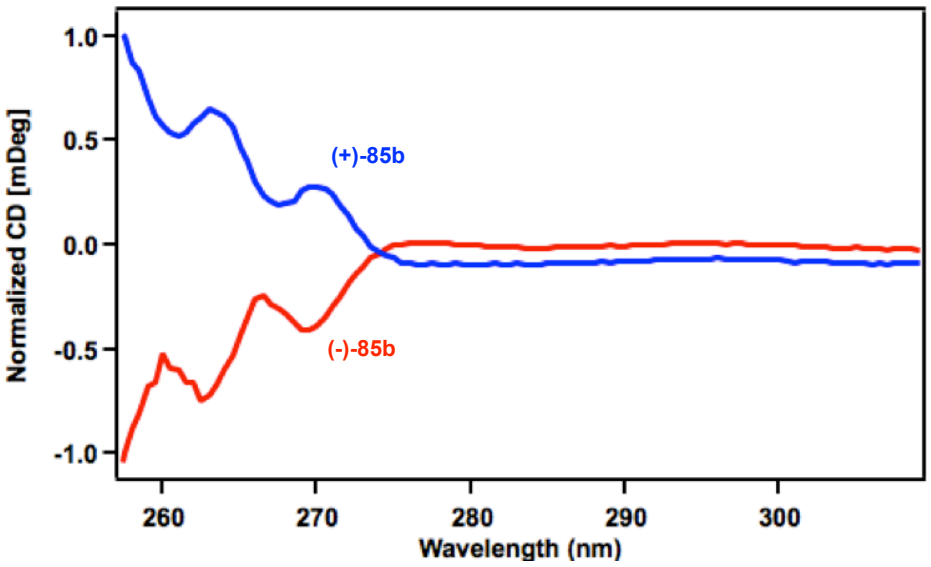

Figure 8.16: CD spectra for isomers of **85b.**

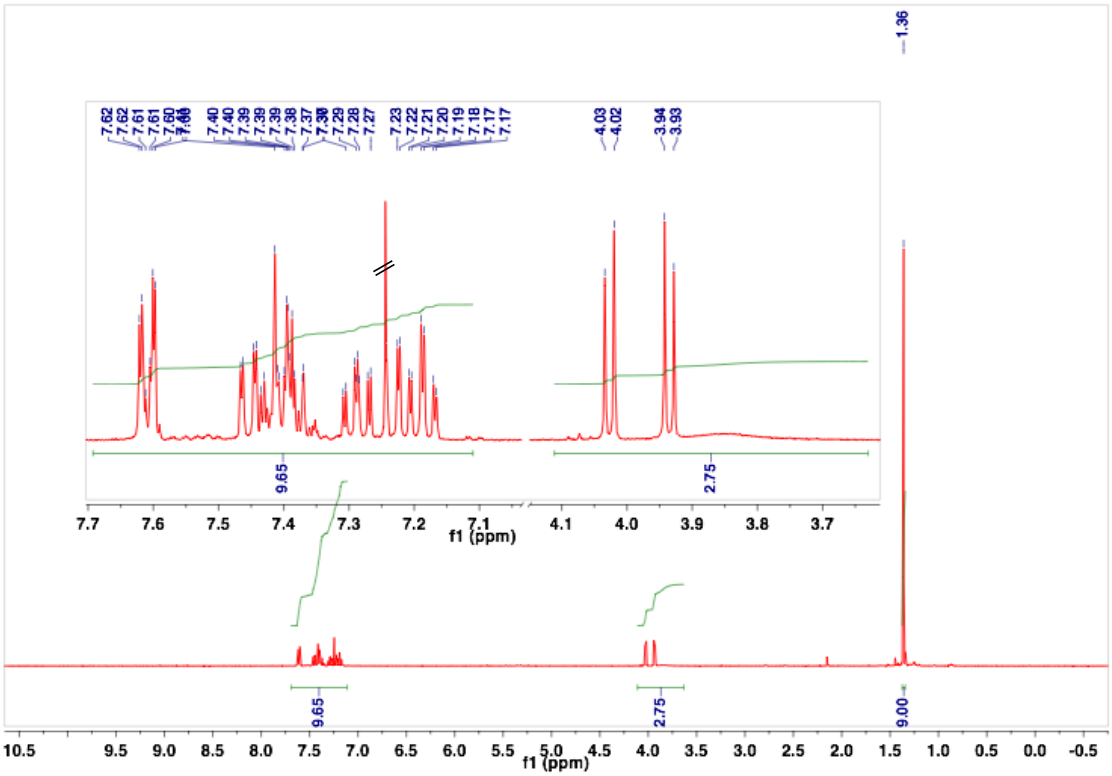

Figure 8.17: ^{1}H NMR (400 MHz, $CDCl_3$, δ ppm) spectrum for β-lactam **85b**.

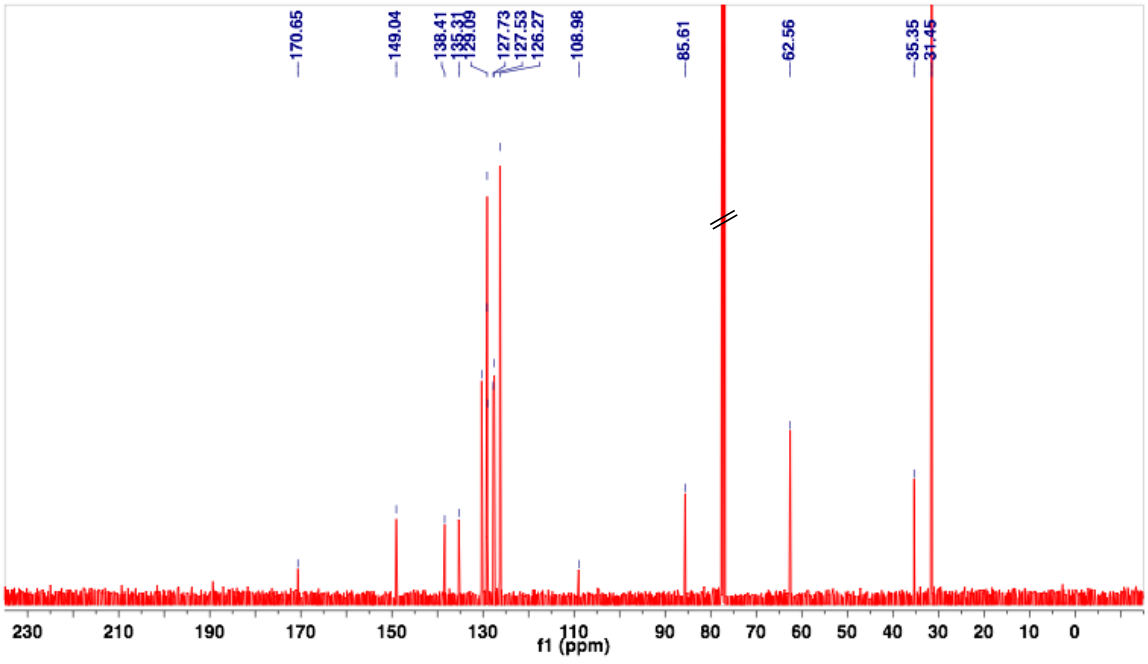

Figure 8.18: ^{13}C NMR (100 MHz, $CDCl_3$, δ ppm) spectrum for β-lactam **85b**.

^{13}C DEPT spectra: Analysis of ^{13}C DEPT did not show any C-H carbon corresponding to the carbocycle (apart from aromatic C-H). This confirms the formation of the 4-membered β-lactam product **85** instead of the 5-memberd oxazolidin-4-ones **88.**

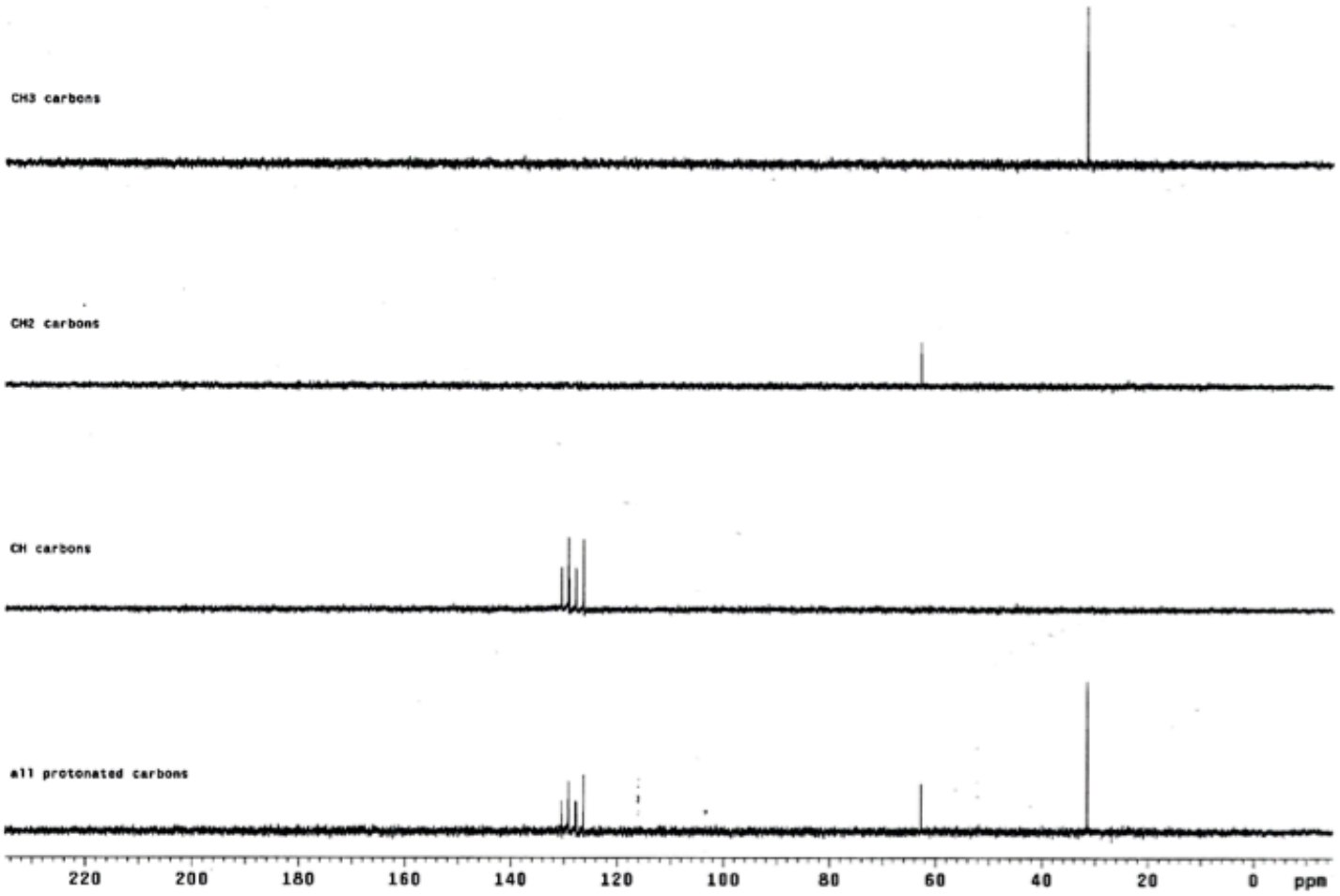

Figure 8.19: ^{13}C NMR DEPT (100 MHz, $CDCl_3$, δ ppm) spectrum for β-lactam **85b**.

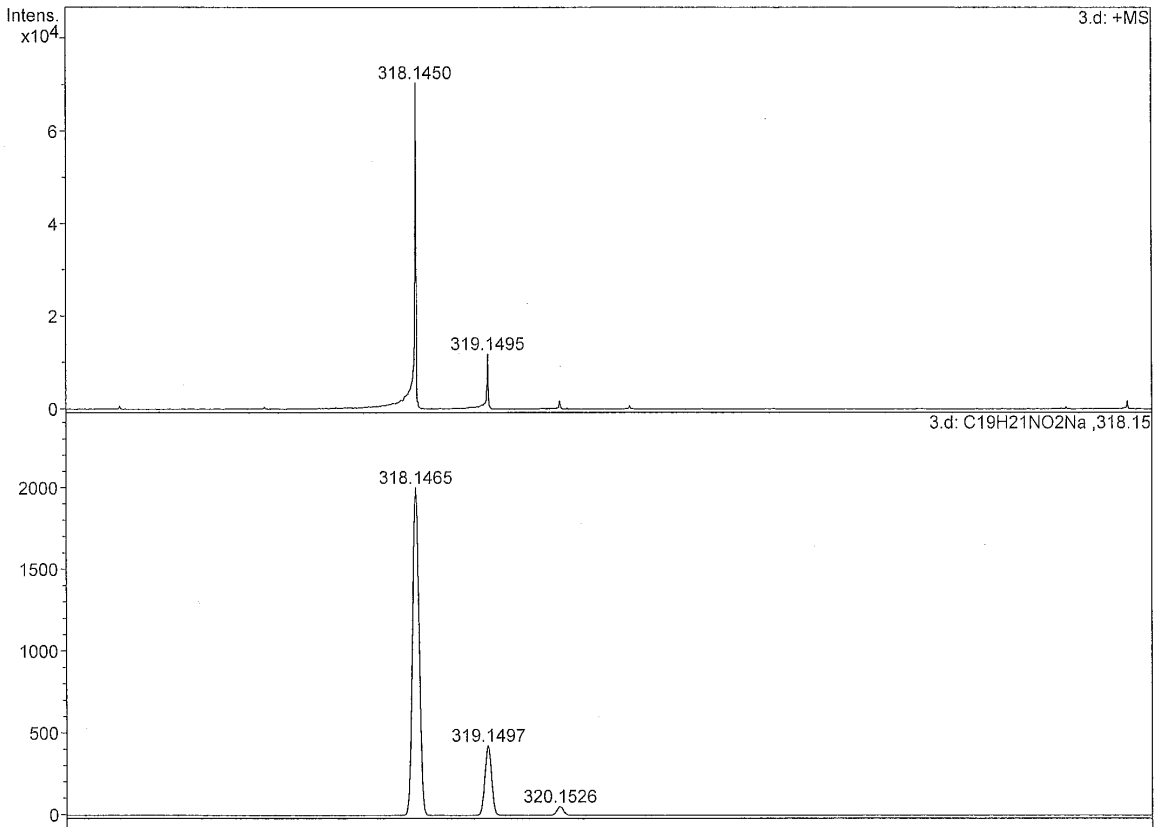

Figure 8.20: HRMS spectrum for β-lactam **85b**.

Mandelamide derivative **86b:** R*f* = 0.25 (20% EtOAc-Hexanes)

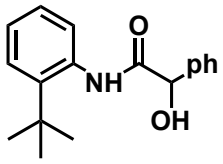

86b

Photoproducts **86b** were isolated by chromatography

Solvent system: 20% EtOAc-Hexanes.

^{1}H NMR (400 MHz, $CDCl_3$, δ ppm): 8.05 (bs, 1H), 7.8 – 7.0 (Ar, 9H), 5.2 (s, 1H), 3.72 (bs, 1H), 1.23 (s, 9H)

^{13}C NMR (100 MHz, CDCl3, δ ppm) 170.0, 141.5, 139.1, 134.9, 129.3, 129.2, 127.2, 127.0, 126.7, 126.0, 125.9, 75.0, 34.4, 30.5

HRMS-ESI ([M + Na]$^{+}$): Calculated: 306.1465; Observed: 306. 1477; Δm = 1.6 ppm

HPLC analysis conditions: Column: CHIRALPACK IC; Abs. detector: 220 nm and 254 nm; mobile phase: Hexanes: IPA = 92.4:7.6; Flow rate: 0.5 mL/min

Retention times (min): ~ 28.27 (**86b**) and ~ 28.89 (*ent*-**86b)**

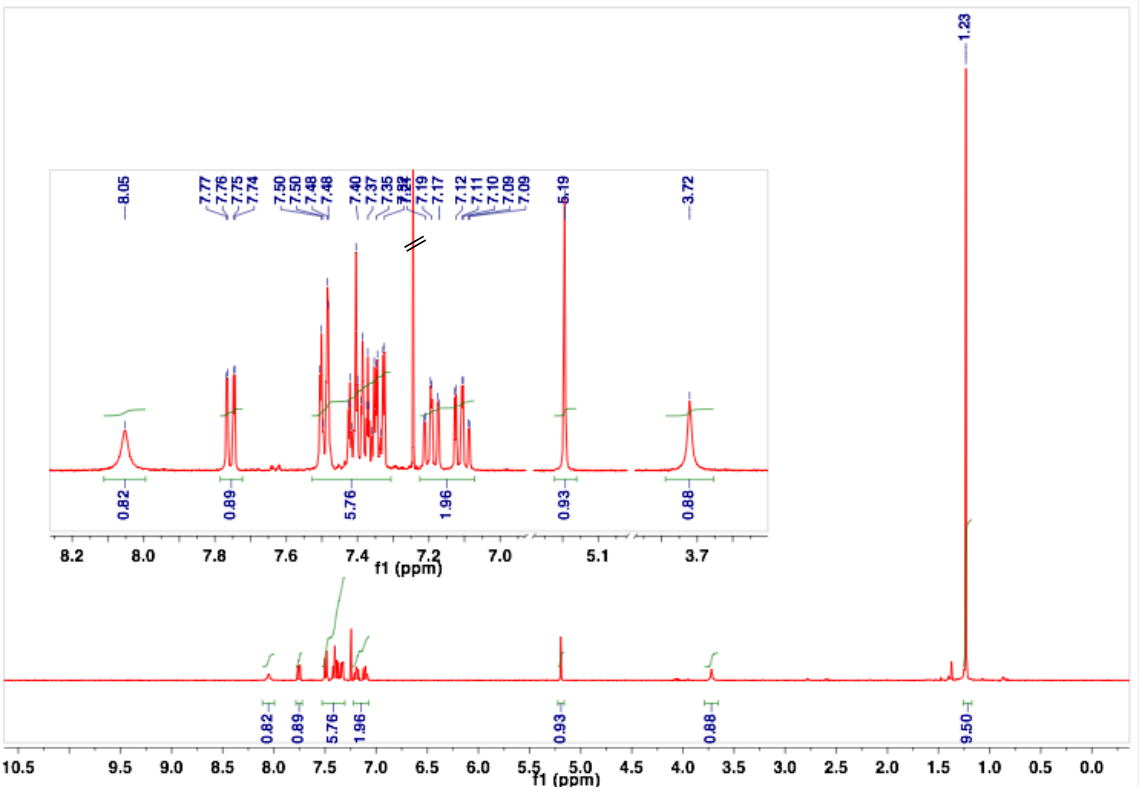

Figure 8.21: ^{1}H NMR (400 MHz, $CDCl_3$, δ ppm) spectrum for mandelamide **86b**.

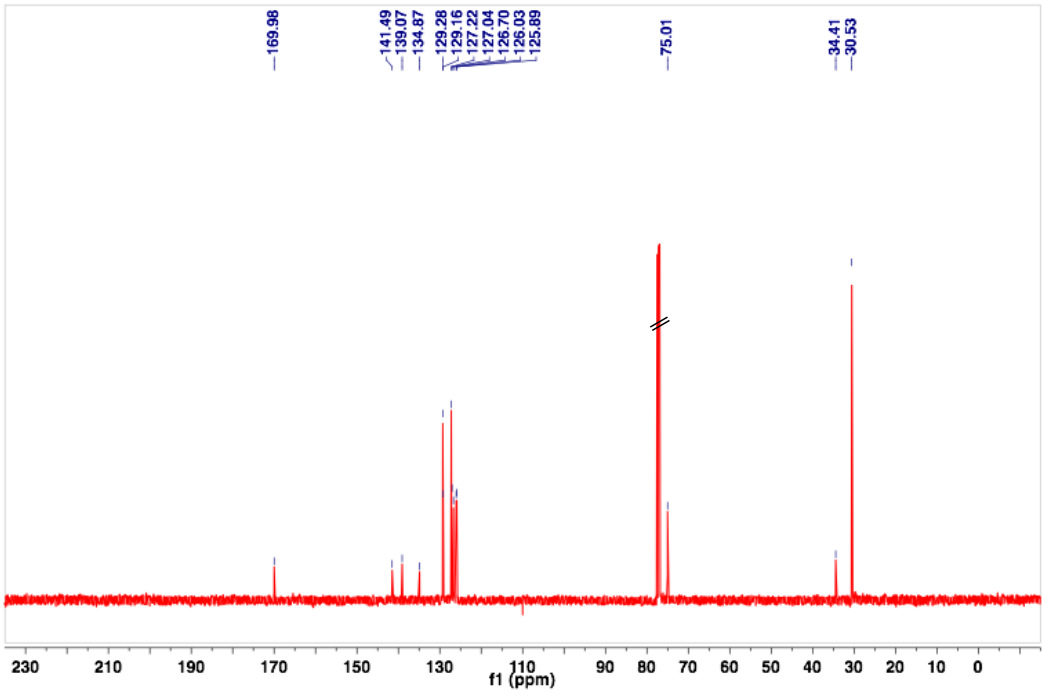

Figure 8.22: ^{13}C NMR (100 MHz, $CDCl_3$, δ ppm) spectrum for mandelamide **86b**.

^{13}C DEPT

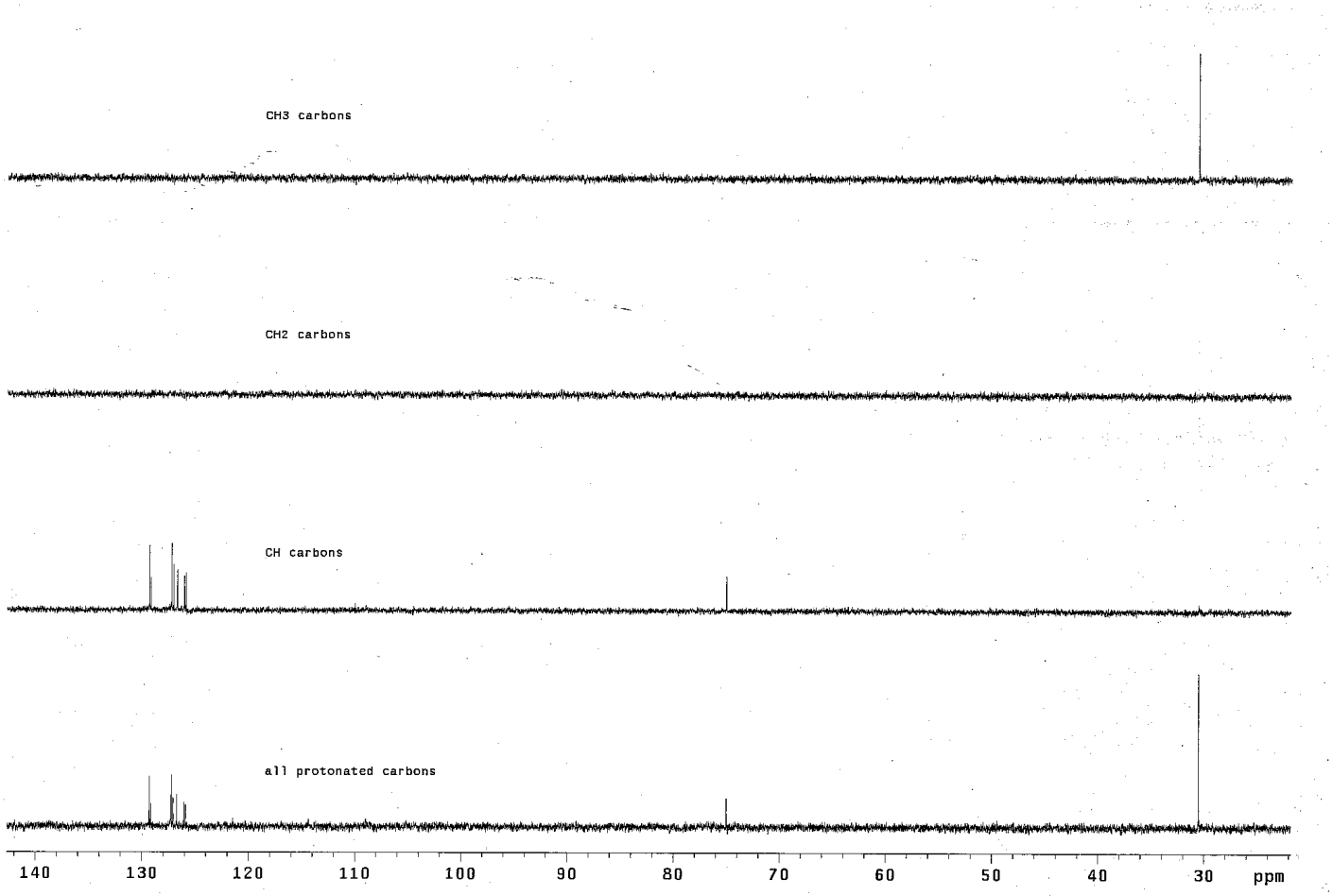

Figure 8.24: ^{13}C NMR DEPT (100 MHz, $CDCl_3$, δ ppm) spectrum for mandelamide **86b**.

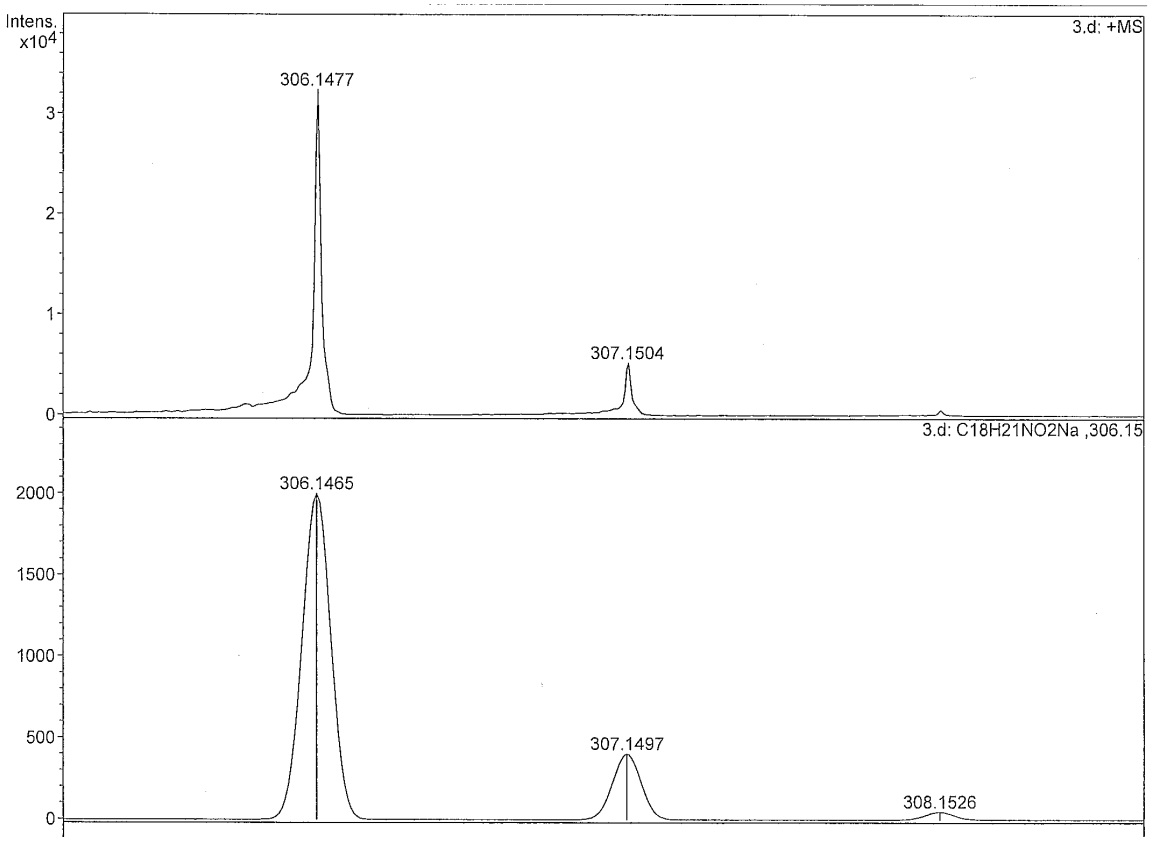

Figure 8.25: HRMS for mandelamide **86b**.

8.5. References

(1) Clayden, J. Atropisomers and near-atropisomers: achieving stereoselectivity by exploiting the conformational preferences of aromatic amides. *Chem. Commun.* **2004**, 127–135.

(2) Honda, A.; Waltz, K. M.; Carroll, P. J.; Walsh, P. J. Atropisomeric Amides: Achiral Ligands With Chiral Conformations. *Chirality* **2003**, *15*, 615–621.

(3) Aoyama, H.; Sakamoto, M.; Kuwabara, K.; Yoshida, K.; Omote, Y. Photochemical Reactions of α-Oxoamides. Norrish Type II Reactions via Zwitterionic Intermediates. *J. Am. Chem. Soc.* **1983**, *105*, 1958–1964.

(4) Wagner, P. J.; Park, B. S. Photoinduced hydrogen atom abstraction by carbonyl compounds. *Org. Photochem.* **1991**, *11*, 227−366.

(5) Chesta, C. A.; Whitten, D. G. Photocyclization of alpha-keto amides in homogeneous solution and aqueous cyclodextrin media. The role of zwitterions and diradicals in photoinduced electron transfer reactions. *J. Am. Chem. Soc.* **1992**, *114*, 2188–2197.

(6) Wang, R.; Chen, C.; Duesler, E.; Mariano, P. S. β-Lactam-Forming Photochemical Reactions of N-Trimethylsilylmethyl- and N-Tributylstannylmethyl-Substituted α-Ketoamides. *J. Org. Chem.* **2004**, *69*, 1215–1220.

(7) Natarajan, A.; Mague, J. T.; Ramamurthy, V. Asymmetric Induction during Yang Cyclization of α-Oxoamides: The Power of a Covalently Linked Chiral Auxiliary Is Enhanced in the Crystalline State. *J. Am. Chem. Soc.* **2005**, *127*, 3568–3576.

(8) Kitagawa, O.; Fujita, M.; Kohriyama, M.; Hasegawa, H.; Taguchi, T. Stereoselective synthesis of diastereomeric atropisomeric lactam with various ring sizes and their structural characterization. *Tetrahedron Lett.* **2000**, *41*, 8539–8544.

(9) Wolf, C. *Dynamic Stereochemistry of Chiral Compounds. Principles and Applications*; RSC publishing: Cambridge, UK, 2008.

(10) Curran, D. P.; Hale, G. R.; Geib, S. J.; Balog, A.; Cass, Q. B. ScienceDirect.com - Tetrahedron: Asymmetry - Rotational features of carbon-nitrogen bonds in axially chiral o-tert-butyl anilides and related molecules. Potential substrates for the “prochiral auxiliary” approach to asymmetric synthesis. *Tetrahedron* **1997**.

(11) Gudmundsdottir, A. D.; Lewis, T. J.; Randall, L. H.; Scheffer, J. R.; Rettig, S. J.; Trotter, J.; Wu, C.-H. Geometric Requirements for Hydrogen Abstractability and 1,4-Biradical Reactivity in the Norrish/Yang Type II Reaction: Studies Based on the Solid State Photochemistry and X-ray Crystallography of Medium-Sized Ring and Macrocyclic Diketones. *J. Am. Chem. Soc.* **1996**, *118*, 6167–6184.

(12) Havinga, E.; Schlatmann, J. L. M. A. Remarks on the specificities of the photochemical and thermal transformations in the vitamin D field. *Tetrahedron* **1961**, *16*, 146.

CHAPTER 9. CONCLUSION

The quest to find alternatives and sustainable strategies to conventional methodologies in the chemical science has led chemists to utilize environmentally friendly and abundant reagents such as “light”. The science of using light to cause chemical reactions or photochemistry is regarded as a promising technology to complement conventional methodologies. However, when it comes to create chiral molecular scaffolds, photochemistry has relatively failed to achieve high stereoselectivities albeit chiral auxiliaries/inductors could be employed in this regard.

Chapter 1 highlighted the fundamental dichotomy between asymmetric thermally controlled reactions and asymmetric photochemical transformations. The drawback for the later one is that the rate and energetics for the chiral induction and bond breaking or bond/group migration processes are not synchronized. This is due to the relatively short lifetime of reactive species in the excited states where other phenomena *viz.* luminescence and radiationless decays could compete with photochemistry. Still, to achieve high stereoselectivities via photochemistry many strategies have been developed in recent years with varying degree of success. Nevertheless, the reaction conditions *viz.* reaction phase and prolonged irradiation time are not cost effective to compete with their established thermal counterparts.

To achieve high stereoselection using photochemistry, this dissertation describes a novel and viable strategy to employ atropisomeric photo-substrates that display built-in chirality i.e. the geometry of the systems of interest would be preset to undergo a stereospecific transformation upon light excitation. In the ground state, atropisomeric molecular systems have the propensity to have restricted or slow bond rotation (which translate with racemization) with respect to the temperature. However, upon photolysis, racemization in the excited state is forbidden or hindered; and thus, optically pure atropisomers could then undergo stereospecific transformation(s), which can lead to enantiopure photoproduct(s). This strategy of employing atropisomeric systems to achieve stereoselectivity draws inspiration from Havinga’s NEER (Non-Equilibrating Excited Rotamers principle.

As model systems, this dissertation focused on using atropisomeric acrylanilides and α-oxoamides in light induced 6π-electrocyclization and γ-H abstraction respectively. In chapters 2 to 5, we showed a new type of 6π-photocyclization, where the photo-substrates under study underwent a transformation with removal of the *ortho* chiral bias group *viz. tert*-butyl. Atropisomeric acrylanilides were

then shown to undergo stereospecific cyclization with respect to their spin states and phase of the reaction. For example, the dissertation demonstrated that in the case of α-substituted acrylanilide lacking a β-alkyl group upon direct irradiation reacted via the singlet excited state resulting in racemic 3,4-dihydroquinolinone photoproduct(s). On the other hand, reactivity from the triplet manifold by sensitized irradiation produced enantiopure product(s) with enantioselectivity as high as 92%. Similarly, the photoreaction of α-substituted acrylanilide under solvent-free irradiations (by direct irradiation) gave chirally enriched photoproduct(s). Other strategies *viz*. reaction under elevated pressure and reaction mediated by Lewis acid(s) and heavy cations to achieve high enantioselectivities were illustrated in chapters 6 and 7 respectively. To broaden the methodology described in this dissertation, the photochemical Norrish cyclization or γ-H abstraction with atropisomeric α-oxoamides leading to enantiopure β-lactam photoproducts was detailed in chapter 8.

In summary, the methodology described in this dissertation is a breakthrough in asymmetric solution phase photochemistry, where substrates with built-in chirality were effectively employed to achieve high stereoselectivities during photochemical transformations. The research work reported in this dissertation is a stepping-stone for developing novel stereospecific photochemical transformation in the research group of Prof. Sivaguru at North Dakota State University.